THE UNIVERSITY OF ADELAIDE

MECHANICAL ENGINEERING DEPARTMENT

FLUID DYNAMIC MEANS OF VARYING THE THRUST VECTOR FROM AN AXISYMMETRIC NOZZLE

submitted by

Steven Slavko Vidakovic

for the Degree of Doctor of Philosophy

February 1995

Awarded 1995

Summary

The use of jets to control the attitude of airborne and space vehicles has developed progressively during the past two decades. Typically gimbal mounted nozzles, or spoiler tabs introduced into the emerging jet flow have been used, the first for systems which require a relatively slow response time as in VTOL or STOL aircraft, the later where a rapid control response is required, as in the Australian designed *NULKA* hovering rocket missile decoy system in which the decoy rocket is 'balanced' on its jet like a pole on a finger. The life of the tabs in the corrosive high temperature, high velocity jet is short and such systems are restricted to a single mission of short duration. This type of rocket decoy requires precise, short time response control of both the magnitude and angle of the thrust to maintain the rocket in hover mode or to manoeuvre it to a new position. For future fighter aircraft entering the post stall domain during close combat, thrust vectoring or directing thrust to produce responses simultaneously in the yaw, roll and pitch directions, may be a deciding factor in surviving the encounter. On the other hand, the agility and manoeuvrability of the attacking missile determines the success of its mission. These are some of the aeronautics related stimuli for investigating novel ways of vectoring thrust from a nozzle.

Several researchers have investigated jet distortion in a convergent-divergent nozzle using secondary fluid injection downstream from the throat. The effectiveness of the secondary fluid injection depends on the divergence angle, nozzle geometry, position and orientation of the secondary fluid injection and the secondary to primary jet mass flux ratio. The common aim however is to form a separation bubble at the mixing region of the primary and secondary jets and so to alter the shape of the primary, initially axisymmetric, jet into an asymmetric jet at the nozzle exit.

Present research originated with Nathan and Luxton (eg. Luxton, Nathan and Luminis Pty. Ltd. (1987)) when it was discovered that a jet precesses from an axisymmetric Orifice-Cavity-Orifice nozzle configuration incorporating a large area ratio. It was found that for a wide range of geometric parameters the flow would precess but when a small asymmetry was introduced at the upstream orifice, the flow was deflected and remained stationary in an azimuthal direction which was determined by the azimuthal position of the disturbance. The applications of such a system were apparent. In particular, applications to VTOL/STOL aircraft, attitude control of airborne and space craft and the positioning of decoy hovering rockets were considered worthy of further study. This led to secondment of the author from the Defence Science and Technology Organisation to the University of Adelaide to undertake the study presented in this thesis.

The original nozzle configuration had large losses associated with the use of a primary orifice at entry to the cavity of the nozzle. It was therefore decided to use a smoothly contoured convergent-divergent nozzle, closely resembling that in a rocket motor, to lead into the cavity. Pressure tappings at the throat of this nozzle double as ports through any one of which can be introduced a small disturbance secondary jet to provoke from that point partial separation of the primary flow and so to produce an asymmetric wall jet in the divergent section leading into the cavity. As in the initial case, an orifice plate at the nozzle exit modifies the flow field inside the nozzle causing the asymmetric wall jet to deflect to large angles. The arrangement provides a novel method of deflecting a jet of fluid through large angles from the nozzle axis by purely fluid dynamic means. In the present thesis the mechanism that causes the deflection and the parameters which determine its magnitude have been investigated using surface flow visualisation, smoke visualisation captured on a high speed video recorder, laser sheet flow visualisation, nozzle surface pressure measurements, hot wire anemometry and laser Doppler velocimetry.

The results of a parametric study of the convergent-divergent nozzle, in which the length of the cavity and the diameter of the exit orifice have been separately varied, show that the azimuthal direction of the thrust can be controlled by fluid injection at the throat. The thrust magnitude reduces as the length of the cavity increases for a given exit orifice and the conical angle at which the jet is deflected can be set by altering the diameter of the exit orifice. The minimum momentum losses are incurred when there is no cavity and this also gives the maximum angle of deflected jet for a given exit orifice.

It is postulated that the large jet deflections result from impingement of the distorted wall jet on the lip at the nozzle exit. This angle through which the jet is deflected is influenced by a number of factors such as lip height, wall jet thickness and the nozzle exit area occupied by the deflected jet. When the wall jet, which occupies only part of the inner circumference of the nozzle, meets the lip at the exit plane, a stagnation line is formed. Below this line the flow is forced to form a vortex, the strength of which depends on the velocity, the lip height and the azimuthal extent of the impinging wall jet. The line defining this vortex must be closed and this is achieved by merging with the streamwise " legs " of the horseshoe vortex whose origin is at the initial disturbance at the throat. The combination forms a very strong vortex which loops outwards from the surface and over the wall jet causing it to deflect towards the nozzle centreline after separating upstream from the exit orifice. The vortex loop is further reinforced by the vortex which forms behind the exit lip as ambient fluid is entrained into the nozzle to replace fluid which has been entrained by the wall jet. Most of this entrained fluid moves upstream almost to the throat where it mixes with the wall jet. A tight streamline curvature over the lip as the entrained fluid enters the cavity produces an associated low pressure region locally around the exit plane which further assists the deflection of the primary jet.

When the fluid dynamic disturbance at the nozzle throat is large enough it causes an asymmetric separation of the primary flow at the throat which then follows the wall distal from the point where the secondary flow is introduced. As the attached primary flow moves downstream from the throat, it distorts into a thick wall jet as it passes through a positive streamwise curvature of the nozzle wall. As the streamwise curvature becomes negative, the wall jet becomes thinner and spreads azimuthally over a large portion of the surface, becoming relatively thin as it approaches the nozzle exit. This azimuthal spreading influences the magnitude of the affect of the lip at the exit of the nozzle as it influences the proportion of the primary flow momentum which is deflected into the vortex loop, hence influences its strength and hence influences the jet deflection. The azimuthal spread and consequent thinning of the wall jet varies with the length of the nozzle. Hence both the thrust and the angle of deflection of the jet are strongly influenced by the addition of an extension cavity at the end of the profiled divergent section of the nozzle. The effect of the exit ring (ie, the height of the lip of the exit orifice) is simultaneously dependent on the nozzle length. With no exit ring attached, the jet occupies part only of the nozzle exit. But with the exit ring, the deflected jet occupies a larger portion of the exit area and reduces the available area through which ambient fluid can be induced into the nozzle to satisfy the entrainment by the primary wall jet within the nozzle. This in turn reduces the pressure within the nozzle and causes an increase in the velocity of the induced ambient flow, an intensification of its streamline curvature and hence an increase of the transverse pressure gradient at the exit plane. This in turn augments the jet deflection. But clearly the strength of these effects depend on the

amount of thinning of the wall jet which occurs through azimuthal spreading, and this in turn depends on the nozzle length and expansion ratio.

Deflected jet angles in excess of 80° have been observed and these results appear to confirm the potential of the system for application in highly manoeuvrable fighters, VTOL/STOL aircraft and super manoeuvrable missiles and rockets. Thrust vector measurements, with the nozzle mounted on the end of a long flexible tube, indicate thrust vectoring efficiencies η as high as 70% for a deflected jet angle α of 50° and η as low as 45% at α of 80°.

Thrust vectoring capabilities of several forms of the nozzle have been explored and are presented. They confirm the potential of the system is such as to justify further development leading to possible use in super-manoeuvrable aircraft and missiles. Work in the supersonic flow regime in particular remains to be evaluated and validated. The flow is extremely complicated but it is believed that the contribution of the present thesis is providing phenomenological descriptions of the flow fields, and of the broad effects of the many parameters and variables which enter the system, opens the way to numerical modelling and hence to the design of practical systems.

Page

Contents

5 CD10 and CD20 Nozzle and their flow mechanisms 115

Statement of Originality

The material in this thesis is original and has not been submitted or accepted for the award of a degree or diploma at any other university and to the best of my knowledge and belief, the thesis contains no material previously published or written by another person except where due reference is made in the text of the thesis.

Steven S. Vidakovic

(February 1995)

Permission to Copy

The author consents to the thesis being made available for loan and photocopying provided that the thesis is accepted for the award of the degree.

Steven S. Vidakovic

(February 1995)

List of Figures

List of Tables

Acknowledgments

The work associated with this project has been monitored and directed meticulously by my supervisor Prof. R.E. Luxton. I am particularly grateful for his keen interest, enthusiasm and support in the project since its inception. With his insight, guidance and lengthy discussions on turbulent mixing and fluid flow in general, my understanding of the subject has greatly increased. This helped me to resolve the intricate flow characteristics associated with the flow studied in this thesis. A sincere thanks to Dr G.J. Nathan for his constructive comments and lengthy discussions with respect to the precessing jet and associated flows. I would also like to thank the Combustion Group members, Mr. S.J. Hill, Mr. G.J. Newbold and Mr G.M. Schneider for their contribution as well as the technical staff members in the electronics department, Mr S. DeIeso, Mr A. Mittler, the instrumentation department, Mr H. Bode and Mr G. Osborne and the workshop, Mr R. Jager and Mr C. Price, who have helped in the acquisition and manufacture of the experimental apparatus and associated components and maintained the equipment during my research. Also I would like to thank Department of Defence, Guided Weapons Division, D.S.T.O. Salisbury for their financial support and the Cadet Research Scientist Scholarship that I was awarded, which made it possible to do the research. In particular I am grateful to Mr P.H.O.Pearson, Dr D.Brown, Dr D.Gambling and Mr D.Thomson for their support and interest in the project over the years, as well as A.R.C. for their financial support of the project. I am also grateful to C.S.I.R.O. and in particular to Dr.J.Symons who encouraged me at the completion stages of the thesis. Finally to my family and especially to my wife Gordana who encouraged and supported me throughout the turbulent periods of the project, I thank you.

Dedication

I dedicate this thesis to my wife Gordana and our two sons, Nikolas and Alexander.

Notation

$\mathbf{A}$	Cross sectional area.
$\mathbf{AR}$	Ratio of exit to cavity area A_e/A_c.
$\mathbf{atm}$	Atmospheric or ambient.
$\mathbf{D}$	Diameter.
$\mathbf{D_o}$	Flow meter orifice plate diameter.
$\mathbf{f}$	Frequency.
$\mathbf{F}$	Total thrust.
$\mathbf{F_s}$	Side thrust.
$\mathbf{F^*}$	Total thrust at sonic conditions.
$\mathbf{h'}$	Pressure drop across the orifice plate (mm of water).
l_c	Length of cavity.
l_d	Length of divergent section.
$\mathbf{m}$	Mass flow rate.
$\mathbf{m^*}$	Mass flow rate at sonic conditions.
$\mathbf{P}$	Pressure.
$\mathbf{P_{atm}}$	Atmospheric pressure.
$\mathbf{P_{dr}}$	Driving or supply pressure.
$\mathbf{P_o}$	Stagnation pressure.
$\mathbf{P_r}$	Pressure ratio (P_d / P_{atm}).
$\mathbf{P_s}$	Static pressure.
$\mathbf{Q_t}$	Dynamic pressure based on throat velocity and density.
$\mathbf{r_{1/2}}$	Radial distance where the axial velocity is half the centre line value.
$\mathbf{Re_t}$	Reynolds Number - based on the throat mean velocity and diameter.
$\mathbf{T}$	Temperature.
$\mathbf{U_x}$	Mean time average velocity vector in x direction.
$\mathbf{U_y}$	Mean time average velocity vector in y direction.
$\mathbf{U_z}$	Mean time average velocity vector in z direction.
$\mathbf{u'_x}$,$\mathbf{u'_y}$, $\mathbf{u'_z}$	Mean turbulence intensities in x, y and z directions respectively.

x	Axial nozzle co-ordinate.
y	Transverse nozzle co-ordinate.
z	Cross-transverse co-ordinate.
α	The angle of the jet velocity vector w.r.t. the nozzle axis.
ν	Dynamic viscosity (kg m/s).
ρ	Density (kg/m^3).
μ	Kinematic viscosity (m^2/s).
β	The expansion angle from the throat w.r.t. the nozzle axis.
θ	Azimuthal angle.

Subscripts

atm	Based on atmospheric conditions.
c	Cavity.
dr	Drive or Supply pressure.
e	Exit conditions.
t	Throat conditions.
o	Stagnation conditions.
j	Refers to jet.

CHAPTER 1

Introduction

The ability to control thrust and vehicle orientation are very important factors in highly manoeuvrable rockets, hovering rocket decoys, such as the Australian designed *Nulka*, missiles **[304]**, tactical fighter aircraft and vertical and short take off and landing (VTOL\STOL) aircraft **[274]**. The aerodynamics of such vehicles have been studied, tested, documented and modelled quite extensively. The mission effectiveness of a vehicle depends very strongly on its range, speed and agility **[273]**. Both cruise and terminal velocities are affected by the aerodynamics, thrust availability and material properties. The agility of a missile can determine the success or failure of its single mission, especially for a surface to air missile (SAM) or an air to air missile (AAM).

Directional control of a conventional airborne vehicle is achieved by moving surfaces in the air stream to adjust the aerodynamic force vector. The alternative which is discussed in the present thesis is to control the thrust vector by novel means. Presently vectoring thrust may be achieved in a number of ways: using gimbals, by inserting tabs **[35]**, deflector plates or targets in the flow to deflect the thrust in a desired direction **[314]**, or physically modifying the shape of the nozzle **[168,169,318]**. Modern tactical fighters, such as Harrier jump jets, are utilising mechanical thrust vectoring to take off and land vertically and to enhance the performance of the aircraft in the post stall regime **[103,104]**. As missile targeting systems become "smarter" the future tactical fighter aircraft will depend primarily on manoeuvrability for survival. These considerations have provided the stimulus to investigate novel means of thrust vectoring.

Research carried out at the D.S.T.O. by the author, on the effects of the high temperature flow on the distortion of a control tab when inserted into a rocket motor plume, led him to the Mechanical Engineering Department of the University of Adelaide and to the work undertaken by Nathan and Luxton on the precessing jet from an axisymmetric nozzle.

The present thesis describes a thrust vectoring nozzle (TVN) which produces a jet which may be deflected at angles in excess of 80° from the nozzle axis by fluid dynamic means while maintaining total thrust efficiency of the order of 50%, or at 50° with an efficiency of the order of 70%. Vidakovic and Luxton thrust efficiency of the order of 50%, or at 50° with an efficiency of the order of 70%. Vidakovic and Luxton (1992) have compared thrust vectoring efficiencies for a range of nozzle configurations and full details are presented in this thesis. The thrust vectoring by fluid dynamic means is achieved by injecting secondary fluid at the nozzle throat and partially separating the primary jet causing it to deform into a wall jet on the wall opposite from that of the secondary fluid injection port.

The subject nozzle derives from a more general nozzle in which a naturally occurring instability causes the issuing jet both to deflect sharply from the axis and to precess. As a by-product of the present vectored jet study, an attempt is made to describe the mechanism by which the precession of the jet is generated. Various types of flow visualisation techniques have been implemented to investigate the flow both inside and outside the nozzle, Vidakovic and Luxton (1991). To quantify these flows a number of parameters have been measured. Velocity vectors were measured using hot wire anemometry, pitot probes and a two channel L.D.V. system. Both static and total pressures were also measured for a variety of driving pressures and nozzle configurations. In this thesis the above results are documented and examined in detail for driving pressures relative to the atmosphere of up to 100 kPa and some results are extended to driving pressures up to 680 kPa.

A number of **[26,56,69,314]**have been carried out by others of the effects of the secondary fluid injection downstream from the throat on the flow characteristics and relevant details of these are discussed in detail in Chapter 8. The research reported by Porzio and Franke (1989) and that by Friddell and Franke (1992) each describe overexpanded supersonic flow generated by a confined jet thrust vector control nozzle of a specific configuration which is not too dissimilar from one of the configurations in this thesis. Their thrust vectoring control was achieved by injecting a secondary fluid some distance downstream from the throat to produce a wall jet which was then deflected by a lip at the exit. Both of these cases are discussed in detail in the Chapter 8. The use of an overexpanded nozzle in the present work may appear to limit applications of the present phenomenon to smaller nozzles such as sustainer rocket motors, but it should be noted that the lower bound for the expansion ratio required to achieve the dramatic jet deflection angles found in the present work is yet to be determined. There have been numerous studies of jets in cross flows and of the two-dimensional fluid "flip-flop", but apart from the work of Franke and his co-workers, to the author's knowledge there has not been any study reported on the deformation of a primary jet from an axisymmetric nozzle by fluid injection at the throat. Nor has there been any detailed study of the phenomenon by which the primary wall jet is deflected at a sharp angle across the nozzle centre line by a small lip at the exit plane.

1.1 Nozzles That Generate Strong Mixing

Fluid exiting from a nozzle produces thrust and, if designed appropriately, can generate high rates of mixing over a range of scales, as is required between a fuel and an oxidant, for stable combustion. A common aim of most gas phase nozzle designers is to increase the rate of mixing between the jet and its surroundings. For aerospace applications such mixing is important for noise reduction and to modify the infra red signature of the jet and this must often be achieved without significantly reducing the thrust efficiency of the nozzle. Two basic means of mixing enhancement are used. In the first a blockage is introduced into the flow to create a large recirculation zone behind the blockage. The blockage may involve the introduction of a solid body **[148,167,234,240,276]**, or the generation of an aerodynamic blockage either to act directly in a manner similar to a solid body but without the generation of additional vorticity, or to create a recirculation zone by means of swirl **[65,66,67,78,283,284]**. In the second case the mixing is enhanced by modification of the dynamics of the entrainment process through the introduction of large-scale vortical structures **[47,48,79,130,140,142,205,229]**. One way of producing large scale vortical structures is by causing a jet to precess. This generates mixing on a scale which is much larger than that of the nozzle itself **[113,206,207,208,209]**.

1.1.1 Large Scale Mixing in Recirculating Flows

Bluff body flame holders and swirl burners both generate a recirculation zone down stream from the nozzle exit. The recirculation zone is produced by a strong adverse pressure gradient leading to separation of the boundary layer which develops from the stagnation point on a bluff body flame holder. Swirling flow generates a recirculating vortex surrounding a low pressure core due to centrifugal motion of the air. If the swirl is strong enough and the externally imposed pressure gradient is correctly set a recirculation zone is established and strong mixing occurs **[6,97,101,166,184,284]**. The use of swirl has also been proposed to control core nozzle mass flux in low by-pass-ratio ducted fan engines, in some cases with little or no loss of thrust over a variable-area nozzle **[141]**. On the other hand the addition of swirl in a nozzle may reduce the thrust efficiency by an amount which depends on the swirl intensity and the swirl profile **[289]**.

The redistribution of the axial momentum of the jet from the above nozzles from its concentration around the nozzle axis to the radial and azimuthal directions produces a low pressure core which in turn produces a recirculation zone in which strong mixing can occur. This has been a prime aim in burner design. The axisymmetric redistribution of momentum to create a swirling annular jet which has a significantly larger shear layer surface area is one of the factors that causes strong fine scale mixing in such nozzles. The formation of the recirculation zone is influenced by geometric parameters such as the burner quarl **[67,101]** and furnace shape. The influence of the recirculation zone on fluid flow is complex. This complexity increases when a flame is being maintained by this type of nozzle despite the fact that it is well known that swirl burners and bluff body flame holders stabilise the flame. Spalding (1953) suggested that when combustion occurs in the recirculation zone, the hot combusting material is carried upstream in the recirculating zone and acts as a source of ignition for the oncoming mixture. This is only one component of the more general observation by Leuckel and Fricker (1976) and Fricker and Leuckel (1976). The high velocity gradients found near the edge of the internal reverse flow zone improve turbulent mixing between fuel and air and give a more complete mixing and stable flame. Each burner has a critical swirl requirement and it has been found that there is no advantage in exceeding this value since no improvement in flame stability results. This has been confirmed by Claypole and Syred (1981,1982) who measured mass flux in the recirculation zone and found that only 5% to 12% of the total mass flux is recirculated. The result indicates that the recirculation zone is probably not an ignition source as has been indicated by Spalding (1953).

Hallett and Gunther (1984) performed experiments on swirling air flows in a sudden expansion at entry to a model chemical reactor. Their study revealed a precessing flow in which the flow entering the expansion was deflected away from the axis of symmetry and caused to precess around it. Independently Nathan (1988) during his Ph.D. studies, Luxton, Nathan and Luminis Pty. Ltd. (1987) and Nathan and Luxton (1989) had been investigating the precessing jet phenomenon to determine the parameters effecting and affecting precession and the mechanism by which the precession is driven. The nozzle configuration tested was an Orifice-Cavity-Orifice configuration with an area ratio substantially larger than that used by Hallet and Gunther. An extensive range of flow visualisation techniques including representation of the mean surface flow were used to determine a plausible flow topology. A model of the flow patterns inside the nozzle was developed and the geometric parameters determined for maximum likelihood of precession to occur. This research is currently being continued by a number of investigators in the University of Adelaide and elsewhere. Nathan (1988) found that when a small asymmetry is placed at the primary orifice, the flow ceases to precess and locks to one side of the downstream cavity. When a small lip is placed at the exit of the nozzle, the flow is deflected across the nozzle axis at a sharp angle. It is this type of deflected jet, which may have potential applications in the control of agile missiles, rockets and STOL/VTOL aircraft, which is investigated in detail in the present thesis.

1.1.2 The Precessing Jet Flow

The observation of an unsteady asymmetric flow downstream from a small abrupt axisymmetric expansion, Hallet and Gunther (1984), relied on the introduction of weak swirl into the flow upstream from the expansion. Nathan (1988) had found that upstream swirl was not needed but could be used to stabilise the direction of precession, which otherwise tended to be intermittent in the range of area ratios then being studied. Luxton and Nathan (1989) later showed that the swirl was not needed (other than to fix the sense of precession) for area ratios greater than about 20. Hallet and Gunther's research was primarily concerned with the effects of the swirl intensity on the downstream flow and mixing. It was observed that as the swirl exceeded a critical intensity, the precession ceased and mixing was further enhanced by the formation of a reversed flow zone, a phenomenon they related to vortex breakdown **[94,172]**. Dellenback et.al. (1988), following Hallet and Gunther, had also observed the precession at low swirl levels through a small expansion and measured a precession frequency of the order of 1 Hertz in their apparatus.

The understanding of the phenomenon at the time at which author joined the Department of Mechanical Engineering may be summarised as follows:

- A precessing jet flow occurs in an axisymmetric cavity downstream from an abrupt axisymmetric expansion and gives rise to a precessing jet at outlet through a small lip at outlet from the nozzle.
- The main thrust of the overall research program was aimed at enhancing the mixing and optimising the burning characteristics of a gas jet through the nozzle. Nathan and Luxton had found that when an asymmetry is introduced at the primary orifice (or at the throat of a profiled nozzle) the jet ceases to precess and remains deflected in a particular azimuthal direction controlled by the azimuthal position of the asymmetry. The thesis builds on these initial observations and contributes to the longer term aim of producing a non-intrusive means of controlling VTOL\STOL aircraft and highly manoeuvrable rockets and missiles.

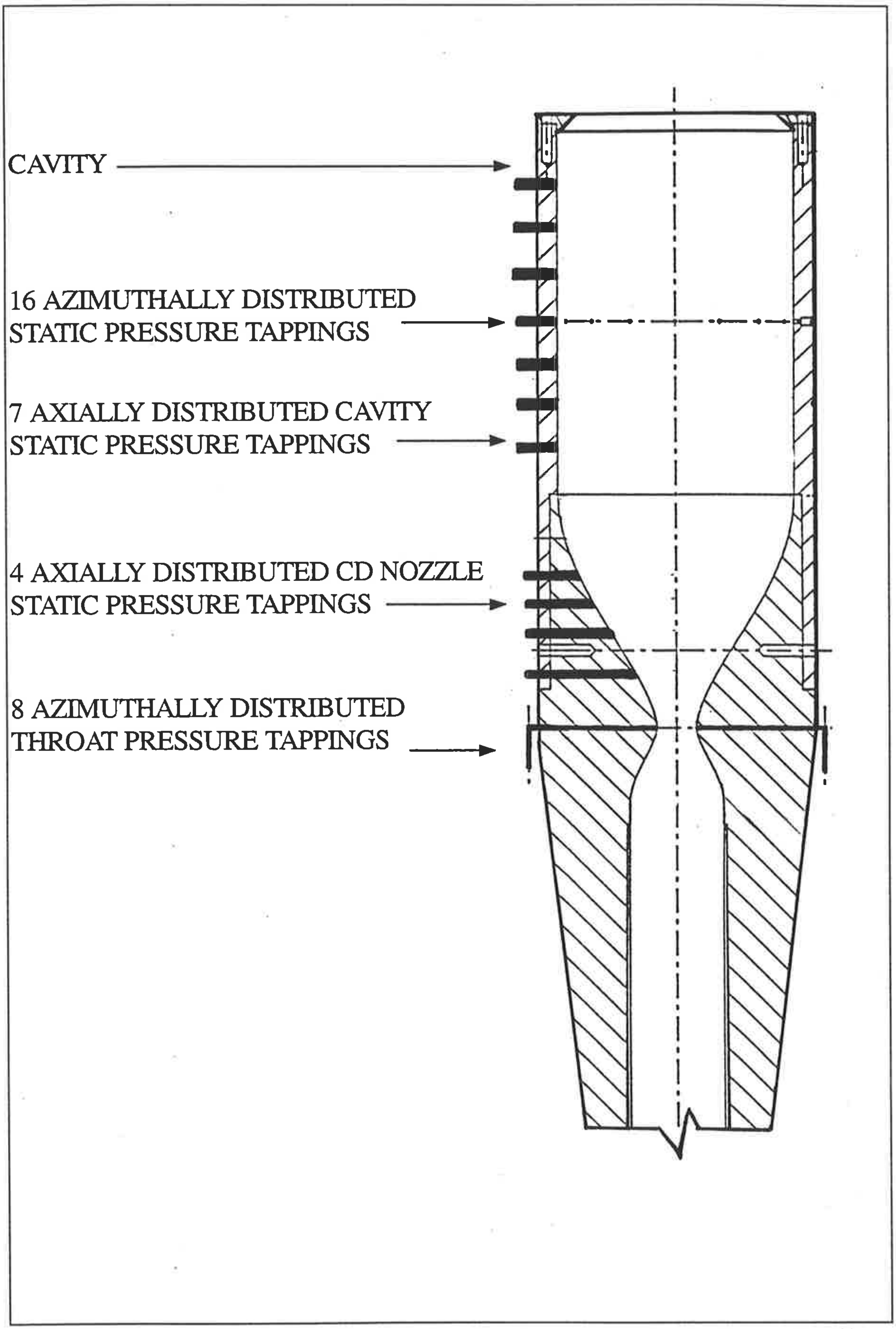

Figure 1.1. Diagram of the convergent-divergent nozzle and pressure tapping locations on the 100mm cavity of the CD10 nozzle.

1.1.3 The Non Precessing Fluid Dynamically Deflected Jet

A description of the asymmetric flow produced in an axisymmetric convergent-divergent nozzle, deduced from various methods of flow visualisation, from velocity and pressure flow field measurements and supported by some theoretical predictions, is presented here. The respective influences of Reynolds number, cavity length, exit ring diameter and primary and secondary mass fluxes on the flow characteristics are described. The over-expanded nozzle used in the experiments is derived from the geometry selected by Nathan (1988). It has smoothly profiled axisymmetric convergent-divergent walls, in contrast to an abrupt expansion and closely resembles a typical rocket motor geometry. The exit walls of the nozzle were made parallel to the nozzle axis allowing cavities of different lengths to be attached to the downstream end. The axisymmetric cavities are made from optical quality acrylic so that laser Doppler velocimetry could be used to measure velocities inside the cavity and to allow laser sheet visualisation. The initial nozzle length to diameter ratio investigated was 2.67, length being measured axially from the nozzle throat, and the nozzle exit to throat diameter ratio was 6, with throat diameter of 10 mm as shown in **Figure 1.1.** This configuration had been found to produce a deflected jet which precessed, albeit intermittently. Cavities considered in this study had nozzle length to diameter ratios l_n / D_c of 1, 2, 2.67 and 4.33 corresponding to no cavity, 60mm, 100mm and 200mm cavities respectively each with 60mm internal diameter. The nozzle converges from the 25mm diameter brass air supply tube to a 10mm throat diameter and then smoothly expands to 60mm to accommodate a smooth transition to the internal diameter of the cavity. The length of the divergent section leading from the nozzle throat to the entry of the cavity is 60mm. The nozzle configurations tested are defined as shown in **Table 1.1.**

As has been shown in flow investigations with a two dimensional backward facing step **[286,294,295]**, double backward facing steps **[84,213,267]**, and with an axisymmetric abrupt expansion **[57,322]**, the reattachment length downstream from the step varies, is unstable and is Reynolds number dependent. Numerical methods have also been employed to compute the flow in the separated region behind backward facing steps **[17]** using both upwind and central difference schemes for laminar and turbulent flows. This instability in the flow over two-dimensional double backward facing step can lead to the two dimensional flip-flop phenomenon. In an axisymmetric case, the reattachment length instability may lead to

Table 1. 1 Nozzle configurations tested.

Nozzle Name	Definition	Researcher
Abell Nozzle:	Short Cavity Nozzle	(Abell)
MLC Nozzle:	Mid-Length Cavity Nozzle	(Nathan)
LC Nozzle:	Long Cavity Nozzle	(Nathan)
CD Nozzle:	Convergent-Divergent Nozzle	(Vidakovic)
CD6 Nozzle:	60 mm Cavity attached to CD Nozzle	(")
CD10 Nozzle:	100 mm Cavity attached to CD Nozzle	(")
CD20 Nozzle:	200 mm Cavity attached to CD Nozzle	(")
RP45 Nozzle:	Square 100 mm Plate, 45° to Convergent Nozzle exit	(")
RP60 Nozzle:	Square 100 mm Plate, 60° to Convergent Nozzle exit	(")
B45 Nozzle:	45° Bend 10 mm ID at Convergent Nozzle exit	(")
B90 Nozzle:	90° Bend 10 mm ID at Convergent Nozzle exit	(")

Note: *Nozzles RP45, RP60, B45 and B90 were only investigated to compare their thrust vectoring capabilities with those of CD family of nozzles.*

a precession of the exiting jet, Nathan (1988), which is the three-dimensional equivalent of the two-dimensional flip-flop.

The reattachment length in the cavity of the MLC nozzle is unstable and a similar instability was noted with the asymmetric separation in the contoured nozzle, which increased with increasing Reynolds number based on the throat velocity and diameter. In the CD Nozzle at Reynolds numbers below about 30,000, the jet remains predominantly axisymmetric. Above this Reynolds number it switches back and forth intermittently from an axisymmetric to an asymmetric flow indicating clearly that the jet separation in the adverse pressure gradient downstream from the throat is unstable. This continues up to a Reynolds number of around 50,000 above which the flow is asymmetric and changes its azimuthal position randomly, since there can be no preferred azimuthal direction in a perfectly axisymmetric nozzle. If the flow is not disturbed the jet precesses periodically around the nozzle, exiting the nozzle as a wall jet, pauses, and then precesses again in an apparently randomly determined direction. This intermittent flow may be described as the three dimensional equivalent of an untuned two-dimensional fluid "flip-flop". Similar flow characteristics are exhibited when the cavity is attached, CD6, CD10 and CD20 Nozzles, but the different cavity lengths can cause changes to occur at lower Reynolds numbers. The longer the cavity, the greater is the diffusion of the wall jet inside the cavity. This reduces the centre line velocity and hence reduces the momentum of the jet at the exit of the nozzle. The exit lip is located at the end of the nozzle and it is the combination of the lip height and the length of the nozzle, which consequently determines the wall jet thickness, that determines the angle at which the jet exits from the nozzle.

The large streamline curvature observed when smoke is used to visualise the flow at the nozzle exit plane indicates the presence of a strong radial pressure gradient across the jet at exit. Random variations in the local entrainment of fluid into the asymmetric jet in the confinement of the axisymmetric nozzle generates azimuthal pressure gradients. These unstable pressure gradients cause the apparently random changes in the azimuthal direction of the deflected jet. The azimuthal direction can be controlled by injection of secondary fluid at the throat. The fluid dynamic means of control considered in detail in this thesis is achieved by continuous injection of air normal to the primary flow at the throat. The injection is through a pressure hole which also serves as one of the pressure tappings at the throat when not being used for injection. Due to the fluid dynamic disturbance, the flow through the throat is forced to separate partially in the region where the disturbance is introduced. Opposite the disturbance the jet remains attached to the wall up to the exit lip, where it is forced to deflect at a large angle. Initially it was thought that this was due to the impingement on the exit lip. As will be demonstrated in the thesis, the flow structures which cause the deflection are both extremely intricate and remarkably resilient. These structures deflect the jet across the nozzle axis. Since the jet does not occupy the whole of the exit plane, ambient fluid is drawn into the cavity and this induced flow contributes to the intricate three-dimensional flow patterns within the nozzle. The deduced flow patterns are shown to be consistent with the surface shear stress patterns on the nozzle wall and are discussed in detail in Chapter 3. The entrained fluid mixes with the issuing primary jet and leaves the nozzle enfolded into a pair of concentrated streamwise vortices.

1.2 The Thesis Structure

The original aims of the present study were quantification of the thrust produced by the deflected air jet from this nozzle, examination of the effects of nozzle parameters on the thrust and jet deflection angle and development of an understanding of the flow phenomena involved. In the event, definition of the flow topology has proved to be a major scientific challenge. While the topological description of the flow which has been developed is sufficient to guide the interpretation of the parametric studies of jet thrust and deflection, it does not constitute a full fluid dynamic description. The present thesis has established the feasibility of the jet vectoring system and its potential benefits justify investment in developing the system further. In scientific terms it has provided the starting point for the full dynamic analysis which will be required for reliable practical design.

The mechanism by which the jet develops from an axisymmetric flow inside an axisymmetric nozzle to a highly deflected wall jet at the exit is discussed in detail in the following sections. The parameters that determine the jet deflection angles and thrust magnitudes are derived from the analysis of the experimental data.

Chapter 2 describes the apparatus used in derivation of experimental results. Chapter 3 introduces the concept of thrust vectoring and describes related nozzles evaluated by other researchers. It also discusses three different modes of flow excitation. In Chapter 4 the CD nozzle is evaluated in detail using various experimental techniques and flow mechanism is deduced from the results. In Chapter 5, the CD10, CD20 and other nozzles are evaluated and compared with the mechanisms and performance of the CD nozzle. Thrust was evaluated in Chapter 6 for all the nozzles considered. Factors determining the performance of the CD family of nozzles are summarised in Chapter 7 and compared with other research and presented in Chapter 8. Conclusions and future suggested work is discussed in Chapter 9.

CHAPTER 2

Apparatus

The equipment used in the experiments is described in the present chapter. Where specific apparatus is used in a particular experiment, it is described in the relevant section.

2.1 The Convergent-Divergent Nozzle and Thrust Measurement System

The experiments reported in this thesis relate to an overexpanded convergent-divergent nozzle to which cavities of various lengths can be attached at the exit from the contoured divergent section. A nozzle is here defined as the axisymmetric convergent-divergent section with or without a cavity. CD Nozzle is defined as a convergent-divergent nozzle without a cavity, where as CD6, CD10 and CD20 nozzles are defined as a convergent-divergent nozzle with the addition of a 60mm, 100mm or 200mm length cavity respectively. At the nozzle exit a sharp edged orifice is attached which deflects the wall jet. The thrust vectoring capabilities of four other nozzles have been tested and these are based on the convergent section of the CD nozzle with various attachments at the exit to set the flow direction. RP45 Nozzle has a 100 mm rectangular plate inclined at 45 degrees and RP60 Nozzle has a 100 mm rectangular plate inclined at 60 degrees at the exit from the convergent nozzle. B45 Nozzle has a 45 degree bend of the same diameter as the throat attached at the exit and B90 Nozzle has a 90 degree bend attached at the exit from the convergent section.

The experimental apparatus is illustrated in **Figure 2.1. 1** and consists of a convergent-divergent section equipped with eight equally spaced throat static pressure ports and four axial static pressure ports along the divergent section of the nozzle. Manufacturing drawings and dimensions of the nozzle and the exit rings can be found in Appendix A. At exit from the divergent section, the rate of change of area is zero and the internal diameter is the same as that of the cavity section so that it couples smoothly. The convergent-divergent nozzle profile has been chosen such that in six throat diameters the nozzle expands following the curve

$$y=C_1\sin(C_2x)^{1.5} + C_3 ,$$

where C_1,C_2 and C_3 are constants. Dry filtered air is supplied to the apparatus via a 25 mm diameter line connected to a 17 m^3 air storage vessel. The storage vessel is maintained at 680 kPa pressure by a compressor capable of delivering 5.8 m^3 per minute.

The convergent-divergent nozzle receives air from a straight 0.9 metre long, 25 mm I.D., 9 gauge brass tube, which is downstream from the orifice plate flow meter described in Section 2.3. They are connected via a length of flexible high pressure hose. Two different apparatus arrangements are used for the acquisition of experimental data. In the first arrangement, **Figure 2.1. 1**, the supply tube is fixed vertically into a heavy steel base plate equipped with four adjustable levelling screws. The base of the brass supply tube is fitted with strain gauges which are used to measure the bending, torsion and compression reaction to the momentum of the vectored jet, details of which can be found in Appendix A. **Figure 2.1. 4** shows the calibration of the strain due to bending caused by the side force applied at the nozzle exit. In the second arrangement, the supply tube is fixed horizontally on a traverse table and coupled to an orifice plate flow meter via flexible high pressure hose. The other end of the supply tube has the attached nozzle orientated so that the L.D.V. beams can traverse the flow in each of the three directions shown in **Figure 2.1. 2** This arrangement was designed to accommodate studies of both 2-D plane jets and wall jets shown in **Figure 2.1. 6.**

At the nozzle throat diameter eight pressure tappings of 1mm diameter are spaced equally around the throat to measure the throat static pressure distribution. One of the pressure tappings is enlarged to 2mm in diameter and doubles as the secondary fluid injection port. Four pressure tappings also of 1mm diameter are placed axially along the divergent part of the nozzle to measure the axial distribution of pressure in the divergent section of the nozzle.

These pressure ports, shown in **Figure 2.1.5**, are in line with the axial pressure ports situated along the CD10 nozzle, shown in **Figure 1.1.** A basic convergent-divergent nozzle was reproduced with identical contour, from the same mould, and used to investigate the effects of secondary injection port diameters ranging from 0.5 mm to 3 mm. The range of secondary injection port diameters were studied to ascertain both their efficacy in causing local jet separation and the degree of geometric interference they impose on the axisymmetric flow and the results of these findings are presented in the following sections.

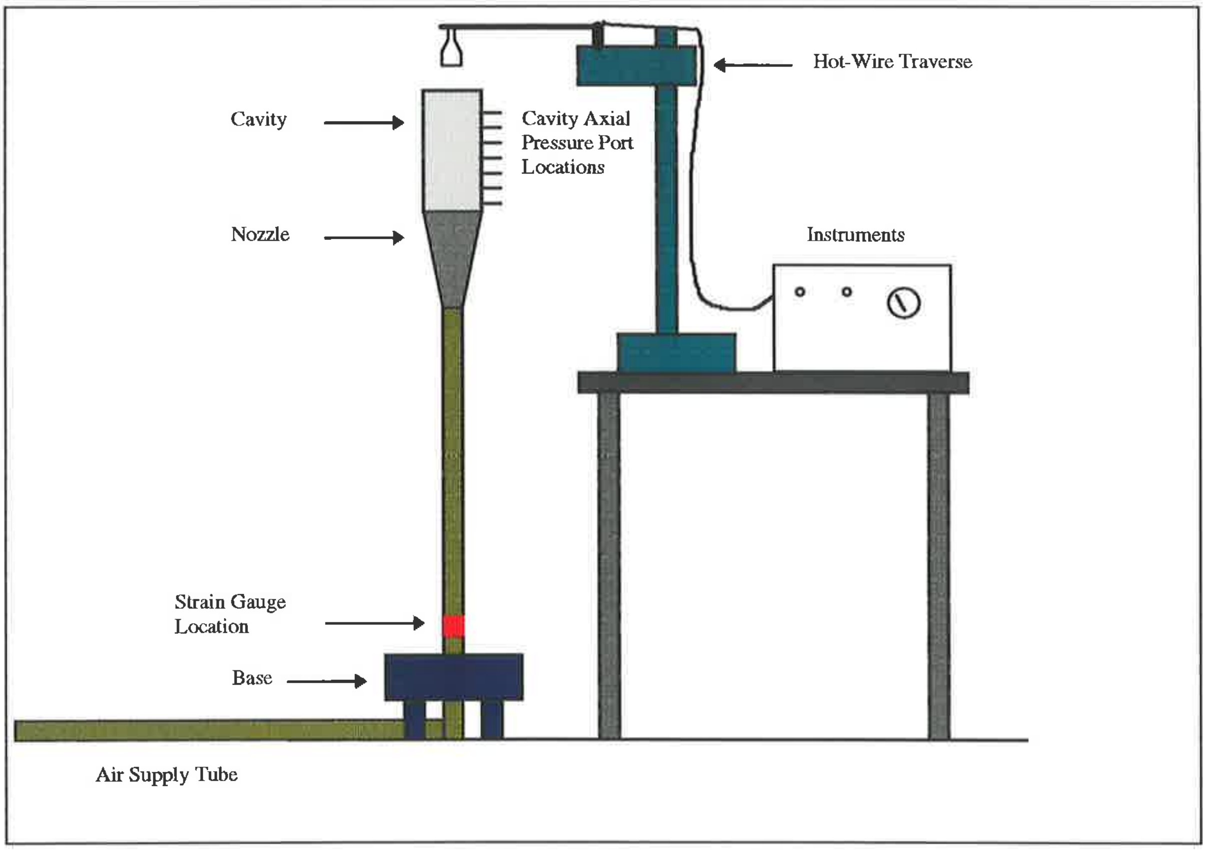

Figure 2.1. 1 Diagram of the main components of the experimental apparatus.

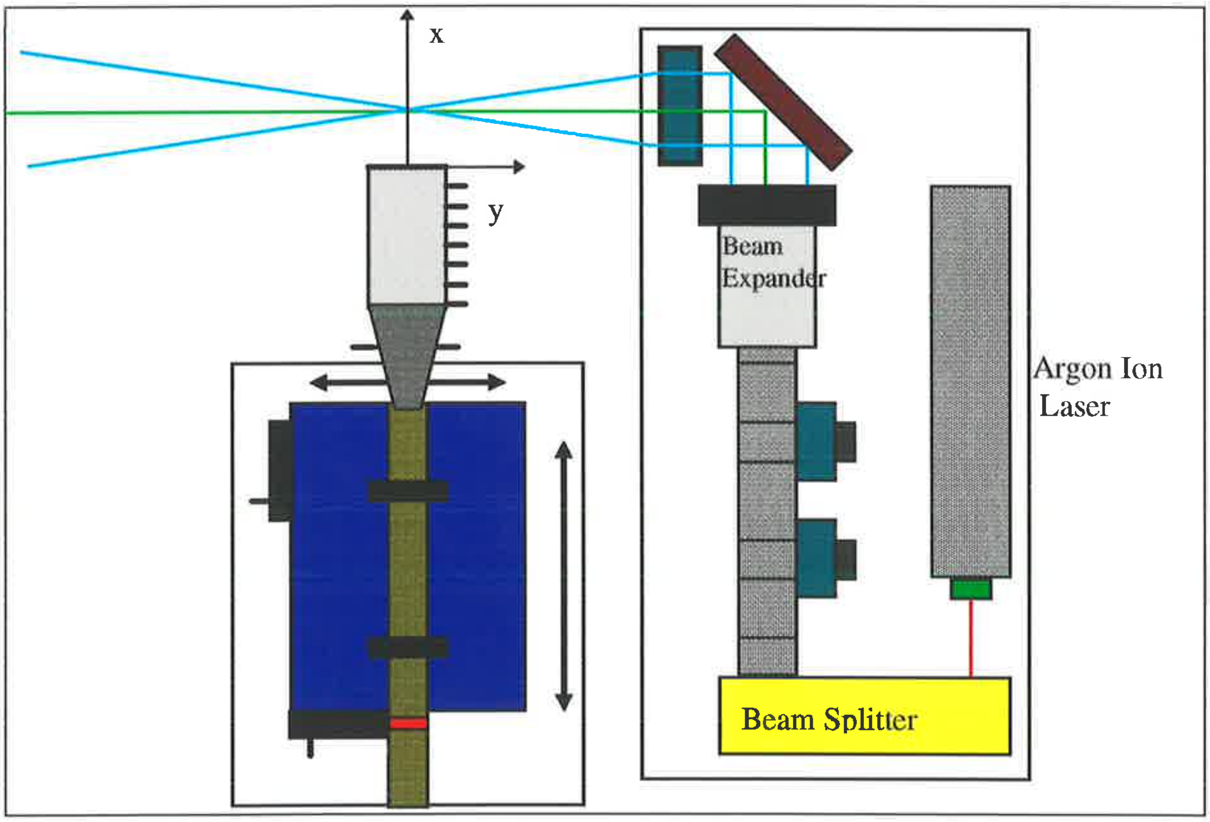

Figure 2.1. 2. Horizontally aligned nozzle apparatus and laser Doppler velocimetry arrangement.

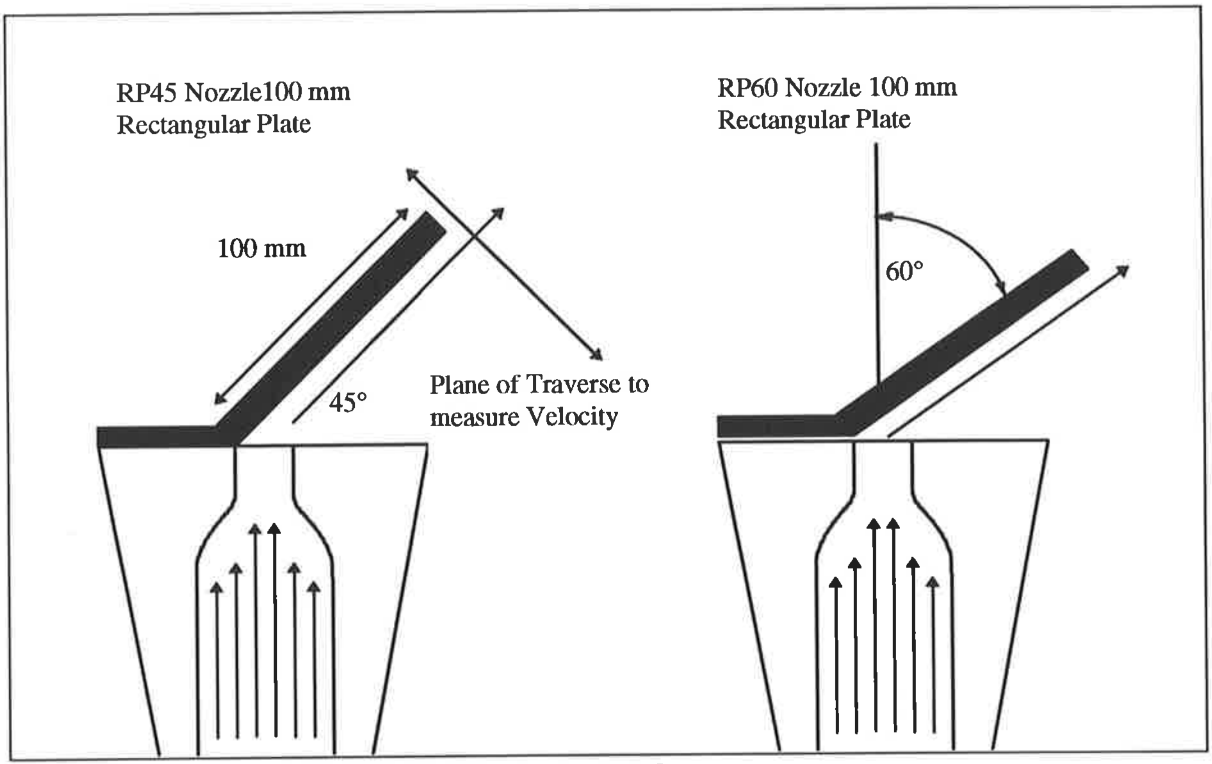

Figure 2.1.3. Schematic diagram of other nozzles tested.

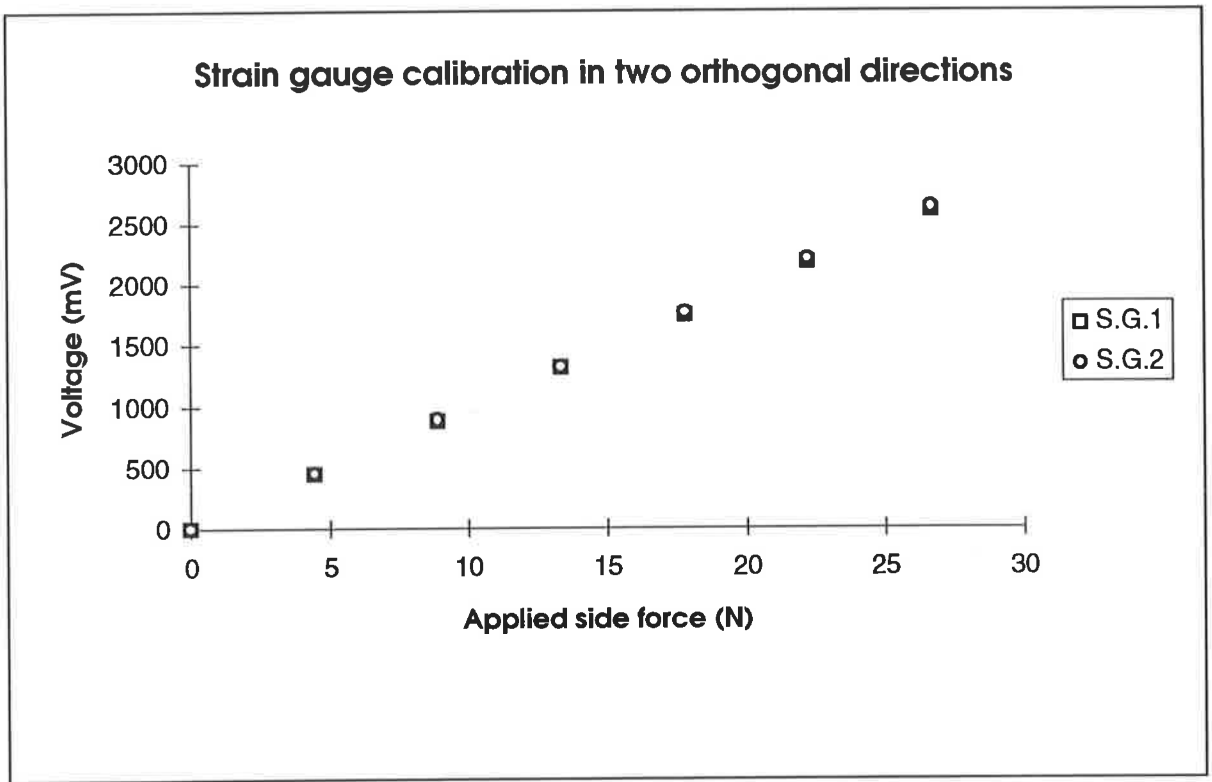

Figure 2.1.4. Calibration plot of strain gauges used to measure bending moment due to side force produced by deflected jet, in two orthogonal directions.

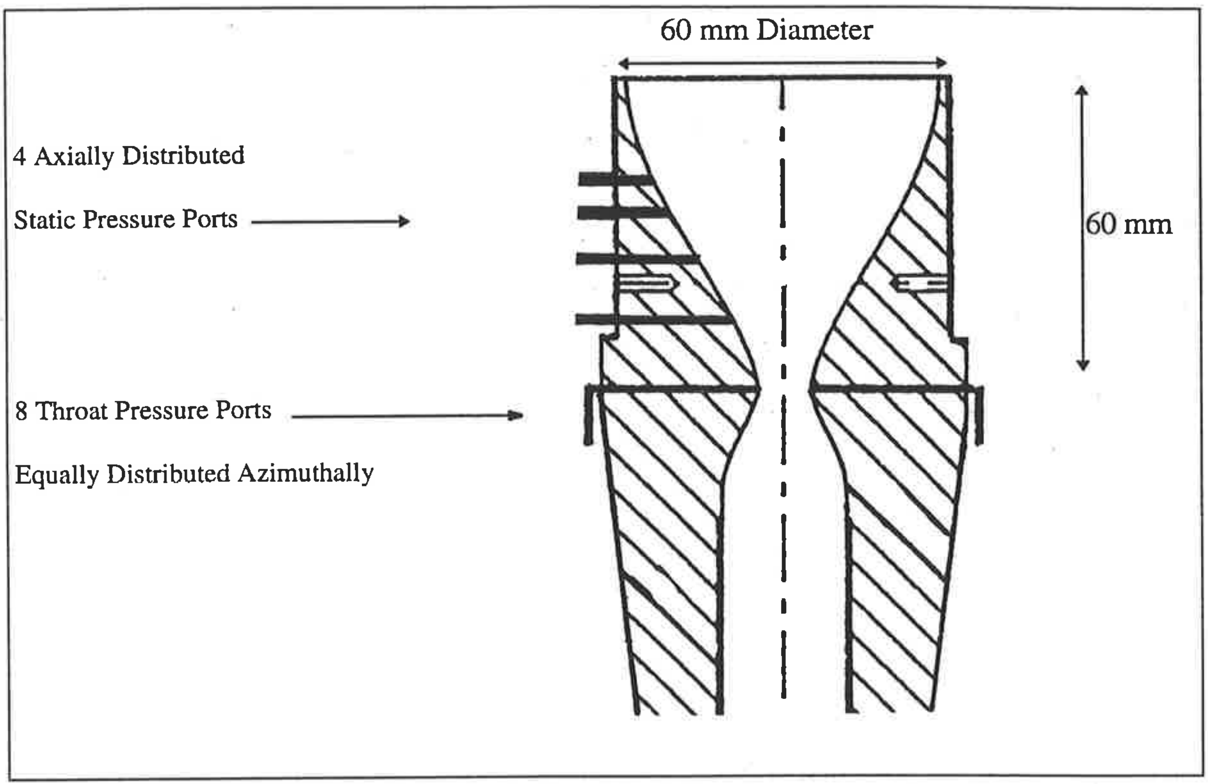

Figure 2.1.5 CD nozzle profile dimensions with axial and throat pressure port locations.

The nozzle has a fluid dynamically smooth surface finish. The 100 mm cavity connected to the divergent part of the nozzle, to give the CD10 nozzle, is manufactured from transparent acrylic resin to allow simultaneous use of laser sheet flow visualisation and LDV velocity measurements in the cavity while measuring cavity wall pressure using 16 equally spaced circumferential pressure tappings at mid-length and 7 equally spaced axial pressure tappings as shown in **Figure 1.1.** This cavity, however, was found to be optically inadequate and three other transparent 60 mm I.D. cavities, 60 mm, 100 mm and 200 mm long, each with only 0.5 mm wall thickness were manufactured to minimise the laser beam distortion through the cavity walls. No wall static pressure ports were fitted to these three cavities. The eight cavity exit rings considered are sharp edged, 20mm to 55mm I.D. and 5mm thick with a chamfer facing the flow. The exit rings are fixed to the 100mm long, 5mm wall thickness cavity by four screws. For the thin wall cavities the fixing arrangement of exit rings is by wires threaded through the exit ring and attached to the nozzle. Full details of the apparatus may be found in Appendix A.

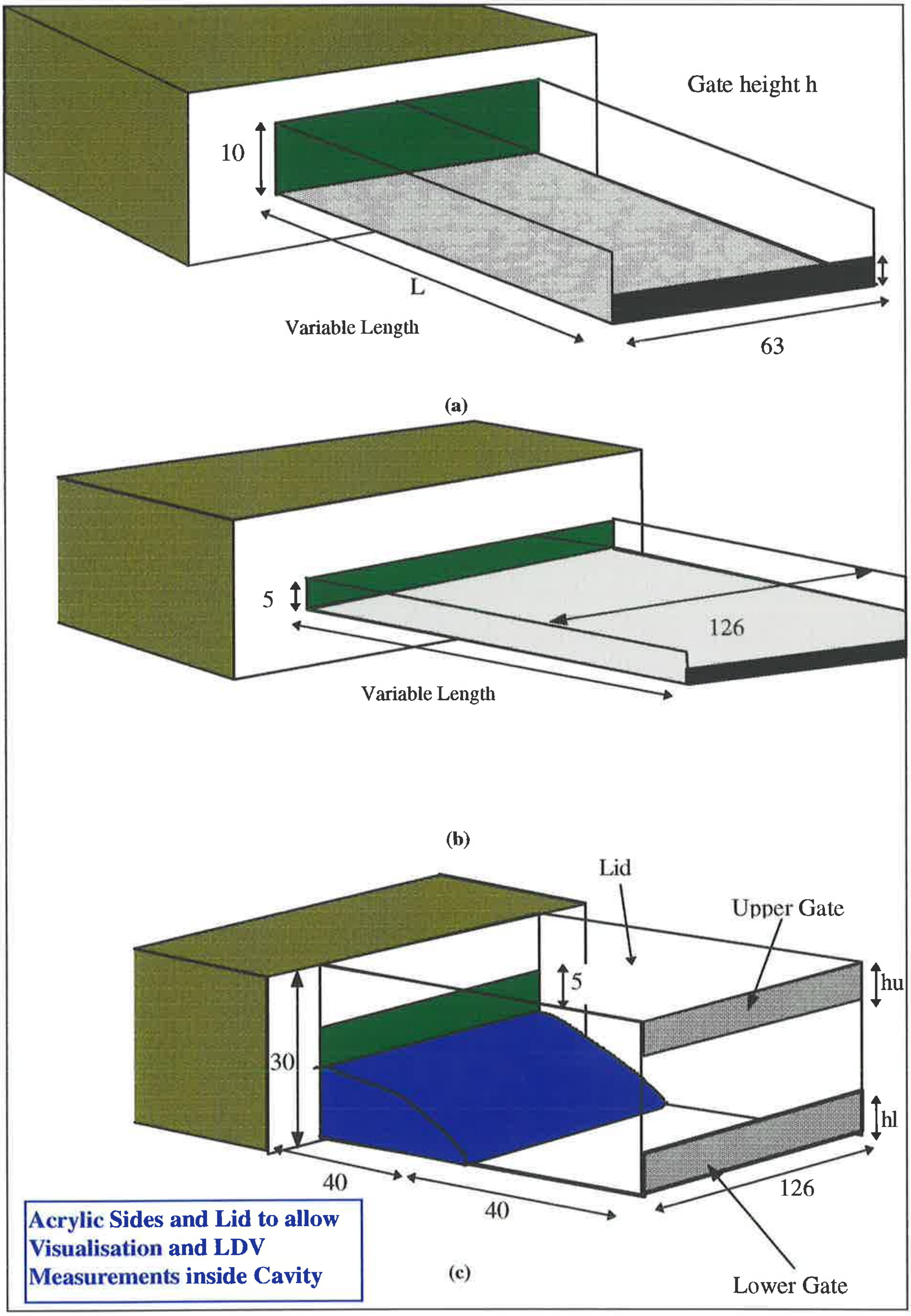

Acrylic Sides and Lid to allow Visualisation and LDV Measurements inside Cavity

Figure 2.1. 6 Diagram of 2-Dimensional configuration channel flows investigated. (a) 63x10 mm, (b) 126x5 mm and (c) 126x5 mm 2-D cavity with lower step contoured and upper step abruptly expanded, including a lower and upper exit gate.

2.2 Calibration nozzle

A calibration nozzle which produces a parallel flow at its exit was used to calibrate the orifice plate flow meter and to measure static pressure in the chamber upstream from the nozzle. The calibrations were initially carried out by Nathan (1988) and by Newbold (1989) , unpublished internal report, and a linear relationship between the flow rate and the orifice plate differential pressure was established. These results were independently confirmed by the author. As the calibration nozzle area contraction ratio was 100, the upstream static pressure measured was effectively the reservoir pressure. The static pressure in the chamber was calibrated with high flow rates so that the upstream static pressure results could be used to evaluate the flow rate at high driving pressures when the relationship between flow rate and the orifice plate pressure differential become non linear.

Since the velocity profile at the exit of the calibration nozzle was found to be uniform, a point measurement at the exit was sufficient to calculate the mass flow rate through the calibration nozzle. The velocity profiles were measured using both pitot-static probe and laser Doppler velocimetry and a sample result of the later method is shown in **Figure 4.8. 3**. The traverses were carried out in both y and z directions to confirm the axisymmetry of the flow.

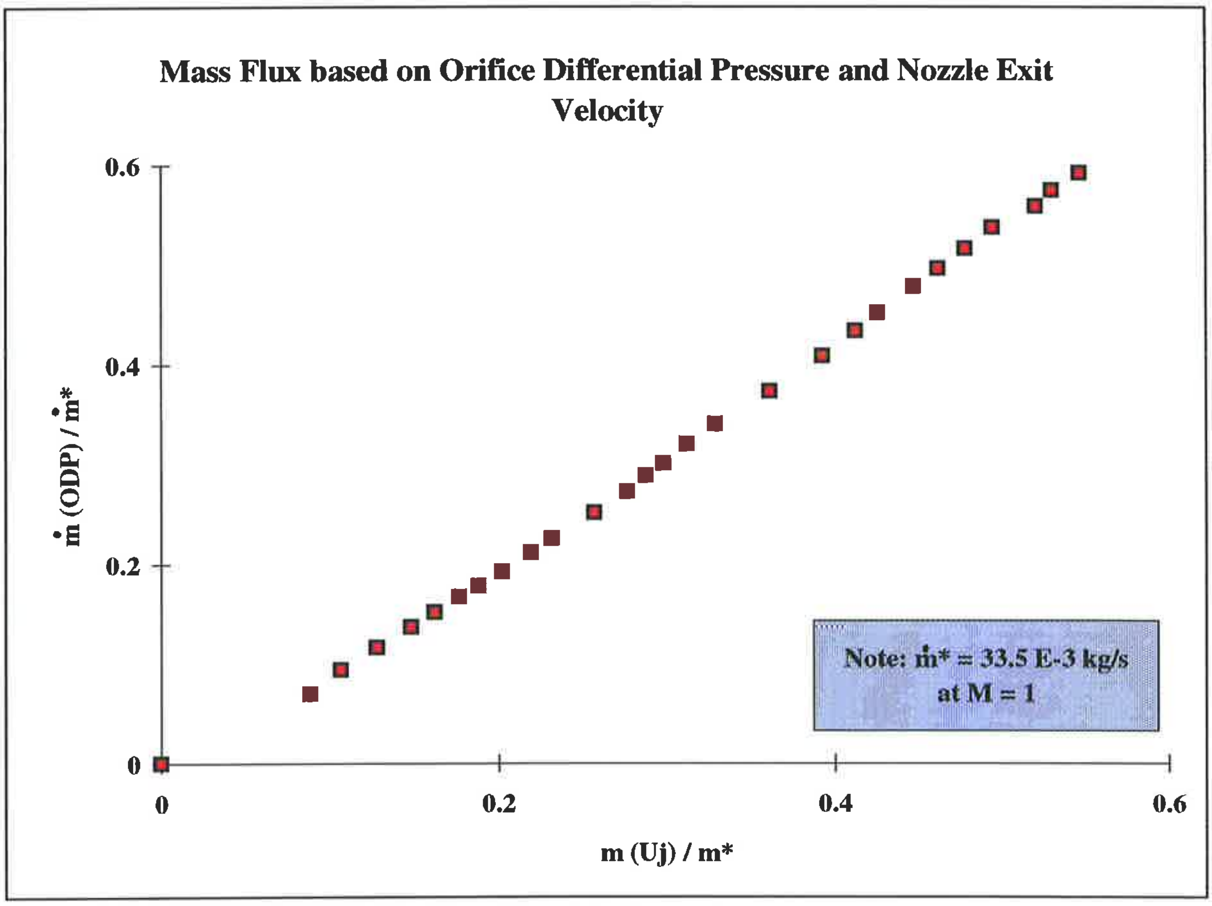

Figure 2.3. 1 Calibration curve for the orifice plate flow meter.

2.3 Orifice plate flow meter calibration

The orifice flow meter and control valve enable the primary flow through the convergent-divergent nozzle to be metered and controlled. A thermometer and a pressure gauge are used to monitor the air conditions downstream from the valve. The differential pressure across the orifice plate flow meter is measured by a "Barocel" pressure transducer with a full scale range of 13.3 kPa and a resolution of 0.01 % FSD. The orifice plate flow meter was designed to conform to BS 1042. Since the discharge pressure from the pressure vessel remains reasonably constant so too does the mass flow rate which is given by the characteristic equation:

$$\textbf{Mass Flow Rate} = \textbf{constant}\ \sqrt{(h'P/T)}$$

The dynamic pressure measured in the exit plane of the calibration nozzle was used to calculate the exit velocity and the mass flow rate through the nozzle. The constant deduced from measurements was 5.44 and thus;

$$\textbf{Mass Flow Rate} = \textbf{5.44}\ \sqrt{(h'P/T)}$$

where h' is the pressure difference across the orifice plate measured in mm of water, P is the absolute static pressure of the fluid and T is the absolute temperature in Kelvin.

This can be related to the subsonic nozzle exit velocity and Reynolds number. The results are valid up to the mass flow rate of 30 x 10^{-3} kg/s, in which range the velocity at the throat is subsonic and compressibility effects are minimal. **Figure 2.3. 1** shows the calibration curve for the orifice plate flow meter used for the primary flow rate. The curve shows the linear relationship between the measured mass flow rate and the mass flow rate that was calculated using the velocity at the nozzle exit.

The orifice plate flow meter was calibrated against the convergent nozzle, the CD, CD10 and CD20 nozzles and the results shown in **Figure 2.3. 2** . The results show that for a constant driving pressure, the flow rate decreases with increase in nozzle length and with reduction of exit area for a given nozzle length. The throat static pressure of each of the nozzles has been recorded for the use in the calculation of fluid properties at the throat. The mass flow rate calculated using pitot-static pressure measurements at the nozzle throat are plotted against the calculated mass flow rate, using the theoretical orifice plate flow meter constants described above, and correlate well for a given range of mass flow rates as shown in **Figure 2.3. 1**.

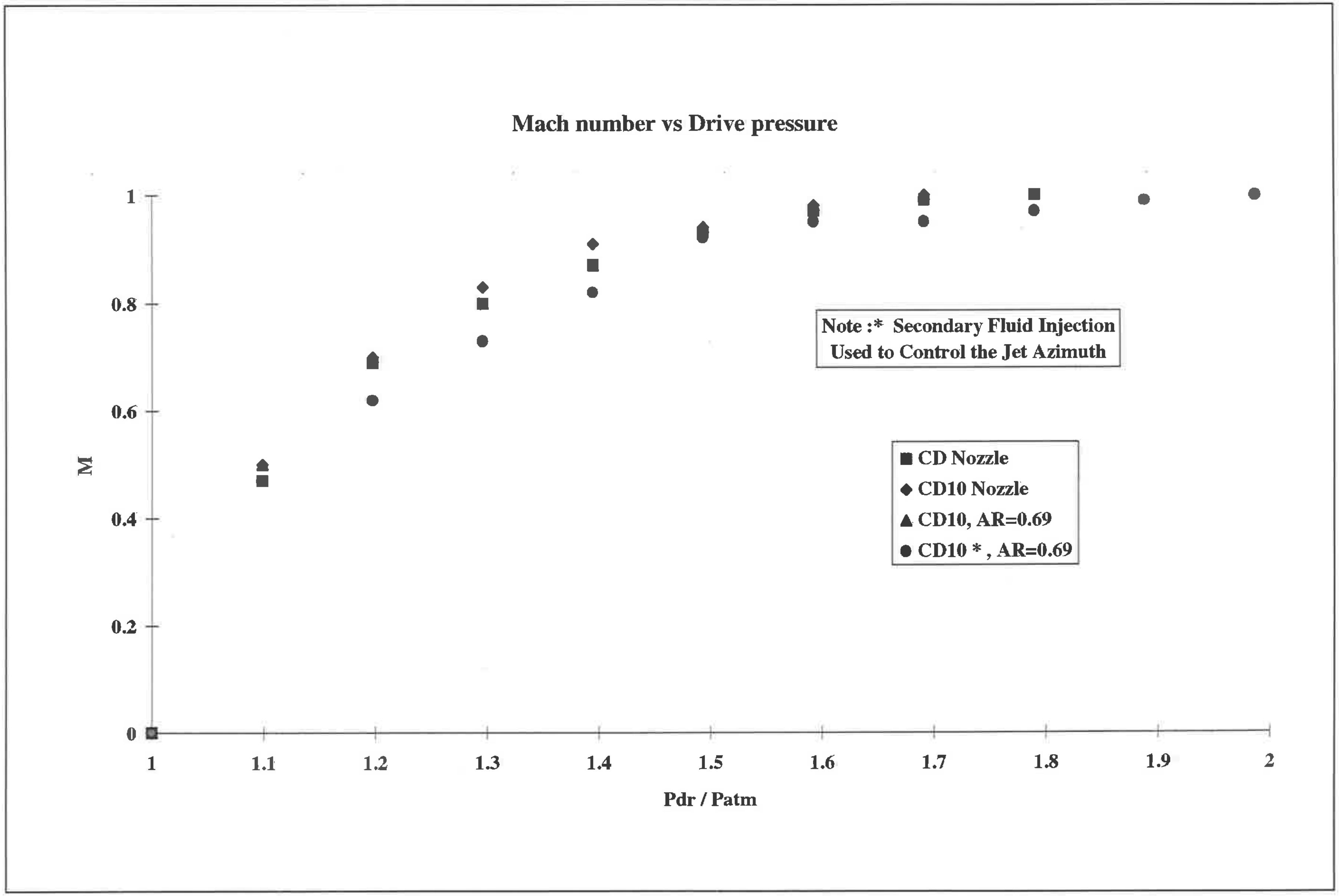

Figure 2.3. 2 Calibration curve for the throat velocity against driving pressure for CD and CD10 nozzles.

2.4 Differential Pressure Transducer and Linear Displacement Transducer Calibration

An array of 16 Honeywell (174 PC) differential pressure transducers, details of which may be found in Appendix B., was used to convert pressure to voltage with linearity of the order of ± 0.5 %, over the full scale range of ± 4 kPa, and a resolution of 0.1 % Full Scale Deflection (FSD). The analogue voltage signals were digitised using an RTI 800 analogue-to-digital card and stored in a PC-based SNAP-SHOT data acquisition and storage system for further analysis. A sample of the calibration plot of applied pressure and voltage output is shown in **Figure 2.4. 1**. The dynamic pressure was measured by total and static pressure probes connected to a single channel Honeywell (174 PC) differential pressure transducer described above. The probe location was measured by means of a linear displacement transducer, calibration of which is shown in **Figure 2.4. 2,** and the output of either the hot-wire, shown in **Figure 2.7. 2,** or the pressure transducer was digitised and recorded for later analysis. **Figure 2.4. 3** shows the CD10 nozzle arrangement with pressure tubing connecting the circumferential pressure ports to 16 channel differential pressure analyser.

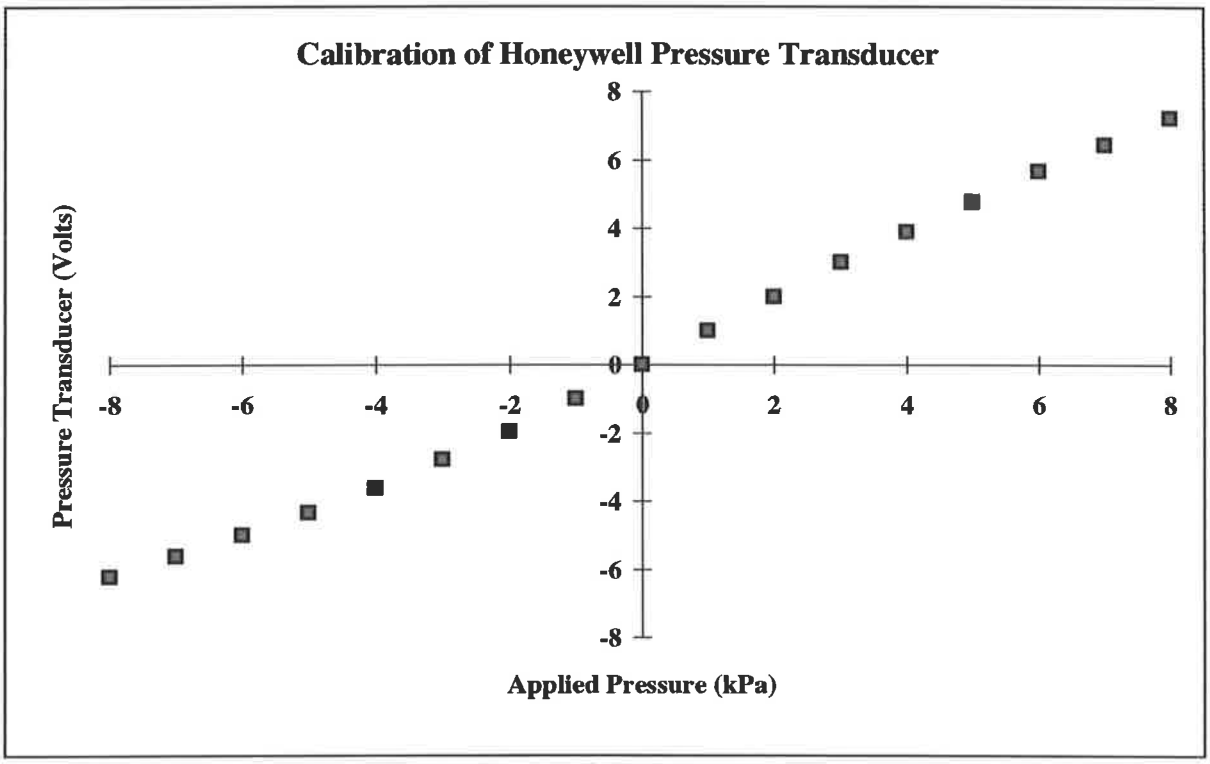

Figure 2.4. 1 Calibration curve for the Honeywell 174 PC differential pressure transducer.

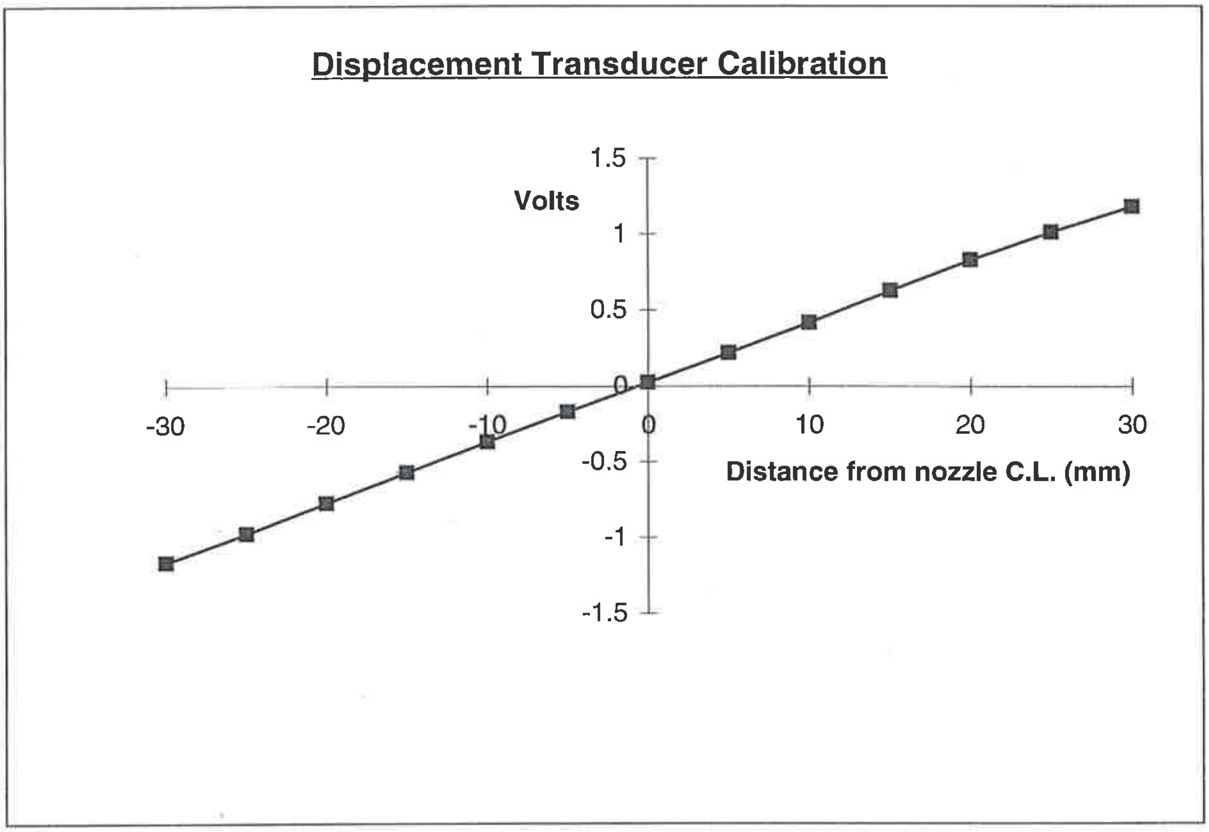

Figure 2.4. 2 Linear displacement transducer output voltage against displacement.

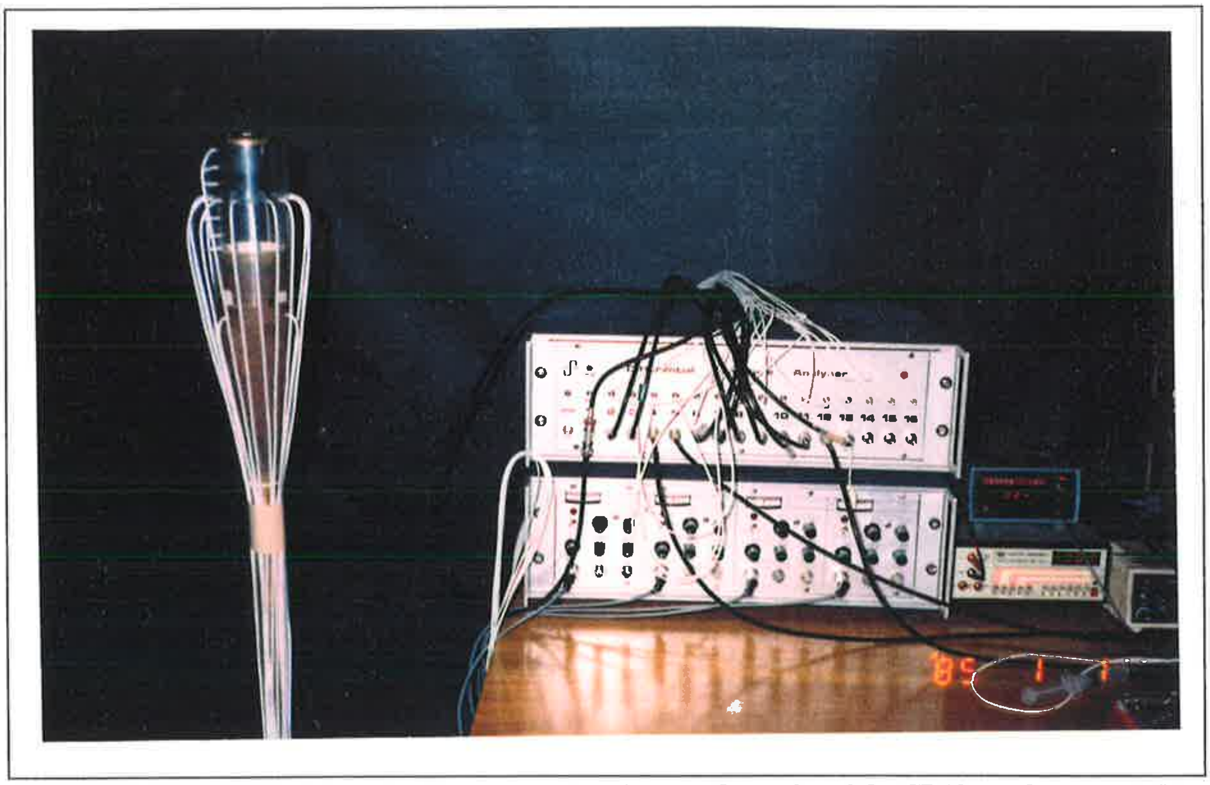

Figure 2.4. 3 Photograph showing the pressure tappings on the cavity of the CD10 nozzle connected to a 16 channel differential pressure transducer array via flexible tubing.

2.5 Laser

The Argon-Ion laser has been used in two capacities. The primary use of the laser system was in the laser Doppler velocimetry (LDV) mode. The other was the use of one of the laser beams passed through a cylindrical lens to produce a sheet of laser light. The laser sheet was then passed through a seeded flow to reveal the various flow structures and images were captured on film using a 35 mm camera.

2.5.1 Laser Doppler Velocimetry (LDV)

The laser Doppler velocimetry equipment used in this thesis is a TSI based 5 watt Argon-ion laser. The 2-colour, 4 beam laser is water cooled and capable of measuring velocity in two directions normal to each other, as shown in the system layout in **Figure 2.5. 1**. Directional ambiguity is resolved by frequency shifting and the whole system was placed on a mobile platform to accommodate its use at different locations. The laser beam is separated into a number of lines and two dominant wavelengths, namely blue (488 nm) and green (514.5 nm) are chosen for measuring the fluid velocity. Each beam is further split into two beams of equal intensity and one of those beams is frequency shifted. The beams are precisely aligned parallel to the LDV table such that as they pass through the optics and the final lens, they all cross at the focal length of that particular lens. Minor adjustments are carried out in the final alignment to ensure that all beams are coincident. The waist of the intersection of those beams is minimum at the cross over point which ensures that the measuring volume is minimum and high spatial resolution is maintained. The final lens mounted on a 2-D traverse table is controlled by stepper motors so that the position is accurately measured in 0.01mm steps. The LDV signal is collected in a back scatter mode and processed on a PC based data acquisition system. Most of the data collected was processed during the data acquisition using a single channel real time processor. Only the mean velocity, standard deviation and turbulence intensity were taken since only time average values were of interest. Where detailed study of the turbulent structures were of interest, LDV raw data was kept for post processing. Details of the LDV system can be found in TSI manuals.

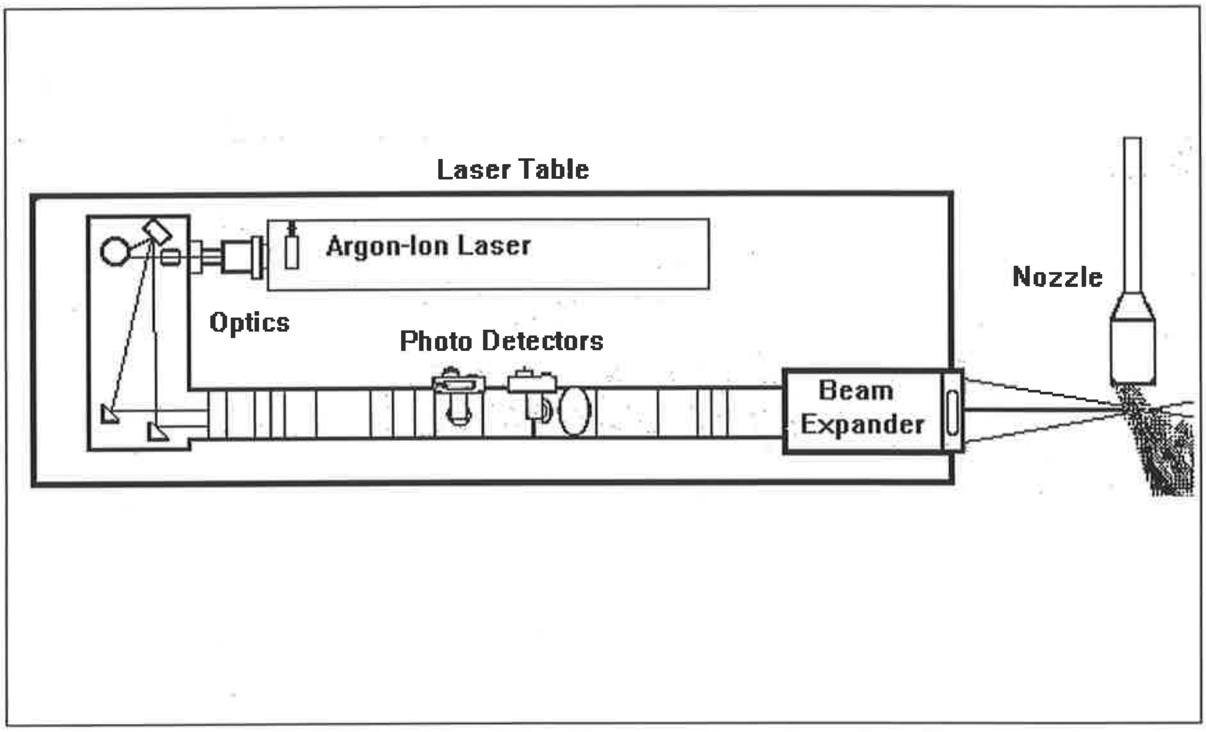

Figure 2.5. 1 Schematic of the T.S.I. laser Doppler velocimetry equipment used to measure the velocity and produce laser sheet.

2.6 Flow Visualisation

A number of visualisation techniques were employed to study the flow. The average wall velocity picture may be obtained using china clay surface flow visualisation. Another method is by capture on a high speed video of the entrainment of smoke into the flow. A further method of studying the flow is by seeding the flow through the nozzle with water vapour using the 6 jet atomiser and illuminate the plane of flow using a laser sheet orientated normally to the viewing direction. A still photo reveals the structures in the flow in the plane of the laser light sheet. All of these techniques contribute to the total understanding of the flow studied and will be discussed in detail in the relevant sections.

2.6.1 Smoke Trace Visualised on High Speed Video

A number of smoke trace attachments were used to visualise the entrainment into the deflected jet and the nozzle. A 12 mm diameter, 300 mm long straight tube with an array of 50 equally spaced holes each 1mm in diameter, termed the smoke rake, was used to pump smoke for a period of up to 5 minutes and visualise the entrainment in to the exiting jet. The smoke rake was positioned at various locations around the nozzle exit to visualise the entrainment flow. The non toxic smoke was stored in a flexible vessel from which it was pumped through the smoke trace attachments. Additionally a 12 mm diameter tube , termed the smoke ring, bent into a 150 mm diameter ring with 40 equally spaced 1mm diameter holes on the upper surface was used. The smoke ring was placed such that the nozzle axis coincided with the smoke ring axis and smoke traces were flowing slowly relative to and in the same direction as the nozzle flow.

2.6.2 China Clay and Oil Surface Flow Visualisation

The china clay surface flow visualisation method is usually implemented by applying a thin film of a solution of "china clay", (Kaolin) in a light oil, to the surface. As the solution dries it attains an opaque white surface. When oil of wintergreen is applied to this surface, by spraying, it matches the refractive index of the clay thereby , making it appear transparent. The flow is then started and the surface flow patterns can be visualised by following the motion of the slurry as it dries. The regions of high mass transfer have a high rate of evaporation and those areas return to original colour first. By contrast the areas of separation have the slowest evaporation and therefore dry more slowly. By taking still photos of the various stages of the process, critical points can be determined, Bradshaw (1970). A variation of the method yields dark areas in regions of high shear and opaque areas where shear is small, Nathan (1988).

The oil streak surface flow visualisation is implemented either by applying a layer of oil on to the surface and starting the flow or introducing the oil at the nozzle throat. At the areas of high shear, and also high mass transfer, the oil is either moved along by the shear or evaporated from the surface. That which is moved by the shear accumulates in areas of separated flow or other low shear or low mass transfer regions. The flow direction on the surface was also determined by the oil droplet orientation. Photographs of the flow were taken for further analysis of the flow patterns inside the nozzle. The alternative to this was to introduce the oil upstream from the nozzle throat and follow the development of the surface flow patterns. The advantage of this method was that the amount of oil introduced can slowly be increased to establish the flow patterns and capture these on 35 mm film.

2.6.3 Laser Sheet Flow Visualisation

Laser sheet photography was used in visualising the flow structures inside and outside the nozzle. The flow was seeded using a "six-jet atomiser" which produced very fine water droplets. The water vapour laden jet is illuminated using a laser sheet produced by the Argon-ion laser and images captured on either black and white or colour film using a conventional 35 mm camera. The laser sheet was produced using a cylindrical lens and the sheet was either passed along the nozzle axis centre line or normal to it. This technique was used on the axisymmetric nozzle flow, plane jet flow and a wall jet flow over a gate to visualise the flow patterns.

2.7 Hot Wire Anemometry

Hot wire anemometry refers to the use of a small electrically heated wire element exposed to the fluid flow the heat loss from which is related to the normal component of the velocity of the flow past it. Typical dimensions of the sensitive element of the wire are of order 0.005 mm diameter by 1.0 to 2.0 mm long. The frequency response of the hot wire can be increased electronically by sensing the changes and rates of change of the wire resistance at constant current, or the electrical current required to keep the wire resistance (temperature) constant. This electronic compensation can increase the frequency response from around 500 Hz to values of around 500,000 Hz. The constant temperature control system operates by utilising a feedback mechanism to maintain the sensor at a constant temperature. Tungsten is the most common material used because of its high temperature coefficient of resistance, (0.004 / °C). Oxidation is the major problem with the use of tungsten wires at high temperature gases, but was used in the present system as temperatures were effectively ambient. A calibration of the wire is shown in **Figure 2.7. 1** in the form (flow velocity)$^{0.5}$ versus (hot wire voltage)^{2}. This is a linear relationship and can be represented by a formula for velocity in terms of voltage as in Equation 2.1.

$$U = [\, \frac{dU^{0.5}}{dV^2} \, (V^2 - V_o^2) \,]^2$$

Eqn. 2.1

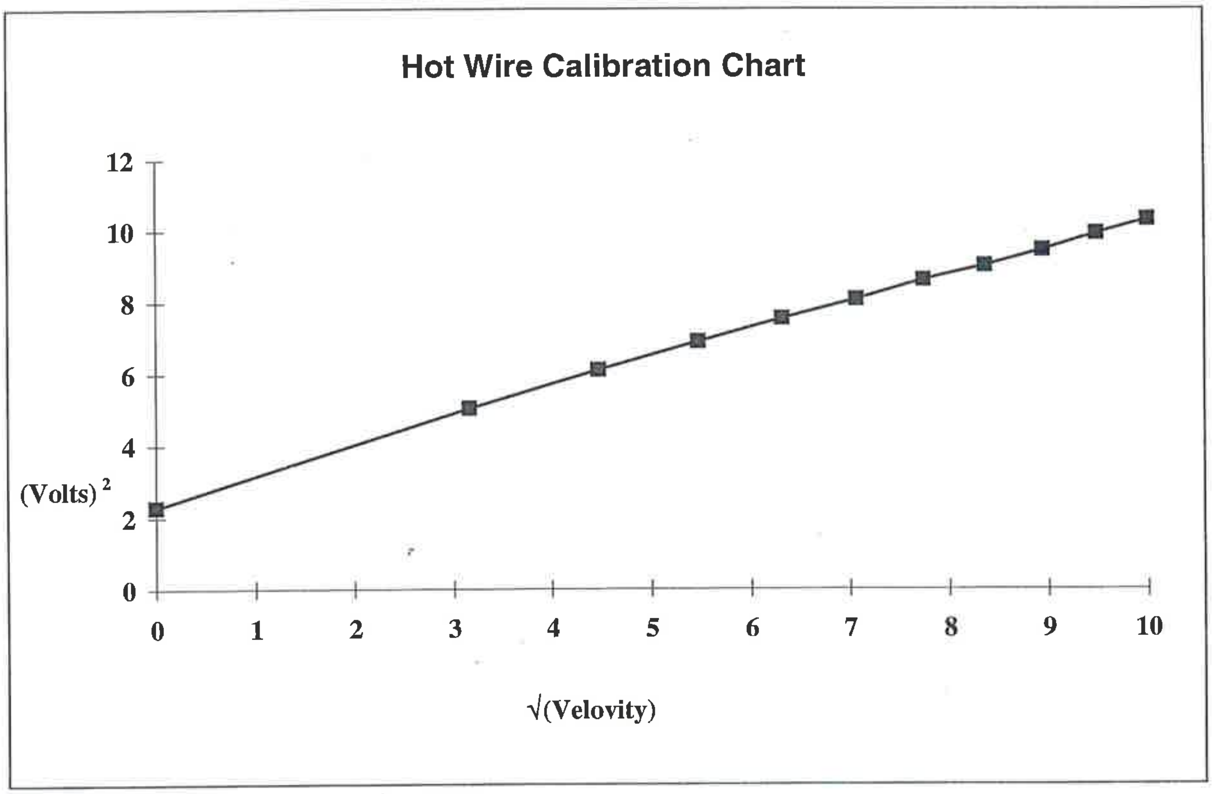

Figure 2.7. 1 Hot-wire calibration curve.

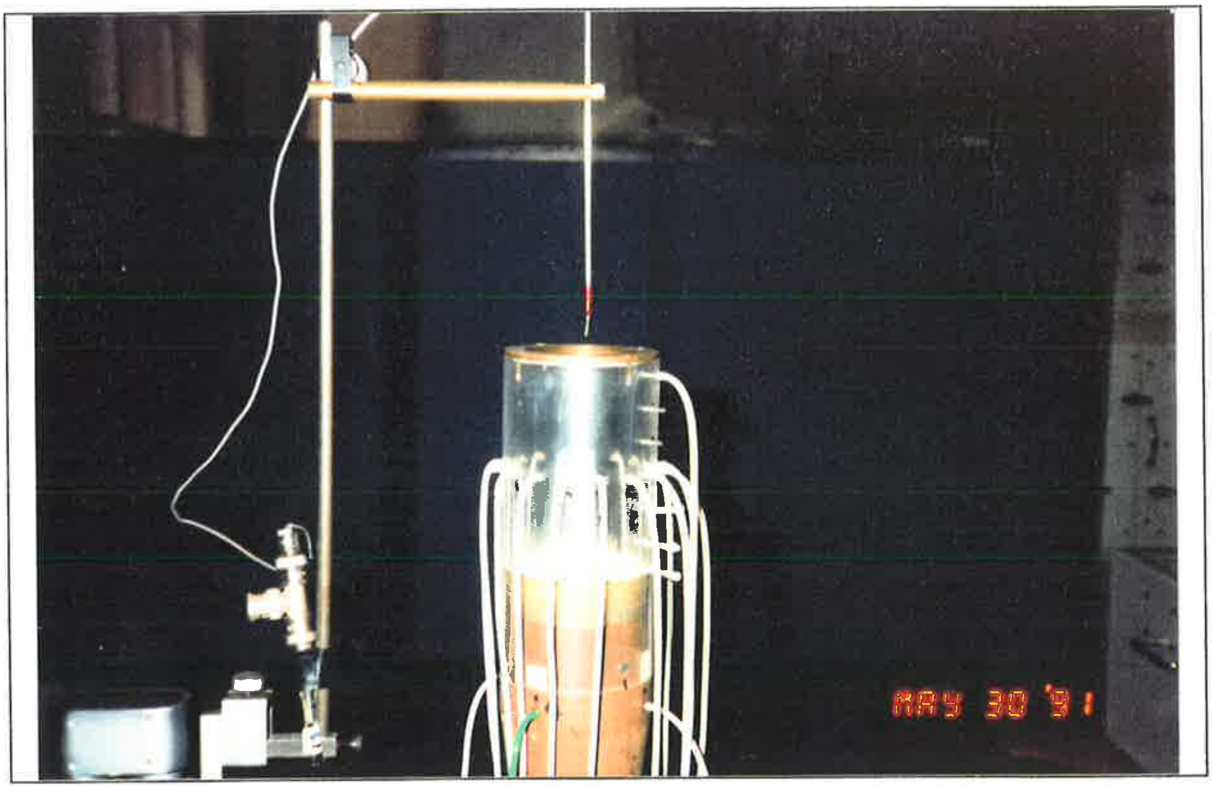

Figure 2.7. 2 CD10 nozzle showing hot-wire at the nozzle exit and circumferential pressure tubes connected to the tappings around the cavity.

where V represents the mean Voltage measured and U represents the mean flow velocity across the element. Since the wire diameter is small, wires are easily damaged especially with high speed flow where even the smallest of particles can destroy the wire. For each of the hot wire probes used the calibration constants were evaluated and the values shown in Equation 2.2 are typical. The constants change with time, especially early in a wires life, and calibration before and after each use was standard procedure.

$$U = (\,0.8852\,(V^2 \;-\; 3.5721)\,)^2 \quad \textbf{Eqn. 2.2}$$

The above equation was used to convert one of the sets of digitised hot wire voltages to velocity values. After the initial "burn in" the constants varied only slightly over a long period but has a very small effect on the accuracy of the measured velocity profiles. A hot wire positioned at the nozzle exit is shown in **Figure 2.7. 2** together with the pressure tubing connected to the cavity pressure ports.

CHAPTER 3

A New Generation of Thrust Vectored Nozzles (T.V.N.)

3.1 Introduction

The vectoring of thrust has been employed by man from prehistoric times. It has been used for millennia by sailors to harness the naturally occurring momentum of the wind by changing its direction locally and so deriving a force to propel their ship in the general direction they wish to travel. Examples such as axial turbines, pelton wheels, wind mills, yachts, planes and ships all use the same principles of altering the momentum direction by redirecting the flow and in the process producing a force in a desired direction. The direction of the thrust produced by a nozzle can easily be changed by changing the orientation of the nozzle as is used in the attitude control of space vehicles. If the nozzle itself cannot be directed, more limited control can be achieved by introducing deflector plates or tabs into the flow to deflect the jet itself by mechanical means. Such systems appear as "*thrust reversers*" for slowing jet aircraft after landing and in the attitude control of the "Nulka" hovering decoy rocket. However the process of deforming an axisymmetric jet from an engine or a rocket motor into an asymmetric jet to produce vectored thrust is greatly complicated by the high dynamic pressures and temperatures associated with the hot gases and the presence of erosive and often corrosive particles.

A nozzle that produces a deflected jet by fluid dynamic means has been developed at the University of Adelaide as a by-product of work on a family of Enhanced Mixing Burner (EMB) Nozzles **[176,207]**. The flow generated by the family of EMB nozzles is characterised by the precession of a deflected jet. The primary motivation of this project was, and still is, the efficient mixing of fluids by non mechanical means. Interest in this work originated with the discovery of what is now termed the Abell nozzle **[1,2]** which produced a flow phenomenon driven by coupling between several flow excited acoustic modes. Initially the flow entering a 2-D nozzle was excited by a speaker driven at a frequency and phase which was locked via on-line frequency analysis to the signal from a hot-wire anemometer placed at the edge of the issuing jet.

The aim was to lock the formation of Brown-Roshko vortices in the jet to the speaker frequency via a phase locked loop. However the whole flow field changed and a set of "pumped" vortices were formed which caused the jet to spread with an included angle of 180 degrees. The same technique was tried with circular nozzles but with limited success. Abell and Luxton [3,4] set out to generate the acoustic signal fluid dynamically by considering an Orifice-Cavity-Orifice (O-C-O) nozzle which produced a {0,1} mode "whistle". This nozzle produced extraordinary diffusion of the jet, but turn down was limited to about 1/2 octave, based on Strouhal number. It was apparent that mixing enhancement by natural acoustic excitation would necessarily be limited to constant flow system.

During a subsequent parametric study of O-C-O system, Nathan (1988) discovered the precessing jet flow within a range of the parameters studied. The only common parameter in the nozzles studied by Abell and Nathan is the Orifice-Cavity-Orifice configuration shown in **Figure 3.1. 1**. The mixing enhancement in the two types of nozzles involve quite different mechanisms, the first being acoustically driven while the second being driven by a fluid mechanical instability. The ratios of the characteristic dimensions which characterise each of the nozzles are presented in **Figure 3.1. 2**, reproduced from Nathan (1988), and the ranges of these characteristic parameter ratios, d_t / d_c, d_e / d_c and l_c / d_c, which have been tested by both Abell and by Nathan are shown. The ratios for the present study of CD, CD10 and CD20 nozzles are indicated within **Figure 3.1. 2** for reference. The different mechanisms which enhance mixing in these two classes of nozzle are summarised as follows:

- The Abell whistling nozzle is a singular case which relies on fluid dynamic excitation and coincidence of discrete acoustic modes.
- The Mid Length Cavity (MLC) nozzle reinforces a naturally occurring fluid dynamic instability inside the nozzle cavity. The instability occurs intermittently over a wide range of configurations but the geometric configuration indicated in **Figure 3.1. 1** is most effective in producing a consistent asymmetric jet which only partially fills the nozzle exit and which precesses.
- The Long Cavity (LC) nozzle also uses the fluid dynamic instability produced inside the nozzle, but increased cavity length causes the exiting jet to fill the whole of the exit plane. Precession is less well defined than for the MLC nozzle but although mixing enhancement is less than for the MLC, it is never the less substantial. Each of the above nozzles has shown potential for gas combustion, producing excellent flame stability, but the Abell acoustic nozzle has very limited turn-down, unlike the MLC and LC nozzles for which turn-down is continuous from choked flow to pilot flame.

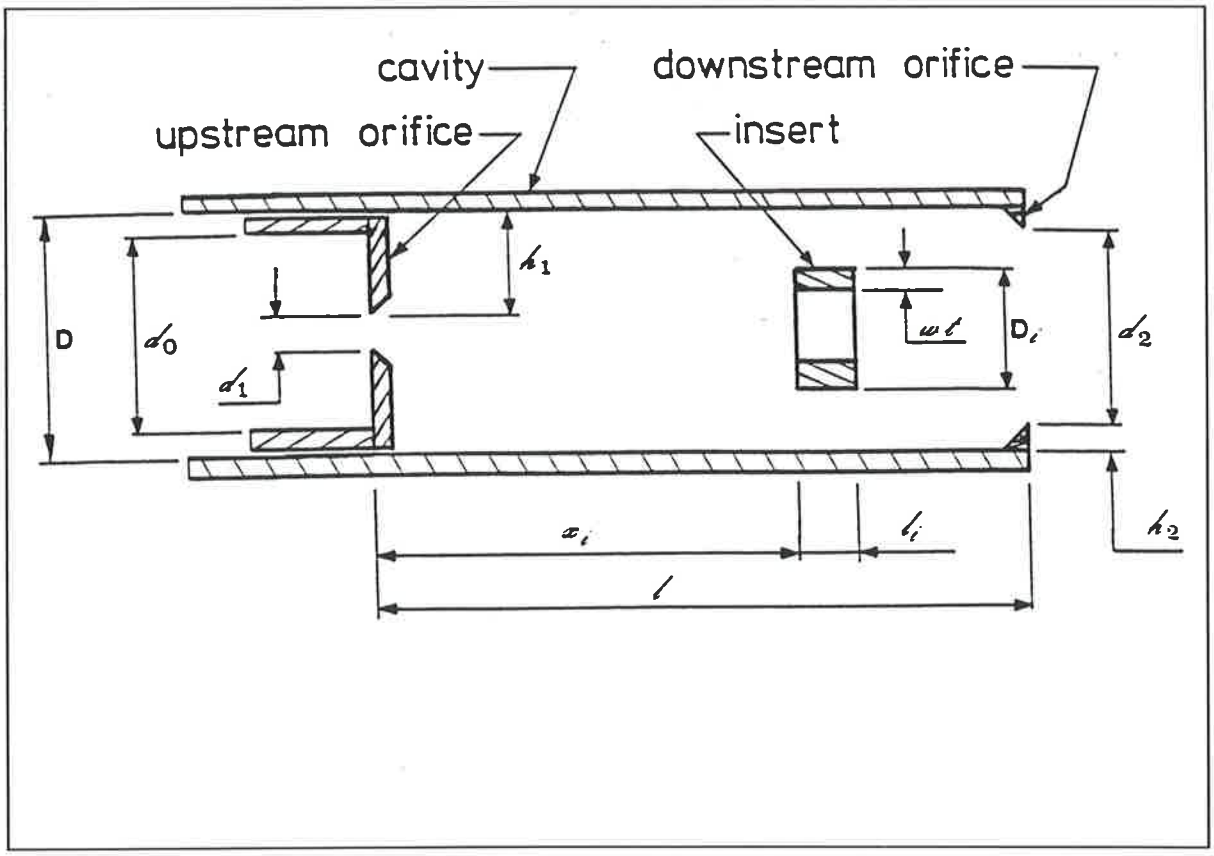

Figure 3.1. 2 Orifice-Cavity-Orifice configuration of the Enhanced Mixing Burner nozzle.

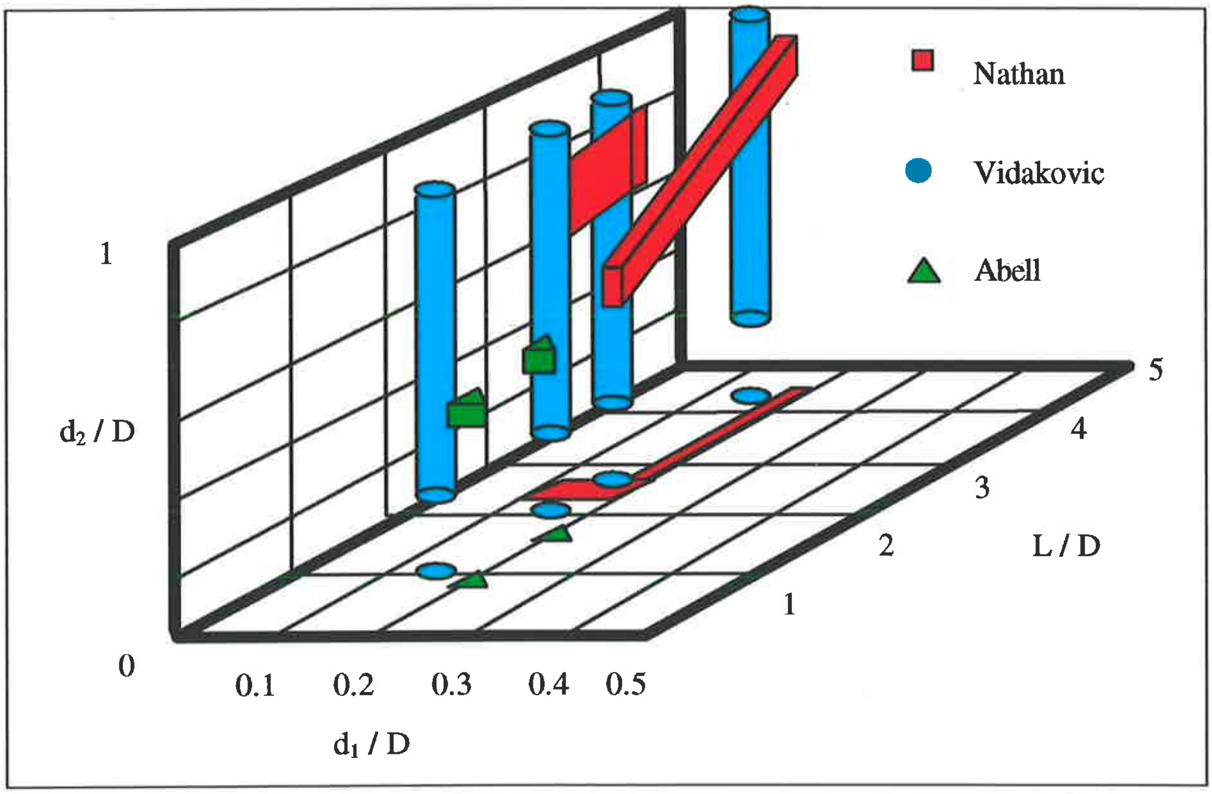

Figure 3.1. 1 Geometric parameters of Orifice-Cavity-Orifice and Convergent-Divergent nozzles tested.

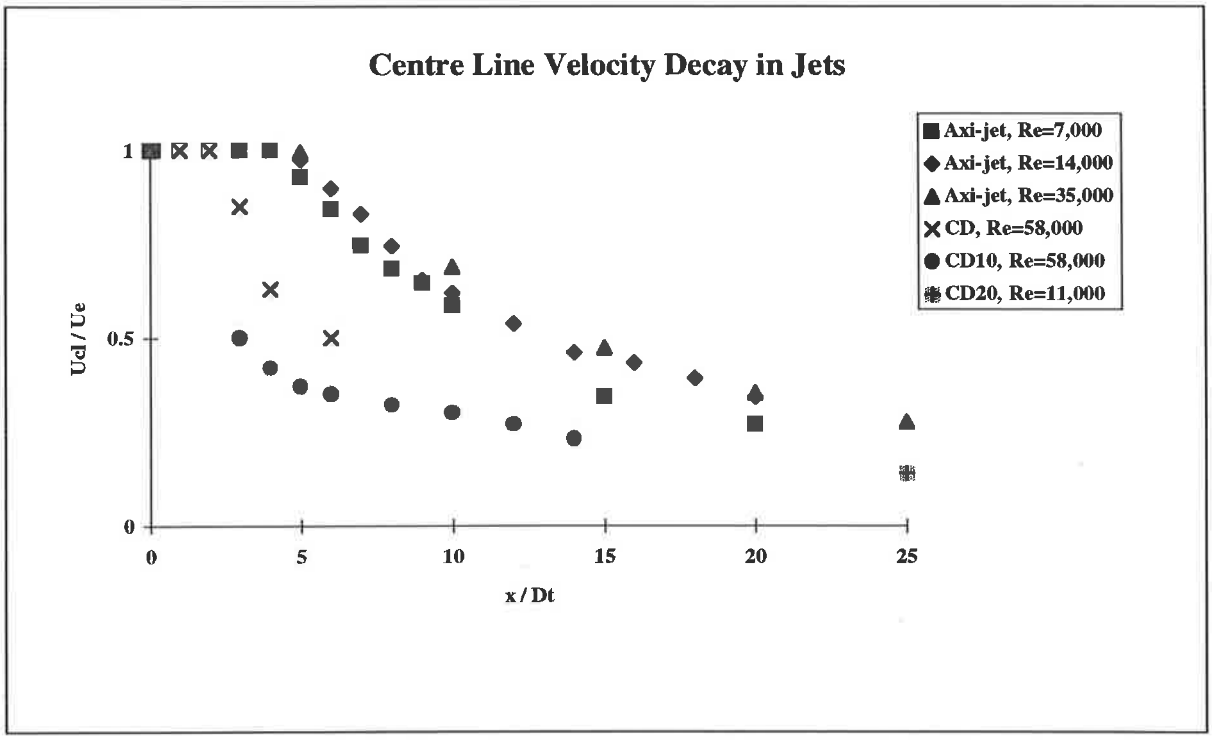

Figure 3.1. 3 Centre line velocity decay comparison between a turbulent jet exiting a convergent nozzle, axisymmetric jet exiting a CD nozzle and an asymmetric wall jet exiting a CD nozzle.

- The CD Nozzle produces an intermittently precessing jet which can be stabilised in a chosen azimuthal direction by secondary fluid injection at the throat. The angle at which the jet is deflected across and away from the nozzle axis, one of the primary parameters of interest in thrust vector control, depends on a combination of the expansion ratio, nozzle length and exit lip height. The non-precessing deflected jet produces large scale entrainment of ambient fluid into the free shear layer. Two stream-wise vortices which originate inside the nozzle and which appear to be caused by the combination of the axial and radial curvature of the nozzle wall are the main cause of the enhanced mixing.
- The CD6, CD10 and CD20 Nozzles similarly produce intermittently precessing jets which enhance large scale entrainment but to degrees which decrease in the order indicated. The parameters for these configurations were evaluated as part of the study of the effect of nozzle length on thrust efficiency.

By definition, increased rates of mixing occur simultaneously with increased spreading angle of the flow. In conventional jets, an increased mixing results in a quicker decay of the centre line velocity and hence the centre line velocity decay has become a common way of measuring the degree of mixing rate improvement in nozzles [22]. However the method is only applicable if the velocity profile of the jet is and remains largely self similar with the characteristic bell-shaped distribution. **Figure 3.1. 3** shows a comparison between the centre line velocity decay of a conventional axisymmetric turbulent jet from a convergent nozzle, of the undisturbed jet from the CD nozzle and of the mean flow centre line velocity of the deflected jet from a CD nozzle with throat disturbance. It is clear that the wall jet centre line velocity decays more rapidly than does the centre line velocity in a simple jet due to the transverse expansion of the jet inside the nozzle caused by the axial and radial wall curvature.

3.2 The Abell Nozzle

As indicated above, the Orifice-Cavity-Orifice developed by Abell and Luxton **[1,2,3,4,174]**, here referred to as the Abell "Whistling" Nozzle, utilises an acoustic feedback mechanism such that the cavity is the primary exciting source. This is driven by the coupling of at least one acoustic mode in the cavity with an upstream Strouhal shedding caused by the separation of the flow from the upstream orifice and its interaction with the downstream orifice. The nozzle dimensions were precisely chosen such that the Strouhal shedding from the primary orifice was matched to the {0,1} radial mode of the cavity, which in turn drives, reinforces and strengthens the vortex shedding and so enhances the mixing characteristics of the nozzle. With the whistling nozzle there is no evidence of ambient fluid being induced into the cavity. The Abell nozzle has a relatively short cavity compared with the MLC, LC, CD, CD10 and CD20 Nozzles, as shown in **Figure 3.1.2** and its optimum dimensions were chosen primarily to maximise the fundamentally poor turn-down ratio without unduly compromising the mixing enhancement. The chosen ratios were:

$$d_t \;/\; d_c \;=\; 0.2\,, \qquad d_e \;/\; d_c \;=\; 0.45\,, \qquad 0.6 \;\leq\; L_c \;/\; d_c \;\leq\; 0.7$$

Eqn 3.1

Nathan's (1988) investigation of the effects of varying cavity length on flame stability revealed that as the cavity length increased, the number of resonant modes which were able to reinforce the Strouhal shedding also increased. Details of this study can be found in Nathan (1988)(in Figure 3.3), which shows the stability map and the range of flow rates over which the EMB is able to stabilise a flame (for a given cavity length). Nathan also concluded that while the extra resonances in longer cavity means that it is possible to maintain a stable flame over a larger operating range, the nozzle is not well suited for combustion. It was also concluded that the several resonances were of unequal strengths and did not produce the same degree of flow stability. In combustion applications this would lead to oscillations of the flame between the adjacent modes. As pointed out by Nathan, an inherent characteristic of all acoustically excited nozzles is their limited turn-down ratio. He summarised his investigation of the acoustic nozzles in a following manner for d_t / d_c = 0.2 and d_e / d_c = 0.45 :

Summary of Acoustic Nozzles

1. Acoustically induced enhanced mixing occurs throughout the dimensional range of:

$$0.45 \leq L_c \ / \ d_c \leq 1.5 \qquad \textbf{Eqn 3.2}$$

2. For $L_c / d_c < 0.45$ acoustic resonances are detectable, but do not cause an improvement in flame stability.
3. For $0.45 < L_c / d_c < 0.8$ "cut-on" of an acoustic resonance (presumably the {0,1} mode) with or without coincident modes as found by Abell and Luxton for $0.6 < L_c / d_c < 0.7$) occurred over a small operating flow range, and was associated with a dramatic improvement in flame stability.
4. For $0.8 < L_c / d_c < 1.5$ different acoustic resonances can be excited over different flow ranges. This results in several stable and unstable combustion zones in the operating range of a single geometry with different flame shape in each range.
5. A "cut-on" of flow patterns which produce improved flame stability is always accompanied by an acoustic resonance.
6. Flame blow-out is not necessarily accompanied by a corresponding "cut-off" of an acoustic resonance.

In summary, the Abell nozzle could have applications in combustion if for given fixed primary and secondary orifice diameters, the burner length could be mechanically adjusted as a function of mass flux, so to give the maximum coupling of the Strouhal shedding and in turn to enhance mixing to produce a stable flame.

3.3 The Mid Length Cavity (MLC) nozzle

The MLC nozzle is the nozzle explored in detail by Nathan. This nozzle, he found, involved no acoustic resonances of measurable magnitude yet produced excellent mixing over a wide operating range. He postulated that the MLC nozzle generates its enhanced mixing by large scale engulfment due to precession of an asymmetric jet from an Orifice-Cavity-Orifice nozzle configuration. The precession produced by the asymmetric jet was investigated in detail by Nathan by examining the results from a large number of flow visualisation experiments in both air and water, together with pitot tube, hot-wire anemometry and acoustic spectra measurements in air. The results appear to agree with and greatly extend the results of independent research by **[113]** and **[78]** which investigated a flow in an abrupt expansion of smaller area ratio than that used by Nathan and found precession to occur only when a swirl is introduced upstream of the primary orifice. The flow phenomena, it should be stressed, are unrelated to the acoustic feedback mechanism used by Abell et,al.

For the configuration of the MLC nozzle tested, it was found that the instantaneous jet leaves the secondary orifice exit plane with a mean angle in excess of 65° from the nozzle axis with the jet edge nearest the exit plane being almost at right angles to the axis. It was shown that when such a jet of gas precesses, it produces a short bulbous flame with high mixing rates due to the large scale folding of ambient air into the vortex structures produced by the precessing gas jet. The precession in such a nozzle is generated fluid-mechanically and is not completely stable. The flow may cease to precess for a brief moment and then start again in a direction which is statistically random unless the upstream flow contains swirl, in which case the direction of the precession is always the opposite from that of the swirl.

The flow produced in and by the MLC nozzle was shown to support a highly stable flame. The stand-off distances were shown to be an order of magnitude lower than that of a free turbulent jet, and blow-off velocities were four times greater. The results were obtained in free air but indications were that this type of burner could be used equally well in the confined space of a furnace or a cement kiln. When the configuration was tested in cold flow, the entrainment rates measured were five fold those of the free turbulent jet entrainment. The projected performance in service has subsequently been proved **[180]**.

3.4 The Long Cavity (LC) nozzle

The Long Cavity (LC) nozzle has flow characteristics which are not too dissimilar from those of the MLC nozzle. The flow generated by the LC is a rapidly mixing, rapidly spreading jet originating from a naturally asymmetric jet which is directed at a smaller angle from the nozzle axis than is the jet from the MLC nozzle for the same mass flux. Nathan (1988) showed by detailed measurements of the acoustic spectra that the LC nozzle is not an acoustically excited phenomenon, since no dominant frequencies were present, no sudden change in spectrum occurs in any part of the operating range and the phenomenon is unchanged when the nozzle is operated as a submerged water jet. If the acoustic feedback mechanism was present, there would have been sudden changes in the frequency spectrum and the large difference in the speeds of sound in water and in air would surely have caused the flow character to be different for the two fluids. This result further supported the conclusion drawn from experiments that LC does not suffer from the problem of limited turn-down ratio.

The nozzle was found to be tolerant of minor dimensional imperfections indicating good durability and low maintenance of the nozzle even in a hostile environment. A number of lengths of cavity were evaluated but limits to the geometric configuration were not found. When Nathan discovered the even larger mixing possible with the MLC nozzle, that nozzle became the focus of attention causing the premature cessation of experiments on the LC nozzle. Thus it cannot be claimed that the nozzle has been optimised. Very recently, commercial consulting has suggested that the LC nozzle may have applications in the process industry and work is to be regenerated.

The results from total and static pressure profiles indicate that there is no recirculation zone in the jet. It also shows that the mean velocity profile at the exit of the nozzle is bell-shaped, not "top hat" which indicates that the jet has diffused and the potential core has been consumed inside the cavity. The jet is never the less instantaneously asymmetric as it passes through the exit plane. This differs from the MLC velocity profiles, where a recirculation zone exists due to the exiting deflected "wall jet". It was shown that the half jet spreading angle for the LC nozzle is of the order of 28° from the nozzle centre line compared with approximately 10° for the free turbulent jet produced by the convergent nozzle in the present project with an infinite abrupt expansion.

3.5 The CD Nozzle

The results of the author's initial evaluation of nozzle geometric parameters was that the CD Nozzle produced the highest momentum deflected jet of the nozzles tested. The work carried out on this nozzle followed on from the initial flow investigation on the CD10 nozzle configuration, which was modelled on the MLC nozzle geometric configuration and which produced a deflected jet when a secondary orifice was placed on the nozzle exit. Both short and long nozzles have their advantages, as will be shown later, and it is envisaged that, in the practical application of this type of controlled flow nozzle, there may be a need to vary the length of the nozzle and the diameter of the secondary orifice to satisfy the mission requirements.

It is postulated that the CD Nozzle generates efficiently a precessing, highly deflected jet by means of an asymmetric jet impinging on a small lip at the nozzle exit assisted by a radial pressure gradient. The postulate has been derived from a large number of flow visualisation, pitot tube, hot-wire anemometry, laser Doppler velocimetry and wall static pressure measurements. The postulate is consistent with results of other researchers and in particular with those by Nathan (1988). The flow phenomenon is produced by injecting a secondary fluid through a pressure port at the throat and across the primary flow which may impinge on the throat wall opposite and downstream from the injection point. The secondary fluid entrains primary fluid as it leaves the port and produces an adverse pressure gradient at the throat near the secondary injection. On the opposite side, as the secondary fluid is transported downstream by the primary fluid, it impinges on the wall producing locally a region of favourable pressure gradient. This flow promotes a Coanda like entrainment causing the streamlines of the primary jet to follow the curvature of the nozzle wall and remain attached on that side of the nozzle but to separate in the region downstream from the secondary injection port. The primary flow thus forms a wall jet on the nozzle wall diametrically opposite from the injection port of the secondary fluid. This wall jet deforms as it proceeds downstream from the throat and spreads over about half the nozzle circumference by the time it reaches the nozzle exit. The jet has been visualised by laser sheet photography as shown in **Figure 4.3. 2** to **Figure 4.3. 18**. The thickness of the wall jet at the nozzle exit is about twice the throat diameter and increases at a higher rate as it leaves the nozzle exit plane, as shown in **Figure 4.3. 3**, indicating a high degree of mixing outside the nozzle.

When the exit ring is placed at the nozzle exit, it causes the jet to deflect across the nozzle axis. The size of the exit lip determines the angle to which the jet is deflected and has been measured to exceed 80° for a particular configuration. The exit ring focuses the kidney shaped wall jet towards the nozzle axis. For smaller exit ring diameters, that is with larger step at the exit, mass flow is squeezed through a diminished exit area. This causes the fluid exit velocity to increase to maintain constant mass flux. The increase in exit velocity also affects the deflection angle of the jet due to a change in radial pressure gradient which is caused by changed entrainment into the nozzle.

3.6 The CD10 Nozzle

The postulated flow in the CD Nozzle largely applies for the CD10 Nozzle. The CD10 Nozzle generates an asymmetric wall jet which, at Reynolds numbers below around 30,000, is unstable and switches from axisymmetric to asymmetric flow. A fully asymmetric flow is established at a Reynolds number of around 45,000. The precession direction is not predictable at the nozzle exit but if the flow upstream from the throat is given a slight swirl, the precession is always in the direction opposite from that of the swirl. The flow exiting the nozzle is more diffuse than is the flow exiting the CD Nozzle for a given mass flux, and when an exit ring is attached, the flow is deflected across the nozzle axis but at a lesser angle than for the CD nozzle.

The velocity distribution at the exit occupies a proportionally larger portion of the exit area than in the CD nozzle for a given mass flux and exit ring diameter. This reduction in the area available for induction of ambient fluid into the nozzle in response to the sub-atmospheric cavity pressure, produces an acceleration of the entrained fluid at the exit plane which in turn produces a pressure gradient across the exiting jet and so deflects it further away from the nozzle axis. The radial pressure gradient is a secondary influence in the deflection of the jet, the primary effect being the impingement of the high momentum wall jet on the exit ring.

Due to the increase in nozzle length, the wall jet is thicker at the nozzle exit compared with the CD nozzle. The primary flow momentum is thus distributed over a larger cross-sectional area such that when the wall jet meets the exit ring the momentum which can be deflected into the horseshoe vortex, which seems to be one of the agents causing the jet to be deflected and which is discussed at length in subsequent sections, is reduced. Its intensity is therefore less than in the CD nozzle and hence the jet deflection is smaller. Also the more diffuse momentum produces a lower thrust. The character of the flow may be compared with that noted by Nathan (1988) in his MLC nozzle. The above process is more obvious in the CD20 nozzle due to the greater distance available for the wall jet momentum to be diffused as indicated below. The process is discussed in more detail in Chapter 6.

3.7 The CD20 Nozzle

The CD20 Nozzle generates a rapidly spreading jet that occupies the whole of the exit area. The jet at the exit is mildly asymmetric and the exit ring at the exit plane produces some deflection. The jet is well mixed at the exit and the magnitude of the momentum vector is much lower than that for the CD and CD10 nozzles. This low momentum flow produces a relatively low thrust and a well mixed flow at the nozzle exit. Flow is generated by the secondary injection of fluid at the throat which produces a wall jet as in previous cases. The development length of the jet in this case is however much greater than for the other two cases causing the jet to occupy virtually the whole of the exit area. This prevents the ambient fluid from being entrained into the nozzle and causes the jet to deflect at a much lesser angle due to the absence of a radial pressure gradient. The flow is similar to the that described by Nathan for the LC nozzle. The thrust produced by this nozzle is also lower than the thrust produced by CD and CD10 nozzles for the same mass flow rate.

3.8 Other Nozzles Tested

The two configurations, RP45 and RP60 employ the same convergent section as used for all nozzles but have respectively, a 45° or 60° deflector plate positioned at the exit plane (equivalent to the throat) to deflect the flow in a manner comparable with that used in some conventional jet vectoring systems. The nozzles were tested to provide base-line thrust vectoring capabilities with which to compare the present range of nozzles over a range of mass flow rates. The other two configurations, the B45 and B90 Nozzles, consist of the convergent nozzle with respectively a 45° or 90° bend positioned at the exit to deflect the jet. Again these were tested to provide comparison with another conventional configuration. The tests were performed using the thrust measuring apparatus described earlier in Chapter 2. and the results of these measurements are discussed and compared with the results of other thrust vectoring nozzles in Chapter 6.

3.9 Conclusions

Three modes of flow excitation, namely acoustic, fluid mechanic and fluidic disturbance, have been identified for the nozzles discussed.

The acoustic excitation produces large scale vortical structures resulting from a flow through a primary orifice producing vortex shedding which stimulates a {0,1} radial mode in coincidence with a resonant mode of the cavity which is amplified sufficiently to produce strong, large scale vortical structures at the nozzle exit.

The MLC Nozzle produces large scale structures by engulfment of ambient fluid into the vortex structures produced by the asymmetric precessing jet from an O-C-O nozzle configuration. The mechanism of precession is currently being studied by other researchers in the department. The process by which the precession is initiated and sustained is not yet fully understood but it is suspected that the asymmetry of entrained fluid at the back of the cavity sets up a swirl that is sensitive to the entrained fluid. In the LC nozzle case, the primary jet diffuses much more than that in the MLC Nozzle and it occupies the whole of the exit plane. The primary jet appetite upstream from the exit is satisfied by the shear layer recirculation back towards the primary orifice. This lower momentum flow produces a much weaker swirl at the base of the cavity and consequently the precession of the primary jet is weaker.

The non-precessing fluid dynamically deflected jet produced by the CD nozzle results from an injection of a secondary fluid which imposes a preferred direction on the system. This prevents the primary jet from precessing. The azimuthal position of the primary flow is determined by the azimuthal position of the secondary injection point. The exit ring diameter determines the angle of deflected jet at the nozzle exit. The CD10 and CD20 have similar flow characteristics near the throat but the flow changes downstream, mainly due to the increased nozzle length. The diffusion of the wall jet distributes the momentum over a larger cross-sectional area and the impact of the lower momentum fluid on the exit ring decreases the effect on the streamline curvature. This produces a jet deflected at an ever diminishing angle as the nozzle length is increased with other parameters held constant. Details of the investigations of these flows on which the above qualitative interpretation have been based are presented in the following Chapters.

CHAPTER 4

CD Nozzle and its Flow Mechanism

It is postulated that the CD Nozzle generates highly deflected precessing jet effectively as a result of the impingement of an asymmetric wall jet on a lip at the nozzle exit so feeding primary flow momentum into an intense vortex loop which generates a strong transverse pressure gradient. The postulate has been derived from a large number of flow visualisation, pitot tube, hot-wire anemometry, laser Doppler velocimetry and wall static pressure measurements. The postulate is consistent with the results obtained by Nathan and other researchers but differs significantly in the matter of interpretation. It is also postulated that the mechanism by which a ***non-precessing*** deflected jet is produced is similar in character to the precessing jet flow. The ***non-precessing*** deflected jet is azimuthally steered by the injection of a secondary fluid through a pressure tapping at the throat producing an adverse pressure gradient at that point and a favourable pressure gradient diametrically opposite and slightly downstream from the nozzle throat. Coanda like mixing of primary flow momentum allows the streamlines of the primary wall jet to follow the curvature of the nozzle and to maintain contact with the wall. When an exit ring is placed at the nozzle exit, the same intense vortex loop postulated for the precessing case generates a strong transverse pressure gradient which causes the jet to deflect sharply across the nozzle axis. These postulates are consistent with the findings from experiments as discussed below.

4.1 A Characteristic Description of the Flow Patterns Generated Inside and Outside the Nozzle

The following description of the flow generated inside the nozzle is applicable to all forms of CD Nozzle, ie., the CD, CD6, CD10 and CD20 Nozzles for fully developed smooth wall pipe flow in the supply to the nozzle and for throat Mach numbers less than 0.7 in which range compressibility had little effect on the flow structure. The effects of Mach number on nozzle thrust, on the other hand, was significant due predominantly to the reduction in density (see Chapter 6.). The flow characteristics have been derived from flow visualisation photographs, velocity profiles and wall static pressure measurements.

In the absence of any throat disturbance, below a Reynolds number of about 45,000, the jet leaving the nozzle throat initially separates axisymmetrically downstream from the throat. As the Reynolds number increases above 45,000 the jet separation switches intermittently between axisymmetric and asymmetric and at Reynolds numbers greater than about 55,000 it separates asymmetrically and precesses intermittently in an apparently random direction.

To allow study of the flow patterns in detail, the deflected jet can be locked in an azimuthal position by introduction of a local disturbance, namely the injection of a secondary jet through a pressure tapping at the throat. The primary jet then remains attached to one sector of the nozzle wall and expands both transversely and radially. The absolute momentum of the primary jet is increased only marginally by the radial injection of the secondary fluid, but this change is sufficient to produce a side force which deflects the primary jet, causing it to be biased toward the wall diametrically opposite from the injection port. The secondary jet sets up a complex local pressure field in the region of the injection port, Lim, Kelso and Perry (1992), which includes a region of adverse pressure gradient. The secondary jet is convected downstream by the primary, so its trajectory is curved. When and if it reaches the opposite side of the nozzle throat, the wall curvature is such that the trajectory of the secondary jet could be such that it is almost aligned with the wall. This could regenerate the boundary layer before the primary jet, which is now a wall jet, can separate.

The wall jet continues downstream, expanding azimuthally and entraining ambient fluid which has been induced into the nozzle. The wall jet is then forced to separate and deflect by the exit ring at the exit plane of the nozzle. The deflection is enhanced by the existence of radial pressure gradient at the exit of the nozzle. Due to entrainment by the primary jet, the pressure inside the nozzle is sub-atmospheric and as a consequence, ambient fluid is induced into the nozzle. The flow of ambient fluid into the nozzle almost reaches the throat immediately downstream of the secondary jet as is clearly shown in the surface flow visualisation shown in **Figure 4.5. 8**. The surface shear stress patterns, which indicate the direction of the flow near the surface, is visualised by oil and graphite mixture as shown in **Figure 5.5. 3 (a)**. These patterns, it will be seen, show both the negative bifurcation surface of the primary jet and the entrained fluid in the absence of the exit ring. These surface flow patterns indicate the flow direction and the spread of the primary jet downstream from the throat. When an exit ring is attached to the nozzle exit, observation is more difficult, but the surface flow patterns shown in the following section indicate that the wall jet is deflected across the nozzle axis and the flow inside the nozzle is changed significantly . As the exit area is made progressively smaller, the surface flow patterns reveal that high streamline curvature is present at the nozzle exit and this appears to be the result of a very strong vortex upstream from the exit lip. The induced ambient fluid velocity increases with the reduction of the exit area, based on the observations of a tuft at the nozzle exit and on marked ambient fluid entrained from the base of the apparatus shown in **Figure 4.3. 1**. These observations are discussed in detail in the following Sections.

4.2 Total and Static Pressure Profiles

A number of total and static pressure measurements have been taken using a pitot-static probe inside and outside the CD nozzle configuration with various diameter exit rings added at the nozzle exit. The diametrical traverse inside the nozzle was limited by the size of the exit ring since the probe was aligned parallel to the nozzle axis. Both total and static pressures were taken simultaneously using the pitot-static probe. The nozzle without the attached exit ring was the only exception in the total pressure case, but the static pressure could not be measured close to the wall using the static-pressure probe due to the nozzle curvature and the fact that the static pressure holes are some distance downstream from the probe tip. For this reason, the pressure inside the cavity was interpolated from the obtained data.

The pressure results were also used to calculate the velocity profiles using the measured dynamic and interpolated static pressure and these velocity measurements were repeated using hot wire anemometry. The wall static pressure at the curved wall downstream from the nozzle throat was measured using 4 axial pressure tappings along the nozzle wall. A set of 8 equally spaced pressure tappings is located at the nozzle throat as described below. The pressure measurements were taken for the flow rate up Mach 1 at the throat and are presented in the following Sections.

4.2.1 Apparatus and Experimental Techniques

A pitot-static pressure probe of 3 mm O.D. was used in the measurement of the total and static pressure. The 2mm inside diameter pressure lines were connected to a differential pressure transducer to measure the difference between total and static pressures, ie. the dynamic pressure. The differential pressure transducer, described in Section 2.4, was calibrated to give a linear relationship between the pressure and voltage with zero offset, as shown by **Figure 2.4. 1**. The voltage produced by the pressure sensor was digitised and stored on a PC based data acquisition system for further analysis.

Seven 1 mm diameter plus one of 2 mm diameter pressure tappings are equally spaced around circumference at the throat. Four further pressure tappings are located axially along the nozzle wall as shown in **Figure 2.1.5** All tappings are connected to a 16 channel pressure transducer via flexible tubing, described in Section 2.4.

Table 4. 1 Variation of axisymmetric and asymmetric gauge pressure (Pa) inside CD nozzle

x / D_t	6	5	4	3
Reynolds No.				
Axisymmetric Flow				
35,000	**-40**	**-36**	**-28**	**-20**
46,500	**-91**	**-89**	**-70**	**-51**
49,000	**-120**	**-115**	**-95**	**-72**
55,000	**-147**	**-151**	**-123**	**-110**
Asymmetric Flow				
58,000	**-200**	**-280**	**-380**	**-420**
60,000	**-230**	**-330**	**-440**	**-500**
65,000	**-260**	**-378**	**-500**	**-530**
68,500	**-275**	**-412**	**-530**	**-640**

4.2.2 Nozzle Static Pressure

The static pressure variation across the CD nozzle centre line in the plane of symmetry of the axisymmetric flow at various distances from the nozzle throat is shown in **Figure 4.2. 1** for a Reynolds number of 35,000, which corresponds to a mass flux of $5x10^{-3}$ kg/s, and Reynolds number of 55,000, corresponding to a mass flux of $7.7x10^{-3}$ kg/s is shown in **Figure 4.2. 2**. The flow remains tentatively axisymmetric with some distortion of the static pressure profiles visible in the later figure. The axisymmetric static pressure profiles collapse onto a common curve at a given axial location downstream from the throat and a comparison of the results between Reynolds number of 35,000 and 55,000, is shown in **Figure 4.2. 3**. The results indicate that the static pressure inside the nozzle becomes more sub-atmospheric with increase in primary mass flux causing more ambient fluid to be induced into the nozzle and entrained by the primary flow. There is some tendency for the jet to become asymmetric prior to reaching the Reynolds number of 55,000 and the slightest asymmetry at or near the throat, such as an incompletely sealed static pressure hole, can produce an asymmetric flow.

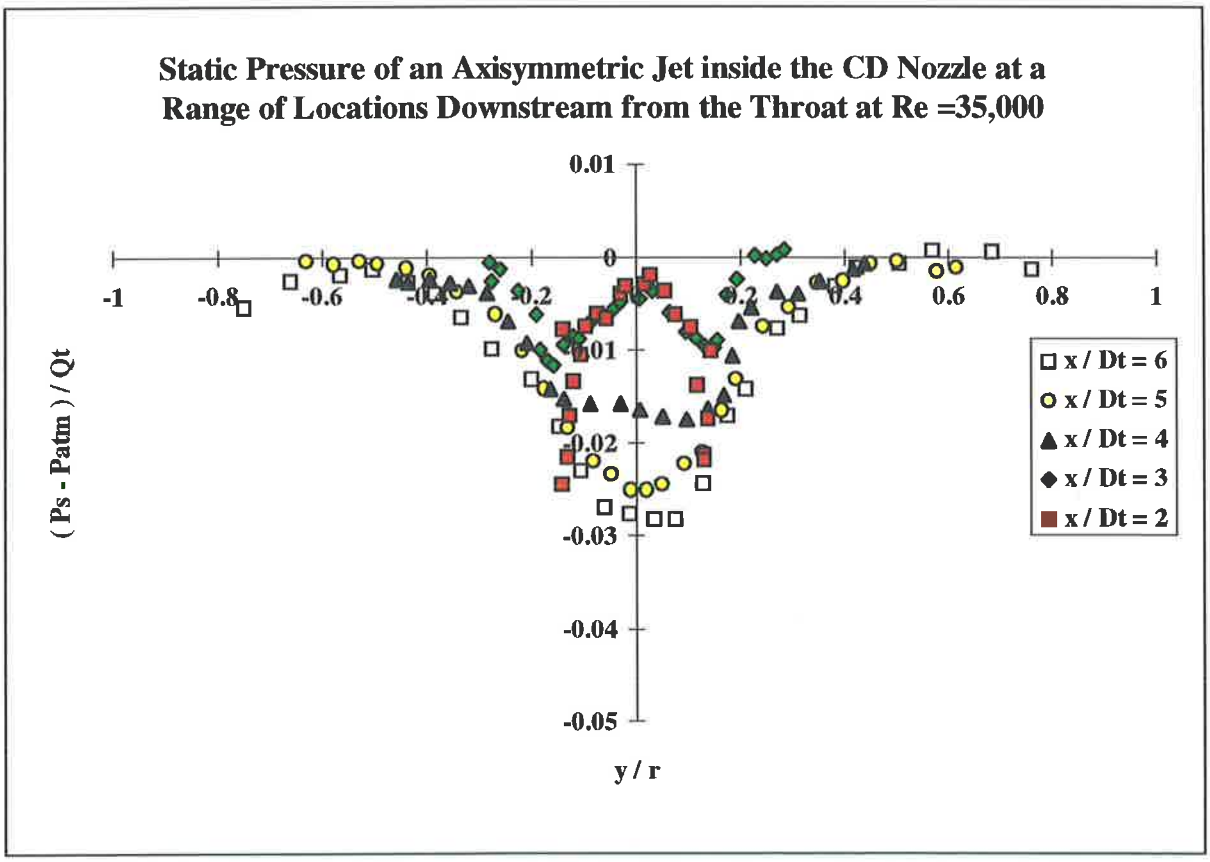

Figure 4.2. 1 Axisymmetric static pressure inside the CD nozzle normalised by the centreline dynamic pressure at $Re_t = 35,000$.

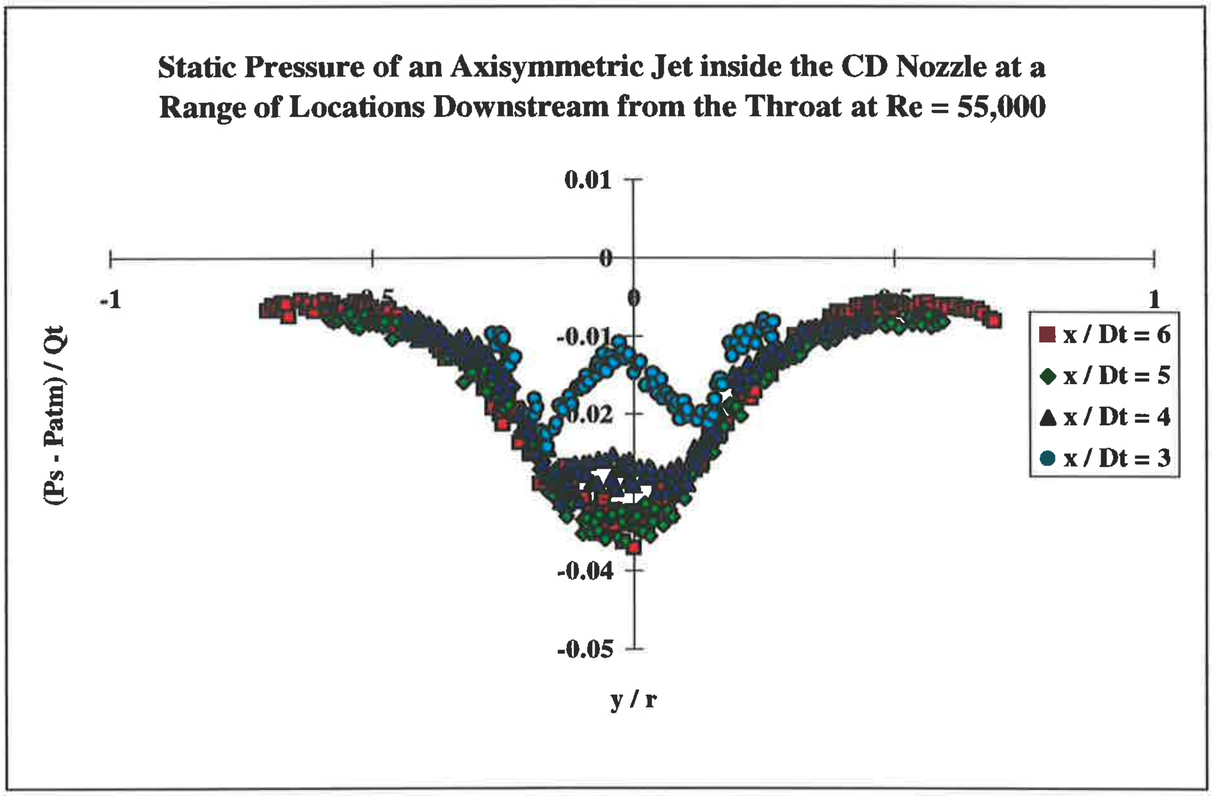

Figure 4.2.2 Axisymmetric static pressure inside the CD nozzle normalised by the centreline dynamic pressure at Re_t = 55,000.

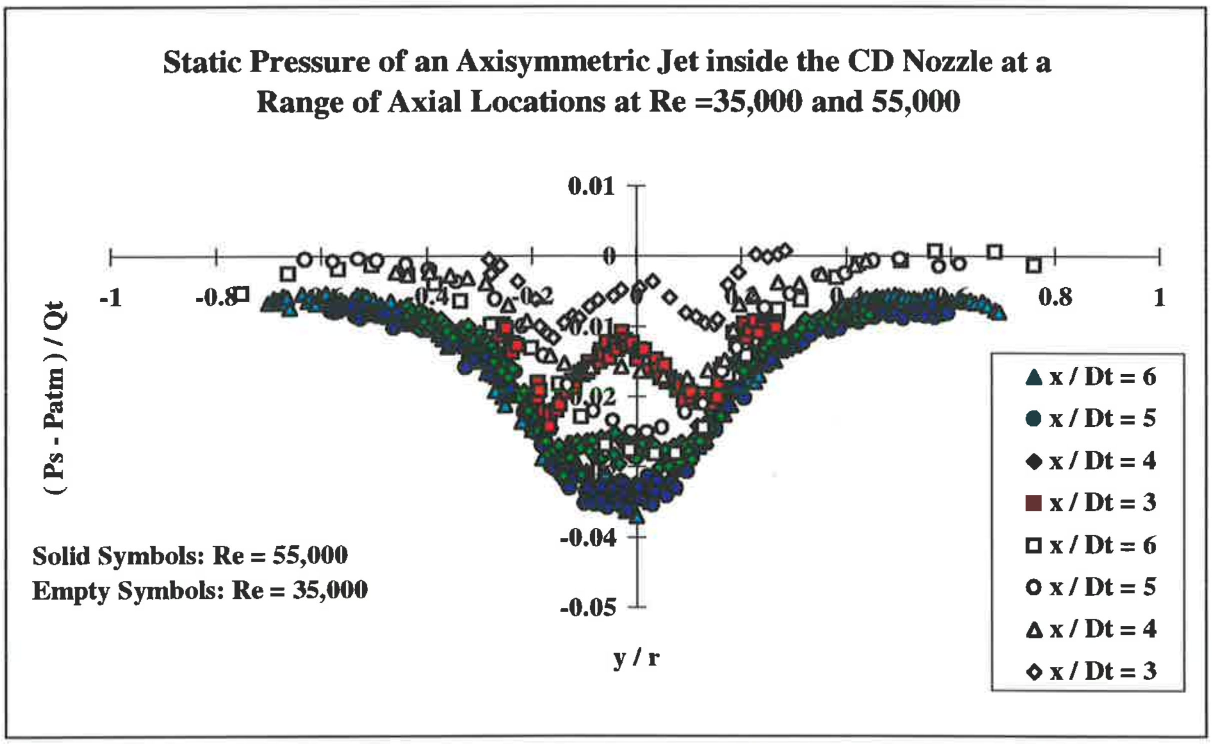

Figure 4.2. 3 Comparison of axisymmetric static pressure inside the CD nozzle at Re_t= 35,000 and 55,000 normalised by dynamic pressure, at a range of locations downstream from the throat.

When the Reynolds number is greater than 55,000 the flow becomes asymmetric and unstable in its azimuthal direction. This instability is eliminated by injecting a secondary fluid through the throat pressure tapping to maintain the azimuthal orientation of the jet so that stable jet pressure measurements could be taken. The static pressure profiles of the asymmetric flow at a Reynolds numbers above 55,000 are shown below in **Figure 4.2.4** for a number of stations downstream from the throat .

The static pressure profiles of the asymmetric flow at higher flow rates, for a given distance downstream from the throat are of similar shape. Generally they are more sub-atmospheric for the higher flow rates. The minimum static pressures measured inside the nozzle at various distances are tabulated in **Table 4.1**. The static pressure probe could not be inserted into the nozzle any closer than 1 throat diameter downstream from the throat without altering the very nature of the instability being studied. Therefore the static pressure data is not available for distances closer then 2 throat diameters from the throat due to the location of the static pressure holes on the probe.

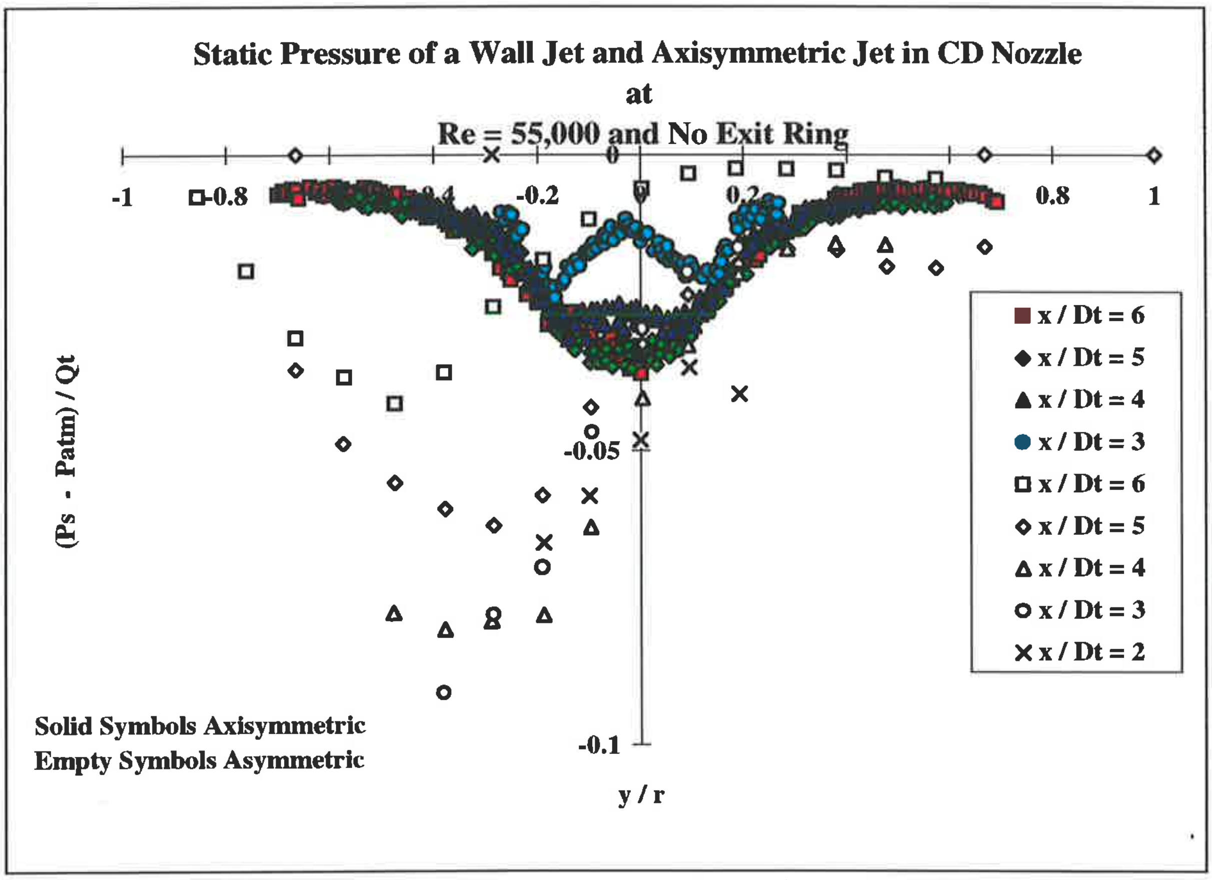

Figure 4.2. 4 Static pressure profiles of two types of flows inside CD nozzle at Re_t=55,000, AR=1.

4.2.3 Nozzle Wall Static Pressure

The static pressure on the nozzle wall was measured at four axially spaced locations, details of which are shown in **Figure 2.1.5**, the first of which is 15 mm, the next is 25 mm, the third is 35 mm and the fourth is 40 mm downstream from the throat. The measurements taken at these four locations include the effects on wall pressure due to variation in mass flux and change in exit area. The results indicate the dependence of nozzle static pressure on the exit area relative to the cavity area, AR.

Results from mcasurements taken at the 4 axial locations downstream from the throat are presented in **Figure 4.2. 5** to **Figure 4.2. 8,** for Reynolds number of 41,000 and 75,000. It can be seen from these figures that the static pressure initially reduces with the reduction of exit area for both Reynolds numbers measured. The minimum measured static pressure was reached when the exit area was around AR=0.69 which coincides with the maximum entrainment from ambient into the nozzle. As the exit area was further reduced, the static pressure increased ,as expected, due to further restriction on the exiting wall jet, which now occupies the whole of the exit area and a significant amount of primary jet is recirculated inside the nozzle. The wall static pressure measurements, shown in **Figure 4.2. 9,** were repeated at four equally spaced azimuthal locations to ascertain the wall static pressure on the surface not in contact with the wall jet . The results show that, for the case of AR = 1 at Re_t= 75,000, a good agreement with the previous set of results is achieved. It can be seen that static pressure is sub-atmospheric everywhere except under the wall jet where it reattaches to the surface. The results suggest that for the case where there is no exit ring present, and Reynolds number is 41,000, the jet leaving the throat separates fully and reattaches between 1.5 and 2 throat diameters downstream. This is also the case for the higher Reynolds number, but the reattachment location is shorter. The reattachment length reduces with increase in Reynolds number, shown by the above figure. The overall trend of the wall jet static pressure, along the surface where it is attached to the wall, is that it increases with reduction of exit area beyond AR = 0.69. The results are summarised in **Figure 4.2. 10**

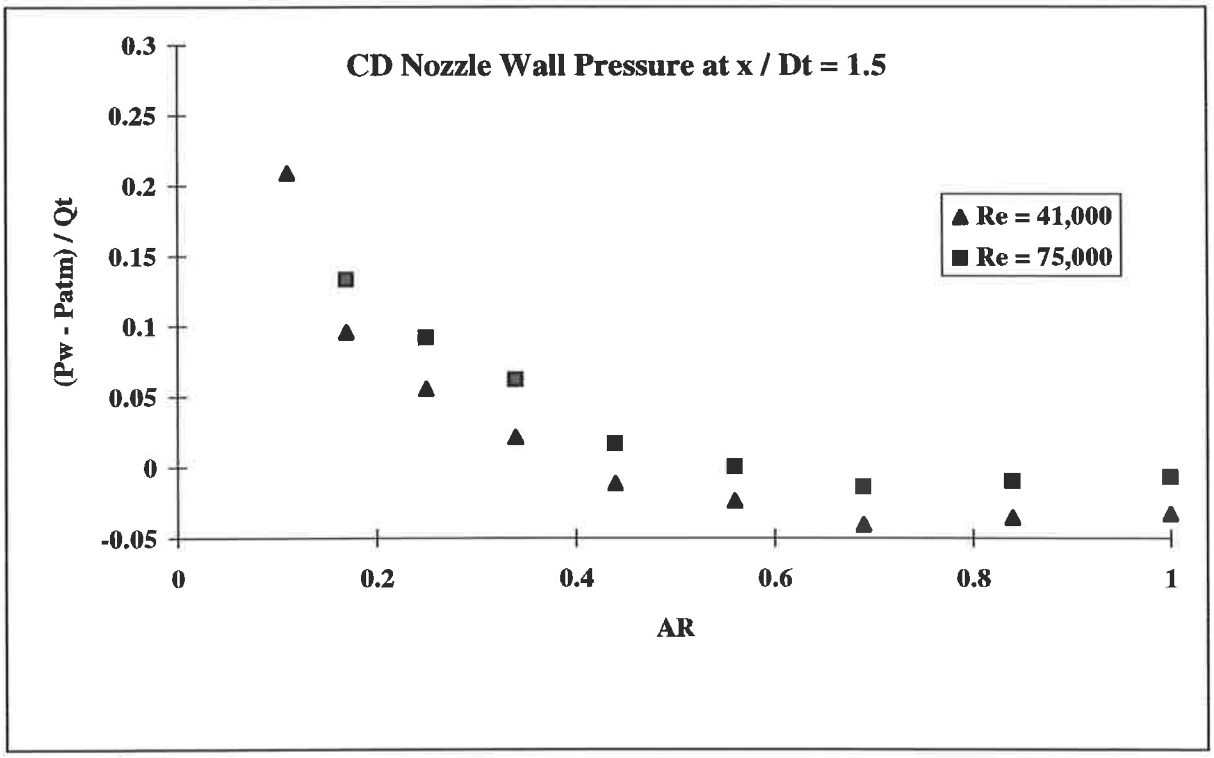

Figure 4.2. 5 **CD nozzle static pressure, wall jet side, at 1.5 throat diameters downstream from the throat for a range of exit areas.**

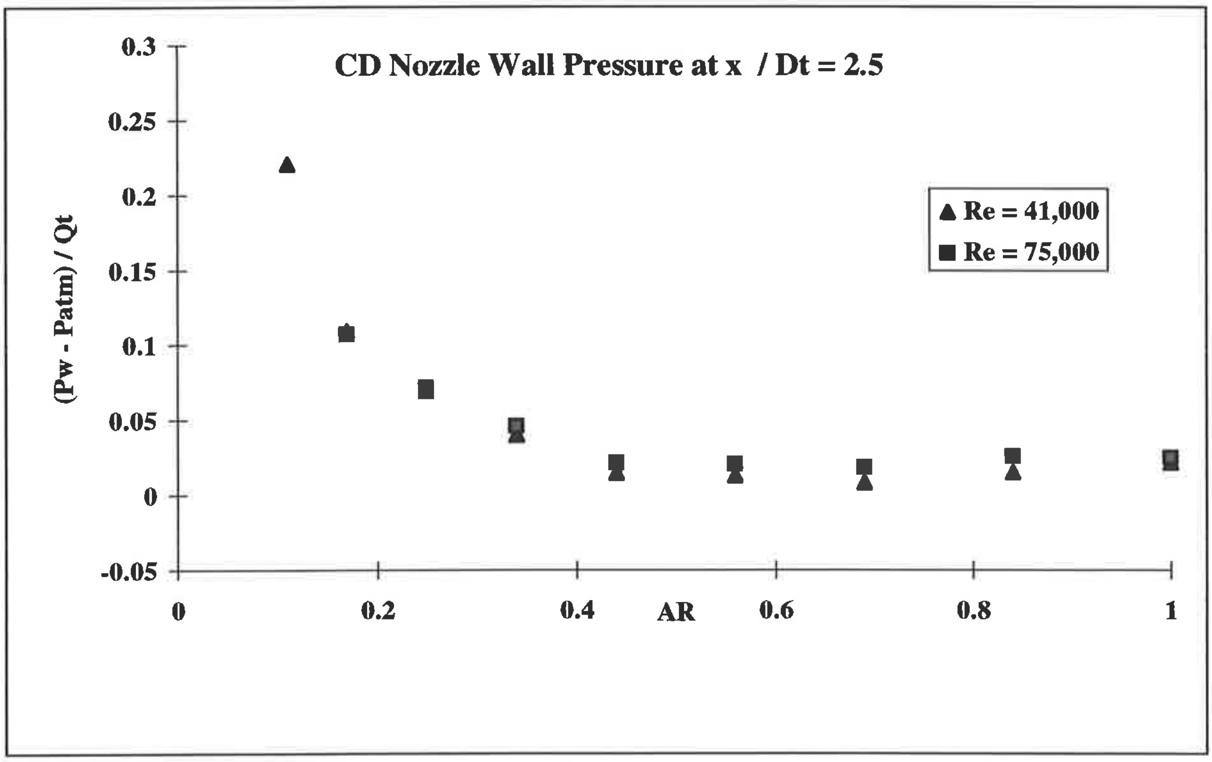

Figure 4.2. 6 **CD nozzle static pressure, wall jet side, at 2.5 throat diameters downstream from the throat for a range of exit areas.**

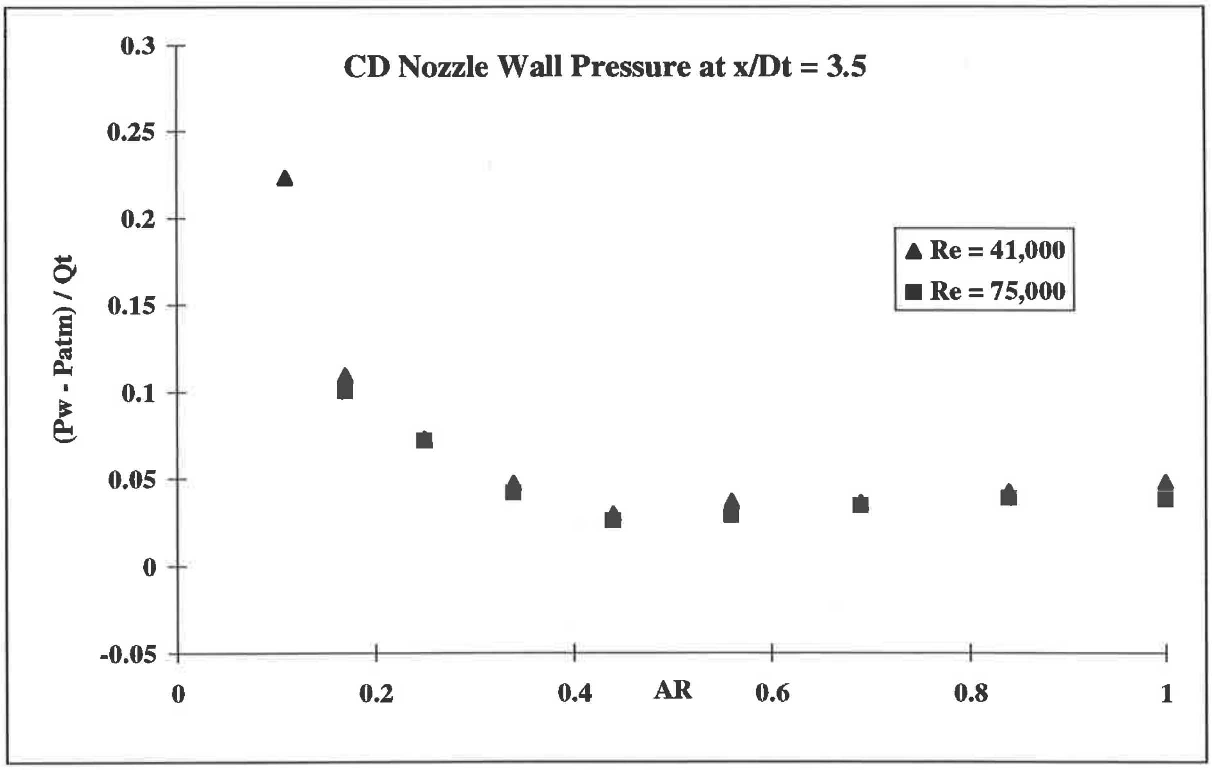

Figure 4.2. 7 CD nozzle static pressure, wall jet side, at 3.5 throat diameters downstream from the throat for a range of exit areas.

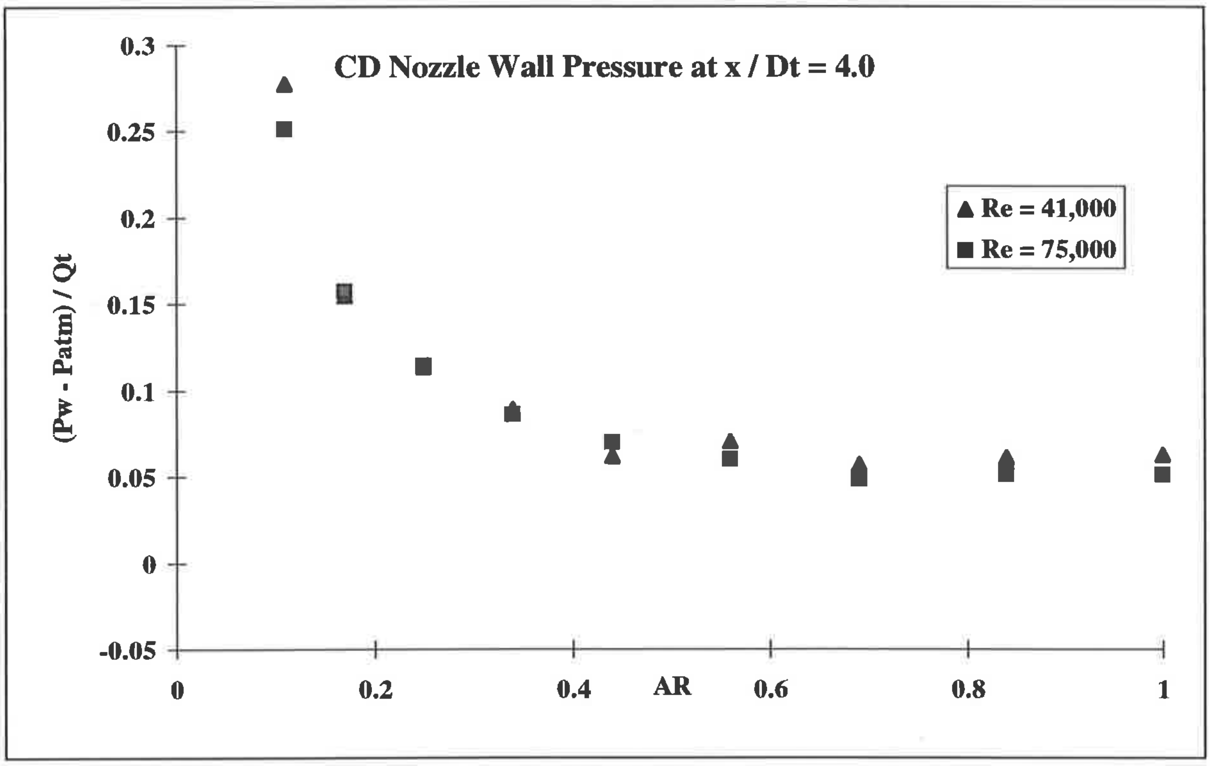

Figure 4.2. 8 CD nozzle static pressure, wall jet side, at 4 throat diameters downstream from the throat for a range of exit areas.

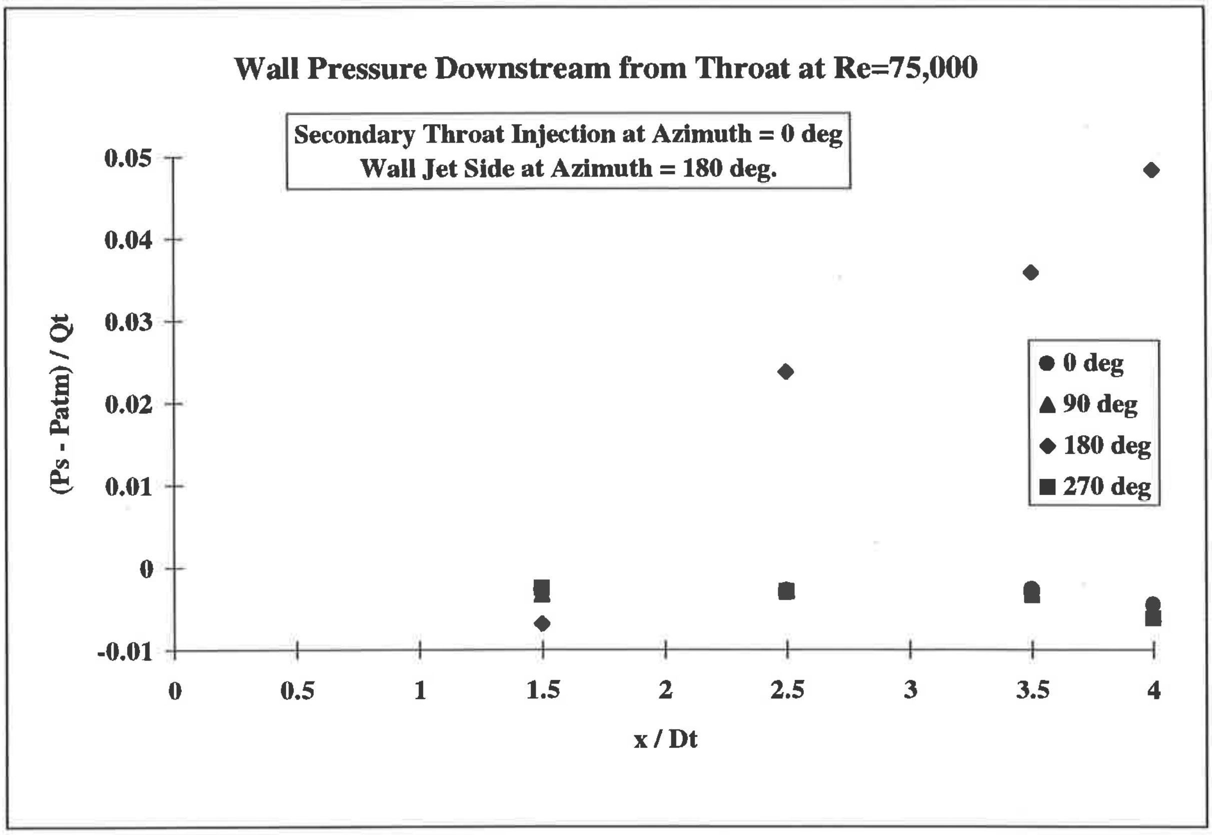

Figure 4.2. 9 CD nozzle wall pressure at four azimuthal locations, AR = 1 and Re_t = 75,000.

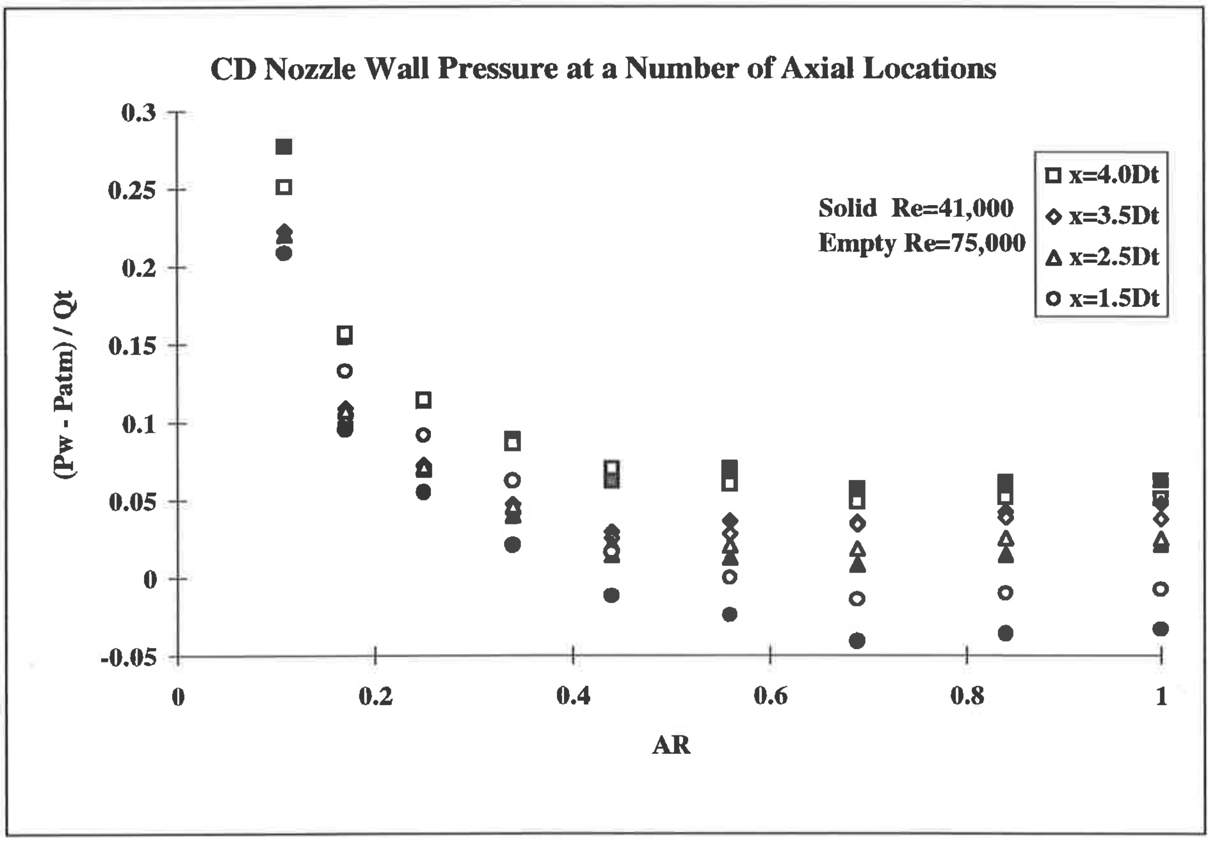

Figure 4.2. 10 CD nozzle wall pressure at a number of axial locations for Re_t = 41,000 and 75,000.

4.2.4 CD Nozzle Total Pressure

The total pressure measurements were taken diametrically across the axisymmetric jet leaving the throat at intervals of one throat diameter (1 D_t) up to the nozzle exit for most of the flow rates considered. As mentioned above, the probe interferes with the flow near the throat, especially when the Reynolds number exceeds about 50,000, which corresponds to a flow rate of 7.2 x 10^{-3} kg/s. The flow remains axisymmetric for the flow rates below this value as shown by the axisymmetric total pressure profiles in **Figure 4.2. 11** to **Figure 4.2. 15** showing that the jet mixing layer turbulence increases with Reynolds number as would be expected.

At flow rates above 7.2 x 10^{-3} kg/s ($Re_t > 50,000$), the flow is asymmetric but requires a secondary fluid injection to maintain a given azimuthal position, although the jet could be "forced" into asymmetric flow at lower flow rates by injection of secondary flow at the throat. This is shown in the flow visualisation of the deflected jet for Re_t as low as 1400. The total pressure profiles of the asymmetric jet at a number of locations inside the CD nozzle for the Reynolds number of 58,000 are shown in **Figure 4.2. 16**. The jet, which initially has the approximate top hat profile near the throat deforms, as is shown in this figure, into a 3 throat diameters thick wall jet. At the higher mass flux, the wall jet thickness decreases and the jet spreads azimuthally, as shown in **Figure 4.2. 17**. The characteristic feature of these profiles is that the wall jet becomes progressively thinner at the nozzle exit as the mass flux is increased possibly due to an increase of the Coanda-like effect which keeps the wall jet attached as shown in **Table 4.2**.

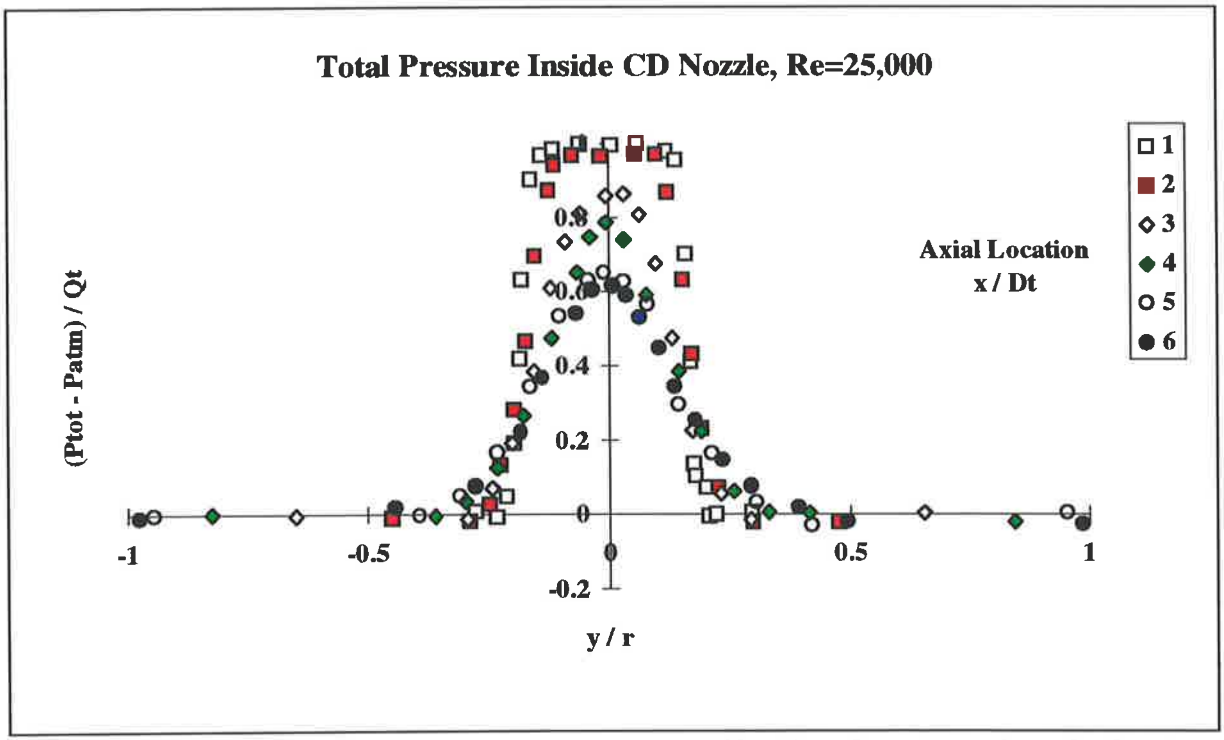

Figure 4.2. 11 CD nozzle total pressure profiles at a range of locations downstream from the throat without an exit ring at Re_t = 25,000.

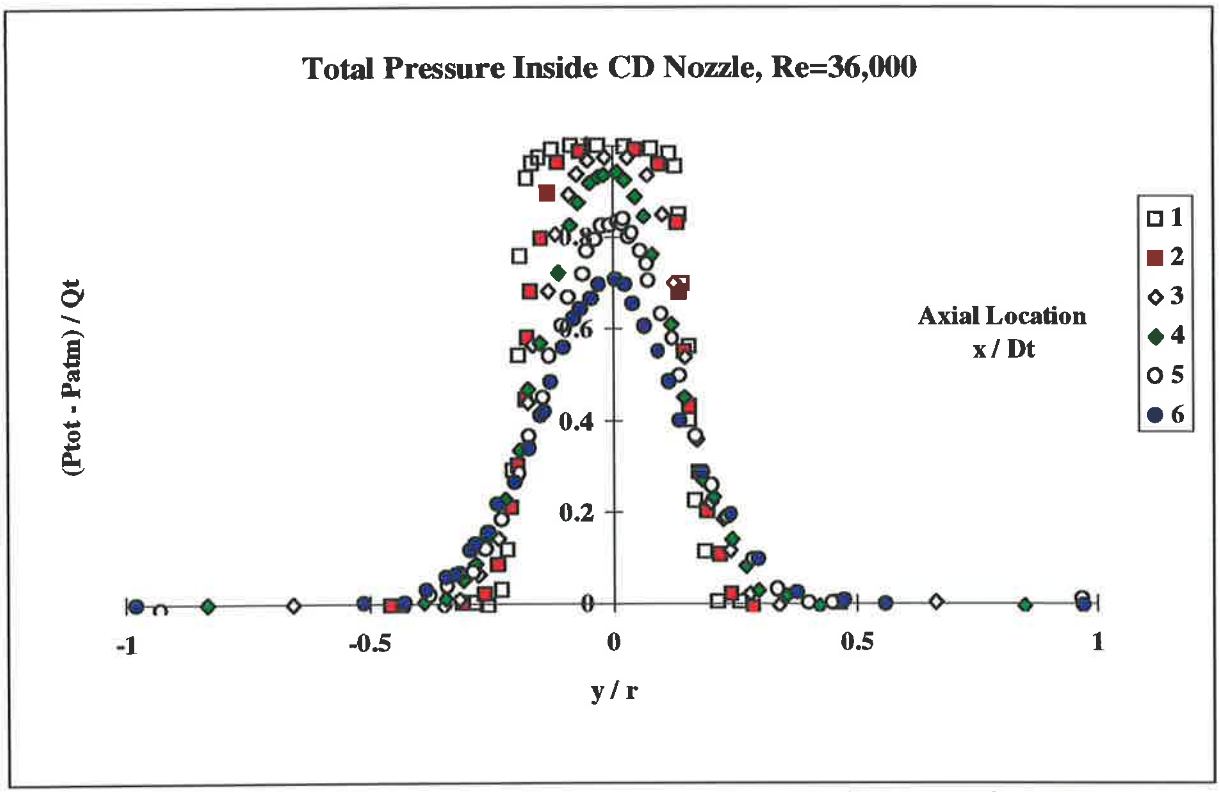

Figure 4.2. 12 CD nozzle total pressure profiles at a range of locations downstream from the throat without an exit ring at Re_t = 36,000.

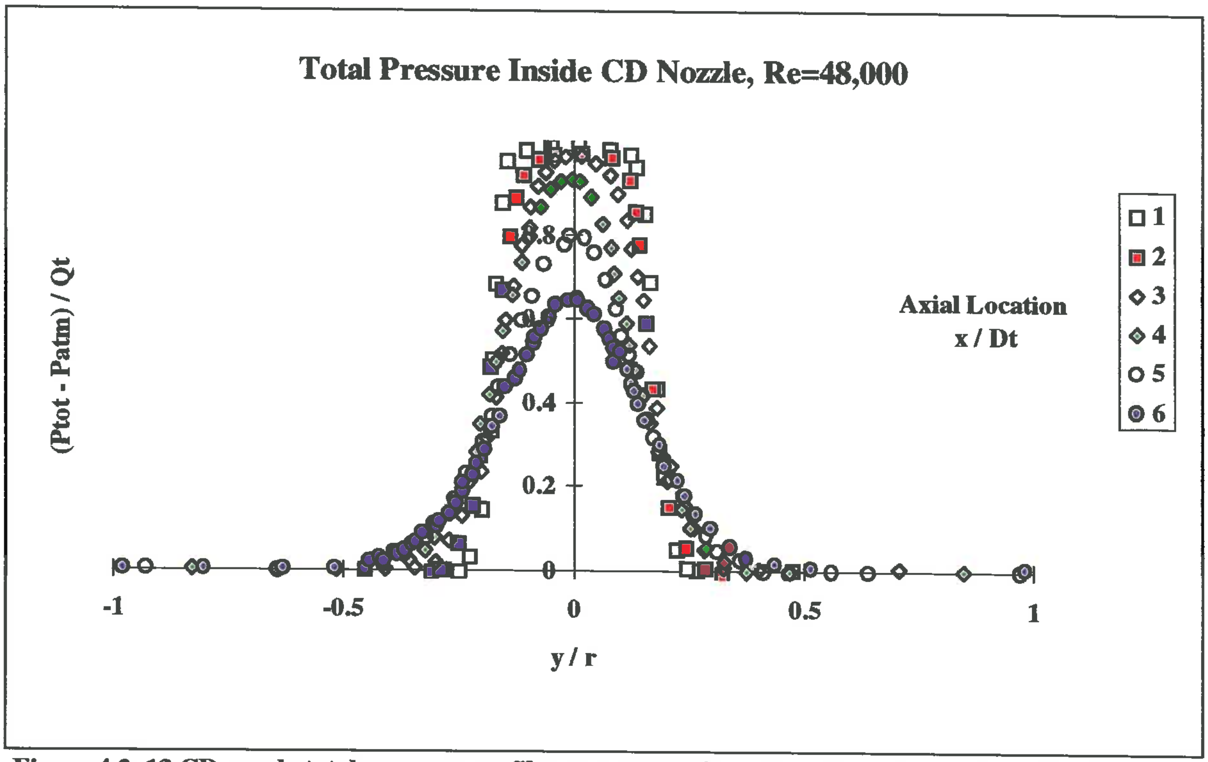

Figure 4.2. 13 CD nozzle total pressure profiles at a range of locations downstream from the throat without an exit ring at $Re_t = 48,000$.

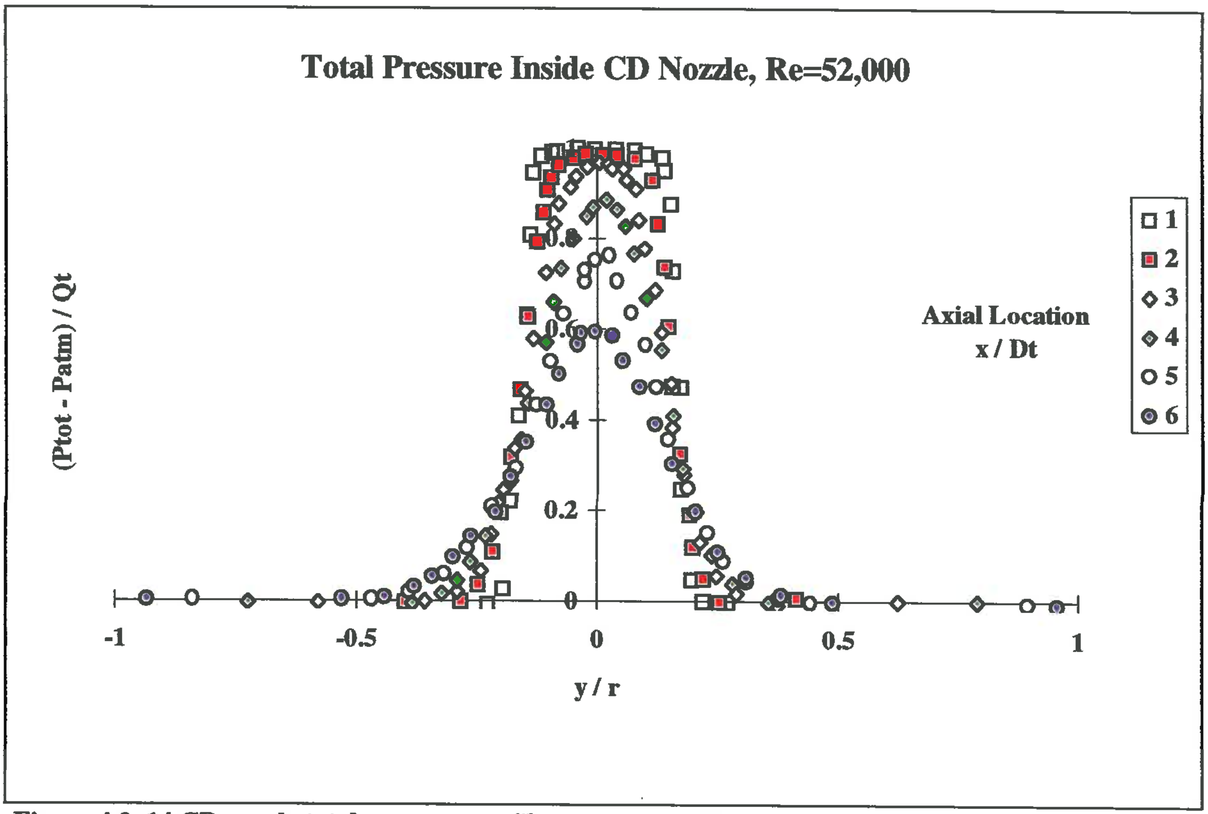

Figure 4.2. 14 CD nozzle total pressure profiles at a range of locations downstream from the throat without an exit ring at $Re_t = 52,000$.

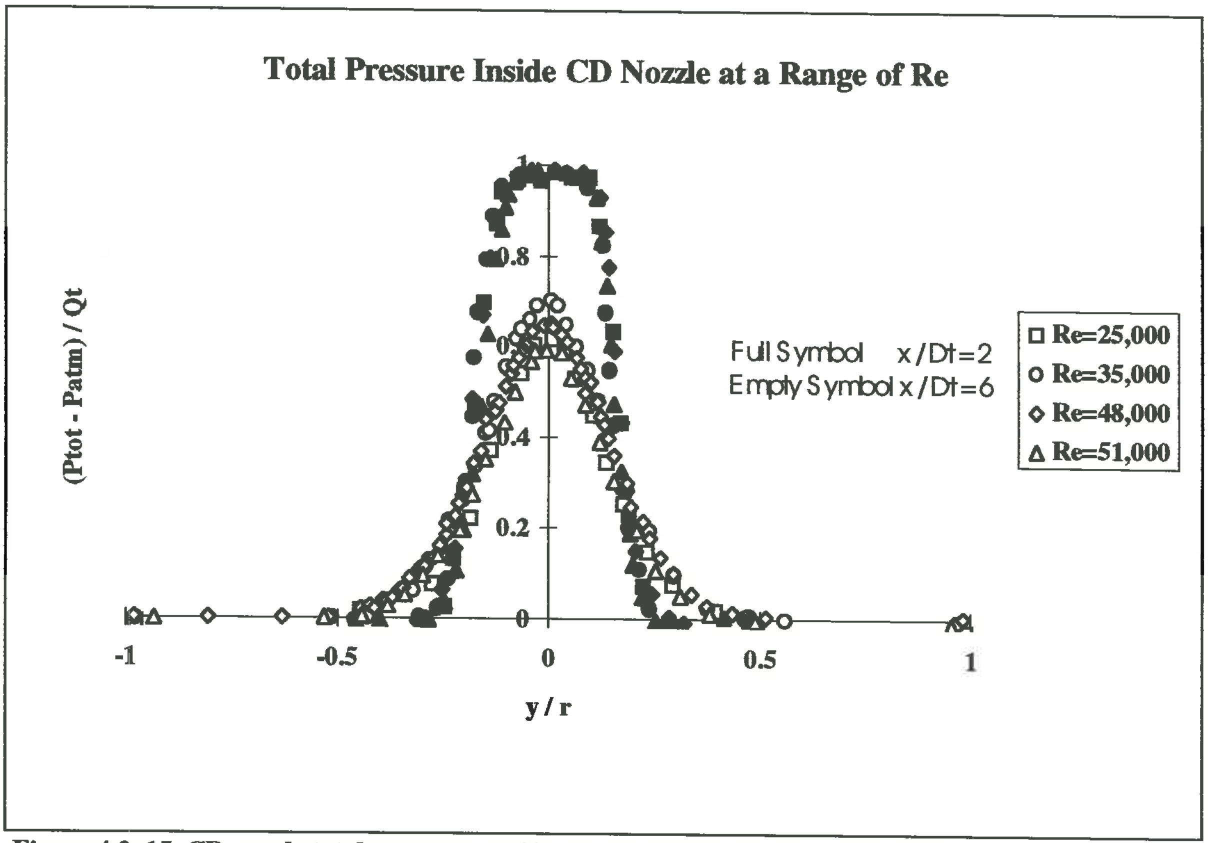

Figure 4.2. 15 CD nozzle total pressure profiles at the nozzle exit at a range of Re_t and no exit ring.

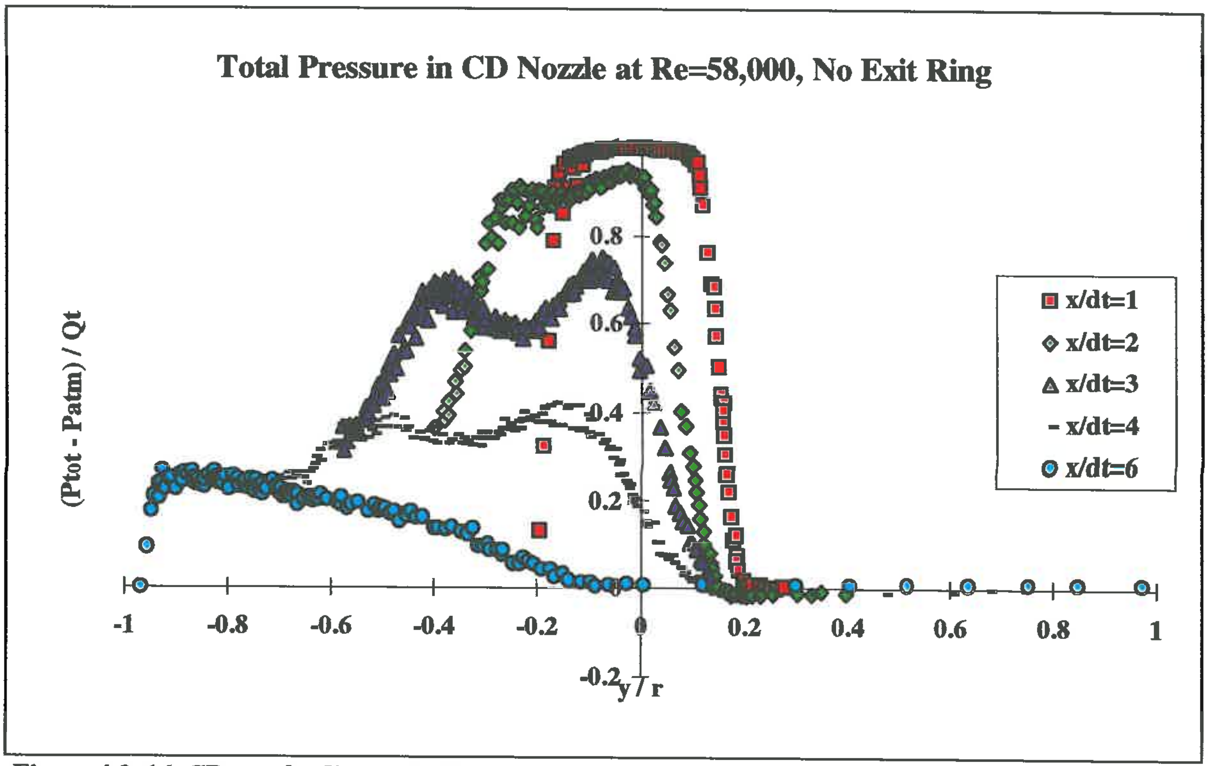

Figure 4.2. 16 CD nozzle, diametrically traversed across asymmetric jet, total pressure profiles at a range of locations from the throat without exit ring, Re_t = 58,000.

Table 4. 2 Wall jet thickness at the plane of symmetry at a number of locations downstream from the throat without the exit ring.

Reynolds Number	at x = 2 D_t	at x = 4 D_t	CD nozzle exit
49,000	1.76 D_t	2.50 D_t	2.35 D_t
58,000	1.80 D_t	2.60 D_t	3.00 D_t
60,000	1.90 D_t	2.94 D_t	3.00 D_t
65,000	1.90 D_t	2.80 D_t	3.00 D_t
72,000	1.90 D_t	2.70 D_t	2.79 D_t
187,000	1.00 D_t	1.47 D_t	1.53 D_t

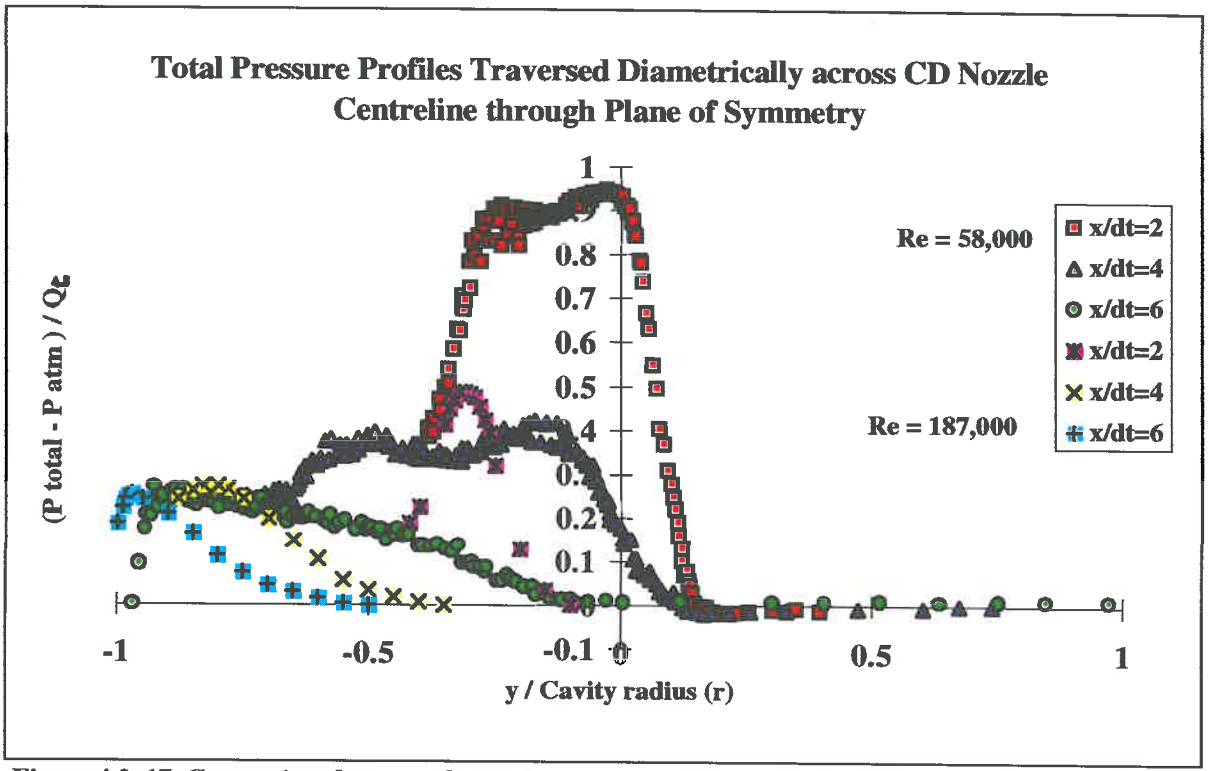

Figure 4.2. 17 Comparison between the total pressure profiles inside the CD nozzle, diametrically traversed across asymmetric jet, at a range of locations from the throat without exit ring for : Re$_t$=58,000 and 187,000.

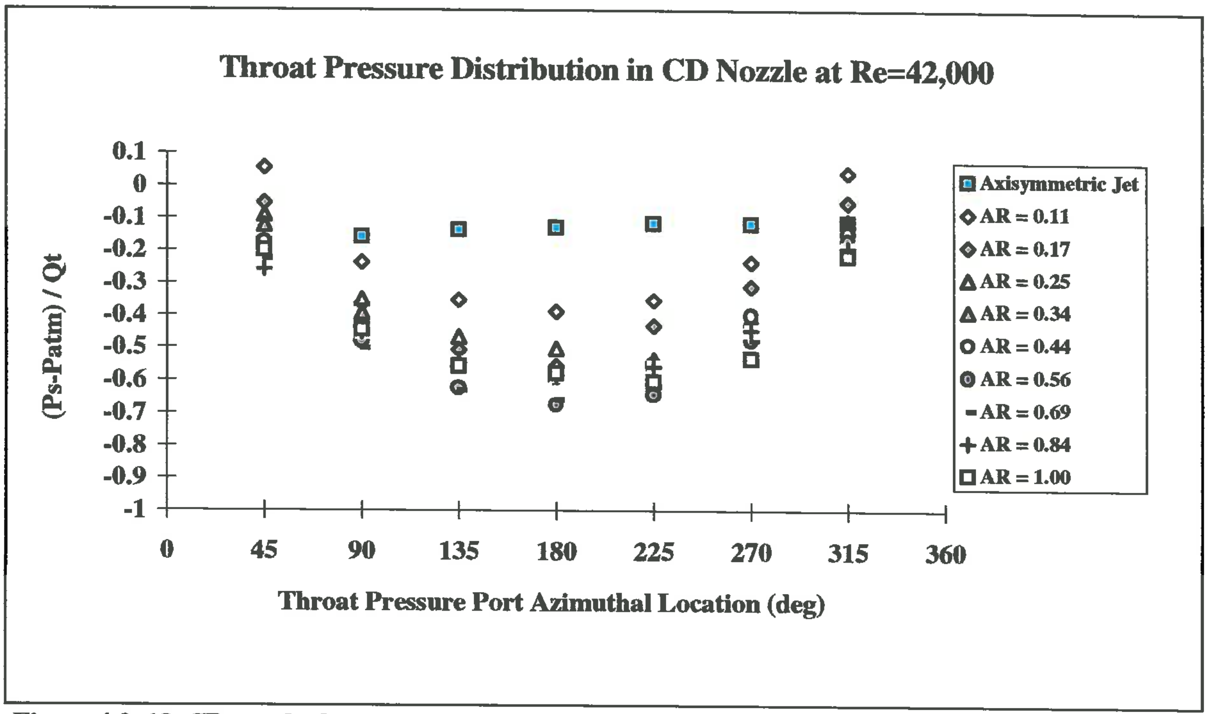

Figure 4.2. 18 CD nozzle throat static pressure distribution at $Re_t = 42,000$ and a range of AR.

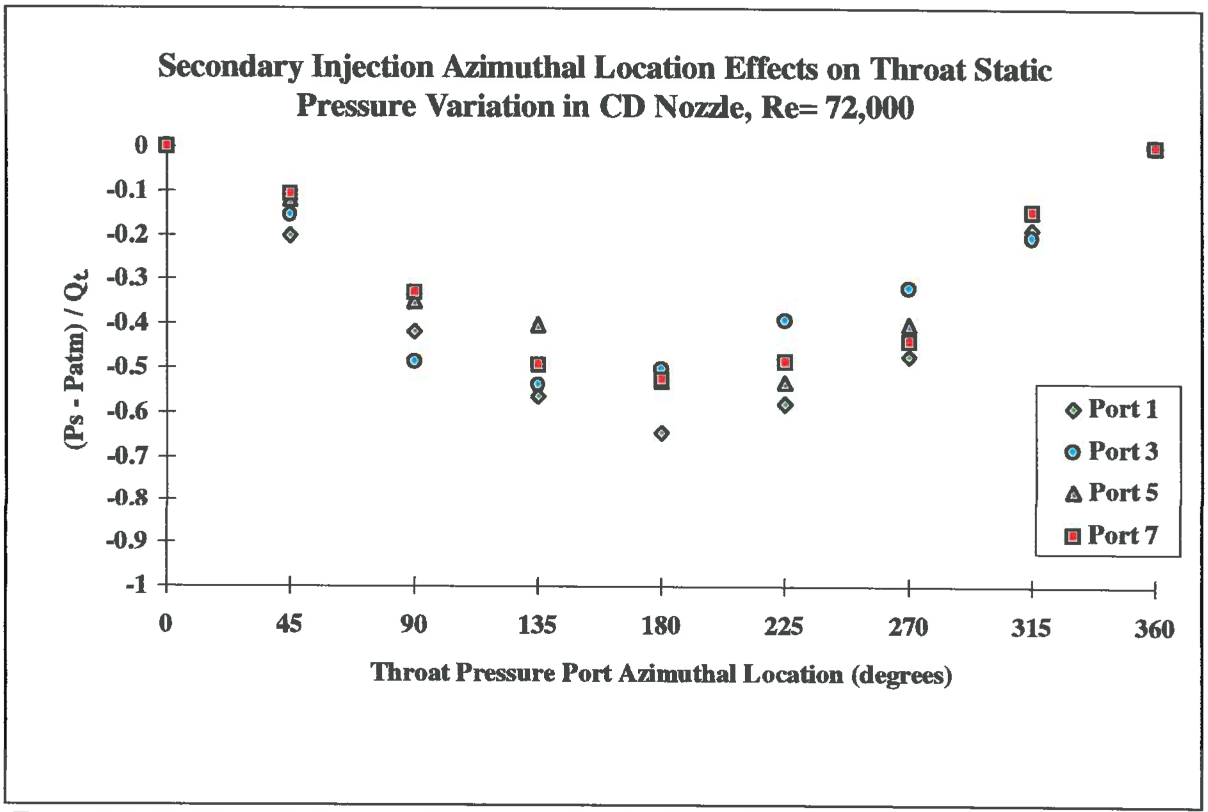

Figure 4.2. 19 CD nozzle throat static pressure distribution at $Re_t = 72,000$, AR = 1 and a range of azimuthal secondary injection points.

4.2.5 CD Nozzle Throat Static Pressure

The throat pressure was measured for both the CD and CD10 nozzles. Initially there were 4 pressure tappings at the nozzle throat and the measurements for the CD10 nozzle consisted of only 4 pressure readings. At the later stage of the project a new nozzle was manufactured which incorporates 8 pressure tappings at the throat. This nozzle was used to assess the static pressure distribution around the throat for various combinations of flow rates and exit ring diameters. For the axisymmetric flow at Reynolds numbers < 50 000, the throat static pressure distribution is constant, as shown in **Figure 4.2. 18**. The injection of secondary fluid at the throat produces a stable asymmetric primary flow and this in turn produces a non-uniform throat static pressure distribution, also shown in the above figure. The lowest static pressure was measured at the azimuthal position of $\theta = 180°$ from the point of secondary injection, which is the location where the jet attaches to the wall, shown in both **Figure 4.2. 9** and **Figure 4.2. 18**. As was shown in previous section, the static pressure distribution, along the nozzle wall where the jet is attached, has the lowest value at the throat but rises very quickly toward atmospheric a short distance downstream from the throat. This is true for the case where no exit ring is attached and Reynolds number is below 80,000. At the Reynolds number of 42,000 where the secondary fluid injection was used to provoke asymmetric separation, the static pressure at the throat is generally sub-atmospheric for all the exit rings tested except for the AR = 0.11, the pressure ports nearest secondary injection port show above atmospheric reading. At the other azimuthal locations, even for this exit area, the pressure remains sub-atmospheric. To test for possible asymmetry due to the geometric imperfection, the experiment was repeated using other secondary fluid injection locations and the results are shown in **Figure 4.2. 19**. These reveal that the measured pressure distribution is the same for all cases considered when the estimated experimental uncertainty is included in the plot. The differences in the measured pressure at the throat, using different azimuthal locations to provoke separation downstream from the injection port, may be attributed to the larger diameter (2mm) of that particular throat pressure tapping at port number one. This tapping was used for the secondary fluid injection in most of the experiments.

4.3 Measure of Deflected Jet Mean Flow Direction

The angle to which the jet is deflected as it exits the nozzle is needed to evaluate the thrust produced by the nozzle since only the transverse reaction on the nozzle was measured. Several methods were used to measure the deflected jet angle and these are discussed in detail in the following sections.

4.3.1 The Use of Tufts

A tuft placed in the flow was the simplest method used to determine the angle at which the jet was deflected. The angle was measured visually against a protractor in the background. Only the angles of the high momentum flow across the plane of symmetry were measured and results summarised in **Table 4.3.** The deflection angle assigned to a particular jet angle is an average of the values across that jet and was reproducible to within ± 5 degrees over three runs. These results were found to be sufficiently accurate for comparison of the various geometric configurations. The values also compared to within ± 5 degrees with other more accurate means of measuring the deflection angle, such as by resolution of the two velocity vectors obtained by LDV. Tufts were initially used only to indicate the general flow direction, but were used for the majority of deflected jet angle measurements as shown in **Figure 4.3. 1**. This figure also illustrates the use of water vapour to mark the fluid being entrained into the nozzle.

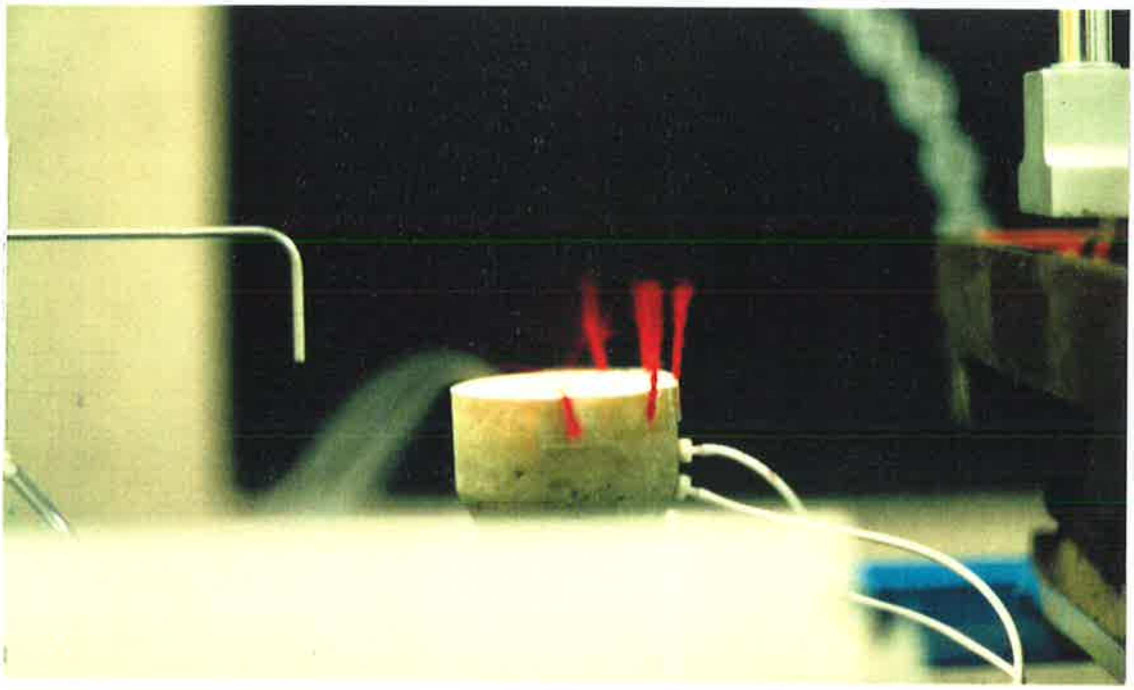

Figure 4.3. 1 Flow visualisation of the marked fluid induced into the nozzle with the jet exiting the right side shown by tuft direction.

Table 4. 3 Summary of deflected jet angles exiting from CD nozzles measured using a tuft

Exit Area Ratio AR	0.84	0.69	0.56	0.44	0.34	0.25	0.17	0.11
Exit Diameter d_e mm	55	50	45	40	35	30	25	20
CD nozzle $\alpha°$	25	45	60	70	80	75	65	45
CD6 nozzle $\alpha°$	25	45	60	70	75	75	65	45
CD10 nozzle $\alpha°$	20	35	50	60	65	60	45	30
CD20 nozzle $\alpha°$	35	40	40	40	35	30	20	10

4.3.2 Laser Sheet Flow Visualisation

Extensive use of the laser was made to visualise the flow both inside and outside the nozzle. The flow velocity at the throat had a maximum value of 10 m/s while at the nozzle exit the velocity was less than 5 m/s. The flow was seeded by the six jet atomiser which produces a fine mist of water with good reflective properties so that when the laser sheet illuminates the particles in the flow they reflect the laser light. The light reflected by the particles in the flow was sufficient at the this low exit velocity to use a standard 35 mm, 100 ASA colour or black and white film to capture the images clearly.

4.3.2.1 Apparatus

The apparatus shown in **Figure 2.1. 2** and **Figure 2.5. 1** was used for the evaluation of the deflected jet angle exiting the CD, CD6, CD10 and CD20 Nozzles. The same apparatus and photographic technique were also used in the evaluation of deflected angle of a two-dimensional wall jet past a gate. The laser beam was passed through a cylindrical lens to produce a laser sheet about one mm thick in the region where measurements were taken. The laser sheet was aligned with the plane of symmetry of both the axisymmetric and asymmetric jet. It was also used to illuminate the flow at the exit normal to the nozzle axis. The photographs were taken at an angle of approximately 20° off the normal to the laser sheet to optimise the illumination of the flow. Again the flow seeding was provided by the six jet water atomiser described earlier.

4.3.2.2 Results

The method of seeding the primary jet and measuring the mean deflected jet angle was limited to a throat velocity of up to 10 m/s. The mass flow rate for this type of flow visualisation was restricted by the limited pressure of the six jet atomiser that was introduced upstream from the throat. This limitation however does not invalidate the results of the measured deflected jet angles since it has been found that the angle at which the mean jet leaves the nozzle exit is only mildly dependent on mass flow rate, in the range considered, and therefore Reynolds number, as discussed in Section 4.3. The deflected jet mean flow direction measured at low velocity apply equally, therefore, to the high velocity flow. The angle of the deflected jet exiting a nozzle with a particular exit ring diameter is visualised by illuminating the seed droplets with a 1 mm thick laser sheet passing upstream along the nozzle axis and in the plane of symmetry of the deflected jet. The intensity of the reflections from the seed droplets in the flow is proportional to their population. Hence relatively unmixed primary jet appears bright while the well mixed regions of the jet are less intense. For the low velocity flow, some primary jet structures are visible. The flow was captured on a 35 mm film in an otherwise dark laboratory. Most of the captured images were taken using the maximum shutter speed possible for the amount of light available from the laser, typically in the range of 1/30 sec and 1/60 sec.

The laser sheet flow visualisation photographs reveal a number of features of the flow. The diffuse angles at which the jet leaves the nozzle exit can be estimated from the total speed and the average angle by applying a weighting factor related to the intensity of the reflected laser light, as the intensity of the seeded jet is an indication of the amount of mixing with the ambient air both inside the nozzle and in the external field. **Figure 4.3. 2** shows the axisymmetric jet leaving the CD nozzle exit plane with the jet spreading half angle of about 10° which is consistent with past findings **[5]**. The jet spreading half angle of a simple jet is quoted to be of the order of 4°. Since the jet in the present study leaves the throat and is surrounded by the divergence, which increases the mixing at the shear layer, it is reasonable to expect the spreading angle to be greater than that for the simple jet case. **Figure.4.3. 3** shows an asymmetric jet leaving the same nozzle with the jet spreading half angle β of about 20° if the unweighted "best fit" common origin for the "attached" and "free" sides of the emerging wall jet is used, also about 20° if separate origins are taken on the extension of the intensity weighted centreline of the jet is used, or ranging from 10° on the "attached" side to almost 30° on the "free" side if the common origin is forced to be on a line parallel to the nozzle axis. The second of the interpretations is the most appropriate. The second interpretation however may be expected since only the free side of the jet is mixing while the jet in contact with the wall is spreading radially to take the shape of the nozzle. It is during this process that the edges of the jet are turned towards the nozzle geometric centreline to form the vortex loop, the cross section of same shown in **Figure 4.3. 10.**, and produce an apparent increase in the spreading half angle shown in **Figure 4.3. 3**.

When the jet exiting the CD Nozzle is disturbed by the addition of an exit ring, the effects are dramatic as is clearly shown in **Figure 4.3. 4** to **Figure 4.3. 9** . The angles measured and indicated in the figures are an intensity weighted mean of the deflected jet trajectories. It can be seen that the deflected jet angle initially increases with decreasing exit area to a maximum value of $\alpha = 80°$. As the exit area continues to decrease below AR of about 0.3 the jet deflection angle now also decreases from its maximum value. The minimum ratio of exit area to nozzle area considered was 0.11 which corresponds to a 20mm diameter exit ring and a diameter ratio of 1/3. The flow at the nozzle exit was also visualised by passing a laser sheet normal to the nozzle axis at various distances from the exit plane. **Figure 4.3. 10** shows the asymmetric jet cross-section contour at 1 mm downstream from the exit and **Figure 4.3. 11** and **Figure 4.3.12** show the jet contour respectively at 5 mm and 10 mm downstream from the exit plane. Note in **Figure 4.3.12** there exist a “pair” of large counter rotating streamwise vortices dominating the jet cross-section. These are discussed in later sections of the thesis.

As the exit rings are added to the nozzle, the flow deflects across and away from the nozzle axis as shown in previous figures. **Figure 4.3.13** to **Figure 4.3.18** show the cross sectional area of the seeded jet at 10 mm above the nozzle exit when it is deflected by various diameter exit rings. The circular images in the background are not related to the flow, they are probably due to a very small droplet of water from the nozzle landing on the lens. Additional data on CD nozzle deflected jet may be found in Appendix C.

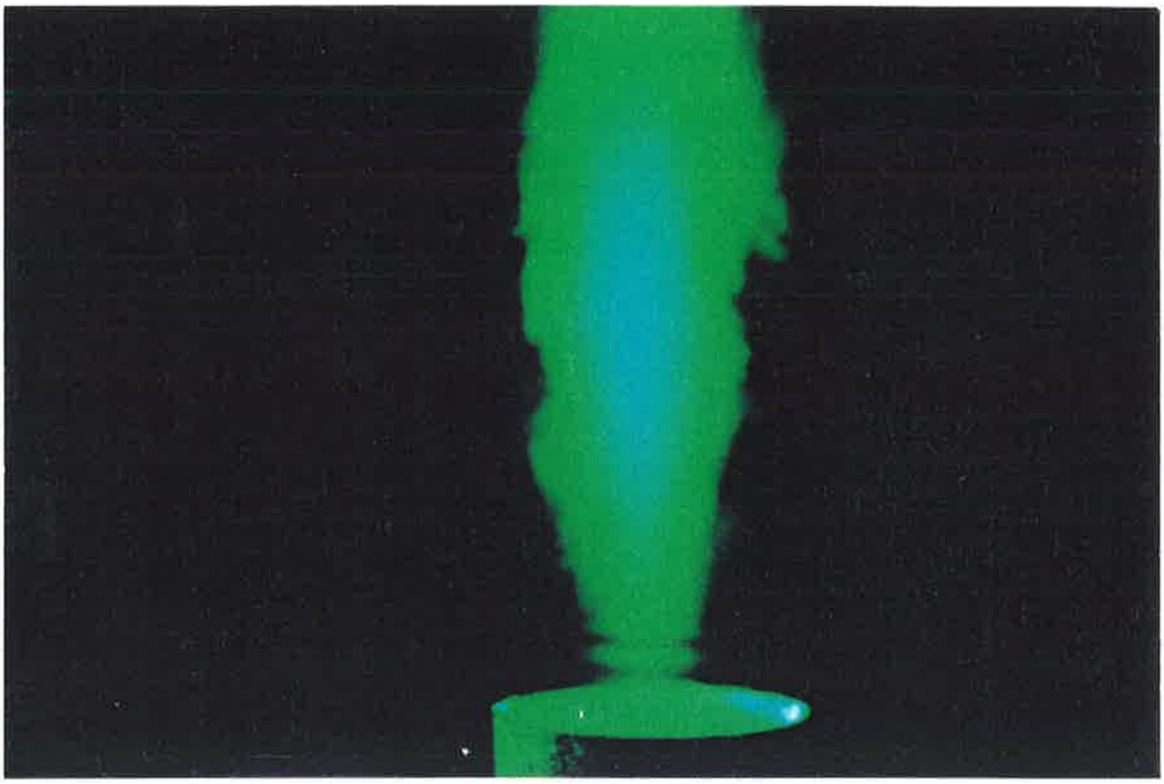

Figure 4.3. 2 **Laser sheet flow visualisation illuminating the axisymmetric jet leaving the CD nozzle at Re_t=7,000 with jet half angle of 10°.**

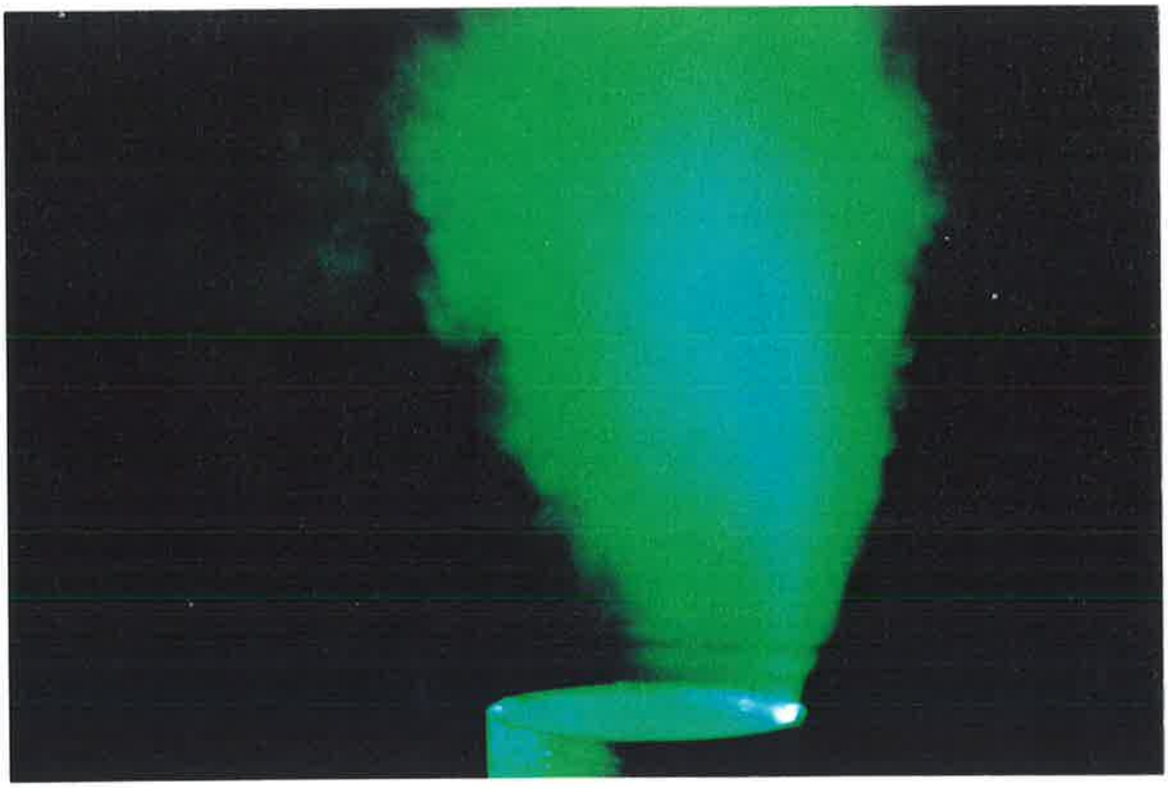

Figure 4.3. 3 **Laser sheet flow visualisation illuminating the asymmetric jet leaving the CD nozzle at Re_t=7,000 with jet half angle of at least 20°.**

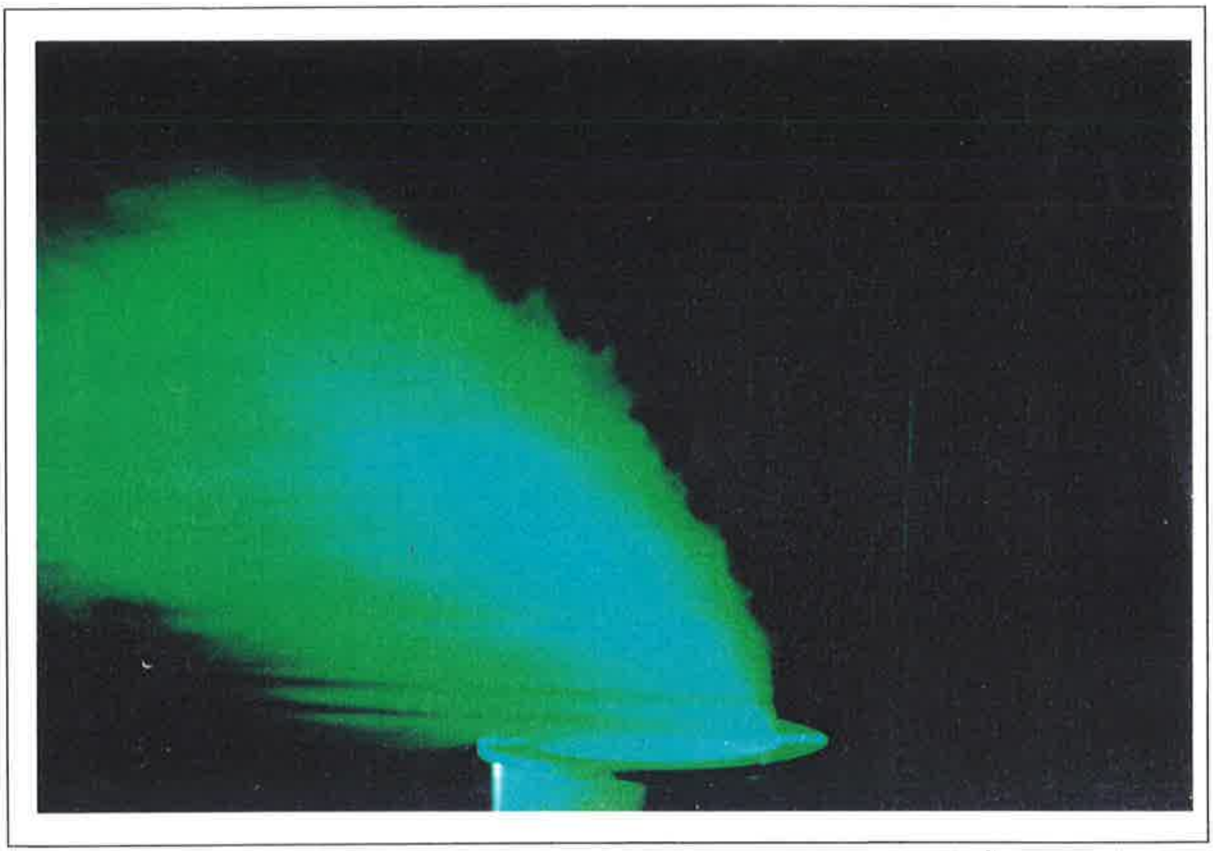

Figure 4.3. 4 Laser sheet flow visualisation illuminating the asymmetric jet leaving the CD nozzle at $\alpha = 45°$ with AR = 0.69 and $Re_t = 7{,}000$.

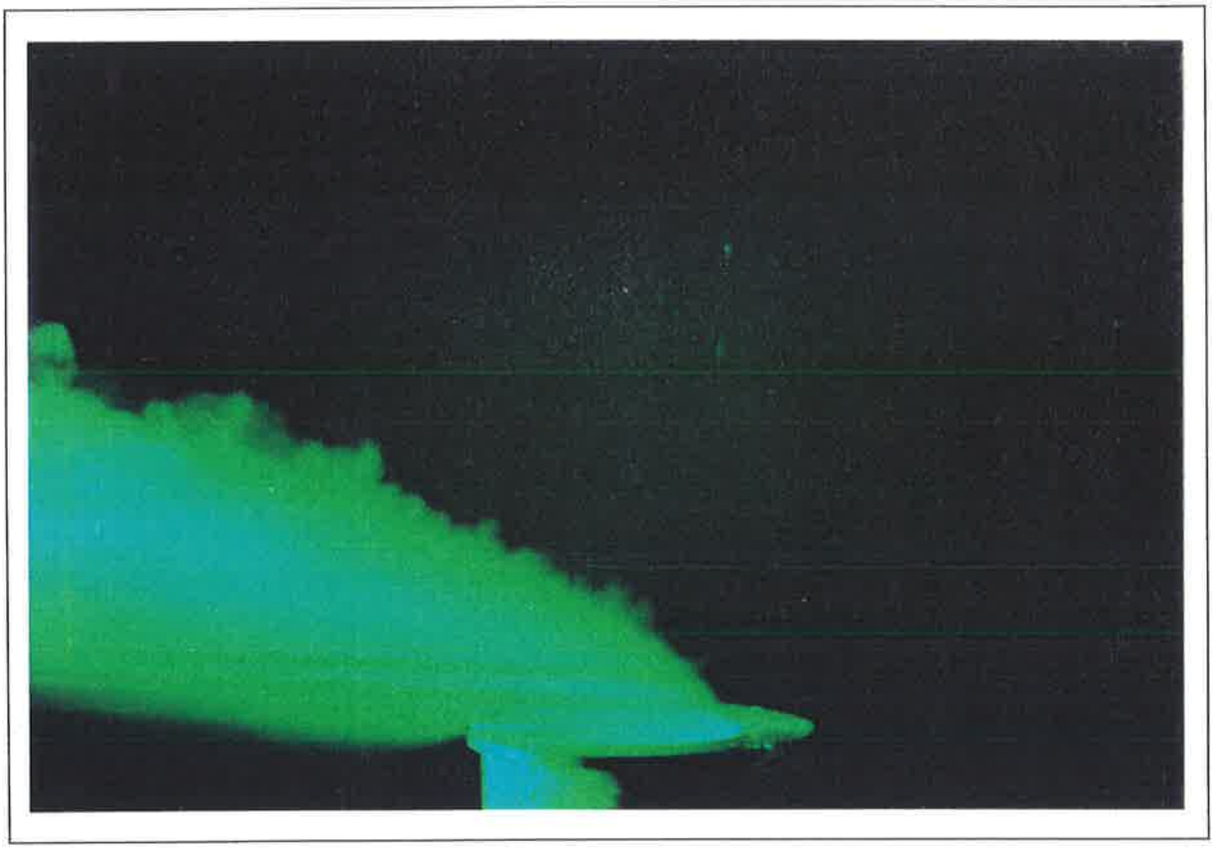

Figure 4.3. 5 Laser sheet flow visualisation illuminating the asymmetric jet leaving the CD nozzle at $\alpha = 70°$ with AR = 0.44 and $Re_t = 7{,}000$.

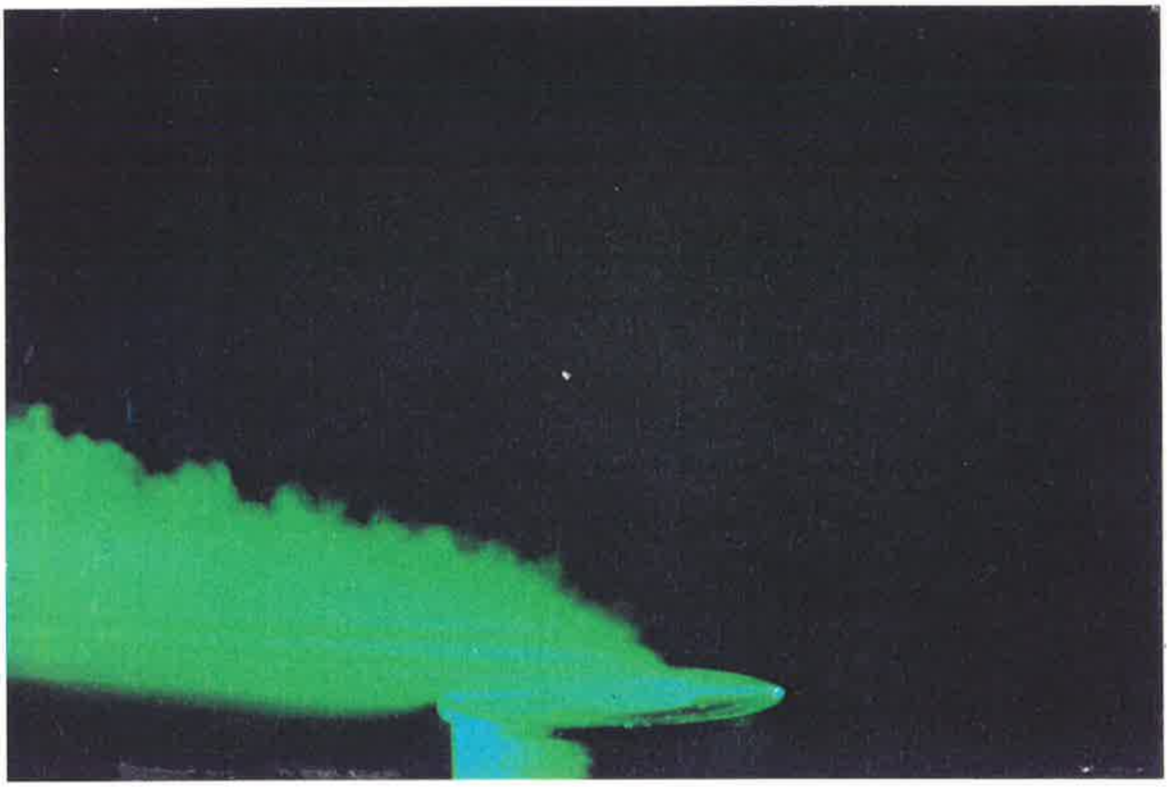

Figure 4.3. 6 Laser sheet flow visualisation illuminating the asymmetric jet leaving the CD nozzle at $\alpha = 80°$ with AR = 0.34 and $Re_t = 7{,}000$.

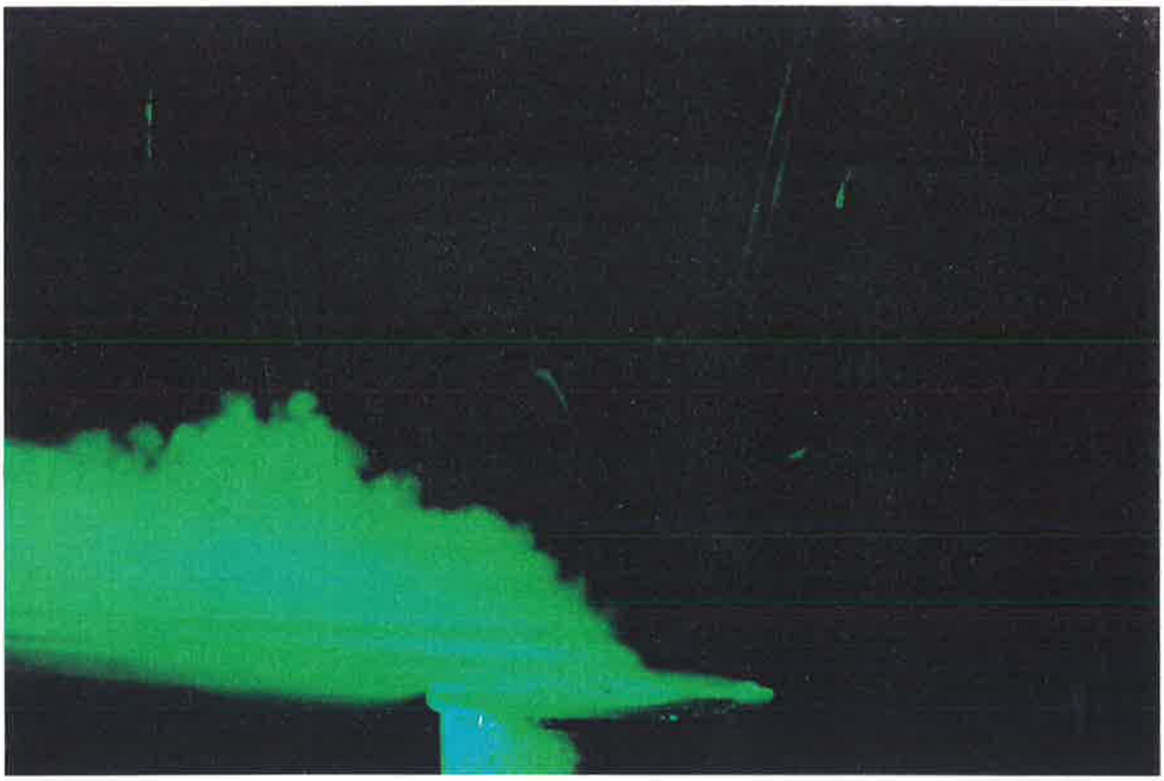

Figure 4.3. 7 Laser sheet flow visualisation illuminating the asymmetric jet leaving the CD nozzle at $\alpha = 75°$ with AR = 0.25 and $Re_t = 7{,}000$.

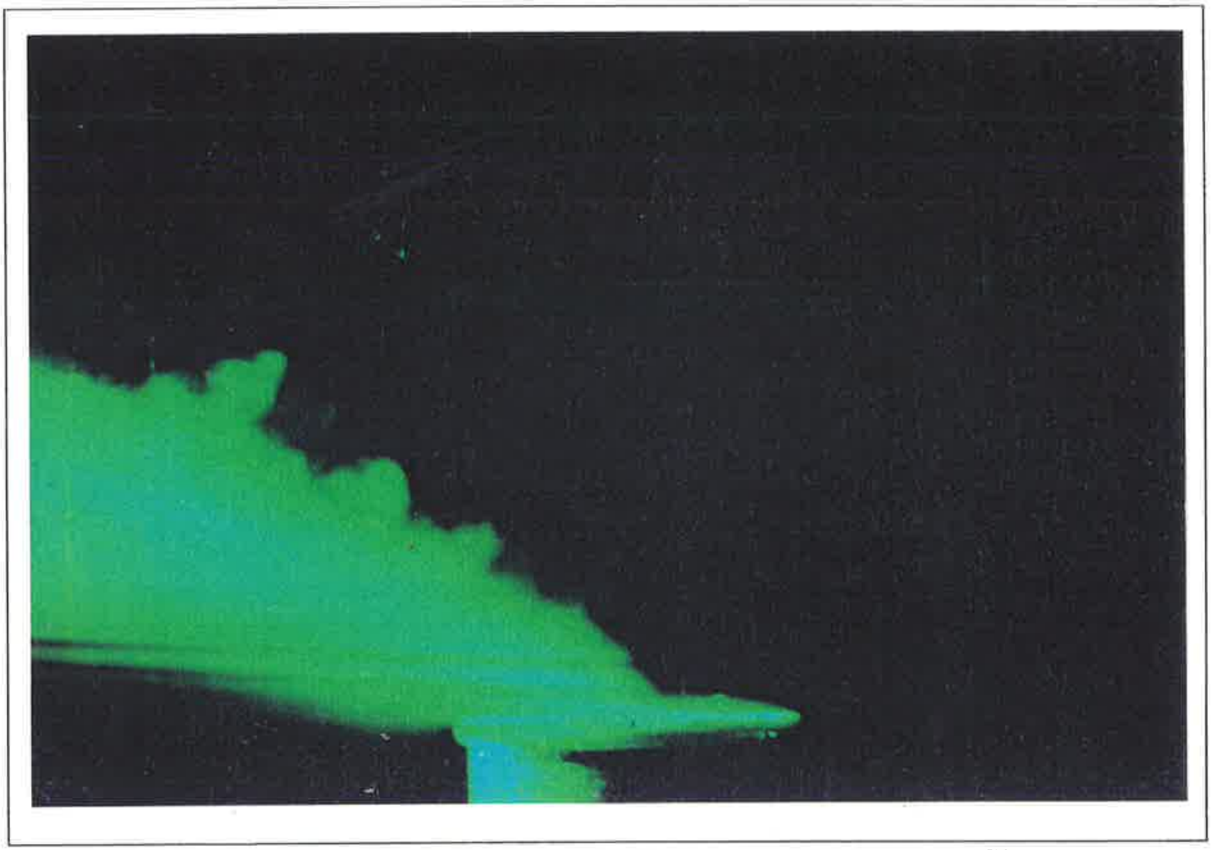

Figure 4.3. 8 Laser sheet flow visualisation illuminating the asymmetric jet leaving the CD nozzle at $\alpha = 65°$ with AR = 0.17 and Re_t = 7,000.

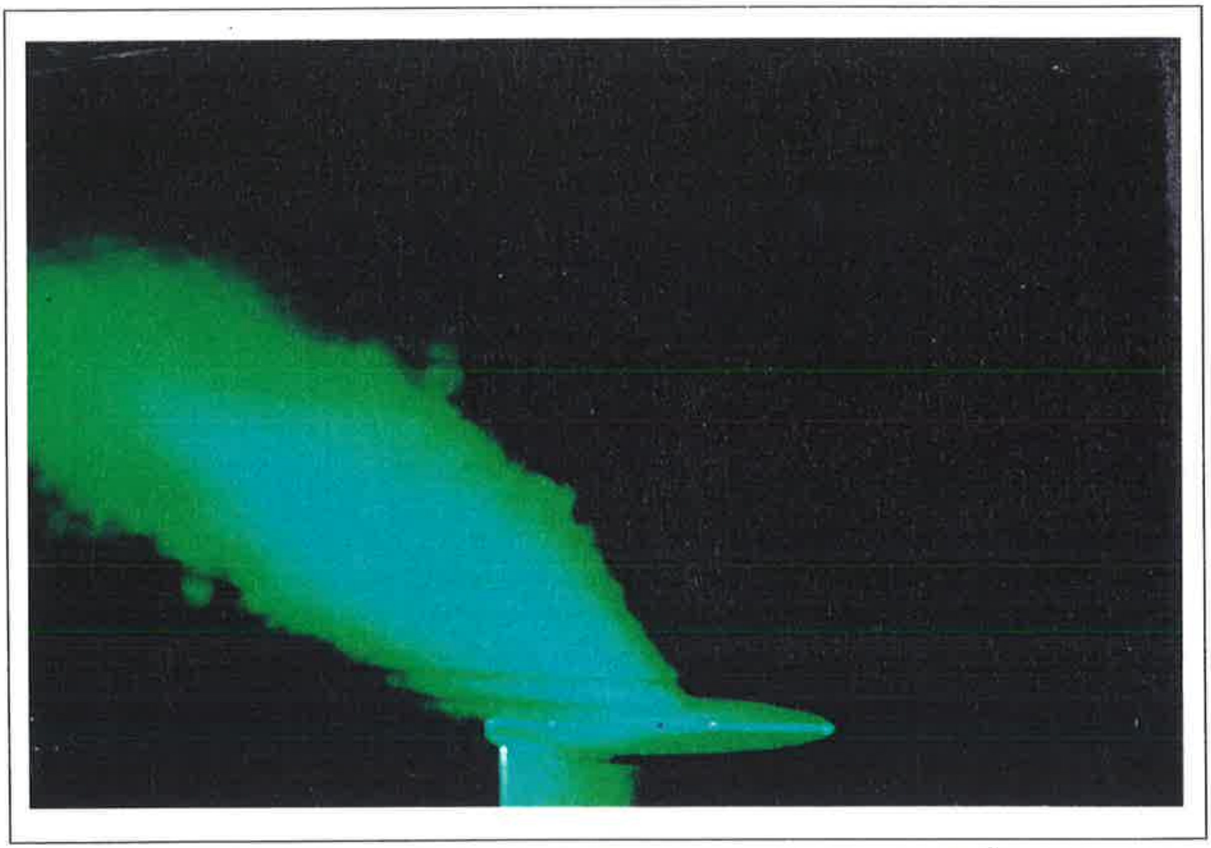

Figure 4.3. 9 Laser sheet flow visualisation illuminating the asymmetric jet leaving the CD nozzle at $\alpha = 55°$ with AR = 0.11 and Re_t = 7,000.

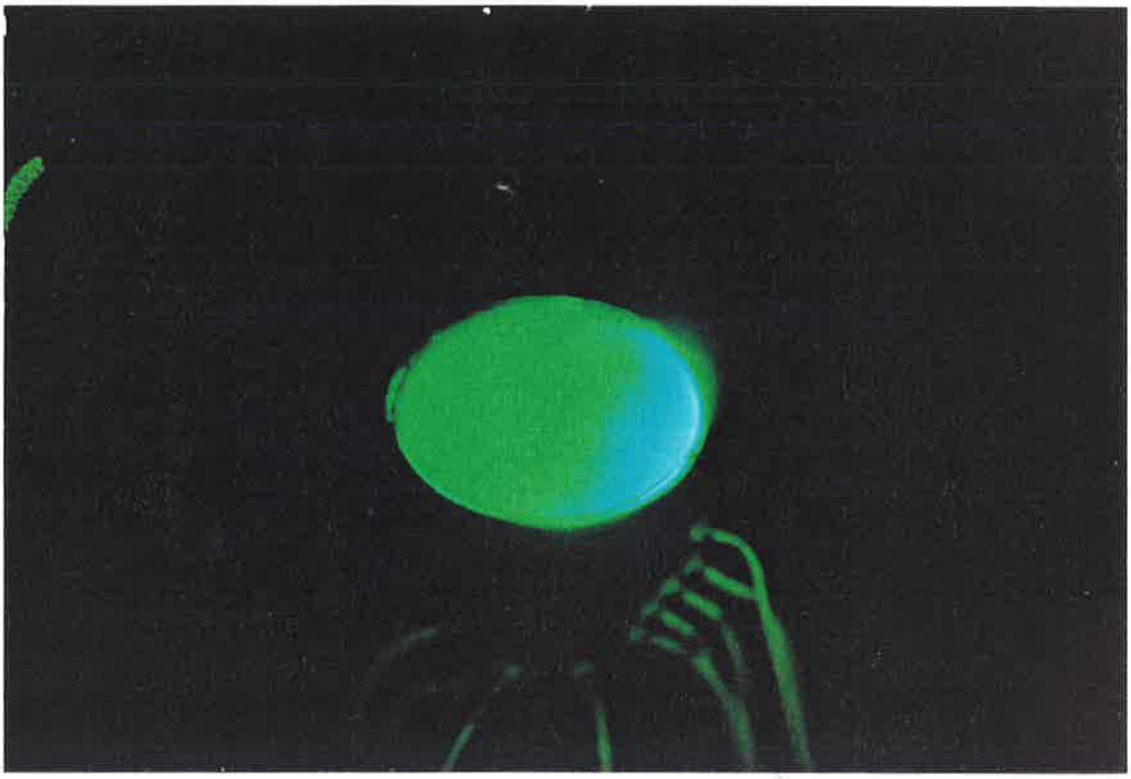

Figure 4.3. 10 Wall jet cross-section visualised by laser sheet 1 mm above the exit plane; CD nozzle with no exit ring. Note streamwise vortices in jet.

Figure 4.3. 11 Wall jet cross-section visualised by laser sheet 5 mm above the exit plane; CD nozzle with no exit ring. Note streamwise vortices in jet.

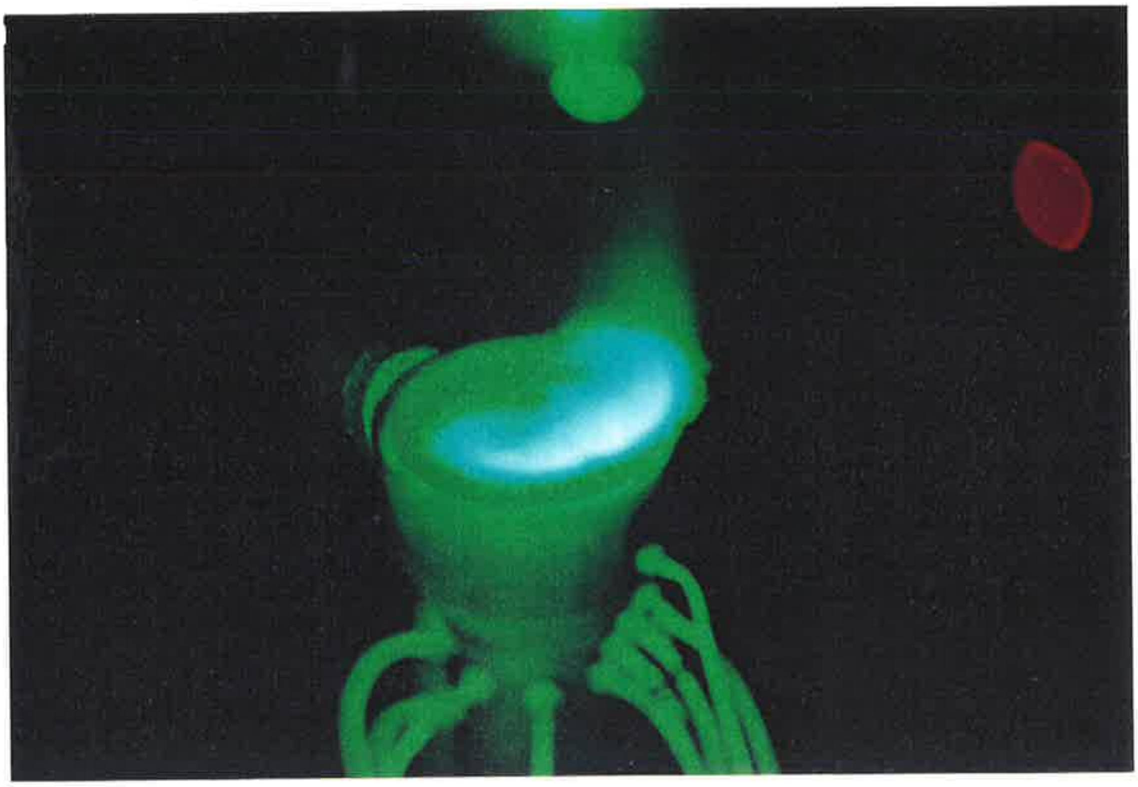

Figure 4.3. 12 Wall jet cross-section visualised by laser sheet 10 mm above the exit plane; CD nozzle with no exit ring. Note streamwise vortices in jet.

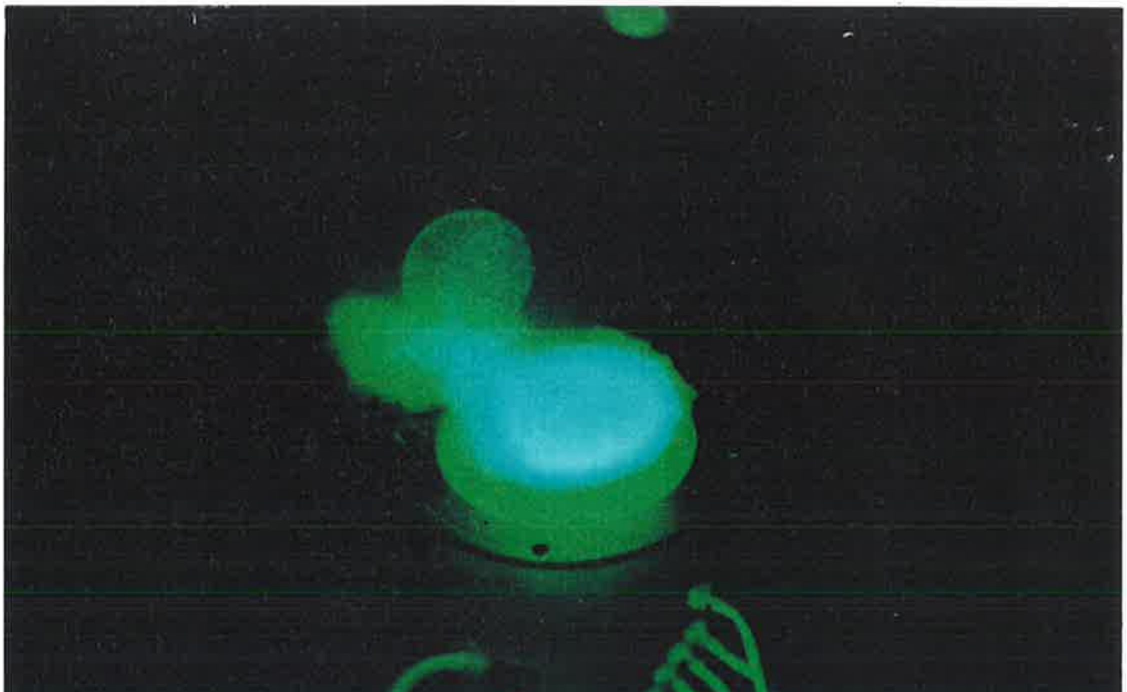

Figure 4.3. 13. Wall jet cross-section visualised by laser sheet 10 mm above the exit plane; CD nozzle with AR = 0.69 and Re_t = 7,000.

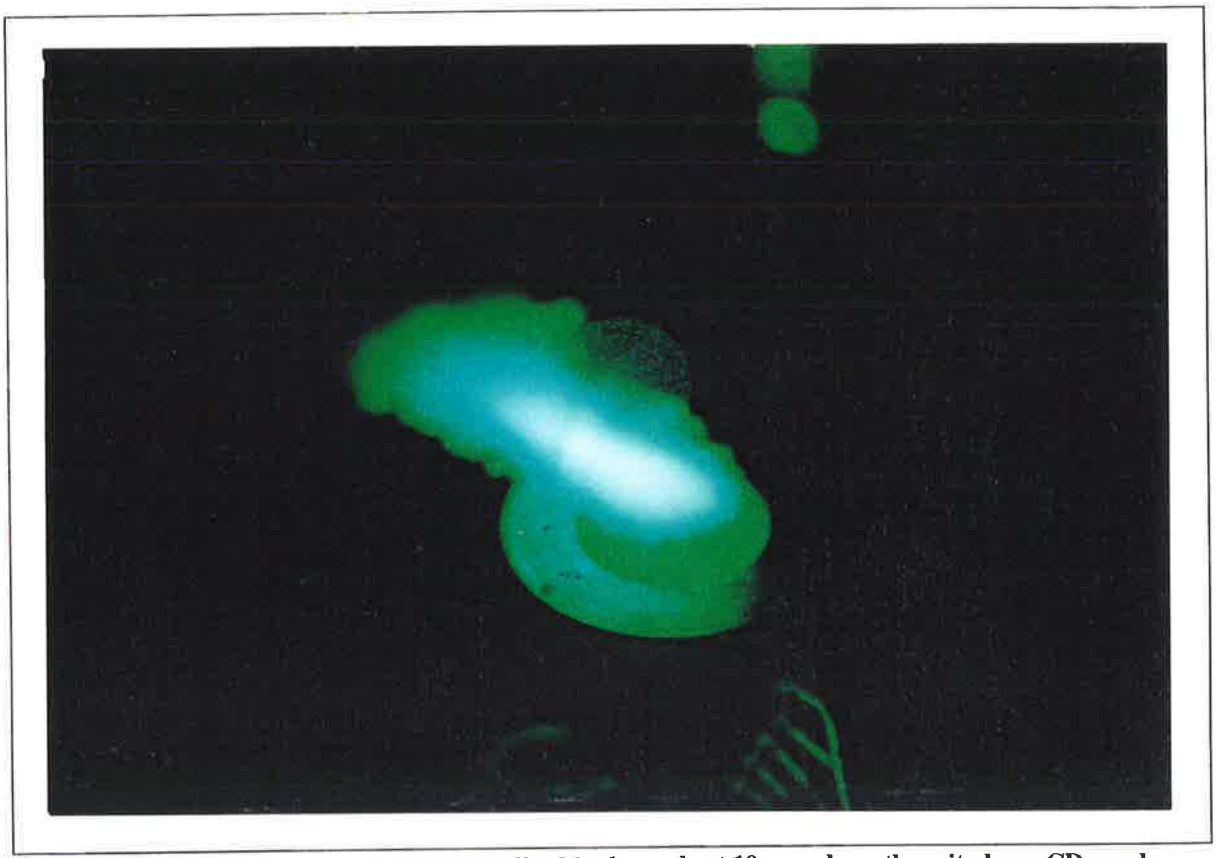

Figure 4.3. 14. Wall jet cross-section visualised by laser sheet 10 mm above the exit plane; CD nozzle with AR = 0.44 and Re_t = 7,000.

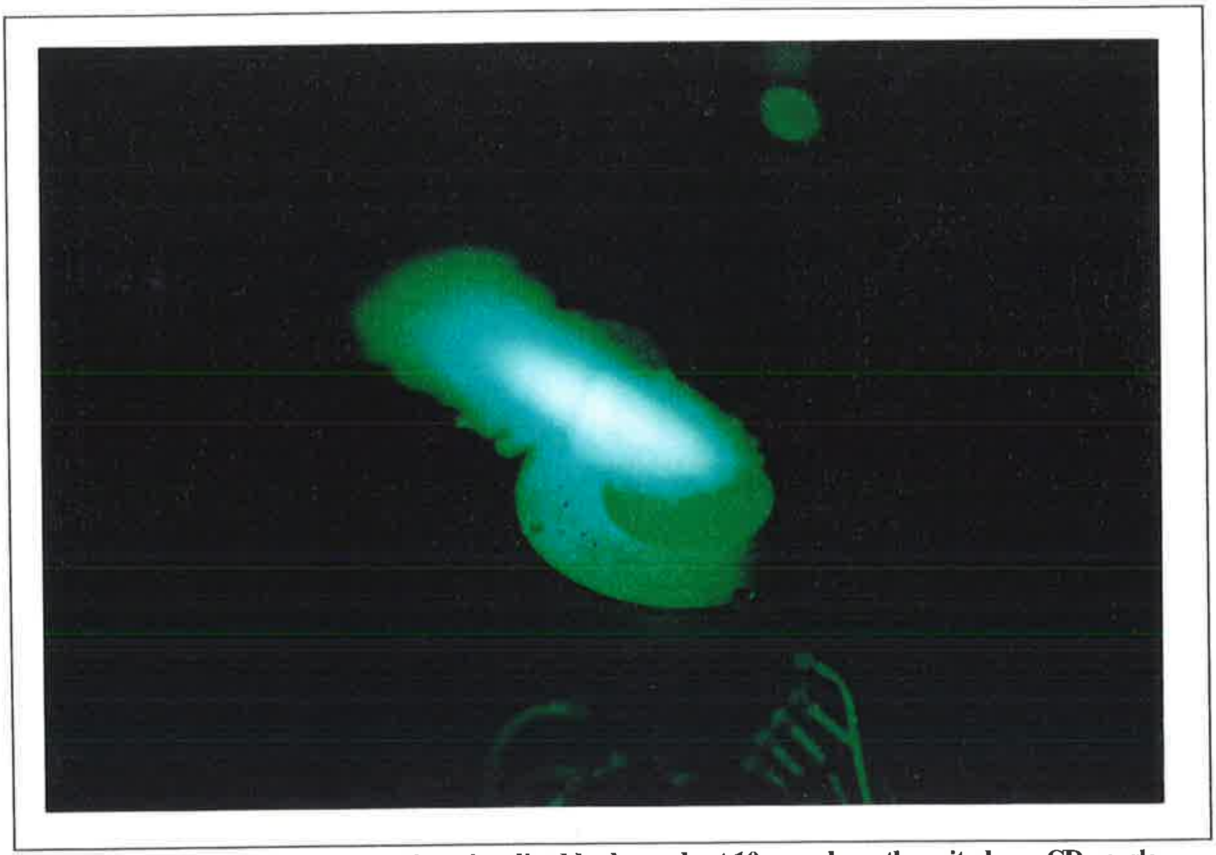

Figure 4.3. 15. Wall jet cross-section visualised by laser sheet 10 mm above the exit plane; CD nozzle with AR = 0.34 and Re_t = 7,000.

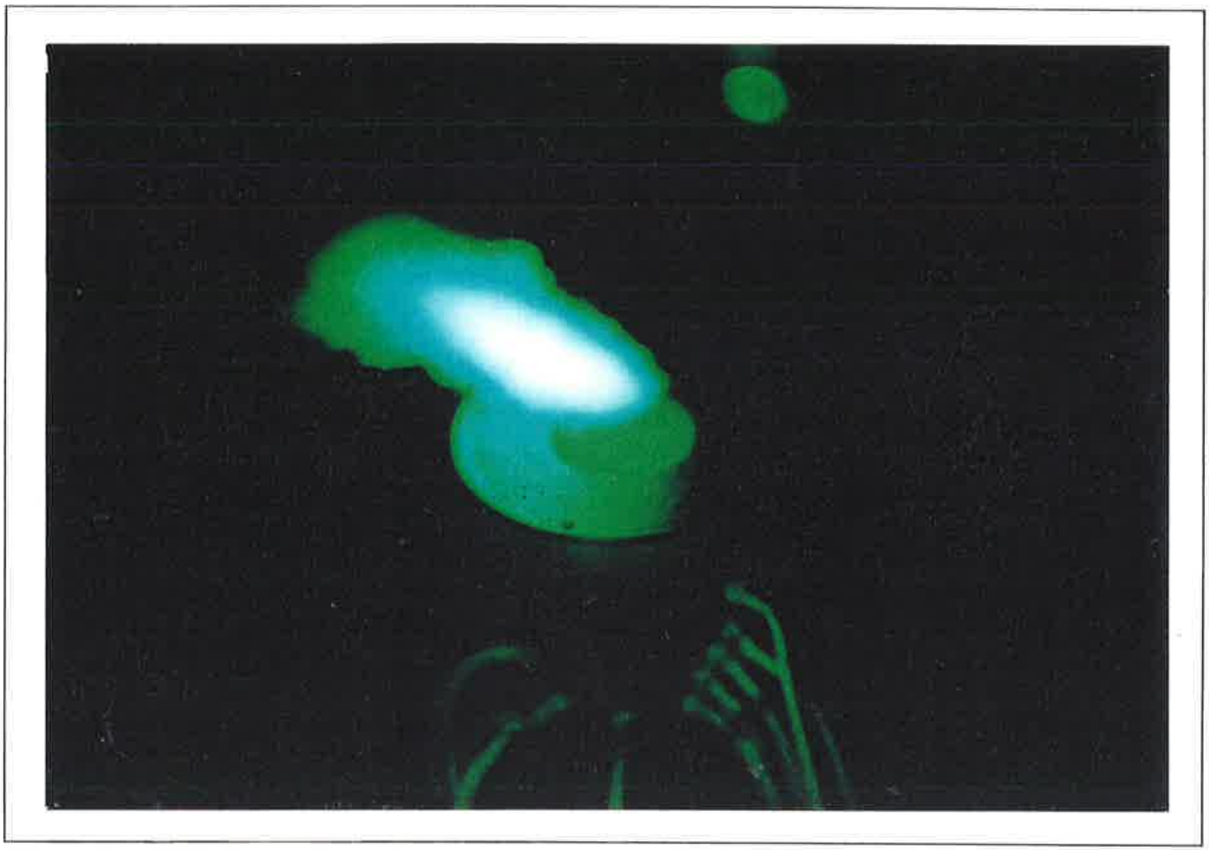

Figure 4.3. 16 Wall jet cross-section visualised by laser sheet 10 mm above the exit plane; CD nozzle with AR = 0.25 and Re_t = 7,000.

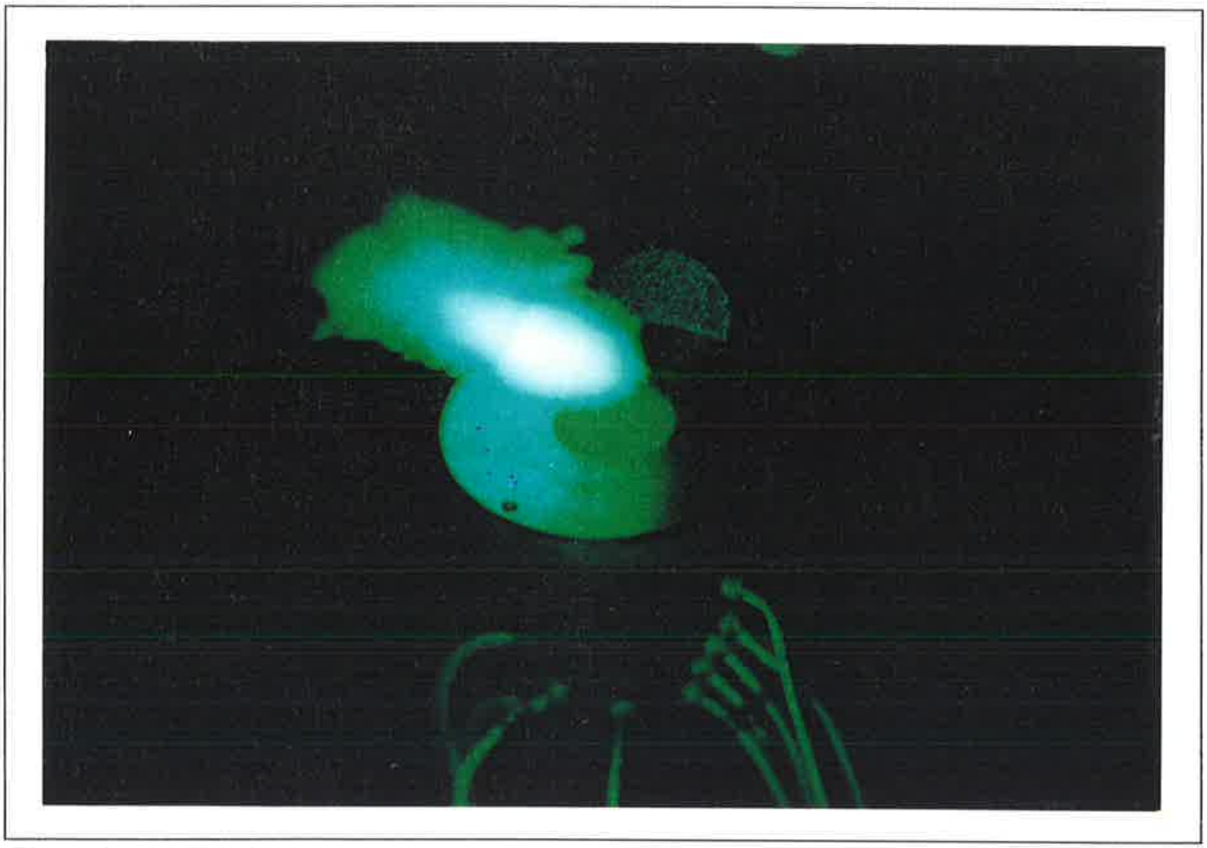

Figure 4.3. 17 Wall jet cross-section visualised by laser sheet 10 mm above the exit plane; CD nozzle with AR = 0.17 and Re_t = 7,000.

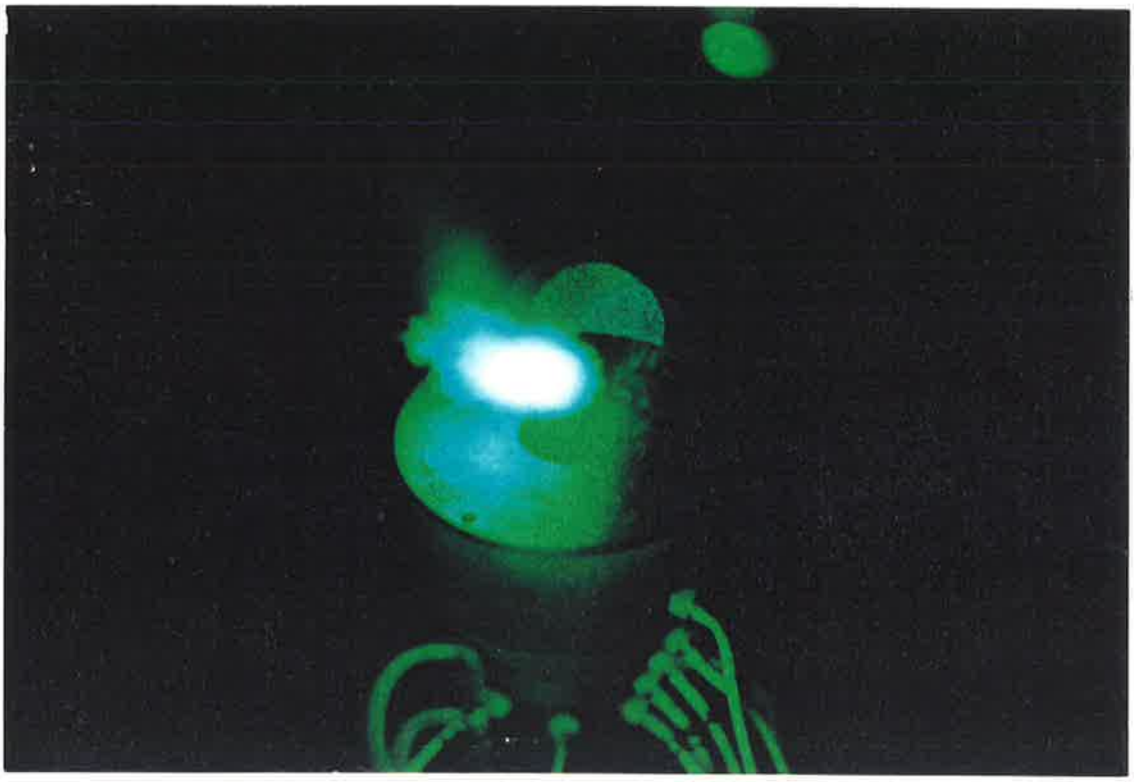

Figure 4.3. 18 Wall jet cross-section visualised by laser sheet 10 mm above the exit plane; CD nozzle with AR = 0.11 and Re_t = 7,000.

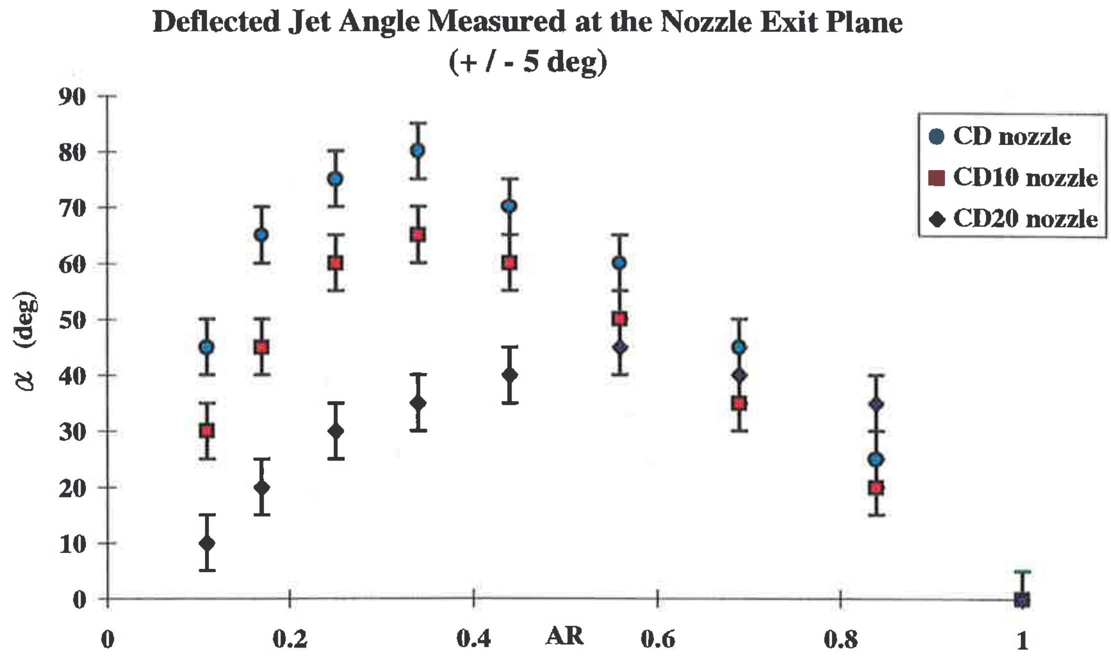

Figure 4.3. 19 Mean deflected jet angles from a family of CD nozzles measured by various methods.

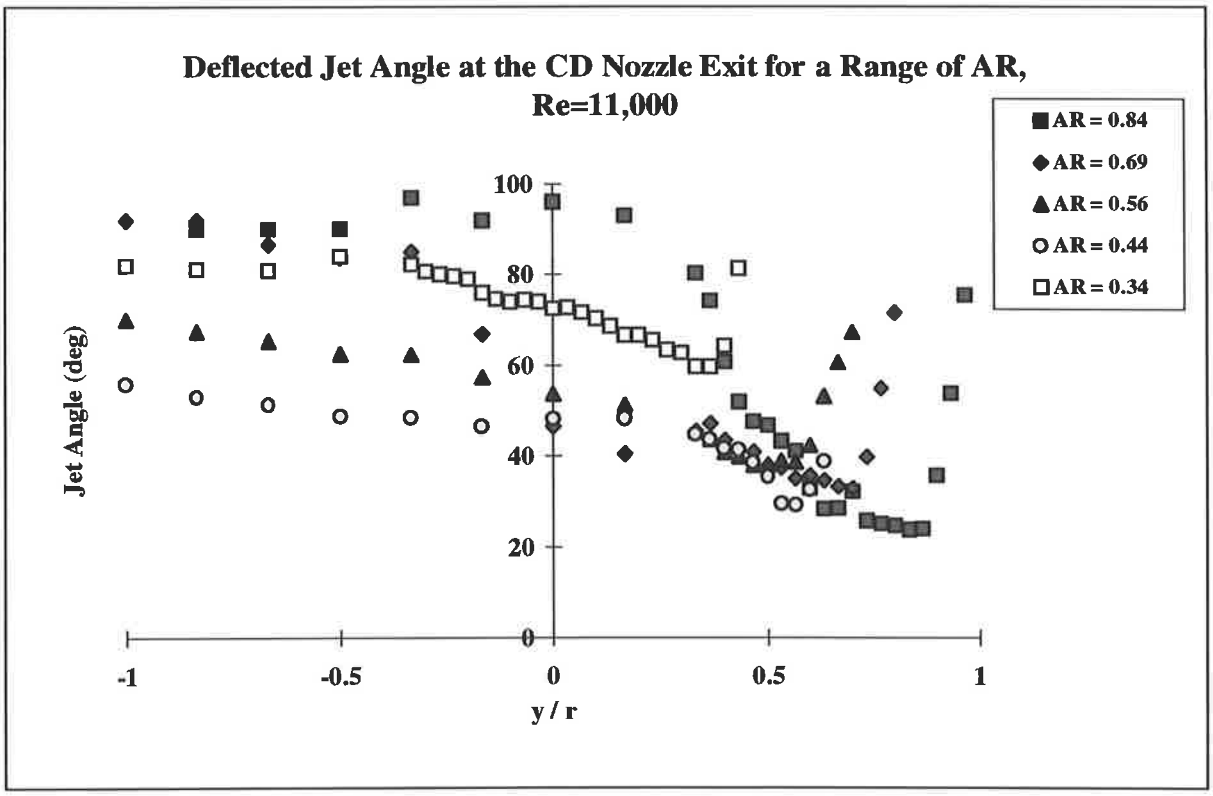

Figure 4.3. 20 Variation of deflected jet angle across the CD nozzle exit plane and plane jet symmetry using 2-component laser Doppler velocimetry to resolve the angles.

4.3.3 L.D.V. Two Component Velocity Measurement used to determine the Mean Flow Direction of Deflected Jet

The laser Doppler velocimetry was used for determining the angle of deflection of the jet to validate the data obtained by the tuft method. A number of velocity measurements were systematically taken at the nozzle exit for various exit ring diameters and nozzle lengths. The results in **Figure 4.3. 19** shows the measured mean angles obtained using a tuft. The LDV measurements support the visual observation that the angle varies across the deflected jet, as shown in **Figure 4.3. 20**. These velocity vectors were measured using a two component LDV system described earlier and the angles calculated from the independent magnitudes of the vectors. The figure shows that, for the exit area ratio AR = 0.84, the angle at which the jet leaves the nozzle exit varies from about $\alpha = 25^\circ$ at the edge of the exit lip, and increases to $\alpha = 50^\circ$ at the jet thickness $t_{1/2}$ where the velocity is half the centre line velocity ($U/U_{C.L.} = 1/2$). The high momentum flow is at the edge closest to the lip edge at a value of y/r = 0.8 and here the angle of the deflected jet is $\alpha = 25^\circ$ which agrees with the result presented in **Table 4.3** for the CD nozzle with a 2.5 mm lip. For AR = 0.69 the deflected jet angle calculated from the LDV measurements is between $\alpha=35^\circ$ and $\alpha=40^\circ$ compared to $\alpha=45^\circ$ in **Table 4.3**. For the AR = 0.34 the deflected jet angle from the LDV measurements is $\alpha=80^\circ$ compared with 80° shown in the previous table. Thus it can be concluded that the angles calculated using the LDV velocity vector measurements correlate well with the measurements obtained from the measured tuft angle, when tuft is placed in the flow and the angles measured for the range of exit areas considered. Good agreement is also found with the laser sheet flow visualisation results of deflected jet angles.

4.3.4 Analysis of Results

The deflected jet angles measured by the three methods correlate well and show that , while the accuracy and detail are greatest with the LDV data, those given by the humble tuft are of adequate accuracy to identify the exit angle of the jet for use in the topological study which has been necessary to unravel the main features of a very complex flow which causes the deflection. In summary, the tuft method is the simplest method of acceptable accuracy for measuring the angles of the deflected jet for various exit velocities and exit areas. The laser sheet method shows not only the angles of deflection of the seeded jet but the evolution of the structures of the flow at low velocity could also be studied in detail with the aid of a high speed camera or still images photographed on a high speed film. As will be seen, sufficient understanding of the flow has been established, and such a detailed study can now be justified and is highly recommended. The LDV provides the most accurate measurement of the deflected jet angle, but it is also the most time consuming. The advantage of LDV velocity measurement is that in a single set of measurements it yields the mean angle, the local flow directions, information about flow structures and turbulence levels which are sufficient to determine the local flow, especially inside the CD nozzle near the throat. A three component LDV is desirable to allow definition of the vortex flow field in detail and to answer some key questions that exist about the strength and direction of vortex lines.

4.3.5 Conclusions

The methods for determining the deflected jet angle, discussed above, have proved to be adequate for the purpose of establishing the effects of nozzle length and exit ring diameter on the deflected jet angle. The use of tufts has been found to be the quickest and easiest method which yields adequate accuracy in the determination of the mean angle of the deflection of the jet. The other two methods, laser Doppler velocity measurements and laser sheet flow visualisation, have confirmed the adequacy of the tuft method and these data have been used in other facets of the overall research program. Detailed LDV velocity measurements were also used as a datum for comparison of the accuracy of the pitot-static and hot-wire velocity measurements.

4.4 Nozzle Throat Secondary Fluid Injection

The secondary fluid injection plays an important part in the control of the non-precessing fluid dynamically deflected jet. The momentum ratio of primary to secondary flow influences the flow pattern of the primary flow downstream from the injection point. For a given primary mass flux there is a minimum requirement for the secondary mass flux necessary to fix the azimuthal position of the primary asymmetric jet. If the secondary mass flux is increased, the total mass flux of the fluid carried downstream is increased and the secondary flow penetrates the primary flow further causing a substantial pressure loss by creating an aerodynamic blockage. An effort has been made to separate the secondary flow mass and momentum effects on the primary flow by progressively increasing the secondary exit area. The diameters selected for this investigation included ports of up to 3 mm in diameter tapped at the throat normal to the nozzle axis. The ports above 2 mm in diameter had an adverse effect on the flow and caused unwanted flow asymmetry at the throat. The maximum secondary injection diameter reported in this thesis is 2 mm with other pressure ports at the throat of 1 mm in diameter. The secondary injection mass flow rates were estimated from the secondary injection measured supply pressure and static pressure at the throat. It has been found that the secondary mass flow rate required to maintain the azimuthal location of the primary jet is less than 5% of the primary mass flux.

4.4.1 Influences of Secondary Fluid on Primary Flow

The secondary fluid injected across the primary flow at the throat produces an adverse pressure gradient at the point of injection by entraining fluid from the higher pressure region downstream. It also produces a favourable pressure gradient on the opposite side of the throat by blowing the boundary layer as it impinges on the diverging nozzle wall downstream from the throat. This produces a stable primary wall jet that expands and deforms into a wall jet which takes on the shape of the transverse contour of the nozzle. The secondary injected fluid is a typical jet in a cross flow and the point of impact on the opposing nozzle wall is determined by the momentum ratio of the primary and secondary flow **[18,32,56,69,149,215]**. This may explain the limited range of secondary fluid mass flux required for stable operation. The penetration of the secondary jet through the primary jet and its impingement on to the opposite wall can be seen in the total pressure profiles inside the cavity as shown in **Figure 4.2. 16**. The high turbulence region near the wall and a double peak in the profile are probably due to the secondary fluid although no definitive experiments were conducted to prove this due to visibility constraints and the disturbance caused by probes near the throat. If the secondary flow momentum is too low, the fluid does not penetrate the primary momentum far enough to reach the opposing wall before it is washed downstream. Therefore only the adverse pressure gradient locally near the injection point is produced and this alone may or may not be sufficient to produce a stable deflected jet. As the secondary fluid momentum is increased, it penetrates almost diametrically across the throat and reaches the opposite wall just downstream from the throat. This produces a stagnation point which distorts the primary jet and causes a fluidic blockage and a complex three-dimensional flow at the throat. At an appropriate intermediate secondary to primary momentum ratio the secondary fluid has enough momentum to penetrate the primary jet but is deflected such that it contacts the opposing diverging wall almost tangentially. This regenerates the boundary layer and prevents the boundary layer separation in that region of the primary wall jet.

4.5 China-Clay and Oil Surface Flow Visualisation

China clay surface flow visualisation is a well known and often used technique of capturing surface shear stress patterns. The technique is particularly useful when the patterns which need to be captured are in enclosures and cavities which can not be viewed directly. Another useful surface flow visualisation technique is the use of a coating of oil on the surface exposed to the flow. This gives a slow response but nevertheless a dynamic image of slowly changing patterns. The oil used in the present apparatus was mixed with graphite powder to give a high contrast against the white nozzle wall. The use of oil was limited to the studies of the effects of small reductions of exit area as the photographs must be taken while the flow is in progress. The china-clay provides frozen patterns of the mean surface shear stress and hence could be photographed and analysed after the flow had been turned off.

It is a well established fact that if the surface flow patterns on the body are known, the topology of the entire flow field can be deduced, as shown by Tobak and Peake (1982). A practical technique of determining experimentally the "*critical points*", and from these deducing a vortex skeleton of the flow which satisfies the topological constraints limiting the number of ways in which streamlines can be joined, was presented by Perry and Hornung(1984) and Perry and Chong (1987). From this skeleton the complete velocity field can be approximated by using the Biot-Savart law.

The type of surface flow patterns which can occur in three-dimensional separated flow are fully described and defined by Hornung and Perry (1984). Following are some of the pattern definitions reproduced from Perry and Chong (1987):

- A positive stream surface bifurcation at the wall is defined as a line from which the normal component of the surface flow moves away in both directions, as shown in **Figure 4.5. 1.**
- A negative stream surface bifurcation at the wall is defined as a line toward which the normal component of the surface flow moves in both directions, as shown in **Figure 4.5. 2.**
- A possible configuration of an open negative stream surface bifurcation at the wall is shown in **Figure 4.5. 3.**
- A vortex has its stream lines at the surface moving toward a focus at the surface from which the fluid separates, moving away from the surface due to a pressure gradient normal to the surface along the low pressure core of the vortex, as shown in **Figure 4.5. 4**. This is a critical point with complex eigen values and is a pattern that often occurs in three-dimensional separation from the surface.

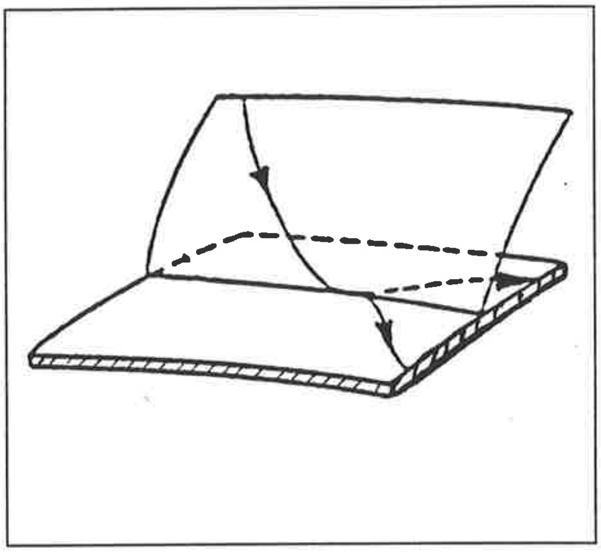

Figure 4.5. 1 A positive stream surface bifurcation at the wall.

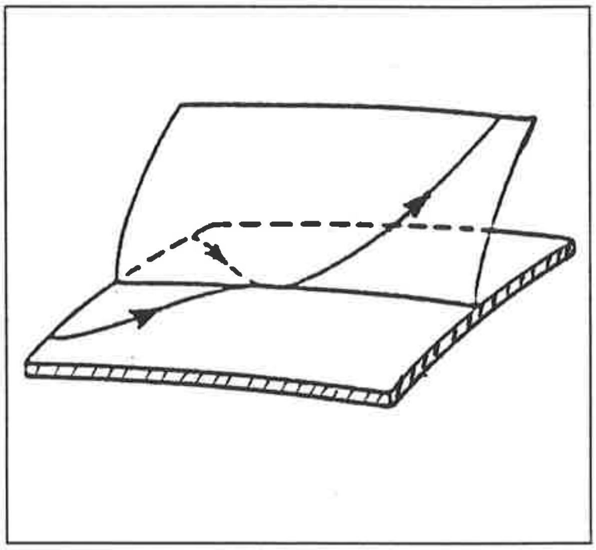

Figure 4.5. 2 A negative stream surface bifurcation at the wall.

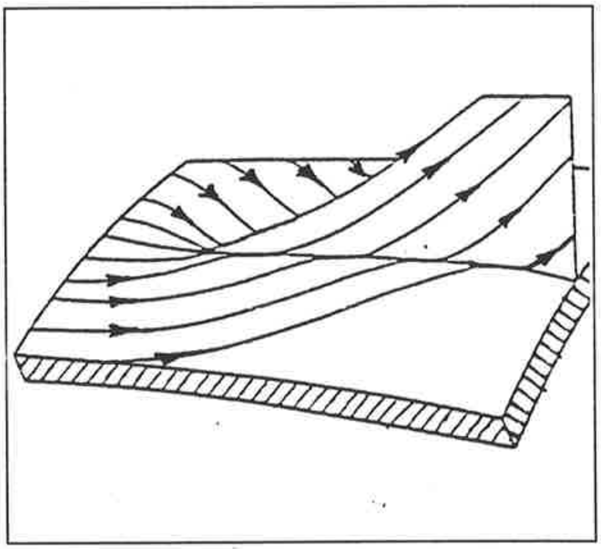

Figure 4.5. 3. A possible configuration of an open negative stream surface bifurcation at the wall.

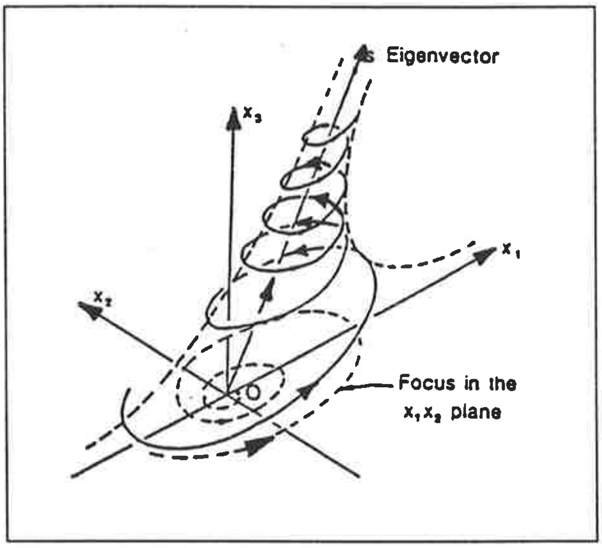

Figure 4.5. 4. A vortex with its stream lines moving towards the focus at the surface where the fluid separates away from the surface.

4.5.1 Apparatus

The flow visualisation was achieved by coating the nozzle wall with a mixture of china-clay (Kaolin) and oil of wintergreen. A quantity of graphite powder was added to the mixture to enhance the contrast against the white background of the nozzle wall. When the china-clay dries, due to the evaporation of the oil of wintergreen during the exposure to the flow, the frozen flow patterns can be photographed. This technique was used for the flow with exit rings attached to the nozzle exit. The exit rings were removed to allow the frozen surface flow patterns to be photographed.

The oil surface flow visualisation was implemented in a similar manner. The flow was this time started and the oil introduced either through the secondary fluid injection tapping or by coating the surface prior to start-up. Once the flow patterns had established the photographs were taken in those cases where the exit ring did not restrict the view. The technique was used where the surface flow patterns were visible during the operation, as in the CD nozzle with an exit ring of diameter not less than 45mm and in the CD10 nozzle where the clear perspex cavity provided a viewing window. The method also has an advantage in that it shows at least the more slowly responding dynamic changes in the surface flow patterns when the jet is intermittently unstable or when it is precessing.

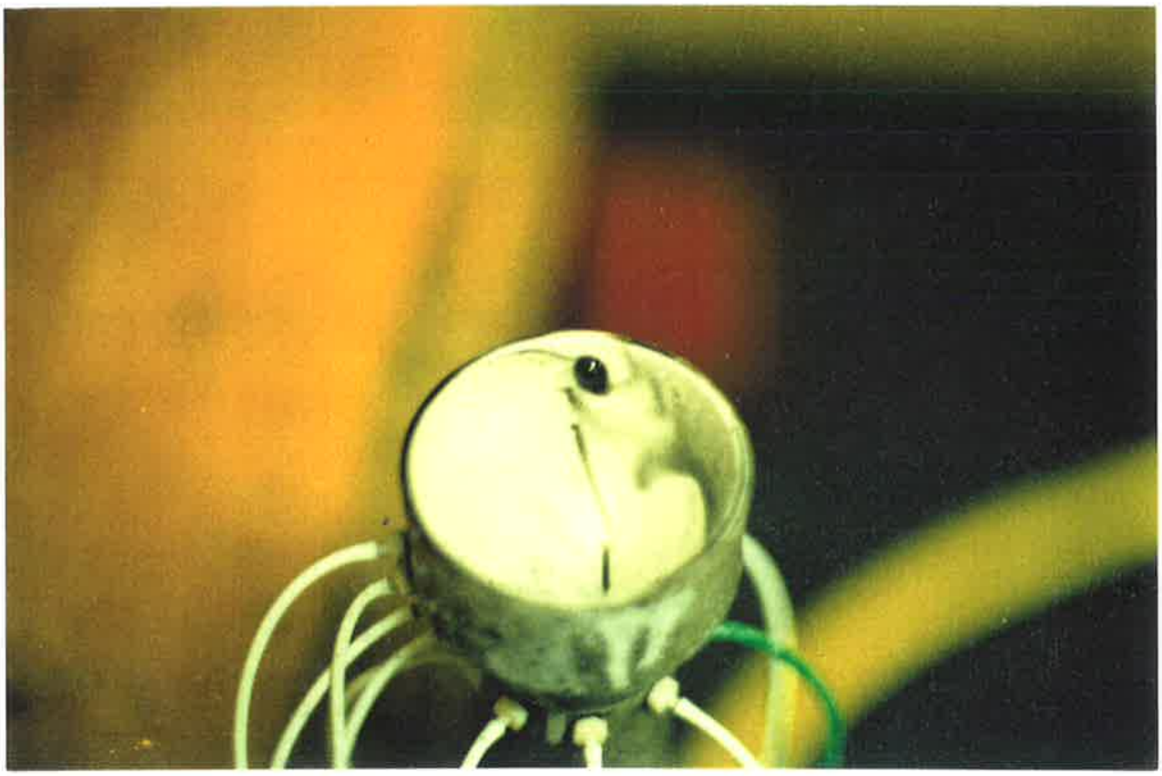

Figure 4.5. 5 **Formation of focus inside the nozzle at Re_t=70,000 with out exit ring. Asymmetric flow, visualised using oil, jet leaving the nozzle along the left wall.**

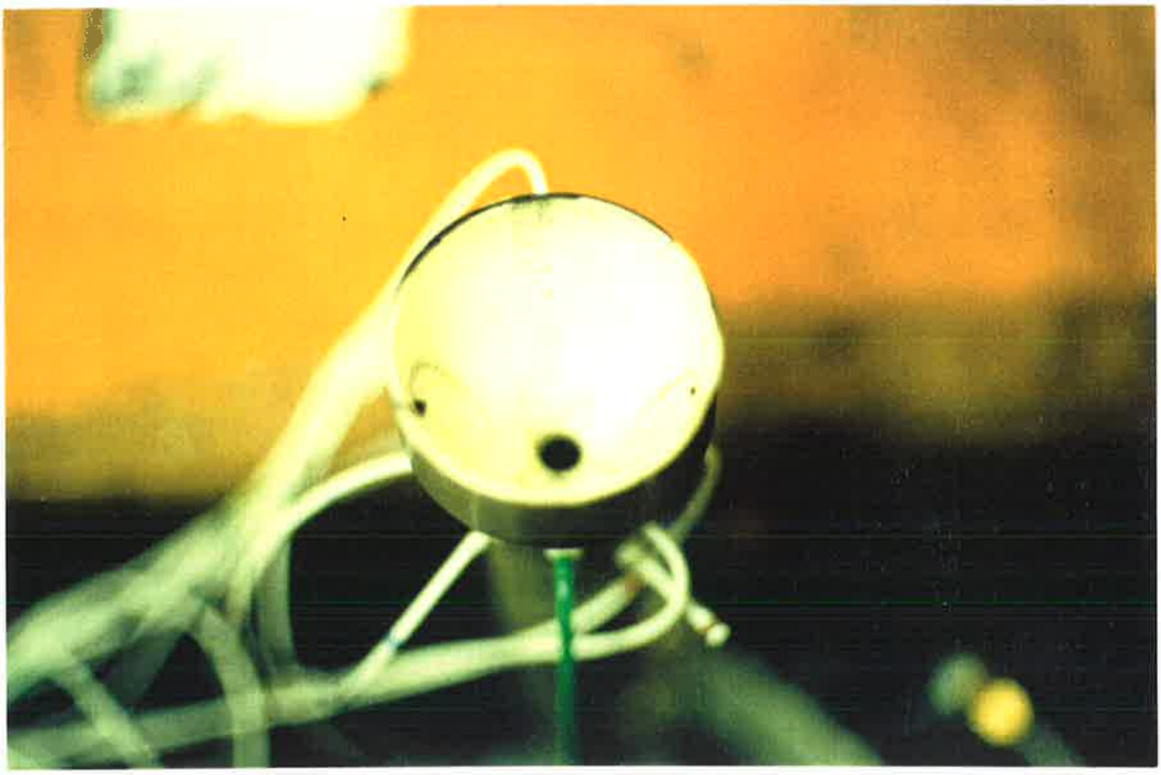

Figure 4.5. 6 **Two foci on opposite sides of the nozzle exit at Re_t=70,000 with out exit ring. Asymmetric flow, visualised using oil, jet leaving the nozzle along the wall furthest away from viewer.**

Figure 4.5. 7 Surface flow patterns inside the nozzle at AR = 0.84 and Re_t=200,000 visualised using oil and graphite powder with jet exiting from left to right.

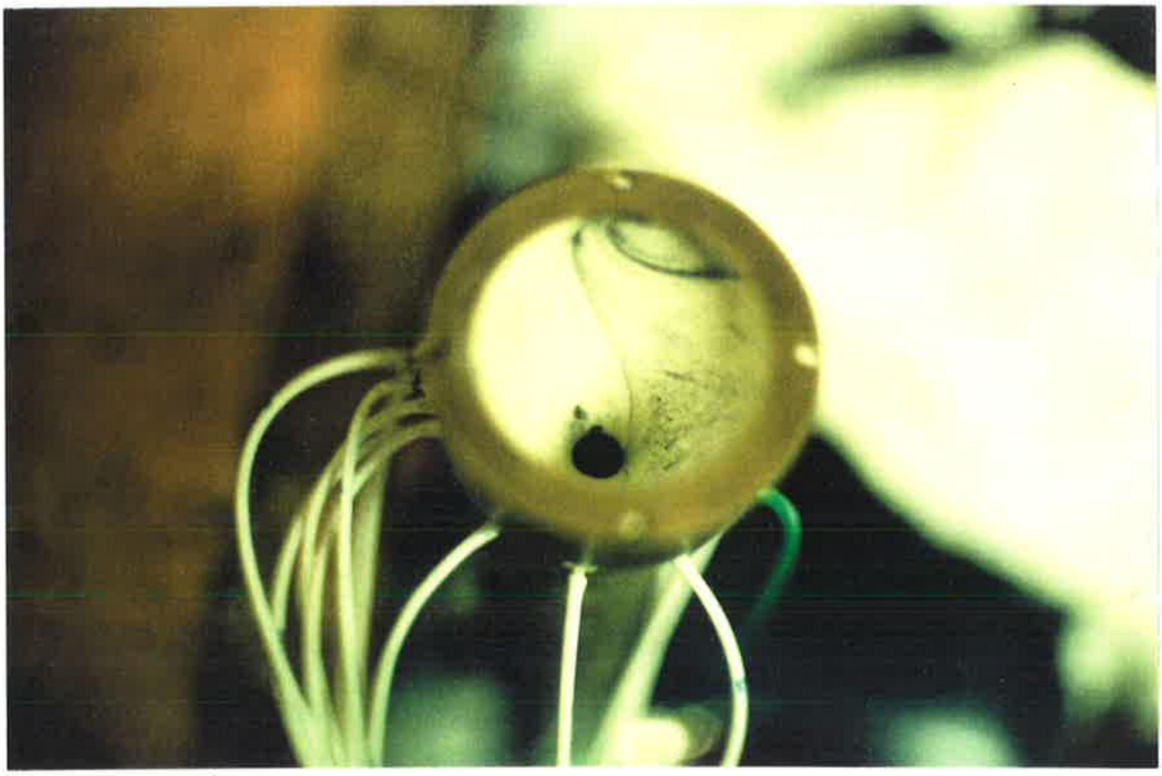

Figure 4.5. 8 Surface flow patterns inside the nozzle at AR = 0.69 and Re_t=200,000 visualised using oil and graphite powder with jet exiting from left to right.

4.5.2 Jet Separation Inside the Nozzle and Interpretation of Surface Flow Pattern Results

It has been found that for a Reynolds number below 45,000 the primary jet can separate axisymmetricaly or asymmetrically downstream from the throat, the results being determined by the momentum of the secondary injection. The flow in the CD nozzle separates asymmetrically for Reynolds number above 55,000 with its azimuthal direction fixed by the azimuthal location of the secondary injection point. The asymmetric flow produces a pair of foci diametrically opposite each other on the nozzle surface near the exit. One of the foci is shown in **Figure 4.5. 5** and is clearly marked by oil entrained into the low pressure core of the vortex. Both foci can just be seen in **Figure 4.5. 6**. This figure also shows the two stream surface bifurcations extending from the throat to the two foci. This flow pattern appears to be produced by the expansion of the primary flow laterally around the transverse curvature of the nozzle and interaction with the ambient fluid which is induced into the nozzle.

When an exit ring is placed at the nozzle exit, the primary wall jet is deflected across the nozzle axis due to an impingement of the wall jet on the exit lip. This reduces the available exit area for the ambient fluid to be induced and therefore increases its velocity as it enters the nozzle. Streamlines are tightly curved as the induced fluid negotiates the exit lip and these features require a radial pressure gradient which deflects the primary jet further. A portion of the primary fluid is recirculated back into the nozzle by the exit ring and feeds into the vortex as can be seen in **Figure 4.5.9. 9** . With a decrease in the exit area, the amount of primary fluid recirculated back toward the throat increases, **Figure 4.5. 7** and **Figure 4.5. 8**. The first figure shows the surface flow patterns produced at a high Reynolds number of 200,000 for a nozzle exit area ratio AR = 0.84. The foci are close to the exit lip and the negative stream surface bifurcation which feeds into the vortex is also just behind the exit lip. In the second figure, for the same Reynolds number but AR = 0.69, the flow patterns show the portion of the stream surface bifurcation to be located further inside the nozzle when compared with the previous case. This supports the postulate that more of the primary fluid is recirculated. This indicates that the vortex strength increases with the reduction of exit area at least within this range of area ratios. The flow patterns presented in , **Figure 4.5.9. 1** to **Figure 4.5.9. 8,** show the change in surface flow patterns as the exit area is reduced from AR = 0.84 to AR = 0.11 and confirms that for a reduced exit area, the induction of ambient fluid is reduced to the point that at AR = 0.34 the induction becomes zero. This interpretation is confirmed independently by static pressure measurements which show the pressure inside the nozzle is positive for AR ≤ 0.34 as discussed in detail in Section 4.2.2. **Figure 4.5.9. 1 (a)** shows the induced ambient fluid surface flow patterns in the upper part of the circle occupying about 60% of the area. **Figure 4.5.9. 2 (a)** shows the reduced area of the induced ambient fluid surface flow patterns now occupying only about 40% of the area in the upper central portion of the circle. **Figure 4.5.9. 4 (a)** shows that the surface flow patterns associated with the induced ambient fluid reduced to an area now occupying only about 10% of the total area inside the nozzle. This is located just above the throat. The area on either side shows the large recirculation of primary fluid. **Figure 4.5.9. 5** shows that the surface flow patterns in the upper part of the picture are produced by the recirculated flow only. This situation persists for further reduction of exit area. The sequence of following figures; **Figure 4.5.9. 3 (b)** to **Figure 4.5.9. 8 (b),** shows that the reduction of exit area does not significantly alter the point of separation of the wall jet upstream from the exit lip. The flow pattern inside the nozzle are interpreted in **Figure 4.5.9. 9** . The general picture is of the two negative bifurcation surfaces produced by the interaction between and mixing of the primary and entrained ambient fluids, two further negative bifurcation surfaces which arise from interaction between and mixing of the primary fluid and the recirculated portion of primary fluid and two foci into which the negative bifurcations feed. It is postulated that these foci are the footprints of a strong vortex loop which passes over the primary fluid wall jet providing the interface with the induced ambient fluid which flows into the nozzle. The surface flow patterns are similar to the surface flow patterns produced in the CD10 nozzle for which it is possible to both view and measure through the cylindrical cavity extension. These data are discussed in the following sections. As the exit area is reduced, the foci appear to move upstream toward the throat and are pushed apart by the spreading wall jet. This is attributed to the large recirculation of the primary fluid imposed by the exit lip and it is this high momentum recirculated fluid which produces the increase in vortex strength.

4.5.3 Discussion of Results

From the china-clay and oil streak surface flow patterns it has been possible to construct postulates of the general flow patterns inside the nozzle. An important feature of the postulated flow topology is the vortex loop which imprints its signature on the nozzle wall as two strong foci at the junction of negative bifurcations. The vortex loop can be envisaged as a horse-shoe vortex which probably extends out of the nozzle and has as its return loop the starting vortex at infinity downstream when no exit ring is attached. These legs of the horse-shoe vortex have been visualised at the nozzle exit as a pair of streamwise vortices; shown in **Figure 4.3. 12.**

When the exit ring is attached to the nozzle exit, the jet is deflected across the nozzle axis as it impinges on the upstream face of the exit lip. This increases the vortex strength within the nozzle and the jet is deflected further. Measured jet deflection angles α from a CD nozzle for a range of exit diameters, summarised in **Table 4.3**, shows that the maximum angle of deflected jet produced by the CD nozzle α = 80° when the exit area ratio AR = 0.34.

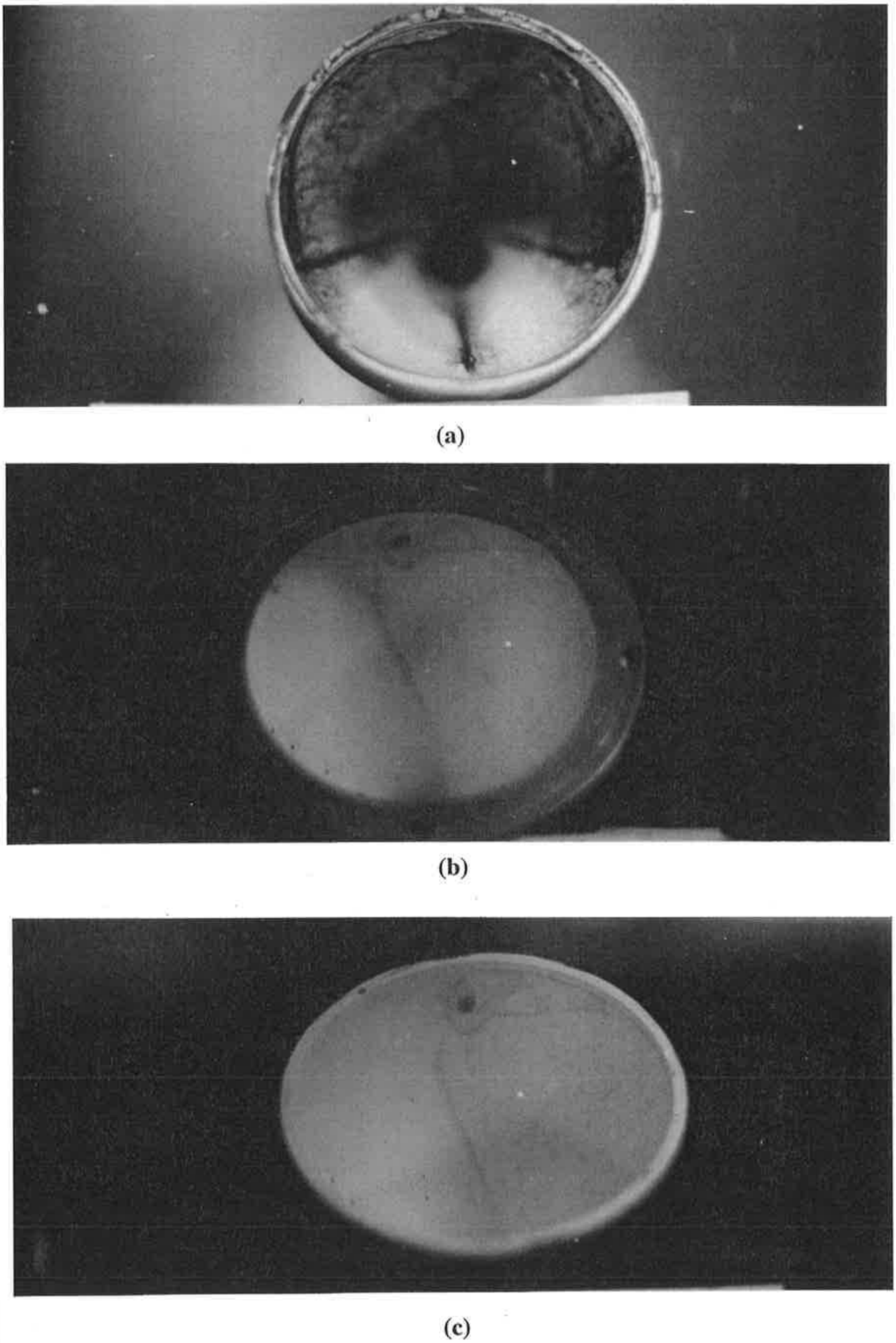

Figure 4.5.9. 1 China clay surface flow visualisation inside CD nozzle at Re_t=72,000 and AR = 0.83; (a) top view, and (c) side view, exit ring removed;(b) side view; exit ring in place

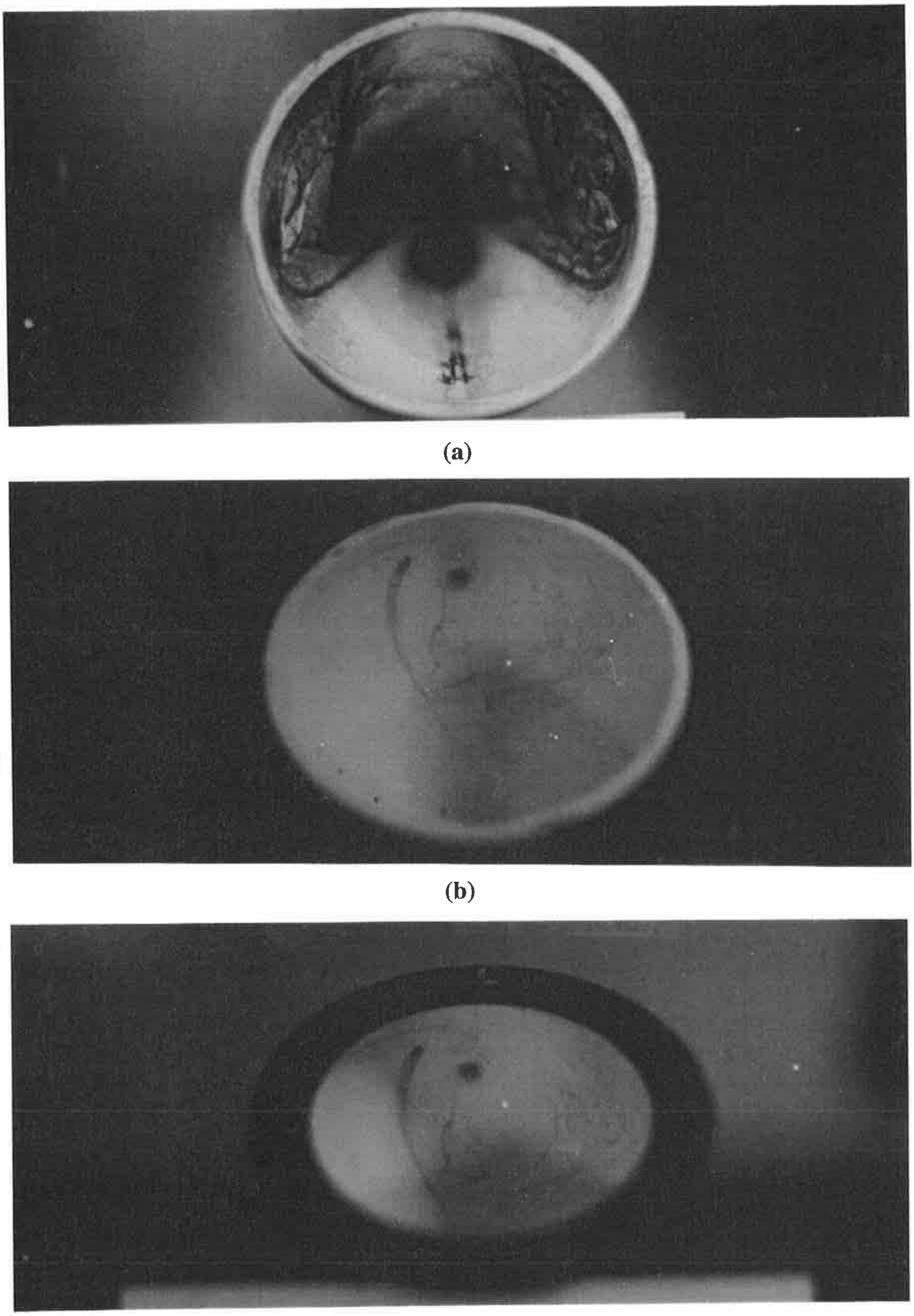

(a)

(b)

(c)

Figure 4.5.9. 2 China clay surface flow visualisation inside CD nozzle at Re_t=72,000 and AR = 0.69; (a) top view, and (b) side view.; exit ring removed, (c) side view; exit ring in place.

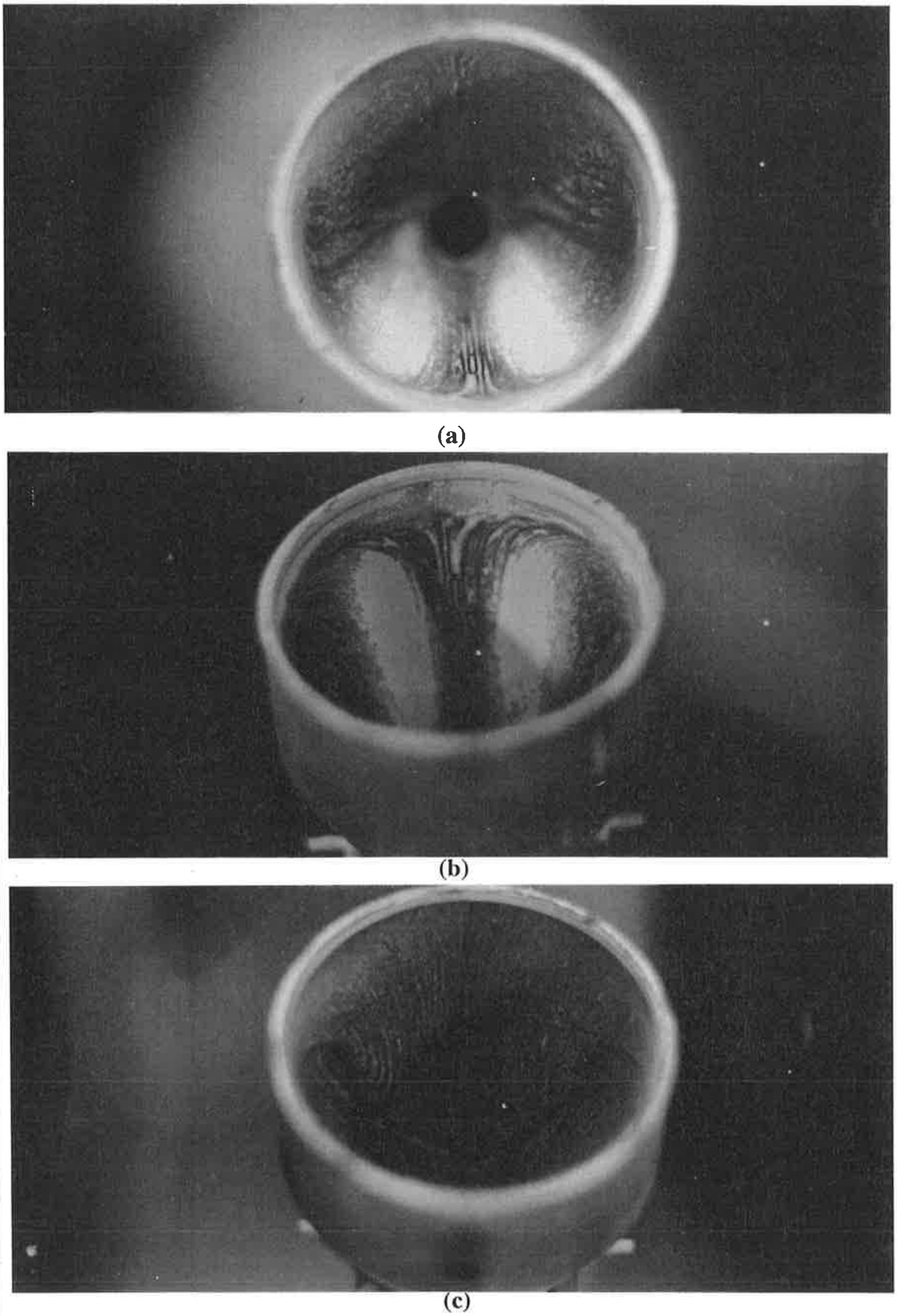

(a)

(b)

(c)

Figure 4.5.9. 3 China clay surface flow visualisation inside CD nozzle at Re_t=72,000 and AR = 0.56; (a) top view, (b) wall jet side(c) focus; exit ring removed.

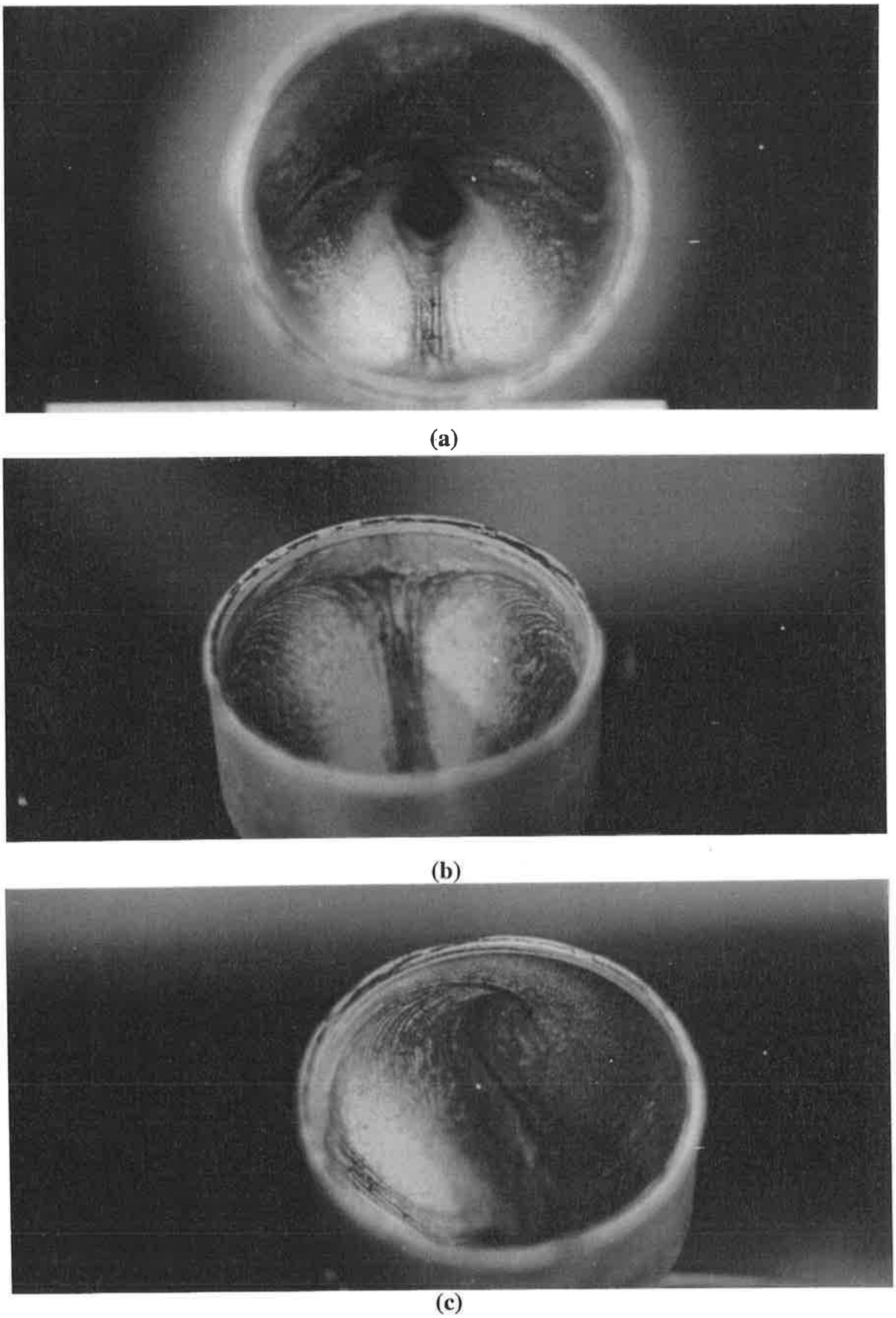

Figure 4.5.9. 4 China clay surface flow visualisation inside CD nozzle at Re_t=72,000 and AR = 0.44; (a) top view, (b) wall jet side, (c) focus; exit ring removed.

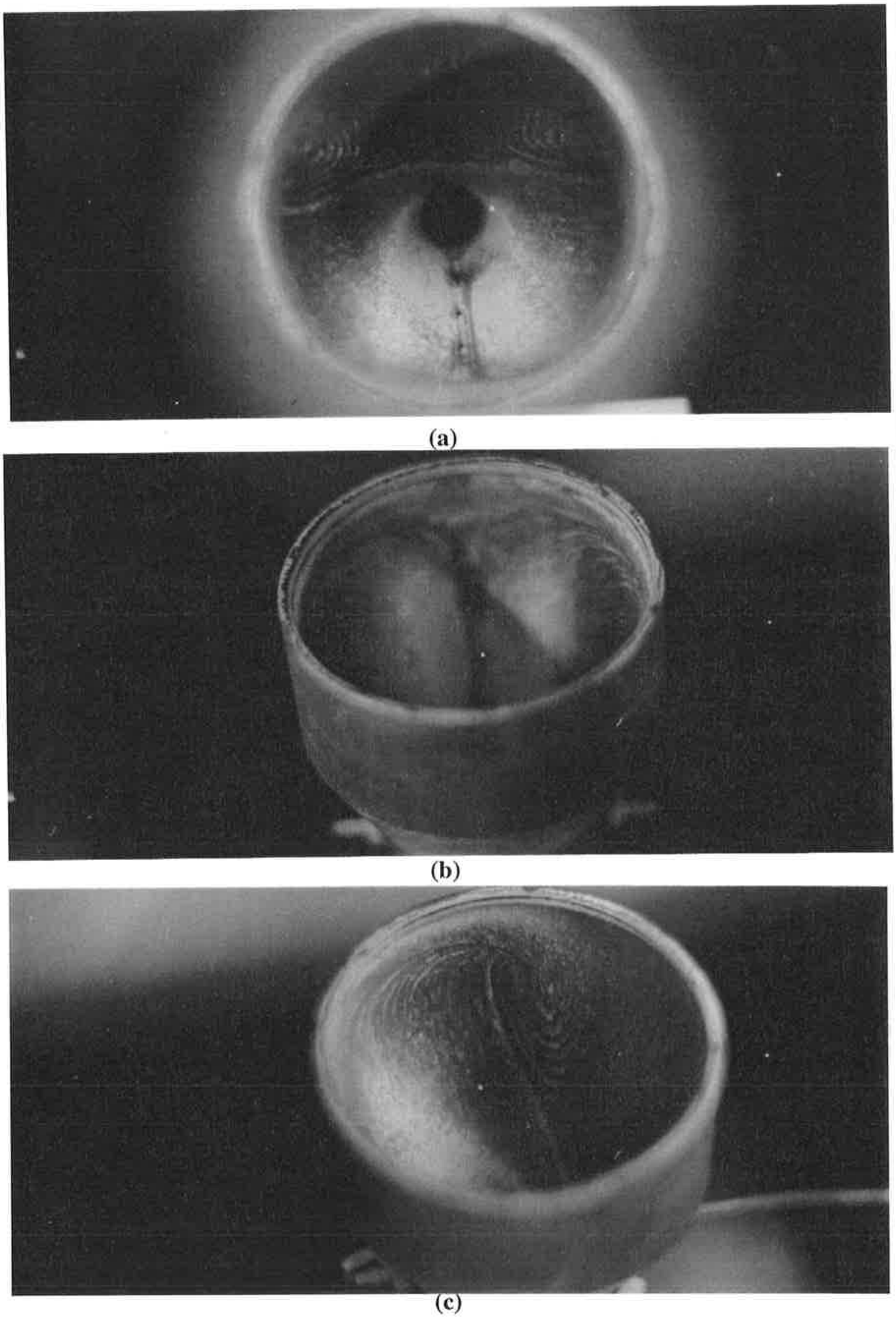

Figure 4.5.9. 5 China clay surface flow visualisation inside CD nozzle at Re_t=72,000 and AR = 0.34; (a) top view, (b) wall jet side , (c) focus; exit ring removed.

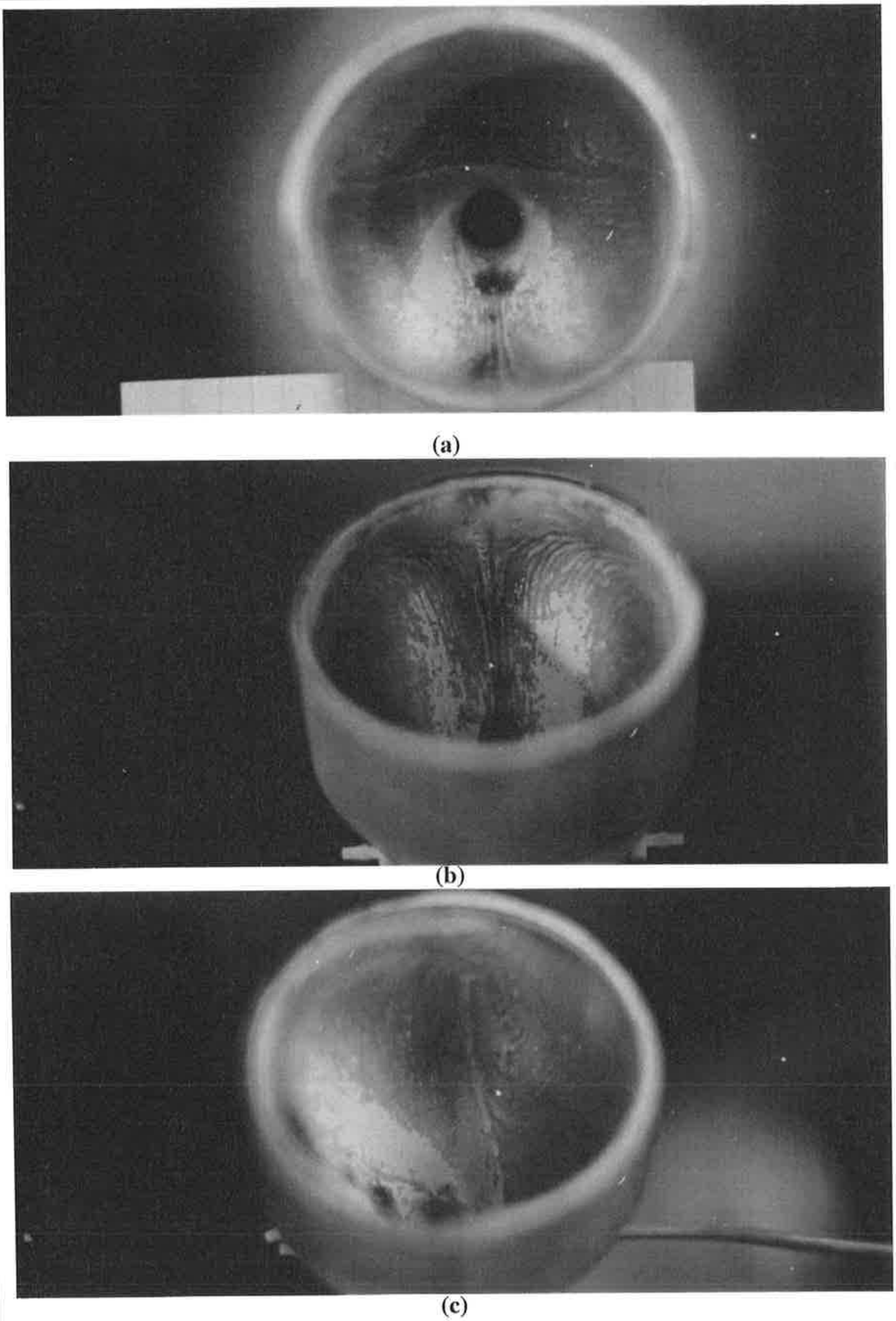

(a)

(b)

(c)

Figure 4.5.9. 6 China clay surface flow visualisation inside CD nozzle at Re_t=72,000 and AR = 0.25; (a) top view, (b) wall jet side , (c) focus; exit ring removed.

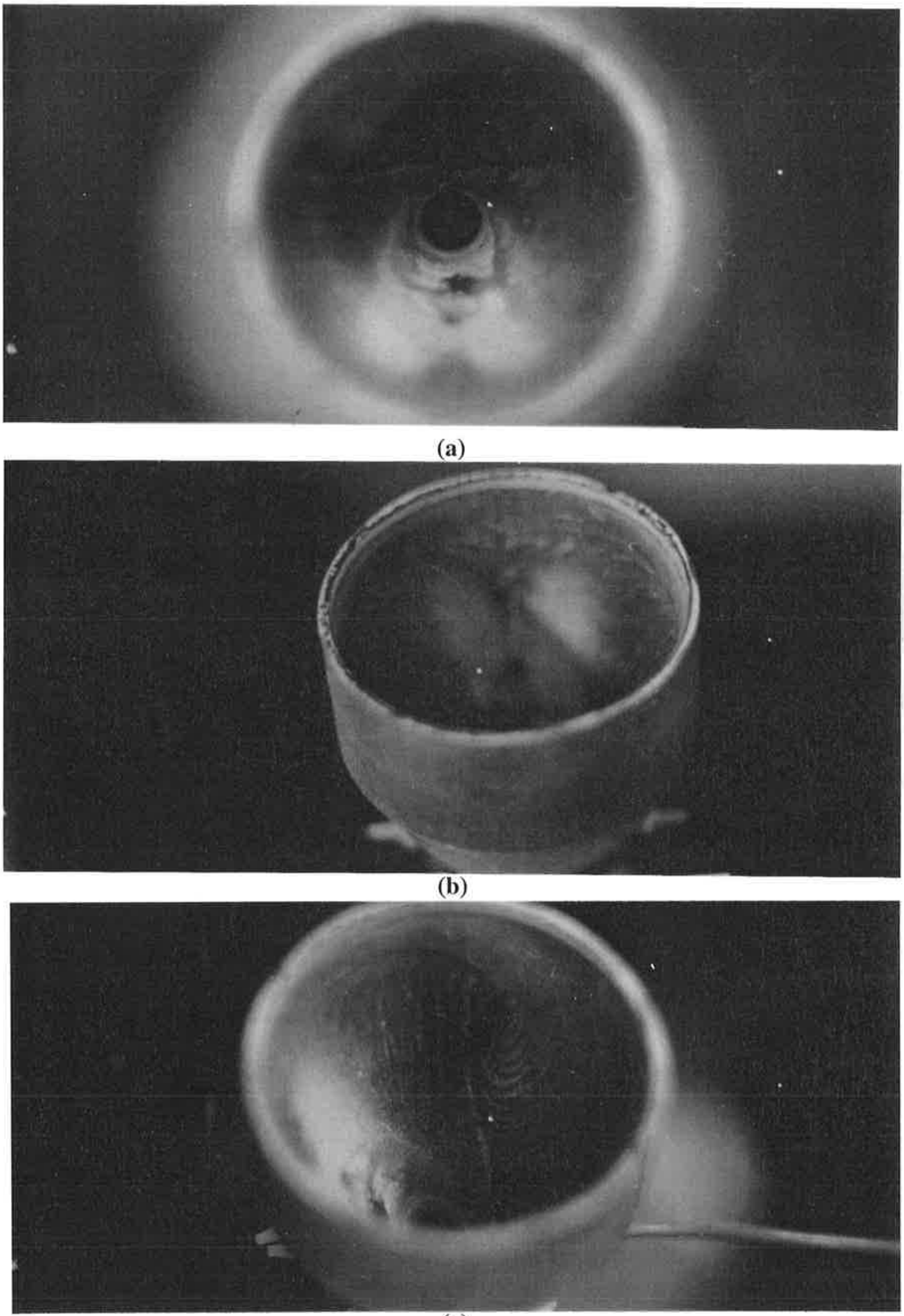

(a)

(b)

(c)

Figure 4.5.9. 7 China clay surface flow visualisation inside CD nozzle at Re_t=72,000 and AR = 0.17; (a) top view, (b) wall jet side , (c) focus; exit ring removed.

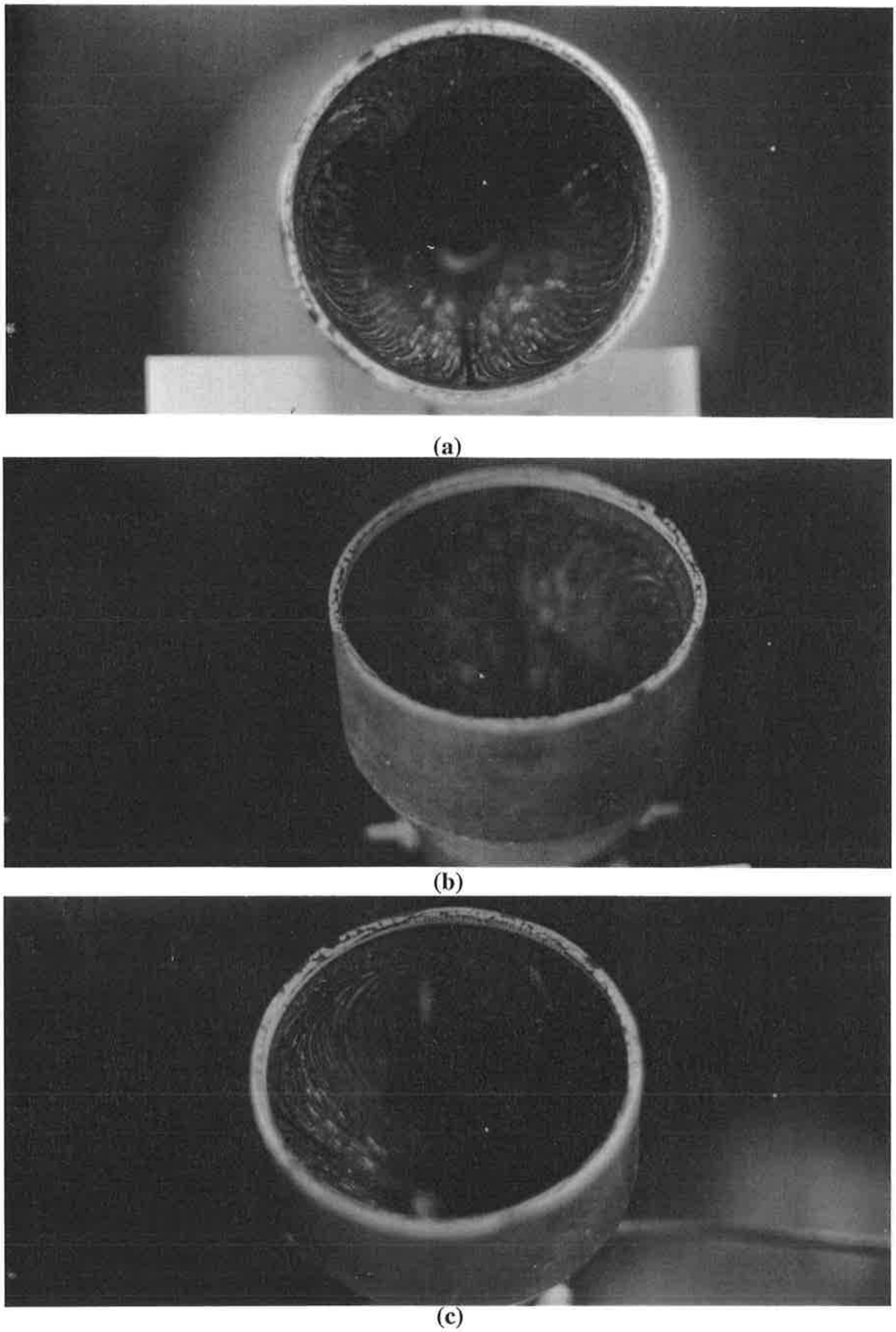

Figure 4.5.9. 8 China clay surface flow visualisation inside CD nozzle at Re_t=72,000 and AR = 0.11; (a) top view, (b) wall jet side , (c) focus; exit ring removed.

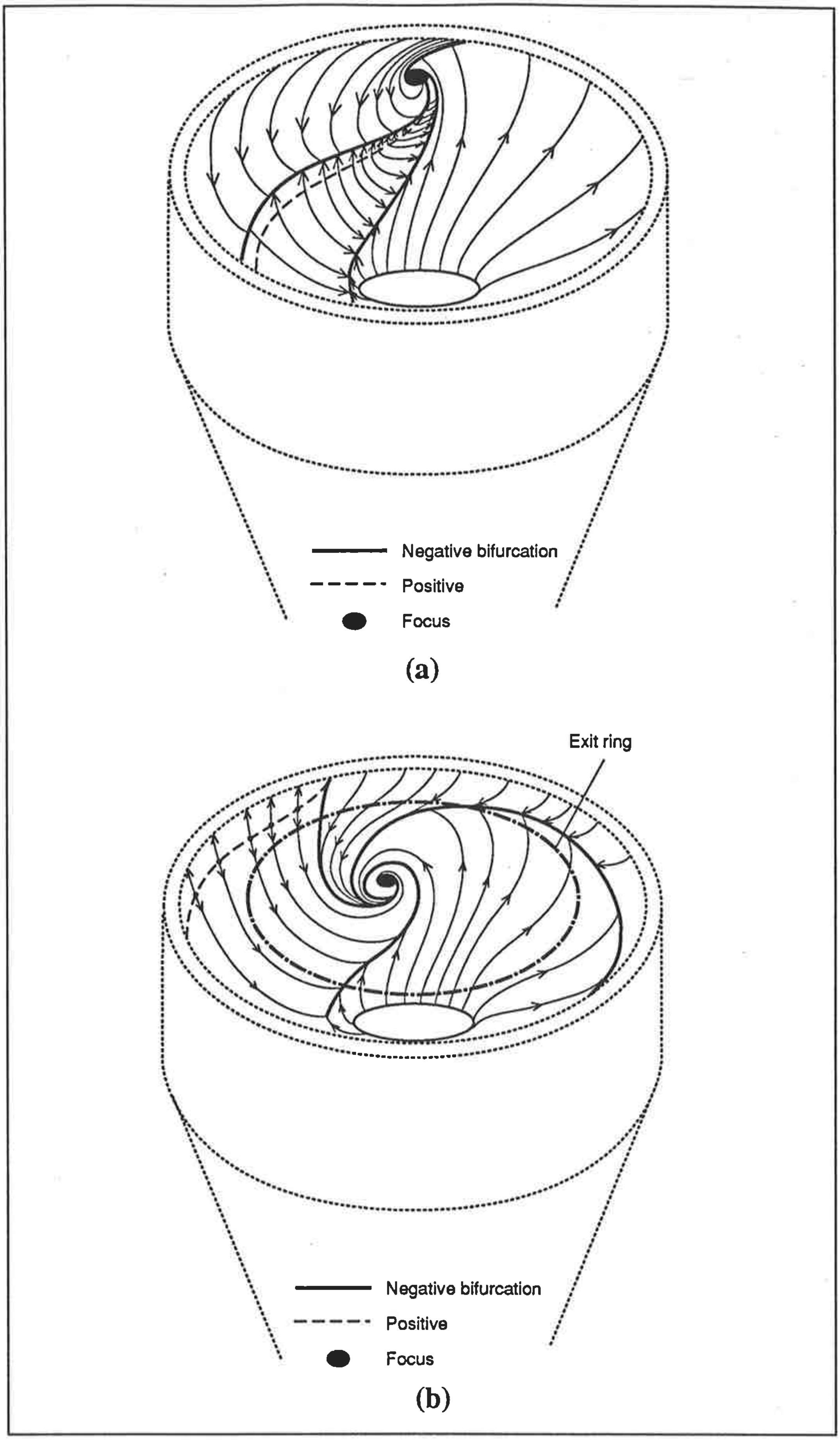

Figure 4.5.9. 9 General interpretation of the nozzle flow patterns from the china clay figures above, (a) No exit ring (b) Moderate exit ring in place.

4.6 Effects of Nozzle Configuration on Mass Flux and Driving Pressure

The mass flow rate through the orifice plate flow meter has been calibrated up to the maximum flow rate of 30 x 10^{-3} (kg/s). Above this value driving pressure was calibrated against mass flux as discussed in Section 2.3. The flow at the throat of the CD nozzle varies with driving pressure and geometric configuration of the nozzle. The relationship between driving pressure and mass flow rate for a convergent nozzle and CD nozzle are shown in **Figure 4.6.1**. It has been found that for the same throat diameter and driving pressure, the mass flow rate is slightly lower for the convergent nozzle with an abrupt expansion at the throat than that through the convergent-divergent nozzle configuration without the exit ring confirming results found by Nathan (1988) for the MLC, LC nozzle and primary orifice discharging into the atmosphere. These differences in mass flow rate are probably due to the difference in the back pressure in the nozzle downstream from the throat.

For a given convergent-divergent nozzle configuration and driving pressure, the mass flow rate decreases as the exit area is reduced due to an increase in back pressure inside the nozzle. This was however not considered a problem since the orifice plate flow meter and not the nozzle pressure ratio, was used to sense the mass flow rate through the nozzle.

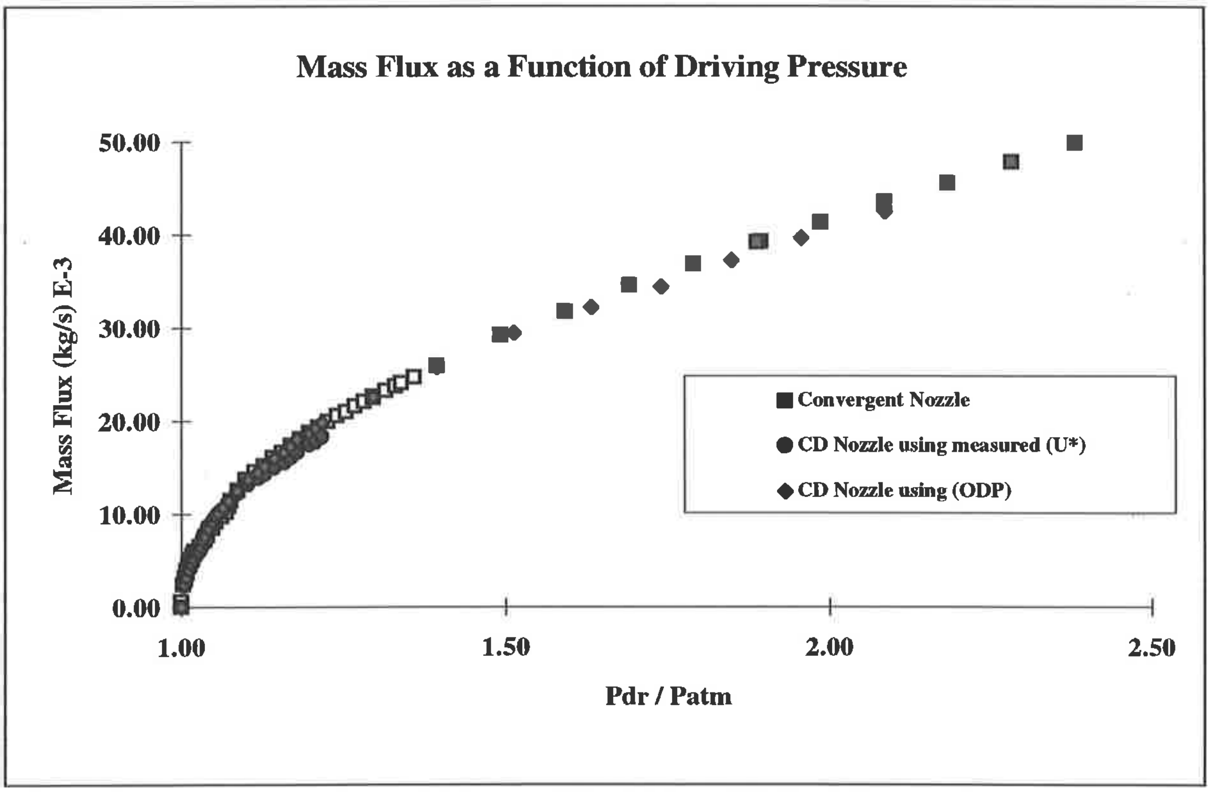

Figure 4.6.1 Relationship between driving pressure and mass flux for various nozzle configurations.

4.7 Velocity Profiles Inside and Outside the Nozzle

A large number of pitot-static pressure profiles have been taken both inside and outside various nozzle configurations and results related to the CD nozzle presented and discussed in this section. The calculated velocities were derived from the dynamic pressure and the calculated density at that point in the nozzle. The density ρ^* was calculated using Eqn. 4.1 , where P^* is the static pressure in the flow, T^* is the fluid temperature and R is the universal gas constant. Because of the separation between the total and static sensing holes of the pitot-static probe, both hot wire and LDV was used where possible to supplement the pitot-static measurements.

$$P^* = \rho^* R T^* \qquad \textbf{Eqn. (4.1)}$$

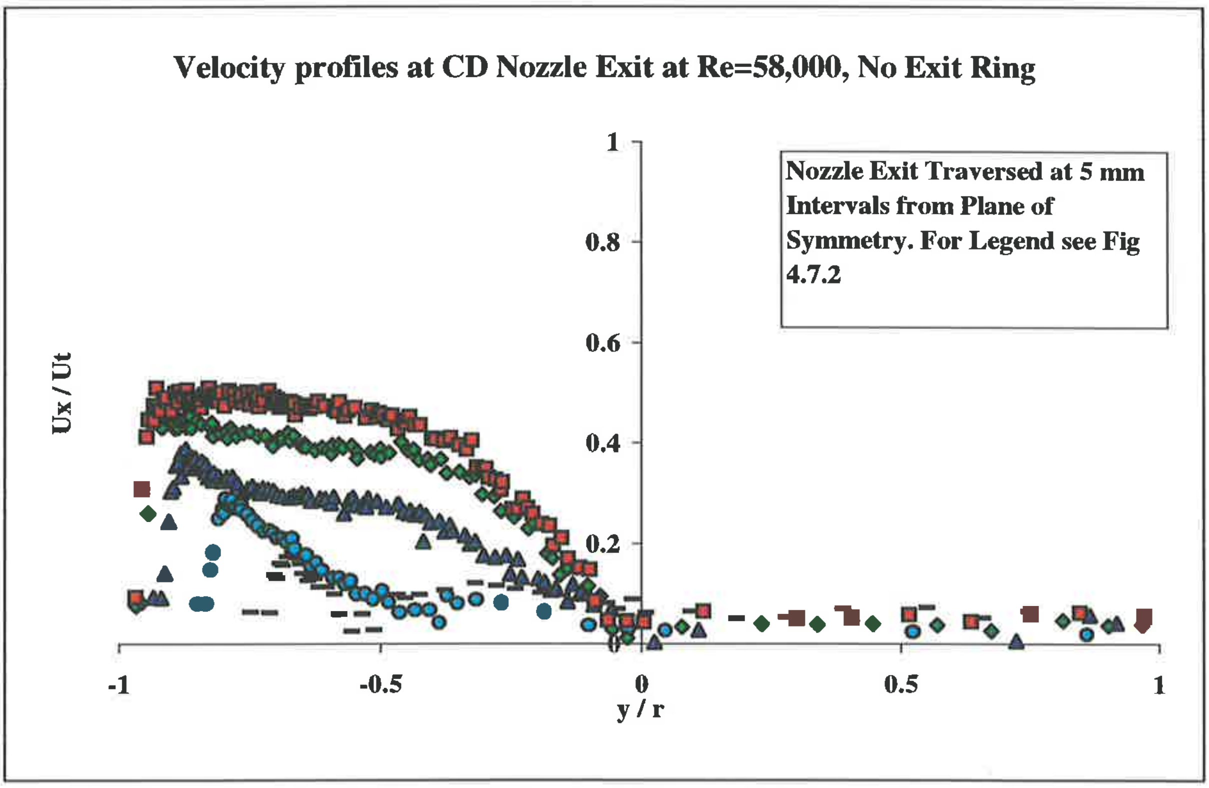

Figure 4.7. 1 Asymmetric velocity at the CD nozzle exit using pitot-static pressure measurements, AR=1 and Re_t=58,000.

4.7.1 Dynamic Pressure Measurements

Before using the pitot-static tube to obtain a measure of the velocity profiles inside the nozzle, the direction of the flow inside the nozzle was determined from both the surface flow visualisation and tufts inserted into the flow. The measured flow velocity using the LDV eliminates the directional bias by using frequency shifted beams to distinguish the flow direction, as discussed in Chapter 2. The pitot-static velocity measurements have been validated using both hot-wire and LDV measurements. From a large number of experiments main features of the flow both inside and outside the nozzle have been deduced and the effects of the nozzle length and the exit ring diameter assessed. The initial total pressure profiles inside the nozzle revealed both the asymmetry and the areas of high turbulence in the flow, shown in **Figure 4.2. 16**. The asymmetry of the velocity profile is found to be dependent on the flow rate through the nozzle. From the pitot pressure profiles the jet thickness reduces as the mass flux increases. This reduction is most noticeable at the initial stage of the flow asymmetry. The primary jet leaving the throat moves downstream and deforms asymmetrically. It is partially attached to the wall downstream from the throat and appears to deform from the initial axisymmetric cross-section into a jet that has the cross-section which resembles a semi-circle at the exit plane. As the flow rate is increased, the jet cross-section at the exit plane changes as it spreads transversely to form a kidney shape cross-section. The velocity profiles across the exit plane of the CD nozzle at $Re_t = 58{,}000$ are shown in the **Figure 4.7. 1**. This initial thick wall jet at the exit plane may affect the angle at which the wall jet leaves the nozzle at lower flow rates when the exit ring is attached and this change in deflected angle appears to be less than the uncertainty of the adopted angle measurement technique using tufts. Measurement of a wall jet thickness inside the CD nozzle, when the exit ring is smaller than 50 mm diameter, was not possible with a pitot-static probe due to the nozzle and exit ring geometry. It is unlikely to change significantly with decreasing exit ring diameter for the first four throat diameters downstream from throat.

The velocity profiles at the CD nozzle exit, without exit ring present, shown in **Figure 4.7. 1** are for the $Re_t=58{,}000$ indicate that the wall jet centre line is moving away from the nozzle geometric centreline, as the jet moves toward the nozzle exit. For this Reynolds number, which is just above critical Reynolds number, the wall jet thickness occupies half the nozzle exit diameter. For the same nozzle and a Reynolds number of 100,000 (corresponding to a mass flow rate, $m = 15 \times 10^{-3}$ kg/s) the wall jet at the nozzle exit spreads more and in effect the wall jet becomes thinner at the nozzle exit, as shown in **Figure 4.7. 2**. This confirms the laser sheet flow visualisation observations, of the jet cross-section at the nozzle exit, made in the previous section.

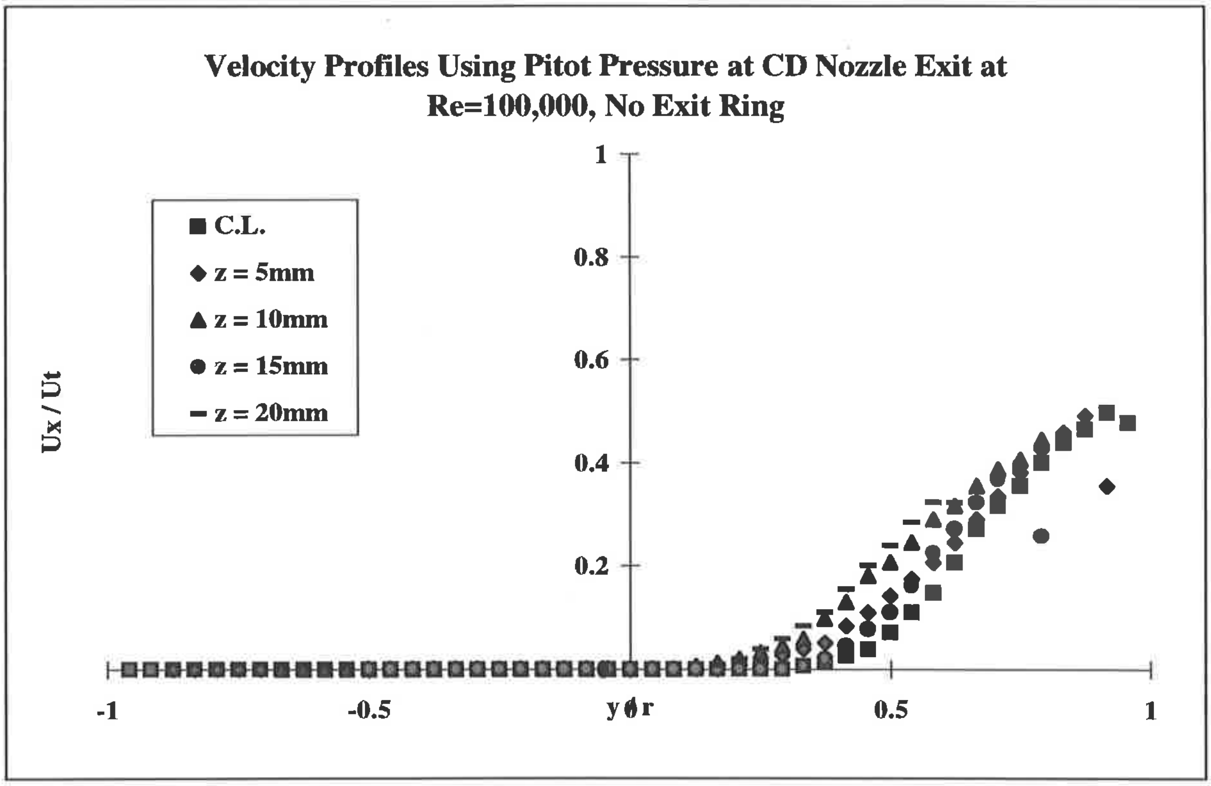

Figure 4.7. 2 Asymmetric velocity at the CD nozzle exit using pitot-static pressure measurements, AR=1 and Re_t=100,000.

4.7.2 Hot Wire Anemometry

A large number of hot wire measurements have been made outside the nozzle for several nozzle configurations. For example, at Re_t=27,000 diametral traverses in the planes of symmetry of both the axisymmetric and asymmetric jets exiting the CD nozzle without an exit ring at the nozzle exit, are shown in **Figure 4.7. 3.** The figure shows the dramatic change in the velocity profile when the jet becomes asymmetric. The centre line velocity in the axisymmetric jet has reduced to $U_{cl}/U_t = 0.85$ by six throat diameters whereas at the same distance downstream, the asymmetric jet has reduced to $U_{cl}/U_t = 0.5$. This result is also confirmed when the velocity profiles measured using LDV, as shown by **Figure 4.7. 6.** A velocity profile across the exit plane of the CD nozzle in the absence of an exit ring has been established and profiles also confirmed by the pitot-static pressure measurements shown in **Figure 4.7. 1.** The jet velocity profiles are verified by the pitot-static and LDV velocity profiles.

When the exit rings are added to the nozzle exit and mass flow rate kept constant, the velocity profiles at the exit plane alter drastically, as would be expected from the flow visualisation results discussed earlier. The velocity profiles across the plane of exiting jet symmetry for each nozzle configuration were measured. Two sets of hot wire measurements were taken with hot wire aligned such that each traverse measured the U_x+U_y and U_x+U_z velocity components respectively. Since the U_z component is assumed to be zero in the plane of flow symmetry, the velocity components in the x and y directions can be resolved. **Figure 4.7. 4** shows the changes in the velocity profile in the x-y plane of symmetry, with change in exit area. **Figure 4.7. 5** shows that the velocity component in the "x" direction at the nozzle exit reduces with decreasing AR until AR = 0.11 when the velocity component in "x" direction increases. This could be explained by the reduction of the angle of the exiting jet from $\alpha = 65°$ to $\alpha = 45°$, when the AR is reduced from 0.17 to 0.11, therefore the "x" velocity component had increased.

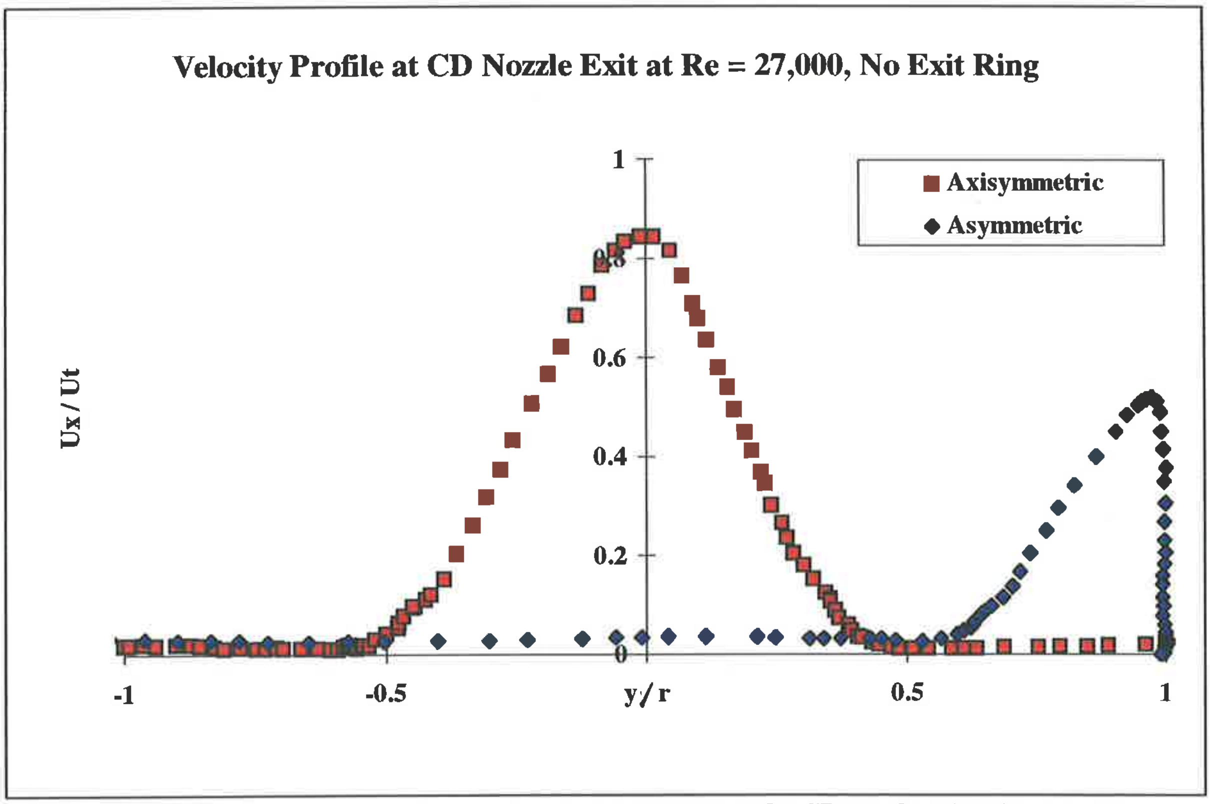

Figure 4.7. 3 Axisymmetric and asymmetric velocity profiles at the CD nozzle exit using hot-wire measurements, AR=1.

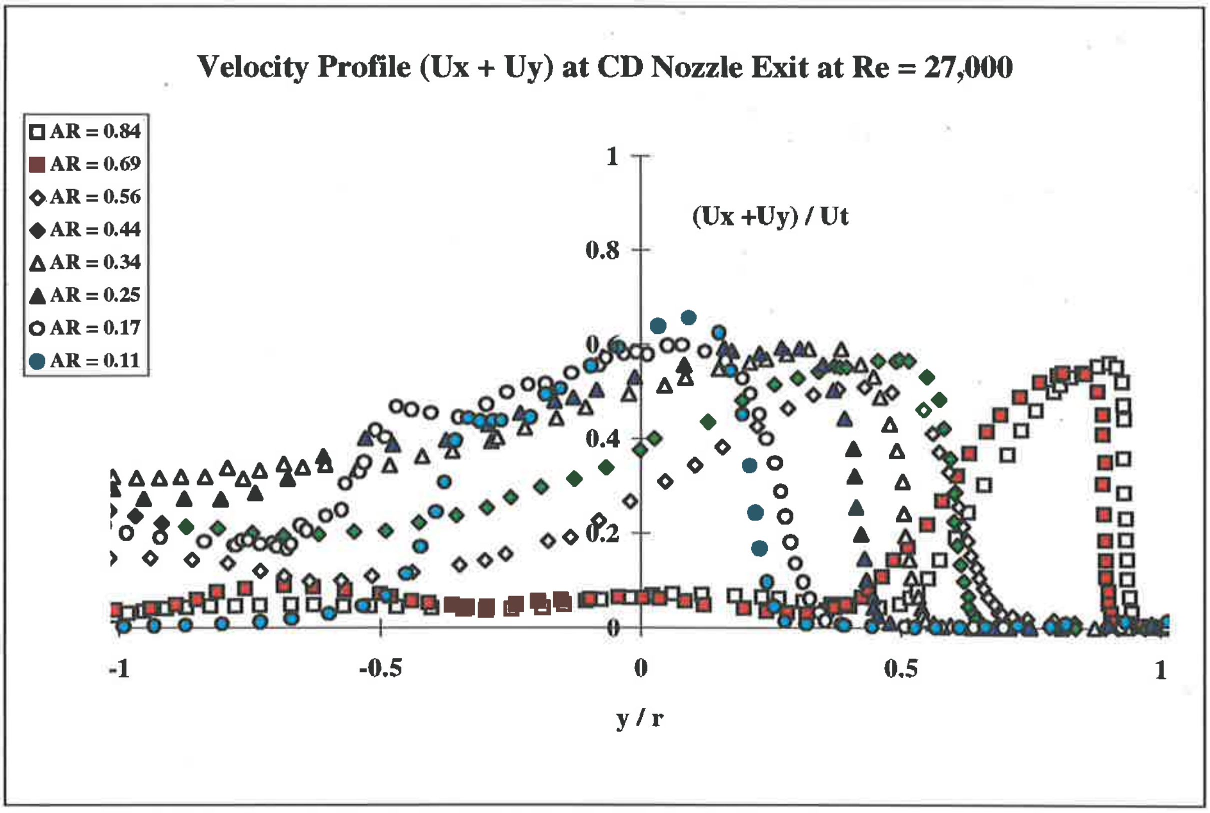

Figure 4.7. 4 Hot-wire velocity profiles showing the total velocity vector of the exiting jet, traversed across the CD nozzle exit plane of symmetry.

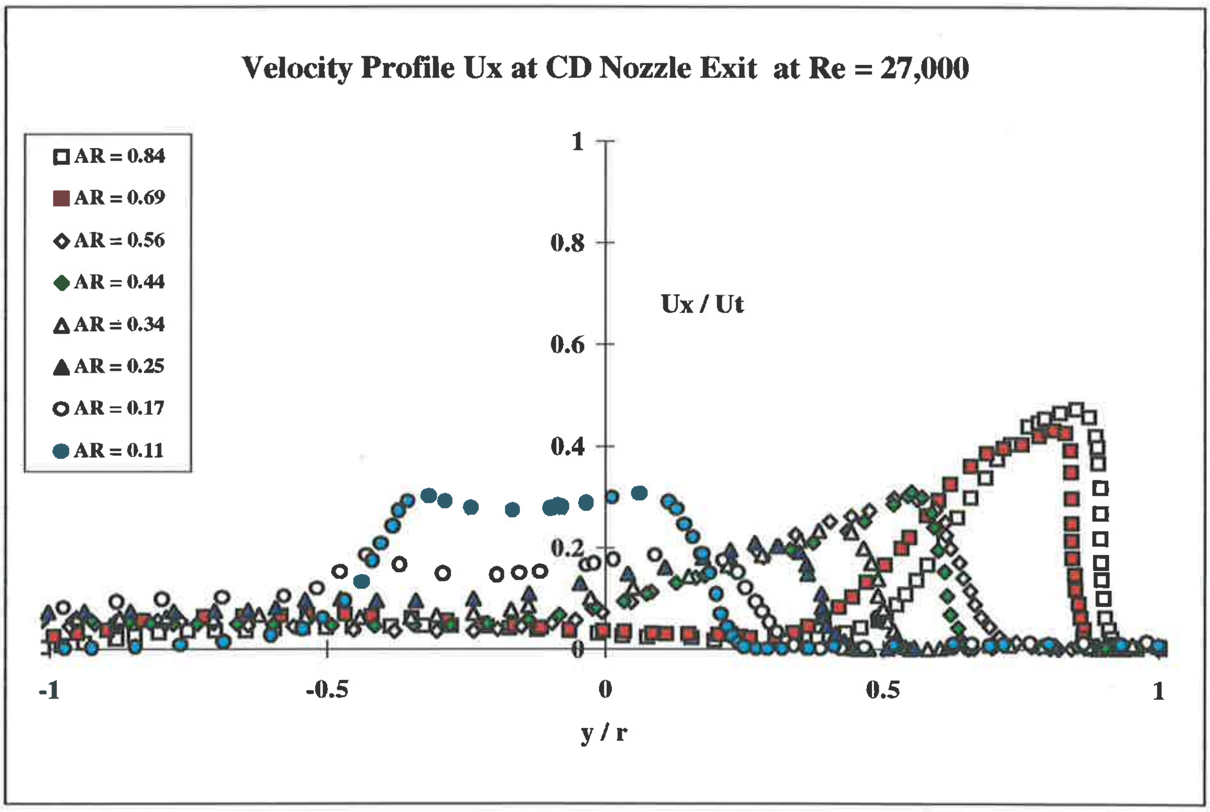

Figure 4.7. 5 Hot-wire velocity profiles showing the U_x component of the velocity vector of the exiting jet, traversed across the CD nozzle exit plane of symmetry at Re_t=27,000.

4.7.3 L.D.V. Velocity Measurements

A number of velocity measurements have been taken at a distance of 5mm downstream from the CD nozzle exit. The measurements could not be taken any closer to the nozzle exit due to the angle at which the beams approach the measuring volume. The velocity profiles, at this distance, would not be too dissimilar from the velocity profiles at the exit. Wall jet velocity vectors across the CD nozzle exit with exit area ratio AR = 1 are shown in **Figure 4.7. 7**. The velocity profiles are similar to the those obtained from the hot-wire and the pitot-static measurements in Sections 4.7.1 and 4.7.2. It is apparent that the wall jet spreads transversely inside the nozzle and that the jet turbulence on the wall side is much less than that in the shear layer, until the jet leaves the nozzle. The turbulent velocity u'_x is much higher in the outer region of the wall jet where a strong shear layer develops between the outgoing jet and the incoming ambient fluid. The intensity of this shear layer is evident from **Figure 4.7. 8**. The high turbulence intensity is partnered by strong entrainment within the nozzle and this in turn causes the strong induction of ambient fluid into the nozzle. This region is also visible in the transverse u'_y turbulent velocity profiles, as shown in **Figure 4.7. 9**. The change in U_y flow direction from positive to negative, shown in **Figure 4.7. 7**, is compatible with the suggested entrainment of fluid from within the cavity into the jet up to the edge of the mixing layer. Within the jet the movement of fluid towards the mixing layer (the negative velocity region) is indicative of the spread of the wall jet as it emerges from the confinement of the nozzle. When the exit area is reduced by placing an exit ring at the nozzle exit, so providing a lip at the exit plane, the wall jet is deflected at an angle primarily determined by the lip height. Initially the angle increases with an increase in exit lip height and reaches a maximum deflected angle of $\alpha = 80°$. This occurs at an exit area ratio AR = 0.34. When the exit area is reduced further the angle at which the jet deflects decreases, as discussed in Section 4.3. The velocity profiles measured at 5 mm downstream from the exit relate to traverses parallel to the exit plane. The velocity profiles in the x direction for the first exit ring of 55mm diameter appear to be similar to the velocity profiles for CD nozzle without the exit ring. However the difference between the profiles becomes increasingly apparent as the exit area reduces, as can be seen in **Figure 4.7. 10**. Since the angle at which the jet deflects varies with exit area, the profiles measured at the exit also change quiet dramatically, as shown in **Figure 4.7. 11** to **Figure 4.7. 16**. These figures show the total velocity vector magnitudes at the exit of the CD nozzle. When the angles are analysed it can be seen that the spreading jet half-angle β deviates from the mean by up to 20°, confirming previous observations in Section 4.3.

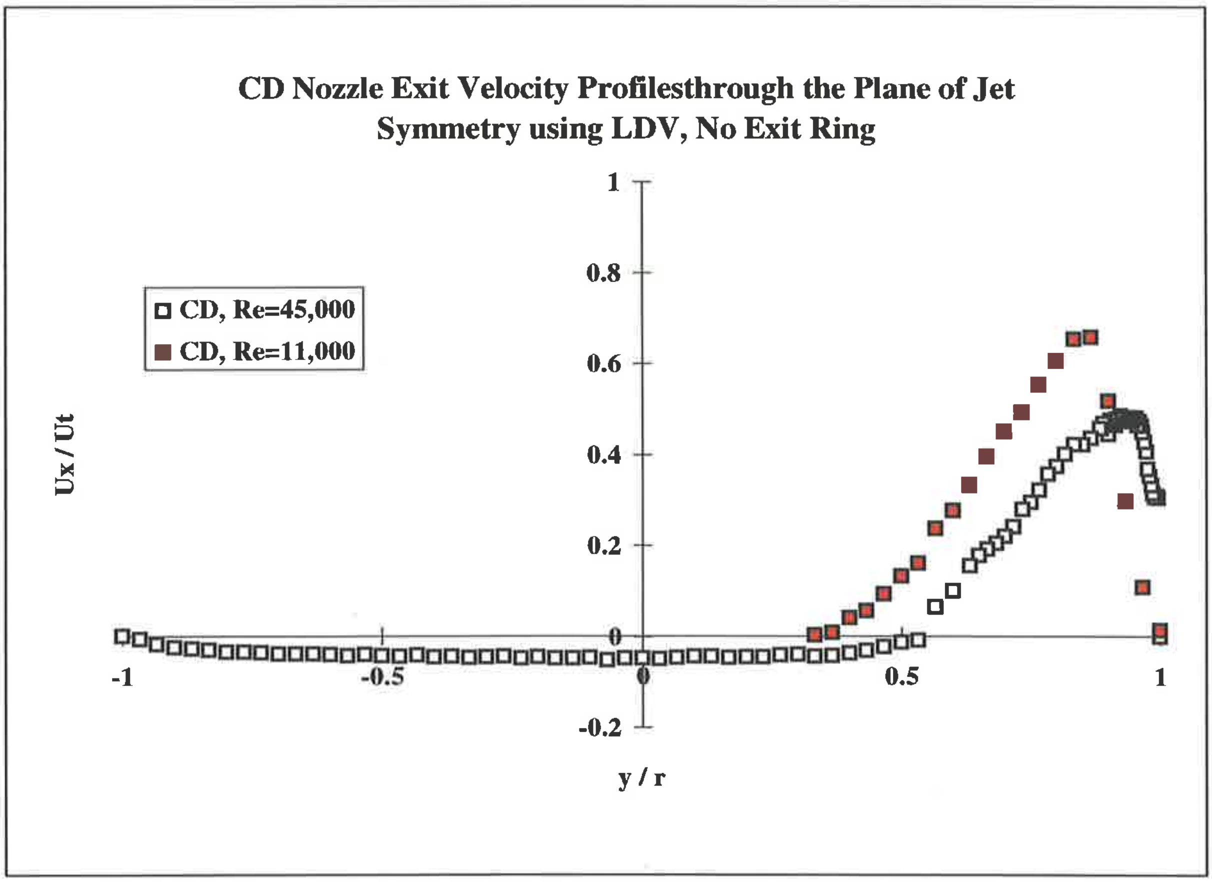

Figure 4.7. 6 Velocity profiles at the CD nozzle exit for Reynolds numbers of 11,000 and 45,000.

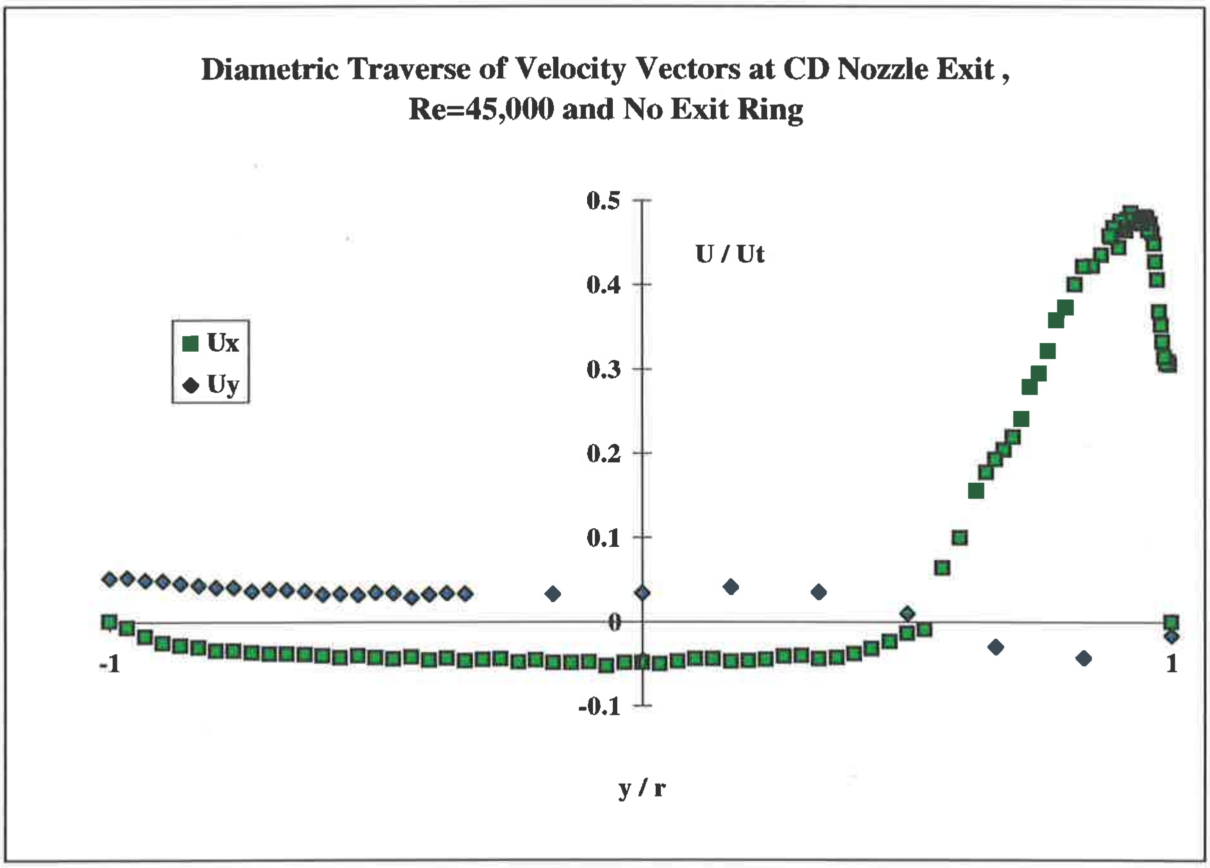

Figure 4.7. 7 LDV velocity vectors U_x and U_y across the plane of jet symmetry at the CD nozzle exit.

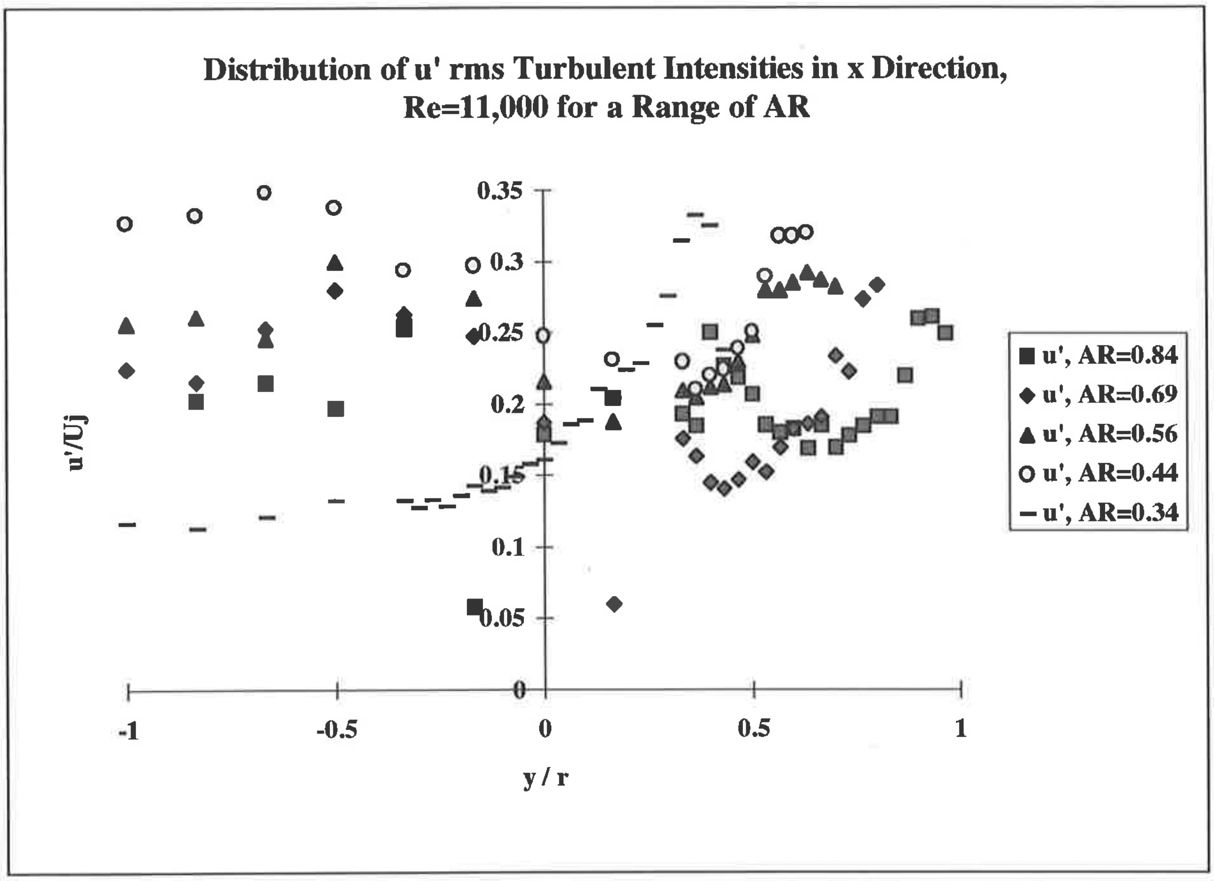

Figure 4.7. 8 LDV turbulent intensity profiles of u'_x/U_j at the CD nozzle exit for a range of exit areas.

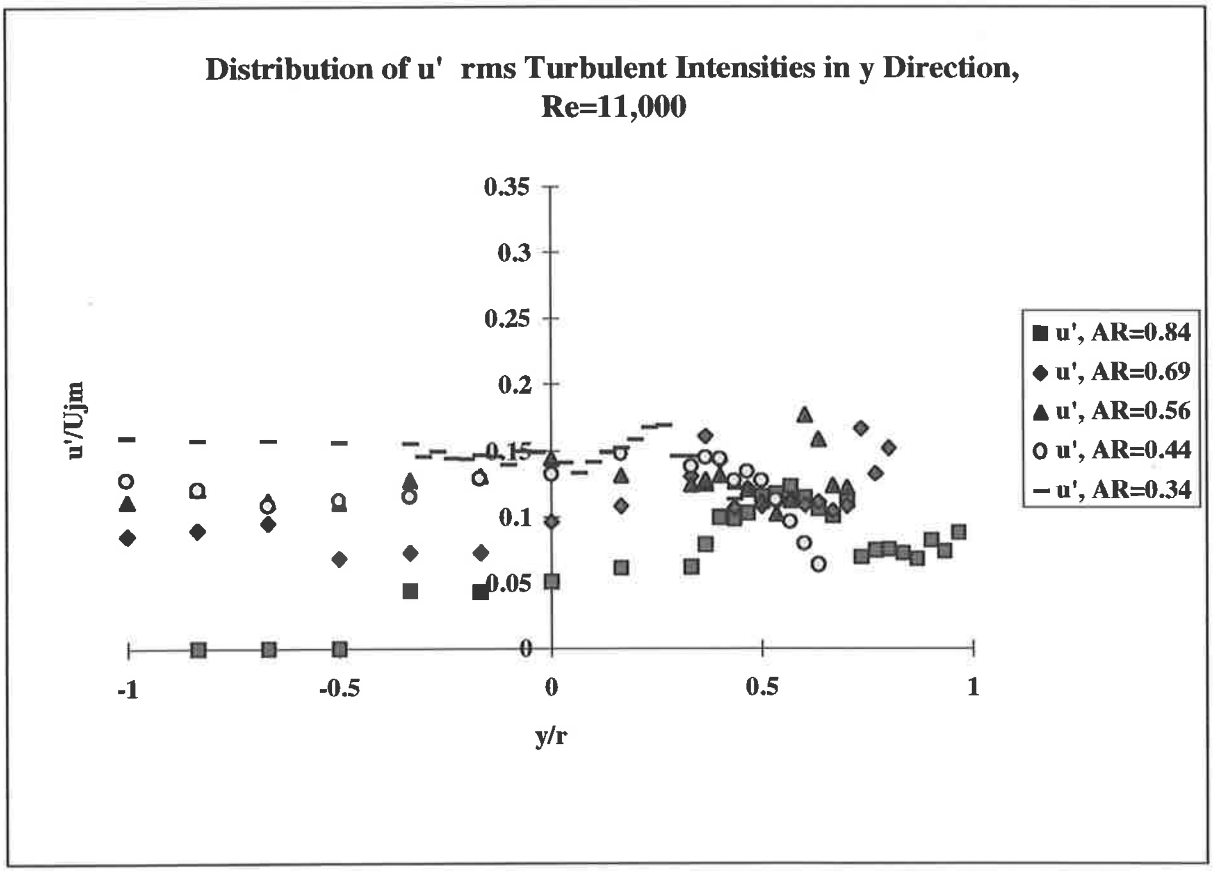

Figure 4.7. 9 LDV turbulent intensity profiles of u'_y/U_j at the CD nozzle exit for a range of exit areas.

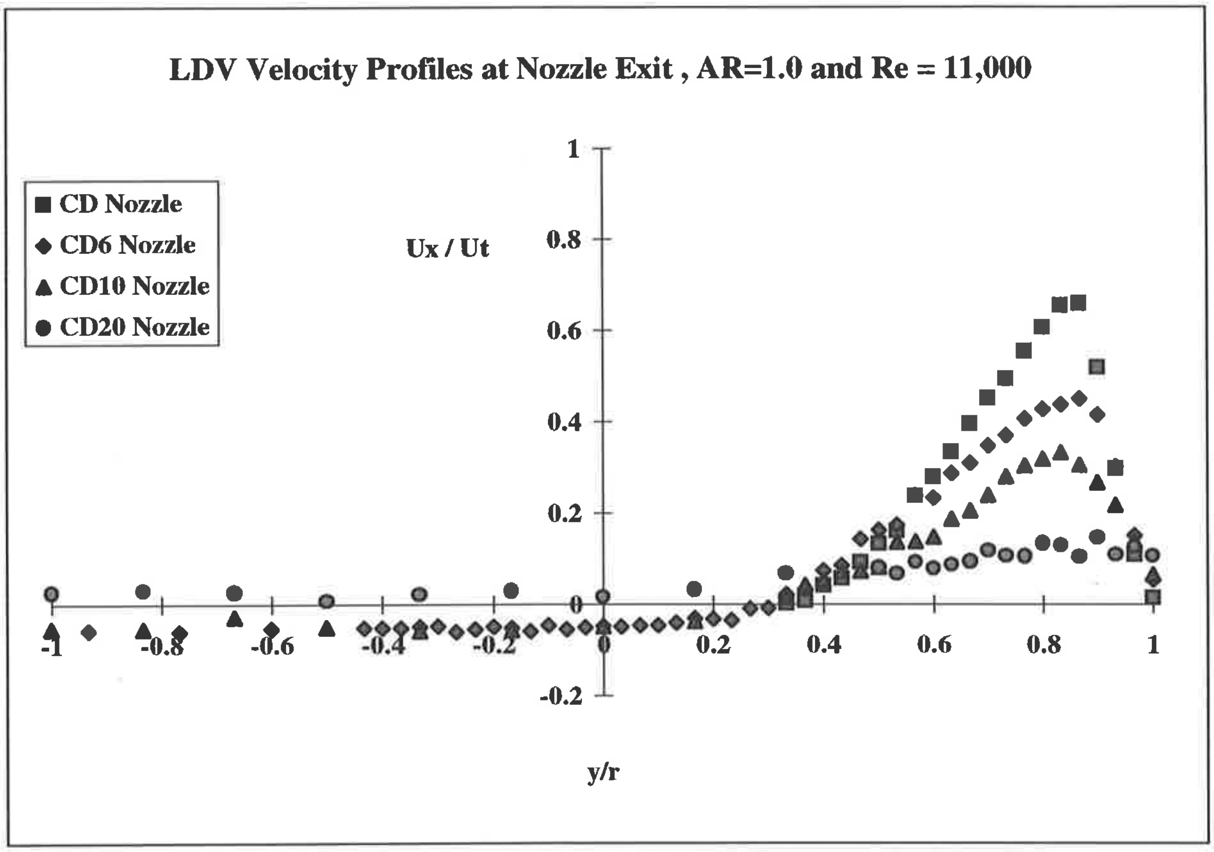

Figure 4.7. 10 LDV velocity vectors at the exit of the CD, CD6, CD10 and CD20 nozzles; AR = 1 and Re_t = 11,000.

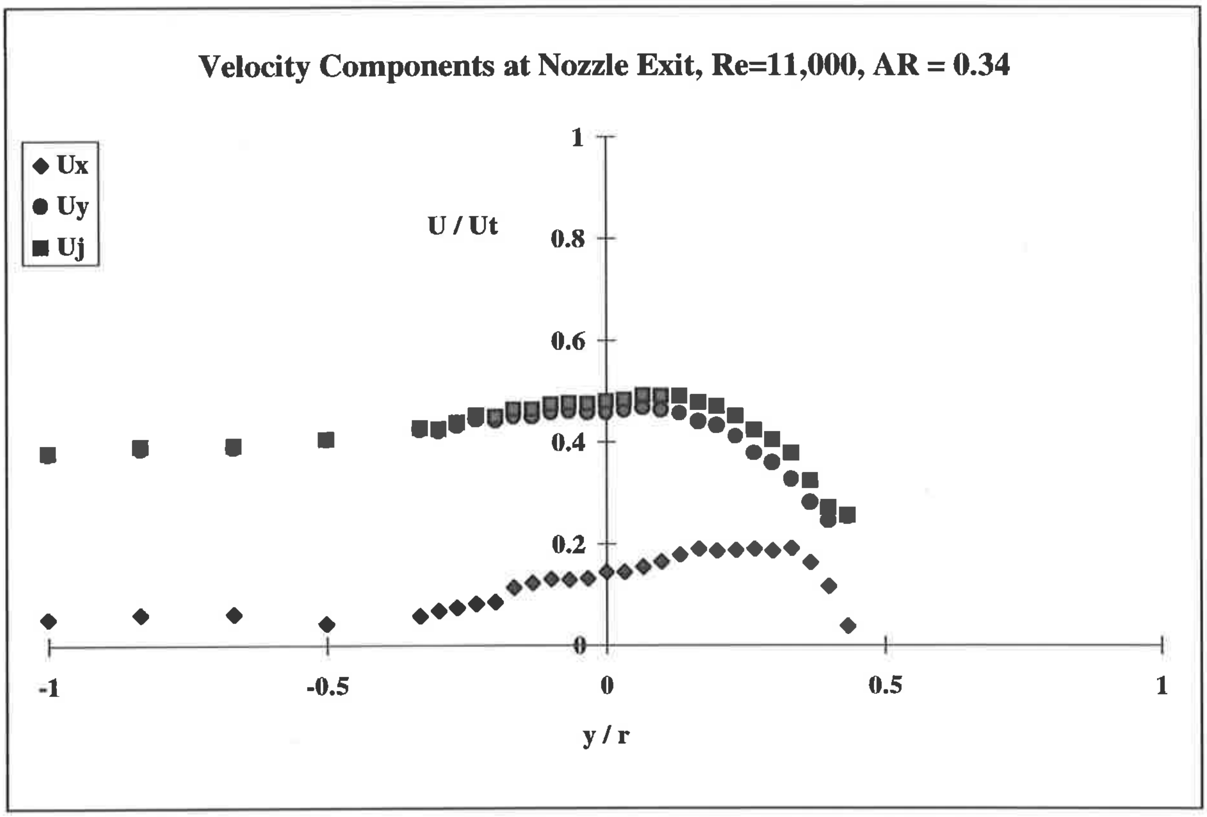

Figure 4.7. 11 LDV velocity vectors at the CD nozzle exit at Re_t=11,000 and AR=0.34.

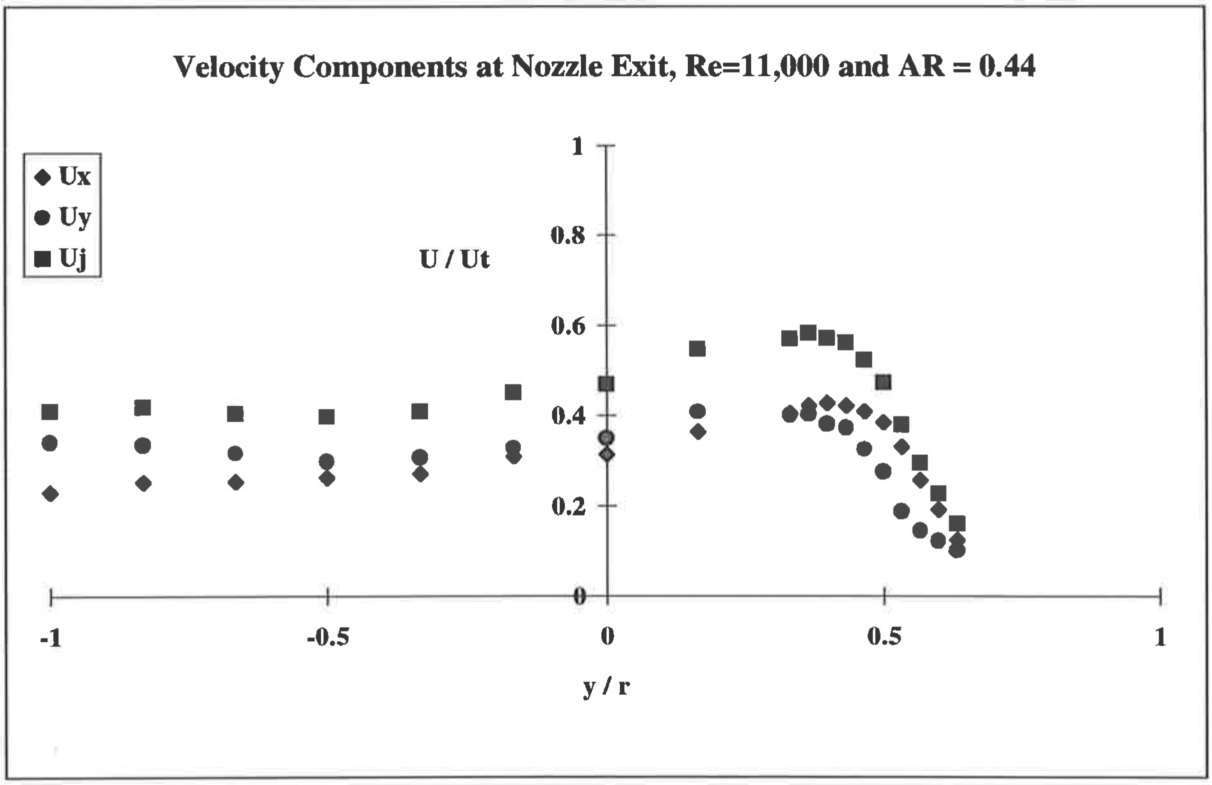

Figure 4.7. 12 LDV velocity vectors at the CD nozzle exit at Re_t=11,000 and AR=0.44.

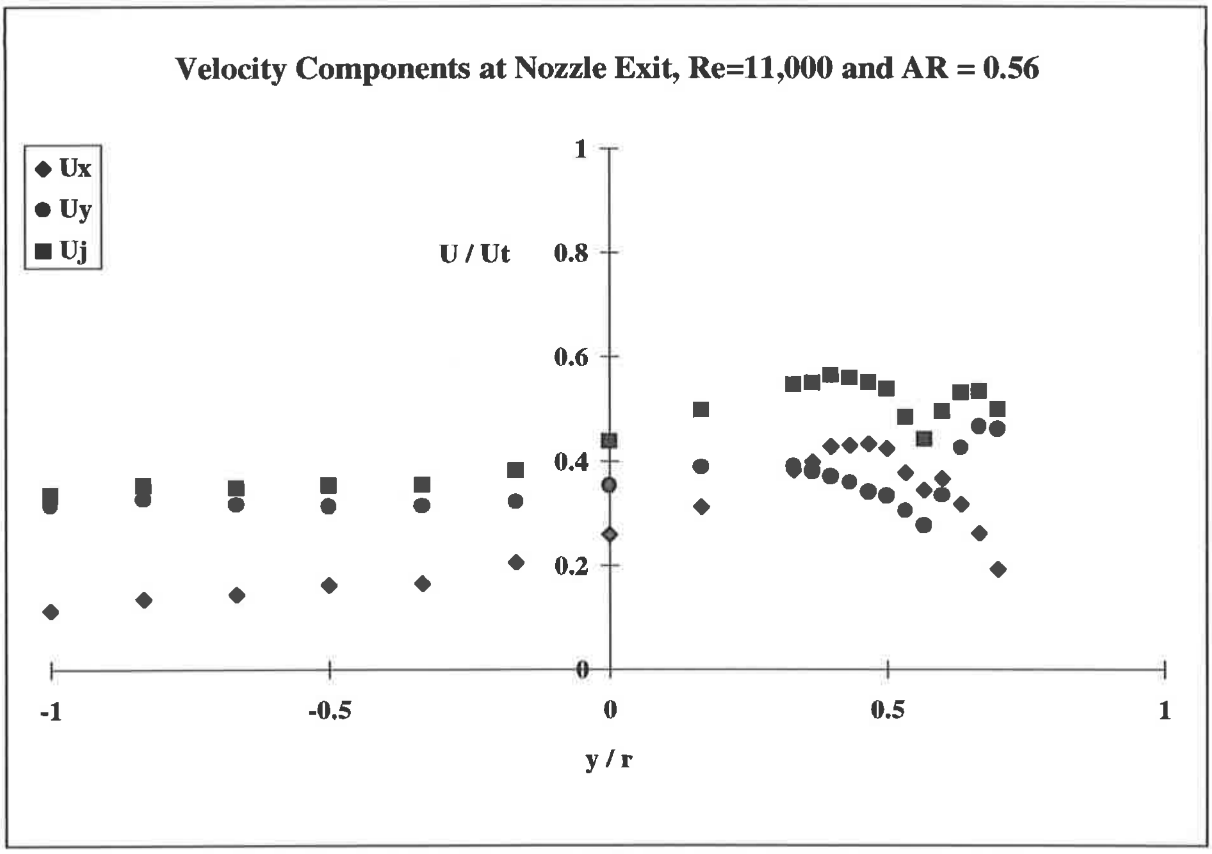

Figure 4.7. 13 LDV velocity vectors at the CD nozzle exit at Re_t=11,000 and AR = 0.56.

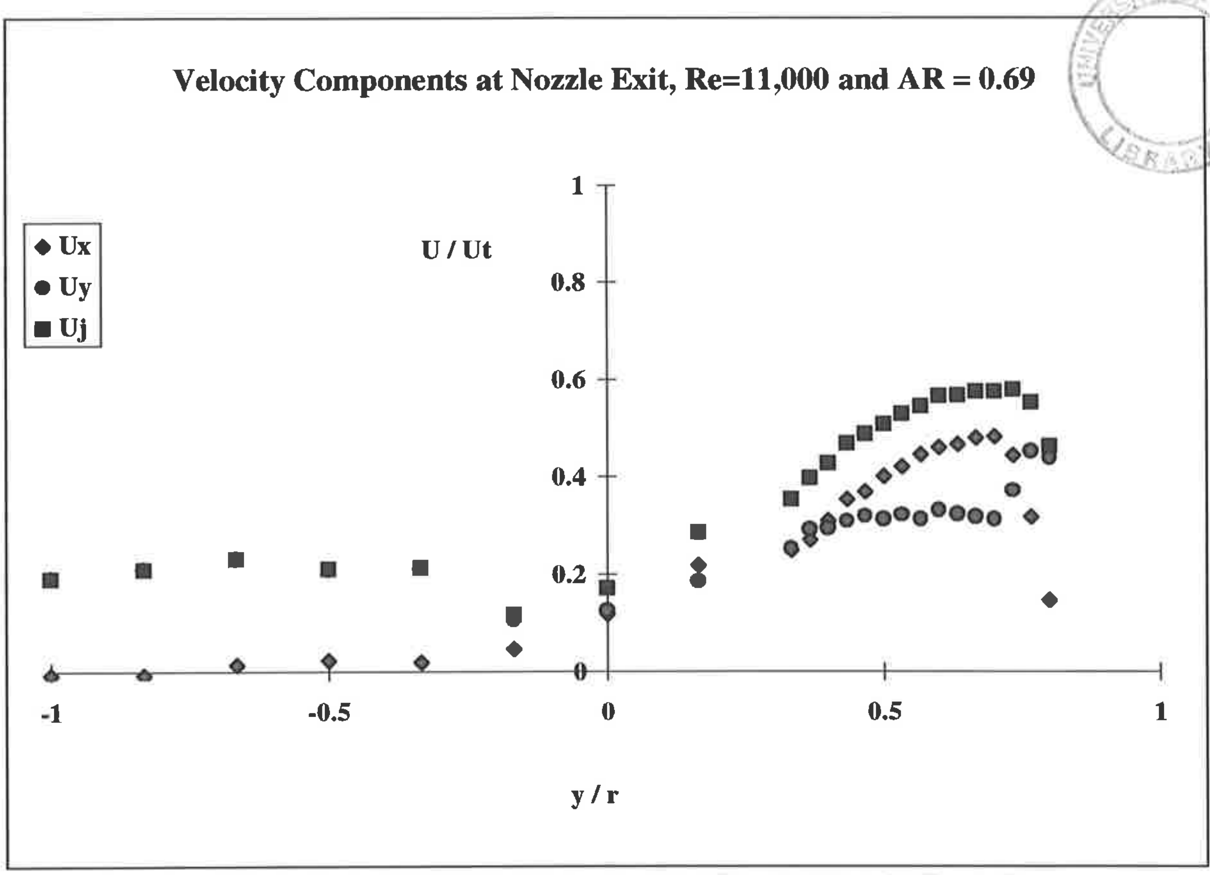

Figure 4.7. 14 LDV velocity vectors at the CD nozzle exit at Re$_t$=11,000 and AR = 0.69.

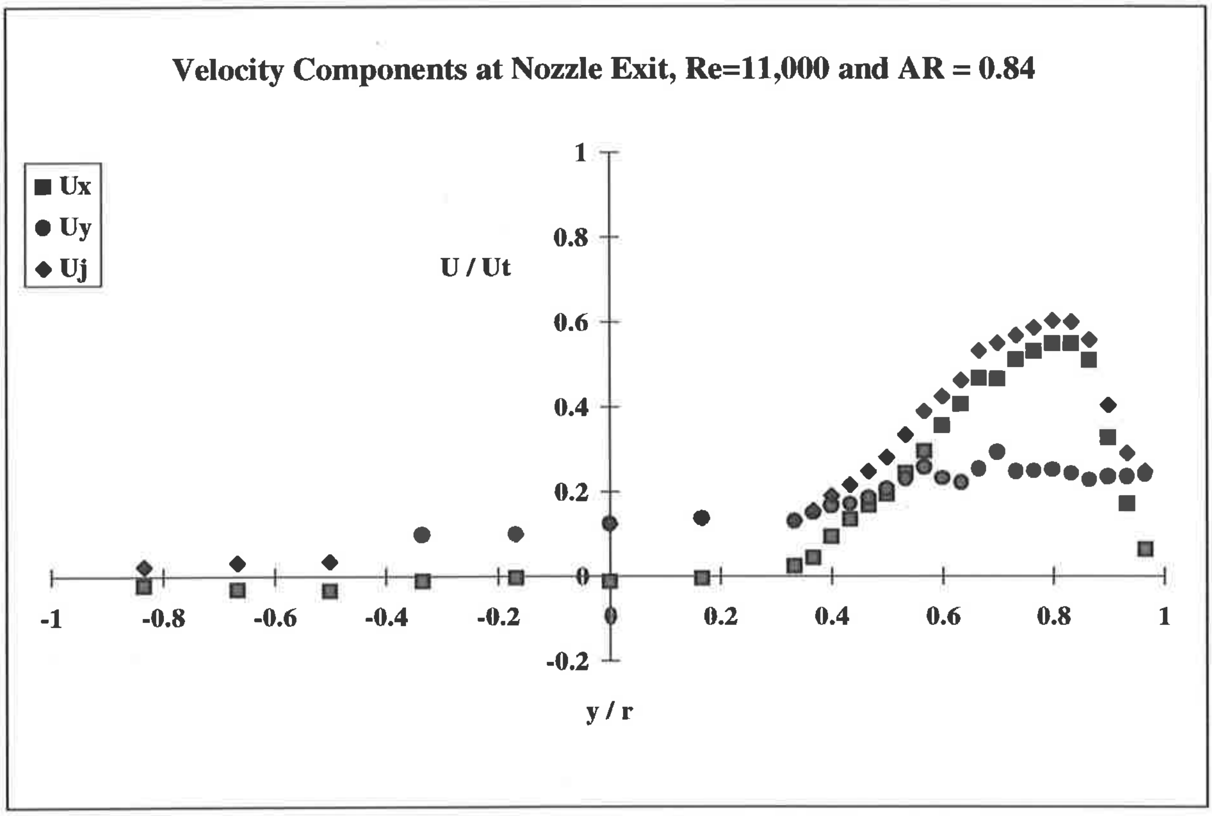

Figure 4.7. 15 LDV velocity vectors at the CD nozzle exit at Re$_t$=11,000 and AR = 0.84.

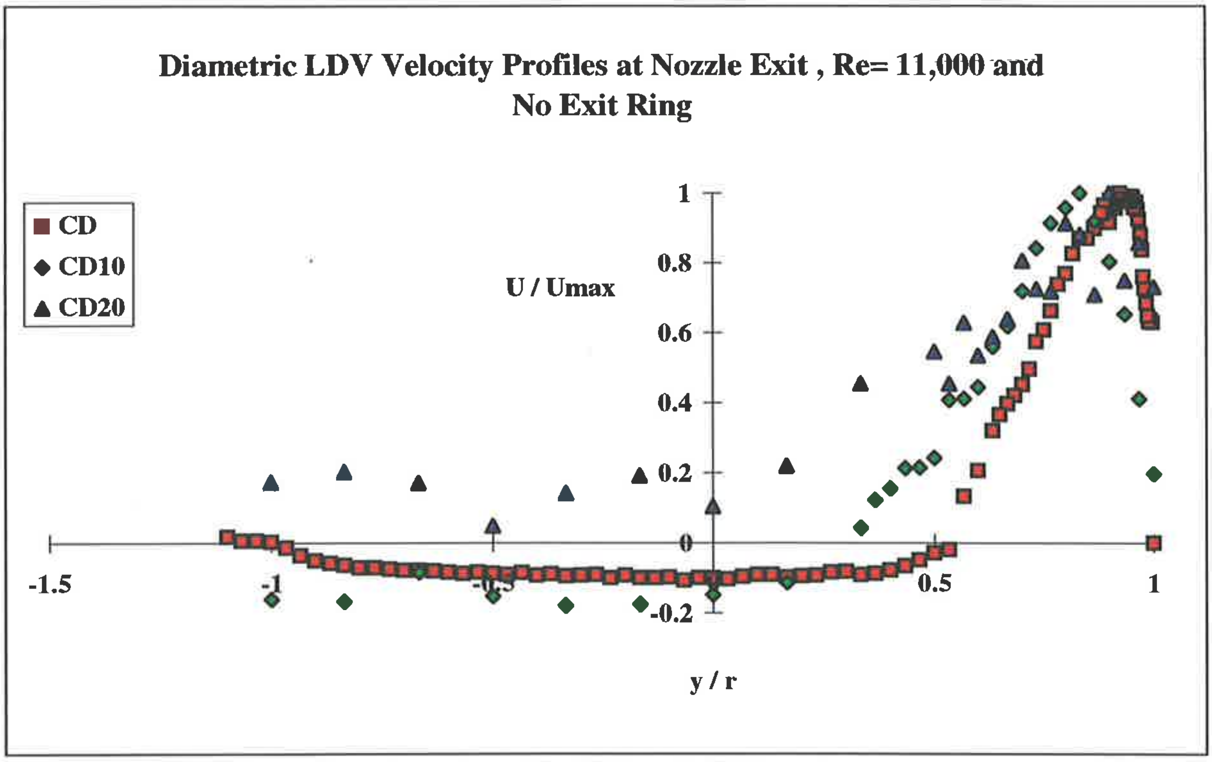

Figure 4.7. 16 LDV velocity vectors at the CD, CD10 and CD20 nozzle exit at Re_t=11,000 and no exit ring. Velocity normalised by maximum exit velocity.

4.8 Asymmetric Flow Compared with Subsonic Turbulent Jet and Plane Wall Jet Flows

In order to understand how the asymmetric jet evolves from the axisymmetric throat the axisymmetric jet and a plane wall jet velocity profiles have each been studied. The wall jets considered in this comparative study had aspect ratios 6.3 : 1 (63mm x 10mm) and 25 : 1 (126mm x 5mm) rectangular cross-sections. The axisymmetric jet analysed was from a convergent 10 mm diameter nozzle expanding abruptly into the atmosphere. The other jets included for comparison are axisymmetric and asymmetric jets exiting the CD nozzle. The convergent nozzle has the same contraction ratio as the CD nozzle. The two wall jets have the same exit areas which is 8 times the CD nozzle throat area.

The asymmetric flow in the CD nozzle develops downstream from the throat, starting as an axisymmetric jet. There are some similarities between the axisymmetric jet from the convergent nozzle and the asymmetric flow which exits from the CD throat of the nozzle. These are discussed later. The asymmetric flow derived from the axisymmetric throat of the nozzle forms a wall jet characteristic velocity profile of which at the nozzle exit resembles a plane wall jet flow. It was therefore decided to undertake a brief study of the plane wall jet, and in particular, the effects of placing an obstruction, or gate, at a distance from a two-dimensional origin of the plane wall jet. A parametric study of the effects of gate height on the jet deflection angle yielded the results presented below which are compared with the jet deflection angles caused by the lip at the exit of the CD family of nozzles. The similarities between the three flows are discussed in some detail and the effect of the gate height on the response of the wall jet characterised. The experimental evidence is presented in the following section. The velocity profiles in the 2-D flow were first measured to establish the similarities between the flow profiles and the flow inside the test nozzles. The effect of varying either or both of the gate height and the distance from the jet exit is then discussed.

4.8.1 Axisymmetric Jet

The axisymmetric jet exiting from both a convergent 10 mm diameter nozzle and the CD nozzle was analysed in detail by measuring the velocity profiles and turbulence characteristics of each at various distances downstream from the throat. The flow characteristics of such flows are well documented, Schlichting (1955), and it is well known that the flow becomes self-similar about six throat diameters from the origin. The turbulence structures of round jets have been explored by many researchers using multiple hot-wire **anemometry [62,76,91,142,325]**, microphones **[159]**, laser Doppler velocimetry and planer laser induced fluorescence **[63]**. The self similarity in the free axisymmetric jets is also established at a distance of about six throat diameters and the turbulence levels are of the same order of magnitude. The present results for the jet from the convergent nozzle agree well with the published data, **[74,254]**. The shear layer develops from the exit plane and grows in a streamwise direction. The potential core is clearly observed and the centre line velocity is constant up to six throat diameters after which the self similarity is observed. Schlichting has shown that the self similarity is sustained in both two-dimensional and axisymmetric jets as well as in two-dimensional wakes behind circular cylinders. The self similarity was observed in the velocity distribution measurements carried out on both the axisymmetric convergent and the convergent-divergent nozzles, as well as in the plane two-dimensional jet. The velocity distribution in an axisymmetric jet and plane jet in **Figure 4.8. 1** correlate well with the results produced in Schlichting (1955)(in figures 2.37 and 2.38).

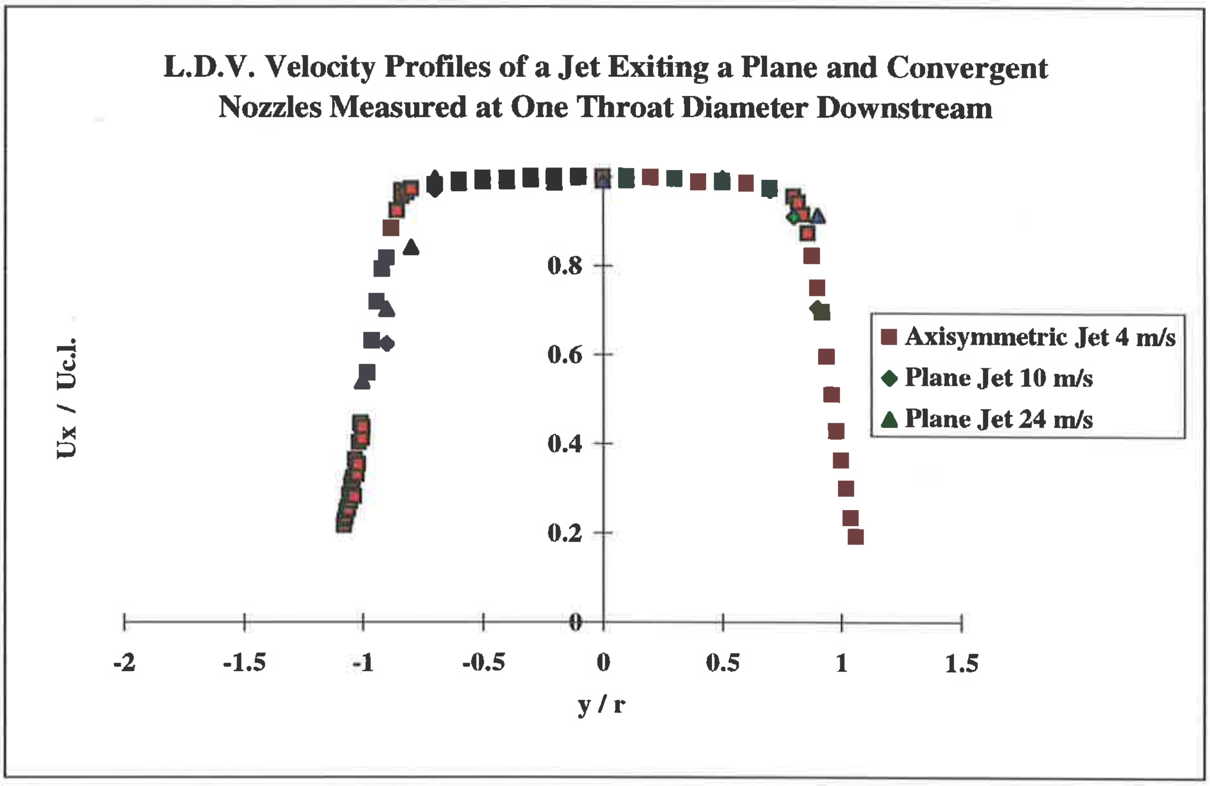

Figure 4.8. 1 Axisymmetric and Plane jet velocity profiles at the nozzle exit traversed in the plane of jet symmetry for $Re_t = 2,700$.

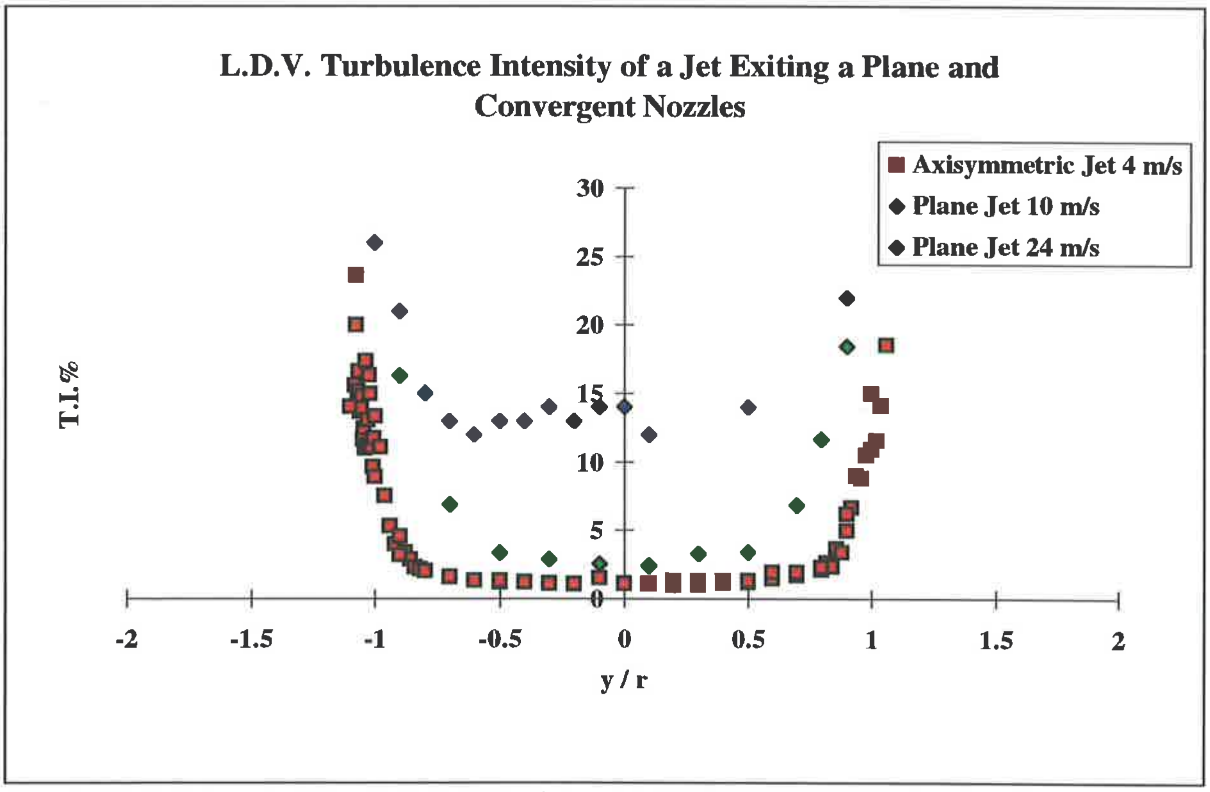

Figure 4.8. 2 Axisymmetric and Plane jet turbulence intensity profiles at the nozzle exit traversed in the plane of jet symmetry for $Re_t = 2,700$.

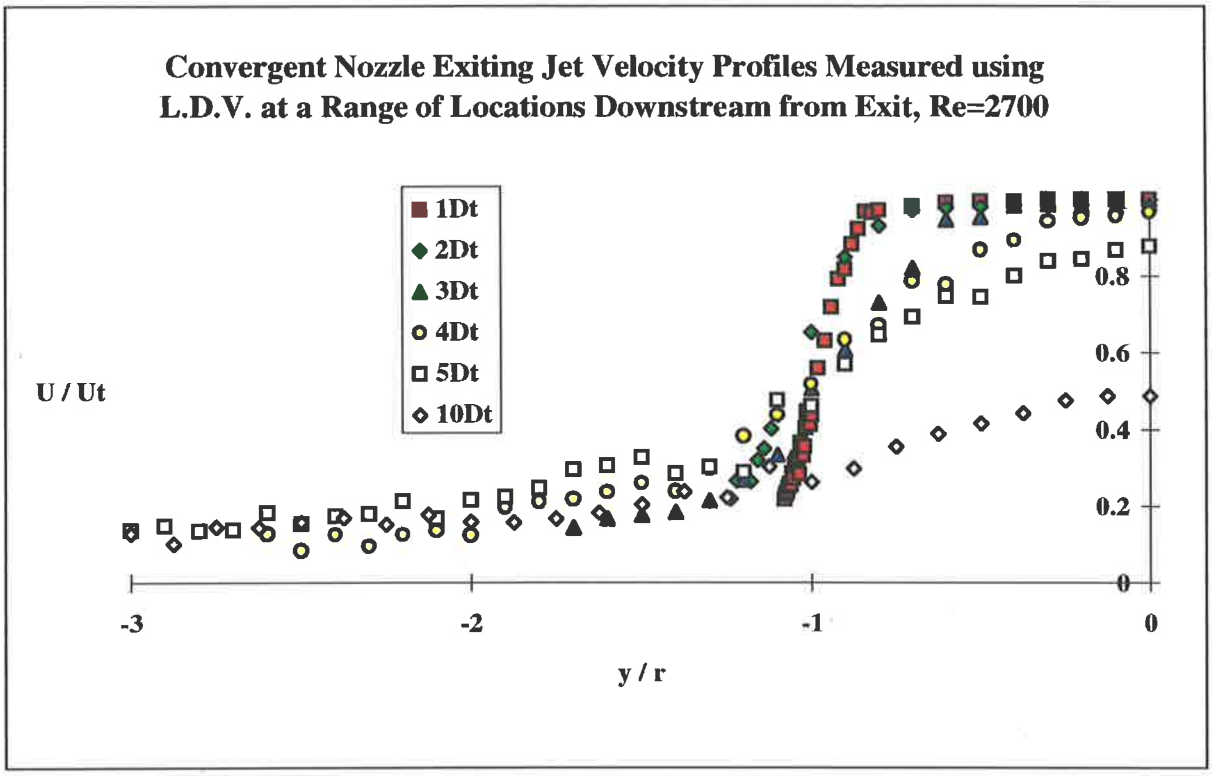

Figure 4.8. 3 Axisymmetric jet velocity profiles at the nozzle exit measured at a range of locations downstream from the throat in the plane of jet symmetry, Re_t = 2,700 and no exit ring.

4.8.1.1 Velocity

A large number of measurements using pitot-static pressure, hot-wire anemometry and LDV have been taken to characterise the axisymmetric flow from the convergent and the CD nozzle. The velocity profiles measured at first 10 diameters downstream of a convergent nozzle exit are shown in **Figure 4.8. 3** and the self similarity is established beyond six D_t. The turbulent intensity increases at the shear layer as shown in **Figure 4.8. 2** and indicates the region of mixing between the primary flow and ambient. The velocities measured using the three methods correlate well and the LDV measurements were used to build confidence in measuring the velocity profiles in a well established and thoroughly documented flow.

4.8.1.2 Flow visualisation

A number of flow visualisation techniques were used to determine the spreading angle of the axisymmetric and asymmetric jet. The most useful method was the laser sheet flow visualisation. **Figure 4.3. 2** in Section 4.3.2.2 shows that the spreading half angle of the axisymmetric jet is approximately 10°. This compares well with the measured spreading angle determined using velocity profiles **Figure 4.3. 3** reveals that the spreading angle of the asymmetric jet is around 20° on the previously "attached" side of the jet and between 20° and 30° on the previously "free" side of the jet, depending on which origin is used, see earlier discussion.

4.8.2 Two-Dimensional Plane Wall Jet

4.8.2.1 Introduction

Jets from two plane nozzles, one with an outlet 10mm high and 63mm wide and the other 5mm high and 125mm wide, shown in **Figure 2.1. 6** have been investigated first by measuring LDV velocity profiles at various distances downstream from the exit and secondly by laser sheet flow visualisation shown in **Figure 4.8. 9**. The nozzles have a smooth contraction with upstream settling screens. A flat plate aligned with the bottom edge of each of the exits from the plane nozzles was then introduced to produce a wall jet, the velocity profiles of which were measured downstream from each of the exits. When a gate of variable height is placed in the flow at a distance from the wall jet exit, the jet is deflected at an angle with a spread of up to 10°. The deflection angles produced by gates of various heights placed in each of the 2-D wall jets were measured and plotted as shown in **Figure 4.8. 8**. These results are compared with the results of deflected jet angles for the CD, CD6, CD10 and CD20 nozzles in **Figure 4.8. 4** .

The laser sheet flow visualisation revealed that, for the particular configurations shown in **Figure 4.8. 10** , the ambient fluid is induced into the 2-D cavity marked by the dark areas inside the cavity, similar to the results discussed in Chapter 4.

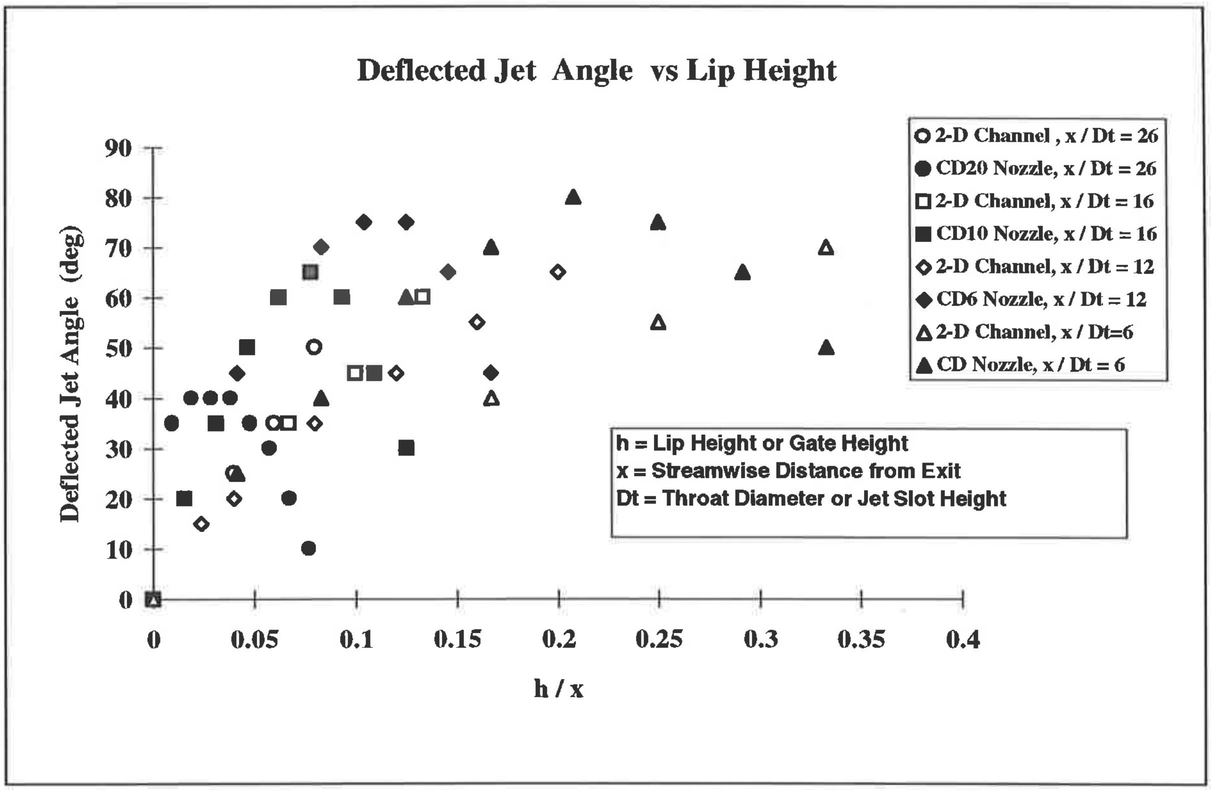

Figure 4.8. 4 Comparison of deflected jet angles produced by 2-Dimensional wall jet over a gate and CD, CD6, CD10 and CD20 nozzles.

4.8.2.2 Apparatus

Two wall jet nozzles were used in this investigation as described above. The first was a 63 mm wide and 10 mm high and the second, 125 mm wide and 5 mm high. Both of these wall jets were evaluated for a range of mass flow rates and gate heights using the LDV to measure the velocity vectors. From these data the deflection angle of the jet was calculated and compared with qualitative tuft observations. The same apparatus was used as for the evaluation of the CD nozzle. **Figure 4.8. 9** shows a deflected 2-dimensional wall jet flow, visualised by laser sheet, exiting one of the nozzle configurations.

4.8.2.3 LDV Velocity Profiles and Deflected Jet Angles

The velocity profiles of the wall jets were measured downstream from the nozzle exit using 2 component LDV and a sample of results for Re_t=1600 are shown in **Figure 4.8. 5**. The velocity at the jet exit has the standard top hat profile. At three slot heights downstream from the exit, the shear layer on the free side of the jet increases noticeably. By six slot heights, the potential core no longer exists and the jet has spread outwards away from the surface. At ten nozzle heights down stream from the exit, the wall jet centre line velocity has decayed to 0.8 of the exit velocity and the velocity decreases away from the surface. The turbulence intensities associated with the flow are shown in **Figure 4.8. 6** which indicates the amount of mixing at the shear layer and the boundary layer in the wall jet. The flow is initially a low turbulence flow of less than 5% and at 10 slot heights downstream, the turbulence increases to above 15%. When a gate is placed in the flow, it deflects the flow to a degree which is determined by the height of the gate and the axial position from the exit. The velocity profiles also change with the introduction of a gate as shown in **Figure 4.8. 7**. The flow over a gate, with a gate height to slot height $(h / t) = 0.5$ is seen as a mild form of deflection and produces downstream a jet deflected at an angle of the order of $\alpha = 20°$, which was measured using a tuft placed in the flow, and the velocity profile does not change significantly across the jet width. When the $(h / t) = 1$, the deflected jet angle increases to a value of $\alpha = 35°$ and the jet centre line velocity is reduced. The same trend is observed for $(h / t) = 1.5$, which causes the jet to deflect to an angle of $\alpha = 50°$. The velocity profile shows the reduction of jet centre line velocity due to its directional change. The deflected jet angles for the wall jet over a range of gate heights at a range of axial distances are summarised in **Figure 4.8. 8**. These deflected jet angles were measured using both a tuft placed into the flow and laser sheet flow visualisation. Both of these methods correlate well with the results presented in **Figure 4.8. 8**.

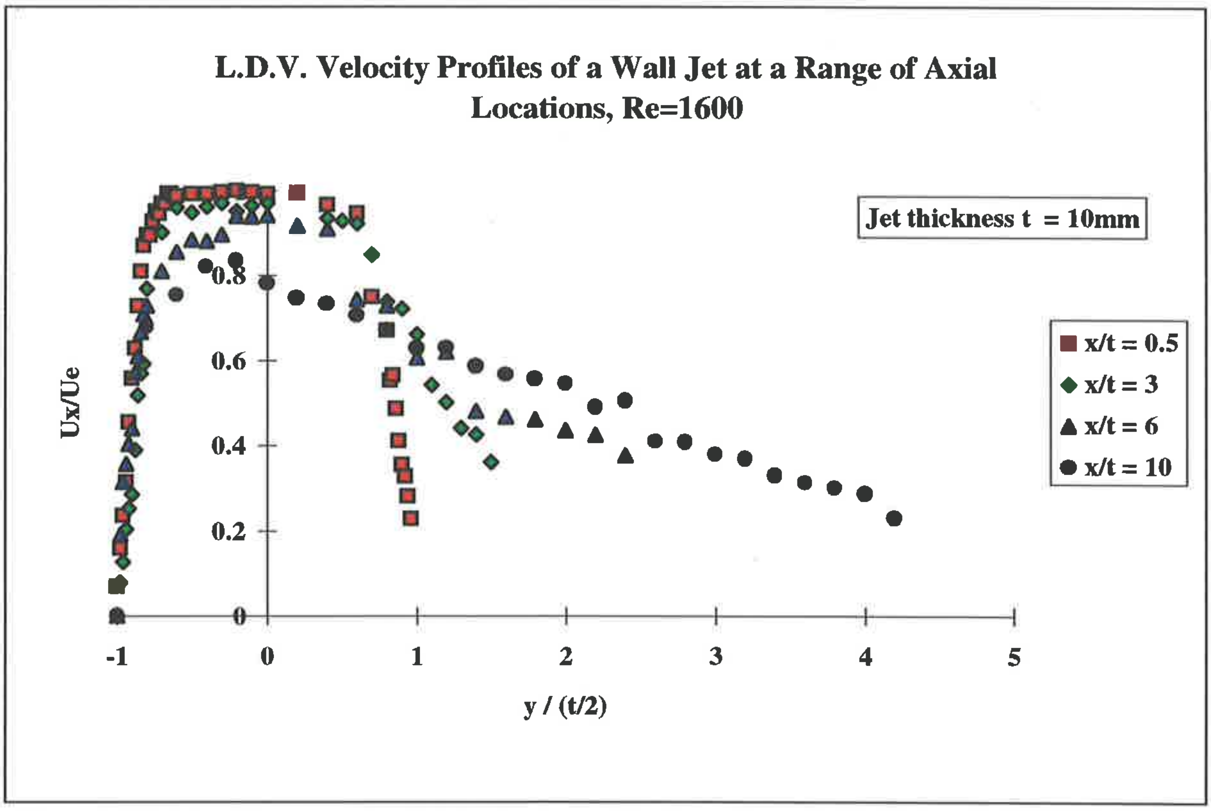

Figure 4.8. 5 Two-dimensional wall jet velocity profiles downstream from the nozzle exit using LDV.

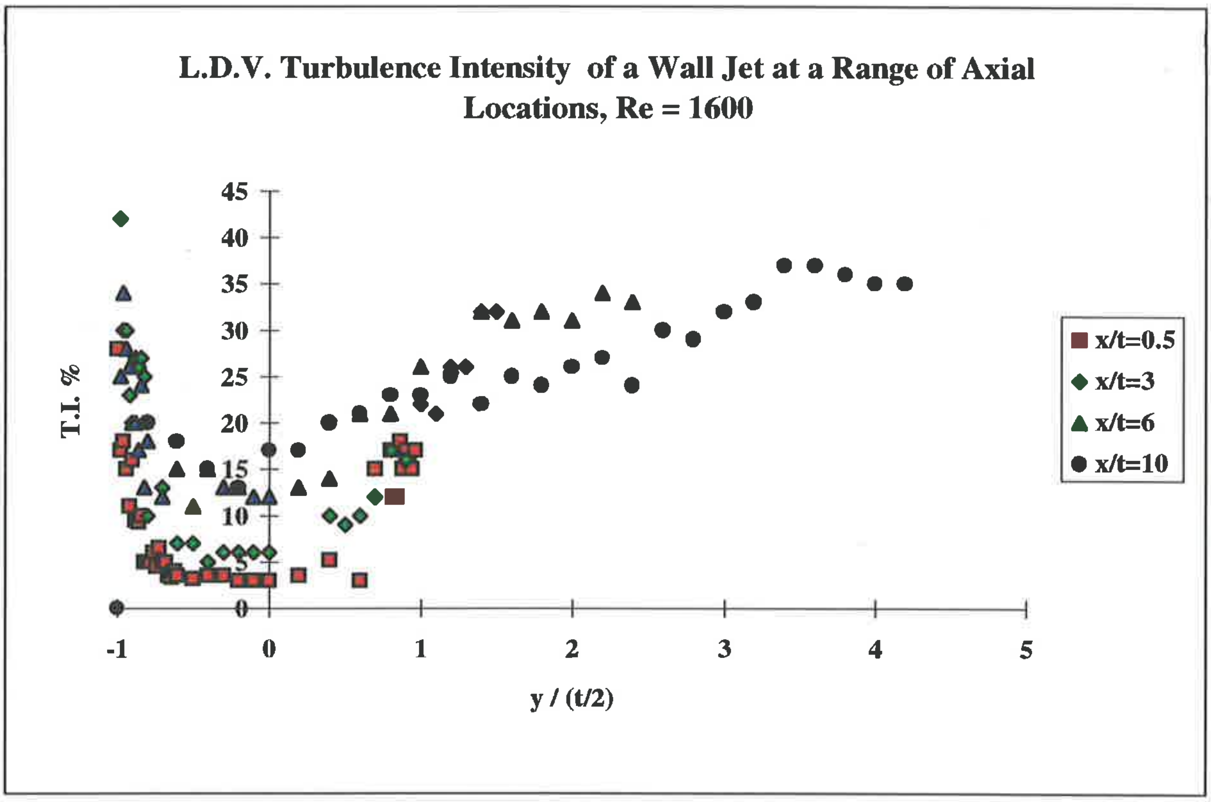

Figure 4.8. 6 Two-dimensional wall jet turbulence intensity profiles downstream from the nozzle exit using LDV.

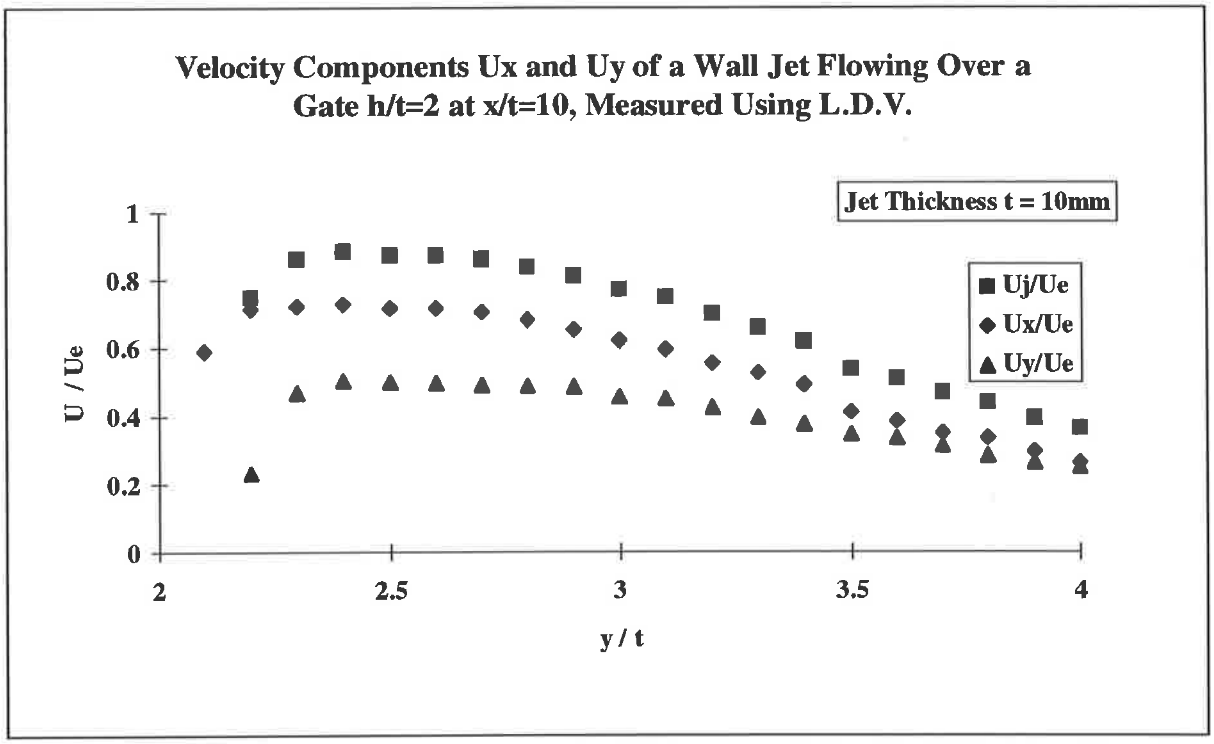

Figure 4.8. 7 Velocity profiles of a 2-dimensional wall jet over a gate measured using a 2 component velocity vector.The angle of a deflected wall jet at the gate was measured to be between 35° and 45°.

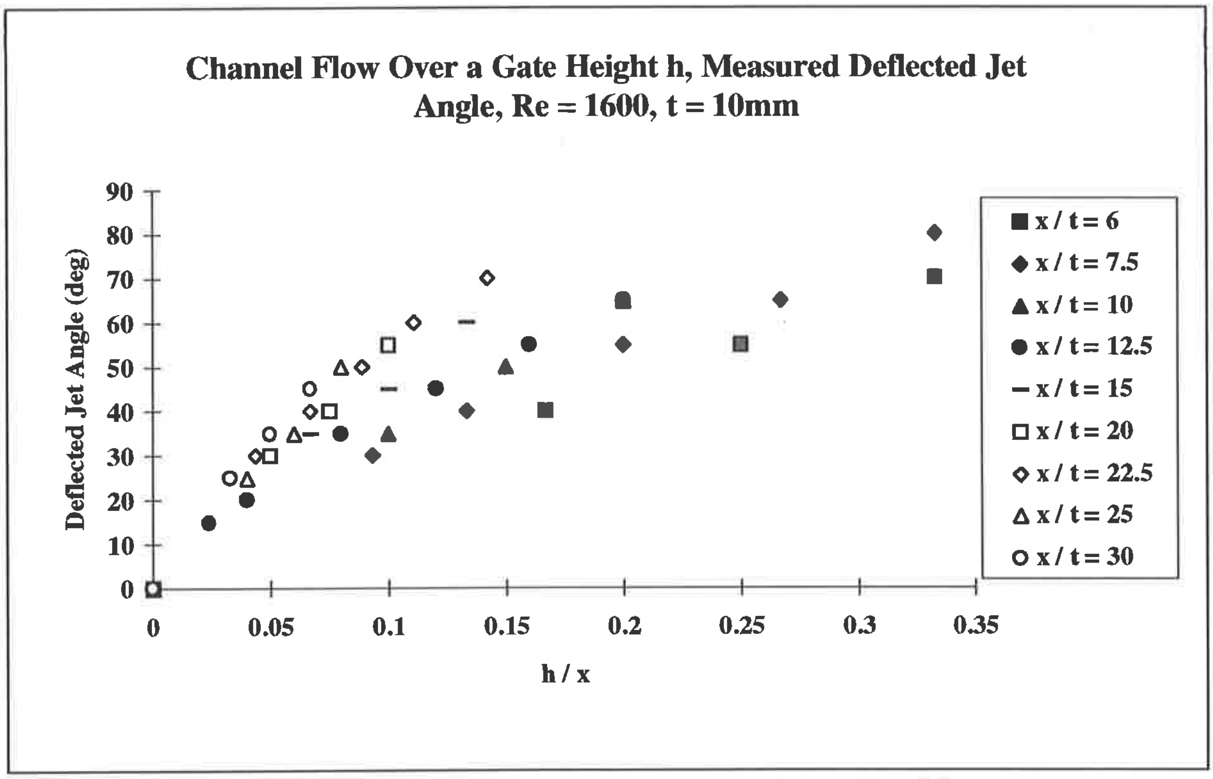

Figure 4.8. 8 Summary of two-dimensional deflected jet angles produced by a gate at a range locations downstream from the nozzle slot, measured using a tuft.

4.8.2.4 Flow visualisation

The flow visualisation using laser sheet photography has been discussed earlier in this Chapter. The flow features revealed using this method of measurement can be seen in **Figure 4.8. 9** and **Figure 4.8. 10.** Both show the angle at which the jet is deflected and in the later figure, the effects of the lid to restrict the amount of ambient fluid for a particular gate height can be clearly seen. A preliminary investigation of the effects of upper gate described in **Figure 2.1. 6 (c)** has been carried out. The results show that at Re_t=200,000, for the lower gate height of 5mm without the lid produces a deflection $\alpha = 20°$ to 35°, with the lid in place $\alpha = 45°$ to 50°. When the upper gate of 10mm is included at the exit plane, the jet is deflected at an angle $\alpha = 60°$. If the upper gate height is increased to 20mm, the jet deflected at an angle of $\alpha = 45°$. These results shows that the reduction in exit area, even in 2-dimensional channel flow, causes an increases in the angle at which the jet deflects at. As the exit area is reduced further, the angle at which the jet is deflected is reduced. This agrees with the postulate that was presented earlier for the CD family of nozzles.

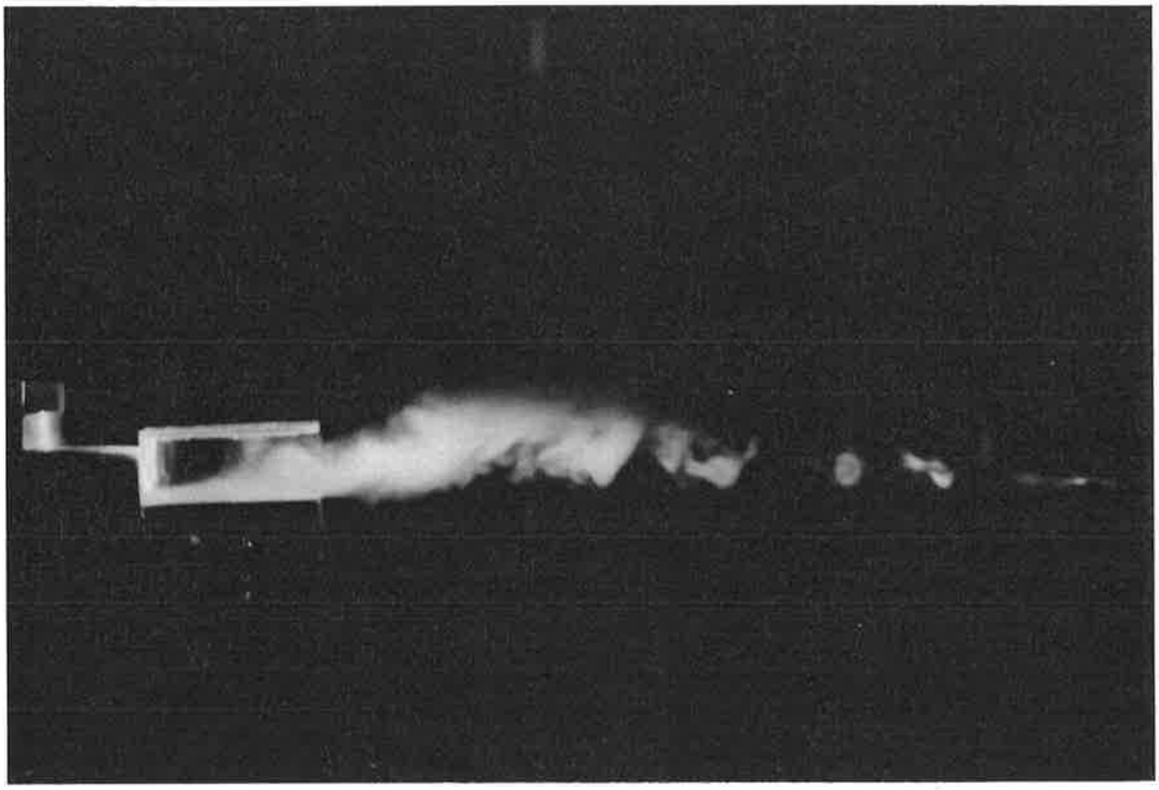

Figure 4.8. 9 Two-dimensional seeded jet deflected at $\alpha = 20°$ to 35° over a gate h = 5mm, without a lid and Re_t=200,000, visualised using a laser sheet.

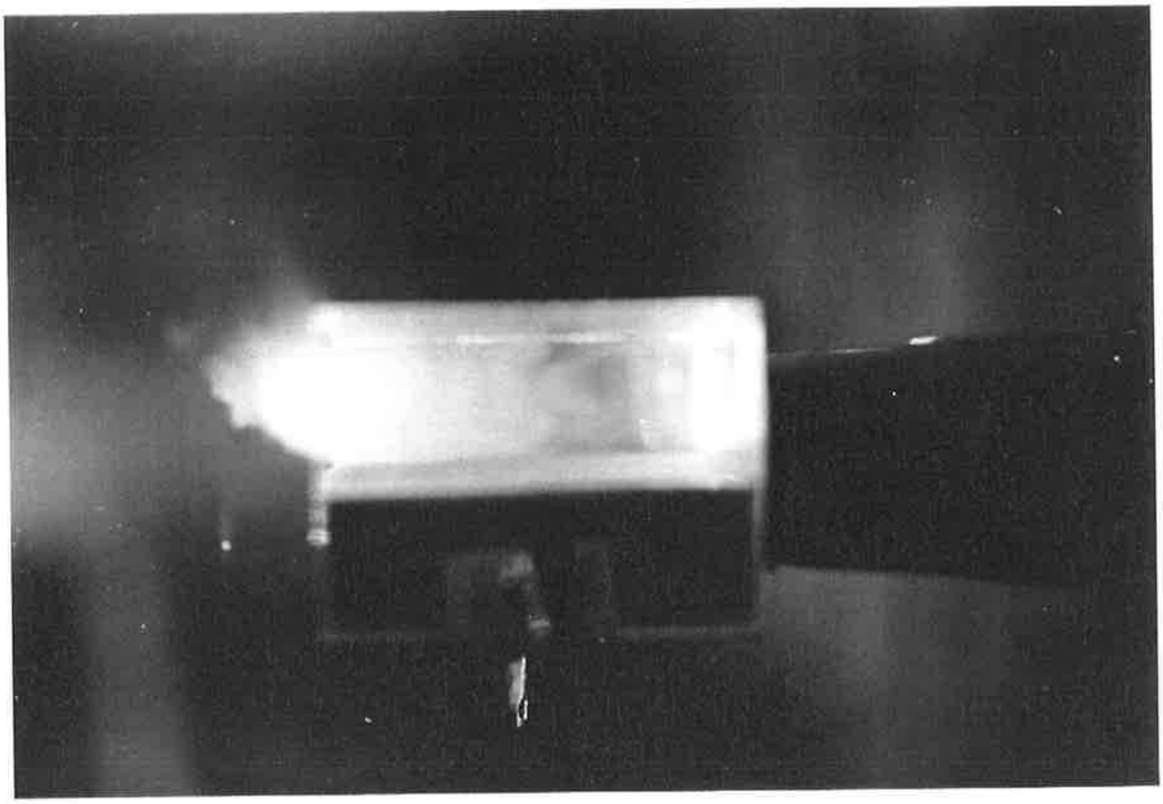

Figure 4.8. 10. Two-dimensional seeded jet deflected at $\alpha = 60°$ over a gate $h_l = 5mm$ and a lid with an upper gate $h_u = 10mm$, $Re_t = 200,000$, visualised without the laser sheet.

4.8.3 Other Nozzles

Other nozzles tested were, RP45 and RP60, the rectangular deflector plates at the exit of the convergent nozzle inclined at 45° and 60° respectively. The velocity profiles at the edge of the rectangular plate for each configuration were measured to compare with the velocity profiles of the CD and CD10 nozzles. The momentum flux has been calculated using these profiles and compared with the measured thrust using the strain gauge arrangement at the root of the supply tube as described in Chapter 2. The schematic of the nozzle configurations is shown in **Figure 2.1. 3.** A typical set of velocity profiles measured using a hot-wire is shown in **Figure 5.4. 3**. Profiles are the result of traversing a hot wire across the jet at the edge of the 45° deflector plate at 5mm intervals parallel to the plane of symmetry. The centreline velocity of the jet at 10 throat diameters downstream from the throat is 0.45 U_t compared to 0.23 U_t at the CD10 nozzle exit , **Figure 3.1. 3,** and 0.5 U_t at the CD nozzle exit shown in **Figure 4.7. 6.** The velocity profiles at the edge of the RP60 are somewhat lower but have similar shape to the RP45 profiles.

The velocity profiles at the exit of the B45 and B90 are very similar to the velocity profiles measured at the exit of the convergent nozzle shown in **Figure 4.7. 3.**

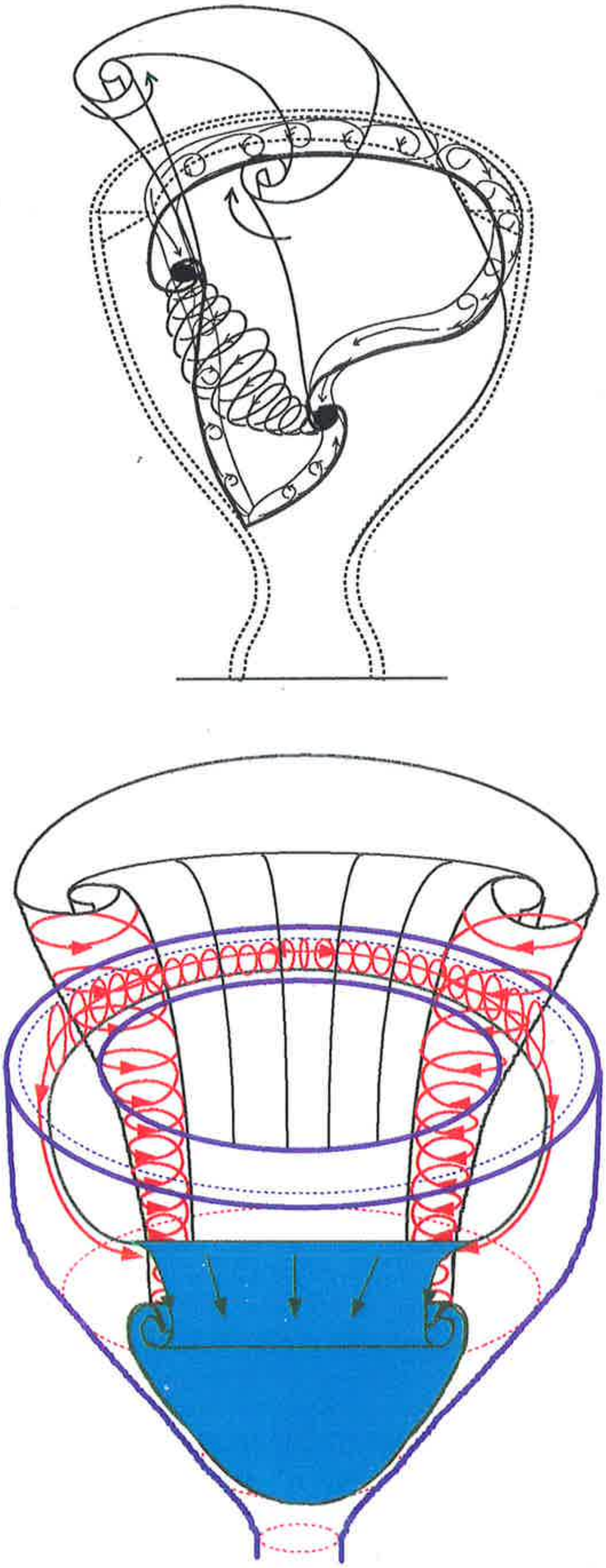

Figure 4.8. 11 Schematic of the postulated vortex system inside the CD nozzle with a moderate lip at the exit causing the wall jet to deflect.

4.9 Conclusions

The flow mechanism inside the CD nozzle has been presented in detail using flow visualisation, pressure profiles and velocity profiles. The flow inside the nozzle may be explained in terms of two-dimensional flow and the effects of exit area ratio has been characterised. The deflection angle of the jet has been characterised in terms of the lip height, lip axial distance from the throat and the wall jet thickness at the exit. It has been established that the deflected jet angle for the CD nozzle could reach 80 ° at an exit area ratio of 0.34. This however coincides with a lower velocity and a lower thrust as will be shown in the Section 6.

The wall jet shows a remarkable resemblance to the asymmetric jet profile inside and just outside the CD nozzle and therefore the comparison between the wall jet deflected over a gate and the jet deflected by an exit ring in the CD nozzle is justified. The deflected jet angles in the two cases increase with increasing *h/l,* the ratio of gate height to gate distance from the exit. For the range tested, the angle at which the 2-D wall jet is deflected is shown to increase as the height of the gate at a given distance from the wall jet exit increases. For the CD nozzle, on the other hand, the jet deflection angle reaches a maximum and then reduces with further increase in lip height. When the effects of lip height, exiting jet thickness and distance of lip from the exiting jet are considered, the major difference is that the CD nozzle deflects the jet more effectively for a given set of parameters. It is postulated that the efficient deflection of the wall jet at the exit of the CD nozzle is due to a combination of deflection due to the lip and the radial pressure gradient produced by a strong vortex loop inside the CD nozzle, just upstream from the exit lip. The vortex loop stretches across the exit diameter and joins the two foci described in this section. The addition of a larger lip produces a stronger vortex and hence a stronger radial pressure gradient resulting in a larger deflection of the exiting jet. The maximum deflection is reached when a balance between the radial pressure gradient and the exiting flow momentum is reached. Therefore the difference between the 2-D wall jet deflection angle and the CD nozzle deflection angle can be attributed to the vortex strength inside the cavity, which, it is postulated, is due to the counter-current flow of the ambient fluid which is induced into the nozzle and the primary jet which feeds into the vortex loop via a vortex loop which forms behind the lip on the wall jet side. Interpretation of the deduced complex vortex system inside the nozzle is presented in **Figure 4.8. 11**.

CHAPTER 5

CD10 and CD20 Nozzles and Their Flow Mechanisms

The basic flows in the CD10 and CD20 nozzles are initially similar to the flow found in the CD nozzle. As the length of the cavity increases, as in the case of CD10 and CD20 nozzles, the flow near the throat changes very little. Further downstream within the nozzle, significant changes take place and by the nozzle exit there has been a substantial azimuthal spread of the jet in the CD10 and very substantial spread in the CD20 nozzle, as will be shown by measurement of the velocity profiles and pressures inside the nozzle. The flow exiting from the CD20 nozzle occupies the whole nozzle exit area most of the time, and ambient fluid only induced into the nozzle intermittently for short periods. The characteristic feature of the flow inside the longer nozzles is the recirculation of the primary fluid back into the nozzle and this first reduces and finally excludes the ambient fluid from being induced. Two effects on the flow are evident. First, the primary flow diffuses more inside the long nozzle and this reduces the amount of thrust that the nozzle produces. Secondly, the fluid momentum is distributed across a larger cross-sectional area. When a lip is placed at the nozzle exit, the jet is deflected to a lesser degree than is the flow from the CD10 nozzle alone, as will be shown in this Chapter.

5.1 A Characteristic Description of the Generated Flow Patterns Inside and Outside the Nozzles

The existence of a cavity extension generates a number of distinct flow features inside the nozzle. The initial fully axisymmetric flow separation just downstream from the throat at low mass flow rates was observed when oil was injected at the throat to identify the separation surface. The laser sheet flow visualisation confirmed that the flow was axisymmetric, as expected. As the flow rate was increased, the separation became asymmetric and the jet reattached itself to one side of the wall with a partial azimuthal separation downstream from the throat. The asymmetric flow continues to entrain fluid as it progresses downstream and increases in cross sectional area. At the exit of the CD10 nozzle, the wall jet occupies about half the exit area and in the CD20 nozzle exit, the wall jet diffuses significantly to occupy almost the whole of the exit area. Only at low flow rates was it observed that the ambient fluid was occasionally entrained. When a laser sheet was introduced diametrically in the plane of symmetry the flow pattern inside the nozzle showed that the expanding wall jet was generating a recirculation of the primary fluid. When the exit area was reduced by placing an exit ring at the nozzle exit, the flow inside the nozzle intensified due to an increased amount of primary fluid being forced to recirculate back into the nozzle. This was revealed in the oil surface flow visualisation experiments. The flow exiting the nozzle, through the reduced exit area was deflected across the nozzle axis by the exit lip and by the vortex loop, as described in Chapter 4. The degree of deflection was determined by the length of the nozzle and the exit lip height. The flow downstream from the nozzle exit leaves the nozzle at an angle and settles into what seems to be a self similar jet. The velocity profiles exiting the CD20 nozzle were measured only for several configurations due to the extremely unsteady behaviour. It was felt that this geometric configuration was very unlikely to be used for thrust control due to its low thrust vectoring efficiency and that analysis using flow visualisation was sufficient.

The CD10, on the other hand, was the first nozzle configuration evaluated and a large proportion of time was invested on this nozzle. It was not until the nozzle length was varied that it was realised that the CD nozzle was the more efficient nozzle by which to vector thrust. By this time a substantial data set, relating to the CD10 nozzle flow, such as surface flow and laser sheet flow visualisation, pressure, velocity and thrust measurements, had been assembled of which only a representative number of results is presented in this thesis.

5.2 Total and Static Pressure Profiles

A number of total and static pressure profiles have been measured inside and outside the CD10 nozzle. The static pressure outside the nozzle is assumed to be atmospheric for the calculation of the dynamic pressure, and hence of the velocity. The static pressure inside the CD10 nozzle was measured along the nozzle wall and circumferentially at an axial distance of 10 throat diameters as indicated in **Figure 1.1.**. Due to the poor thrust vectoring performance it was decided not to do a detail study on the CD20 nozzle hence no pressure or velocity data are presented for that nozzle. The CD10 nozzle however showed promise when thrust vectoring efficiency was measured and it was deemed worth examining in detail, particularly because the transparent cavity allowed extensive flow visualisation to be implemented, therefore only the CD10 pressure details are presented in this Section.

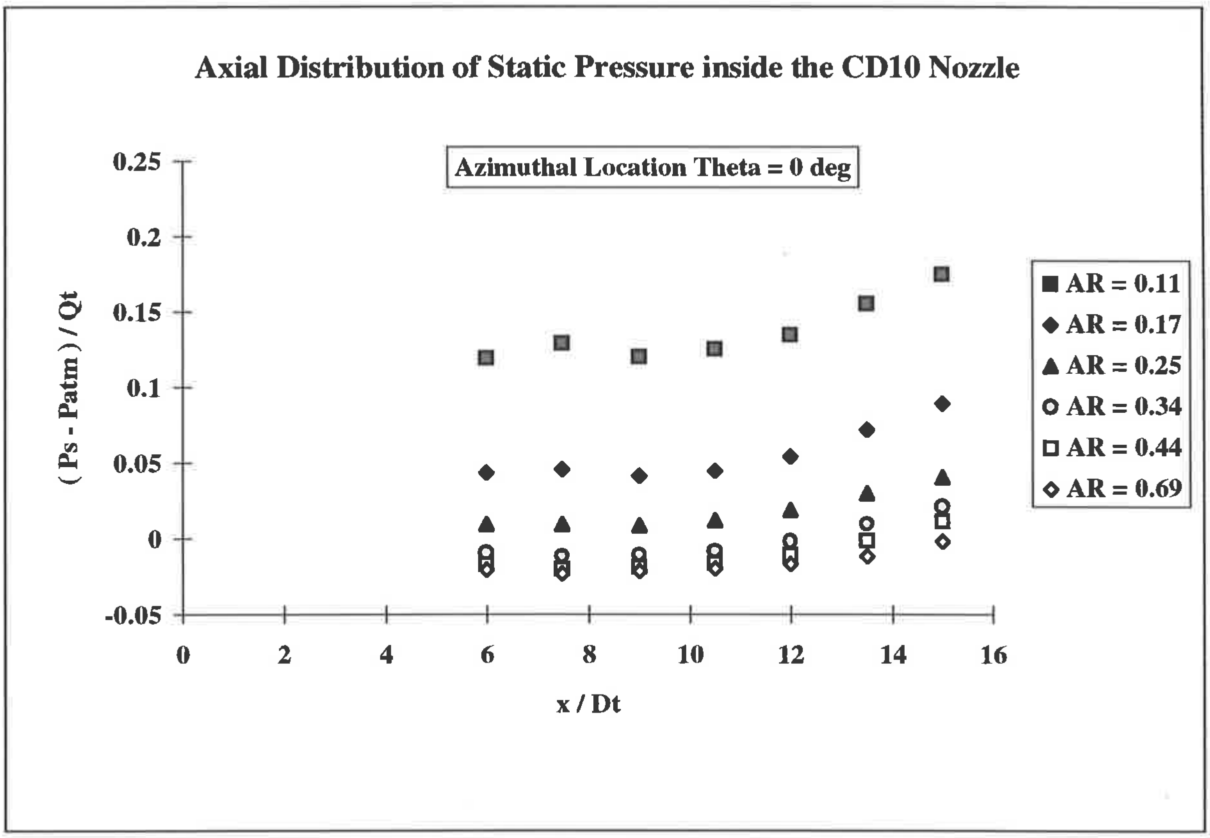

Figure 5.2. 1 CD 10 nozzle axial distribution of pressure along the sector of the cavity wall that is opposite from the azimuthal position at θ=0° relative to the secondary fluid injection position.

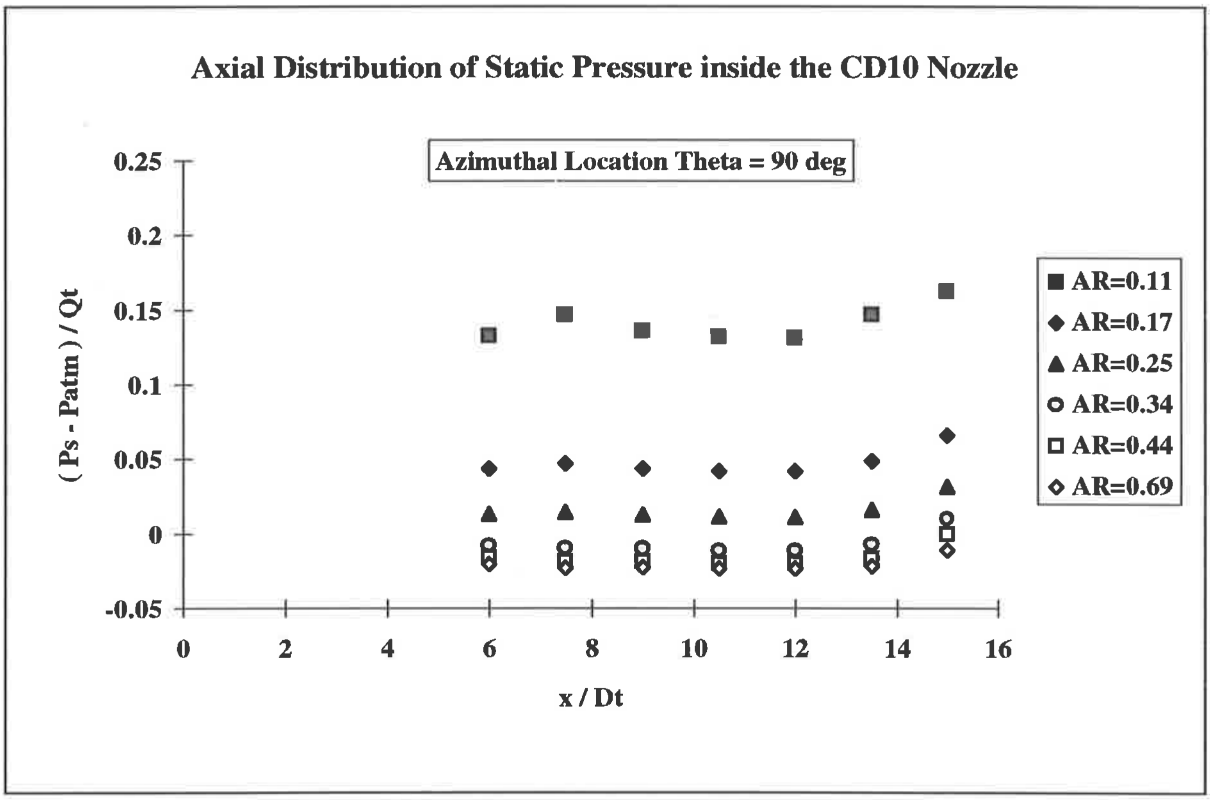

Figure 5.2. 2 CD10 nozzle axial distribution of pressure along the sector of the cavity wall that is at the azimuthal position at θ=90°relative to the secondary fluid injection position.

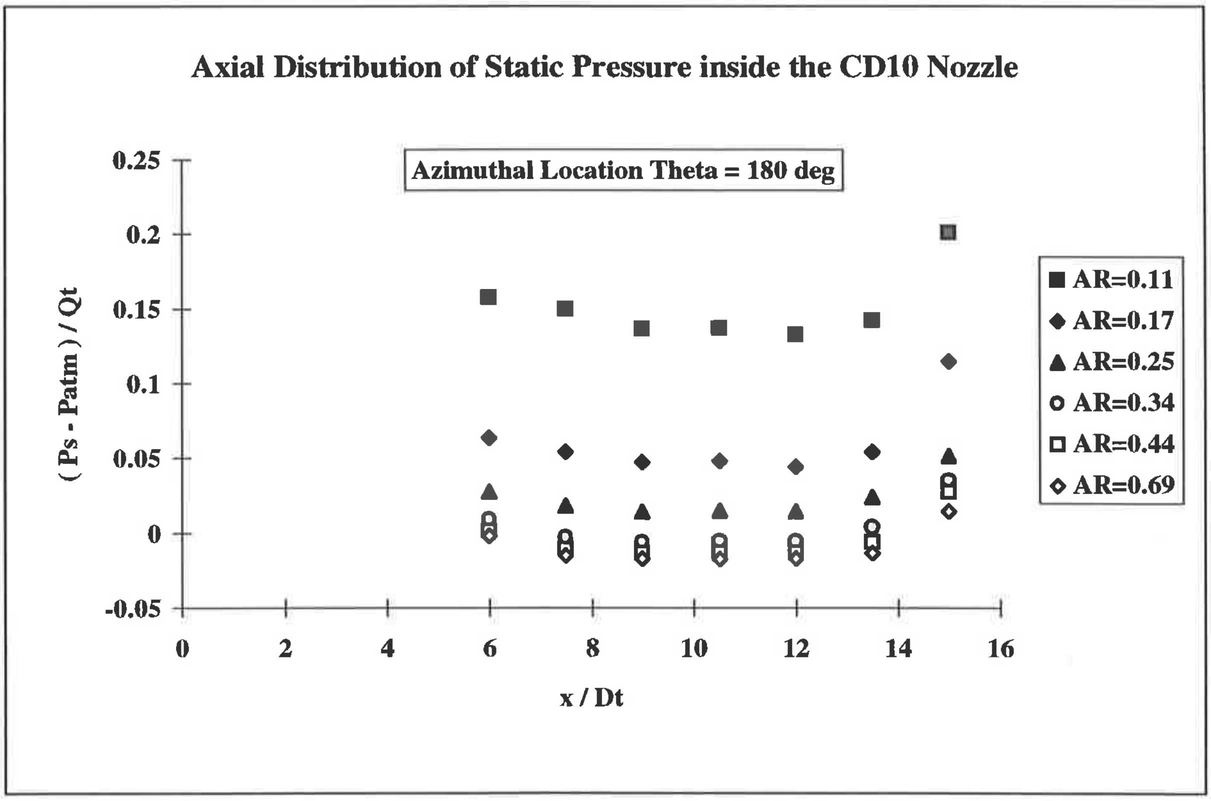

Figure 5.2. 3 CD10 nozzle axial distribution of pressure along the sector of the cavity wall that has the wall jet attached.

5.2.1 CD10 Nozzle Static Pressure

Static pressures have been measured at seven axial positions inside the CD10 nozzle. The wall pressure tappings are 1mm ID and are spaced at 15mm intervals with the mid tapping used as a common tapping for the measurement of circumferential pressure variations. Details of these measuring positions can be found in **Figure.1.1.** The axial wall pressure in the nozzle was measured at 16 equally spaced points with pressure tappings of 1 mm ID. The pressure tappings were connected to a 16 channel differential pressure transducer, described in Section 2, via flexible 1 mm ID tubing. Data in a form of an analogue voltage signal was digitised and recorded on a personal computer data storage and analysis system. For each point measured, data was collected for periods of up to 10 seconds and the reduction and analysis of data was performed at a later time. For each exit ring attached to the CD10 nozzle exit, both axial and circumferential pressure distributions were measured. The static pressure was measured for a range of mass flow rates up to 34 x 10^{-3} kg/s. A set of results measured along the nozzle wall opposite from the wall jet for a select set of the exit rings are shown in **Figure 5.2.1** to **Figure 5.2.3.**

The first of these, **Figure 5.2.1** shows the axial pressure distributions along the sector of the cavity wall along which flows entrained ambient fluid which is induced into the nozzle. Note that this is on the opposite side from the sector occupied by the wall jet. Its azimuthal position relative to the secondary fluid injection point is θ=0°.

The obvious feature of this figure is that the pressure decreases with increase in exit area and becomes sub-atmospheric between the AR = 0.25 and AR = 0.34.

The next set of measurements, **Figure 5.2.2** , represents the flow at the azimuthal position of θ = 90°, that is, pressure near the boundary where the wall jet entrains the ambient fluid. These pressure distributions show the same trend exhibited in the previous figure indicating that streamline curvature is not a major factor in the problem except near the exit lip where the strong curvature associated with separating wall jet causes a marked transverse gradient. The negative bifurcation at the surface in the vicinity of the pressure tappings near the exit, as shown in the china-clay visualisation figures, complements these observations. **Figure 5.2.3** shows the axial distribution of pressure at the azimuthal angle of θ = 180°, that is the pressure under the wall jet. Pressure in this case is sub-atmospheric when the AR is above 0.25, which is consistent with the previous figures. All three of the above observations indicate that the nozzle pressure is sub-atmospheric at AR above 0.34 and above atmospheric at AR of less than 0.25. The sub-atmospheric pressure produces an induction of ambient fluid into the nozzle at AR above 0.34, a result of which is the enhancement of the vortex loop inside the nozzle. In turn this process increases the angle through which the jet is deflected. The opposite is true for the AR below 0.25.

As the exit area ratio is reduced to AR = 0.34, the pressure beyond six throat diameters is initially sub-atmospheric and relatively constant until the exit lip is approached. The pressure in each of these configurations, as shown in **Figure 5.2.1** to **Figure 5.2.3** , has this character. Close to the exit lip where the pressure rises considerably the flow is dominated by the impingement of the wall jet on the exit lip, the related separation from the inner surface of the nozzle and the vortex associated with the reversed flow below the stagnation line on the exit lip. For exit area ratios less than 0.25, the axial static pressure everywhere is above atmospheric indicating that there is no entrainment of ambient fluid into the nozzle. The pressure however exhibits a similar trend as in previous cases and increases near the nozzle exit due to the stagnation line at the exit lip. A set of pressure measurements along the azimuthal locations θ = 0°, 90°, 180° and 270° axis were taken for a range of mass flow rates and exit areas and are presented in **Figure 5.2.4.1 to Figure 5.2.4.11.** It appears that the axial distribution of wall static pressure is Reynolds number independent. At higher flow rates there appears to be a radial pressure difference across the wall jet and this radial pressure gradient is associated with the entrainment of the "free" boundary of the wall jet. The other interesting feature of **Figure 5.2.4.2** and **Figure 5.2.4.4.** is that at the azimuth θ = 90° and 270° the axial distribution of pressure appears to be identical suggesting symmetry of the wall jet across nozzle. On the other hand axial distribution of pressure along the wall jet is different to the distribution on the opposite side , shown in **Figure.5.2.4.1.** and **Figure 5.2.4.3.** , for azimuth θ = 0° and 180°

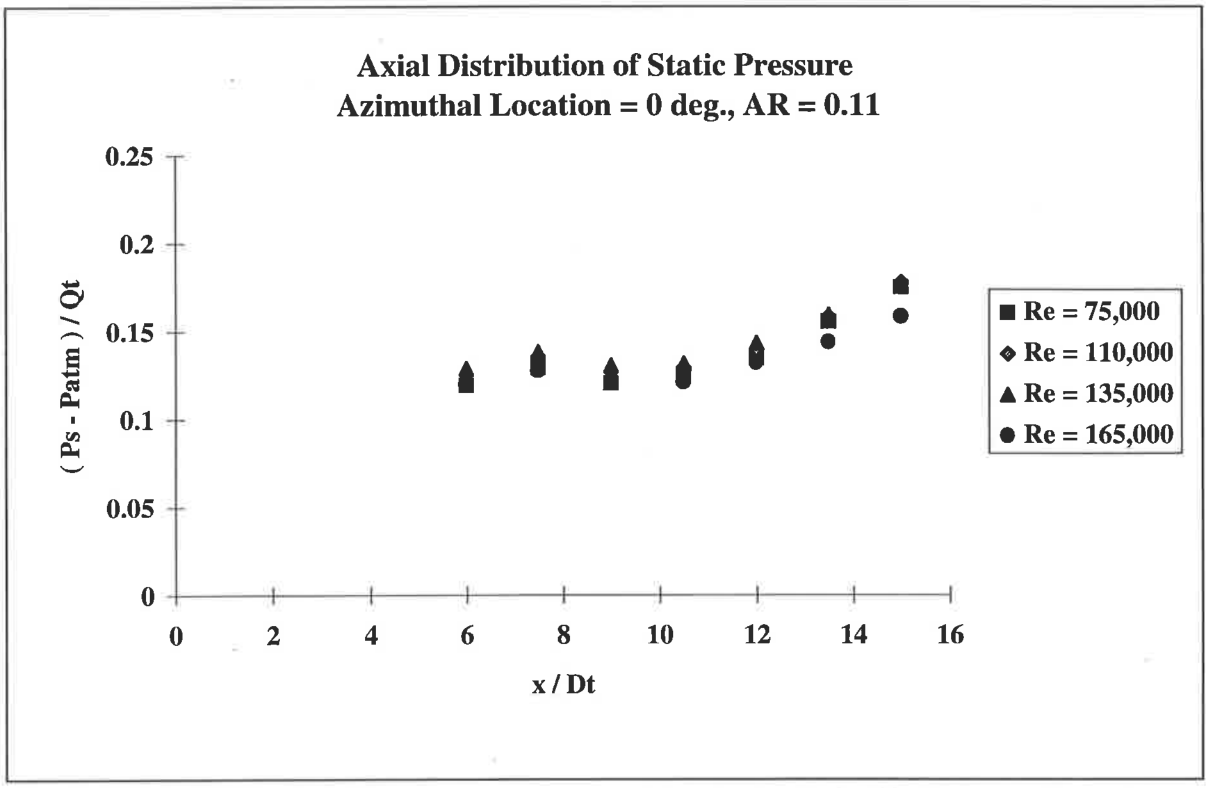

Figure 5.2.4.1 CD10 wall static pressure measured axially, at azimuth θ = 0° at a range of mass flow rates, AR = 0.11.

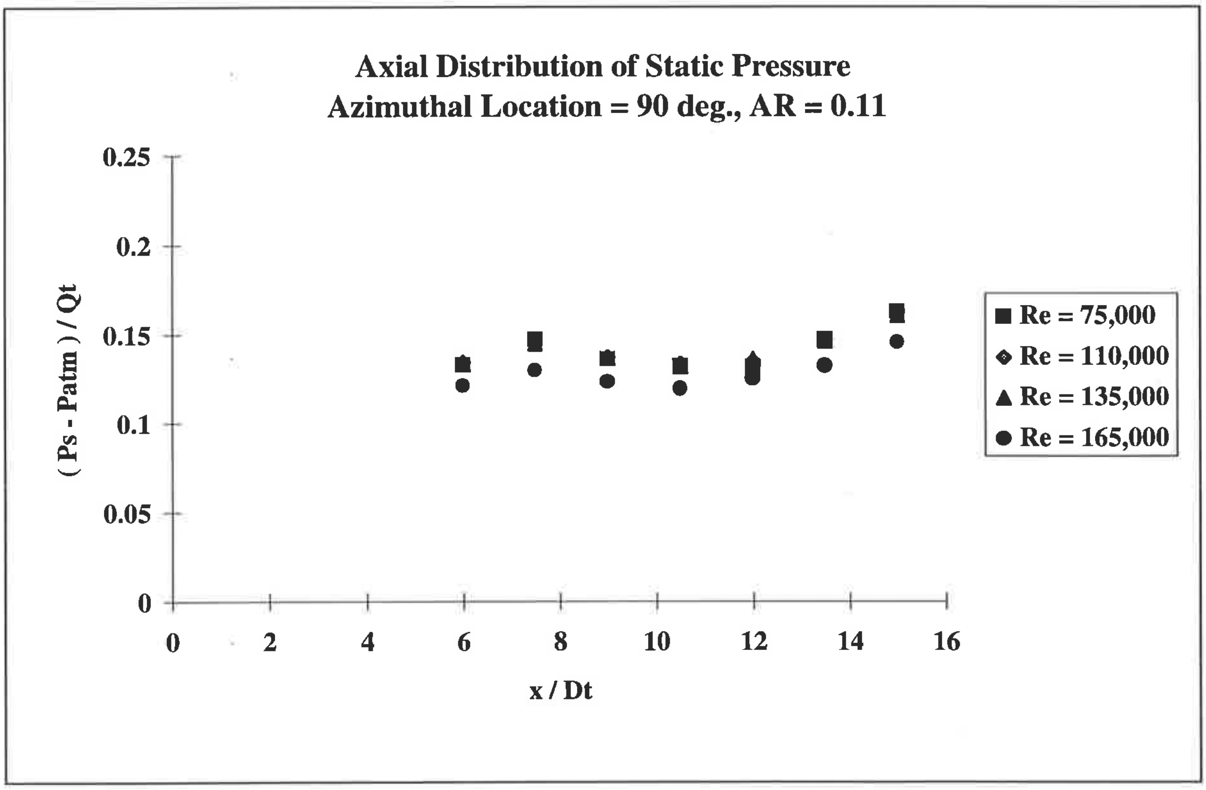

Figure 5.2.4.2 CD10 wall static pressure measured axially, at azimuth θ = 90° at a range of mass flow rates, AR = 0.11.

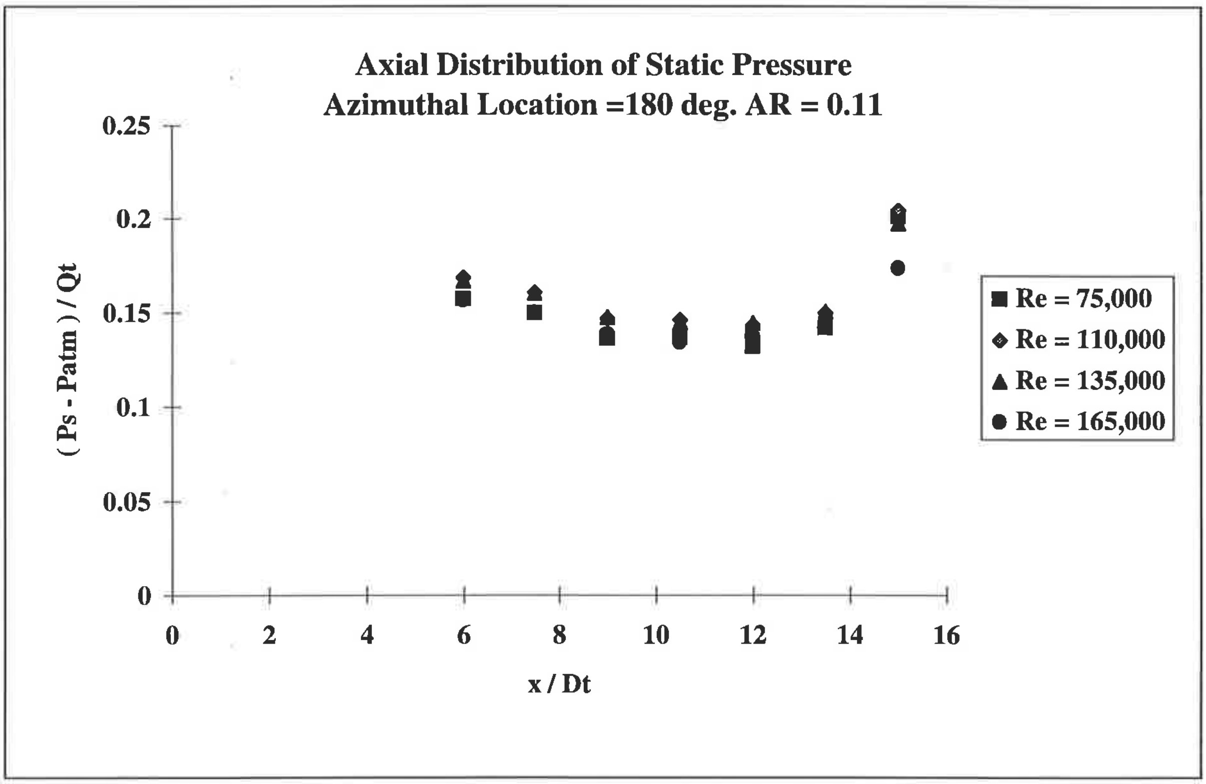

Figure 5.2.4.3 CD10 wall static pressure measured axially, at azimuth θ = 180° at a range of mass flow rates, AR = 0.11.

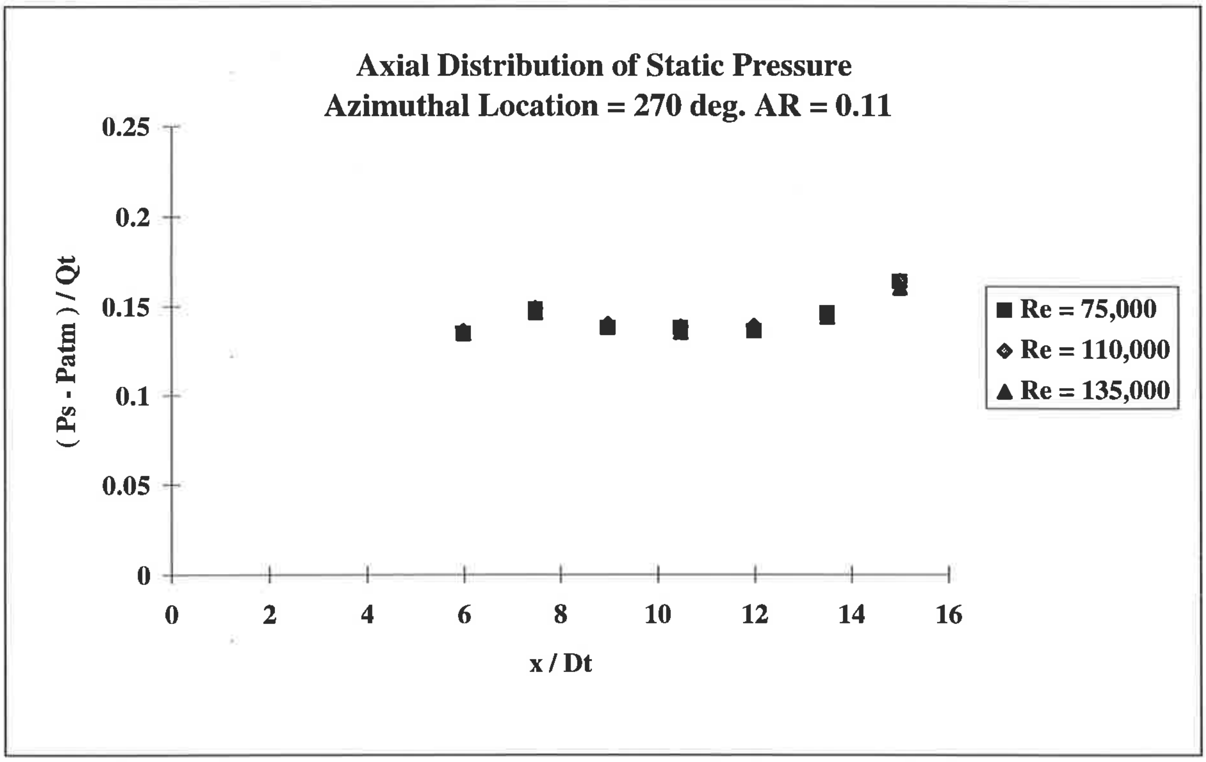

Figure 5.2.4.4 CD10 wall static pressure measured axially, at azimuth θ = 270° at a range of mass flow rates, AR = 0.11.

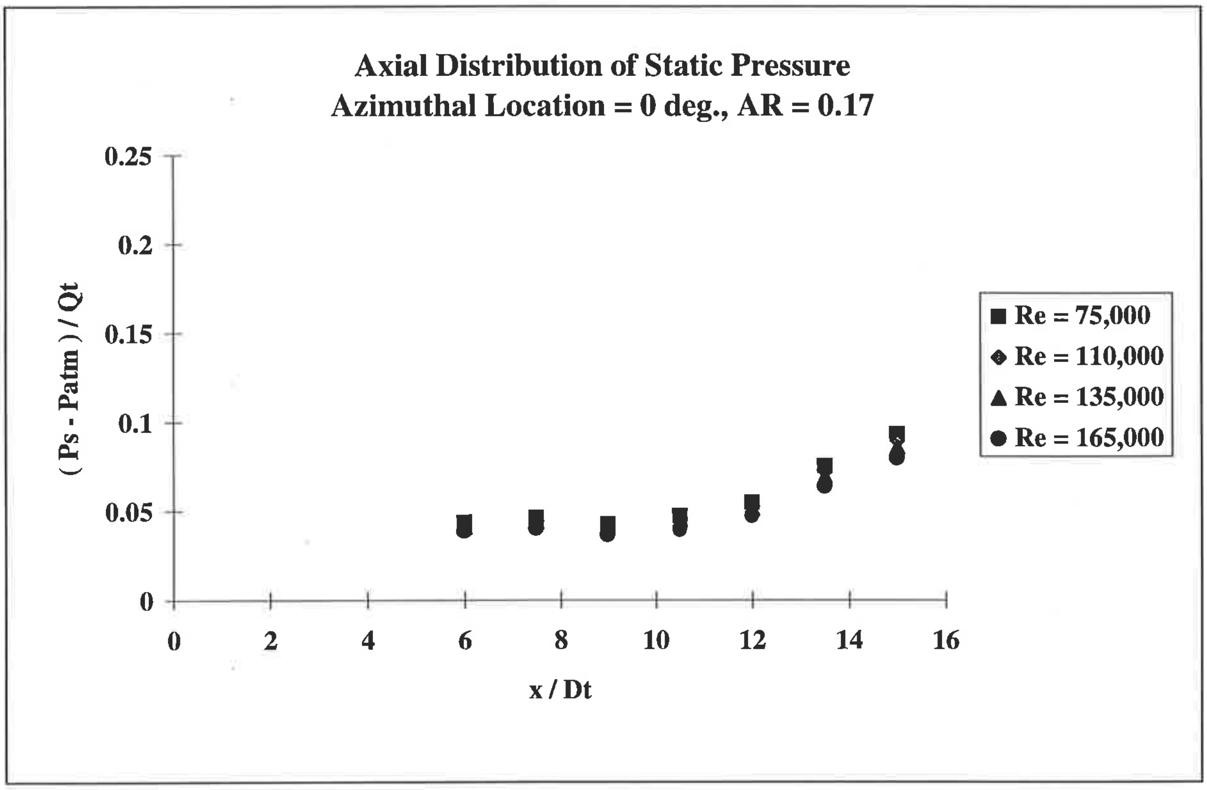

Figure 5.2.4.5 CD10 wall static pressure measured axially, at azimuth θ = 0° at a range of mass flow rates, AR = 0.17.

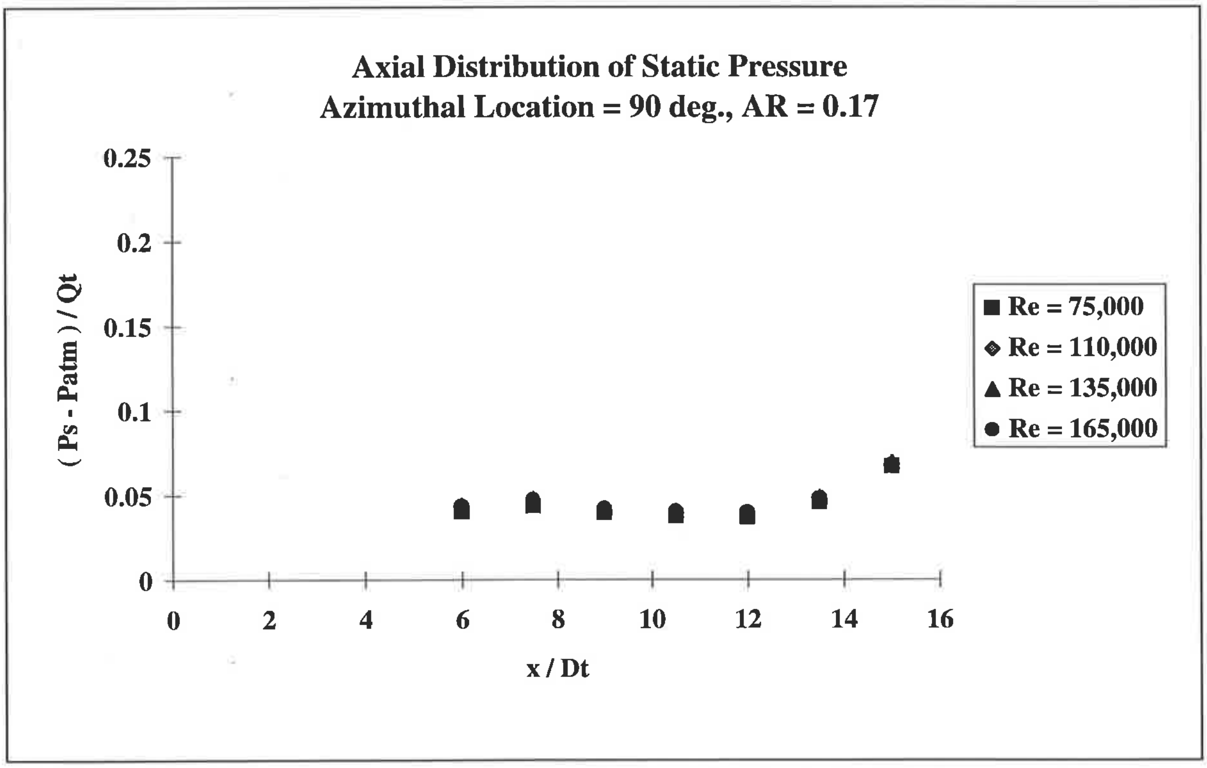

Figure 5.2.4.6 CD10 wall static pressure measured axially, at azimuth θ = 90° at a range of mass flow rates, AR = 0.17.

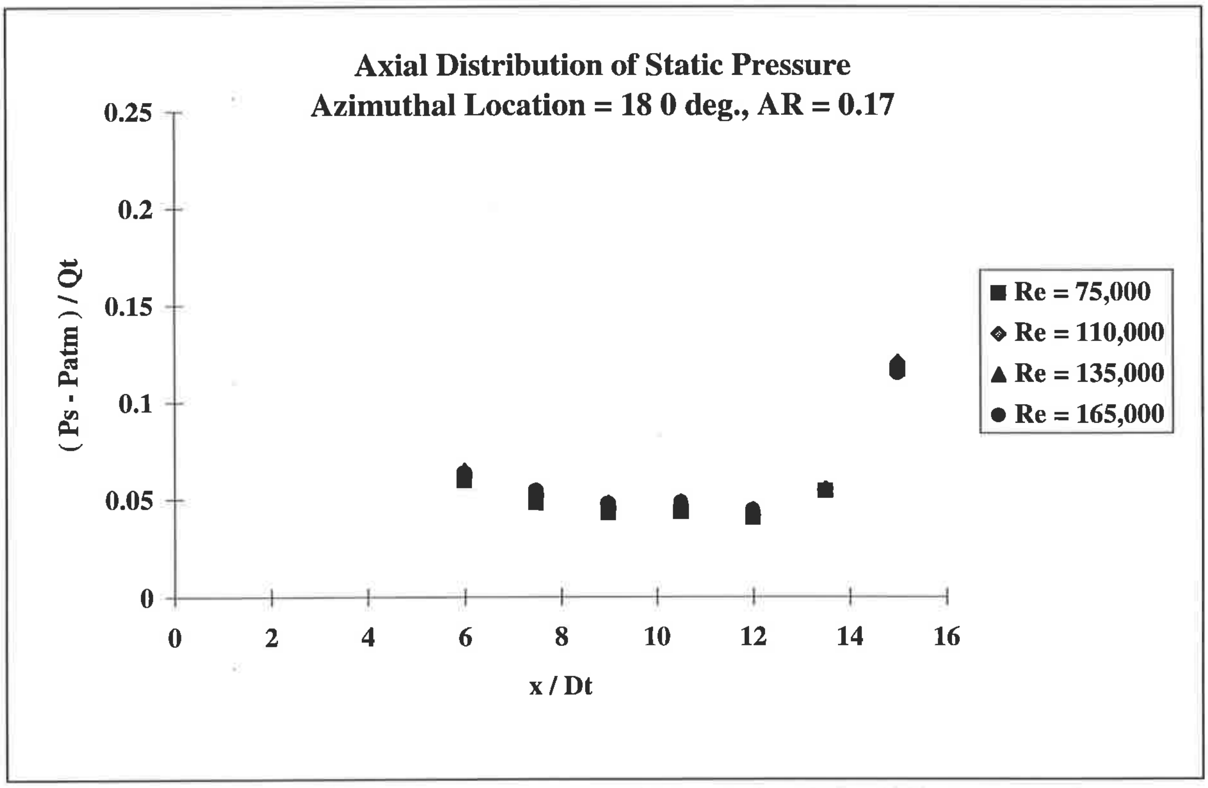

Figure 5.2.4.7 CD10 wall static pressure measured axially, at azimuth θ = 180° at a range of mass flow rates, AR = 0.17.

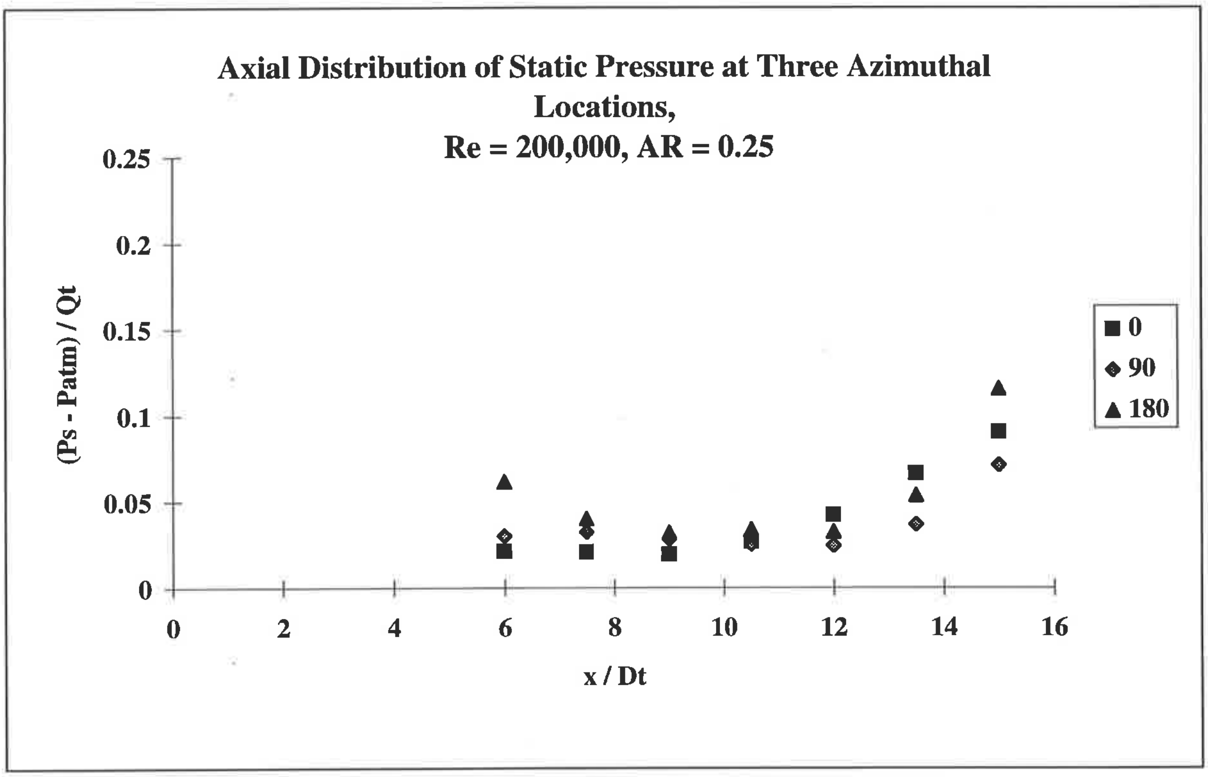

Figure 5.2.4.8 CD10 wall static pressure measured axially, at azimuth θ = 0°, 90°, 180° , at Re_t = 200,000, AR = 0.25.

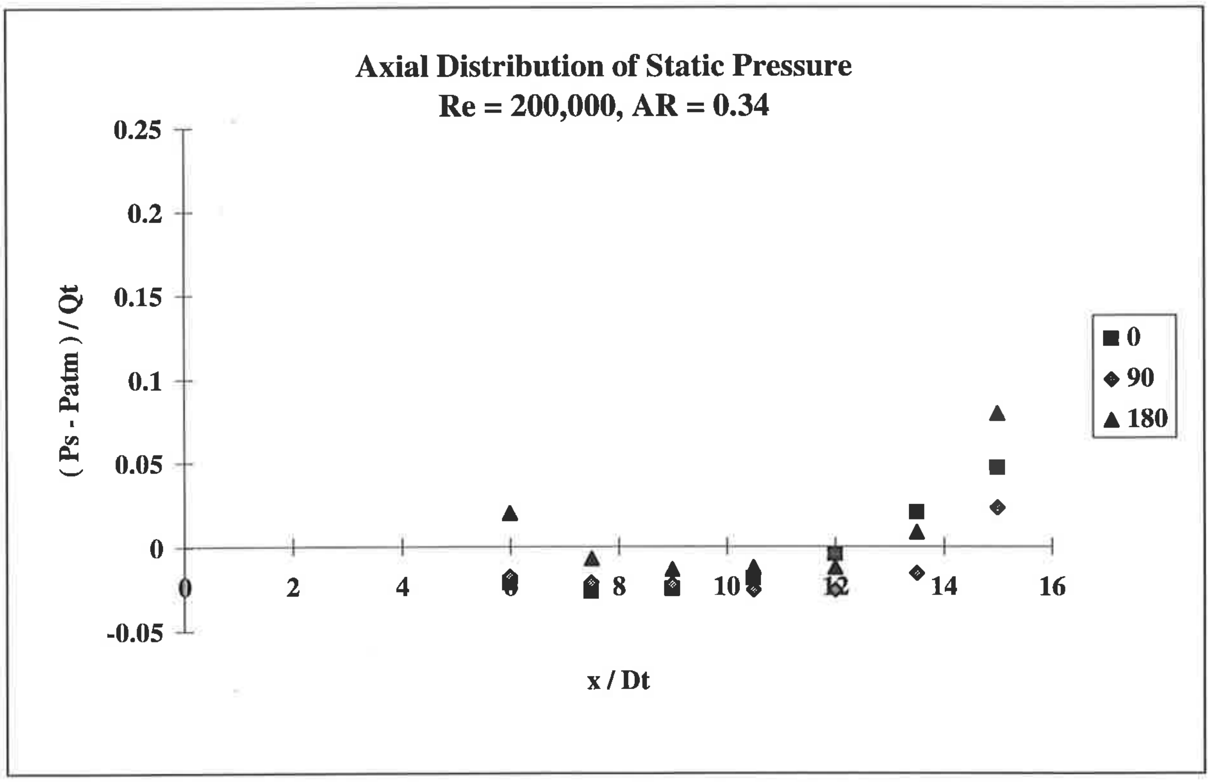

Figure 5.2.4.9. CD10 wall static pressure measured axially, at azimuth θ = 0°, 90°, 180° , at Re_t = 200,000, AR = 0.34.

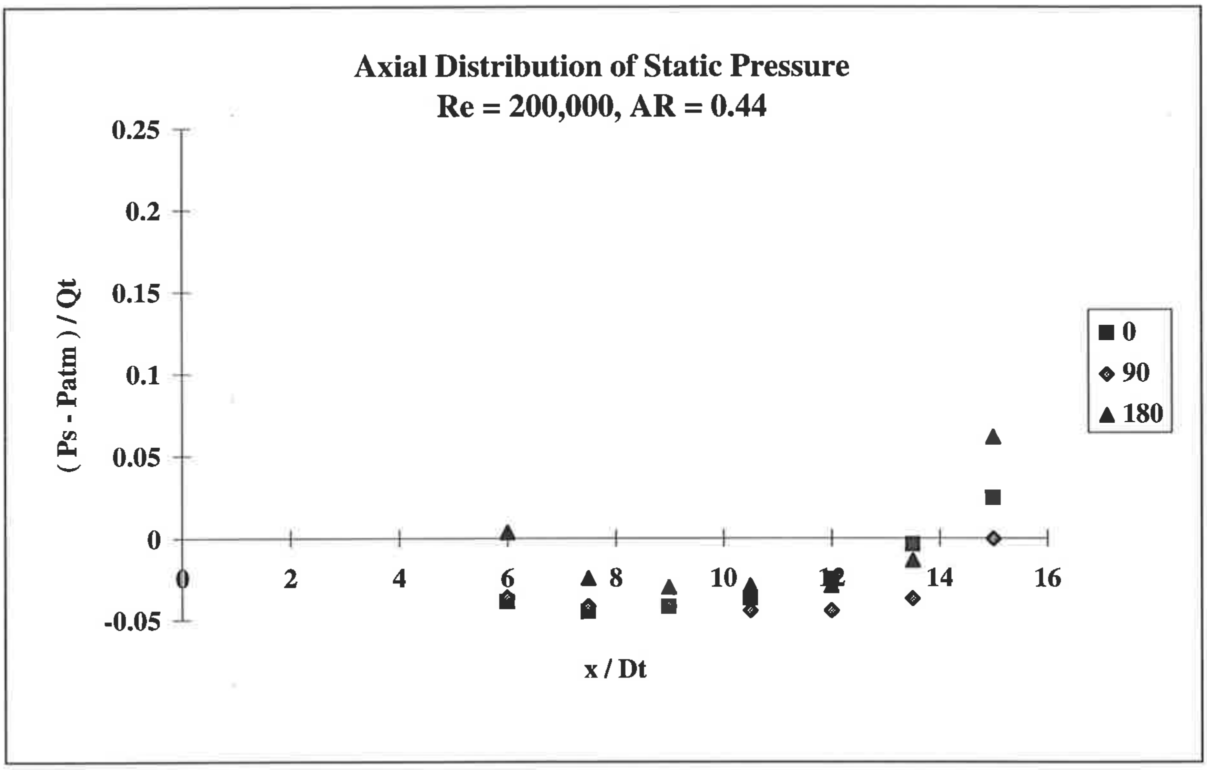

Figure 5.2.4.10 CD10 wall static pressure measured axially, at azimuth θ = 0°, 90°, 180° , at Re_t = 200,000, AR = 0.44.

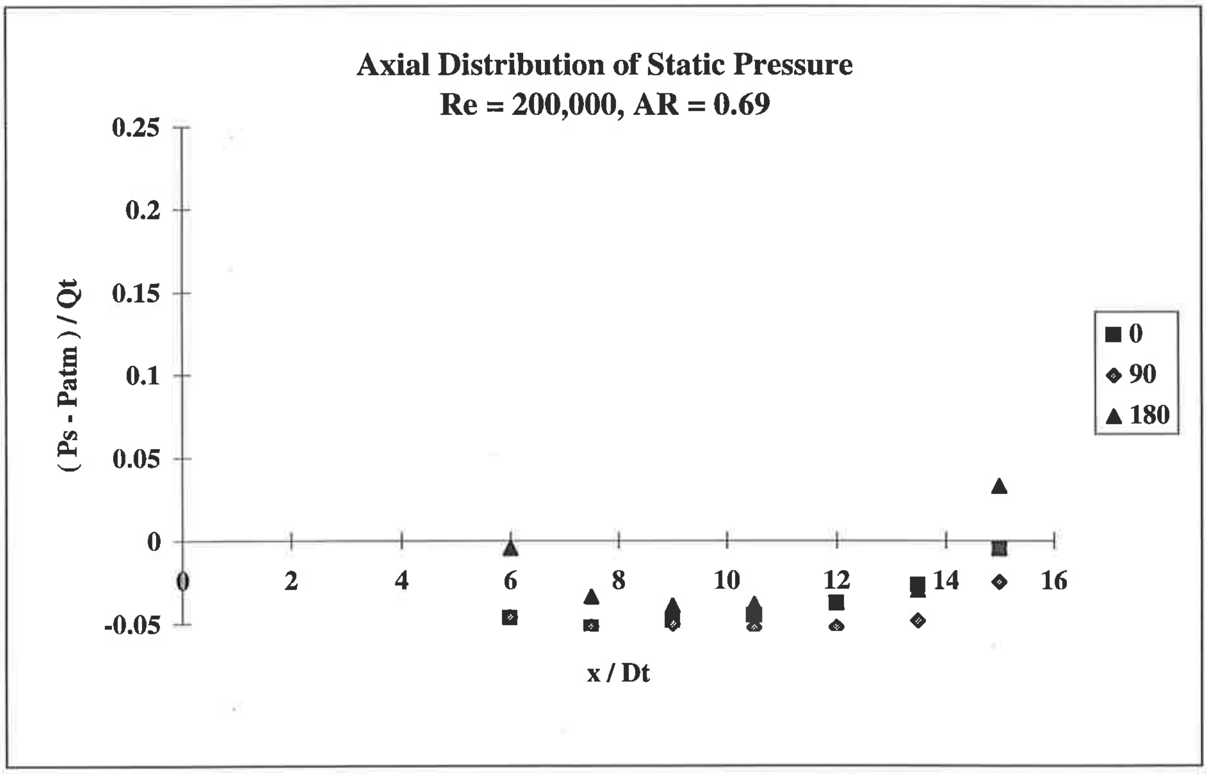

Figure 5.2.4.11 CD10 wall static pressure measured axially, at azimuth θ = 0°, 90°, 180° , at Re_t = 200,000, AR = 0.69

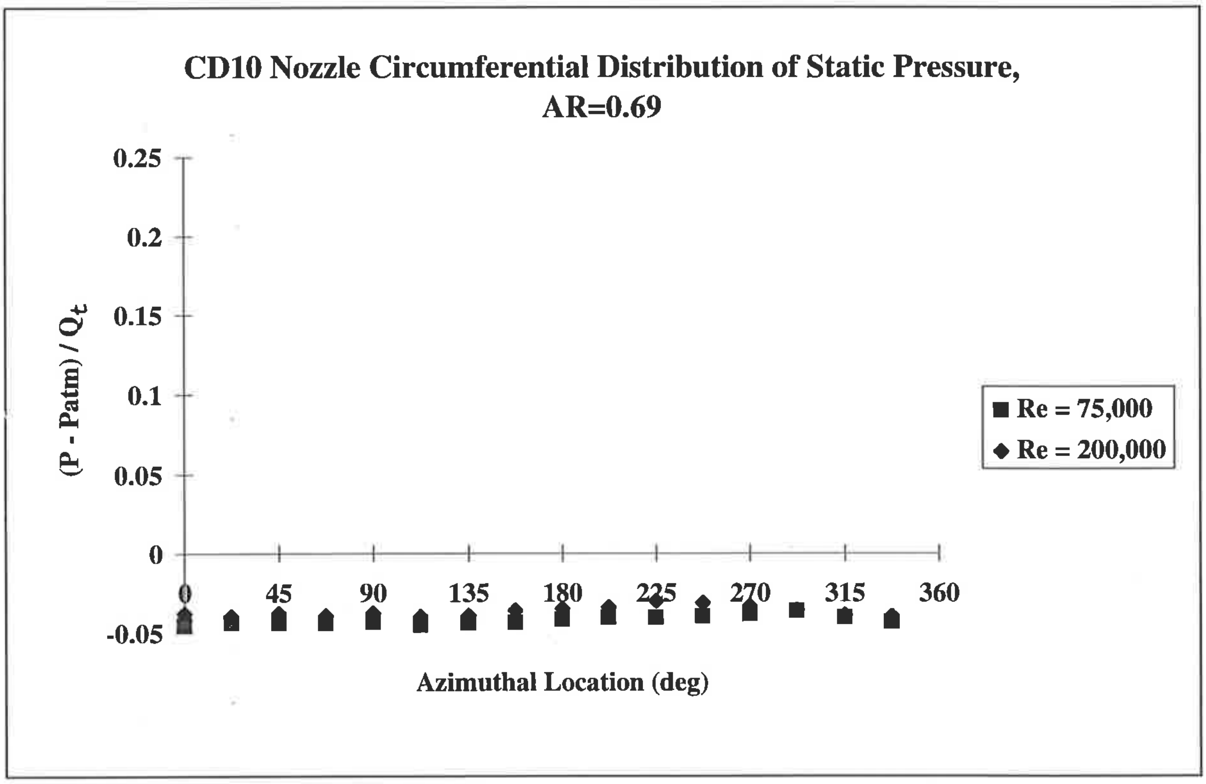

Figure 5.2.5. 1 CD10 circumferential distribution of static pressure measured at a range of mass flow rates, AR = 0.69.

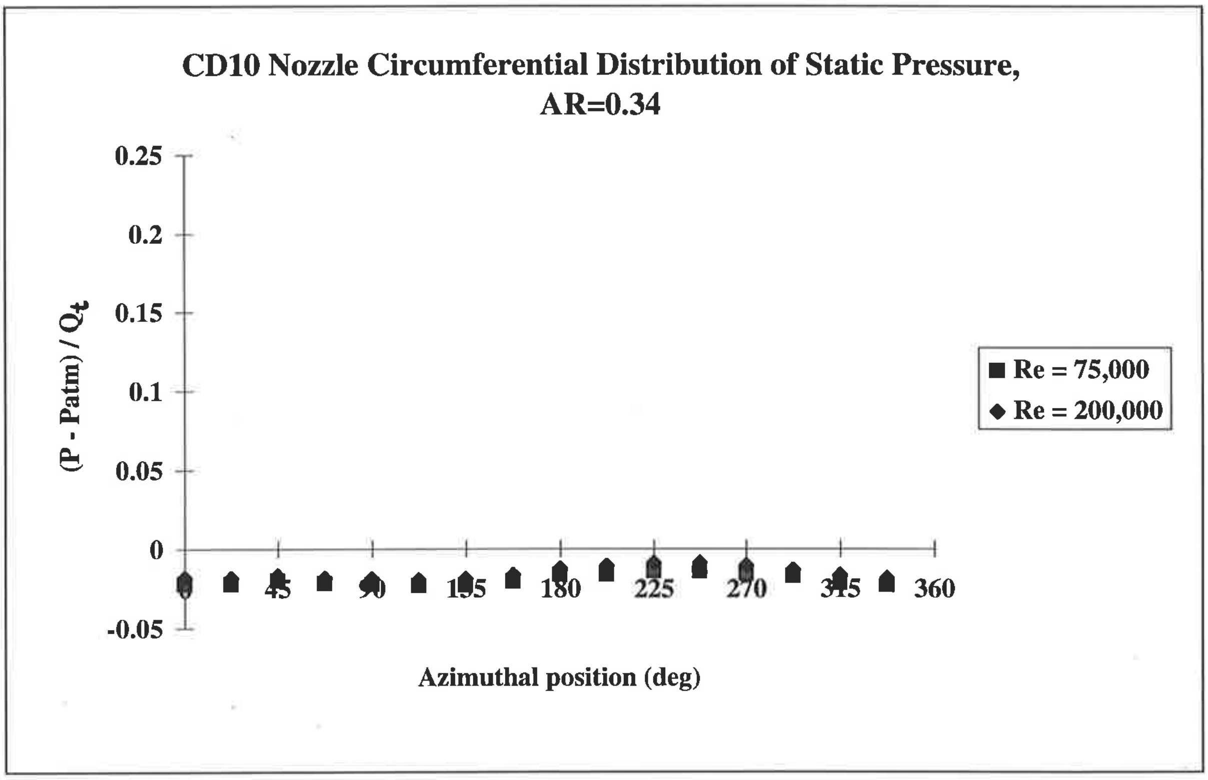

Figure 5.2.5. 2 CD10 circumferential distribution of static pressure measured at a range of mass flow rates, AR = 0.34.

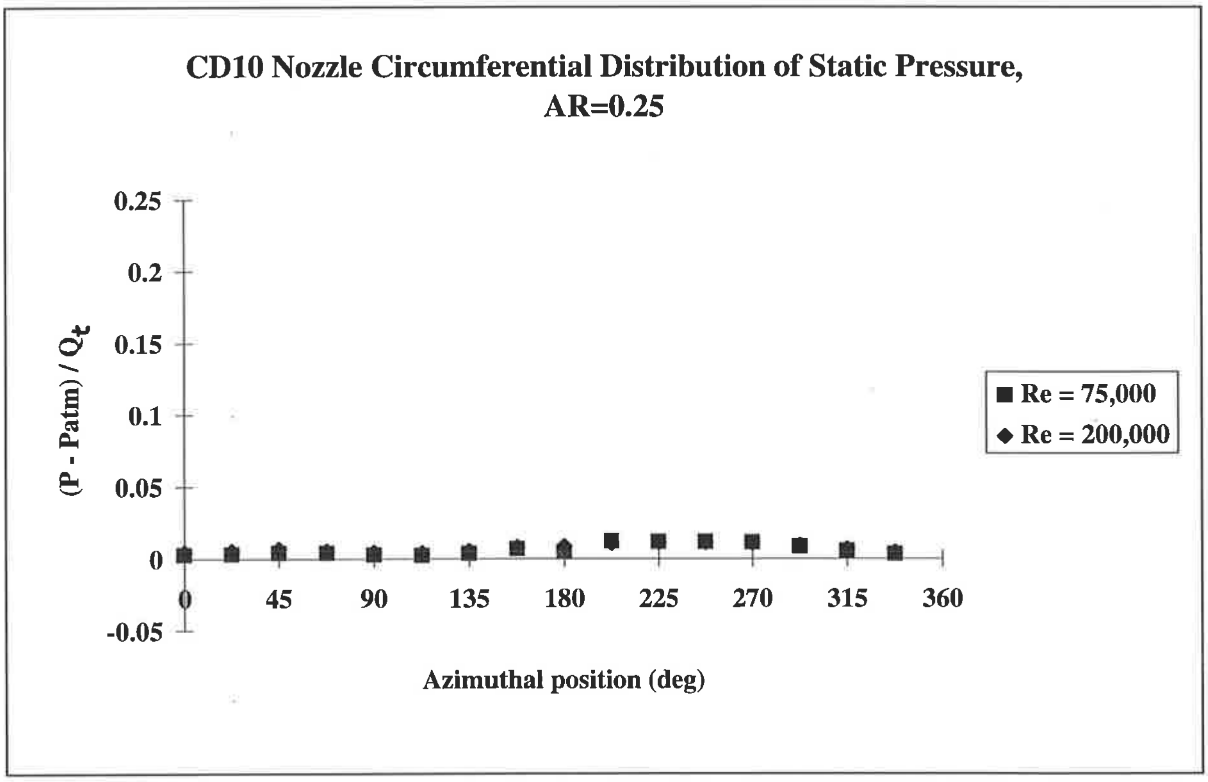

Figure 5.2.5. 3 CD10 circumferential distribution of static pressure measured at a range of mass flow rates, AR = 0.25.

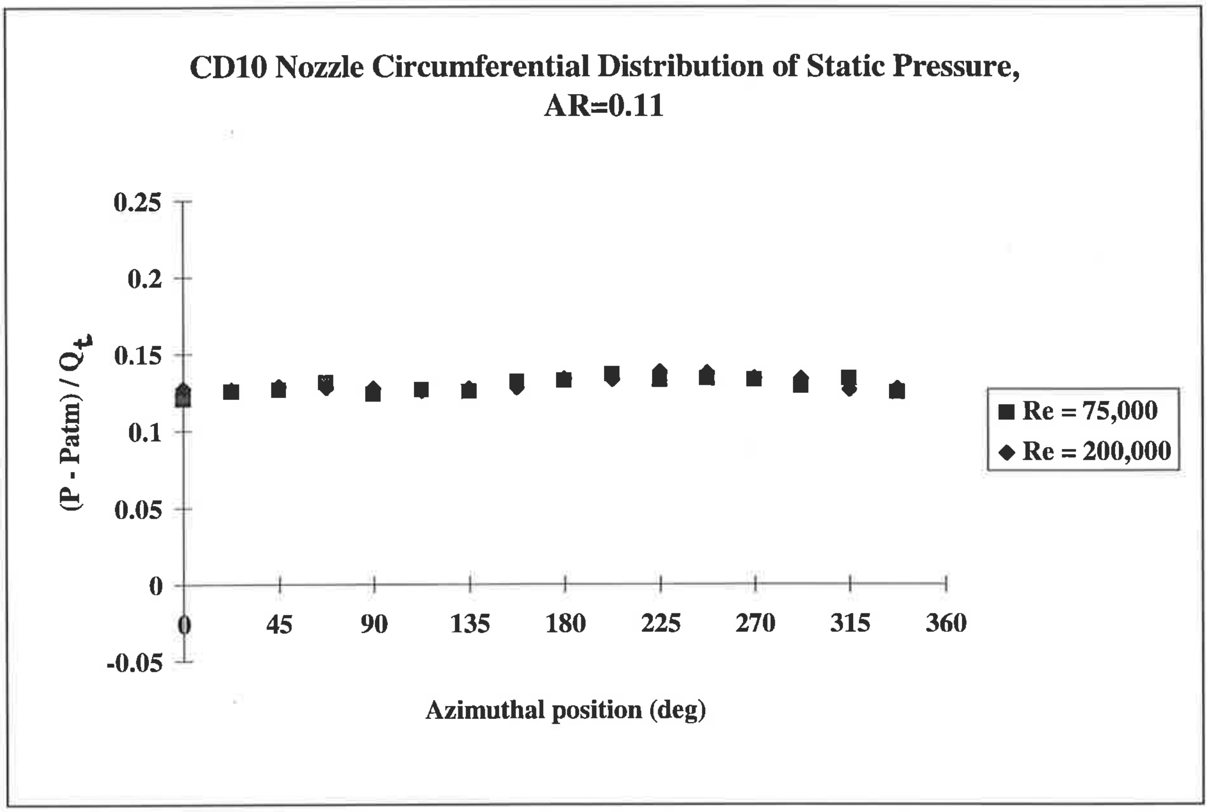

Figure 5.2.5. 4 CD10 circumferential distribution of static pressure measured at a range of mass flow rates, AR = 0.11.

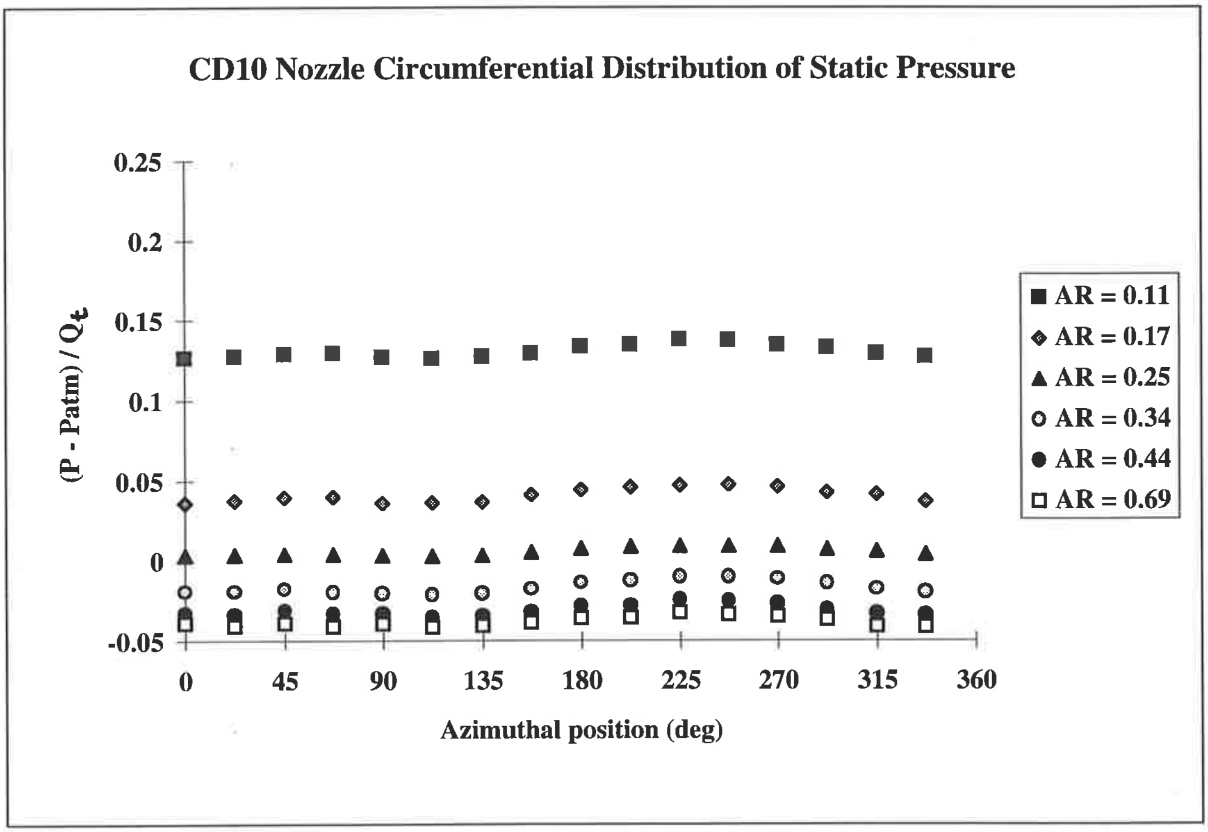

Figure 5.2.5. 5 CD10 circumferential distribution of static pressure measured at a range of AR.

The circumferential static pressures were measured for a range of mass flow rates and exit areas. Variation of circumferential pressure with change in AR at 10 throat diameters downstream from the throat is presented in **Figure 5.2.5. 1** to **Figure 5.2.5. 5**.

The cavity static pressure is only slightly dependent on Reynolds number, as may be deduced from the above figures. The static pressure inside the nozzle has been measured independently at points distributed in axial and circumferential directions and the results are in good agreement at the common measuring pressure tappings, where the axial pressure tappings coincide with the circumferential pressure tappings in four azimuthal positions 0°, 90°, 180° and 270° at about 10 throat diameters downstream from the throat.

5.2.2 CD10 Nozzle Throat Static Pressure

The throat static pressure was initially measured at 4 locations 90° apart. At a later stage it was decided to increase the number of tappings to 8. This was done so that a detailed static pressure distribution at the throat of the CD nozzle could be obtained to act as a datum during interpretation of the downstream pressures. The results produced by each of the four locations indicate the variation of pressure with mass flux in the CD10 nozzle. A sample result for the CD10 nozzle is presented in **Figure 5.2.6. 1** and shows the static pressure variation at the throat for the asymmetric case at AR=0.69 for a range of Reynolds numbers, and the results are in good agreement with the CD nozzle results shown in **Figure 4.2. 18**. The asymmetric flow produces an asymmetric throat static pressure distribution with the lowest pressure experienced at the azimuthal position downstream from the point of separation. When the flow is not controlled by injection of fluid at the throat, the flow may change its azimuthal direction without any warning. The work presented here relates to a flow controlled by secondary fluid injection of sufficient magnitude to maintain the azimuthal direction.

The pressure ratio $(P - P_{atm}) / Q_t$, where Q_t is the dynamic pressure defined as being equal to $1/2\ \rho\ (U_t)^2$, in both the CD and CD10 nozzles for a given AR = 0.69 and Re_t = 75,000 have a value of about 0.6 at the azimuth θ = 180° and a value of about -0.2 at the azimuth θ = 45°.

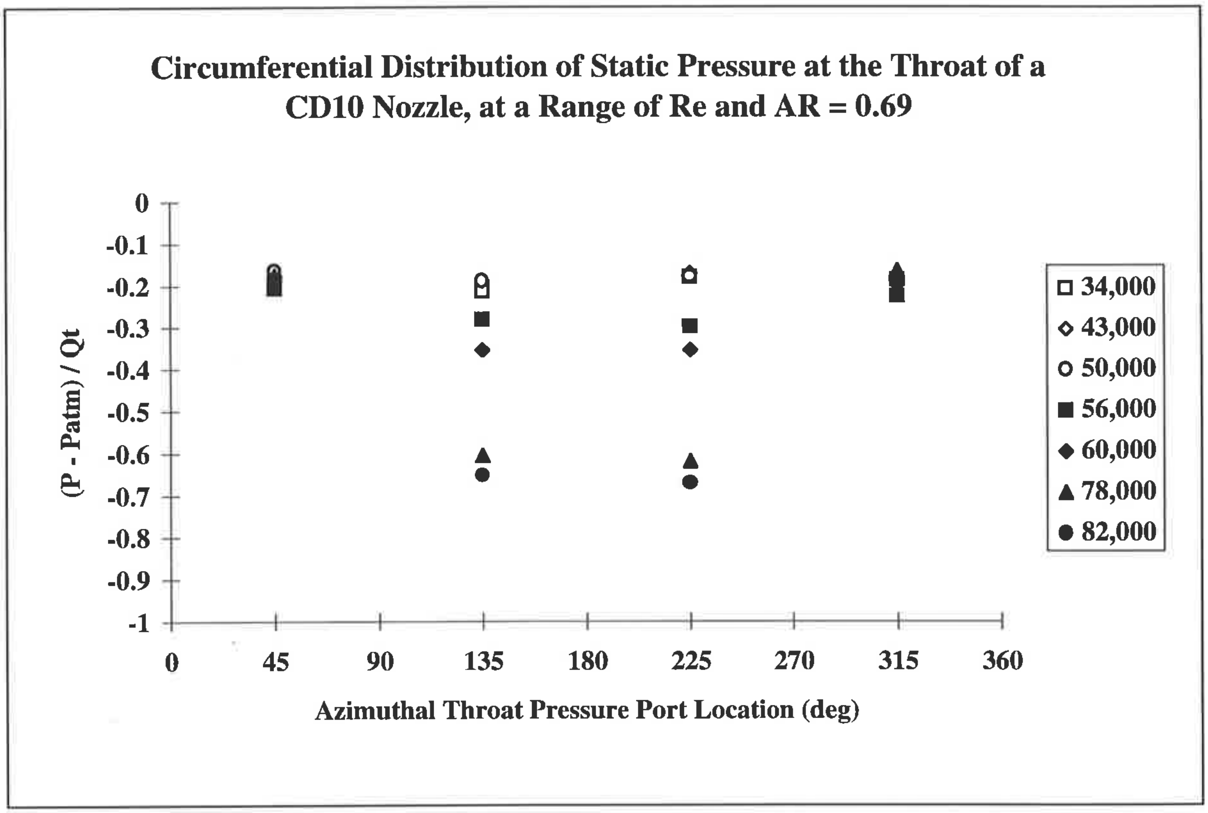

Figure 5.2.6. 1 Static pressure at the CD10 nozzle throat for a range of mass flow rates, AR = 0.69.

5.2.3 CD10 Nozzle Total Pressure

An attempt was made to measure the CD10 nozzle total pressure at a range of axial distances from the throat. The probe was mainly traversed diametrically across the nozzle. The results were inconclusive due to the uncertainty of the flow direction inside the nozzle as this was found to be changing. It is now known that the variations are related to variations in the strength of the vortex loop inside the nozzle which turns the primary fluid back towards the throat. Data for the CD20 nozzle was even more inconclusive. Similar problems were cited by Nathan (1988) in his evaluation of the Long Cavity nozzle. Further study is recommended using LDV to accurately map out the 3-D velocity profiles inside the cavity to determine the vortex strength due to the lip height (exit area ratio) and mass flux.

At the CD10 nozzle exit, the total pressure was measured by traversing across the jet streamlines which were found to be directed approximately at 35° to 45° away from the nozzle axis for the AR=0.69, see Table 4.1 for summary of deflected jet angles. The total pressure profiles, when converted to velocity, gave the "picture" of the exiting jet width and thickness shown in **Figure 5.2.6. 2,** shown as a 3-D surface plot representing the velocity of half the exiting jet, traversed at 45° to the nozzle axis at the exit plane, at $Re_t = 86{,}000$.

The profiles were taken at 5 mm intervals across the stream to give a reasonably complete picture of the exiting jet from one aspect. This result was also used to calculate the momentum flux produced by the particular nozzle configuration and the results were compared with the measured thrust values obtained from the strain gauge apparatus described earlier in Chapter 2. The results from the momentum calculations were presented elsewhere, **[293]** and the results are in good agreement with the results presented in Chapter 6. The total pressure measurements outside the nozzle were useful when the direction of the flow was known so that the probe could be aligned with the flow. It was found that the measurements using total pressure profiles were consistent with the results from both hot-wire and LDV.

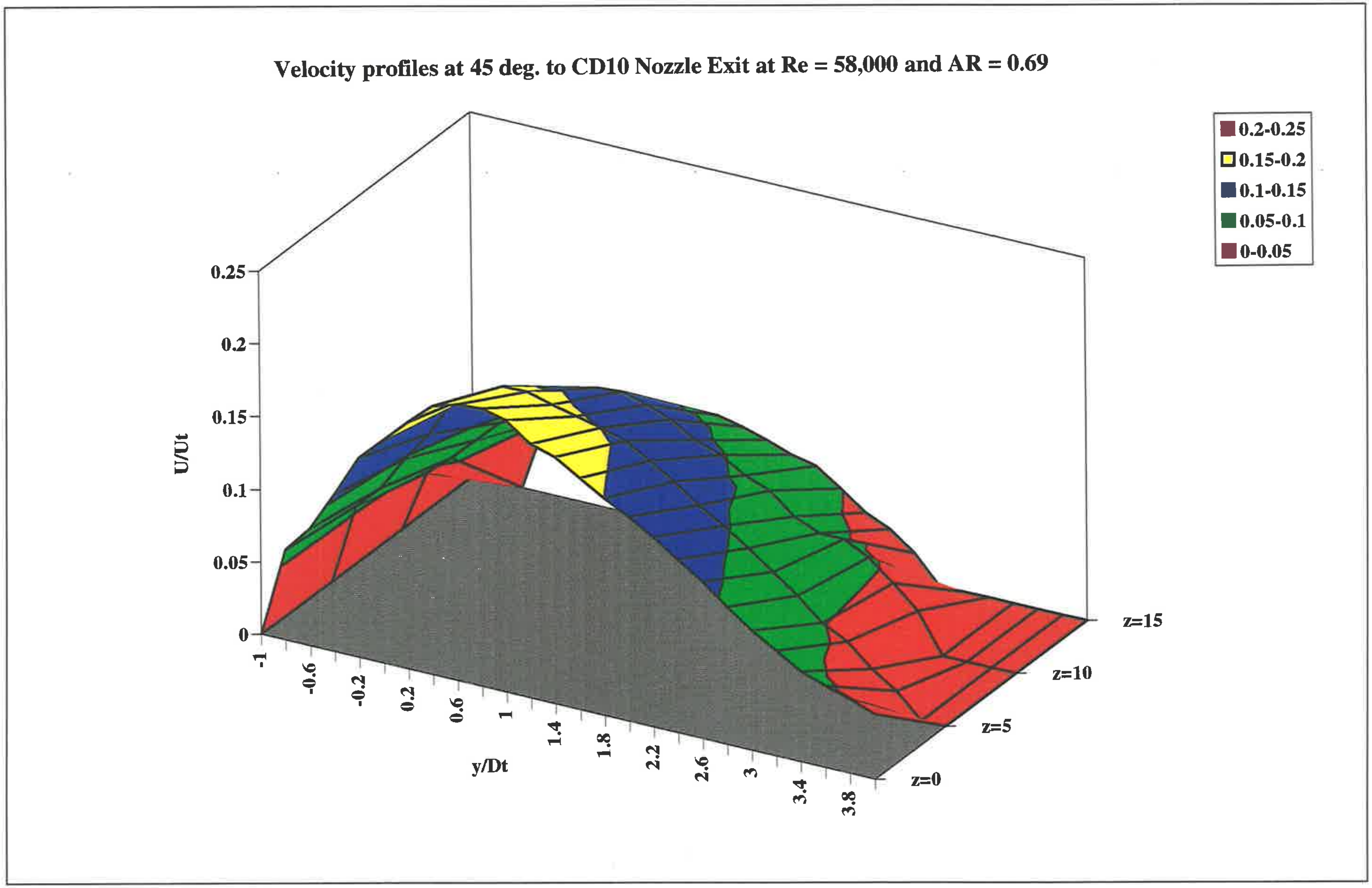

Figure 5.2.6. 2 Velocity profiles measure at 45° to the CD10 nozzle exit plane, AR = 0.69, Re$_t$=58,000, derived from the pitot-static pressure measurements traversed along the plane of jet symmetry.

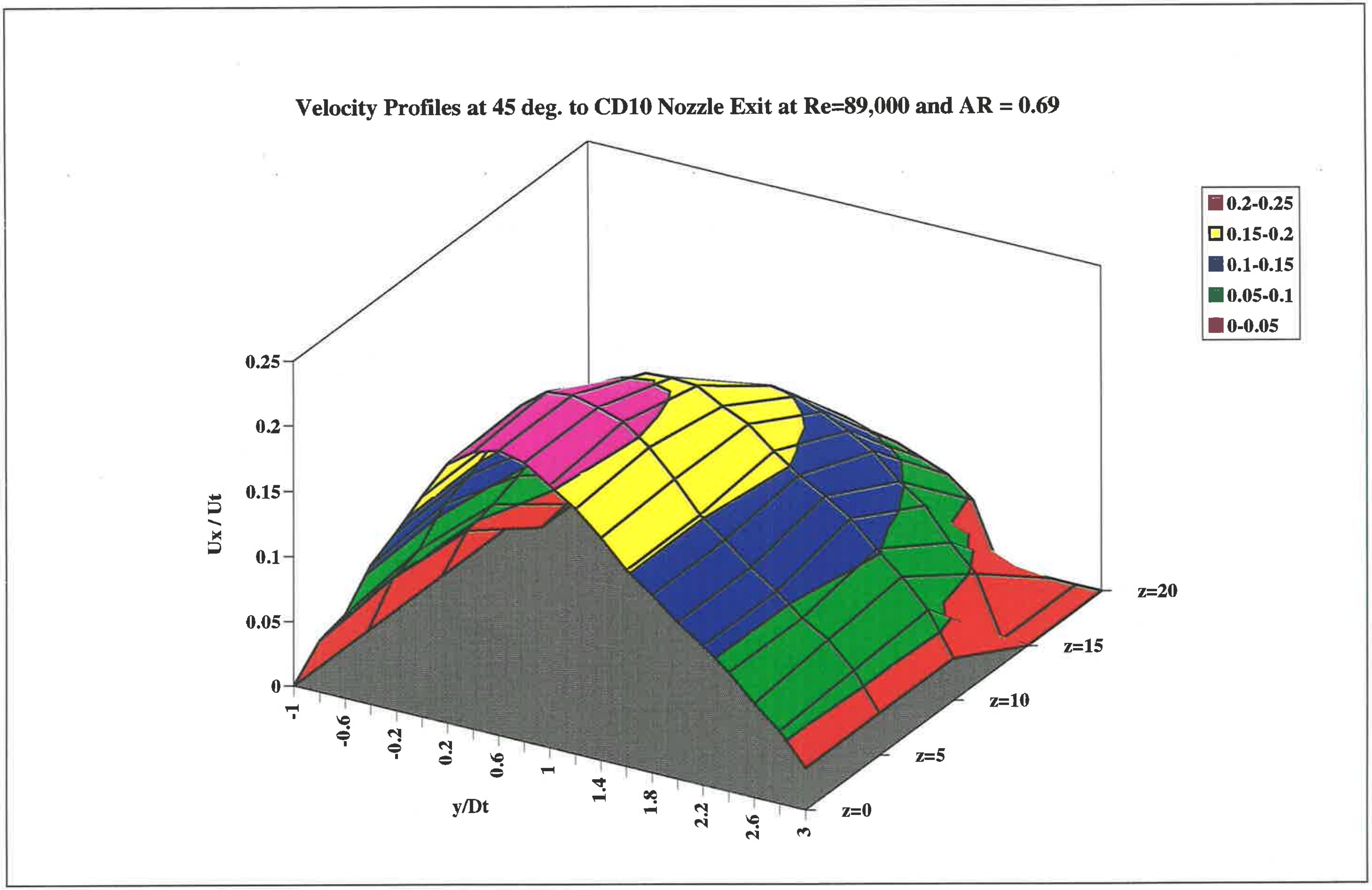

Figure 5.2.6. 3 Velocity profiles measure at 45° to the CD10 nozzle exit plane, AR = 0.69, Re_t=89,000, derived from the pitot-static pressure measurements traversed along the plane of jet symmetry.

5.3 Measurement of the CD6, CD10 and CD20 Nozzle Deflected Jet Mean Flow Direction

The angle at which the jet leaves the CD6, CD10 and CD20 nozzles was measured in a number of ways. As discussed in Section 4, the most suitable and convenient method was to place a tuft in the flow and measure its angle. The other method used was a laser sheet flow visualisation. These two methods were sufficiently accurate to measure the deflected jet angles produced by a lip at the nozzle exit since it has been shown by the use of the LDV 2 component velocity vectors, that the previous two methods give results which are sufficiently accurate for the present interpretive study . The tuft method was used for the CD10 and CD20 nozzles and laser sheet for the CD6 nozzle.

5.3.1 Laser Sheet Photography Results

The laser sheet flow visualisation has been described earlier and the same method was used to capture the deflected jet leaving the nozzle. The flow images of the jet from the CD6 nozzle were recorded on 35 mm film and are shown in **Figure 5.3. 1** to **Figure 5.3. 7**. The captured images show only the width of the jet and the angle at which the jet is deflected by the lip at the exit. The intensity of the image across the centre plane of the jet may be interpreted as being related to the local proportion of primary fluid, as discussed in previous section. Towards the edges of the jet the intensity reduces indicating that the primary fluid is becoming more diluted by ambient fluid due to the entrainment and mixing. The spread of the jet in the asymmetric flow at AR=1 could also be measured. In general the spread is of the same order as for the CD nozzle. The above figures show the effects of exit area on the angle to which the jet is deflected. The feature to notice is that the maximum angle is reached when the AR=0.34, and is the same result observed for the CD nozzle. Note the visible signs that part of the primary jet fluid is induced into the cavity when no exit ring exists at the exit as shown in **Figure 5.3. 1** and a considerably larger proportion of primary fluid recirculated when an exit ring AR = 0.69 is introduced at the CD6 nozzle exit as shown in **Figure** 5.3. 2. Further more it is clear that a large proportion of primary fluid is recirculated, and presumably increases with reduction of exit area, into the cavity ,shown in **Figure 5.3. 3**. It is also of interest to see the formation of the vortex loop cross section and subsequent move upstream as the exit area is reduced, shown in the above figures. These dark areas of induced ambient fluid inside the cavity confirm that the exiting jet does not occupy the whole of the exit area for at least AR = 0.69 anyway. **Figure 5.3. 2** to **Figure 5.3. 7** show how the angle of deflected jet is effected by reduction of exit area.

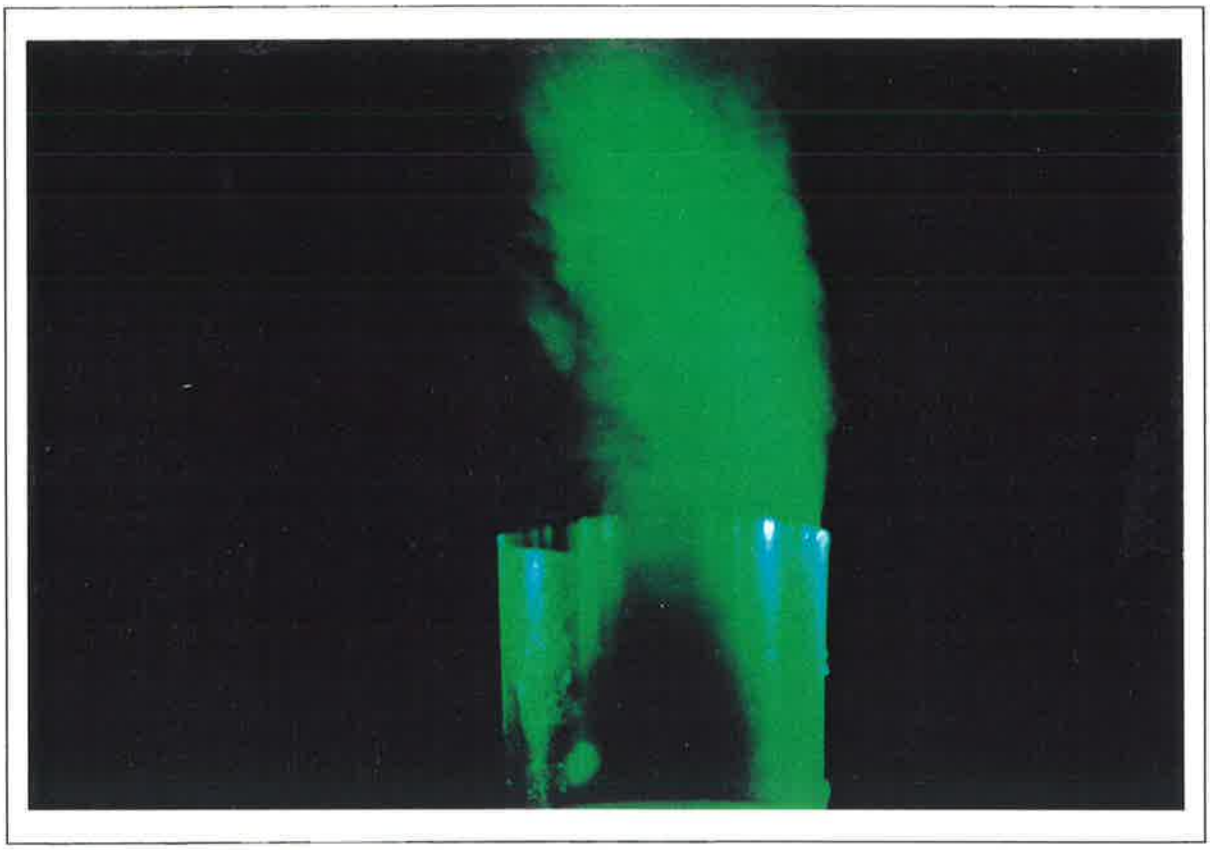

Figure 5.3. 1 Deflected jet from the CD6 nozzle illuminated by a laser sheet: AR =1.0, Re_t = 27,000.

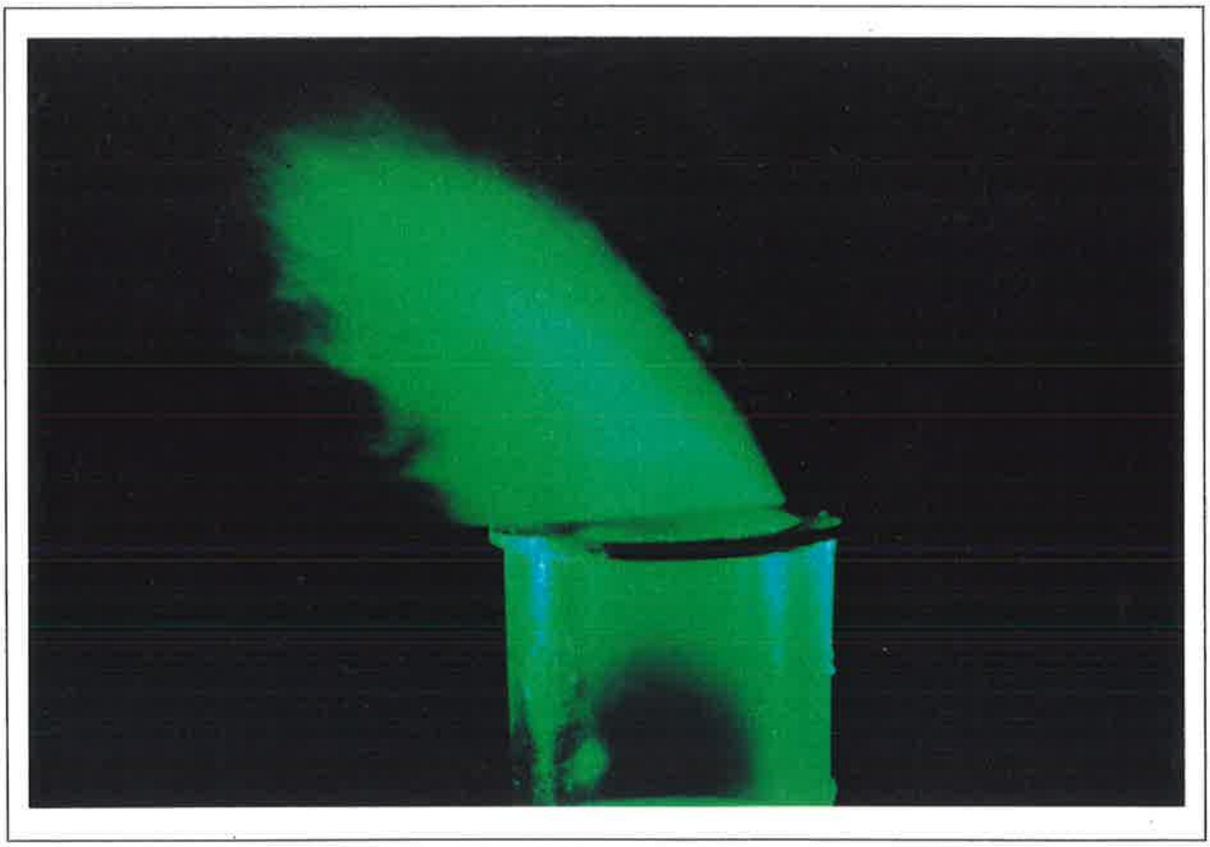

Figure 5.3. 2 Deflected jet from the CD6 nozzle illuminated by a laser sheet: AR =0.69, Re_t = 27,000.

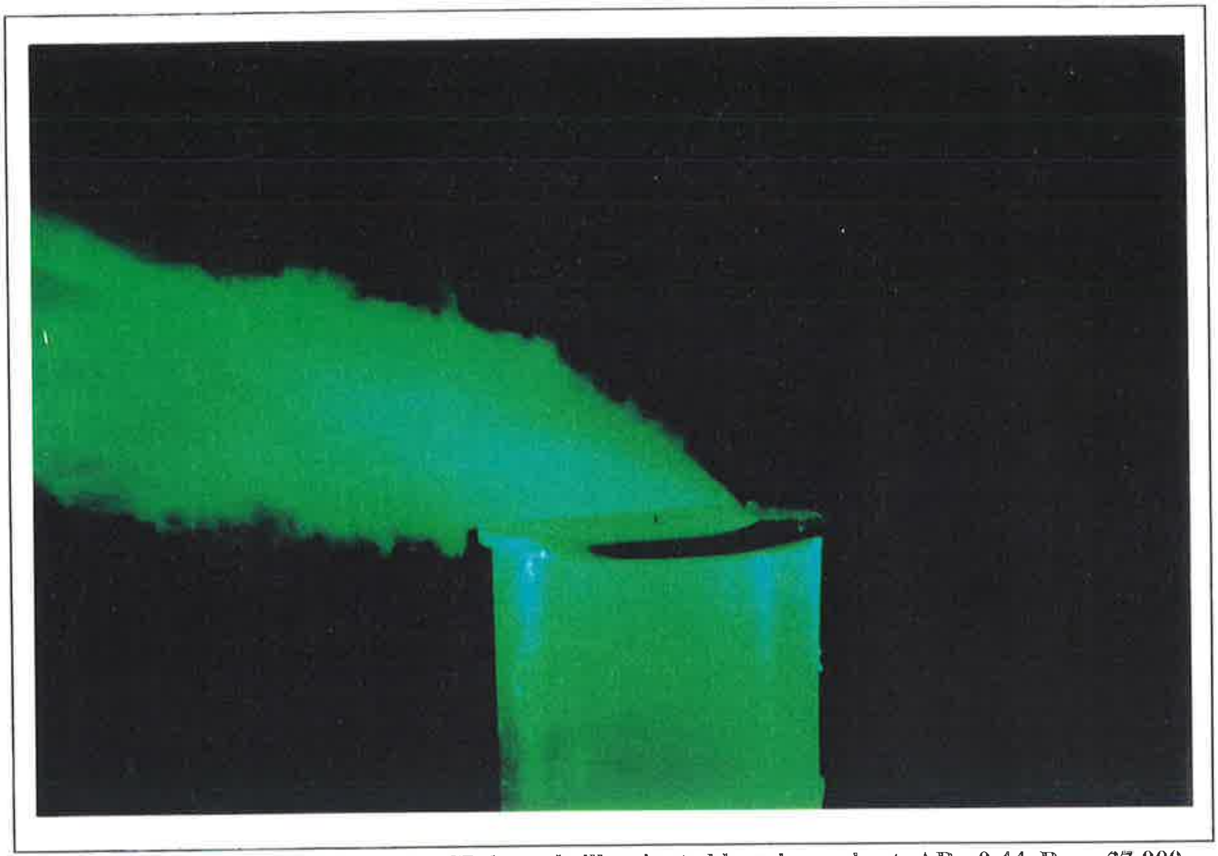

Figure 5.3. 3 Deflected jet from the CD6 nozzle illuminated by a laser sheet: AR =0.44, Re_t = 27,000.

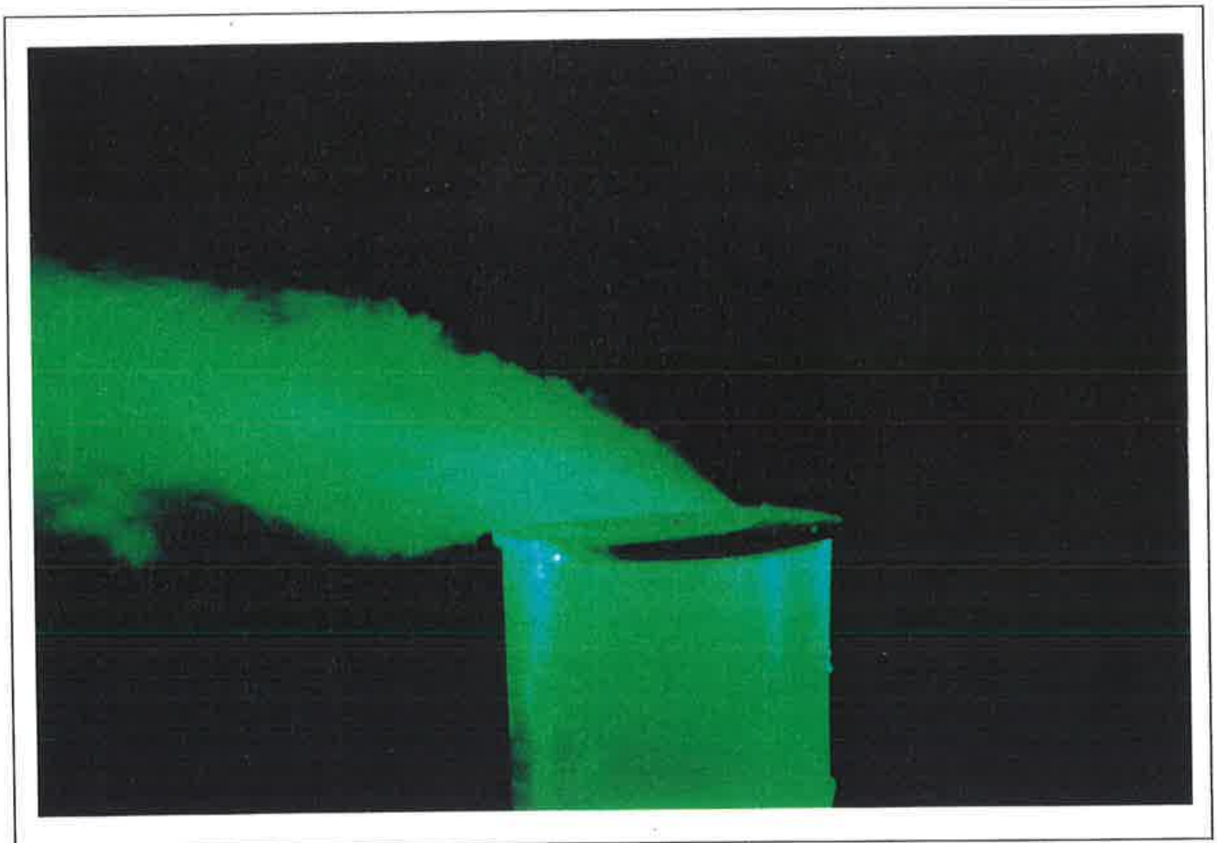

Figure 5.3. 4 Deflected jet from the CD6 nozzle illuminated by a laser sheet: AR =0.34, Re_t = 27,000.

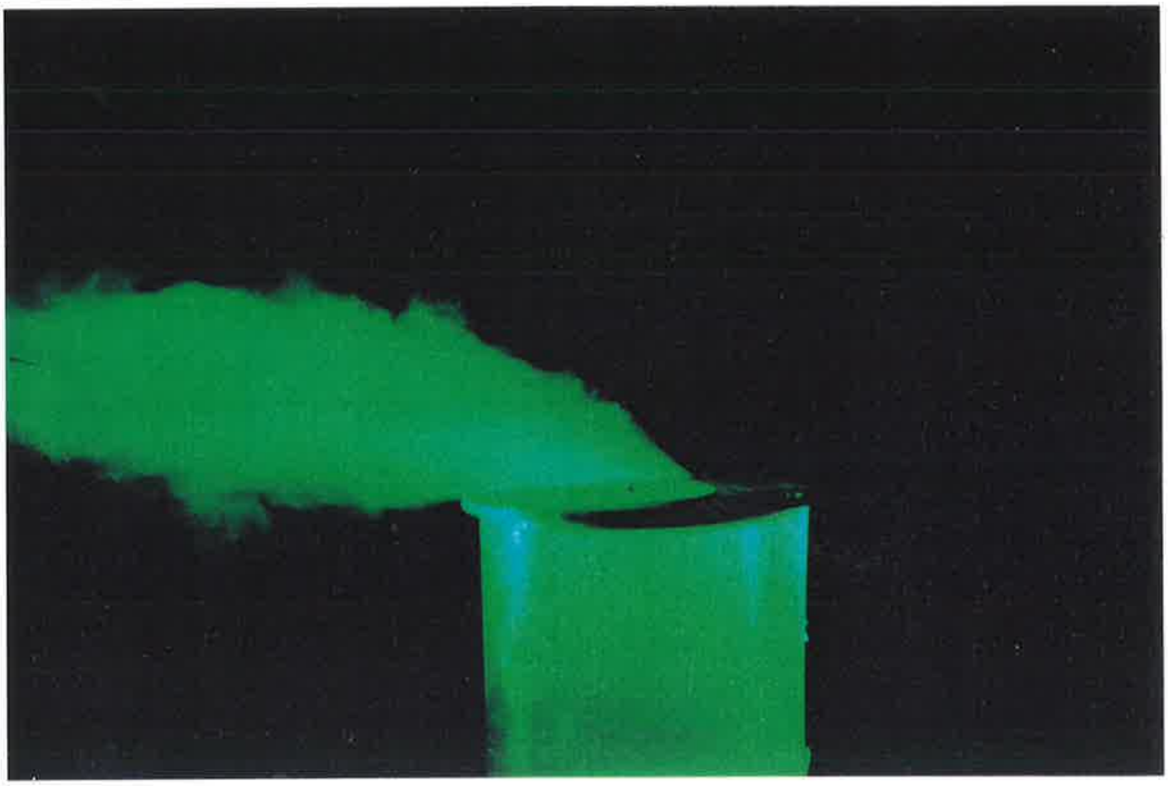

Figure 5.3. 5 Deflected jet from the CD6 nozzle illuminated by a laser sheet: AR =0.25, Re_t = 27,000.

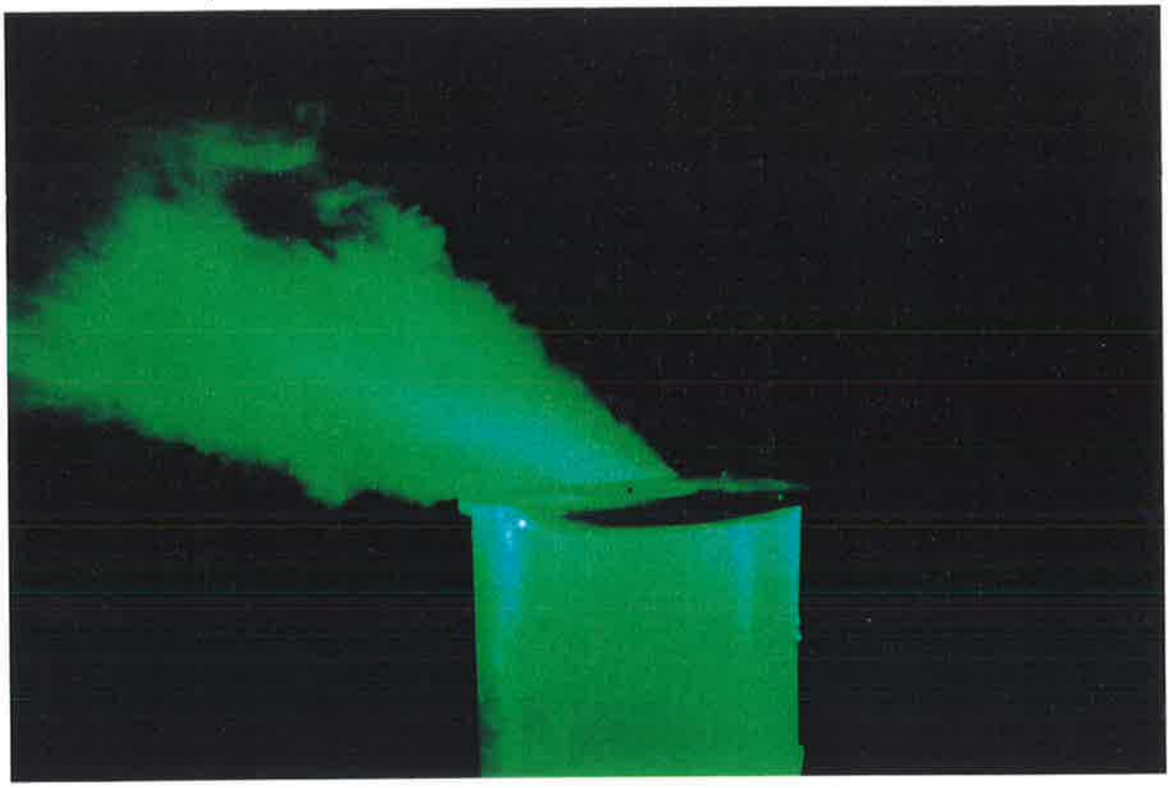

Figure 5.3. 6 Deflected jet from the CD6 nozzle illuminated by a laser sheet: AR =0.17, Re_t = 27,000.

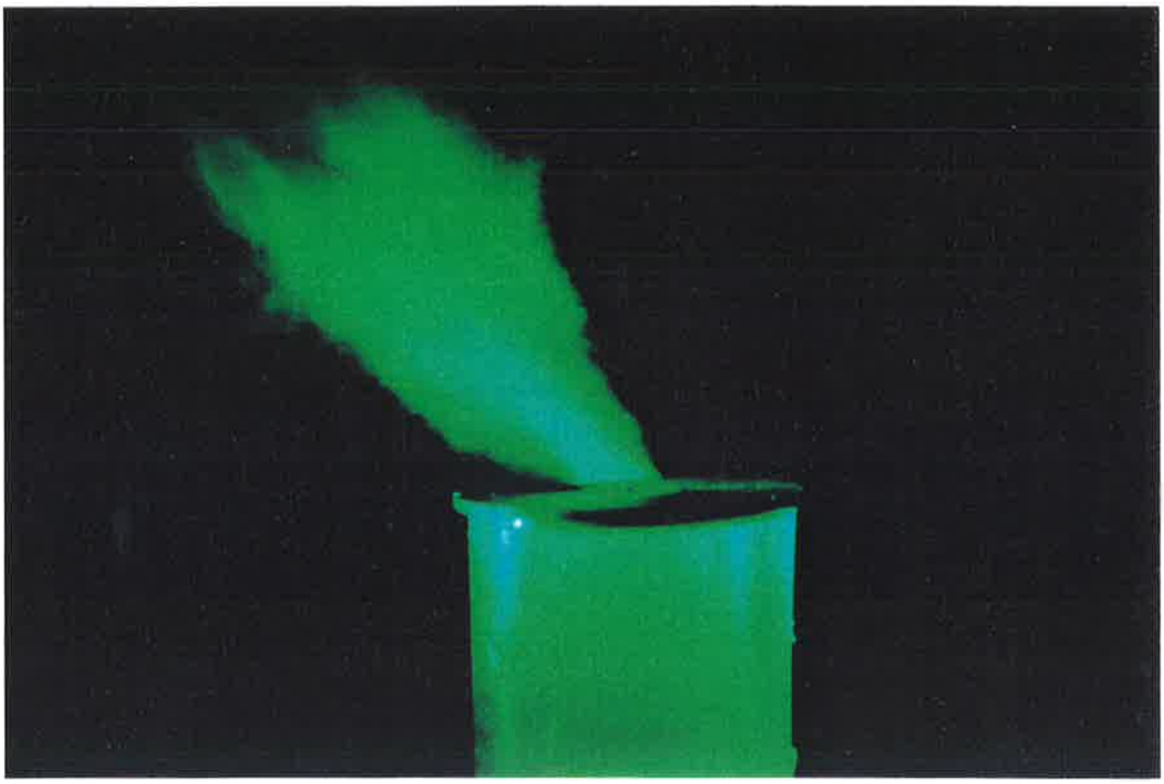

Figure 5.3. 7 Deflected jet from the CD6 nozzle illuminated by a laser sheet: AR =0.11, Re_t = 27,000.

5.4 Measurement of Velocity Inside and Outside the Nozzle

A number of velocity traverses of the jet and its related flow fields have been taken inside and outside the CD10 nozzle. The convergent-divergent nozzle was made of a opaque material so it was not possible to use the LDV to measure the axial velocity profiles in the vicinity of the first 6 throat diameters. Measurements of the velocity profiles were attempted through the perspex cavity of the CD10 and CD20 nozzles and it was found that the water mist seeding system left a deposit of condensate on the cavity walls. This made the experiment very time consuming because the experiment had to be stopped, the cavity wall cleaned, and the experiment restarted, stopped, and the procedure repeated again a short time later. The initial cavity wall was 5mm thick, which produced distortion of the beams and the scattered signal collected in the back scatter mode had a high noise component due to the condensation. New cavity walls were manufactured from 1mm thick perspex (a precision task accomplished by Mr Jager and Mr Price at the Departmental Workshop) and the beam distortion was minimised. The seeding problems could not, however, be avoided due to the type of seeder and the nature of the flow inside the cavity. Solid particle seeding could have been used but this would have required the apparatus to be redesigned to allow the containment and subsequent extraction of the seeding particles to conform with the statutory Occupational Health and Safety legislation. On this basis it was decided to limit the use of the LDV to the region outside the nozzle to avoid the condensation problem. The velocity profiles inside the cavity were measured using a hot-wire probe and the direction of the flow was inferred from the surface flow visualisation as discussed later in this Chapter.

5.4.1 Hot Wire Anemometry

A number of hot-wire traverses were carried out inside the cavity to establish the effect of the cavity on the spread of the jet and the jet centre line decay. **Figure 5.4. 1** shows the development of the velocity profile inside the CD10 nozzle. The initial velocity profile, in this case, was measured at an axial distance of 3 throat diameters downstream from the nozzle throat and indicates that the jet is 1.25 throat diameters thick and has the centre line value of U_x/U_t=0.60 in the plane of symmetry. At the axial distance of 6 throat diameters the jet thickness increases to about 2 throat diameters while the jet centre line velocity has decayed to around 0.35 of the throat velocity, determined by the mass flux and nozzle configuration. This would indicate greater diffusion of the jet than that of a CD nozzle flow where the centre line velocity at 6 throat diameters downstream from the throat maintains a value of close to 0.6 of the throat velocity. The wall jet in general is expected to diffuse a great deal more in the CD20 nozzle because of the greater residence time, and in fact the jet occupies the whole of the exit plane.

The velocity profiles outside the CD10 nozzle for a range of distances from the nozzle exit plane have been measured along a 45° line relative to the nozzle axis, which coincides approximately with the deflected jet centreline. These results are presented in **Figure 5.4. 2** and show the profile of the jet as it moves away from the nozzle exit. The 45° angle was chosen from the laser sheet flow visualisation and tuft measurements which determined the angle at which the deflected jet was leaving the nozzle. From the figure above it is clear that the chosen angle was appropriate since the maximum velocity remains close to the chosen centreline. It is also evident that the jet has a spreading half angle of about 10°. This appears to be in good agreement with an axisymmetric turbulent jet spreading half angle. The spreading half angle of the free side of the jet however is of the order of 15° to 20°.

A number of velocity measurements have been taken at the edge of the rectangular plate of the RP45 nozzle and results presented in **Figure 5.4. 3** and **Figure 5.4. 4** for two Reynolds numbers. The profiles are similar in character to the velocity profiles exiting the CD10 nozzle and the centreline velocity is just over 0.45 of the throat velocity in both cases. The point to note is that the jet has deformed into a jet similar in character to the wall jet discussed in Chapter 4.

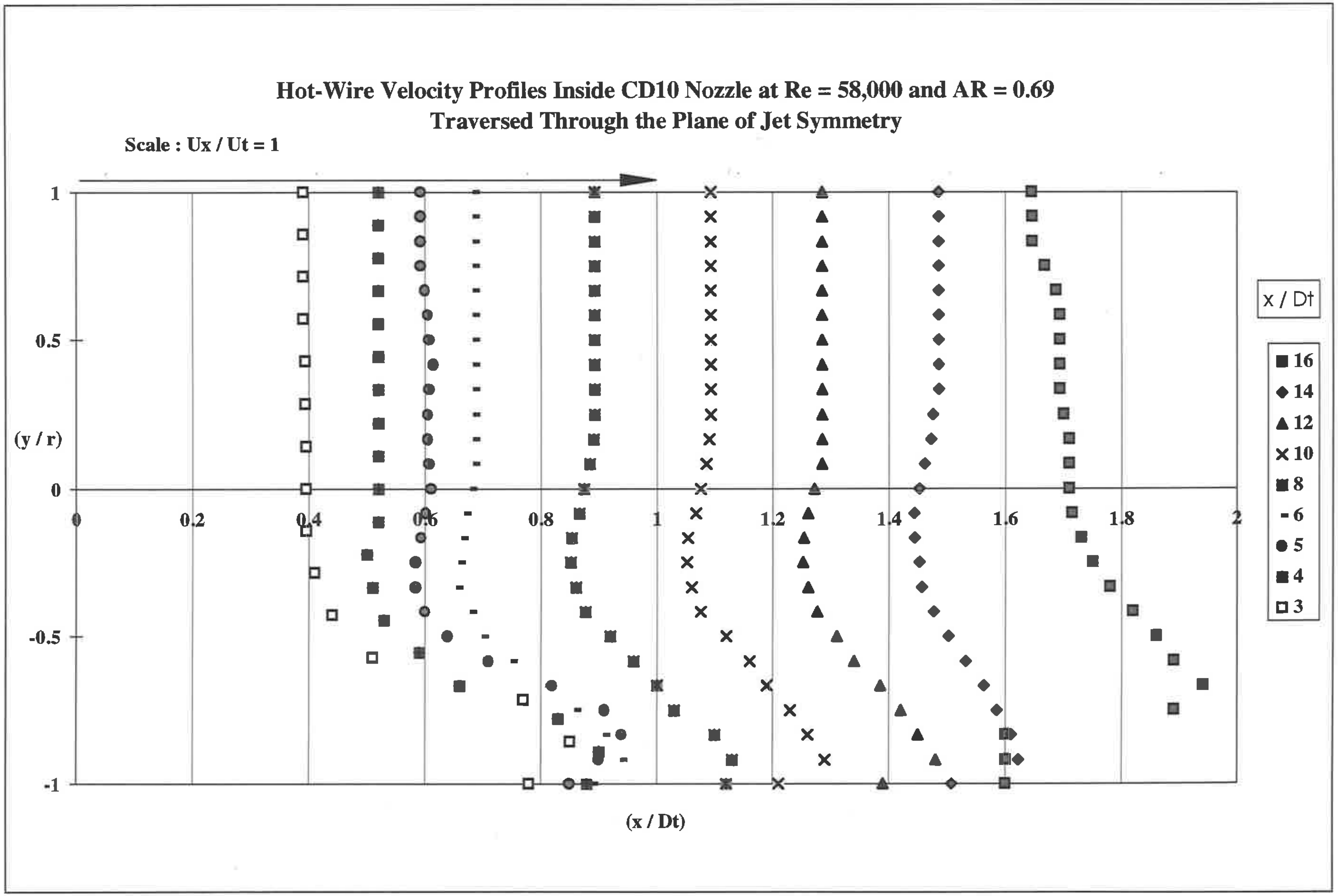

Figure 5.4.1 Hot-wire velocity profiles measured diametrically inside the CD10 nozzle at a range of axial positions downstream from the throat; Re_t = 58,000, AR = 0.69.

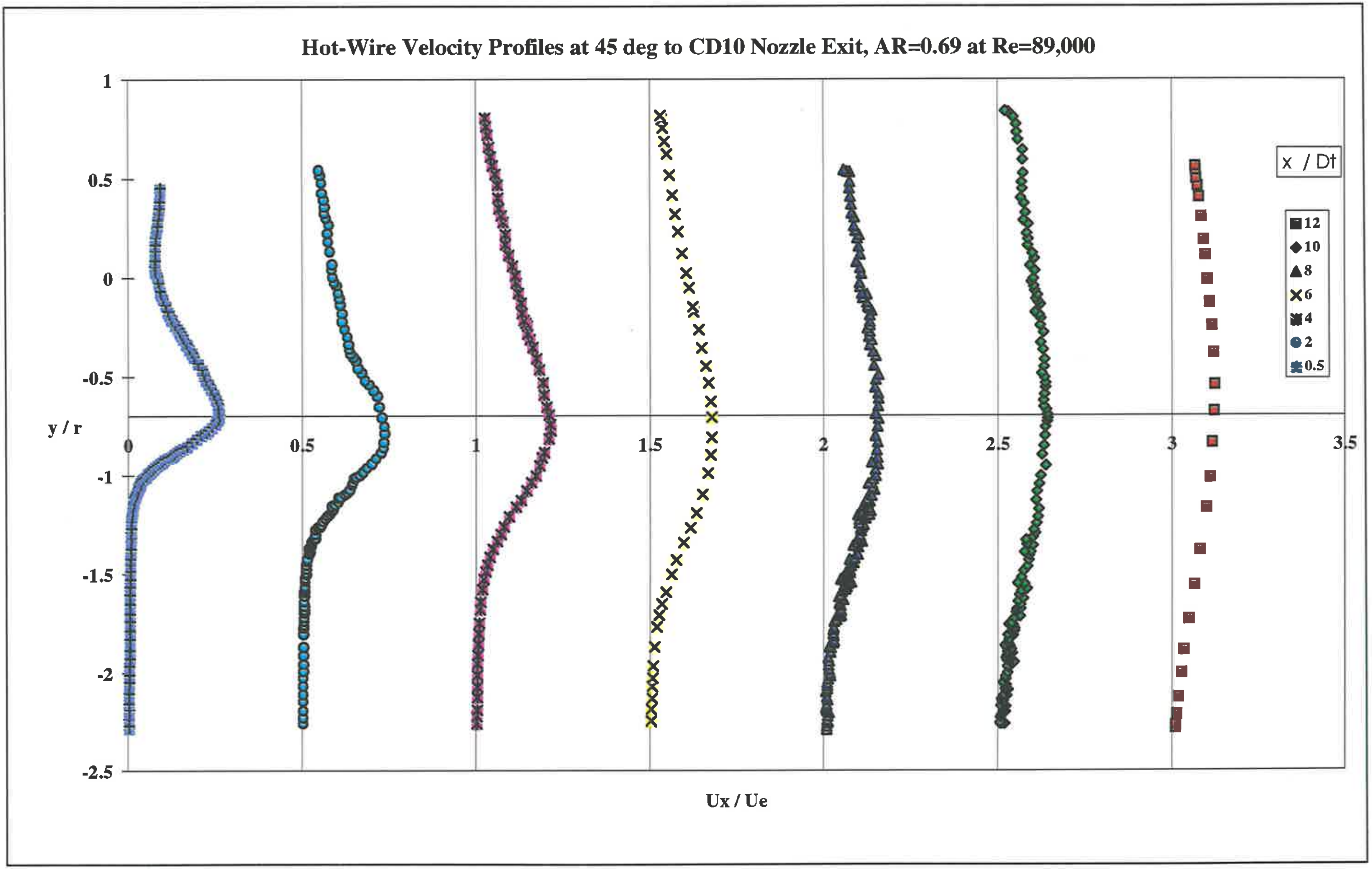

Figure 5.4. 2 Hot-Wire velocity profiles downstream from the CD10 nozzle exit measured at 45° across deflected jet centreline, at a range of locations downstream from the nozzle exit; Re = 89,000, AR= 0.69

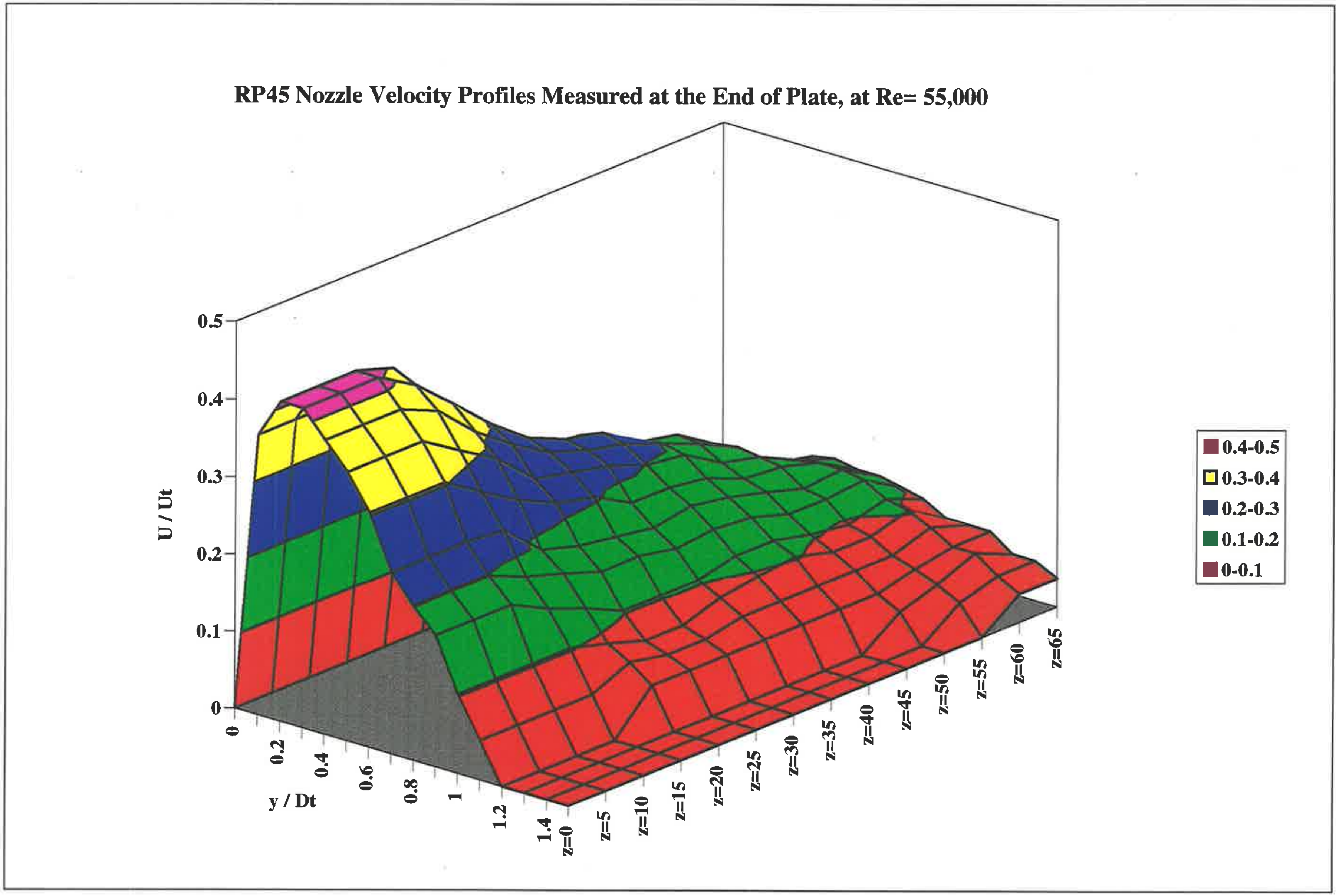

Figure 5.4. 3 Hot-wire velocity profiles at the edge of the RP45 nozzle measured across the deflected jet centreline (45°) at a range of locations across the plate; $Re_t = 55,000$.

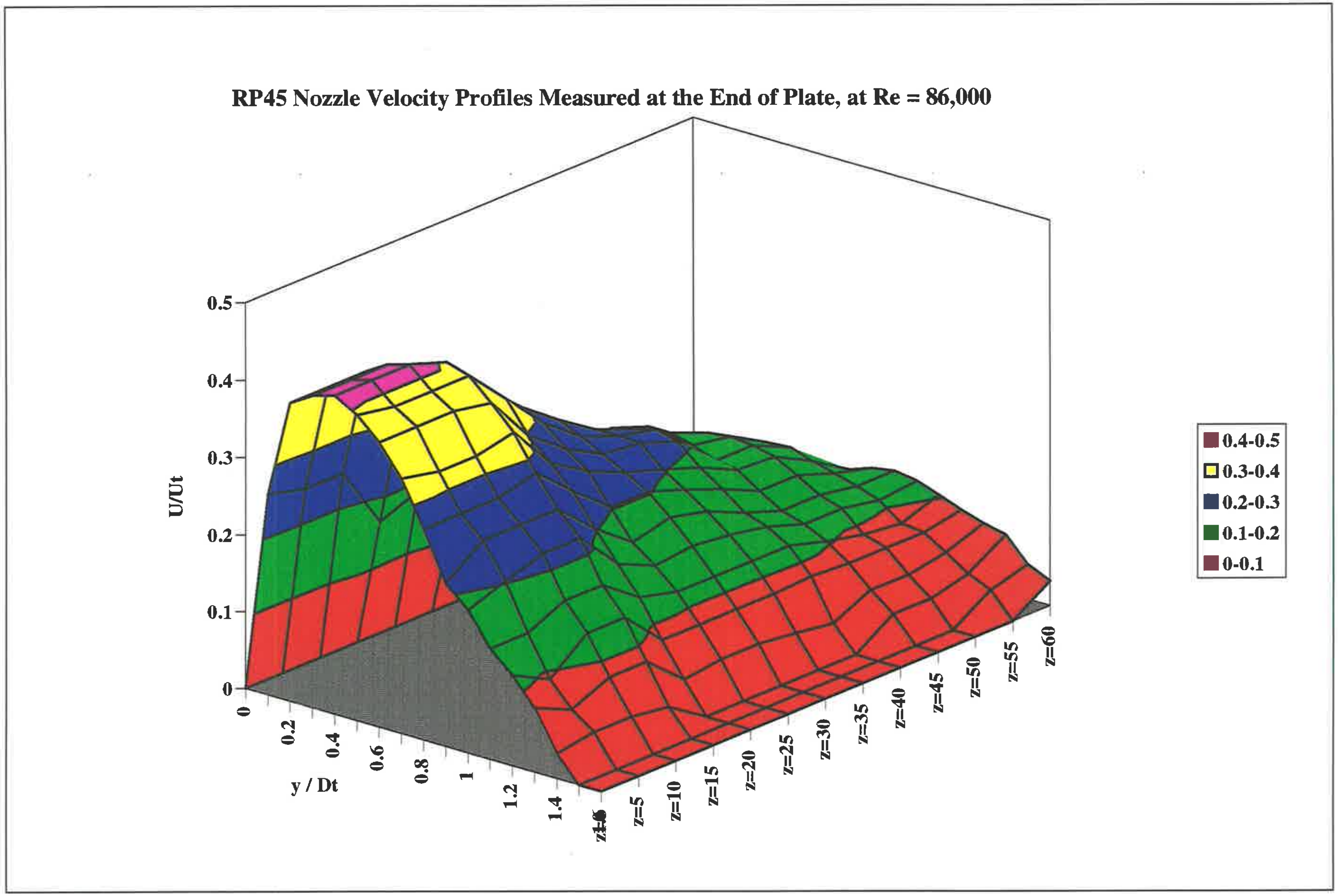

Figure 5.4. 4 Hot-wire velocity profiles at the edge of the RP45 nozzle measured across the deflected jet centreline (45°) at a range of locations across the plate; Re_t = 86,000.

5.5 Surface Flow Visualisation

The major features of the flow topology can be deduced from close examination of the surface flow patterns. The process of interpreting the flow patterns has been outlined in Chapter 4 and only the results will be discussed here. The surface flow patterns, pressure measurements and pitot traverses inside the CD10 nozzle have revealed the flow to be complex and three dimensional with stream surface bifurcations and foci present on the nozzle wall. To study the surface flow patterns, the inside surface of the nozzle is coated with china-clay (Kaolin) solution and exposed to the flow. The differences in the rate of evaporation of the oil from the mixture and the residual depths of Kaolin left on the surface reveal the areas of high and low surface shear stress. The patterns are then photographed for later analysis. As a variation within the cylindrical cavity the surface flow patterns were captured by inserting a thin sleeve coated with china-clay and exposing it to the flow. When the surface is exposed long enough to "freeze" the image, the sleeve is removed and rolled out flat to simplify the photography.

The flow of oil on the surface was used to observe the dynamic mean changes inside the nozzle and in the transparent cavity the patterns were clearly visible from outside the nozzle. The non-toxic oil for this form of visualisation is introduced as smoke and provides some indication of the jet motion. However when the smoke cools down as it comes into contact with the nozzle walls it condenses and leaves a thin film of oil on the surface. The areas of high shear then moves the oil to the areas of low shear where the oil accumulates. An impression of the flow in the region of the throat was captured by viewing the nozzle from downstream along its axis. The oil that was introduced to view the flow patterns in the throat region was mixed with graphite to increase contrast with the white background of the nozzle surface.

5.5.1 China Clay Surface Flow Visualisation

The surface flow patterns revealed by the china-clay surface flow visualisation has shown a number of features of the flow inside the nozzle. **Figure 5.5.1. (a)** is a photograph of the unrolled sleeve that has been coated with china-clay and inserted into the cavity. The flow direction was from bottom to top of the sleeve and the Reynolds number and area ratio were Re_t=72,000 and AR=0.69. The centre of the picture shows the footprint of the entrained fluid as it flows upstream towards the nozzle throat and the outer edges correspond with the centre line of the wall jet. (The left and right edges of the sleeve are adjacent within the cavity).

The dominant feature in **Figure 5.5.1. (a)** is the negative surface bifurcation along the cavity which flares out as it approaches the exit lip. Just below the exit lip in the region occupied by the wall jet the negative bifurcation corresponds with the line of separation where the primary fluid is deflected away from the nozzle wall by the exit lip. Streamwise "legs" of the negative bifurcation are where the primary fluid and the entrained fluid meet and leave the surface. These are the negative stream surface bifurcations described in the discussion of **Figure 4.5. 2**. It can be seen that as the primary fluid flows downstream along the cavity wall the lateral spread noted previously in the basic CD nozzle continues within the cavity at an increasing rate until the flow becomes tangential across the cavity and eventually reverses to carry primary fluid back towards the throat. This reversal of the primary flow to the low pressure inside the cavity is caused by entrainment of cavity fluid at the "free" surface of the primary wall jet. This low pressure also induces ambient fluid into the nozzle but if insufficient ambient fluid can be induced to satisfy the entrainment appetite, some fluid from the primary jet must recirculate back towards the throat. The surface flow patterns also show the very edge of the vortices which are formed just upstream from where the cavity joins the divergent section of the CD nozzle, (see discussion of the oil flow visualisation in Section 4.5).

Near the exit of the nozzle just upstream from the lip, at the top right and left of **Figure 5.5.1. (a)**, the negative stream surface bifurcation is only about 3 mm from the exit lip. This distance increases with the increase of the size of the lip, ie. with the decrease of the diameter of the exit ring, and follows the same trend as was shown in **Figure 4.5.9. 1** to **Figure 4.5.9. 8**. Additional data for other exit area ratios may be found in Appendix C.

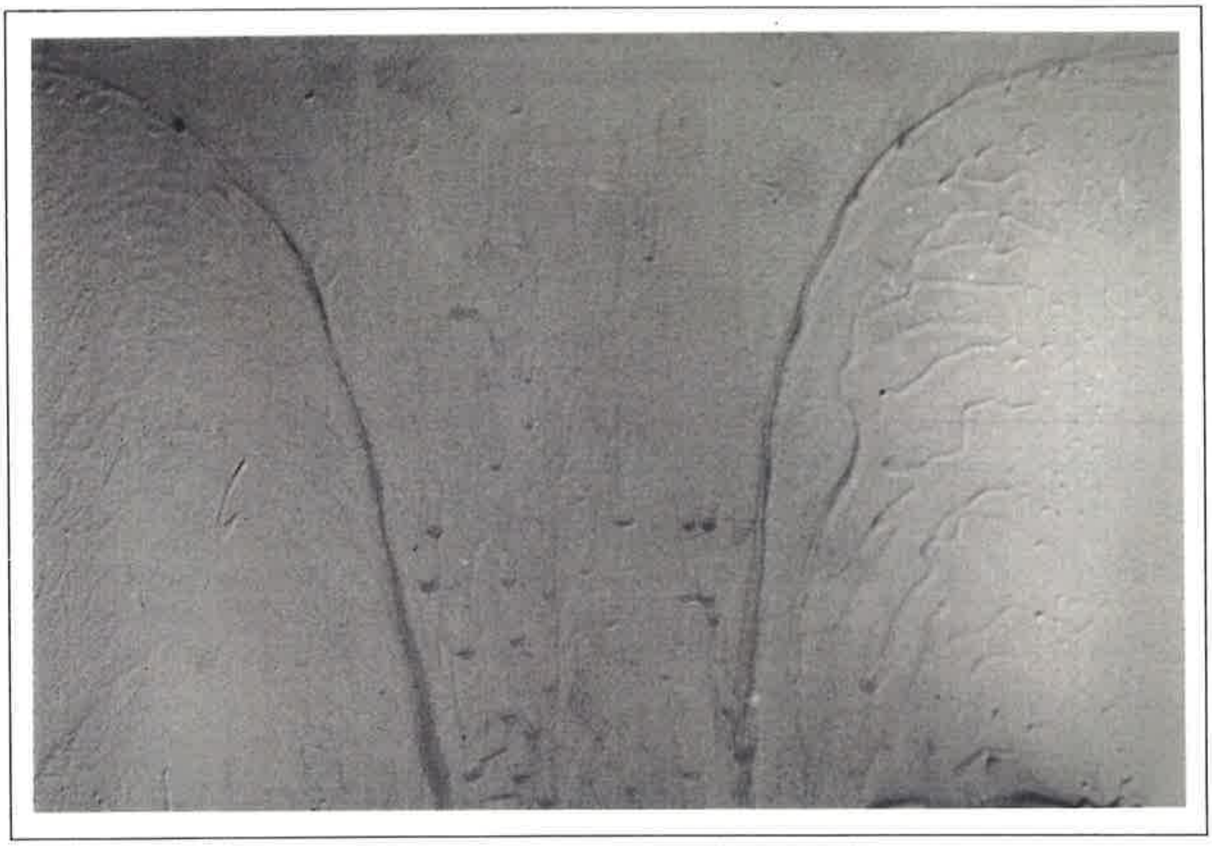

Figure 5.5.1. (a) Photograph of the unrolled sleeve inserted into the cavity of the CD10 nozzle, coated with china-clay and exposed to the flow at Re_t = 72,000, AR = 0.69, the primary jet flows from bottom to top.

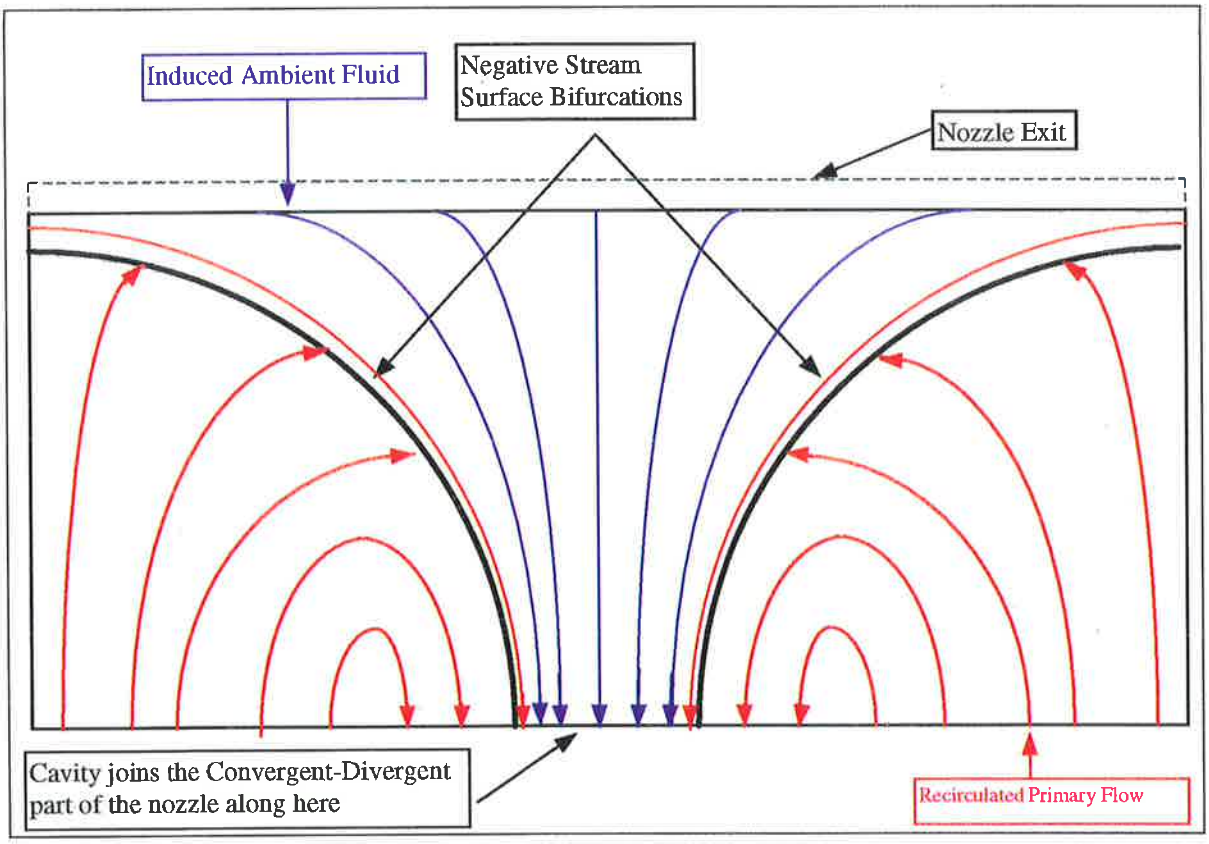

Figure 5.5.1. (b) Interpretation of the flow patterns on the unrolled sleeve at Re_t = 72,000, AR = 0.69.

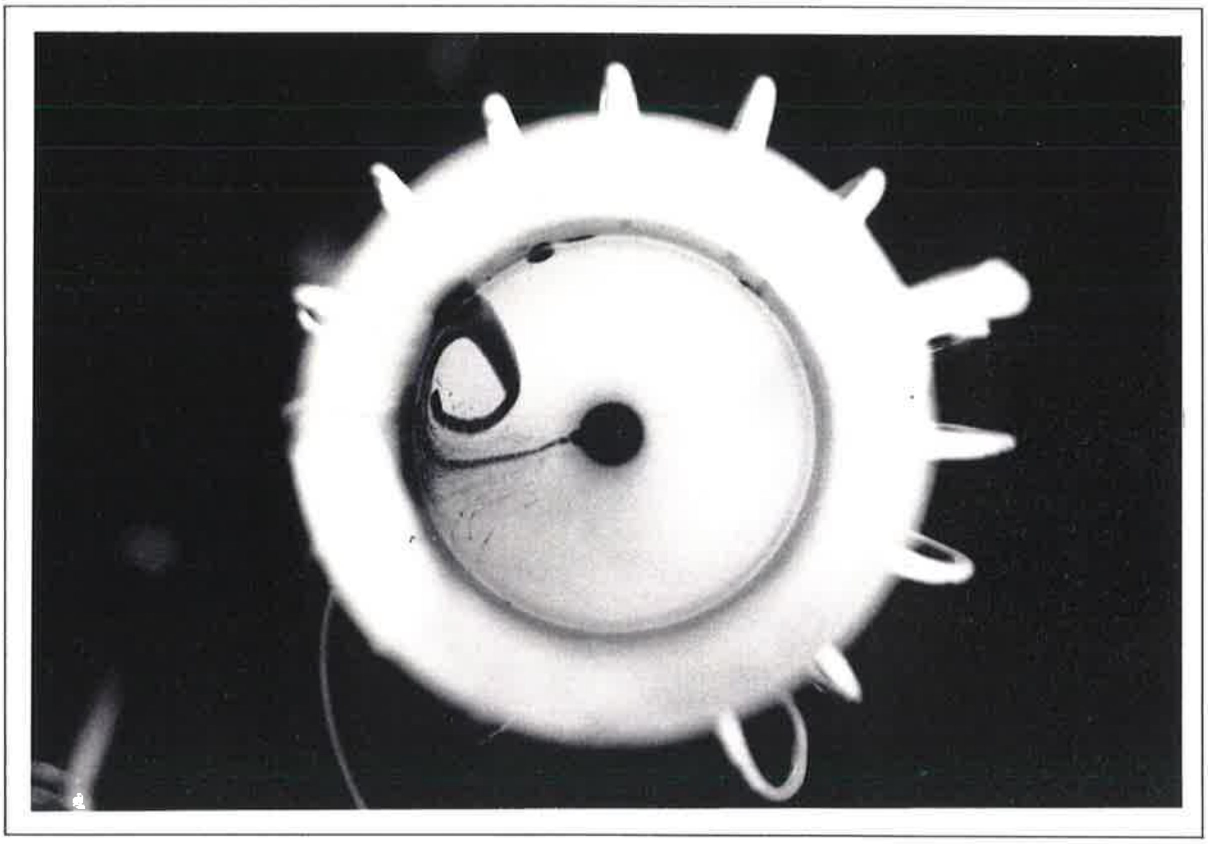

Figure 5.5.2 (a) Oil-surface flow patterns inside the CD10 nozzle near the throat, jet exiting from left to right at Re_t = 55,000 and AR = 0.69.

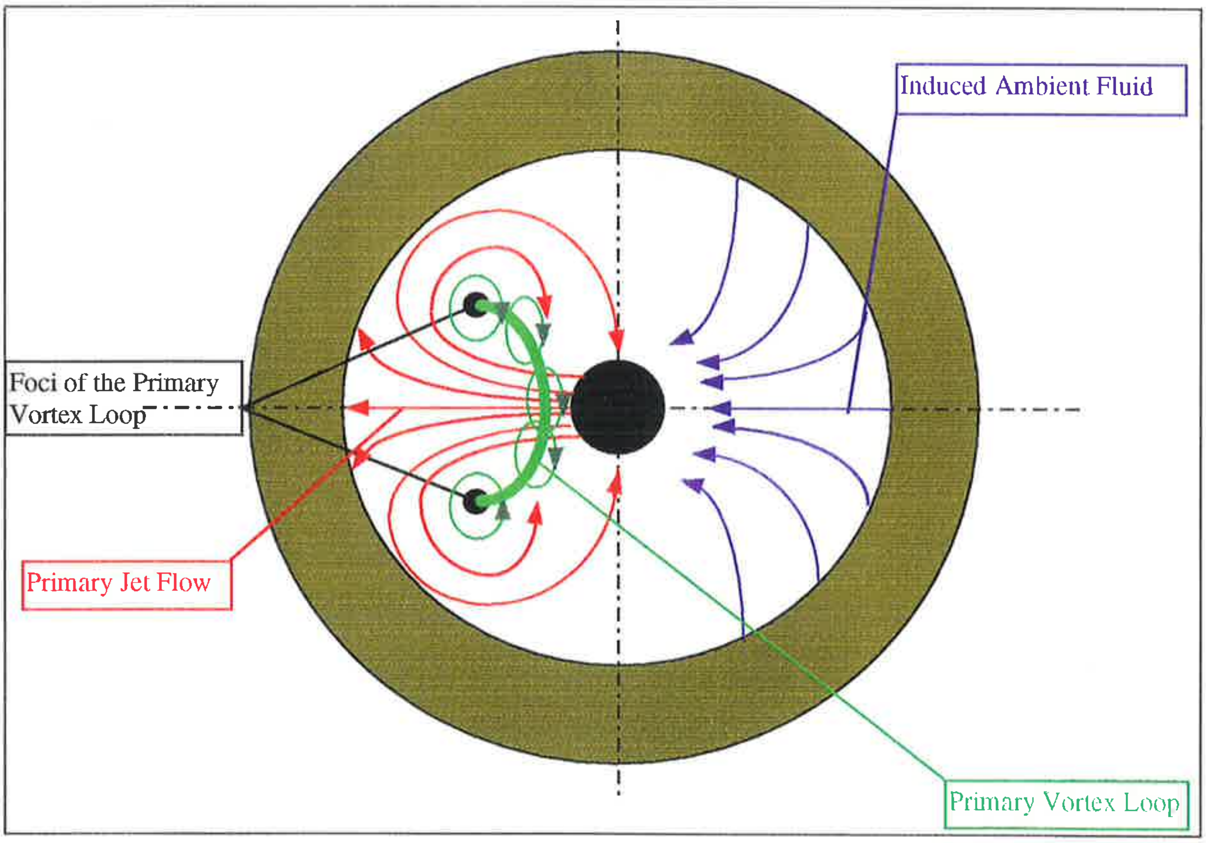

Figure 5.5.2. (b) Interpretation of the oil-surface flow patterns at Re_t = 55,000 and AR = 0.69.

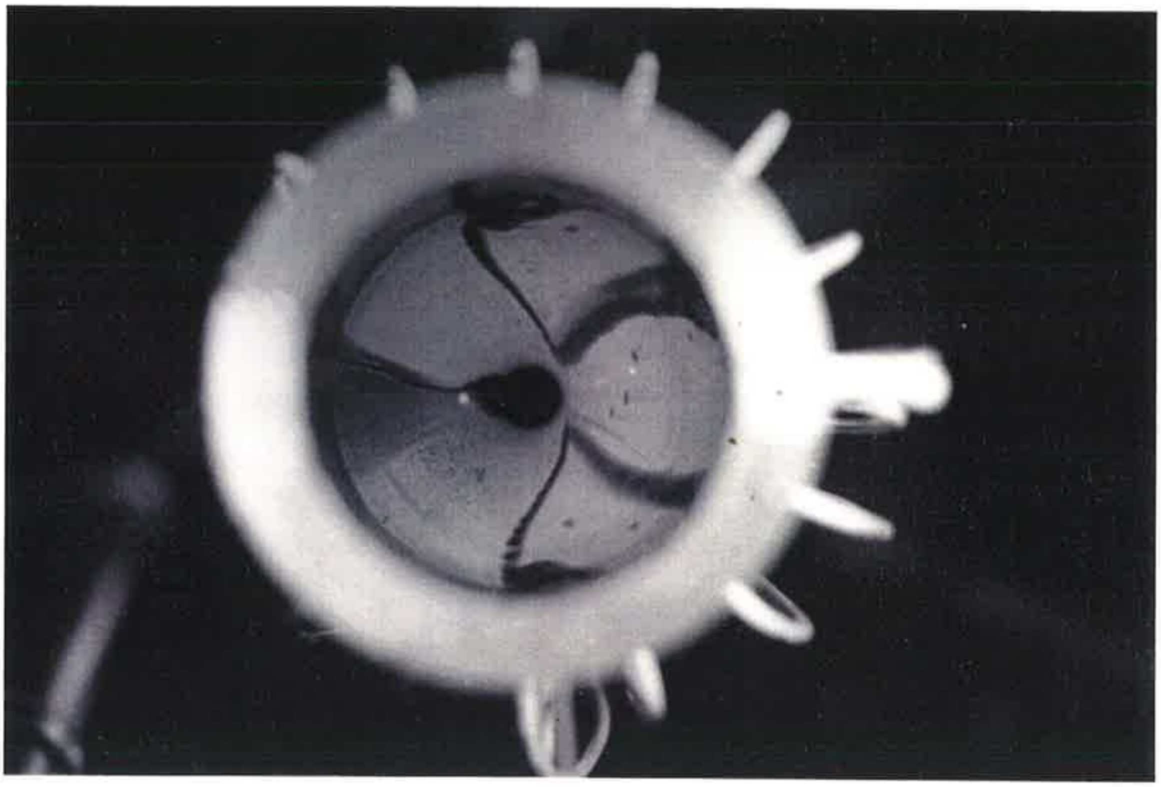

Figure 5.5.3 (a) Oil-surface flow patterns inside the CD10 nozzle near the throat, jet exiting from left to right at Re_t = 72,000 and AR = 0.69.

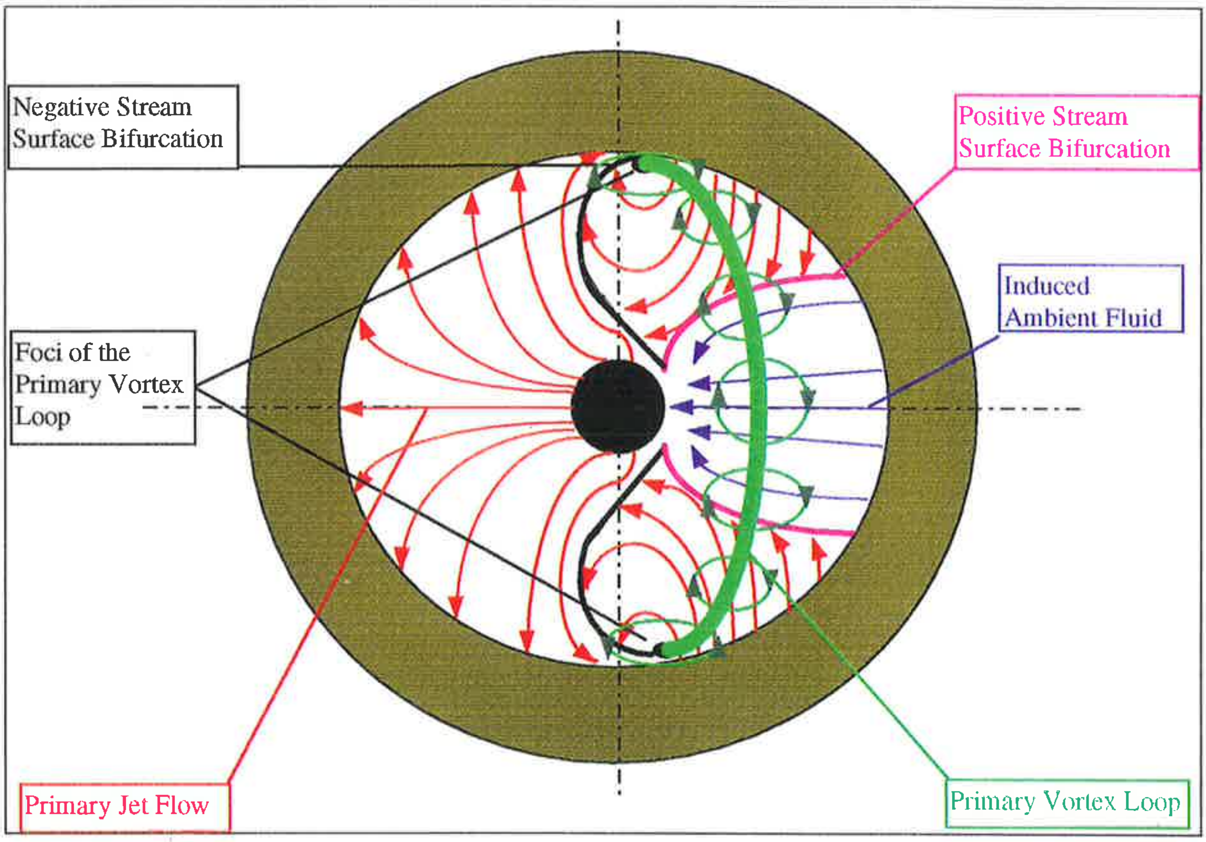

Figure 5.5.3. (b) Interpretation of the oil-surface flow patterns at Re_t = 72,000 and AR = 0.69.

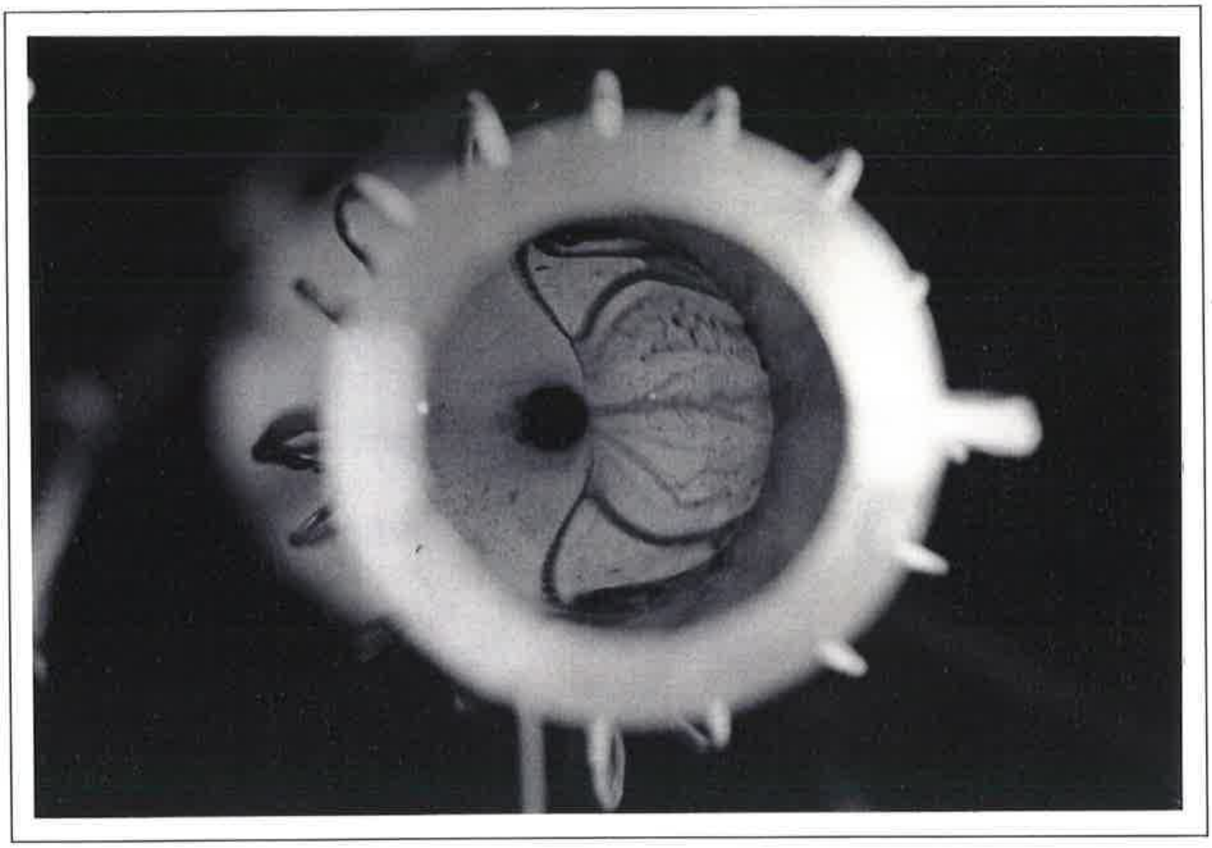

Figure 5.5.4 (a) Oil-surface flow patterns inside the CD10 nozzle near the throat, jet exiting from left to right at Re_t = 130,000 and AR = 0.69.

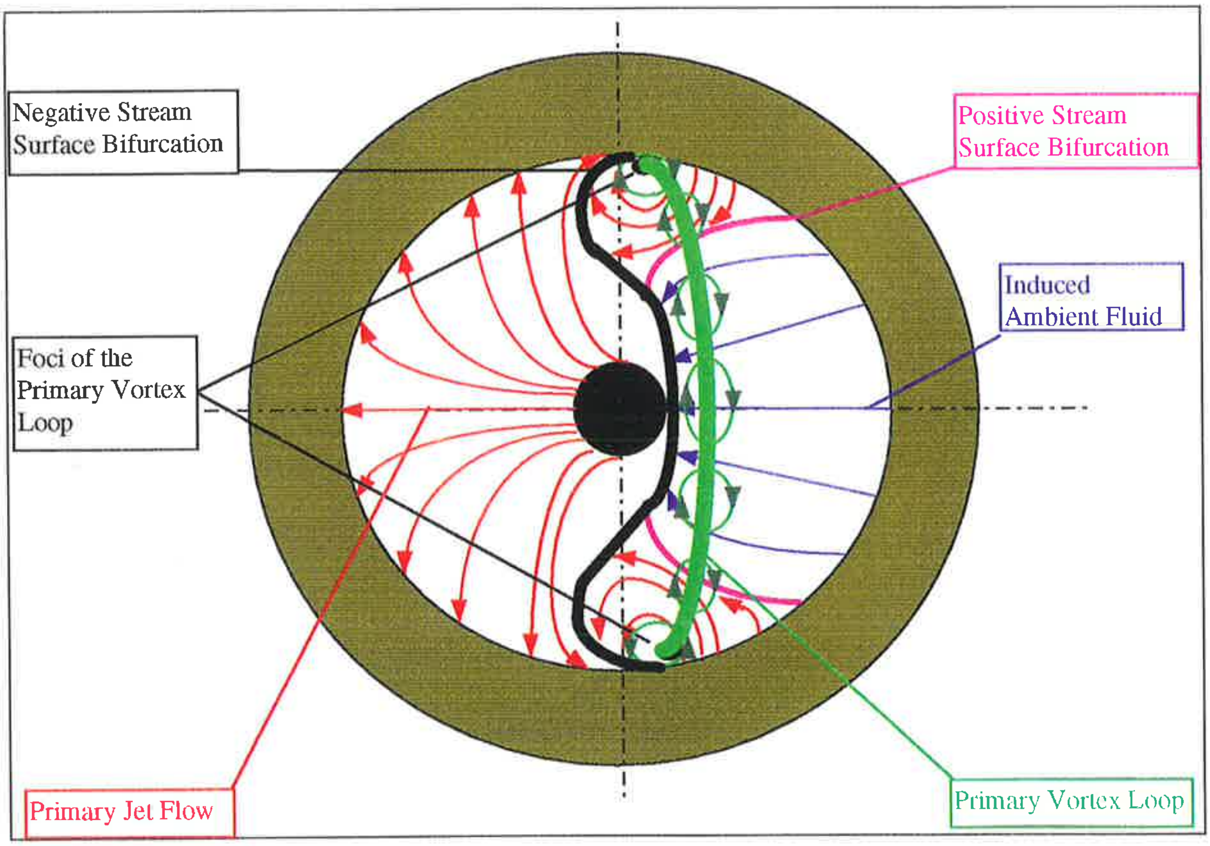

Figure 5.5.4. (b) Interpretation of the oil-surface flow patterns at Re_t = 130,000 and AR = 0.69.

5.5.2 Surface oil flow visualisation

The use of oil to visualise the surface flow was used because the double curvature of the nozzle wall made the china-clay method both difficult and imprecise. To reveal the surface flow patterns in the vicinity of the throat, an oil-graphite powder mixture was injected through a pressure tapping at the throat. The asymmetric flow was kept steady by injecting secondary fluid through a pressure tapping also at the throat, and when a steady state flow pattern was reached a photograph was taken along the nozzle axis looking upstream towards the throat. **Figure 5.5.2.** (a)shows the captured image of the oil surface flow patterns near the throat at Re_t=55,000 and AR=0.69, indicating the initial stages of the formation of one of a pair of foci that appear on the opposite sides of the secondary fluid injection location. The interpreted flow, **Figure 5.5.2. (b)**, shows that the foci are near the throat and only several throat diameters apart. **Figure 5.5.3. (a)** shows the surface flow patterns for the Re_t=72,000 with AR=0.69 and the striking difference when compared with the previous figure is that the pair of foci have moved diametrically opposite from each other and are further away from the throat, as shown in **Figure 5.5.3. (b)**. This is caused by the higher momentum fluid issuing from the throat. The formation of the negative stream surface bifurcation is also revealed in this figure. There are in fact two pairs of stream surface bifurcations present in this figure. The first pair is the continuation of the stream surface bifurcations in the cavity as revealed by china-clay flow patterns in **Figure 5.5.1. (a)** and the second pair rolls up into the foci. As the mass flux is increased, with AR = 0.69 and Re_t=130,000, the flow pattern changes as shown in **Figure 5.5.4. (a).** The area between the negative stream surface bifurcations associated with the ambient fluid moving along the cavity wall towards the throat appears to enlarge perhaps due to the recirculated higher momentum primary fluid moving toward the throat. The foci have moved further away from the wall jet and remain at a distance of around 6 throat diameters downstream from the throat.

The side view of the oil flow patterns inside the cavity shown in **Figure 5.5.5. (a)** and the interpretation shown in **Figure 5.5.5. (b)**, reveals the flow of the primary jet as it expands and encounters the entrained fluid, at which point the flow separates and thus produces the negative stream surface bifurcation which is clearly visible. The flow Reynolds number is 72,000 and the flow exits the cavity from left to right. **Figure 5.5.6.** (a) shows the same flow from a position where the flow is exiting towards the viewer, with interpretation of these flow patterns are shown in **Figure 5.5.6.** (b). It shows the two negative stream surface bifurcations between which the flow is down toward the throat while on the other side the primary fluid is turning along the cavity wall toward the viewer and down. This figure confirms the previous findings using china-clay flow visualisation in **Figure 5.5.1.** (a). Surface flow patterns along the cavity wall, where the wall jet is attached to the cavity, shown in **Figure 5.5.7.** (a), shows the separation region near the exit lip which is the negative stream surface bifurcation that continues down along the opposite side to the wall jet and marks the boundary between the primary and the entrained ambient fluid and or recirculated primary fluid , some of it coming from behind the lip on the side of the attached wall jet. This small sample of the visualisation techniques presented here is representative of the flow patterns at higher Reynolds numbers and other exit areas tested. The changes in flow patterns with exit area is similar to that described in Chapter 4 for the CD nozzle. The effect of cavity is to increase the amount of mixing inside the nozzle such that when the wall jet reaches the exit lip, the jet momentum is more diffuse and the amount of primary fluid recirculated toward, and to strengthen, the main vortex is lower than for the CD nozzle.

5.5.3 Discussion of Results

The surface flow visualisation results presented above are indicative of the flow patterns of the various geometric configurations such as the exit area and would consume a large part of the thesis if presented in detail. Qualitatively the surface flow patterns in the CD10 nozzle compare favourably with those in the CD nozzle. In both cases the flow pattern changes significantly with increase in mass flux as shown above, but features such as the foci remain present but shift with changing flow parameters and nozzle configuration. The stream surface bifurcations are also present in all geometric conditions considered. It can be concluded that the flow patterns in the vicinity of the throat, once established, remain but are shifted due to different quantities of primary fluid being returned towards the throat determined mainly by the size of the exit lip. Flow patterns are comparable with the flow patterns in the CD nozzle and in both cases there appears to be a pair of foci on opposite sides of the nozzle. It is postulated that these foci are the footprints of a strong vortex loop which appears to play the major role in turning the jet as it leaves the nozzle.

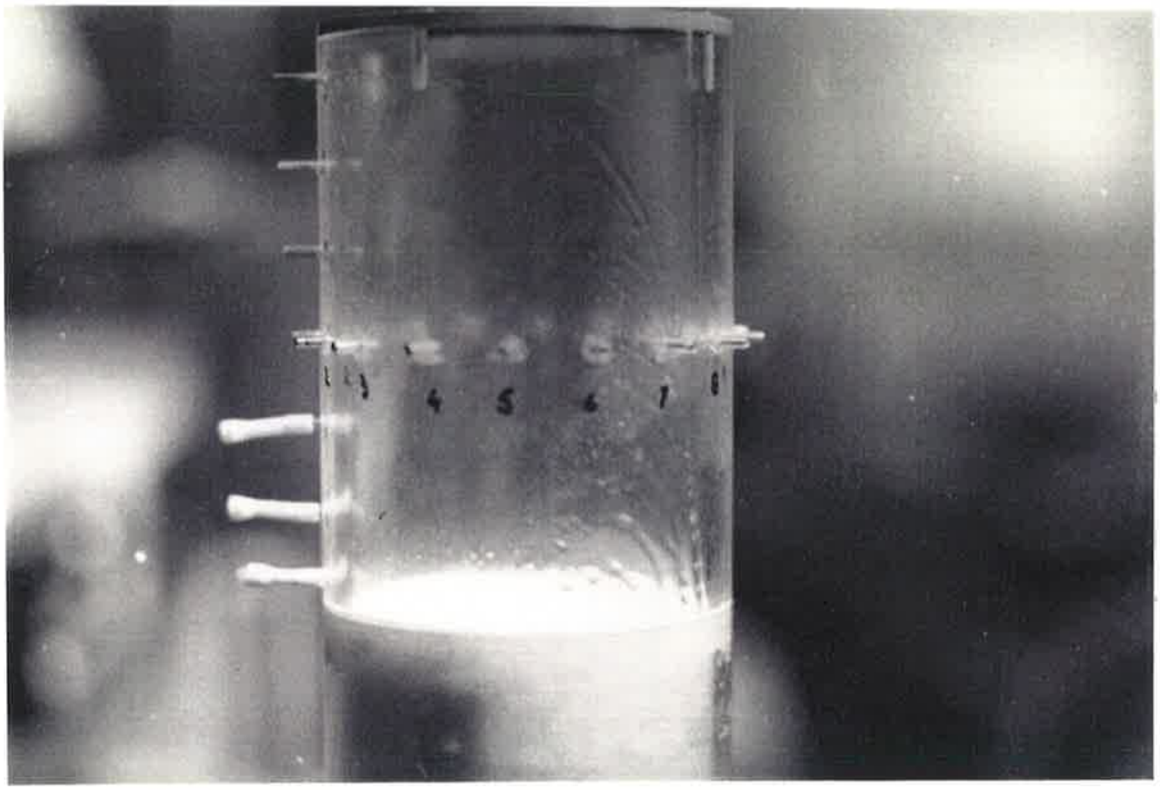

Figure 5.5.5. (a) Side view of the oil-surface flow patterns inside the CD10 nozzle marking the negative stream surface bifurcation, jet exiting from left to right: Re_t = 72,000 and AR = 0.69.

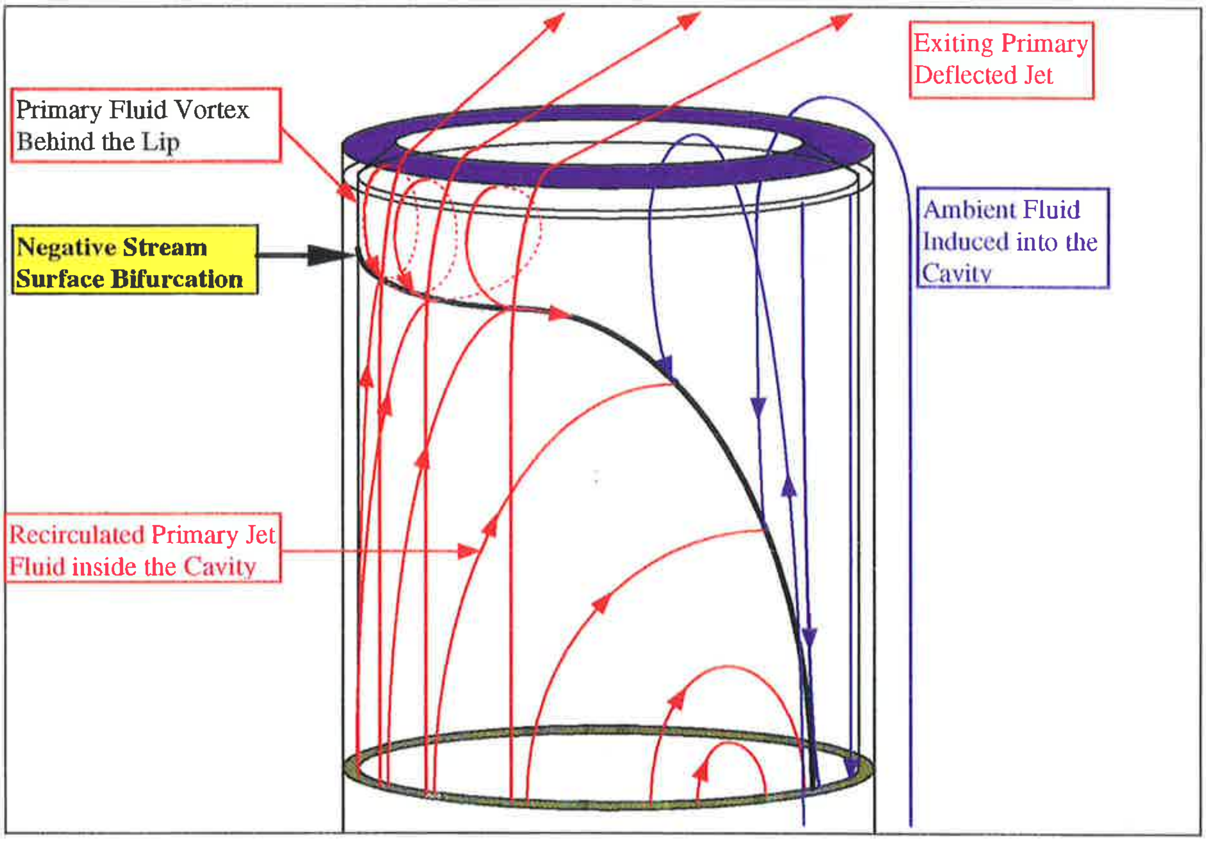

Figure 5.5.5. (b) Interpretation of the oil-surface flow patterns inside the CD10 nozzle marking the negative stream surface bifurcation, jet exiting from left to right: Re_t = 72,000 and AR = 0.69.

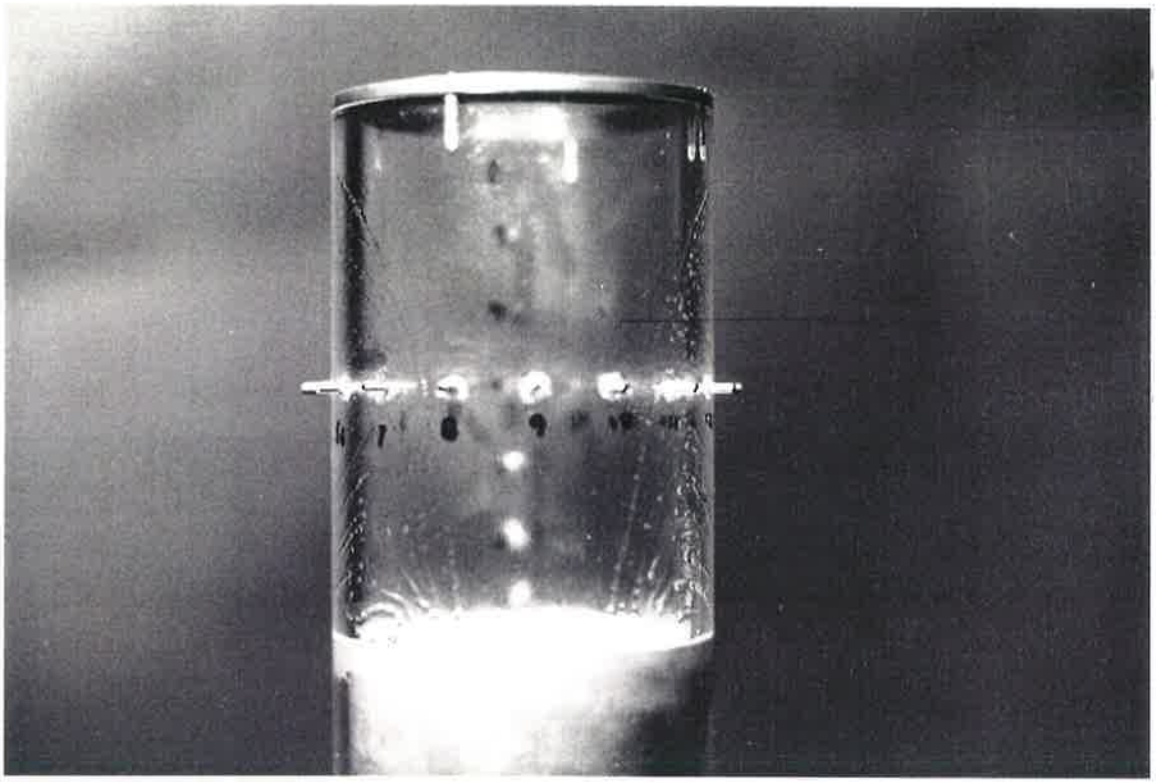

Figure 5.5.6. (a) Front view of the oil-surface flow patterns inside the CD10 nozzle marking the negative stream surface bifurcation, jet exiting toward the viewer: $Re_t = 72{,}000$, $AR = 0.69$.

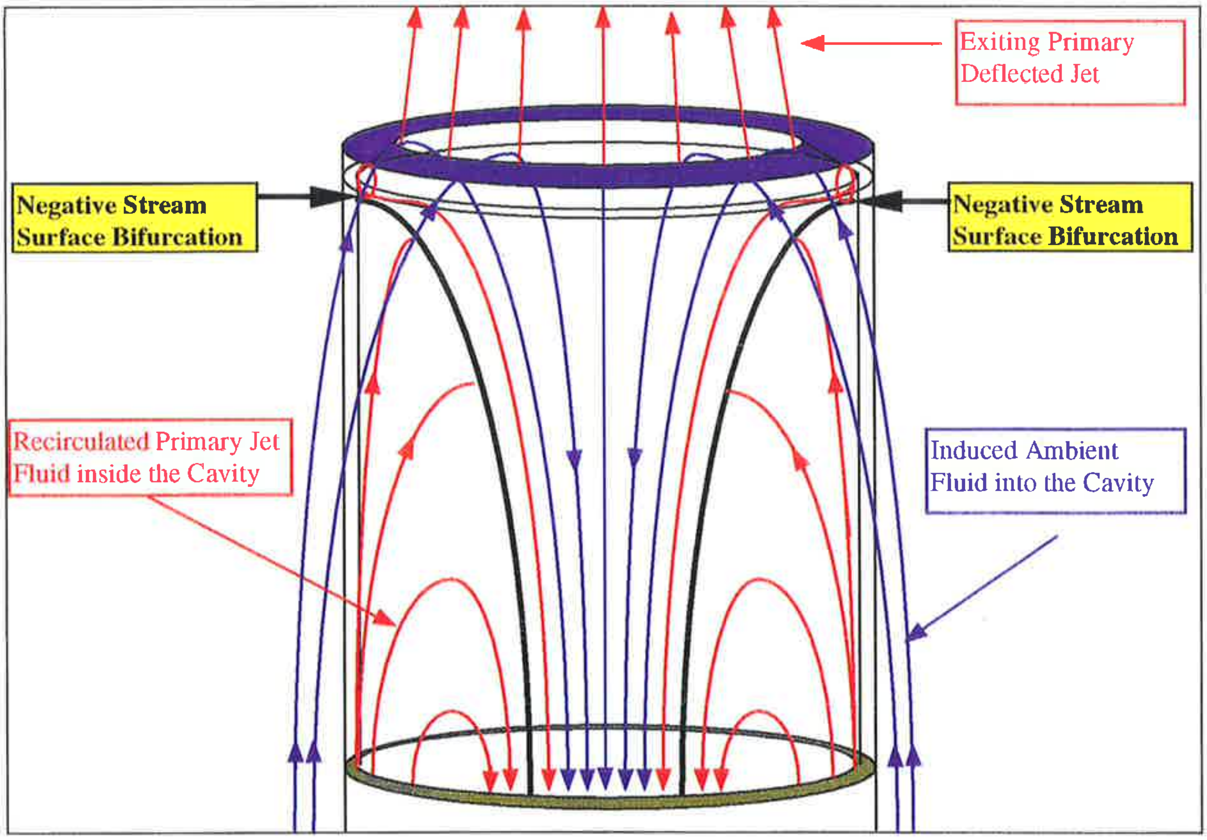

Figure 5.5.6. (b) Interpretation of the oil-surface flow patterns inside the CD10 nozzle marking the negative stream surface bifurcations, jet exiting toward the viewer: $Re_t = 72{,}000$, $AR = 0.69$.

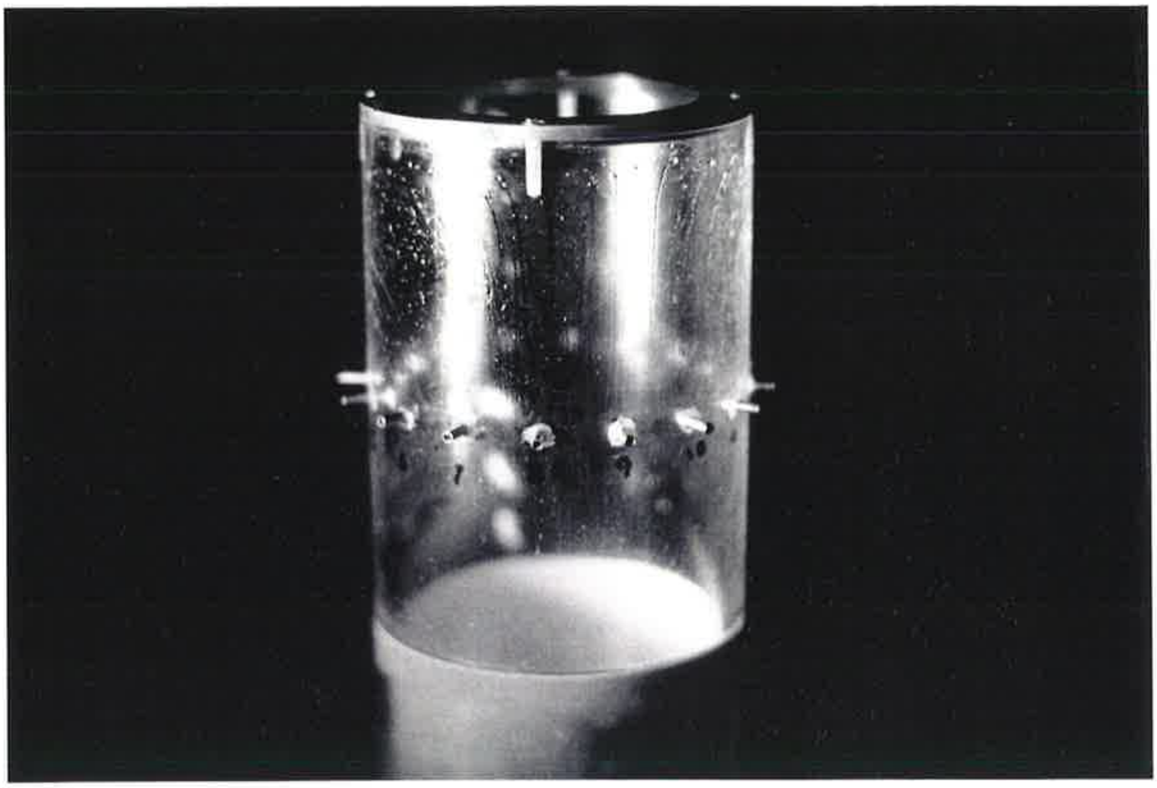

Figure 5.5.7 (a) Oil-surface flow patterns inside the CD10 nozzle showing the wall jet separation near the exit lip, jet exiting away from the viewer: Re_t = 72,000 and AR = 0.69.

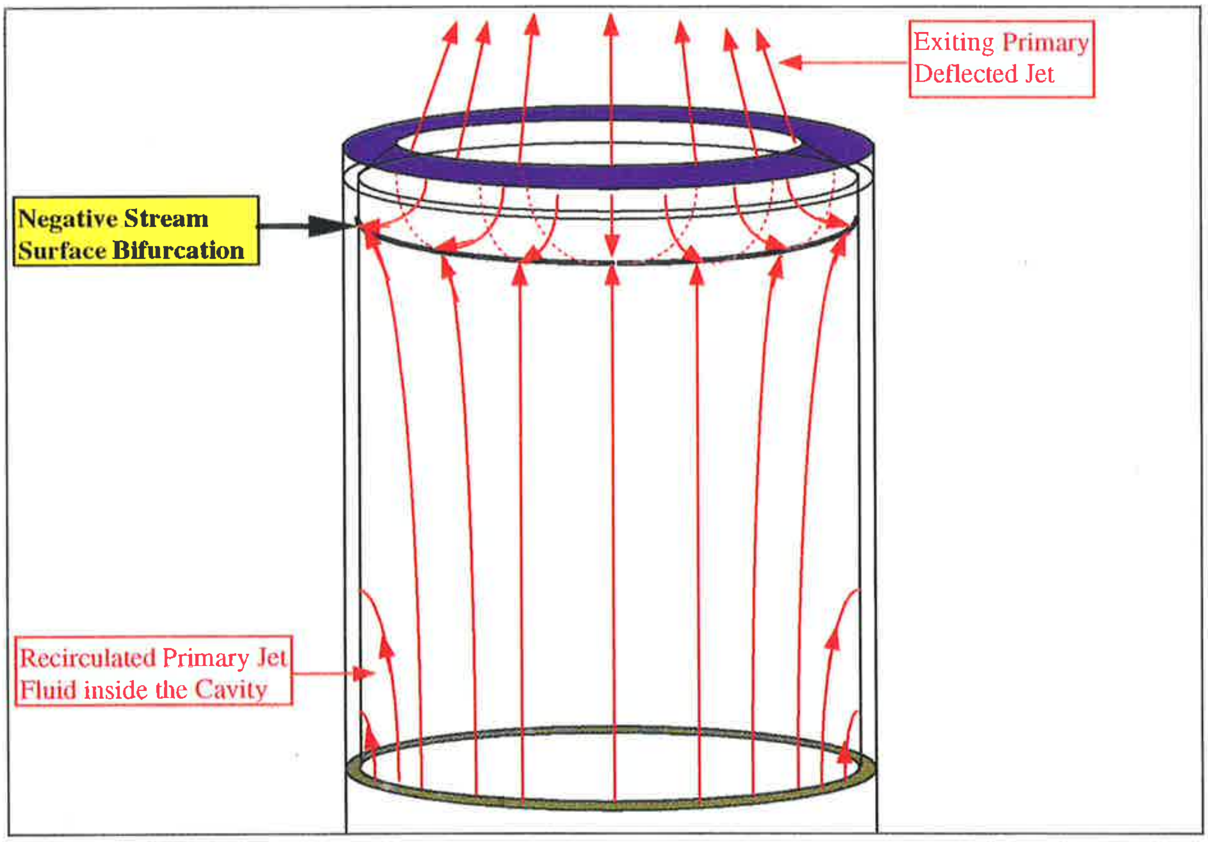

Figure 5.5.7. (b) Interpretation of the oil-surface flow patterns inside the CD10 nozzle with the jet exiting away from the viewer: Re_t = 72,000 and AR = 0.69.

5.5.3.1 Stability of Flow Inside the Nozzle

It has been found that the azimuthal direction of the asymmetric jet is established by the azimuthal position of the secondary fluid injection. Once the azimuthal direction has been established with the secondary injection, the flow inside the cavity is stable. Without any secondary injection the flow is unstable and is liable to change its azimuthal orientation in an unpredictable manner and without warning. The amount of ambient fluid entrained into the cavity depends on the exit area and for a given exit area, the amount of fluid entrained fluctuates due to the apparent instability of the deflected jet exiting across the exit plane. This has been shown by other researchers in the department using hydrogen bubbles in water to visualise the amount of ambient fluid entrained into the cavity. This work has been carried out on a Orifice-Cavity-Orifice (O-C-O) nozzle configuration but results apply equally to the present test nozzles. The instability is more apparent in the O-C-O nozzle configuration than in the CD nozzle due to the reversed flow foot found at reattachment after separation at the upstream orifice in the O-C-O nozzle flow. This does not occur in the CD nozzle flow, except for a very low velocity flow, below Re_t of several thousand, as discussed in Chapter 4, the wall pressure on the wall jet side, just downstream from the throat, is sub-atmospheric for a number of nozzle configurations. The flow from CD nozzle is more stable at high mass flow rates, in any case, the secondary fluid injected at the throat pressure tapping fixes the azimuthal position of the wall jet.

5.6 Influence of Exit Rings on the Flow

The primary function of the exit ring is to deflect the wall jet across the nozzle axis. In the process of doing so, some of the primary fluid is channelled back into the nozzle to feed the two foci of the vortex loop found downstream from the throat. The size of the exit lip determines the deflected jet angle, up to a maximum value of 65° at AR=0.34 for the CD10 nozzle, which corresponds to an exit diameter of 35mm. This is the exit area that also produces larger deflected jet angle in CD and CD6 nozzles. When the exit area is reduced further the static pressure inside the cavity is above atmospheric and the deflected jet angle begins to decrease. The influence of the exit ring diameter is similar to that for the CD nozzle but because the flow has defused more in the CD10 than in the CD nozzle, the maximum angles achieved are less.

The second point to note is that when the exit ring is placed at the nozzle exit, some primary fluid is redirected back into the nozzle and this reduces the ambient fluid required to be entrained. This primary fluid is seen to be directed towards the two foci and appears to feed the vortex loop which joins them. As the lip size increases, a point is reached when the exit area is so restricted that no ambient fluid is induced into the cavity and only primary fluid is redirected back toward the throat. This also occurs with the CD nozzle.

5.7 Conclusions

The CD10 nozzle has been shown to have internal flow patterns similar to those in the CD nozzle. The measured velocity profiles inside the nozzle have the same form as in the CD nozzle but the magnitude of the velocity vectors are reduced due to the nozzle length and the azimuthal diffusion associated with the increase in length. By the time the wall jet reaches the exit plane and the exit ring, its momentum has been spread over a larger cross-sectional area and therefore the stagnation pressure on the ring is less, the vortex loop is weaker and the jet is deflected at a lesser angle. The nozzle interior is sub-atmospheric up to the maximum jet deflection angle, at which point the angle begins to decrease and the pressure inside the cavity increases above atmospheric as the exit area is reduced further. The flow patterns inside the cavity show a pair of foci belonging to a vortex loop downstream from the throat. The vortex line is stretched as it loops downstream due to the diverging wall curvature. The foci are seen to be fed by the primary fluid being returned upstream from the exit lip. The fluid that spirals into a pair of foci leaves the surface via the low pressure core of the vortex loop and transported downstream by the primary fluid. **Figure 5.7. 1** shows the postulated vortex interaction inside the CD10 nozzle for a configuration with a modest exit lip This postulate is similar to the vortex structure deduced in the CD nozzle in Chapter 4.

It has been shown that a range of deflected jet angles can be produced from CD10 nozzle by reducing the exit area, through placement of an exit ring of a particular diameter at the nozzle exit plane. The azimuthal direction of the flow is controlled by the azimuthal position of the secondary fluid injection. The efficiency of the CD10 nozzle is slightly lower than that of the CD nozzle but still produces some very useful thrust. The CD20 nozzle has been found not to be very effective in deflecting the wall jet at large angles. The jet from the CD20 nozzle is deflected at an average angle of around 40°, with the smallest lip, and maintains that angle for a large range of lip sizes. For an exit area ratio greater than 0.25, the jet deflection angle reduces. The flow inside the CD20 nozzle near the exit has been found to be a diffused jet with some high momentum fluid being returned along the cavity wall opposite from the point of secondary fluid injection.

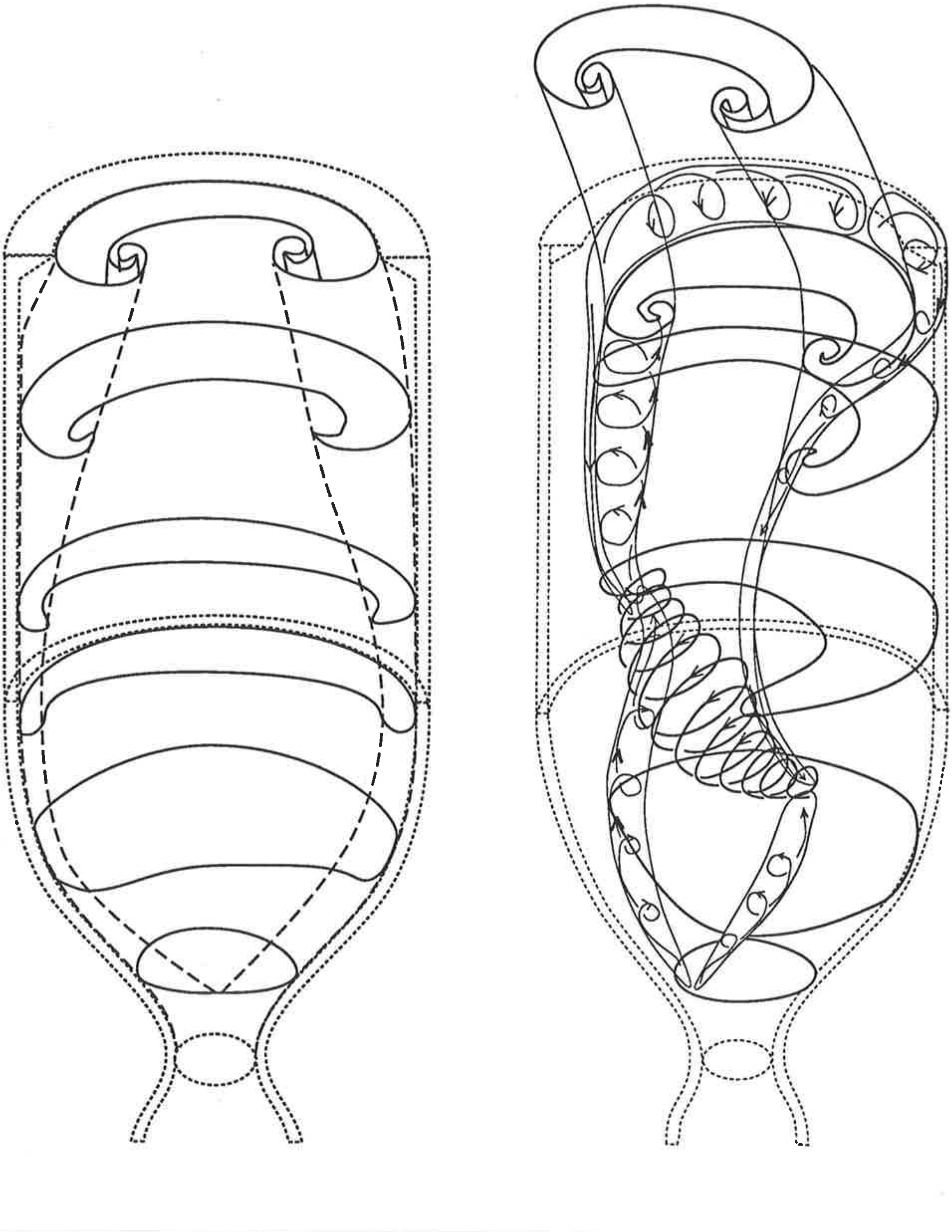

Figure 5.7. 1 Deduced vortex skeleton built from the interpretation of the surface flow visualisation figures inside the CD nozzle showing the interaction between vortex loops.

CHAPTER 6.

Thrust Evaluation of CD, CD10 and CD20 Nozzles

6.1 Introduction

The thrust from a selection of nozzles has been measured using the apparatus described in Chapter 2. A set of strain gauges fitted to the base of the air supply tube, details of which could be found in Appendix A, was connected to yield voltages which were directly proportional to the side force produced by the vectored jet. The set of thrust measurements for each configuration span a range of mass flow rates up to 40×10^{-3} kg/s, corresponding to a driving pressure of 100 kPa gauge. Vibrations excited by fluctuations in the thrust from the nozzle at the end of the flexible supply tube were resolved by applying a continuous known side force and this bias was accounted for in the analysis. Thrust produced by the CD, CD10 and CD20 nozzles with exit ring diameters d_e/d_t from 2 to 5.5 are presented here.

The azimuthal position of the deflected jet in the CD, CD10 and CD20 nozzles is controlled by the azimuthal location of the secondary fluid injection at the nozzle throat. Any one of eight pressure tappings at the throat of the nozzle can be used as the injection point to provoke asymmetric separation of the primary flow immediately downstream from the throat. The injection of air is normal to the primary flow and behaves as a jet in a cross flow **[18,32,53,56,69]** as discussed in previous Chapters. As the secondary jet mixes with the primary jet it produces locally an adverse pressure gradient which causes the primary flow to separate from the diverging wall downstream from the injection position. As the secondary jet penetrates the primary it is bent over and in some cases could be approximately aligned with the surface, when it reaches the diametrically opposite wall, slightly down stream from the throat. This adds momentum to the flow near the wall as does a wall jet and so keeps the primary jet attached to the wall. Reference may be made to the general field of separation control by increasing the momentum in the boundary layer close to the surface, eg. Duncan, Thom and Young (1970).

The primary jet expands to a kidney shape cross-section and impinges on the exit lip as a high momentum wall jet. The exit lip causes the jet to separate immediately upstream. Below the stagnation line on the exit lip the flow forms a strong vortex which feeds back into the other major vortex structures within the nozzle, as described in Chapter 4 and Chapter 5. The structures cause the primary jet to deflect and produce the vectored thrust, the measurements of which are reported in this Chapter.

6.2 Apparatus

The vertically orientated experimental rig, shown in **Figure 2.1. 1**, together with a set of strain gauges mounted at the base of the flexible supply tube, shown in detail in Appendix A, was used to measure the bending moments produced by the vectored thrust issuing from the nozzle. The voltage signal from the input conditioner was digitised using an analogue to digital (A/D) card and the data were stored via a personal computer (PC) for later analysis. The card is capable of sampling 16 channels simultaneously at 2 KHz. Record lengths were varied to establish that required, and it was found that a period of 5 seconds was sufficient to obtain a reliable average. Data were then analysed and are presented as time averaged values of transverse components of the thrust. It should be noted that the stiffness required to maintain stability of the nozzle precluded the use of strain gauges to measure the axial thrust component. Instead, the angle at which the jet leaves the nozzle was measured, and the total vectored thrust calculated.

Thrust has been measured for a number of nozzle configurations and exit areas. Vectored thrust from the CD, CD10 and CD20 nozzles combined have been evaluated for a range of exit areas and mass flow rates. The performance of other nozzles such as RP45, RP60, B45 and B90 have also been evaluated to provide a comparison with conventional thrust vectoring systems.

6.3 Experimental Results

The transverse reaction or side force produced by the vectored jet from each of the nozzles was measured from the strain gauge outputs discussed above. The angle at which the jet leaves the nozzle was measured in a number of ways, as discussed in Chapter 4 and 5. From these two measurements the total thrust has been calculated. The thrust produced by each of the nozzles is presented as a percentage of the total thrust that would have been produced by a convergent nozzle for the same mass flux and same throat diameter expanding abruptly in atmospheric conditions. Thus the thrust efficiency η is here defined as the _ratio_ of the total thrust F, produced by the deflected jet directed at some angle α away from the nozzle geometric centreline, and the thrust F^{*}, that would have been produced by the convergent nozzle for the same mass flux. While other definitions of thrust efficiency are possible, the present definition in terms of mass flow rate is believed to be compatible with the fact that the effectiveness of the rocket motor can be gauged by the effective work done by the jet during the burning time of the fuel, which is the integral of the thrust with respect to the distance travelled. The deflected jet angles produced by the various nozzles are summarised in **Figure 6.3. 1**. The results show that the maximum angle of deflection of the jet is around 80°, for the limited range of nozzles tested. For this situation, the accuracy with which the total thrust is produced by the nozzle is determined primarily by the accuracy of the strain gauge matrix, which is high. On the other extreme, when the deflected jet angle is relatively small, say of the order of 20°, the calculated total thrust depends on the accuracy with which the jet angle can be measured and a small uncertainty in the measured angle has an influence which increases as the angle decreases. Thus a large uncertainty must be accepted in the calculation of the total thrust.

6.3.1 CD Nozzle

The CD nozzle consists of the convergent-divergent section of the nozzle with downstream length from the throat of 6 throat diameters. For the range of mass flow rates considered, the thrust vectoring efficiency for the nozzle is plotted in **Figure 6.3. 2** as a function of mass flux ratio m/m^*, where m is the mass flux and m^* is the mass flux for sonic flow through a convergent nozzle exiting to ambient. **Figure 6.3. 3** shows the effects of both the mass flux and the exit area on the thrust vectoring efficiency as a 3-D surface plot. The results show that for the exit area ratio AR = 0.84, representing the 55 mm exit diameter, an average thrust efficiency η of 70% has been achieved and with the jet deflected $\alpha = 25°$ from the nozzle axis. These values are sustained up to the mass flux ratio $m/m^* = 0.8$ where compressibility begins to effect the flow. This character is typical for all the exit areas tested. For the exit area ratio AR = 0.34, representing the 35 mm exit diameter, the thrust efficiency η reaches a minimum value of 45% but produces the maximum deflection of the jet of $\alpha = 80°$. Again the thrust efficiency is initially constant and as the mass flow rate is increased, the thrust efficiency decreases. As the exit area is reduced further beyond AR = 0.34, the thrust efficiency η increases reaching a value of 60% when AR = 0.11 with the jet deflected to $\alpha = 45°$ away from the nozzle axis, as shown in **Figure 6.3. 1**. These angles were also plotted against the exit to cavity area ratio in **Figure 4.3. 19**. The area ratio AR = 0.11, was the minimum exit area tested, and corresponds to $d_e/d_t = 2$. The thrust efficiency η can be summarised as decreasing with the reduction of exit area, reaching the minimum value at the maximum deflected jet angle of 80°, then increasing again to 60% for the minimum exit area tested.

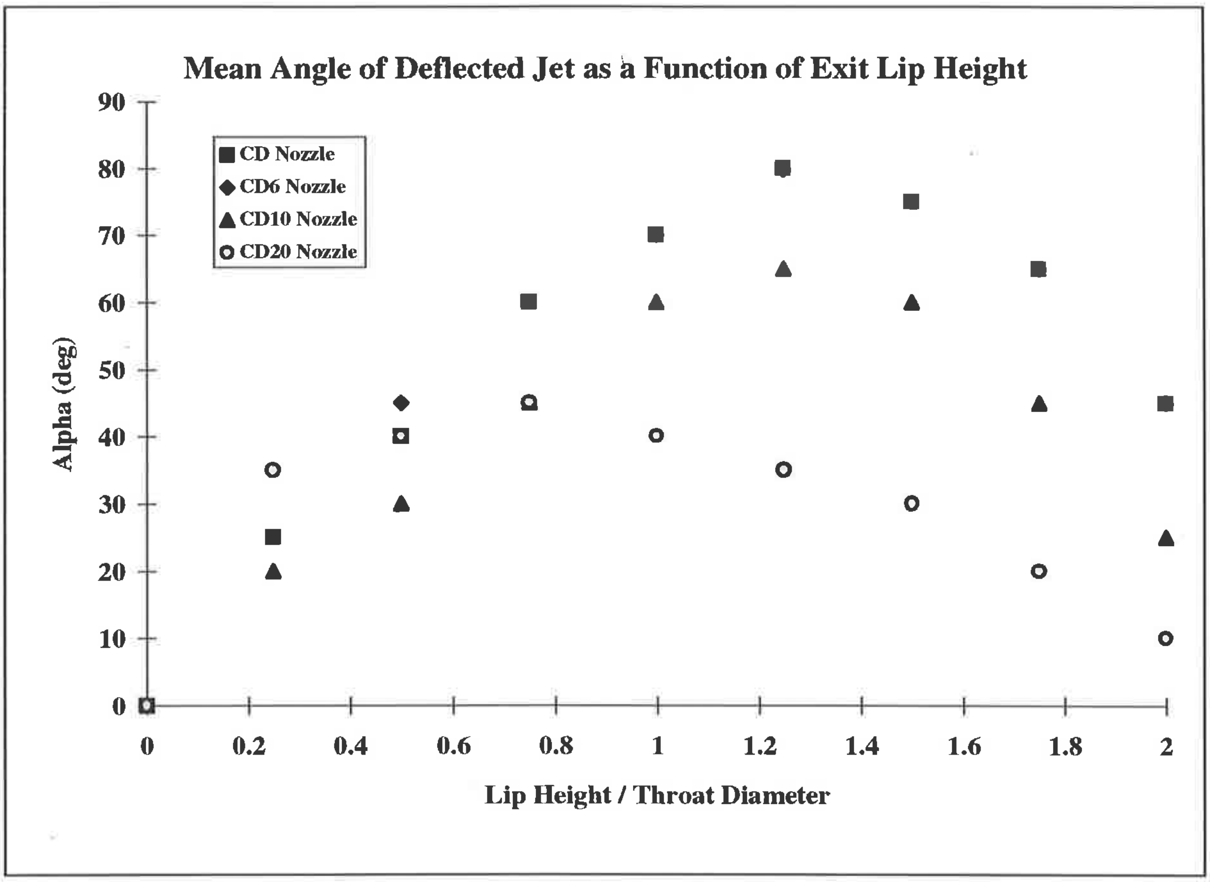

Figure 6.3. 1 CD, CD6, CD10 and CD20 nozzle deflected jet angles plotted against the exit lip height.

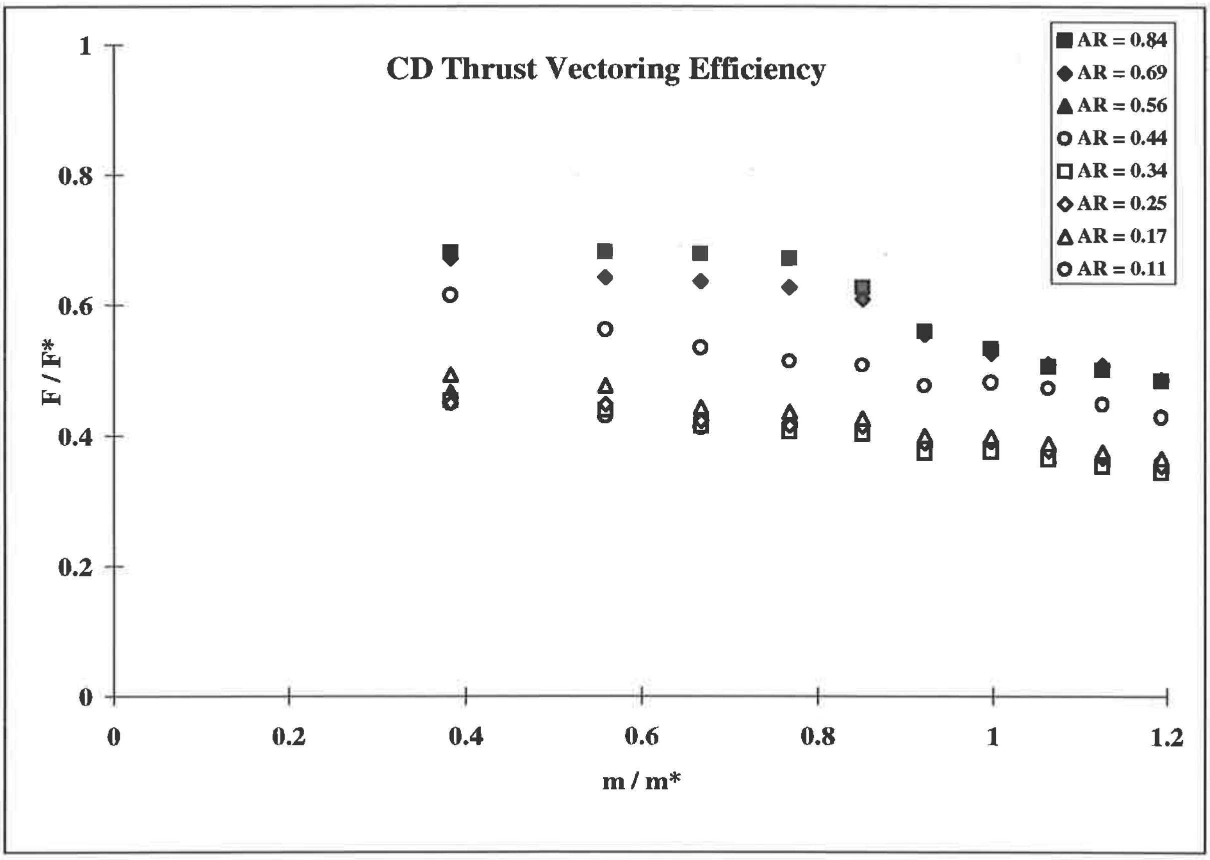

Figure 6.3. 2. CD nozzle thrust vectoring efficiency η plotted against mass flux ratio for a range of exit area ratios tested.

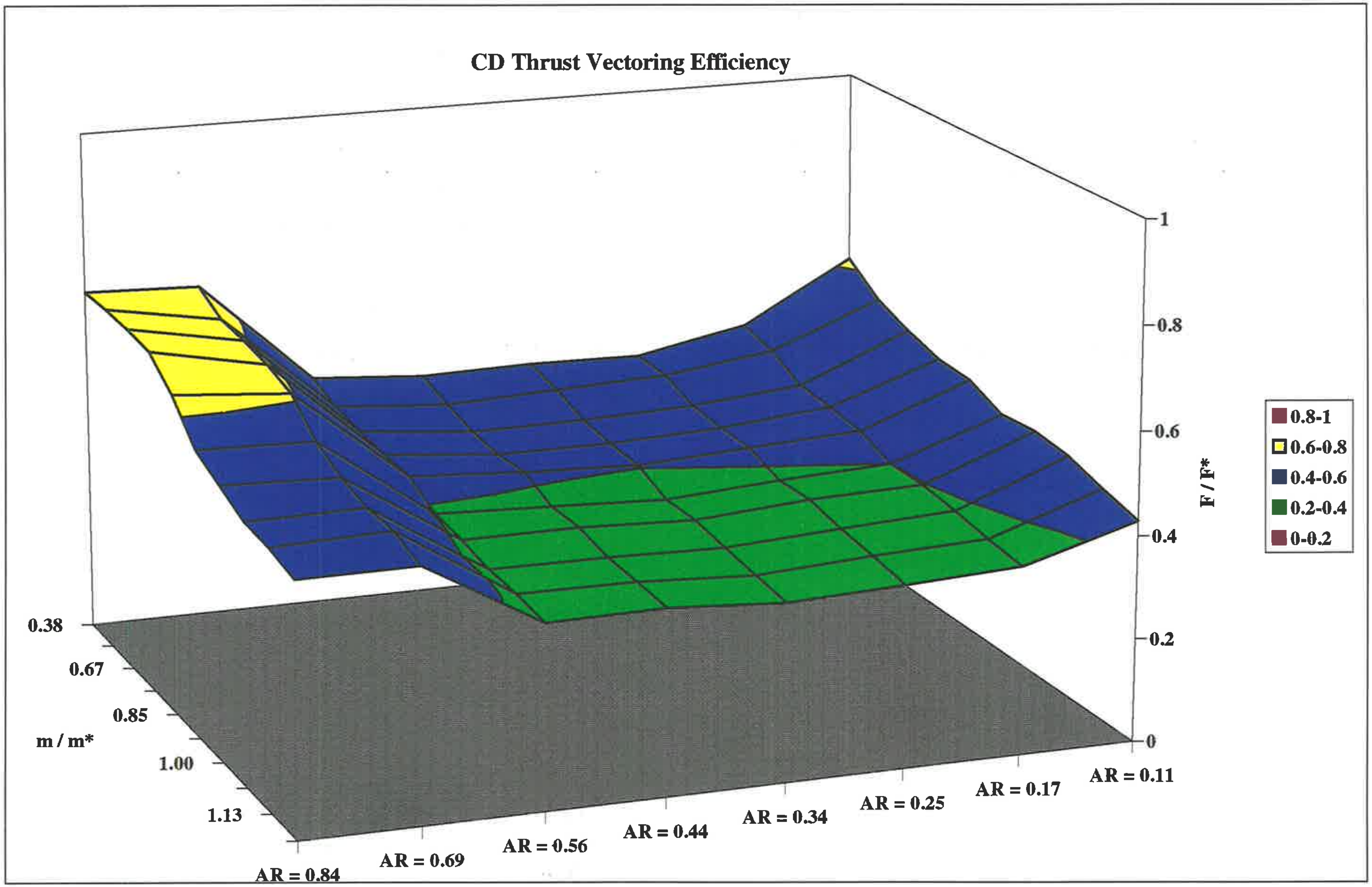

Figure 6.3. 3. CD nozzle thrust vectoring efficiency η plotted against mass flux ratio for a range of exit area ratios tested as a 3-D surface plot.

6.3.2 CD10 Nozzle

CD10 nozzle consists of the basic convergent-divergent nozzle with a 100 mm cavity attached at the exit. The addition of the cavity brings the total length of the nozzle 16 throat diameters. For the range of mass flow rates considered, the thrust vectoring efficiency for this nozzle was measured and the results shown in **Figure 6.3. 4**. They show that the largest exit area AR = 0.84 produces the highest thrust efficiency η of 60%. This is achieved at a deflected jet angle α of 20° and it remains relatively constant until the mass flux ratio m/m^* = 0.8 at which point the efficiency begins to decrease, as for the CD nozzle. The thrust efficiency decreases with the reducing exit area and reaches a minimum η of 25% for the exit area AR = 0.34. Again the thrust efficiency is constant until the mass flux ratio m/m^* of 0.8 is reached at which point the efficiency decreases. The deflected jet angle α for the minimum thrust efficiency is 65° beyond which the deflected jet angle decreases. Efficiency increases with further decrease of exit area such that for the minimum exit area ratio AR = 0.11, the thrust vectoring efficiency η is 50% at a deflected jet angle α = 30°. **Figure 6.3. 5** shows the thrust efficiency data as a 3-D surface plot and shows the effects of exit area as well as mass flux on thrust vectoring efficiency.

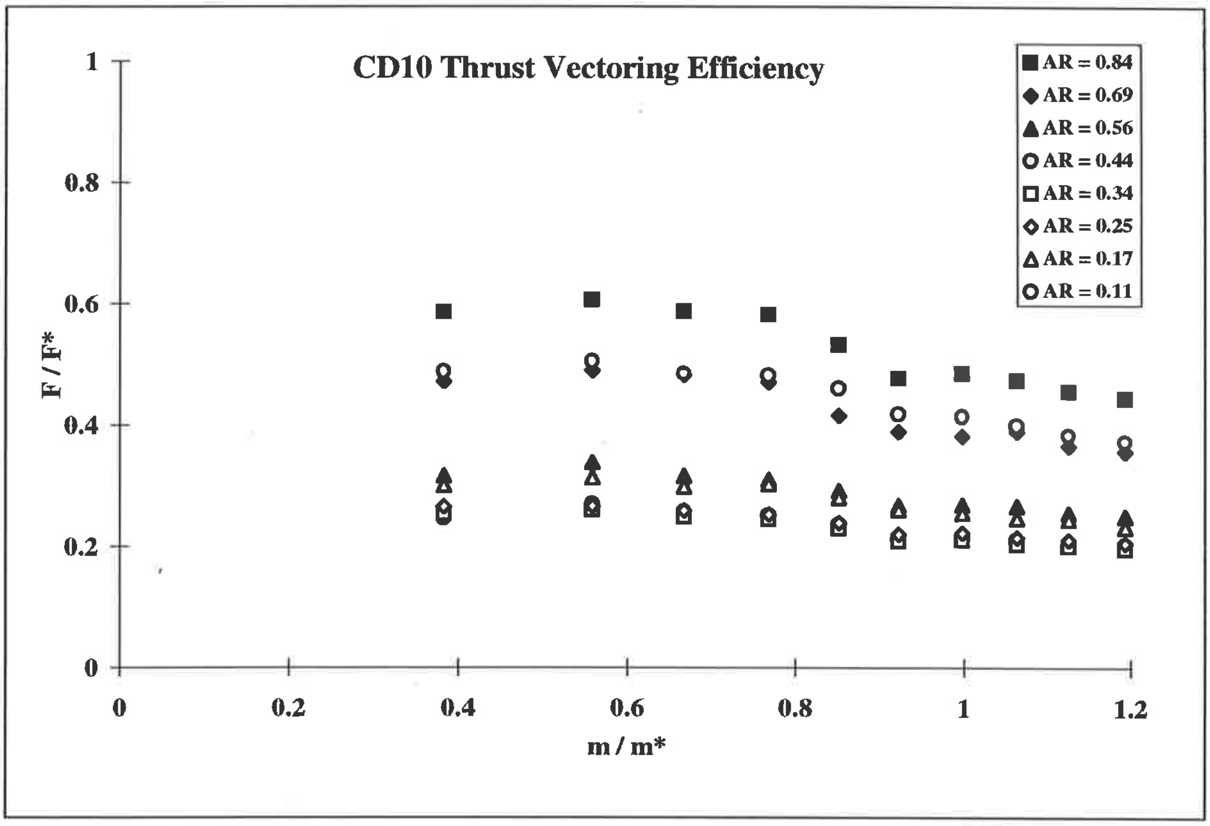

Figure 6.3. 4 CD10 nozzle thrust vectoring efficiency η plotted against mass flux ratio for a range of exit area ratios tested.

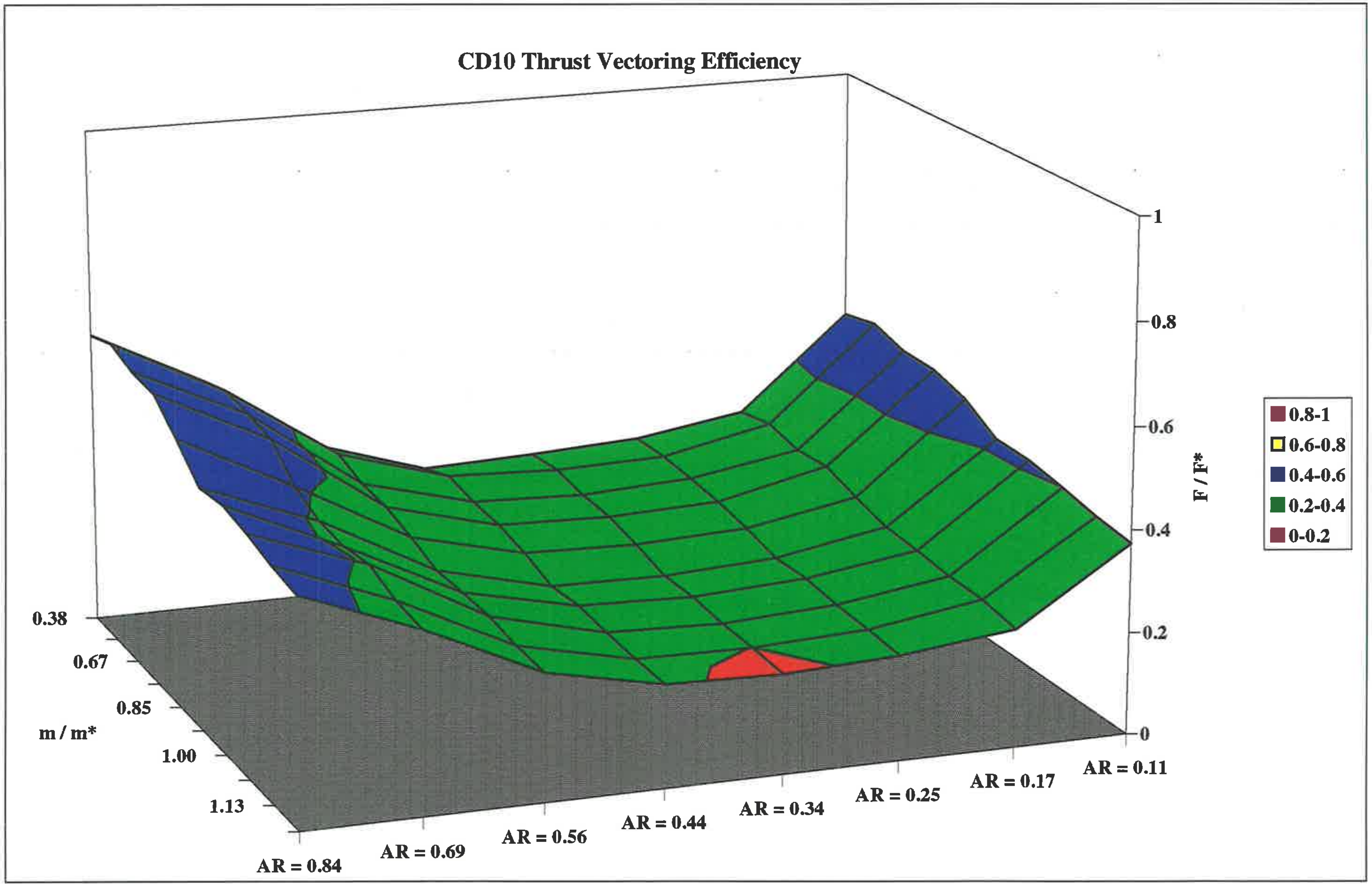

Figure 6.3.5 CD10 nozzle thrust vectoring efficiency η plotted against mass flux ratio for a range of exit area ratios tested as a 3-D surface plot.

6.3.3 CD20 Nozzle

The CD20 nozzle consists of a basic convergent-divergent nozzle with a 200 mm cavity attached at the exit which makes the total length of the nozzle 26 throat diameters. For the range of mass flow rates considered, the thrust vectoring efficiency for this nozzle was measured and the results are shown in **Figure 6.3. 6**. The results show that for the exit area AR between 1.0 and 0.25, the average thrust efficiency η achieved is around 10% and the jet is deflected at $\alpha = 35°$ away from the nozzle axis. The thrust efficiency is maintained at a fairly constant value for the range of mass flow rates considered, but the deflected jet angle increases to a maximum value of 45° at the exit area ratio AR = 0.56 after which the angle decreases. The maximum thrust efficiency η of 45% is achieved at the minimum exit area ratio AR = 0.11 and this produces a deflection α of 10°. The results are also shown in **Figure 6.3. 7** to emphasise the effects of exit area ratio on the thrust efficiency as a 3-D surface plot.

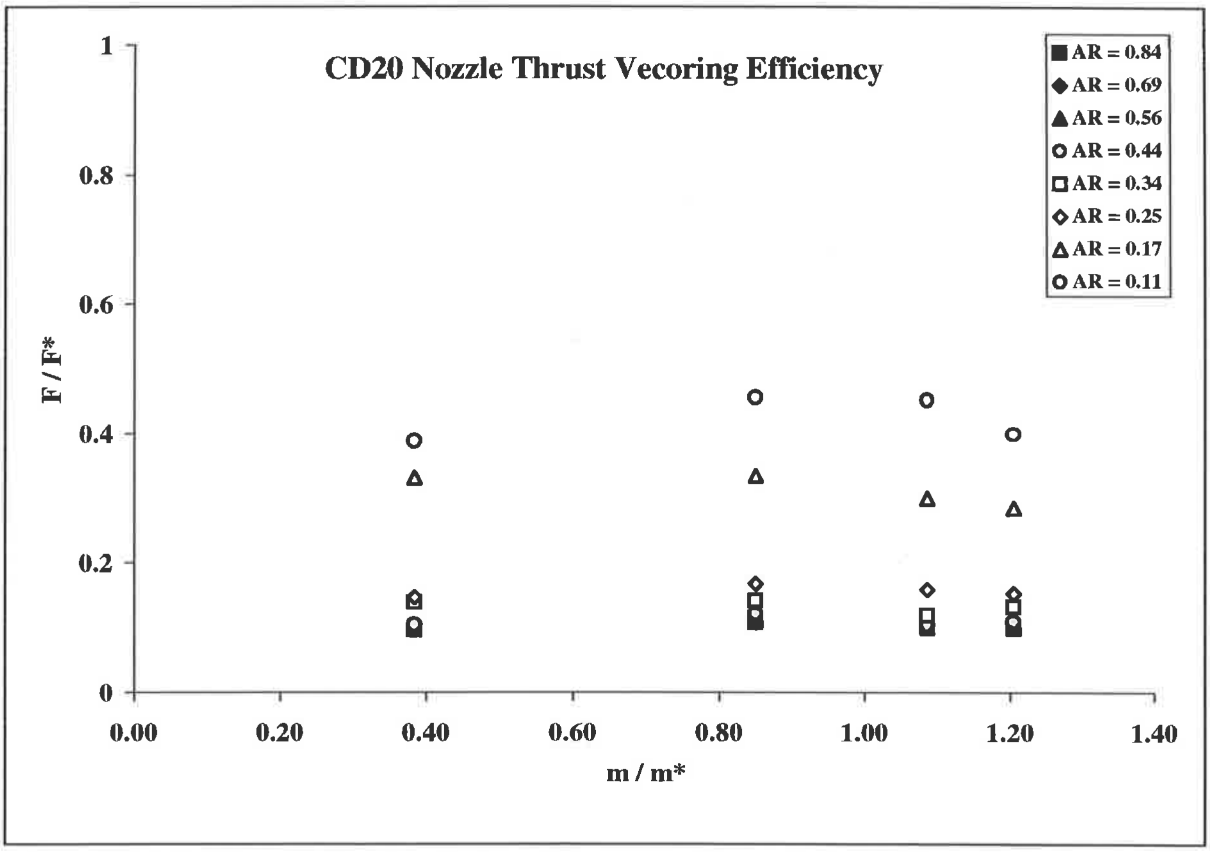

Figure 6.3. 6 CD20 nozzle thrust vectoring efficiency η plotted against mass flux ratio for a range of exit area ratios tested.

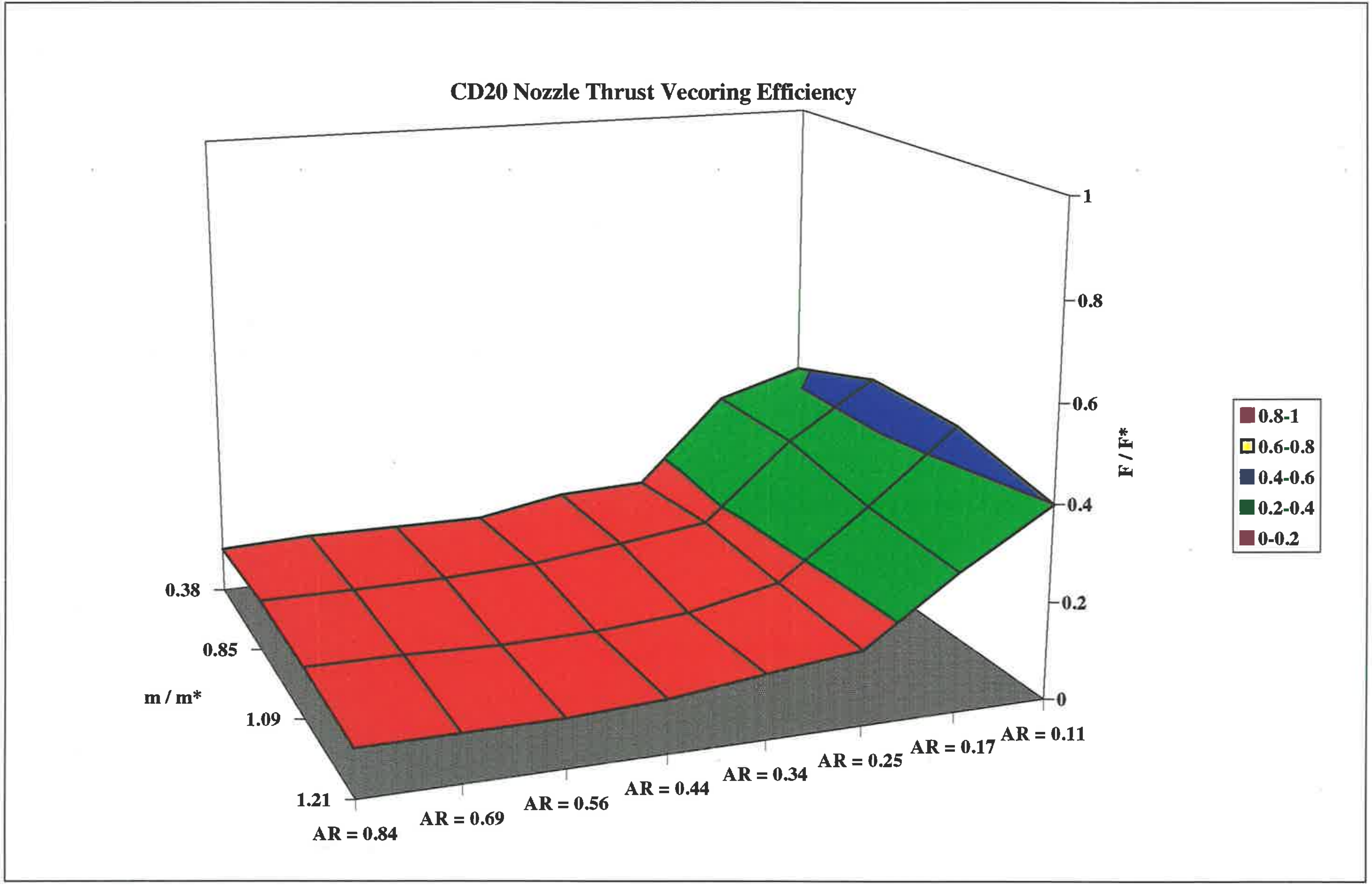

Figure 6.3.7 CD20 nozzle thrust vectoring efficiency η plotted against mass flux ratio for a range of exit area ratios tested as a 3-D surface plot.

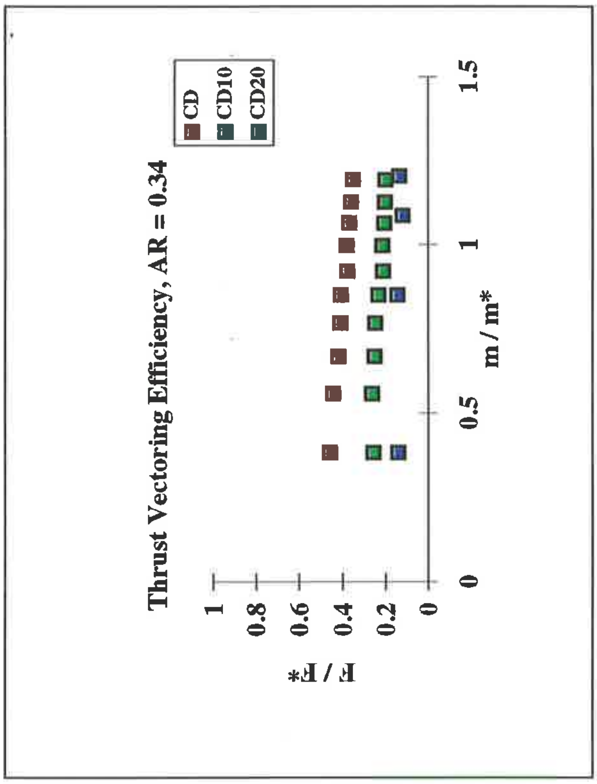

Figure 6.3. 9 Thrust vector efficiency for CD, CD10 and CD20 nozzles at AR = 0.34

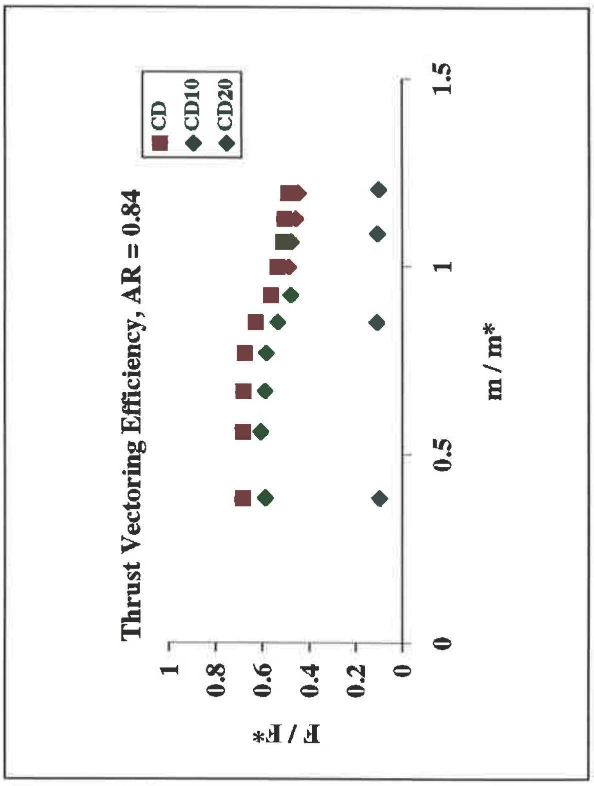

Figure 6.3. 8 Thrust vector efficiency for CD, CD10 and CD20 nozzles at AR =0.84

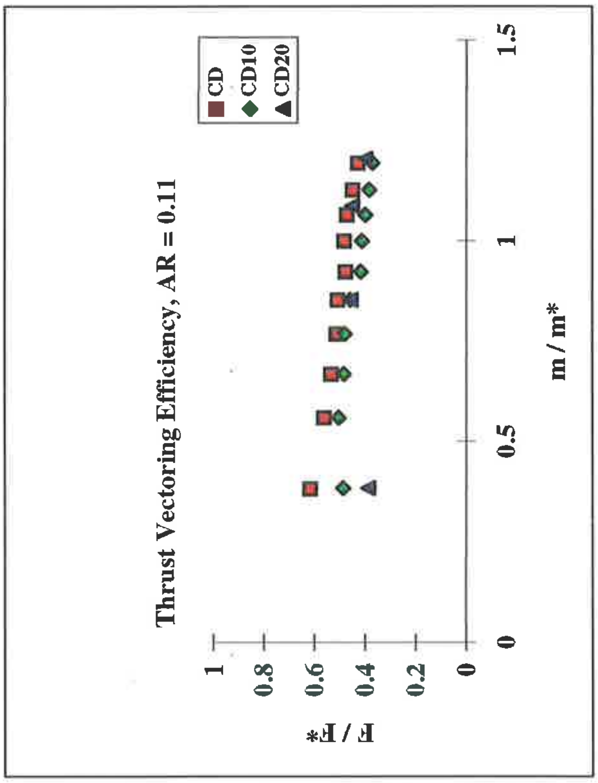

Figure 6.3. 11 Thrust vector efficiency for CD, CD10 and CD20 nozzles at AR = 0.11.

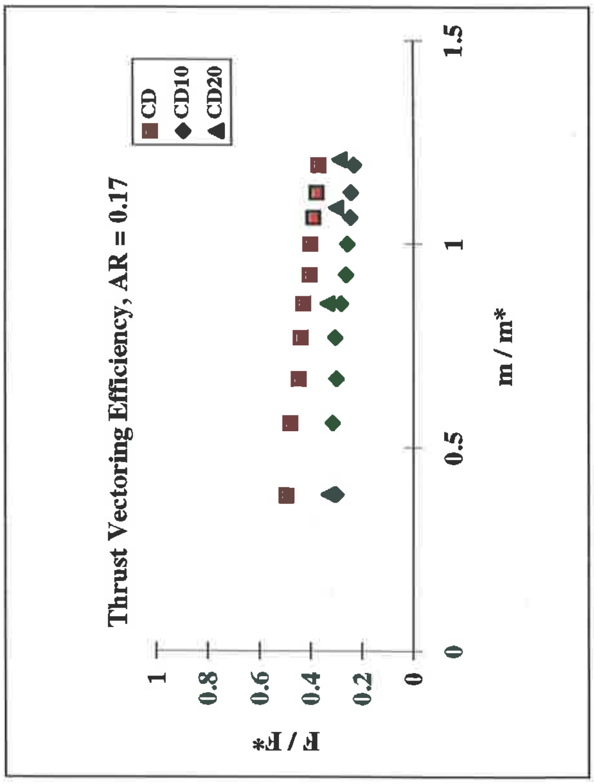

Figure 6.3. 10 Thrust vector efficiency for CD, CD10 and CD20 nozzles at AR = 0.17

6.3.4 Other Nozzles

As described earlier, nozzles RP45 and RP60 consist of a convergent section identical in profile to the convergent section of the CD nozzle to which is added a 100 mm square deflector plate inclined at 45° and 60° respectively across the nozzle exit. The measured thrust efficiency of the RP45 has an average value η of 50% and RP60 has an average value η of 45%. Both remain constant over the range of mass flow rates considered. The flow is deflected at 45° and 60° respectively. A typical profile at the edge of the RP45 nozzle shown in **Figure 5.4. 3** with traverses across the jet axis measured at 5mm intervals and $Re_t = 55,000$. The centreline velocity at 10 throat diameters downstream from the nozzle exit was found to be 0.45 U_t which compares with 0.25 U_t centreline velocity exiting the CD10 nozzle, shown in **Figure 5.4. 1** and 0.5 U_t at the CD nozzle exit shown in **Figure 4.7. 6.**

Nozzles B45 and B90 consist of the convergent nozzle, described above, to which is added a bend with an internal diameter the same as the throat diameter of the convergent nozzle. B45 has a bend at 45° and B90 has a bend at 90°. Both of these nozzles achieved a thrust efficiency η which was measured to be 90% for a range of mass flow rates.

6.4 Conclusions

From the results presented it can be concluded that nozzles CD, CD10 and CD20 can be used for thrust vectoring, at least for cold flow, where the thrust required does not exceed 70% of the total thrust, for a thrust vector angle of $\alpha = 25°$. The maximum deflection possible, using the CD nozzle, is $\alpha = 80°$ with an efficiency $\eta = 45\%$. The thrust vectoring efficiencies and deflected jet angles measured are highest for the CD nozzle, followed by the CD10 and then finally the lowest thrust vectoring efficiencies were given by the CD20 nozzle. From the results for the CD and CD10 nozzles, shown in **Figure 6.3. 3** and **Figure 6.3. 5**, it can be seen that the maximum deflected jet angle is achieved at the minimum thrust efficiency. This however is not the case for the CD20 nozzle and the **Figure 6.3. 7** shows that the thrust vectoring efficiencies are effectively constant until the exit area ratio is reduced to AR = 0.25 after which η increases.

RP45 produces a thrust vectoring efficiency η of 50% at the preset angle α of 45° and RP60 gives η = 45% at $\alpha = 60°$. This is compared with the CD nozzle which produces a deflected jet at an angle α of 45° with η = 70% at AR = 0.69 and $\alpha = 60°$ with $\eta = 50\%$ at AR = 0.56. This indicates that potentially the CD nozzle could have a superior thrust vectoring performance in service then nozzles based on the deflector plate principle embodied in the RP45 and RP60 nozzles. The B45 and B90 have been shown to vector the thrust very efficiently with η = 90%. The efficiency is high due to the relatively low pressure losses associated with redirecting the flow inside the tube compared in comparison with the high degree of mixing involved in the CD, CD10 and especially the CD20 nozzles.

For the range of nozzles tested, CD nozzle performs best due to its capacity to deflect the jet through a large range of angles with relatively high thrust vectoring efficiencies. This trend can be seen in **Figure 6.3. 8** to **Figure 6.3. 11** in which the nozzle thrust efficiencies for CD, CD10 and CD20 are compared for each area ratio. It is clear that the thrust vectoring efficiency η for the CD nozzle is superior in all cases. The decrease in efficiency of the CD nozzle as cavity extensions are added can be explained by reference to Chapter 4. There it is shown that the primary wall jet produced by the secondary jet at the throat spreads azimuthally around the circumference as it moves downstream through the divergent section of the nozzle. This spreading process continues through the 100 mm cavity extension and still further through the 200 mm long cavity extension. Thus although the total mass flux changes very little[1], the momentum is more diffuse and hence the linear momentum leaving the nozzle is decreased. In the profiled nozzle some of this momentum loss could be regained by changes in the pressure distribution within the nozzle. This is unlikely to be significant with the constant diameter cavity extensions.

---

[1] These differences being due to small differences in the mass of ambient air entrained into the nozzle.

CHAPTER 7.

Toward the Optimum Nozzle Configuration

7.1 Summary of Factors Influencing T.V.N. Performance

Many factors can influence the performance of the CD nozzle as a thrust vectoring device. The initial nozzle design was based on the preliminary findings by Nathan (1988) which were based on an Orifice-Cavity-Orifice nozzle. With an exit ring attached to the nozzle, the reattached jet downstream from the primary orifice is deflected to large angles across the axis as it leaves the nozzle. Initial findings by Nathan revealed that in the O-C-O nozzle, the required l/d_c was of the order of 2.7 for the reattachment of the jet and hence the precession, for this application, to occur. The throat area expansion ratio A_t/A_c, for the above configuration, was found to be 36. Using these ratios as the initial design for the convergent-divergent nozzle, it is probable that the nozzle efficiency has increased relative to the simple O-C-O nozzle because of the smooth contraction and expansion of the CD nozzle since there is only a partial separation of the jet downstream from the throat and not a total separation such as occurs downstream from the primary orifice in the O-C-O design. Other factors that could influence the nozzle performance are the cavity length, exit lip height and shape , secondary fluid injection point, secondary mass flux, angle of secondary fluid injection to the main jet, nozzle throat axisymmetry, turbulence intensity of the primary jet and expansion ratio of the throat to maximum nozzle diameter.

7.1.1 Effects of Cavity Length

Three cavity lengths have been tested to ascertain the role they play in the development of the wall jets prior to their reaching the exit lip. From velocity profiles and laser sheet flow visualisation it has been shown that the length of the cavity determines the wall jet thickness at the nozzle exit. The short cavity, as in the CD nozzle, produces a wall jet which is relatively thin, is of high momentum and has a relatively low turbulence level. This thin wall jet leaves the CD nozzle as a jet with high momentum concentrated near the nozzle surface, as shown by laser sheet flow visualisation at the exit of the nozzle, **Figure 4.3. 10**. When the exit area is reduced by addition of an exit ring, the wall jet is caused to separate from the wall and to be deflected sharply across and away from the nozzle axis.

The addition of the medium length cavity, as in the CD10 nozzle, allows the mixing layer to grow and the overall wall jet cross section to increase. The wall jet thickness increases and the jet also spreads laterally around the curved inner surface of the cavity such that the wall jet momentum is distributed across a larger cross section. To a first order this reduces the potential thrust inversely with the jet cross section, a result which assumes one-dimensional flow and ignores skin friction. Eventually, the expanding wall jet will occupy the whole of the exit plane. This is the case for the CD20 nozzle. When the exit area of the CD10 nozzle is reduced, beyond the value which produces maximum deflected jet, the wall jet is deflected, but due to the lower momentum of the wall jet, the lip vortex is weaker and hence the strength of the main vortex loop within the nozzle is reduced. Thus the deflection of the jet is reduced. With a small exit area, the wall jet occupies the whole of the outlet area and the stream lines converge towards the nozzle axis causing the wall jet to separate further upstream from the exit, further reducing the strength of the lip vortex and further reducing the jet deflection.

The above discussion reinforces the conclusions drawn in Chapter 4 that the prime influence in deflecting the jet is the strength of the vortex loop within the nozzle and this in turn depends on the efficiency with which part of the linear momentum of the primary jet can be converted into angular momentum, via processes such as the lip vortex, and fed into that vortex loop.

With a long cavity, as in the CD20 nozzle, the weakening of the wall jet as it spreads, and the fact that the now diffused jet occupies the whole of the exit plane, even before an exit ring is attached, together result in the poor performance as a thrust vectoring nozzle. When the exit area is reduced to a value of around AR = 0.25, the wall jet is deflected only mildly and the thrust efficiency is low. The efficiency is improved marginally by reducing the exit area still further as discussed in Chapter 6.

7.1.2 Exit Lip

The exit lip plays a very important role in deflecting the wall jet across the nozzle axis. The angle of the jet deflection is determined by the ratio of lip height to the wall jet thickness. This is the dominant factor in determining the angle at which the jet will deflect as it leaves the nozzle.

In an attempt to understand the dominating influences of the exit lip a number of experiments were carried out on the interaction of two dimensional wall jets with gates of several different heights placed at various distances from the exit plane of the wall jet. The results for the 2-D wall jet have been discussed in detail in Chapter 4. They show that the deflected jet angle is proportional to the ratio of the lip height to the jet thickness. It was also shown that the axial distance of the gate from the jet exit also has an influence. The velocity profiles at the exit of one 2-dimensional wall jet and axisymmetric jet are shown in **Figure.4.8.1**. They reveal the similarity between the velocity profiles. This led the author to investigate further the effects of gate heights on wall jets at various distances from the jet exit and to note the jet deflection angles achieved by these means. The 2-dimensional configuration was investigated to simplify the geometry, hopefully without altering the main features of the deflection process. From various velocity measurements, laser sheet flow visualisation and tuft flow visualisations, deflected jet angles were measured. The interesting feature of these data is that for subsonic flow the angles at which the jet deflects at, appear to be Reynolds number independent in both 2-D and 3-D flows, or at least not very Reynolds number dependent, due to large variations of the spreading angles of the exiting deflected jet. Data for the 2-D wall jet flow over a gate shows that for a given gate height the angle of deflection of the wall jet varies with distance from the exit . This was anticipated from the CD20 nozzle data. It was also established that the thickness of the 2-D wall jet increases with the axial distance from exit due to mixing layer growth. The mixing depends on the ambient conditions, and in our test case, the cavity pressure and the proportion of exit area occupied by the jet also influence the mixing. If the exit area of the CD nozzle through which ambient fluid is entrained is small, then the entrained fluid, which does enter the nozzle, must do so at a much higher velocity. This promotes mixing with the shear layer which increases both the turbulence level and jet thickness. The results from the 2-D experiments show that the deflected jet angle decreases with distance from the origin of the wall jet. This is due to the thickening of the wall jet and diffusion of the wall jet momentum as it flows over the surface between the origin and the gate. The reduced effects of gate height on deflection jet angle in 2-D case is due to the absence of communication between the lip vortex loop and the primary vortex loop which exists in the CD family of nozzles, shown in **Figure 4.8. 11** and **Figure 5.7. 1.**

7.1.2.1 Influence of Exit Lip Shape on the Flow

The exit rings tested had an upstream facing chamfer from the inside nozzle diameter to the exit diameter. This produced a sharp edged orifice at the exit of the nozzle with a shallow angle except the 55 mm diameter exit ring which had a 22.5 degree chamfer. Two other 50 mm diameter exit ring types were tested, a square edge and a reverse chamfer so that the upstream face was normal to the nozzle wall and the results compared with the test lip. They produced no noticeable changes in the flow direction at the nozzle exit. The results are inconclusive since only these two exit rings of 50 mm diameter were tested. Further investigation into the effects of the exit lip shape should be carried out on the remaining exit ring diameters but it is suspected that they will have secondary effects on both thrust efficiency and the angle at which the jet is deflected. One feature in particular which is worthy of further study is the suggestion in **Figures 5.3.3** to **5.3.6.** that the Coanda-like effect causes the jet to attach to the outer face of the sharp edged exit lip for the range of aspect ratios represented.

7.1.3 Primary Mass Flux

The influence of the primary mass flux on the efficiency has been established in Chapter 6. It has been shown that the mass flux does not alter the angle to which the jet is deflected. Thus the vectored jet is not, to the first order at least, Reynolds number dependent. The primary mass flux has been shown to have a secondary effect during the initial stages of establishing the asymmetric flow at low flow rates, below say $5\text{x}10^{-3}$ kg/s, but beyond that flow rate the primary flux does not influence the thrust efficiency until the compressibility effects come into effect. It is postulated that as the primary momentum increases, the proportion of that momentum which is converted to angular momentum via the lip vortex, and is hence fed back into the main vortex loop, remains approximately constant so providing sufficient circulation in the main vortex loop to deflect the higher momentum primary flow to an angle which is approximately independent of flow rate. It is recommended that this postulate be tested. The effects of supersonic flow need to be investigated to determine the effects of shock waves on the thrust vectoring performance of the nozzle.

7.2 Conclusion

The nozzle configuration plays a critical part in determining the thrust efficiency and magnitude of the deflected jet angle. To produce maximum thrust, the nozzle should be short, yet long enough to deform the axisymmetric jet into an asymmetric wall jet after the injection of the secondary fluid. The lip height can be chosen to suit the particular thrust vectoring requirements of the nozzle. As mentioned previously, the secondary mass flux required for stable operation of the deflected jet is below 5% of the primary mass flux. The effectiveness with which the throat separation is induced in the nozzle and hence the ability to control the thrust vectoring are dependent on the secondary mass flux direction. This has been shown by Azevedo (1993) who studied the performance of a two-dimensional convergent-divergent nozzle and showed that the performance was improved if the secondary fluid was directed upstream at 10 degrees from the normal. It was also shown by Bis et.al., (1990) that the jet inclined at 30 degrees toward the upstream in cross flow penetrates the primary flow further than when the jet is normal to the cross flow. This last result was predicted by C.F.D. and later confirmed by experiments. The momentum ratio of the primary to the secondary fluid determines the spread, deformation and penetration of the secondary fluid jet which should be investigated further.

CHAPTER 8

Comparison of Results With Other Research

8.1 Introduction

Very little research has been carried on controlling the direction of jets from an axisymmetric nozzle by fluid dynamic means. Consequently few direct comparisons of the present findings can be made with data in the public domain. The initial research carried out by Nathan (1988) had the aim of enhancing the characteristics of non-pre-mixed gas burners by improving the mixing of the fuel with the surrounding air. The large scale precessing motions produced by the O-C-O configuration were found to increase flame stability and reduce undesirable emissions. The emphasis of the present research, even though it had its origins in the work of Nathan **[207]** and Luxton and co-workers **[174, 175, 176, 180, 119, 204, 205, 206, 208, 209, 262]** has been control of the thrust vector from a nozzle by purely fluid dynamic means. The common theme of these two research projects has been that they both produce a deflected jet by means of a lip at the nozzle exit. The other published research on the topic has been carried out by Franke and co-workers **[102,225]** and others **[314]** and this has concentrated solely on supersonic flow through a nozzle of a particular geometric configuration. Secondary fluid injection is used but is located downstream from the throat.

8.2 Comparison of CD Family of Nozzles With Other Similar Nozzles

Franke and his co-workers: The work by Friddell and Franke (1992), which extended the earlier findings of Porzio and Franke (1989), involved a nozzle which has some similarities to one of the nozzles tested in the present investigation. Porzio and Franke investigated thrust vector controlled by injection of secondary fluid at a station downstream from the throat. The nozzle however had a 20° conical divergence and was tested at supersonic flow conditions, while the present investigation has related only to the subsonic conditions. The nozzle had following specifications: d_t=12.7mm , L/d_t=10.4, A_c/A_t=24, A_e/A_t=6 . The angle of reconvergence was 55° and the lip height to throat diameter was 1.2. The deflected jet angle varied from 25° at 465 psia primary driving pressure to 45° at 115 psia primary driving pressure. The thrust efficiency η varied from 65% to 60% respectively. The results obtained by Fridell and Franke are for the same throat diameter and nozzle length, L/d_t=10, A_c/A_t=17, A_e/A_t=7.8 , with the angle of reconvergence at 45° and the lip height to throat diameter of 0.67 . The deflected jet angle also varied from 25° at 465 psia primary driving pressure to 45° at 115 psia primary driving pressure. In their study, thrust efficiency η varied from 80% to 60% respectively. The nearest to equivalent test nozzle studied in the present investigation is the CD nozzle with L/d_t=6, A_c/A_t=36, an exit to throat area ratio A_e/A_t=6, (AR=0.17) which represents the 25 mm diameter exit ring and the lip height to throat diameter of 1.75. This particular configuration has been shown to produce a deflected jet angle of 65°, and a thrust efficiency η of 50%, compared with the same CD nozzle and an exit ring of 20 mm diameter, A_e/A_t=4, (AR=0.11), and the lip height to throat diameter of 2, which produced a thrust efficiency η of 60% and a deflected jet angle of 45°.

These results compare well when differences in nozzle shape, exit lip shape as well as the expansion and contraction ratios are considered and are summarised below. The point to remember is that the present results are for the subsonic flow with driving pressures up to 200 kPa(abs), where as Franke and co-workers have explored their nozzle from 600 kPa (abs) to above 6.5 MPa (abs) primary driving pressure. The results emphasise that this type of nozzle could be used to vector thrust at large angles very efficiently at both subsonic and supersonic regimes.

Porzio and Franke (1989) results
D_t=12.7mm , L/D_t=10.4, A_c/A_t=24, A_e/A_t=6, η =60% to 65%.

P_p (psia)	115	215	315	415	465
α°	45	35	30	27	25

Friddell and Franke (1992) results
D_t=12.7mm L/D_t=10, A_c/A_t=17, A_e/A_t=7.8, η = 60% to 80%.

P_p (psia)	90	115	165	215	315	415
α°	45	35	26	26	24	24

CD nozzle,(present study results Primary driving pressure up to 200 (kPa abs))
D_t=10mm L/D_t=6, A_c/A_t=36,

A_e/A_t	36	30	25	20	16	12	9	6	4
α°	0	25	45	65	70	80	75	65	45
η %	-	70	65	45	45	45	45	50	60

CD10 nozzle results
D_t=10mm L/D_t=16, A_c/A_t=36,

A_e/A_t	36	30	25	20	16	12	9	6	4
α°	0	20	35	50	60	65	60	45	30
η %	-	60	50	35	27	27	27	30	50

CD20 nozzle results
D_t=10mm L/D_t=26, A_c/A_t=36,

A_e/A_t	36	30	25	20	16	12	9	6	4
α°	0	35	40	40	40	35	30	20	10
η %	-	10	10	10	12	14	17	33	45

Wishart and Krothapalli (1993) investigated supersonic flow from an axisymmetric nozzle. The results for nozzle with a solid body obstruction on the wall between the throat and the nozzle exit were presented qualitatively. The aim of the small blockage was to produce distortion and hence side force from the axisymmetric jet. The results show that it is possible to contour the jet shape via the number and location (axial and azimuthal) of disturbance. They also note that even though mechanical disturbance generators (rods) were used, the same effect can be obtained by the use of fluid-mechanic disturbance such as a jet in a cross-flow leading to possible active control of the vectored jet. The disturbance rods projected upstream at an angle of 28° to the jet centreline and emits a cone shaped disturbance wave. The intersection of cone and the nozzle lip produces two regions of pressure mismatch that cannot be sustained by the shear layer and a pair of streamwise vortices are formed, the result noted in the present thesis shown in flow visualisation **Figure 4.3. 12**. Bradbury and Khadem have investigated axisymmetric flow disturbed by tabs at the jet exit plane. The angle of the wedge shaped tabs influence the local flow exiting the nozzle such that a 45° wedge deflects the local flow above the tab by about 12°, where as the 90° tab deflects the local flow by about 15°.

This shows how effective a small tab, with jet exit to tab area ratio of about 200:1, is for deflecting the flow at moderate angles.

Balu, Marathe, Paul and Mukundas (1990) have investigated a similar problem computationally and compared the predictions with the experimental results of Newton and Spaid (1962). They predicted pressure distribution generated by secondary injection between the throat and the exit by solving the 3-D Euler equations (unsteady) with appropriate boundary conditions. The axial thrust augmentation was deduced from integrating the nozzle wall pressure distribution obtained as part of the flow field solution and predictions compared with measured pressures. An inviscid model was justified by the fact that the separation of the upstream boundary layer has a comparatively insignificant effect on the total side force, as shown by the experiments of Newton and Spaid. The predicted and experimental side force reaches the maximum value at the secondary to primary mass flux ratio of **5%** which compares well with the results by Franke and co-workers and the results obtained in the present thesis.

Other researchers like Lilley and Arszman (1990) and Lilley (1992) investigated the effects of scarfed-nozzles on the thrust vectoring of jets. They found that the thrust from these nozzle can be vectored by up to 34° for scarf angle of 30° and expansion ratio 2 and at about 12° for higher pressure ratios. Wu and Chow (1985) also investigated flow from an asymmetric two-dimensional convergent nozzle and found that with the upper wall deflected at 30° and lower wall at 0°, the jet deflected at about 24° for the pressure ratio of 10. Wassom, Faupell and Perley (1990) investigated the thrust vectoring capabilities of an aero-fin and found that it can deflects the flow at about 15°.

A two-dimensional jet oscillations or flip-flop jet nozzle has been investigated extensively by Badri Narayan and co-workers, Viets (1975), Binder and Favre-Marinet (1981), and Lai and co-workers, amongst others. They all show that the mixing of the jet by mechanical or other means is beneficial to improved combustion and reduction of pollutants. This was the aim of the original study by Nathan(1988) which was the origin of this thesis.

The research to date has , with the exception of Franke and co-workers, presented results for jets deflected up to 35°. The present thesis has shown that the jet exiting a CD nozzle can be deflected up to 80°.

8.3 Comparison of CD Family of Nozzles With the EMB Family of Nozzles

The flow inside the CD family of nozzles has been investigated in detail and it has been found that there are many similarities with the O-C-O configuration investigated by Nathan and Luxton. Geometrically the CD10 nozzle has some comparability with their MLC (Mid Length Cavity) nozzle while the CD20 nozzle has some with their LC (Long Cavity) nozzle. The MLC nozzle exit total pressure profiles as shown in Nathan (1988)(in his Figure 4.7), show that the maximum total pressure occurs at a distance of 0.5 d_c from the nozzle outlet which indicates that the jet is exiting at $\alpha = 45°$. This angle was confirmed in the Figure 4.9 of the same reference where the angle was measured using a static pressure yaw meter. For the same exit lip to cavity diameter ratio the jet from the CD10 nozzle is deflected to ≅ 35°, as shown in **Figure 6.3. 1**. The slight difference between the two deflected jet angles could be attributed to the fact that the O-C-O nozzle reattaches to the cavity wall and due to entrainment of primary fluid into the wall jet and the formation of the reverse foot, the reattachment length decreases. The "free" surface of the primary jet is greater than for the CD10 nozzle and therefore the entrainment appetite is greater. This would suggest that the wall jet at the exit lip is thinner and spread out azimuthally more than CD10 nozzle which in turn would increase the angle of deflected jet when compared with CD10 nozzle. Greater appetite would induce more ambient fluid into the nozzle and increase the radial pressure gradient across the nozzle exit which further increases the deflected jet angle.

The static pressure inside the cavity of the MLC nozzle has been shown to be approximately 500 Pa below ambient for a P_d = 20 kPa and for the similar geometry CD10 nozzle the static pressure inside the cavity was found to be approximately 450 Pa below the ambient which tends to support the above postulate. The results of the wall static pressure variation in the MLC nozzle show similarity with the results for the wall static pressure in the CD10 nozzle. That is, as the jet approaches the exit lip, the wall static pressure increases to above ambient due to the stagnation region on the inner face of the exit ring. This gives some confidence that comparison of the results acquired by Nathan with those acquired in the present investigation for the two related, but seemingly different, nozzles is meaningful. The results show that the major features of the flow inside the two nozzles are similar but have marked differences. The china clay surface flow visualisation for the MLC nozzle has revealed that the negative stream surface bifurcation exists and that it moves due to the precession of the exiting jet. With a bluff body inserted into the cavity, the flow is stabilised enough to obtain an average china-clay surface flow picture (as in Nathan (1988) Figure 4.44), showing a surface flow pattern which has some similarity to the flow patterns found in the CD10 nozzle, shown in **Figure 5.5.1. (a)**. In both cases the striking features are the footprint patterns of the entrained fluid moving toward the throat, the primary jet moving toward the exit lip with the two being separated by the negative stream surface bifurcation. The difference between them is that there is no reattachment point of the primary jet on to the cavity wall in the CD10 nozzle, for $Re_t > 58,000$, since the wall jet is fully attached on that side of the wall, hence there is no reverse flow foot associated with the CD10 nozzle. The flow characteristics of the two nozzles are similar in the way in which the flow behaves downstream from the reattachment point when the azimuthal position of the MLC nozzle jet is fixed. The nozzle relies on the flow instability inside the nozzle for the precession to begin and to be maintained as in a limit cycle. This instability is suppressed in the CD10 nozzle by the injection of the secondary fluid which fixes the azimuthal position of the jet. When the secondary injection is not implemented, the jet tends to change its azimuthal position but not in a consistent manner like the MLC nozzle. This may be put down to the non-existence of the reverse flow foot described in detail by Nathan. This flow was analysed by Hill (unpublished) who biased the direction of the jet entering the cavity through the upstream orifice so it was misaligned by approximately 15° from the axis. This flow did not precess and showed surface flow visualisation patterns which were remarkably like those shown in **Figure 5.5.3. (a)**. When the initial bias was decreased to 10°, the flow was on a verge of precession and the surface flow patterns showed two dominant foci were displaced, one up and one down relative to each other such that the vortex loop, discussed earlier in Chapter 4, is no longer perpendicular to the nozzle axis and now has a component of circulation in line with the nozzle axis which may be the driving force for precession to occur. The direction of precession is therefore determined by which of the foci moves towards the throat. It is therefore postulated that this is the driving force behind precession.

8.4 Flow separation in nozzles and diffusers

The CD family of nozzles has been designed with a single profile based on a sinusoidal curve. The separation of the jet is initially axisymmetric, as has been shown in previous sections, followed by an asymmetric separation at higher mass flow rates. It is this asymmetric flow that is the driving force behind the high thrust vectoring efficiency and it is envisaged that the ease by which the flow is forced to become asymmetric will determine the efficiency of the flow. The simplest nozzle uses a conical expansion which separates axisymmetrically unless provoked to turn into an asymmetric flow **[102,225]** by secondary fluid injected downstream from the throat. A large amount of research has been done on design of supersonic nozzles **[19,112,182]** and on prediction of separation points within the nozzle. Back, Massier and Gier (1965) have investigated the flows through conical supersonic convergent-divergent nozzles both theoretically and experimentally. They have considered the conical half angle of convergence of 30° and 45°, with conical half angle of expansion of 15°. The wall pressures, for a range of driving pressures, have been measured upstream and downstream of the nozzle throat. The results show that the flow separation could be predicted by knowing the convergence and divergence angles and driving pressures. This could prove to be a useful tool in designing an appropriately contoured nozzle to achieve the required asymmetric separation in the nozzle with a minimum of secondary fluid injection. Their research has also revealed the dependency of the pressure ratio on the ratio of streamwise radius of throat curvature (r_c) and the throat radius (r_{th}). The smaller the ratio of (r_c) / (r_{th})., the larger the difference between the measured results and one-dimensional isentropic flow predictions. This suggests that a small streamwise radius of curvature of the throat, compared with the throat radius, should be avoided in the design of nozzles. This however may not be possible in some instances where the geometric restrictions require the nozzle to be short. The nozzle contour of the CD family of nozzles needs to be explored if the performance is to be optimised.

CHAPTER 9

Conclusions

9.1 Evidence of Postulated Flow

A large portion of the experimental effort was used to develop a postulate to describe the flow in the CD10 nozzle. This remained elusive. After some parametric investigation with the CD nozzle alone (ie. without any cavity), it was discovered that the CD nozzle was capable of deflecting a jet efficiently when secondary fluid was injected at the throat. This diverted attention to the later nozzle and most of the remainder of research has been concentrated on the CD nozzle. The postulated flow patterns and flow mechanisms for both nozzles have many similarities. The postulated patterns in the CD20 nozzle have been investigated with less vigour since it was less efficient than the CD10 nozzle and much less efficient than the CD nozzle. Hence the experimental data to back the postulate is not as strong but the conclusions drawn for the CD and CD10 nozzle can be extrapolated to strengthen the postulate.

The experimental evidence on which the postulated flow structures are based on is listed below:

- Visualisation of the surface flow patterns inside the nozzle using china-clay.
- Visualisation of the flow outside the nozzle using marked fluid and laser sheet.
- Visualisation of the surface flow patterns using oil in the divergent part of the nozzle.
- Visualisation of the flow both inside and outside the nozzle using a tuft.
- Hot wire anemometry measurements of the flow both inside and outside the nozzle.
- LDV velocity measurements in both the CD nozzles and 2-D wall jet flow.
- Total and static pressure profiles both inside and outside the nozzle.
- Wall static pressure measurements at the throat, along the wall and around the circumference of CD and CD10 nozzle.

It has been shown that the results are in agreement with those produced by Nathan (1988) on the geometrically different MLC and LC nozzles. Good agreement has also been shown with the research by Franke and co-workers which confirms the practical applications that this type of nozzle may have. Both thrust efficiencies and the angles to which the jets are deflected are a significant advance on present jet vectoring systems. On this basis alone the flow warrants further investigation to optimise the nozzle geometry. As a fundamental problem in fluid mechanics, the complexity presents a major challenge for analytical study.

9.1.1 Major Experimental Results

In both the CD and CD10 nozzles both flow mechanism and performance characteristics were evaluated while for the CD20 nozzle only the performance has been evaluated. The flow mechanism outside the CD6 nozzle was used to complete the evaluation of deflected jet angles for a range of nozzle lengths.

Some of the major nozzle performance findings for the CD nozzle are:

- The maximum angle to which the jet has been deflected has been measured to be 80°.
- The maximum thrust efficiency produced by a CD nozzle has been measured as 70%.
- The deflected jet angle increases with the decrease of exit area, to a limit beyond which the angle decreases.
- Correspondingly, the thrust efficiency decreases with the decrease of exit area.
- The maximum deflected jet angle is achieved at an Exit Area Ratio AR = 0.34 which is equivalent to a step height of 1.25 throat diameters located at 6 throat diameters from the injection point.
- The thrust efficiency is minimum when the deflected jet angle is maximum.
- The deflected jet angle decreases beyond AR < 0.34.
- Correspondingly the thrust efficiency increases with further decrease of exit area.

Some of the major thrust performance findings for the CD10 nozzle are:

- The deflected jet angle increases with the decrease of exit area.
- The thrust efficiency decreases with decrease of exit area.
- The maximum deflected jet angle is achieved at an Exit Area Ratio AR = 0.34. as with the CD nozzle, but the 1.25 throat diameter step is now 16 throat diameters downstream from the secondary injection point.
- The thrust efficiency is a minimum at maximum deflected jet angle.
- The deflected jet angle decreases with further decrease of exit area.
- The thrust efficiency increases with further decrease of exit area.

Some of the major thrust performance findings for the CD20 nozzle are :

- The deflected jet angle increases slightly with the decrease of exit area.
- The thrust efficiency remains relatively constant up to maximum deflected jet angle.
- The maximum deflected jet angle is achieved at AR = 0.56.
- The deflected jet angle decreases with further decrease of exit area.
- The thrust efficiency increases with further decrease of exit area.

The performance characteristics of the nozzles with respect to the pressure distribution inside the nozzle can be summarised as follows:

- For the no lip case, the CD nozzle wall static pressure is sub-atmospheric.
- The wall static pressure is linearly proportional to the ratio of exit area and local area.
- It appears that the wall static pressure is not Reynolds number dependent but is set by the ambient reference.
- The throat static pressure distribution is axisymmetric for the axisymmetric flow separation and asymmetric for the asymmetric wall jet flow.
- The CD10 nozzle wall static pressure is sub-atmospheric for AR ≥ 0.34
- The presence of radial pressure gradient was revealed by measurements of the circumferential pressure distribution in both CD and CD10 nozzles.

The flow visualisation findings can be summarised as follows:

- China-clay surface flow visualisation has revealed the existence of the vortex that spans the nozzle with its foci clearly visible downstream from the throat.
- Oil surface flow visualisation has revealed the areas occupied by the primary jet and the entrained ambient fluid within the nozzle and that the separation lines between them are negative stream surface bifurcations.
- Laser sheet flow visualisation has shown what appear to be a pair of streamwise vortices within the jet as it leaves the CD nozzle.
- The deflected jet angle for the test nozzles has been found to be maximum at an exit area ratio of 0.34, which coincides with the minimum thrust efficiency of the CD and CD10 nozzle but not the CD20 nozzle.
- The spreading angle of the wall jet after leaving the CD nozzle is twice that of the axisymmetric jet.

9.2 Conclusions

Through the results presented it has been confirmed that the flow through an axisymmetric convergent-divergent nozzle of a particular expansion ratio will separate axisymmetrically up to a particular mass flow rate. When this mass flow rate is exceeded, the separation downstream from the throat becomes asymmetric and unstable, in the sense that its azimuthal position of the separation changes without warning or bias and hence the direction in which the jet leaves the nozzle fluctuates randomly. This can be overcome by injection of a secondary fluid at the throat with sufficient momentum to promote a local separation at the throat and inhibit separation from the diverging section of the diametrically opposite surface of the nozzle. The momentum of the primary jet is thus concentrated into a wall jet. The asymmetric wall jet leaves the nozzle as a jet of kidney shaped cross-section, formed by the wall curvature and the downstream legs of the horseshoe vortex. When a lip is placed at the exit of the nozzle, the jet is deflected at a large angle to produce *vectored thrust.* The direction of the *vectored thrust* is primarily determined by the geometric configuration of the nozzle and its magnitude by the momentum of the primary flow.

Two broad types of behaviour have been encountered in the evaluation of the nozzles. The first type is where the flow inside the nozzle does not occupy the whole of the exit area. This allows ambient fluid to be induced into the nozzle and entrained by the wall jet. The interaction between the induced ambient fluid, the high momentum primary fluid and the vortex structures generated by the secondary fluid injection causes a strong vortex loop to form inside the nozzle. This vortex loop is partially responsible for the deflection of the exiting jet. This type of flow was found to occur for the nozzles with lengths of between 1 and 3 times the maximum diameter of the nozzle. In the second type of flow the primary jet occupies the whole of the nozzle exit area and no ambient fluid enters the nozzle. When this occurs, a significant proportion of the primary fluid is redirected back towards the throat to satisfy the entrainment appetite of the primary wall jet, and in the process the primary jet momentum is distributed more uniformly across the nozzle exit reducing the thrust. This type of flow occurs when the nozzle length is greater than 4 maximum nozzle diameters.

For the CD and CD10 nozzles, it has been found that the static pressure inside the cavity is below atmospheric until the exit area ratio is reduced to 0.34. In the CD20 nozzle, on the other hand, the pressure inside the nozzle was always above atmospheric in the parallel section when any exit ring was attached (AR<1) as the jet occupied the whole of the exit plane. With no exit ring (AR=1) the pressure fluctuated from just less than atmospheric to just greater than atmospheric allowing ambient fluid to be induced into the nozzle intermittently. LDV velocity profiles at the CD and CD10 nozzle exits have shown that the ambient fluid is induced into the nozzle, and these results are consistent with the wall static pressure measurements. The induction and subsequent entrainment of the ambient fluid has also been shown by flow visualisation of marked ambient fluid as it is induced into the nozzle.

It has also been found that the formation of a vortex loop inside the nozzle has a significant influence on the angle of the exiting jet, especially in the CD nozzle. It has been established that the strength of the vortex is determined by the size of the exit lip and the mass flux, which enhances the angle at which the exiting jet deflects. The vortex loop is formed through a complex interaction, the details of which are yet to be defined, between the primary wall jet, the secondary injection jet and the ambient fluid which is induced into the nozzle. Certainly the vortex structure which forms around the secondary jet injection point (which should not be confused with that which would result if the secondary jet was replaced by a solid cylinder of the same shape) has an important influence as can be seen from the strong pair of foci which form on the surface downstream from the throat. The addition of an exit ring causes a lip vortex to be formed which extracts its angular momentum from the linear momentum of the primary wall jet. The terminations of the lip vortex merge with the previously mentioned foci and the **two** vortex systems become **one.** It is concluded that the foci are the footprints of the end of a vortex loop and that the strength of this loop is increased by the circulation fed back from the lip vortex with which it becomes contiguous. When the lip is not present the strength of the loop vortex is insufficient to cause any appreciable jet deflection. As the height of the lip is increased, the strength of the lip vortex first increases, reaches a maximum and then begins to decrease as the separation in front of the exit ring moves further upstream. Accordingly the circulation fed into the vortex loop follows, first increases and then decreases. Such an interpretation is compatible with the initial increase in the angle of deflection of the primary jet as the height of the step at the exit plane increases, ie. as AR decreases. It then begins to decrease when the jet occupies the whole of the available exit area.

The two-dimensional studies of the interaction of a wall jet with a gate, Section 4.8.2 showed the vortex loop contributes to a large degree towards turning the finite aspect ratio jet as it passes over the gate. The circulation in this vortex loop derives solely from the lip vortex. In the nozzle it is augmented by the loop which derives from the secondary fluid injection. The jet deflection may also be augmented independently by the radial pressure gradient that exists at the nozzle exit, though it has not been possible to determine if this pressure gradient is also caused by the vortex loop. Once the jet leaves the nozzle at a given angle, it diffuses and appears to be self similar downstream from the nozzle exit. This conclusion is based on the limited number of velocity profiles measured through the plane of symmetry.

9.3 Future Work on Thrust Vectoring

The work should be tackled at two fronts; the fundamental aspects of thrust vectoring such as the effects of vortex loop formed by the exit lip on the primary flow and the interaction between various structures formed within the nozzle, and the application of such flows in industry as well as domestic use..

9.3.1 Fundamental Research

The work presented in this thesis has succeeded in identifying the major flow structures within the very complex flow in the nozzle. Parallel work by Hill, Nathan and Luxton (1992) is doing likewise for the O-C-O configuration of the precessing jet nozzle. Both studies have found flows to be governed largely by vortex interaction. An example found in the present study is the interaction between the vortex loop which forms as the result of interactions between the primary flow, the secondary flow and the ambient fluid which is induced into the nozzle, and the lip vortex which forms below the stagnation line of the finite aspect ratio wall jet on the exit ring. A significant body of work exists on the vortex structures which form when a finite width obstruction is placed in a boundary layer but no studies have been found of the behaviour of a finite width wall jet impinging on an infinitely wide fence. This is a basic building block in developing an analytical description of the flow in the vectored thrust nozzle and is well suited to a more conventional Ph.D. research program. Such work needs to be extended to the interaction of the lip vortex structures with a vortex generated by placing a sharp edged "doorway" upstream from the fence. More generally, the important role played by vortex interactions in the fluid mechanics has been known for many years, but only recently have non-intrusive measuring systems, such as the 3-D laser Doppler velocimetry and computational techniques and computing power become available to allow their detailed study. The study suggested above, while being of direct value in understanding of vortex interactions and their analytical modelling, in a manner being adopted by Hussain and his co-workers **[130,188]**, should be carried out in the next phase of research.

9.3.2 Applied Research

The research thus far has characterised the flow associated with the CD based nozzles of various lengths and of a particular profile which produces a fluid dynamically controlled jet deflected at a large angle without drastic loss of thrust efficiency. The CD nozzle is almost certainly not the optimum configuration and more research is needed to characterise other parameters, such as nozzle profile, not evaluated in this investigation. The present study is a first step in understanding the exceedingly complex flow phenomena involved in the nozzle. As is necessary when taking the first step into an unknown area a large amount of data has been accumulated and much of it has proved subsequently to be either irrelevant or redundant as the flow topology began to emerge. For this reason only those data which contributed directly to the interpretation of the flow have been included in this thesis.

The asymmetric separation downstream from the throat is controlled by the injection of secondary fluid at the throat. The diameter of the injection port is restricted by the diameter and streamwise curvature of the throat. The effects of moving the secondary fluid injection point downstream from the throat to accommodate a larger secondary exit area and possibly to improve the controllability of the deflected jet, should be evaluated. The profiles of nozzle convergence and divergence need be characterised to optimise the location of the *natural* separation point of the primary flow within the nozzle. The shape of the exit lip requires detailed investigation to minimise the losses across the lip.

This is particularly important if large deflections, involving large lips, are required. For particular applications, means of varying the lip height in service, for example by means of an iris construction, should be investigated. The research reported in this thesis has been concerned with subsonic flow and extension to supersonic flow, in which the flow field will be further complicated by shock and expansion wave interaction, will be essential before practicality can be claimed. For such flows it is probable that the best location of the secondary fluid injection port will be downstream from the throat as found by Franke and his co-workers.

For practical applications as a thrust vectoring device, the nozzle will be required to operate with hot combusting flow. While small scale, short term research of this type may be possible in the university facilities, the larger scale, long term durability testing is necessarily in the provinces of Government Laboratories and Industry.

9.4 Potential Applications

The fluid dynamically deflected jet has many potential applications in both combusting and cold flow regimes. The areas of possible application of the system could involve military, industrial and domestic use. The potential application of the system which gave rise to the present study was the attitude and altitude control of hovering rockets. It originated when the author was evaluating the performance characteristics of a system which controlled thrust by insertion of tabs at the nozzle exit. It was found that the high temperature and corrosive environment of the by-products from the solid propellant propulsive system meant that the life of the tabs was short and their geometry deteriorated during that life due to abrasive action of the plume, which introduced an undesirable time dependencies into the control algorithm. This posed the question of how the thrust could be controlled by non-mechanical means, and hence to the topic of this thesis. Other applications of the vectored thrust nozzle may be in the use of highly manoeuvrable aircraft by allowing pitch, roll and yaw to be controlled by vectoring the thrust from two or more engines. This would simplify the aircraft design and remove some of the large, inefficient control surfaces and in the process reducing the total drag of the aircraft. The added advantage of the low drag aircraft is its high performance envelope which should allow it to out-manoeuvre other aircraft. If the system is developed it is probable that the early applications would be to rockets and missiles. The conventional manoeuvrability of missiles is determined by the size of the control surfaces and the missile speed. The vectored thrust missile could do away with aerodynamic control surfaces and use the vectored thrust to direct it to the target. It is also conceivable that the missile could turn rapidly through 180° from its initial direction at any velocity. Conventional missiles need a large radius and time to re-orientate an attack on a moving target if it is not successful on its first pass. Fuel limitations usually preclude such re-orientation of an attack.

A primary wall jet could be controlled in the azimuthal direction to act as a three dimensional flip-flop valve. The primary fluid could be re-directed in any one of say four or possibly even eight equally spaced directions by injecting a small quantity of secondary fluid at the throat. One possible industrial application of this type of system envisaged is the pumping of fluids to different areas as required. Depending on the response time required, such a system could form the basis of a new type of fuel injection system. Other potential application is in the spray painting and powder coating industry where access between the components to be coated is limited. The direction of spray could be controlled by secondary fluid injection to allow difficult places to be coated. When combined with robotic spray system this could eliminate from industry an activity known to be a serious health risk.

A possible use of the system in the domestic environment could be a fluid dynamically controlled sprinkler system. The system could allow continuous change in orientation of the exiting spray or jet by continuous change of the azimuthal position of the secondary fluid injection point.

To conclude, it is probable that some or even all of the above applications may precede a full analytical description of the extraordinarily complex set of flow interactions which occur within the thrust vectoring nozzle.

REFERENCE

[1] **Abell, C.J.** (1977) "Acoustic coupling in a turbulent flow", Sixth A.H. and F.M.C. Adelaide, Australia, pp 415-417.

[2] **Abell, C.J. and Luxton, R.E.** (1979) "Progress Report SENRAC Project P45 to June 1979", Dept. of Mech. Eng. University of Adelaide.

[3] **Abell, C.J. and Luxton, R.E.** (1980) 'NERDDP/SENRAC Grant 79/9174, "Mixing enhancement in combustion flows, Progress report June 1980.", Dept. of Mechanical Eng. University of Adelaide.

[4] **Abell, C.J. and Luxton, R.E.** (1981) 'NERDDP Projects 79/9174, 80/0336, SENRAC Project P45., "Mixing enhancement in combustion flows, Technical Progress Report June 1980-Dec 1981", Dept. of Mech. Eng. University of Adelaide.

[5] **Abramovich, G.N** (1963) "The Theory of turbulent jets", Ed. Schindel, L.H., MIT Press.

[6] **Ahmad, N.T., Andrews, G.E., Kowkabi, M. and Sharif, S.F.** (1984) "Centrifugal mixing forces in enclosed swirl flames", Twentieth Symposium on Combustion, pp 259-267.

[7] **Ahmed, S.A., So, R.M.C. and Mongia, H.C.** (1985) "Density effects on jet characteristics in confined swirling flow", Experiments in Fluids 3, pp 231-238.

[8] **Alvi, S.H., Sridharan, K. and Lakshmana Rao N.S.** (1978) "Loss characteristics of orifices and nozzles", J.Fluids Engineering, vol.100, pp 299-307.

[9] **Anderson, A.B.C.** (1955) "Metastable jet-tone states of jets from sharp-edged, circular, pipe-like orifices", The journal of Acoustical Society of America, vol 27, No.1, pp 13-21.

[10] **Anderson, J.S., Grabitz, G., Meier, G.E.A., Jungowski, W.M. and Witczak, K.J.** (1978) "Base pressure oscillations in a rectangular duct with an abrupt enlargement", Arkives of Mechanics, Warszawa, vol 30, pp 337-351.

[11] **Anderson, R. and Bejan, A.** (1985) "The instability of a round jet surrounded by an annular shear layer", Journal of Fluids Engineering, vol 107, pp 258-263.

[12] **Andrews, G.E., Bradley, D. and Lwakabamba, S.B.** (1975) "Turbulence and turbulent Flame propagation - a critical appraisal", J.Combustion and Flame 24, pp 285-304.

[13] **Antcliff, R.R.** (1985) "CARS system for turbulent flame measurements", J.Propulsion, vol.1, No.3, pp 205-209.

[14] **Ardonceau, P.L.** (1984) "The structure of turbulence in a supersonic shock-wave/boundary-layer interaction", A.I.A.A. Journal, vol 22, No.9, pp 1254-1262.

[15] **Armaly, B.F., Durst, F., Pereiera, J.C.F. and Schonung, B.** (1983) "Experimental and theoretical investigation of backward-facing step flow", J.F.M., vol 127, pp 473-496.

[16] **Armstrong Jr., R.R**. (1981) "Influence of mach number on coherent structure relevant to jet noise", A.I.A.A. Journal, vol.19, No.6, pp 677-683.

[17] **Atkins, D.J., Maskell, S.J. and Patrick, M.A.** (1980) "Numerical prediction of separated flows", International Journal for numerical methods in Engineering, vol 15, pp 129-144.

[18] **Azevedo, D.** (1993) "Measured losses associated with secondary air injection through nozzle walls", Journal of Propulsion and Power, vol 9, No.1, pp 43-50.

[19] **Back, L.H., Massier, P.F. and Grier, H.L.** (1965) "Comparison of measured and predicted flows through conical supersonic nozzles, with emphasis on the transonic region", A.I.A.A. Journal, vol 3, No.9, pp 1606-1614.

[20] **Badri Narayanan, M.A. and Platzer, M.F.** (1987) "Jet excitation by a bivane system and its application to an ejector for thrust augmentation", Naval Postgraduate School, Monterey, California, NPS-67-87-004.

[21] **Badri Narayanan, M.A. and Platzer, M.F.** (1987) "The mixing mechanism by organised turbulence structures in a plane jet excited by a novel method", IUTAM Symp. on Turbulence Management, Jan. 1987, Bangalore, India.

[22] **Badri Narayanan, M.A. and Raghu, S.** (1982) "Two dimensional jet subjected to periodic oscillations in the potential core region", Report number 82 FM2, (March 1982).

[23] **Badri Narayanan, M.A.** (1987) "Excitation of plane jet by twin vane oscillator: A preliminary investigation", Report No.AE 87FM1, Fluid Dynamics Lab., Dept.of Aerospace Eng., Indian Inst. of Sci., Bangalore, India.

[24] **Ballal, D.R. and Lefebvre, A.H.** (1974) "Turbulence effects on enclosed flames", Acta Astronautica, vol.1, pp 471-483.

[25] **Ballal, D.R. and Lefebvre, A.H.** (1975) "The structure and propagation of turbulent flames", Proc.R.Soc.Lond.A. 344, pp 217-234.

[26] **Balu, R., Marathe, A.G., Paul, P.J. and Mukunda, H.S.** (1991) "Analysis of performance of a hot gas injection thrust vector control system", Journal of Propulsion, vol 7, No.4, pp 580-585.

[27] **Batchelor, G.K.** (1960) "Homogeneous Turbulence", Cambridge University Press, 1960.

[28] **Benedict, R.P., Carlucci, N.A. and Swetz, S.D.** (1966) "Flow losses in abrupt enlargements and contractions", J. of Eng.Power, Jan. 1966, pp 66-81.

[29] **Benjamin, T.B.** (1962) "Theory of the vortex breakdown phenomenon", J.F.M., vol.14, part 4, pp 593-629.

[30] **Bilger, R.W.** (1976) "Turbulent jet diffusion flames", Prog.Energy Combustion Sci., vol. 1, pp 87-109.

[31] **Binder, G. and Favre-Marinet, M.** (1981) "Some characteristics of pulsating or flapping jets", Unsteady Turbulent Shear Flows, edited by R.Mitchel, J.Cousteix and R.Houdeville, Springer-Verlag.

[32] **Bis, Z., Blasiak, W., Collin, R, Magnusson, L. and Vaclavinek, J.** (1991) "Fundamental characteristics of a turbulent jet within a crossflow", The Royal Institute of Technology, Dept. of Heat and Furnace Technology, S-10044 Stockholm, Sweden.

[33] **Bloxsidge, G.J., Dowling, A.P. and Langhorne, P.J.** (1988) "Reheat buzz: an acoustically coupled combustion instability. Part 2. Theory", J.F.M., vol 193, pp 445-473.

[34] **Bogdanof, D.W.** (1983) "Compressibility effects in turbulent shear layer", A.I.A.A. Journal, vol 21, No.6, pp 926-927.

[35] **Bradbury, L.J.S. and Khadem, A.H.** (1975) "The distortion of a jet by tabs", J.F.M., vol 70, part 4, pp 801-813.

[36] **Bradshaw, P. and Wong, F.Y.F.** (1972) "The reattachment and relaxation of a turbulent shear layer", J.F.M., vol 52, pp 113-135.

[37] **Bradshaw, P.** (1983) "Complex three-dimensional turbulent flows", 8th A.F.M.C., pp k5.1-k5.7.

[38] **Bradshaw, P.** (1973) "Effects of streamline curvature on turbulent flow", AGARD 169, Ed.Young,A.D.

[39] **Bradshaw, P.** (1971) "An Introduction to Turbulence and its Measurement", Pergamon Press, 1971.

[40] **Brainerd, J.J. and Levinsky, E.S.** (1963) "Viscous and nonviscous nonequilibrium nozzle flows", A.I.A.A. Journal, vol 1, No.11, pp 2474-2481.

[41] **Brain, T.J.S. and Reid, J.** (1973) "Performance of small diameter cylindrical critical-flow nozzles", National Eng.Lab.Report 546, Great Britain.

[42] **Bremhorst, K. and Hollis, P.G.** (1987) "Velocity measurements in a fully pulsed subsonic air jet", Progress Report (March 1987), Dept. of Mech.Eng., Uni. of Queensland.

[43] **Bremhorst, K.** (1983) "Effect of wall heat flux on the longitudinal velocity and temperature fields in initially fully developed flow of air in a pipe", 8th A.F.M.C., pp 10A9-10A12.

[44] **Broadwell, J.E. and Dimotakis, P.E.** (1986) "Implications of recent experimental results for modelling reactions in turbulent flows", A.I.A.A. Journal, vol 24, No.6, pp 885-889.

[45] **Broadwell, J.E. and Breidenthal, R.E.** (1982) "A simple model of mixing and chemical reaction in a turbulent shear layer", J.F.M., vol 125, pp 397-410.

[46] **Broadwell, J.E., Dahm, W.L.A. and Mungal, M.G.** (1984) "Blowout of turbulent diffusion flames", Twentieth Symp. on Comb., pp 303-310.

[47] **Brown, G.L. and Roshko, A.** (1974) "On density effects and large structure in turbulent mixing layers", J.F.M., vol 64, part 4, pp 775-816.

[48] **Brown, G.L.** (1974) "The entrainment and large structure in turbulent mixing layers" Proc. Fifth Australasian Conf., pp 352-359.

[49] **Bull, M.K. and Agarwal, N.K.** (1983) "Characteristics of the flow separation due to an orifice plate in fully-developed turbulent pipe-flow", Eighth Australasian Fluid Mechanics Conf., Newcastle., pp 4B1-4B4.

[50] **Cabelli, A., Pearson, I.G. and Shepherd, I.C.** (1985) "Turbulent diffusion gas flame noise", Proc.Aust.Inst.Energy Nat.Conf., Melbourne, Paper 20, pp 257-268.

[51] **Campbell, I.G., Bray, K.N.C. and Moss, J.B.** (1983) "Combustion oscillations in a ducted premixed flame", I.Mech.E., C69/83, pp 85-94.

[52] **Castro, I.P. and Bradshaw, P.** (1976) "The turbulence structure of a highly curved mixing layer", J.F.M. vol 73, part 2, pp 265-304.

[53] **Catalano, G.D., Mathis, J.A. and Chang, K.S.** (1991) "Higher order statistics of a turbulent jet in a confined crossflow", AIAA Journal, V29, N12, pp 2124-2131.

[54] **Chandrasuda, C. and Bradshaw, P.** (1981) "Turbulence structure of a reattaching mixing layer", J.F.M., vol 110, pp 171-194.

[55] **Chan, Y.Y.** (1974) "Spatial waves in turbulent jets", The Physics of Fluids, vol 17, No.1, pp 46-53.

[56] **Charwat, A.F. and Allegre, J.** (1964) "Interaction of a supersonic stream and a transverse supersonic jet", A.I.A.A. Journal, vol 2, No.11, pp 1965-1972.

[57] **Cherdron, W., Durst, F. and Whitelaw, J.H.** (1978) "Asymmetric flows and instabilities in symmetric ducts with sudden expansions", J.F.M., vol 84, pp 13-31.

[58] **Cherry, N.J., Hillier, R. and Latour, M.E.M.P.** (1984) "Unsteady measurements in a separated and reattaching flow", J.F.M., vol 144, pp 13-46.

[59] **Chien, J.C. and Schetz, J.A.** (1975) "Numerical solution of the three-dimensional Navier-Stokes equations with applications to channel flows and a buoyant jet in a cross flow", Journal of Applied Mechanics,pp 575-579.

[60] **Choi, D.W., Gessner, F.B. and Oates, G.C.** (1986) "Measurements of confined, coaxial jet mixing with pressure gradient", J.F. Eng., vol 108, pp 39-46.

[61] **Chou, S.K.** (1983) "Jet entrainment and compression in compressible flow ejectors", Eighth Australasian Fluid Mechanics Conf., pp 9b11-9b14.

[62] **Chua, L.P. and Antonia, R.A.** (1988) "Flow reversal and intermittency of a turbulent jet", A.I.A.A. Journal, vol 27, number 11, pp 1494-1499.

[63] **Chuech, S.G., Lai, M.C. and Faeth, G.M.** (1989) "Structure of turbulent sonic underexpanded free jets", A.I.A.A. Journal, vol 27, No.5, pp 549-559.

[64] **Clarke, J.F. and McChesney, M.** (1964) "The Dynamics of Real Gases", Butterworth and Co. 1964.

[65] **Claypole, T.C. and Syred, N.** (1981) "The effects of swirl burner aerodynamics on NO_x formation", Eighteenth Symposium on Combustion, pp 81-89.

[66] **Claypole, T.C. and Syred, N.** (1983) "The integration of swirl burners with furnaces for the combustion of low calorific value gases", I.Mech.E., C75/83, pp 139-145.

[67] **Claypole, T.C. and Syred, N.** (1982) "The stabilization of flames in swirl combustors", Journal of Institute of Energy, March 1982, pp 14-19.

[68] **Clemens, N.T. and Mungal, M.G.** (1992) "Effects of sidewall disturbances on the supersonic mixing layer", Journal of Propulsion, vol 8, No.1, pp 249-251.

[69] **Coelho, S.L.V. and Hunt, J.C.R.** (1989) "The dynamics of the near field of strong jets in crossflows", J.F.M., vol 200, pp 95-120.

[70] **Collins, D.J., Platzer, M.F., Lai, L.C.S. and Simmons, J.M.** (1982) "Experimental investigation of oscillating subsonic jets", Numerical and Physical Aspects of Aerodynamic Flow, Springer-Verlag, pp 575-587.

[71] **Crow, C.T., Chung, J.N. and Troutt, T.R.** (1988) "Particle mixing in free shear layer", Prog.Energy Combust.Sci., vol 14, pp 171-194.

[72] **Crow, S.C. and Champagne, F.H.** (1971) "Orderly structure in jet turbulence", J.F.M., vol 48, part 3, pp 547-591.

[73] **Cummings, A.** (1984) "Acoustic nonlinearities and power losses at orifices", A.I.A.A. Journal, vol 22, No.6, pp 786-792.

[74] **Dahm, W.J.A, and Dimotakis, P.E.** (1990) "Mixing at large Schmidt number in the self-similar far field of turbulent jets", J.F.M., vol 217, pp 299-330.

[75] **Davey, A.** (1961) "Boundary-layer flow at a saddle point of attachment", J.F.M., vol 10, pp 593-610.

[76] **Davies, P.O.A.L., Fisher, M.J. and Barratt, M.J.** (1962) "The characteristics of the turbulence in the mixing region of a round jet", Fluid Mechanics, 15, pp 337-367.

[77] **Davies, P.O.A.L.,** (1981) "Flow-acoustic coupling in ducts", Journal of Sound and Vibration, vol 77, No.2, pp 191-209.

[78] **Dellenback, P.A., Metzger, D.E. and Neitzel, G.P.** (1988) "Measurements in turbulent swirling flow through an abrupt axisymmetric expansion", A.I.A.A. Journal, vol 26, No.6, pp 669-681.

[79] **Dimotakis, P.E. and Brown, G.L.** (1976) "The mixing layer at high Reynolds number: large scale dynamics and entrainment", J.F.M., vol 78, part 3, pp 535-560.

[80] **Dracos, T., Giger, M. and Jirka, G.H.** (1992) "Plane turbulent jets in a bounded fluid layer", J.F.M., vol 241, pp 587-614.

[81] **Driver, D.M., Seegmiller, H.L. and Marvin, J.G.** (1987) "Time-dependent behaviour of a reattaching shear layer", A.I.A.A. Journal, vol 25, No 7, pp 914-919.

[82] **Duncan, W.J., Thom, A.S. and Young, A.D.** (1970) "Mechanics of Fluids" Arnold.

[83] **Durrett, R.P., Stevenson, W.H. and Thompson, H.D.** (1988) "Radial and axial turbulent flow measurements with an L.D.V. in an axisymmetric sudden expansion air flow", J.F.Eng. vol 110, pp 367-372.

[84] **Durst, F., Melling, A. and Whitelaw, J.H.** (1974) "Low Reynolds number flow over a plane symmetric sudden expansion", J.F.M., vol 64, part.1, pp 111-129.

[85] **East, L.F.** (1966) "Aerodynamically induced resonance in rectangular cavities", J. Sound Vib., vol 3, No. 3, pp 277-287.

[86] **Eaton, J.K. and Johnston, J.P.** (1981) "A review of research on subsonic turbulent flow reattachment", A.I.A.A. Journal, vol 19, No.9, pp 1093-1100.

[87] **Edelman, R.B. and Harsha, P.T.** (1978) "Laminar and turbulent gas dynamics in combustors - Current status", Prog. Energy Combust. Sci., vol 4, pp 1-62.

[88] **Eickhoff, H., Lenze, B. and Leuckel, W.** (1984) "Experimental investigation on the stabilization mechanism of jet diffusion flames", Twentieth Symp. on Combust., pp 311-318.

[89] **El-Taher, R.M.** (1983) "Experimental investigation of curvature effects on ventilated wall jets", A.I.A.A. Journal, vol 21, No.11, pp 1505-1511.

[90] **Elsner, J.W., Drobniak, S. and Klajny, R.** (1989) "Behaviour of column-mode vortex structures in the near flow region of a round free jet", Turbulence, vol 1, pp 35-50.

[91] **Elsner, J.W. and Drobniak, S.** (1982) "Turbulent structure in swirling jets", IUTAM Symposium Marseille, pp. 219-228.

[92] **Elsner, J.W., Boguslawski, A. and Drobniak, S.** (1989) "The application of variable interval time averaging method in the detection of coherent structures in a round free jet", Turbulence, vol 1, pp 51-68.

[93] **Emmons, H.W.** (1958) "Fundamentals of Gas Dynamics", Princeton, 1958.

[94] **Escudier, M.P. and Keller, J.J.** (1985) "Recirculation in swirling flow: A manifestation of vortex breakdown", A.I.A.A. Journal, vol 23, No. 1, pp 111-116.

[95] **Escudier, M.P., Bornstein, J. and Maxworthy, T.** (1982) "The dynamics of confined vortices", Proc.R.Soc.Lond., pp 335-360.

[96] **Escudier, M.P.** (1987) "Confined vortices in flow machinery", Ann.Rev.Fluid Mech., No. 19, pp 27-52.

[97] **Favaloro, S.C., Nejad, A.S. and Ahmed, S.A.** (1989) "Measurements of swirling flow in a ramjet dump combustor model", Proc.Aero.Conf., Melbourne. 1989., pp 309-313.

[98] **Favre-Marinet, M., Binder, G. and Hac, Te.V.** (1981) "Generation of oscillating jets", Journal of Fluids Engineering, vol 103, pp 609-614.

[99] **Feil, O.G.** (1964) "Vane system for very-wide-angle subsonic diffusers", J.of Basic Eng., pp 759-764.

[100] **Fernholz, H.H. and Krause, E.** (1982) "Three-dimensional turbulent boundary layers", Springer-Verlag, International Union of Theoretical and Applied Mechanics, Symposium, Berlin, Germany.

[101] **Fricker, N. and Leuckel, W.** (1976) "The characteristics of swirl-stabilised natural gas flames. Part 3: The effect of swirl and burner mouth geometry on flame stability", J. of the Inst. of Fuel, pp 152-158.

[102] **Friddell, J.H. and Franke, M.E.** (1992) "Confined jet thrust vector control nozzle studies", Journal of Propulsion and Power, vol 8, No.6, pp 1239-1244.

[103] **Gal-Or, B.** (1990) "Fundamental concepts of vectored propulsion", Journal of Propulsion, vol 6, No.6, pp 747-757.

[104] **Gal-Or, B. and Sherbaum, V.** (1993) "Thrust vectoring: Theory, Laboratory, and Flight Tests", Journal of Propulsion and Power, vol 9, No.1, pp 51-58.

[105] **Galea, S.C. and Simmons, J.M.** (1983) "Excitation of a plane jet by period perturbation of the nozzle area", Eighth Australasian Fluid Mechanics Conf., pp 13C5-13C8.

[106] **Garg, A.K. and Leibovich, S.** (1979) "Spectral characteristics of vortex breakdown flowfields", American Institute of Physics, Phys. Fluids, vol 22, No 11, pp 2053-2064.

[107] **Gerhart, P.M. and Gross, R.J.** (1985) " Fundamentals of fluid mechanics" Addison-Wesley Publication.

[108] **Goldstein, R.J.** (1983) "Fluid Mechanics Measurements", Hemisphere Publishing Corporation, 1983.

[109] **Gouldin, F.C., Depsky, J.S. and Lee, S.L.** (1985) "Velocity field characteristics of a swirling flow combustor", A.I.A.A. Journal, vol 23, No. 1, pp 95-102.

[110] **Grandke, T.** (1985) "Theory and application of the LASER shadow technique: Part 1. Two dimensional turbulent flow", Experiments in Fluids 3, pp 77-86.

[111] **Gupta, A.K., Beer, J.M. and Swithenbank, J.** (1976) "Concentric multi-annular swirl burner: Stability limits and emission characteristics", Sixteenth Symp. on Combust., pp 79-91.

[112] **Haddad, A. and Moss, J.B.** (1990) "Aerodynamic design for supersonic nozzles of arbitrary cross section", Journal of Propulsion, vol 6, No.6, pp 740-746.

[113] **Hallett, W.L.H. and Gunther, R.** (1984) "Flow and mixing in swirling flow in a sudden expansion", The Canadian Journal of Chemical Engineering, vol 62, pp 149-155.

[114] **Harch, W.H.** (1983) "Numerical simulation of flow in ramjet combustor geometries", 8th Australasian Fluid Mechanics Conference, pp 10.9-10.12.

[115] **Harch, W.H., Collins, D.J. and Platzer, M.F.** (1983) "A description of the velocity field of a vane excited jet", 8th A.F.M.C., 8C5-8C8.

[116] **Heister, S.D., Nguyen, T.T. and Karagozian, A.R.** (1989) "Modelling of liquid jets injected transversely into a supersonic crossflow", A.I.A.A. Journal, vol 27, No.12, pp 1727-1734.

[117] **Henbest, S.** (1991) "A study of flow in axisymmetric co-flowing jets", Recent advances in experimental fluid mechanics. ed.,Zhuang,F.G. pp 349-354.

[118] **Hill, Jr.W.G. and Greene, P.R.** (1977) "Increased Turbulent jet mixing rates obtained by self-excited acoustic oscillations", Journal of Fluids Engineering, pp 520-525.

[119] **Hill, S.J., Nathan, G.J. and Luxton, R.E.** (1992) "Precessing and axial flows following a sudden expansion in an axi-symmetric nozzle", 11th A.F.M.C., Hobart, Australia.

[120] **Hitchman, G.J., Strong, A.B., Slawson, P.R. and Ray, G.D.** (1990) "Turbulent plane jet with and without confining end walls", A.I.A.A. Journal, vol 28, No.10, pp 1699-1700.

[121] **Ho, C.M. and Nosseir, N.S**. (1981) "Dynamics of an impinging jet. Part 1. The feedback phenomenon", J.F.M., vol 105, pp 119-142.

[122] **Holdeman, J.D., Srinivasan, R., Reynolds, R.S. and White, C.D.** (1992) "Studies of the effects of curvature on dilution jet mixing", Journal of Propulsion, vol 8, No.1, pp 209-218.

[123] **Hornung, H. and Perry, A.E.** (1984) "Some aspects of three-dimensional separation, Part 1: Stream surface bifurcation", Zeitschrift Fur Flugwissenschaften und Weltraumforschung, pp 77-87.

[124] **Hottel, H.C.** (1950) "Burning in laminar and turbulent jets", Survey Papers, pp 97-113.

[125] **Hunt, J.C.R., Abell, C.J., Peterka, J.A. and Woo, H.** (1978) "Kinematical studies of the flows around free or surface mounted obstacles ; applying topology to flow visualisation", J.F.M., vol 86, part 1, pp 179-200.

[126] **Husain, Z.D. and Hussain, A.K.M.F.** (1983) "Natural instability of free shear layer", A.I.A.A. Journal, vol 21, No.11, pp 1512-1517.

[127] **Husain, H. and Hussain, F. (1993)** " Elliptic jets. Part 3. Dynamics of preffered mode coherent structures", J.F.M. vol 248, pp 315-361.

[128] **Hussain, A.K.M.F. and Clark, A.R.** (1981) "On the coherent structure of the axisymmetric mixing layer: a flow-visualisation study", J.F.M., vol 104, pp 263-294.

[129] **Hussain, A.K.M.F. and Hasan, M.A.Z.** (1983) "The Whistler-nozzle phenomenon", J.F.M., vol 134, pp 431-458.

[130] **Hussain, F., Virk, D. and Melander, M. (1993)** "New studies in Vortex Dynamics: Incompressible and Compressible vortex reconection, core dynamics, and coupling between large and small scales", Sadhana, Vol 18, Parts 3 & 4, pp 477-529.

[131] **Johnson, R.S.** (1990) "Ring wave on the surface of shear layer flows: A linear and nonlinear theory", J.F.M., vol 125, pp 145-160.

[132] **Johnston, J.P. and Nishi, M.** (1990) "Vortex generator jets-means for flow separation control", A.I.A.A. Journal, vol 28, No.6, pp 989-994.

[133] **Johnston, S.C., Dibble, R.W., Schefer, R.W., Ashurst, W.T. and Kollman, W.** (1984) "Laser measurements and stochastic simulations of turbulent reacting flows", A.I.A.A. Journal, vol 24, No. 6, pp 918-937.

[134] **Joos, F. and Vortmeyer, D.** (1986) "Self-excited oscillations in combustion chambers with premixed flames and several frequencies", Combustion and Flames 65:, pp 253-262.

[135] **Jungowski, W.M.** (1978) "Some self induced supersonic flow oscillations", Prog.Aerospace sci., vol 18, No.2, pp 151-175.

[136] **Karamcheti, K. and Tao-Sze Hsia, H.** (1963) "Integral approach to an approximate analysis of thrust vector control by secondary injection", A.I.A.A. Journal, vol 1, No.11, pp 2538-2544.

[137] **Kato, S.M., Groenewegen, B.C. and Breidenthal, R.E.** (1987) "Turbulent mixing in nonsteady jets", A.I.A.A.Tech notes, pp 165-168.

[138] **Kawall, J.G. and Keffer, J.F.** (1981) "The role of coherent structures in the development of a uniformly strained turbulent wake", (Turbulent Shear Flows 3, Ed. Bradbury,L.J.S.ct al) pp 133-144.

[139] **Kehtarnavaz, H., Coats, D.E. and Dang, A.L.** (1990) "Viscous loss assessment in rocket engines", J.Propusion, Vol 6, No.6, pp 713-717.

[140] **Kiya, M. and Sasaki, K.** (1985) "Structure of large-scale vortices and unsteady reverse flow in the reattaching zone of a turbulent separation bubble", J.F.M., vol 154, pp 463-491.

[141] **Knowles, K. and Carpenter, P.W.** (1990) "Use of swirl for flow control in propulsion nozzles", J.Propulsion, vol 6, pp 158-164.

[142] **Komori, S. and Ueda, H.** (1985) "The large scale coherent structure in the intermitted region of the self preserving round free jet", J.F.M., vol 152, pp 337-359.

[143] **Ko, N.W.M. and Cheung, W.T.** (1983) "Mean velocity distribution of an interrupted jet", 8th A.F.M.C., pp 12B5-12B8.

[144] **Koochesfahani, M.M., Dimotakis, P.E. and Broadwell, J.E.** (1985) "A "Flip" experiment in a chemically reacting turbulent mixing layer", A.I.A.A. Journal, vol 23, No. 8, pp 1191-1194.

[145] **Koochesfahani, M.M. and Dimotakis, P.E.** (1989) "Effects of a downstream disturbance on the structure of a turbulent plane mixing layer", A.I.A.A. Journal, vol 27, No. 2, pp 161-165.

[146] **Koochesfahani, M.M. and Dimotakis, P.E.** (1986) "Mixing and chemical reactions in a turbulent liquid mixing layer", J.F.M., vol 170, pp 83-12.

[147] **Koochesfahani, M.M. and Dimotakis, P.E.** (1985) "Laser-induced fluorescence measurements of mixed fluid concentration in a liquid plane shear layer", A.I.A.A. Journal, vol 23, No. 11, pp 1700-1707.

[148] **Kremer, H., Minx, E. and Rawe, R.** (1973) "Stabilization of parallel-flow turbulent jet diffusion flames by means of flame holders", Proc.Combustion Institute, European Symposium, Sheffield University, pp 536-541.

[149] **Krothapali, A, Lourenco, L. and Buchlin, J.M.** (1990) "Separated flow upstream of a jet in a crossflow", A.I.A.A.Journal,vol 28, No.3, pp 414-419.

[150] **Lai, J.C.S. and Lu, D.** (1991) "The near field characteristics of a two-dimensional wall jet", 1st International Conference on Experimental Fluid Mechanics, pp 136-141, Chengdu, China.

[151] **Lai, J.C.S. and Simmons, J.M.** (1983) "Some flow characteristics of mechanically excited plane turbulent free jets", 8th A.F.M.C., pp 8C1-8C4.

[152] **Lai, J.C.S.** (1984) "Unsteady effects in mechanically-excited turbulent plane jets", Int.J. Heat and Fluid Flow, pp 215-221.

[153] **Lai, J.C.S. and Simmons, J.M.** (1985) "Instantaneous velocity measurements in a vane-excited plane jet", A.I.A.A. Journal, vol 23, No. 8, pp 1157-1164.

[154] **Lai, J.C.S. and Simmons, J.M.** (1980) "Instantaneous velocity measurements in a periodically pulsed plane turbulent jet", A.I.A.A. Journal, vol 18, No. 12, pp 1532-1534.

[155] **Lakshminarasimha, A.N., Tabakoff, W and Metwally, M.** (1992) "Laser Doppler velocimetry measurements in the vortex region of a radial inflow turbine", Journal of Propulsion, vol 8, No.1, pp 184-191.

[156] **Lamb, H.** (1932) "Hydrodynamics", Cambridge University Press, 1932.

[157] **Langhorne, P.J.** (1988) "Reheat buzz: an acoustically coupled combustion instability. Part 1. Experiment", J.F.M., vol 193, pp 417-443.

[158] **Lang, W., Poinsot, T. and Candel, S.** (1987) "Active control of combustion instability", Combustion and Flame 70: pp 281-289.

[159] **Lau, J.C., Fisher, M.J. and Fuchs, H.V.** (1972) "The intrinsic structure of turbulent jets", Journal of Sound and Vibration, vol 22, No.4, pp 379-406.

[160] **Launder, B.E. and Spalding, D.B.** (1972) "Mathematical models of turbulence", Academic Press, 1972.

[161] **Law, C.K.** (1984) "Heat and mass transfer in combustion: Fundamental concepts and analytical techniques", Prog. Energy Combust. Sci., vol 10, pp 295-318.

[162] **Lefebvre, A.H. and Reid, R.** (1966) "The influence of turbulence on the structure and propagation of enclosed flames", Combustion and Flame, vol 10, pp 355-366.

[163] **Leibovich, S.** (1983) "Vortex stability and breakdown: Survey and extensions", A.I.A.A.Journal, vol 22, No.9, pp 1192-1206.

[164] **Leibovich, S.** (1978) "The structure of vortex breakdown", Ann.Rev.Fluid Mech.1978, pp 221-246.

[165] **Lepicovsky, J., Ahuja, K.K. and Sallikuddin, M.** (1986) "An experimental study of one-excited heated jets", J.Propulsion, vol 2, No.2, pp 149-154.

[166] **Leuckel, W. and Fricker, N.** (1976) "The characteristics of swirl-stabilised natural gas flames, Part 1: Different flame types and their relation to flow and mixing patterns", Journal of the Inst. of Fuel, pp 103-112.

[167] **Lignola, P.G. and Reverchon, E.** (1988) "A jet stirred reactor for combustion studies: Design and characterisation", Combust.Sci. and Tech., vol 60, pp 319-333.

[168] **Lilley, J.S. and Arszman, J.H.** (1990) "Scarfed nozzles for thrust-vector adjustment", Journal of Propulsion, vol 7, No.3, pp 382-388.

[169] **Lilley, J.S.** (1993) "Reduced-length scarfed-nozzle for thrust vector adjustment", Journal of Propulsion and Power, vol 9, No.2, pp 233-239.

[170] **Lim, T.T., Kelso, R.M. and Perry, A.E.** (1992) "A study of a round jet in cross-flow at different velocity ratios", 11th A.F.M.C. Hobart, Australia, pp 1089-1092.

[171] **Long, D.F., Kim, H. and Arndt, R.E.A.** (1984) "Controlled suppression or amplification of turbulent jet noise", A.I.A.A. Journal, vol 23, No.6, pp 828-833.

[172] **Lopez, J.M.** (1988) "Axisymmetric vortex breakdown, Part 1: Confined swirling flow", A.R.L. Aero. Report 173, AR-004-572.

[173] **Loth, E., Baum, J. and Lohner, R.** (1992) "Formation of shocks within axisymmetric nozzles", A.I.A.A.Journal, vol 30, No.1, pp 268-270.

[174] **Luxton, R.E.** (1985) "Mixing enhancement in combusting flows - End of grant report", National Energy Research, Development and Demonstration Program. Department of Resources and Energy, Australian Government, Canberra.

[175] **Luxton, R.E. and Nathan, G.J.** (1989) "The combustion characteristics of an enhanced mixing nozzle", The Combustion Inst., International Joint Conference, Sept. 89, Sydney, Australia.

[176] **Luxton, R.E., Nathan, G.J. and LUMINIS Pty. Ltd** (1987) "Controlling the motion of a fluid jet", International Patents, 16 April 1987, Australian Patent Office, Adelaide, Australia.

[177] **Luxton,R.E.** (1984) "Prediction and management of flow in ducts and pipes", ESAA Summer School, University of Adelaide, pp 1-50.

[178] **Mabey, D.G.** (1972) "Analysis and correlation of data on pressure fluctuations in separated flow", J. Aircraft, vol 9, pp 642-645.

[179] **Mahmud, T., Wall, T.F. and Truelove, J.S.** (1983) "Aerodynamic studies on jets issuing from swirled double concentric nozzles with divergent exits", 8th Australasian Fluid Mechanics Conference, pp 1B.10-1B.13.

[180] **Manias, C.G. and Nathan, G.J.** (1992) "The precessing jet gas burner - A low NO_x burner providing process efficiency and product quality improvements", International Kiln Association Conference, Toronto, Canada.

[181] **Manias, C.G. and Nathan, G.J.** (1994) "Low NO_x clinker production", World Cement, May 1994.

[182] **Marcum, D.L. and Hoffman, J.D.** (1988) "Calculation of three-dimensional inviscid flowfields in propulsive nozzles with centrebodies", Journal of Propulsion vol 4, No.2, pp 172-179.

[183] **Mason, P.J. and Morton, B.R.** (1987) "Trailing vortices in the wakes of surface-mounted obstacles", Journal of Fluid Mechanics, vol 175, pp 247-293.

[184] **Mathur, M.L. and Maccallum, N.R.L.** (1967) "Swirling air jets issuing from vane swirlers. Part 2: Enclosed jets", J. of the Inst. of Fuel, pp 238-2425.

[185] **Ma, Y., Van Moorehem, W.K. and Shorthill, R.W.** (1991) "Experimental investigation of velocity coupling in combustion instability", Journal of Propulsion, vol 7, No.5, pp 692-698.

[186] **Mehta, R.D.** (1977) "The aerodynamic design of blower tunnels with wide-angle diffusers", Prog.Aerospace Sci., vol 18, pp 59-120.

[187] **Meier, G.E.A., Grabitz, G., Jungowski, W.M., Witczak, K.J. and Anderson, J.S.** (1978) "Oscillations of the supersonic flow downstream of an abrupt increase in duct cross-section", Gottingen, No. 5.

[188] **Melander, M. and Hussain, F. (1994)** "Topological vortex dynamics in axisymmetric viscous flows", J.F.M., vol 260, pp 57-80.

[189] **Melbourne, W.H.** (1979) "Turbulence effects on maximum surface pressures - A mechanism and possibility of reduction", Wind Engineering, vol 1, pp 541-551.

[190] **Menon, R., Larson, C. and Tamburrino, A.** (1989) "Turbulence Measurements in liquid flows using a dedicated L.D.V. system", Tenth Australian F.M.C.

[191] **Mills, R.D.** (1968) "Numerical solution of viscous flow through a pipe orifice at low Reynolds numbers", Journal of Mechanical Engineering Science, vol 10, No.2, pp 133-140.

[192] **Moon, L.F. and Rudinger, G.** (1977) "Velocity distribution in an abruptly expanding circular duct", J. of Fluids Eng., pp 266-230.

[193] **Morgan, R.G. and Stalker, R.J.** (1983) "Experiments on a simple scramjet model", 8th A.F.M.C., Uni. of Newcastle, pp 10C1-10C4.

[194] **Morris, P.J.** 1990) "Instability waves in twin supersonic jets", Journal of Fluid Mechanics, vol 220, pp 293-307.

[195] **Morton, B.R.** (1984) "The generation and decay of vorticity", Geophysics Astrophysics Fluid Dynamics, vol 28, pp 277-308.

[196] **Morton, B.R.** (1969) "The strength of vortex and swirling core flows", Presented as an additional lecture at the 11th A.F.M.C., Hobart,(1992), pp 315-332.

[197] **Moustafa, G.H. and Rathakrishnan, E.** (1993) "Studies on the flowfield of multijet with square configuration", A.I.A.A. Journal, vol 22, No.7, pp 1189-1190.

[198] **Moffat, R.J.** (1988) "Describing the uncertainties in experimental results", Experimental, Thermal and Fluid Science,vol 1, pp 3-17.

[199] **Mungal, M.G., Hermanson, J.C. and Dimotakis, P.E.** (1984) "Reynolds number effects on mixing and combustion in a reacting shear layer", A.I.A.A. Journal, vol 23, No.9, pp 1418-1423.

[200] **Mungal, M.G. and Dimotakis, P.E.** (1984) "Mixing and combustion with low heat release in a turbulent shear layer", J.F.M., vol 148, pp 349-382.

[201] **Mungal, M.G., Dimotakis, P.E. and Broadwell, J.E.** (1984) "Turbulent mixing and combustion in a reacting shear layer", A.I.A.A. Journal, vol 22, No.6, pp 797-800.

[202] **Mungal, M.G. and Frieler, C.E.** (1988) "The effects of Damkohler number in a turbulent shear layer", Combustion and Flame 71: pp 23-34.

[203] **Nakayama, Y., Woods, W.A. and Clark, D.G.** (1988) "Visualized Flow: Fluid motion in basic and engineering situations revealed by flow visualization", Pergamon Press, 1988.

[204] **Nathan, G.J. and Luxton, R.E.** (1992) "The flow field within an axi-symmetric nozzle utilising a large abrupt expansion", Recent Advances in Experimental Fluid Mechanics,ed. F.G.Zhuang, International Academic Publication, pp 527-532.

[205] **Nathan, G.J. and Luxton, R.E.** (1992) "Reduced NOx emissions and enhanced large scale turbulence from a precessing jet burner", 24th Symposium (International) on Combustion. The Combustion Institute, July 1992, Sydney, Australia.

[206] **Nathan, G.J. and Luxton, R.E.** (1988) "A stable, Un-premixed gas burner with infinite turn-down ratio", 1st European Conf. Industrial Furnaces and Boilers, March '88, Lisbon, Portugal.

[207] **Nathan, G.J.** (1988) "The Enhanced Mixing Burner", Thesis for the Degree of Doctor of Philosophy, The University of Adelaide, Mechanical Engineering Department.

[208] **Nathan, G.J. and Luxton, R.E.** (1989) "The combustion characteristics of an enhanced mixing nozzle", The Combustion Institute International Joint Conference, Sydney, Aust.

[209] **Nathan, G.J. and Luxton, R.E.** (1989) "A precessing asymmetric flow field in an abruptly expanding axi-symmetric duct", 10th Australasian Fluid Mechanics Conference, pp 11c2, Melbourne, Australia.

[210] **Newton, J.F. and Spaid, F.M.** (1962) "Interaction of secondary injectants and rocket exhausts for thrust vector control", J. of American Rocket Soc., Aug. 62, pp 1203-1211.

[211] **Nguyen, T.T. and Karagozian, A.R.** (1992) "Liquid fuel jet in subsonic crossflow", Journal of Propulsion, vol 8, No.1, pp 21-29.

[212] **Norton, M.P. and Bull, M.K.** (1984) "Mechanism of the generation of external acoustic radiation from pipes due to internal flow disturbances", Journal of Sound and Vibration, vol 94, No.1, pp 105-146.

[213] **Ouwa, Y., Watanabe, M. and Asawo, H.** (1981) "Flow visualisation of a two-dimensional water jet in a rectangular channel", Japanese Journal of Applied Physics, vol 20, No.1, pp 243-247.

[214] **Parekh, D.E. and Reynolds, W.C.** (1987) "Bifurcating air jets at higher subsonic speeds", Stanford University.

[215] **Patankar, S.V., Basu, D.K. and Alpay, S.A.** (1977) "Prediction of the three-dimensional velocity field of a deflected turbulent jet", J. of Fluids Eng., pp 758-762.

[216] **Pelfrey, J.R.R. and Liburdy, J.A.** (1986) "Mean flow characteristics of a turbulent offset jet", Trans.of A.S.M.E., vol 108, pp 82-88.

[217] **Pelfrey, J.R.R. and Liburdy, J.A.** (1986) "Effects of curvature on the turbulence of a two-dimensional jet", Experiments in Fluids 4, pp 143-149.

[218] **Perry, A.E. and Fairlie, B.D.** (1974) "Critical points in flow patterns", Adv. in Geophysics B 18:, pp 219-315.

[219] **Perry.A.E.** (1986) "A description of eddying motions and turbulence", 9th A.F.M.C., Auckland, N.Z., pp 7-12.

[220] **Perry.A.E. and Chong, M.S.** (1987) "A description of eddying motions and flow patterns using critical-point concepts", Ann.Rev.Fluid Mech., vol 19, pp 125-155.

[221] **Perry, A.E., Tan, D.K.M. and Chong, M.S.** (1983) "Flying hot wire studies of vortex motions in co-flowing jets and wakes", 8th A.F.M.C. Newcastle, Australia, pp 13C1-13C4.

[222] **Perry, A.E. and Hornung, H.** (1984) "Some aspects of three dimensional separation, Part 2: Vortex skeletons", Z. Flugwiss. Weltraumforsch.8, Heft 3. pp 155-160.

[223] **Perry, A.E. and Fairlie, B.D.** (1975) "A study of turbulent boundary-layer separation and reattachment", J.F.M., vol 69, part 4, pp 657-672.

[224] **Piatt, M. and Viets, H.** (1979) "Conditioned sampling in an unsteady jet", A.I.A.A. Aircraft Systems and Technology Meeting, 79-1857.

[225] **Porzio, A.J. and Franke, M.E.** (1989) "Experimental study of a confined jet thrust vector control nozzle", Journal of Propulsion, vol 5, No.5, pp 596-601.

[226] **Presser, C., Greenberg, J.B., Goldman, Y. and Timnat, Y.M.** (1982) "A numerical study of furnace flame root stabilization using conical burner tunnels", Nineteenth Symp. on Combustion, pp 519-527.

[227] **Quinn, B.** (1973) "Compact ejector thrust augmentation", J.Aircraft, vol 10, No.8, pp 481-486.

[228] **Quinn, B.** (1973) "A simple estimate of the effect of ejector length on thrust augmentation", J.Aircraft, vol 10, No.5, pp 313-314.

[229] **Rajagopalan, S. and Antonia, R.A.** (1979) "Some properties of the large scale structure in a fully developed turbulent duct flow", Phys.Fluids, vol 22, No.4, pp 614-622.

[230] **Rajagopalan, S. and Antonia, R.A.** (1983) "Some aspects of the fine structure in a turbulent boundary layer", 8th A.F.M.C. Newcastle, Australia, pp 9A13-9A16.

[231] **Rajakuperan, E, Saxena, S.K. and Ramaswamy, M.A.** (1991) "Experimental study of flow development and mixing in underexpanded free jets issued from elliptical sonic nozzles", 1st International Conference on Experimental Fluid Mechanics, Chengdu, China pp 130-135.

[232] **Raman, G., Hailye, M. and Rice, E.J.** (1993) "Flip-flop jet nozzle extended to supersonic flows", A.I.A.A. Journal, vol 31, No.6, pp 1028-1035.

[233] **Rao, D.M.** (1971) "A method of flow stabilization with high pressure recovery in short, conical diffusers", Aero.Journal, vol 75, pp 336-339.

[234] **Rao, K.V.L. and Lefebvre, A.H.** (1982) "Flame blowoff studies using large-scale flame holders", J. of Eng. for Power, vol 104, pp 853-857.

[235] **Rawe, R. and Kremer, H.** (1981) "Stability limits of natural gas diffusion flames with swirl", Eighteenth Symp. on Combustion, pp 667-677.

[236] **Restivo, A. and Whitelaw, J.H.** (1978) "Turbulence characteristics of the flow downstream of a symmetric, Plane sudden expansion", Journal of Fluids Engineering, vol 100, pp 308-310.

[237] **Reuter, D., Daniel, B.R., Jagoda, J. and Zinn, B.T.** (1986) "Periodic mixing and combustion processes in gas fired pulsating combustors", Combustion and Flame 65: pp 281-290.

[238] **Rho, B.J., Kim, J.K. and Dwyer, H.A.** (1990) "Experimental study of a turbulent cross jet", A.I.A.A. Journal, vol 28, No.5, pp 784-789.

[239] **Ricou, F.P. and Spalding, D.B.** (1961) "Measurements of entrainment by axi-symmetrical turbulent jets", J.F.M., vol 11, pp 21-32.

[240] **Rizk, N.K. and Lefebvre, A.H.** (1984) "Influence of laminar flame speed on the blowoff velocity of bluff-body-stabilised flame", A.I.A.A. Journal, vol 22, No.10, pp 1444-1447.

[241] **Rockwell, D. and Schachenmann, A.** (1982) "Self-generation of organised waves in an impinging turbulent jet at low Mach number", J.F.M., pp 425-441.

[242] **Rockwell, D.** (1983) "Oscillations of impinging shear layers", A.I.A.A., vol 21, No.5, pp 645-664.

[243] **Roquemore, W.M., Tankin, R.S., Chiu, H.H. and Lotters, S.A.** (1986) "A study of a bluff-body combustor using laser sheet lighting", Experiments in Fluids 4, pp 205-213.

[244] **Rosenhead, L.** (1963) "Laminar Boundary Layers", Oxford University Press, 1963.

[245] **Roshko, A.** (1991) "Uses of flow visualisation in research", I.C.E.F.M., pp 3-11.

[246] **Rouse, H.** (1938) "Fluid mechanics for hydraulic engineers" McGraw-Hill Book Company.

[247] **Rouse, H.** (1950) "Elementary mechanics of fluids", John Wiley and Sons.

[248] **Rudd, M.J.** (1972) "Velocity measurements made with a laser dopplermeter on the turbulent pipe flow of a dilute polymer solution", J.F.M., vol 51, part.4, pp 673-685.

[249] **Salam, T.M., Kaji, M., Nakanishi, S. and Ishigai, S.** (1980) "Visualisation of recirculating flows in reversed-flow furnace models", Department of Mech.Eng., Osaka University, Osaka, Japan. pp 57-61.

[250] **Salam, T.M., Kaji, M., Nakanishi, S., Ishigai, S. and Matsumoto, S.** (1980) "Characteristics of reversed flow due to jet issuing to dead-end channel", Tech.Reports Osaka University, vol 30, pp 217-224.

[251] **Samet, M. and Einav, S.** (1988) "Mean value measurements of a turbulent swirling-jet", A.I.A.A. Journal, vol 26, No.5, pp 619-628.

[252] **Samimu, M. and Abu-Hijleh, B.A./K.** (1989) "Performance of laser Doppler velocimetry with polydisperse seed particles in high speed flow", Journal of Propulsion, vol 5, No.1, pp 21-25.

[253] **Schetz, J.A.** (1980) "Injection and mixing in turbulent flows", Pub.AIAA, Ed. Summerfield, M., 1980.

[254] **Shuen, J-S., Solomon, A.S.P., Zhang, Q-F. and Faeth, G.M.** (1984) "Structure of particle-laden jets: Measurements and predictions", A.I.A.A. Journal, vol 23, No.3, pp 396-404.

[255] **Samimy, M. and Langenfeld, C.A.** (1988) "Experimental study of isothermal swirling flows in a dump combustor", A.I.A.A. Journal, vol 26, No.12, pp 1442-1449.

[256] **Samuel, A.E.** (1970) "A boundary layer developing in an increasingly adverse pressure gradient",

[257] **Sayles, D.C.** (1988) "Development of test motors for advanced controllable propellants", Journal of Spacecraft, vol 12, No.3, pp 174-178.

[258] **Schachenmann, A. and Rockwell, D.** (1980) "Self-sustained oscillations of turbulent pipe flow terminated by an axisymmetric cavity", Journal of Sound and Vibration, vol 73, No.1, pp 61-72.

[259] **Schadow, K.C., Gutmark, E., Koshigoe, S. and Wilson, K.J.** (1987) "Combustion related shear-flow dynamics in elliptic supersonic jets", Symp. on Aerodynamics of Hypersonic Lifting Vehicles, Bristol, U.K.

[260] **Schadow, K.C.** (1987) "Turbulent mixing mechanism for ducted rockets", Thirteenth TTCP Meeting, Panel WTP-4, Air Force Astronautics Lab. Edwards Air Force Base, California.

[261] **Schneider, G.M., Nathan, G.J. and Luxton, R.E.** (1992) "An experimental study of a precessing deflected jet", 11th A.F.M.C., Hobart, Australia., pp 1105-1108.

[262] **Schneider, G.M., Vidakovic, S.S., Cooper, J.D., Musgrove, A.R., Nathan, G.J. and Luxton, R.E.** (1993) "Theoretical and Experimental pressure field evaluation downstream of a mechanically precessing jet", Aust. Heat and Mass Trans. Conf., Brisbane , Dec 1993, pp 43.1-43.6

[263] **Schofield, W.H.** (1983) "On separating turbulent boundary layers", Mechanical Engineering Report 162, D.S.T.O., A.R.L.Melb., AR-002-978.

[264] **Schofield, W.H.** (1981) "Equilibrium boundary layers in moderate to strong adverse pressure gradients", J.F.M., vol 113, pp 91-122.

[265] **Schofield, W.H.** (1983) "Separating turbulent boundary layers", 8th A.F.M.C., Newcastle, Australia, pp 9A9-9A12.

[266] **Scott, J.N. and Hankley Jr., W.L.** (1985) "Numerical simulation of cold flow in an axisymmetric centrebody combustor", A.I.A.A. Journal, vol 23, No.5, pp 641-649.

[267] **Seki, N., Fukusako, S. and Hirata, T.** (1976) "Turbulent fluctuations and heat transfer for separated flow associated with a double step at entrance to an enlarged flat duct", Journal of Heat Transfer, pp 588-593.

[268] **Shieh, C.F.** (1992) "Navier-Stokes solutions of transonic nozzle flow with shock-induced flow separation", Journal of Propulsion and Power, vol 8, No.4, pp 829-835.

[269] **Shin, D.S. and Ferziger, J.H.** (1993) "Linear stability of the confined compressible reacting mixing layer", A.I.A.A. Journal, vol 31, No.3, pp 571-577.

[270] **Simmons, J.M., Platzer, M.F. and Smith, T.C.** (1978) "Velocity measurements in an oscillating plane jet issuing into a moving air stream", pp 33-53.

[271] **Simmons, J.M., Lai, J.C.S. and Platzer, M.F**. (1981) "Jet excitation by an oscillating vane", A.I.A.A. Journal, vol 19, No.6, pp 673-676.

[272] **Simpson, R.L.** (1976) "Interpreting laser and hot-film anemometer signals in a separating boundary layer", A.I.A.A. Journal, vol 14, No.1, PP 124-126.

[273] **Skow, A.M.** (1994) "Agility as a contributor to fighter design balance", Combat Systems International Journal, pp 145-149, Sterling Pub. Group.

[274] **Smith, C.F. and McArdle, J.G.** (1992) "Flow in a ventral nozzle for short takeoff and vertical landing aircraft", Journal of Propulsion and Power, vol8, No.2, pp 530-536.

[275] **Smits, A.J., Eaton, J.A. and Bradshaw, P.** (1979) "The response of a turbulent boundary layer to lateral divergence", J.F.M., vol 94, part.2, pp 243-268.

[276] **Spalding, D.B.** (1953) "Theoretical aspects of flame stabilization", Aircraft Eng., XXV, pp 264-276.

[277] **Starner, S.H.** (1983) "Seeding problems in flames and swirling flows, with implications for LDA bias", 8th A.F.M.C., Newcastle, Australia, pp 7C5-7C7.

[278] **Stevenson, W.H., Thompson, H.D. and Craig, R.R.** (1984) "Laser velocimeter measurements in highly turbulent recirculating flows", Journal of Fluids Engineering, vol 106, pp 173-180.

[279] **Steward, F.R. and Tennankore, K.N.** (1976) "Similarity criterion for a confined swirling jet system", Sixteenth Symp. on Combust., pp 1593-1609.

[280] **Stokes, A.N. and Welsh, M.C.** (1985) "Flow-resonant sound interaction in a duct containing a plate, Part 2: square leading edge", J. of Sound and Vibration 103 (1).

[281] **Strykowski, P.J. and Wilcoxon, R.K.** (1993) "Mixing enhancement due to global oscillations in jets with annular counterflow", A.I.A.A. Journal, vol 31, No.3, pp 564-570.

[282] **Su.Y.** (1989) "Mechanism of sidewall effect studied with oil flow visualisation", A.I.A.A. Journal, vol 27, No.12, pp 1828-1830.

[283] **Syred, N. and Beer, J.M.** (1974) "Combustion in swirling Flows: A review", Combustion and Flame 23, pp 143-201.

[284] **Syred, N., Claypole, T.C. and Styles, A.C.** (1981) "The role of centrifugal force fields in the stabilization of swirling flames", J. Energy, vol 6, No.5, pp 344-345.

[285] **Takagi, T. and Okamoto, T.** (1981) "Characteristics of combustion and pollutant formation in swirling flames", Combustion and Flame 43, pp 69-79.

[286] **Taylor, C., Thomas, C.E. and Morgan, K.** (1981) "Modelling flow over a backward-facing step using the F.E.M. and the two-equation model of turbulence", International Journal for Numerical Methods in Fluids, vol 1, pp 295-304.

[287] **Taylor, G.I.** (1923) "Stability of a viscous liquid contained between two rotating cylinders", Royal Soc. of London, Philosophical Transactions, Series A, vol 223, pp 289-343.

[288] **Tennekes, H.** (1968) "Simple model for the small-scale structure of turbulence", The Physics of Fluids, vol 11, No.3, pp 669-671.

[289] **Thompson, H.D. and Hoffmann, J.D.** (1990) "Swirling flow in thrust nozzles", J.Propulsion, vol 6, No.2, pp 151-157.

[290] **Tobak, M. and Peake, D.J.** (1979) "Topology of two-dimensional and three-dimensional separated flows", A.I.A.A. 12th Fluid and Plasma Dynamics Conference, pp 1-29.

[291] **Tobak, M. and Peake, D.J.** (1982) "Topology of three-dimensional separated flows", Ann.Rev.Fluid Mech.14, pp 61-85.

[292] **Townsend, A.A.** (1976) "The structure of turbulent shear flows", Cambridge University Press, 1975.

[293] **Trabold, T.A., Esen, E.B. and Obot, N.T.** (1987) "Entrainment by turbulent jets issuing from sharp-edged inlet round nozzles", J. of Fluids Eng., vol 109, pp 248-254.

[294] **Tropea, C.D. and Gackstatter, R.** (1985) "The flow over two-dimensional surface-mounted obstacles at low Reynolds numbers", J. of Fluids Eng., vol 107, pp 489-494.

[295] **Troutt, T.R., Scheelke, B. and Norman, T.R.** (1984) "Organised structures in a reattaching separated flow field", J.F.M., vol 143, pp 413-427.

[296] **Vidakovic, S.S. and Luxton, R.E.** (1991) "Fluid mechanics of deflected jets: Velocity flowfields in the cavity." Proc.International Aerospace Congress 1991, Vol.2, pp 675-685, 12-16 May, 1991, Melbourne, Australia.

[297] **Vidakovic, S.S. and Luxton, R.E.** (1992) "Fluid mechanics of deflected jets: Evaluation of nozzle thrust vectors", 11th A.F.M.C., pp 1093-1096, Hobart, Australia.

[298] **Vidakovic, S.S. and Luxton, R.E.** (1991) "Fluid mechanics of deflected jets: Flow visualisation within the nozzle", I.S.T.P.4 in Heat and Mass Transfer, pp 50-62, July 14-19 1991, UNSW, Sydney, Australia.

[299] **Vidakovic, S.S. and Luxton, R.E.** (1993) "Effects of exit rings on vectored thrust issuing from a subsonic convergent-divergent nozzle", 5th AHMT, paper 72, Brisbane, Australia.

[300] **Viets, H.** (1975) "Flip-Flop jet nozzle", A.I.A.A. Journal, vol 13, No.10, pp 1375-1379.

[301] **Viets, H., Bethke, R.J. and Bougine, D.** (1983) "Three-dimensional vortex dynamics near a wall", 4th Inter.Symp. on Turbulent Shear Flows, Uni. of Karlsruhe, Eds. Bradbury, L.J.S., Durst, F., Launder, B.E., Schmidt, F.W. and Whitelaw, J.H., Springer-Verlag, pp 34-61.

[302] **Wang, K.C.** (1974) "Boundary layer over a blunt body at high incidence with an open-type of separation", Proc.R.Soc.Lond., vol 340 A, pp 33-55.

[303] **Wang, K.C.** (1972) "Separation pattern of boundary layer over an inclined body of revolution", A.I.A.A., 9th Aero.Sc.Meeting, vol 10, No.8, pp 1044-1050.

[304] **Wassom, S.R., Faupel, L.C. and Perley, T.** (1991) "Integrated aerofin/thrust vector control for tactical missiles", Journal of Propulsion, vol 7, No.3, pp 374-381.

[305] **Weisbrot, I. and Wygnanski, I.,** (1988) "On coherent structures in a highly excited mixing layer", J.F.M., vol 195, pp 137-159.

[306] **Welsh, M.C., Stokes, A.N. and Parker, R.** (1984) "Flow-resonant sound interaction in a duct containing a plate, Part 1: Semi-circular leading edge", J. of Sound and Vibration 95, pp 305-323.

[307] **Welsh, M.C. and Gibson, D.C.** (1979) "Interaction of induced sound with flow past a square leading edged plate in a duct", J. of Sound and Vibration 67, pp 501-511.

[308] **Welsh, M.C. and Stokes, A.N.** (1985) "Transient vortex modelling of flow induced acoustic resonances near cavities or obstructions in ducts", IUTAM Symp. Aero and Hydro-Acoustics, Lyon, July 1985.

[309] **Welsh, M.C.** (1976) "Flow control in wide-angled conical diffusers", J. of Fluids Eng., pp 728-735.

[310] **Westphal, R.V., Johnston, J.P. and Eaton, J.K.** (1984) "Experimental study of flow reattachment in a single sided sudden expansion", NASA Contractor Report 3765.

[311] **Williams, F.A.** (1985) "Combustion instabilities", (Combustion Theory 2nd edition, Benjamin Cummings.) pp 294-372.

[312] **Winter, A.R., Graham, L.J.W. and Bremhorst, K.** (1991) "Effects of time scales on velocity bias in LDA measurements using sample and hold processing", Experiments in Fluids, vol 11, pp 147-152.

[313] **Winter, A.R., Graham, L.J.W. and Bremhorst, K.** (1991) "Velocity bias associated with laser Doppler anemometer controlled processors", Journal of Fluids Engineering, vol 113, pp 250-255.

[314] **Wishart, D.P., Krothapali, A and Mungal, M.G.** (1993) "Supersonic jet control via point disturbance inside the nozzle", AIAA Journal, Vol 31, No 7, pp 1340-1341.

[315] **Wohl, K., Kapp, N.M. and Gazley, C.** (1948) "The flame stability of open flames", Third Symp. on Combust., pp 3-21.

[316] **Wohl, K., Gazley, C. and Kapp, N.M.** (1948) "Diffusion flames", Third Symp.on Combust., pp 288-300.

[317] **Wolf, D.E., Sinha, N. and Dash, S.M.** (1988) "Fully-coupled analysis of jet mixing problems", N.A.S.A. Contract Report 4139.

[318] **Wu, C.C. and Chow, W.L.** (1985) "Study of an asymmetric flap nozzle as a thrust-vectoring device", Journal of Propulsion, vol 1, No.4, pp 286-291.

[319] **Wu, H.I. and Fricker, N.** (1976) "The characteristics of swirl-stabilised natural gas flames. Part 2: The behaviour of swirling jet flames in a narrow cylindrical furnace", J. of the Inst. of Fuel, pp 144-151.

[320] **Wu, J.M., Vakili, A.D. and Yu, F.M.** (1988) "Investigation of the interacting flow of nonsymmetric jets in crossflow", A.I.A.A. Journal, vol 26, NO.8, pp 940-947.

[321] **Wygnanski, I., Katz, Y. and Horev, E.** (1992) "On the applicability of various scaling laws to the turbulent wall jet", J.F.M., vol. 234, pp 669-690.

[322] **Yang, B.T. and Yu, M.H.** 1983) "The flowfield in a suddenly enlarged combustion chamber", A.I.A.A. Journal, vol 21, No.1, pp 92-97.

[323] **Yang, T., Ntone, F., Jiang, T. and Pitts, D.R.** (1985) "An investigation of high performance, short thrust augmenting ejectors", J. of Fluids Eng., vol 107, pp 23-30.

[324] **Yavuzkurt, S.** (1984) "A guide to uncertainty analysis of hot-wire data", Journal of Fluids Engineering, vol 106, pp 181-186.

[325] Yule, A.J. (1978) "Large scale structure in the mixing layer of a round jet", J.F.M., vol 89, part 3, pp 413-432.

[326] Zilker, D.P., Cook, G.W. and Hanratty, T.J. (1977) "Influence of the amplitude of a solid wavy wall on a turbulent flow. Part 1. Non-separated flow", J.F.M. vol 82, part.1, pp 29-51.

APPENDIX A

Detail Drawings of Nozzle, Cavity and Exit Rings

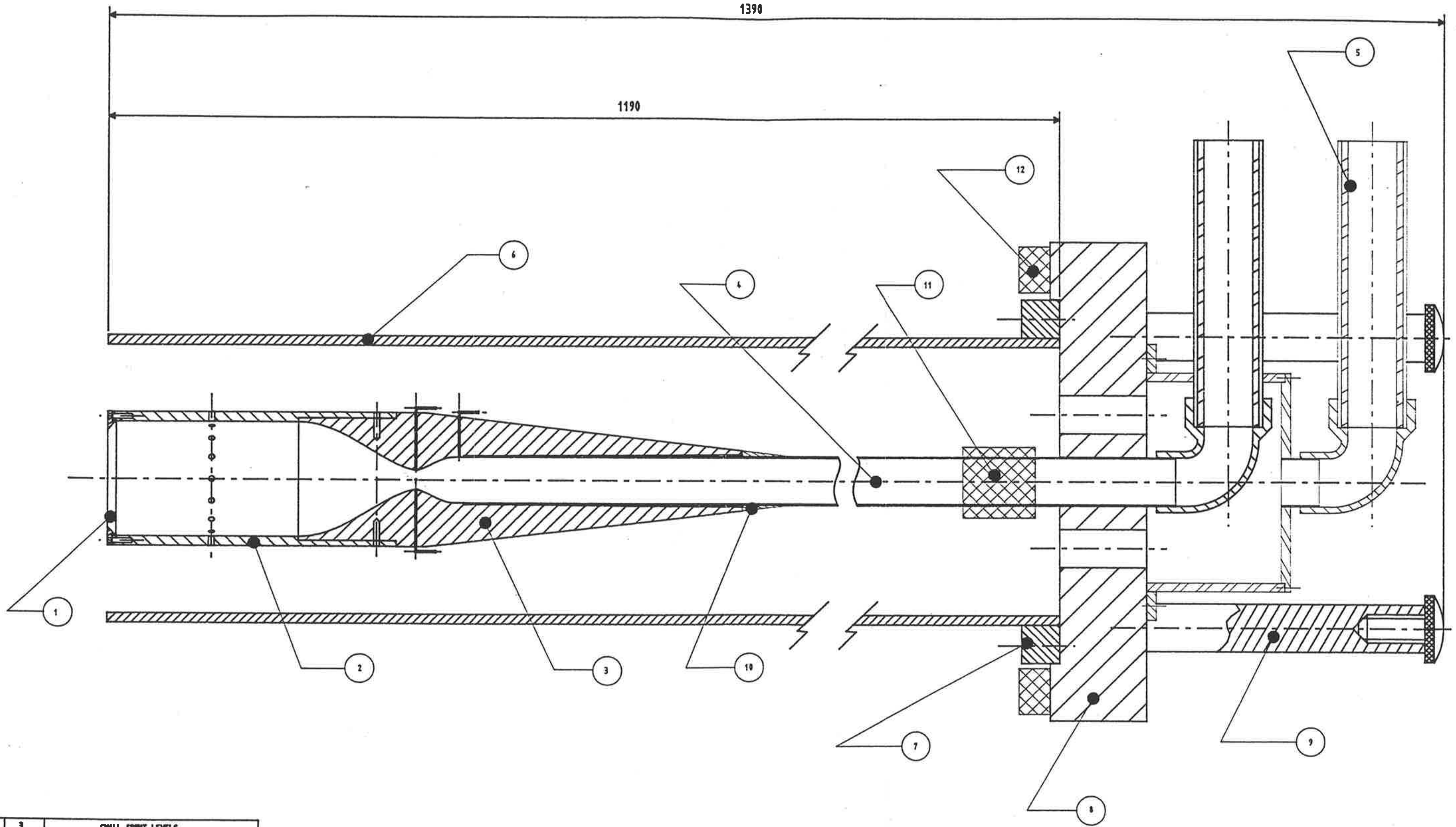

12	3	SMALL SPIRIT LEVELS
11	1	STRAIN GUAGE MATRIX
10	1	NOZZLE SUPPORTING SHIM
9	4	LEGS
8	1	BASE PLATE
7	1	SHROUD MOUNTING RING
6	1	OUTER FLOW SHROUD (SEE NOTE 3)
5	1	OUTER FLOW SUPPLY MANIFOLD
4	1	INNER FLOW SUPPLY MANIFOLD
3	1	FLOW DEFLECTION NOZZLE
2	1	FLOW DEFLECTION TUBE
1	1	DEFLECTOR RING
PART	QTY	DESCRIPTION

NOTE: (1) MOUNTING OF STRAIN GUAGE MATRIX WILL BE ARRANGED FOR AFTER INNER SUPPLY TUBE IS ASSEMBLED TO BASE.

(2) SPIRIT LEVELS WILL BE ATTACHED AFTER RIG IS COMPLETE.

(3) OUTER SHROUD MATERIAL: Ø150 X 1190 LONG PERSPEX TUBING

TITLE: ASSEMBLY OF FLOW DEFLECTION RIG
CLIENT: UNIVERSITY OF ADELAIDE
VIEW: SECTION | SCALE: 1:1 | DATE: SEPT 18 1989
DRAWN BY: THOMAS KIEBERT | DRWG No 1
CHECKED BY: | DATE:

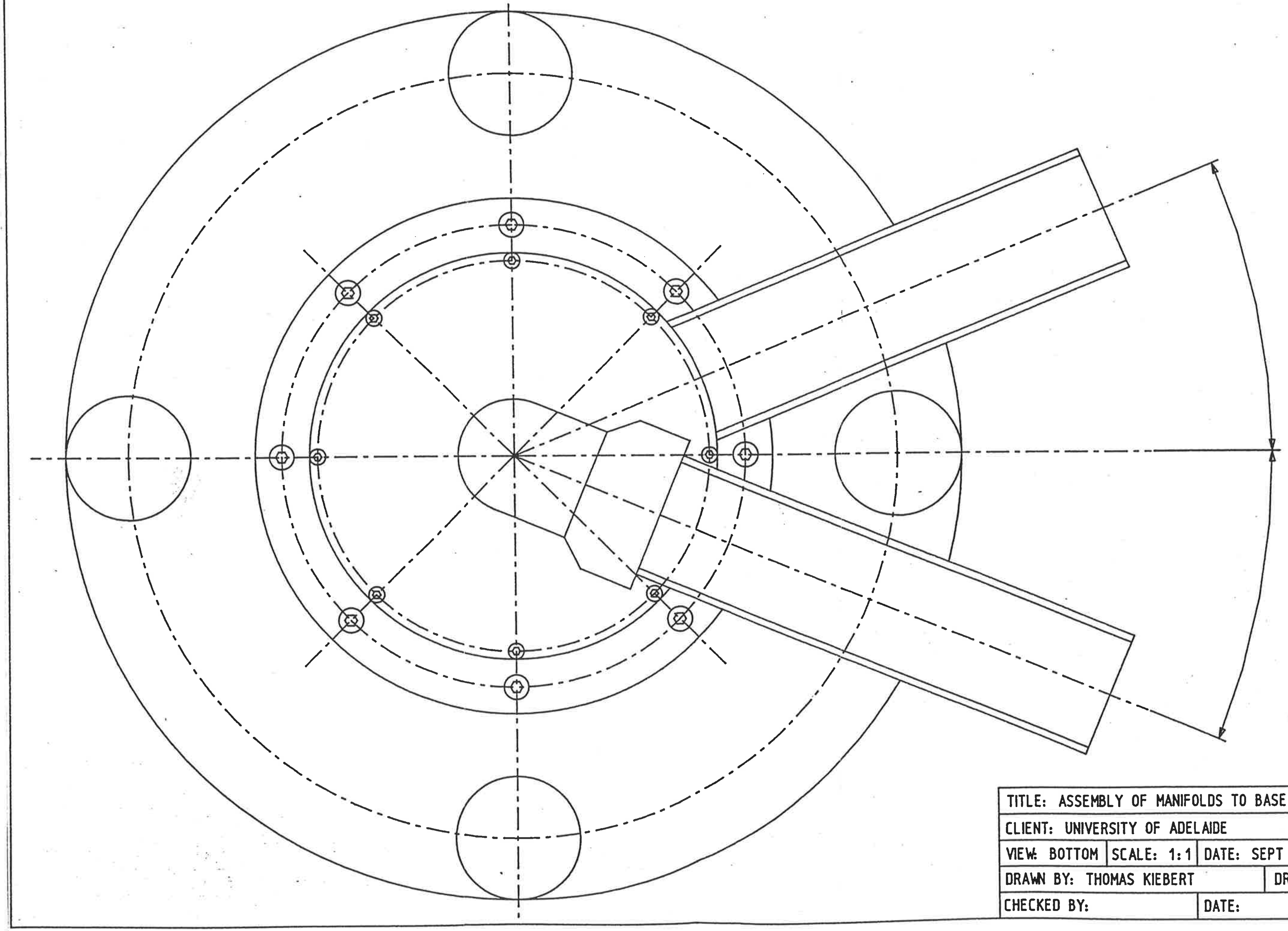

TITLE: ASSEMBLY OF MANIFOLDS TO BASE

CLIENT: UNIVERSITY OF ADELAIDE

VIEW: BOTTOM | SCALE: 1:1 | DATE: SEPT 28 1989

DRAWN BY: THOMAS KIEBERT | DRWG No 2

CHECKED BY: | DATE:

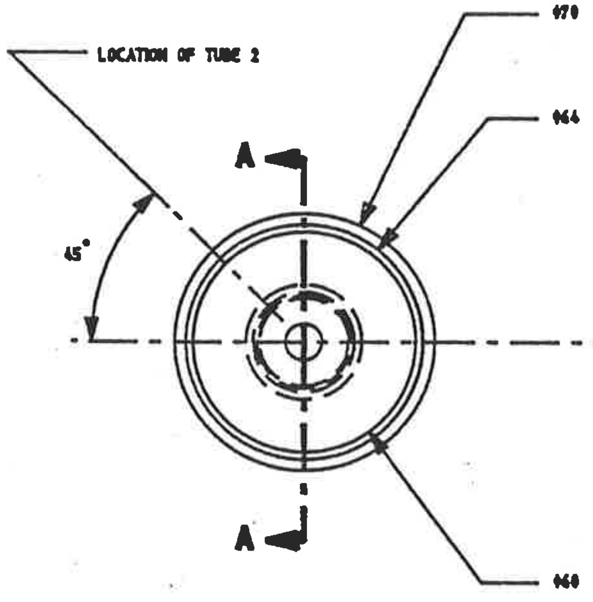

VIEW: FRONT

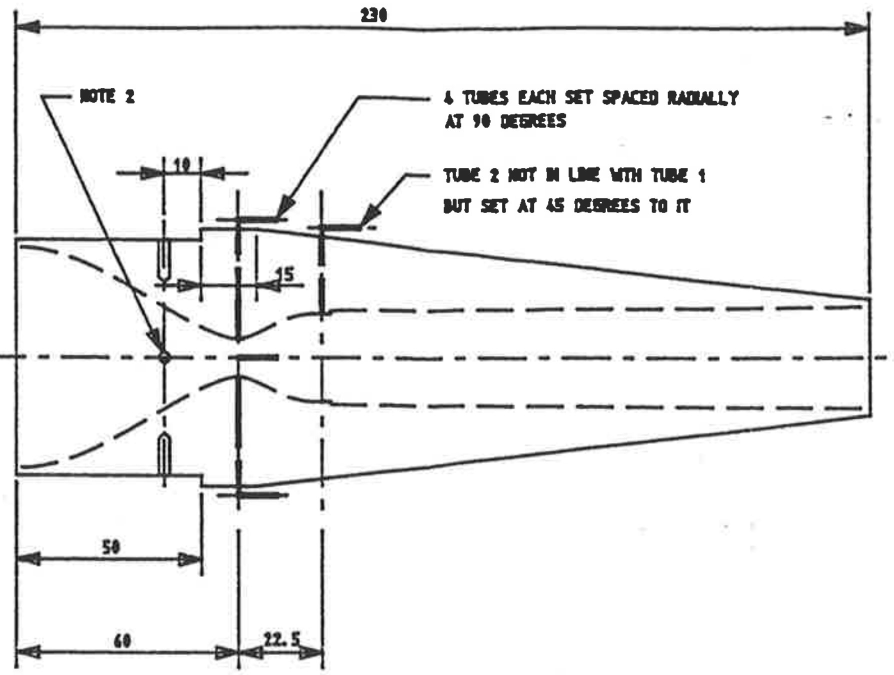

VIEW: RIGHT

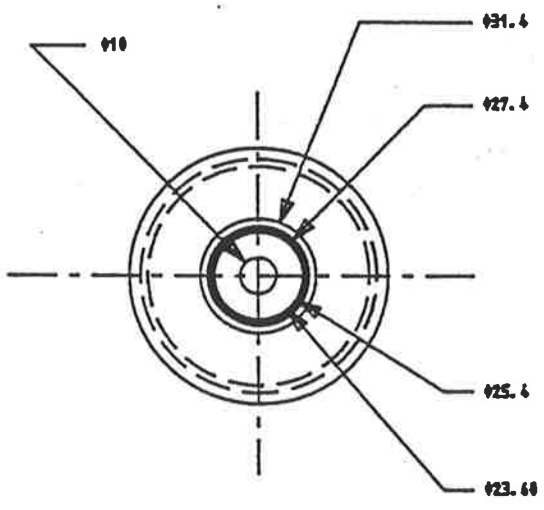

VIEW: REAR

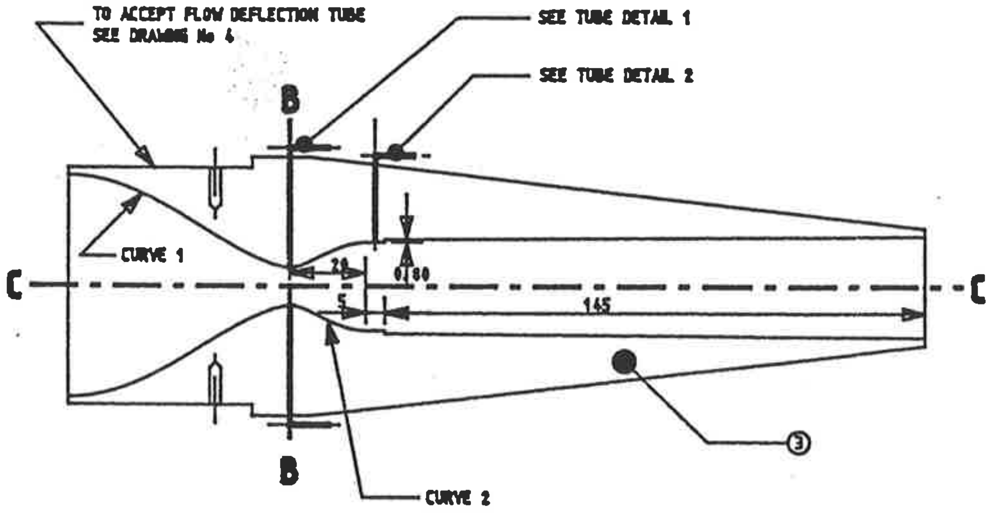

VIEW: SECTION A-A

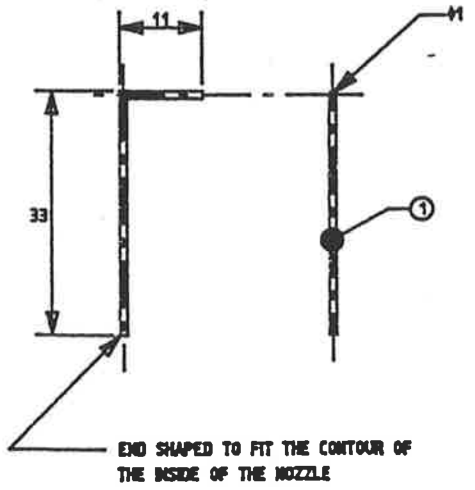

VIEW: TUBE DETAIL 1

SCALE: 2:1

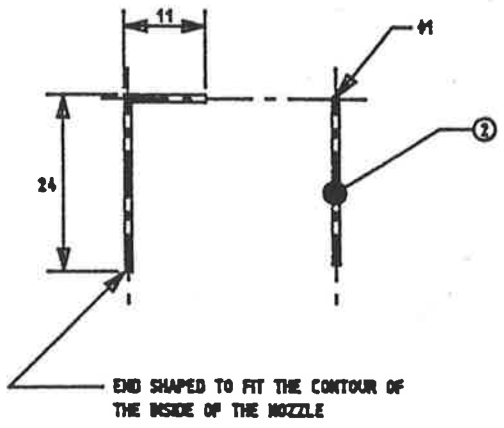

VIEW: TUBE DETAIL 2

SCALE: 2:1

NOTE (1) SCALE 1:1 UNLESS SHOWN
(2) 4 HOLES SPACED RADIALLY AT 90 DEGREES DRILLED AND TAPPED FOR GRUB SCREW M3 X 10 DEEP
(3) ALL DIMENSIONS IN mm

14	10.3630	30	19.8651	46	27.5511		
12	9.2945	28	18.6838	44	26.8291	60	30.0000
10	8.2916	26	17.4810	42	26.0262	58	29.9486
8	7.3701	24	16.2660	40	25.1482	56	29.7949
6	6.5468	22	15.0485	38	24.2011	54	29.5379
4	5.8449	20	13.8388	36	23.1918	52	29.1858
2	5.2993	18	12.6473	34	22.1275	50	28.7332
0	5.0000	16	10.3630	32	21.0159	48	28.1873
X	Y	X	Y	X	Y	X	Y

POINTS FOR CURVE 1: $Y=25(SIN(1.5X))^{1.5}+5$

X MEASURED FROM LINE B-B (SEE SECTION A-A)
Y MEASURED FROM LINE C-C (SEE SECTION A-A)

4	6.1681	10	9.0433	16	11.3069		
2	5.4207	8	8.0643	14	10.7191	20	11.8000
0	5.0000	6	7.0801	12	9.9482	18	11.6748
X	Y	X	Y	X	Y	X	Y

POINTS FOR CURVE 2: $Y=6.80(SIN(4.5X))^{1.5}+5$

PART No	QTY	DESCRIPTION	MATERIAL
3	1	FLOW DEFLECTION NOZZLE	FIBRE GLASS/ARALDITE EPOXY RESIN
2	4	STATIC PRESSURE/AIR SUPPLY TUBE	BRASS TUBE: O.D. 3 I.D. 2
1	4	STATIC PRESSURE TUBE	BRASS TUBE: O.D. 3 I.D. 2

TITLE: FLOW DEFLECTION NOZZLE
CLIENT: UNIVERSITY OF ADELAIDE
SCALE: NOTE 1 | VIEW: SHOWN | DATE: JULY 18 1989
DRAWN BY: THOMAS KIEBERT | DRWG No 3
CHECKED BY: | DATE:

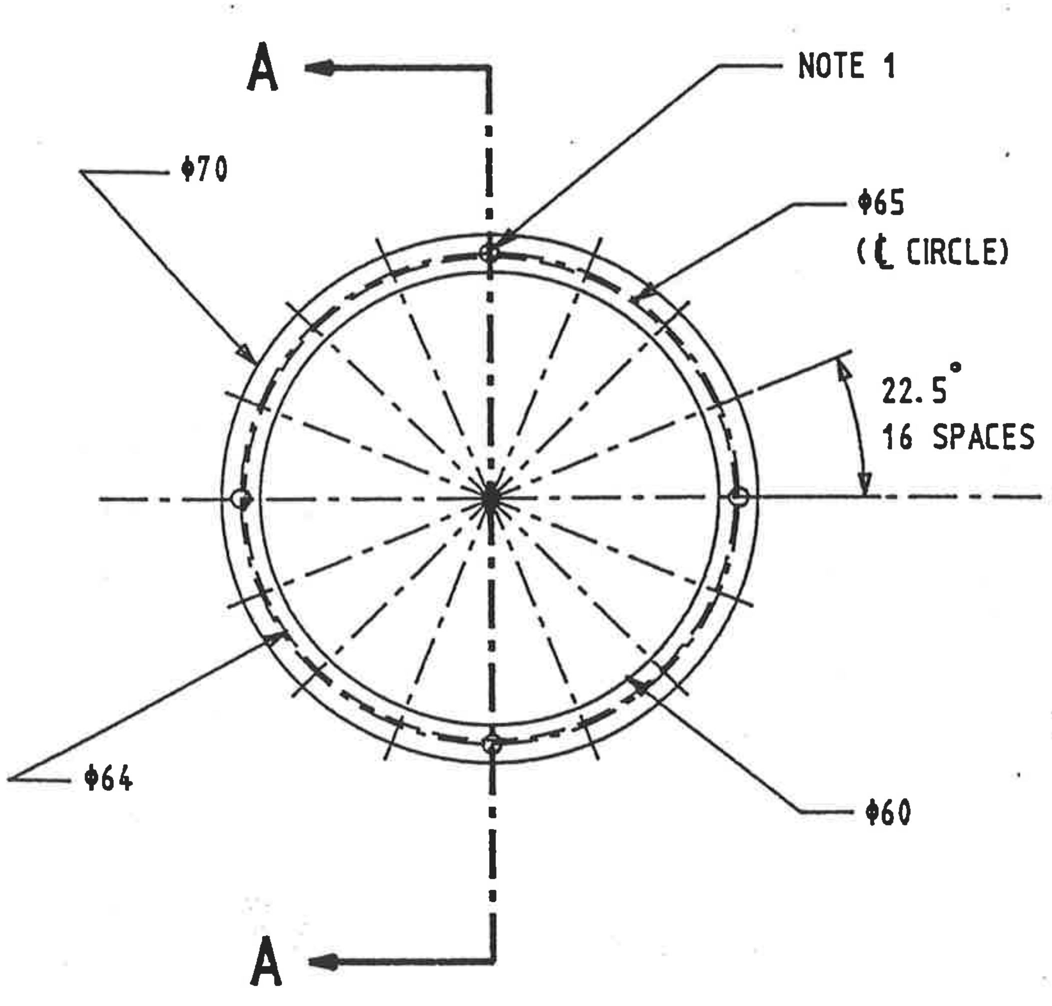

VIEW: FRONT

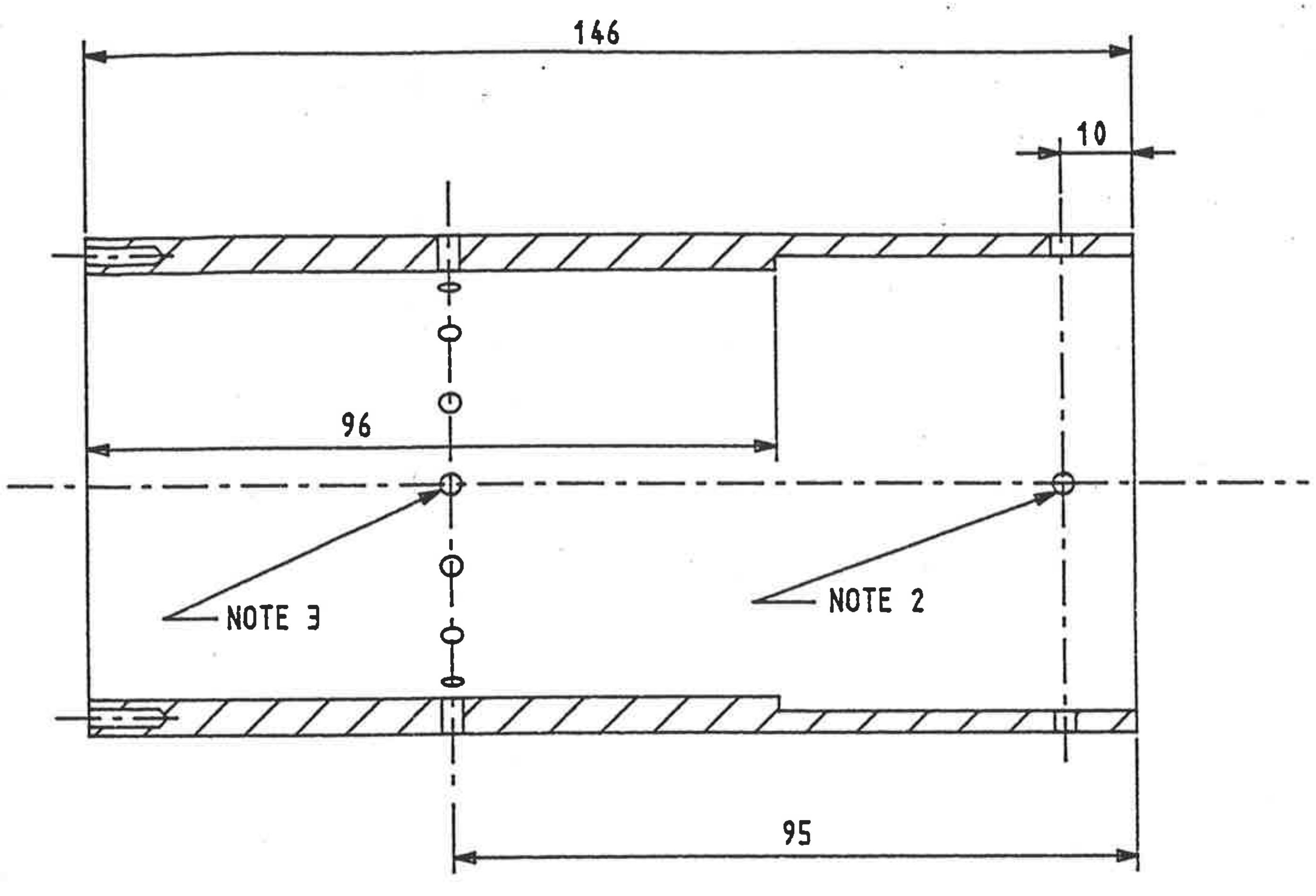

VIEW: SECTION A-A

NOTE: (1) 4 HOLES SPACED RADIALLY AT 90 DEGREES
DRILLED AND TAPPED FOR SOCKET HEAD SCREW M2.5 X 10 DEEP
TO ATTACH DEFLECTION RING (SEE DRAWNG No 5)

(2) 4 HOLES φ3 SPACED RADIALLY AT 90 DEGREES
TO ALLOW PASSAGE OF M3 SOCKET HEAD SCREWS
FOR ATTACHMENT OF TUBE TO FLOW DEFLECTION NOZZLE (SEE DRAWNG No 3)

(3) 16 HOLES SPACED RADIALLY AT 22.5 DEGREES
DRILLED THROUGH AT φ3 TO ACCEPT φ3 FLEXIBLE
PLASTIC TUBING (TO BE GLUED IN).

(4) ALL DIAMETERS TO MATCH SMOOTHLY WTH NOZZLE (SEE DRAWNG No 3)

(5) ALL DIMENSIONS IN mm

MATERIAL: SOLID ROUND PERSPEX O.D. 70 X 150 LONG

TITLE: FLOW DEFLECTION TUBE		
CLIENT: UNIVERTSITY OF ADELAIDE		
SCALE: 1:1	VIEW: SHWN	DATE: OCT 10 1989
DRAWN BY: THOMAS KIEBERT		DRWG No 4
CHECKED BY:		DATE:

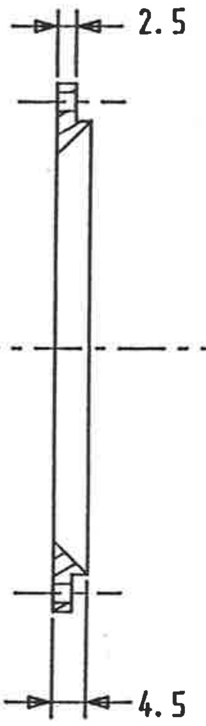

VIEW: SECTION A-A

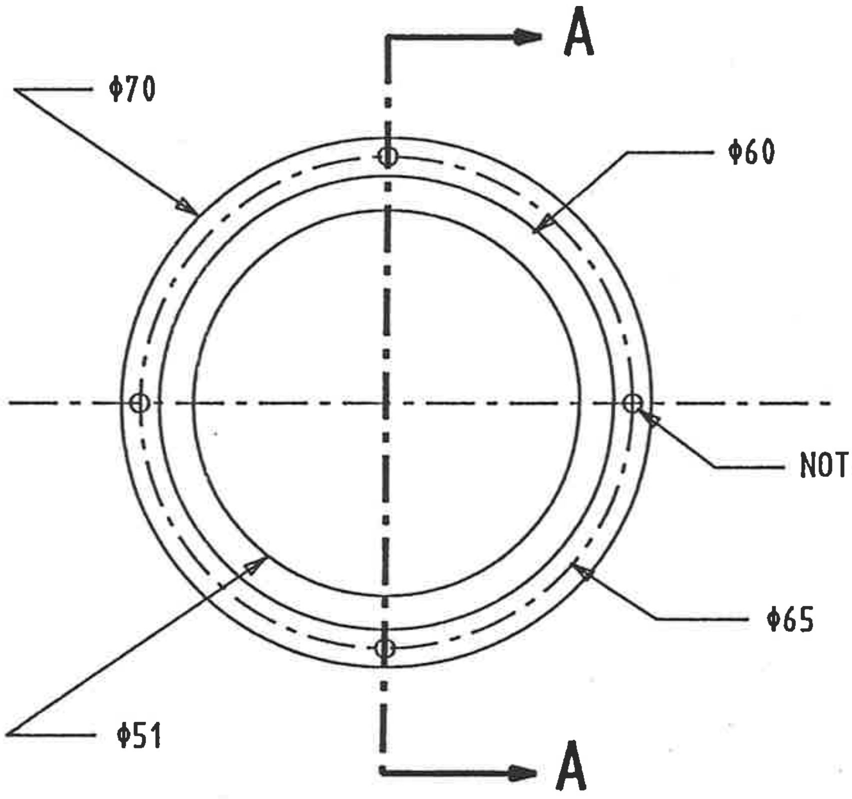

VIEW: TOP

NOTE: (1) 4 HOLES ϕ2.5 DRILLED THROUGH TO ACCEPT M2.5 ALLEN-HEAD SCREWS FOR ATTACHMENT OF RING TO FLOW DEFLECTION TUBE.

(2) MATERIAL: BRASS

(3) ALL DIMENSIONS IN mm

TITLE: DEFLECTOR RING
CLIENT: UNIVERSITY OF ADELAIDE
VIEW: SHOWN | SCALE: 1:1 | DATE: SEPT 19 1989
DRAWN BY: THOMAS KIEBERT | DRWG No 5
CHECKED BY: | DATE:

NOTE: (1) ALL JOINTS BRAZED.
(2) PART No 4 TO BE THREADED INTO ELBOW AFTER OUTER FLOW MANIFOLD IS ASSEMBLED TO BASE PLATE.
(3) ALL DIMENSIONS IN mm.

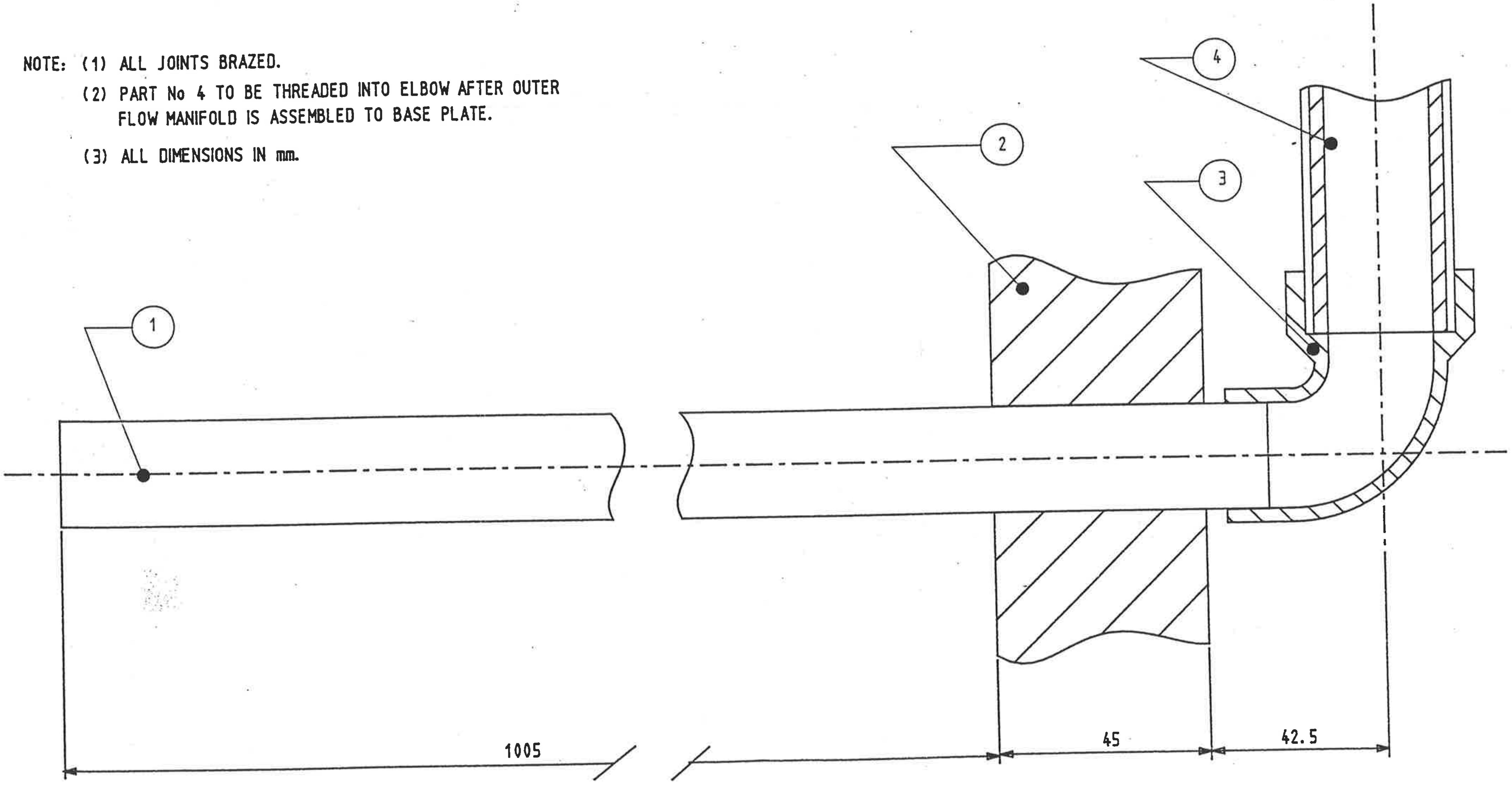

PART	QTY	DESCRIPTION	MATERIAL DIMENSIONS
4	1	THREADED SUPPLY TUBE (STD PIECE)	BRASS - 25.4 X 150 LONG (TO FIT ELBOW)
3	1	PLAIN-FEMALE THREAD END ELBOW (STD PIECE)	BRASS - 25.4 mm (PLAIN END TO FIT PART 1)
2	1	BASE PLATE	STEEL
1	1	INNER FLOW SUPPLY TUBE	BRASS TUBE - 25.4 X 1100 LONG WALL THICKNESS - 0.9

TITLE: INNER FLOW SUPPLY MANIFOLD ASSEMBLED TO BASE PLATE
CLIENT: UNIVERSITY OF ADELAIDE
VIEW: SECTION | SCALE: 1:1 | DATE: OCT 11 1989
DRAWN BY: THOMAS KIEBERT | DRWG No 6
CHECKED BY: | DATE:

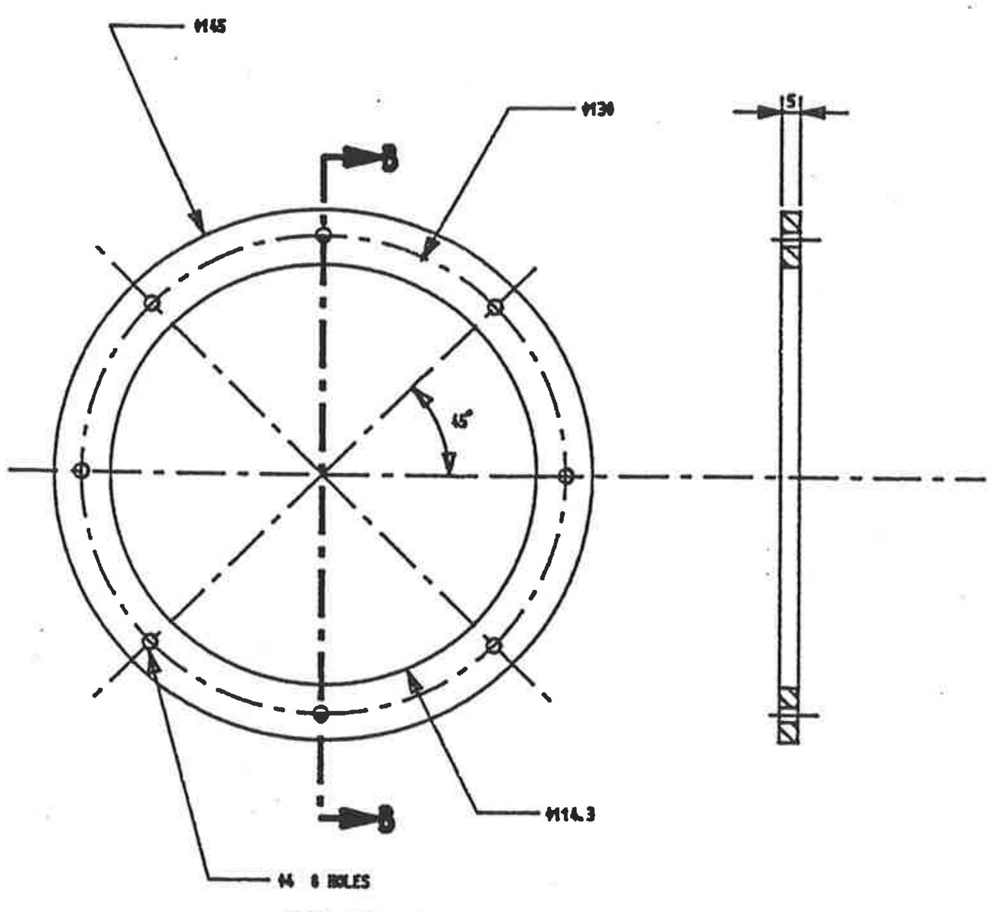

VIEW: TOP

VIEW: SECTION B-B

MOUNTING RING

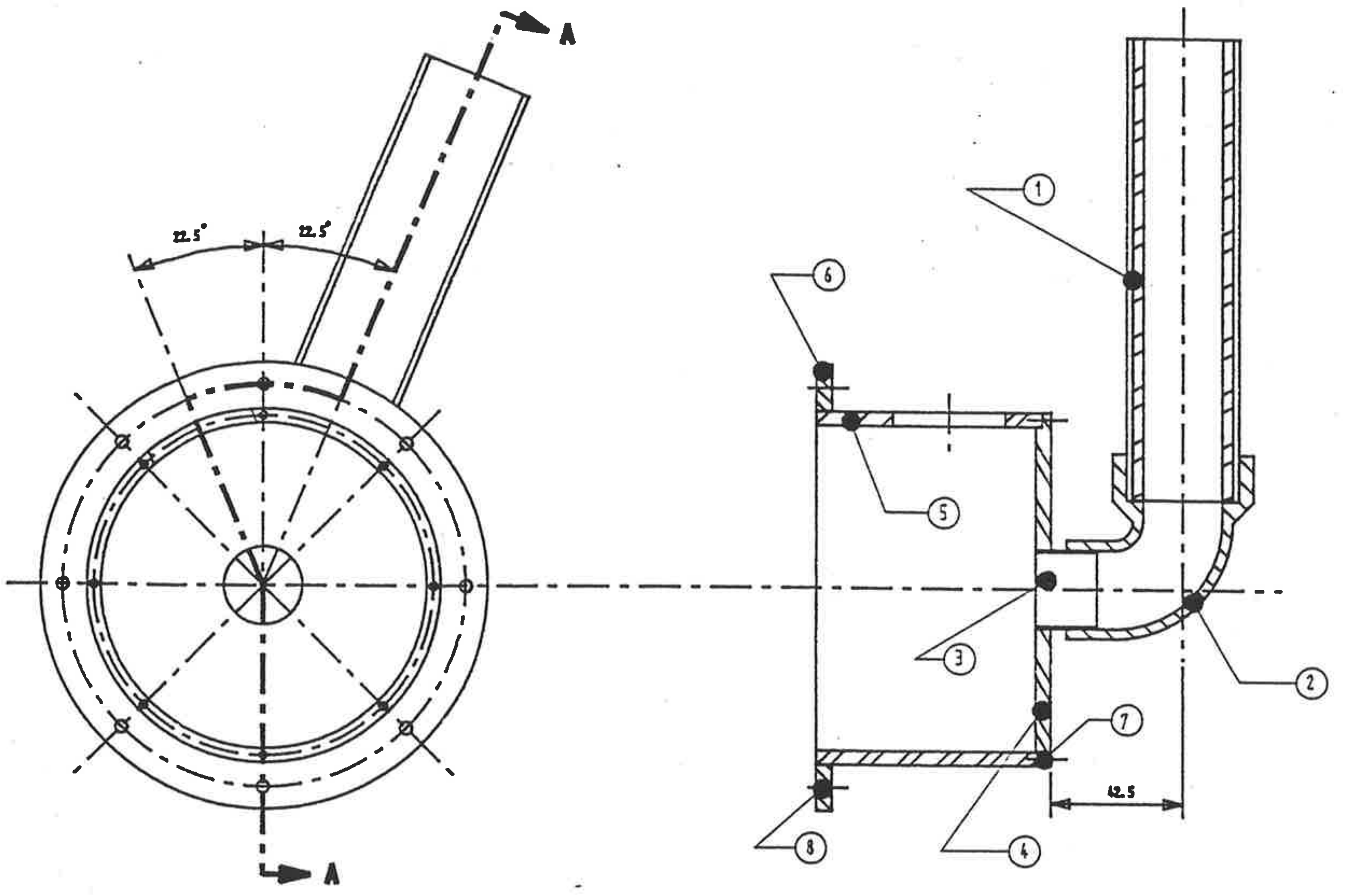

VIEW: TOP

VIEW: SECTION A-A

ASSEMBLY

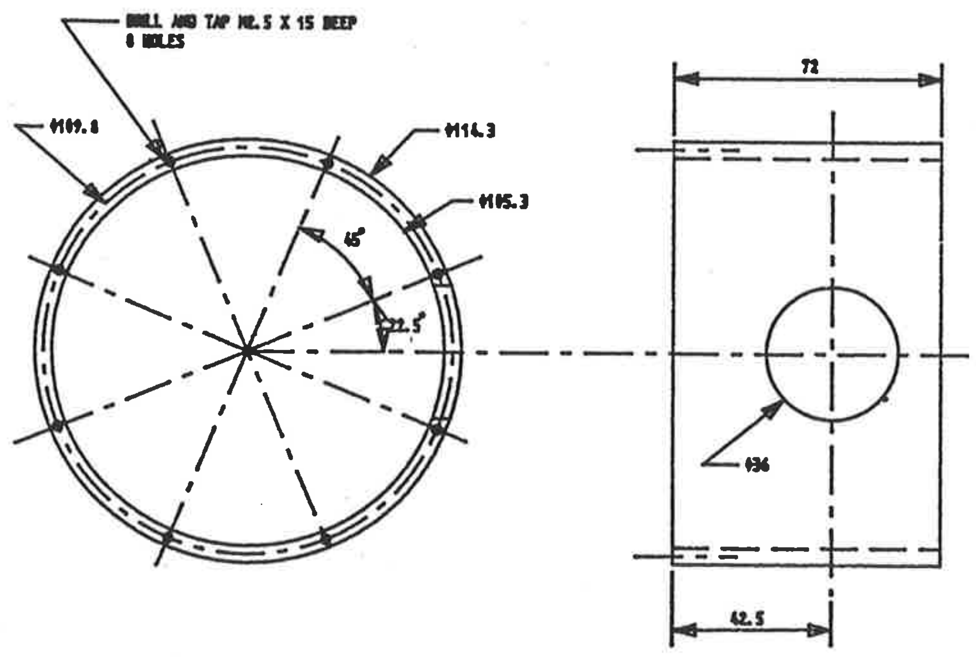

VIEW: BOTTOM

VIEW: RIGHT

MANIFOLD BODY

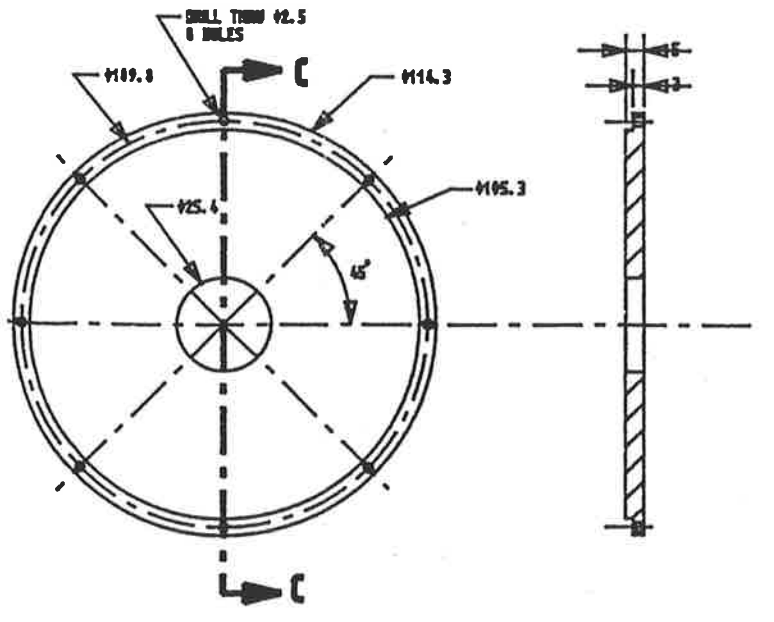

VIEW: TOP

VIEW: SECTION C-C

COVER PLATE

NOTE: (1) PART No 3 PRESS FIT INTO PART No 4.
(2) PART No 2 BRAZED TO PART No 3.
(3) PART No 6 FILLET WELDED TO PART No 5.
(4) ALL DIMENSIONS IN mm.

PART No	QUANTITY	DESCRIPTION	MATERIAL / DIMENSIONS
8	8	MOUNTING RING MOUNTING SCREWS	SOCKET HEAD SCREWS M6 X 10 LONG
7	8	COVER PLATE MOUNTING SCREWS	SOCKET HEAD SCREWS M2.5 X 10 LONG
6	1	MOUNTING RING	PLAIN STEEL
5	1	MANIFOLD BODY	GALVANIZED STEEL TUBE O.D. 114.3 - I.D. 105.3
4	1	COVER PLATE	PLAIN STEEL
3	1	CONNECTING TUBE	BRASS TUBE-Ø25.4 X 40 LONG WALL THICKNESS- 0.9
2	1	PLAIN-FEMALE THREAD END ELBOW (STD PIECE)	BRASS - TO FIT Ø25.4 TUBE
1	1	THREADED SUPPLY TUBE (STD PIECE)	BRASS - 25.4 X 150 LONG (TO FIT ELBOW)

TITLE: OUTER FLOW SUPPLY MANIFOLD		
CLIENT: ADELAIDE OF UNIVERSITY		
VIEW SHOWN	SCALE: 1:1	DATE: SEPT 28 1989
DRAWN BY: THOMAS KIEBERT		DRWG No 7
CHECKED BY:	DATE:	

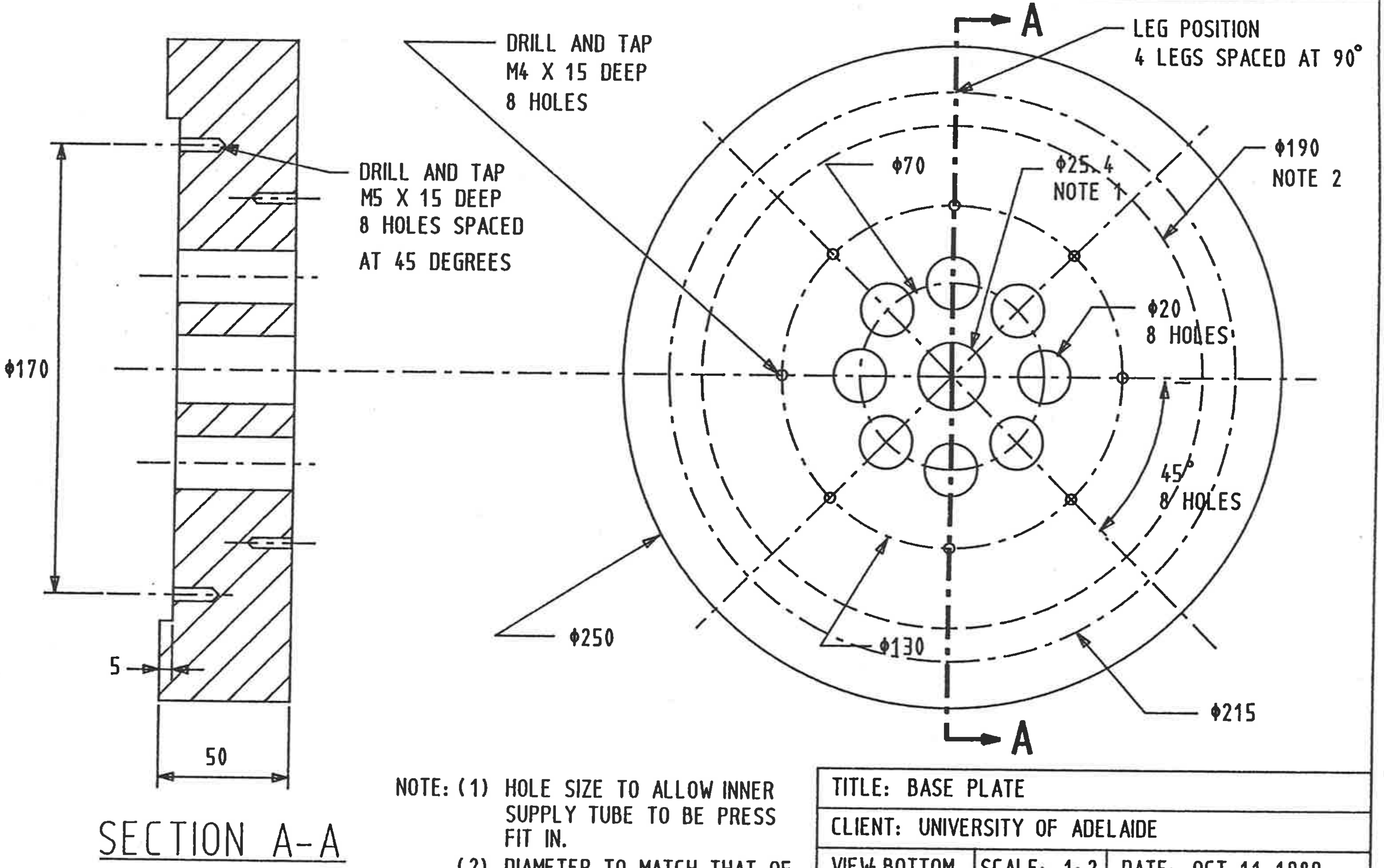

NOTE: (1) HOLE SIZE TO ALLOW INNER SUPPLY TUBE TO BE PRESS FIT IN.
(2) DIAMETER TO MATCH THAT OF THE SHROUD MOUNTING RING.
(3) MATERIAL: PLAIN STEEL.
(4) ALL DIMENSIONS IN mm.

TITLE: BASE PLATE		
CLIENT: UNIVERSITY OF ADELAIDE		
VIEW: BOTTOM	SCALE: 1: 2	DATE: OCT 11 1989
DRAWN BY: THOMAS KIEBERT		DRWG No 8
CHECKED BY:		DATE:

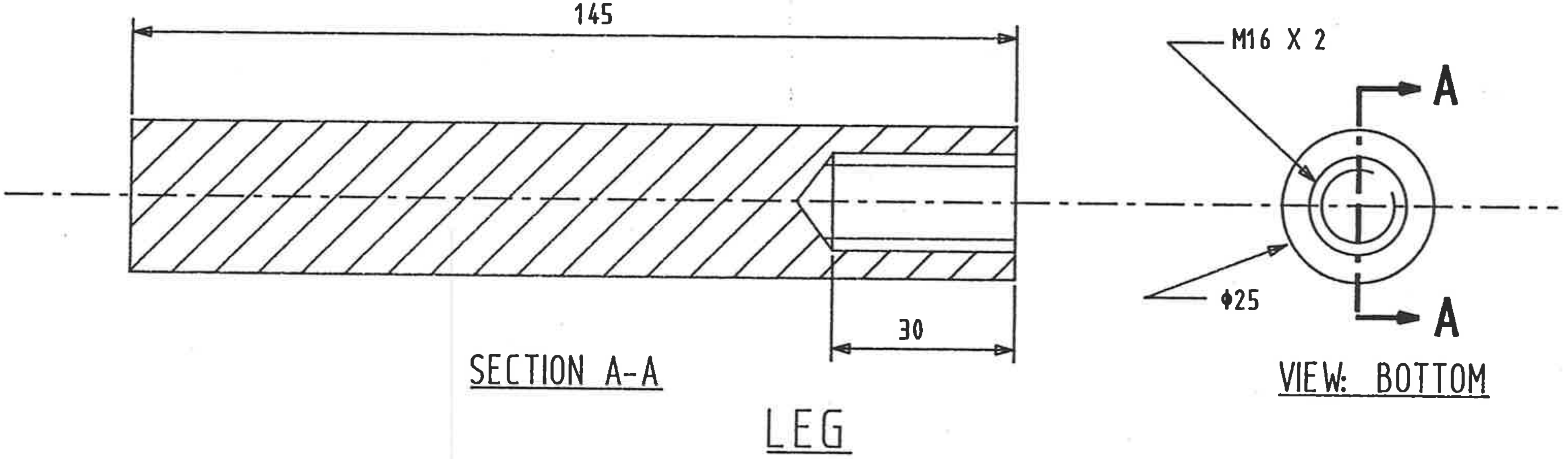

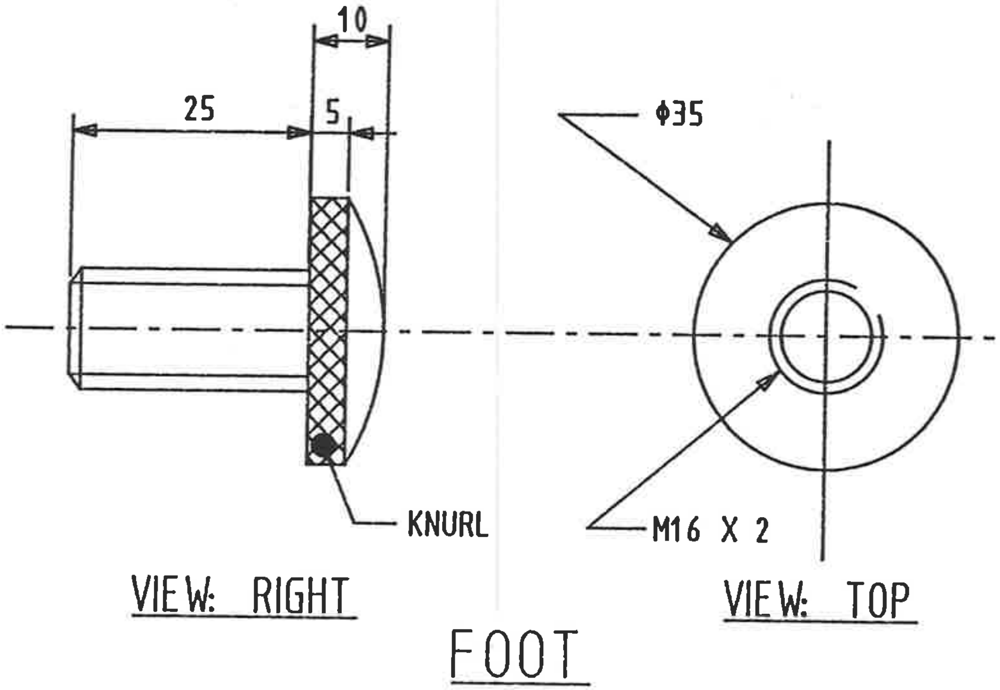

NOTE: (1) MATERIAL: PLAIN STEEL

(2) QUANTITY: 4 OF EACH

(3) LEGS TO BE FILLET WELDED TO BASE PLATE AT POSITIONS SHOWN ON DRWG No 8

(4) ALL DIMESIONS IN mm

TITLE: LEG WITH ADUSTMENT FOOT		
CLIENT: UNIVERSITY OF ADELAIDE		
VIEW: SHOWN	SCALE: 1:1	DATE: SEPT 27 1989
DRAWN BY: THOMAS KIEBERT		DRWG No 9
CHECKED BY:		DATE:

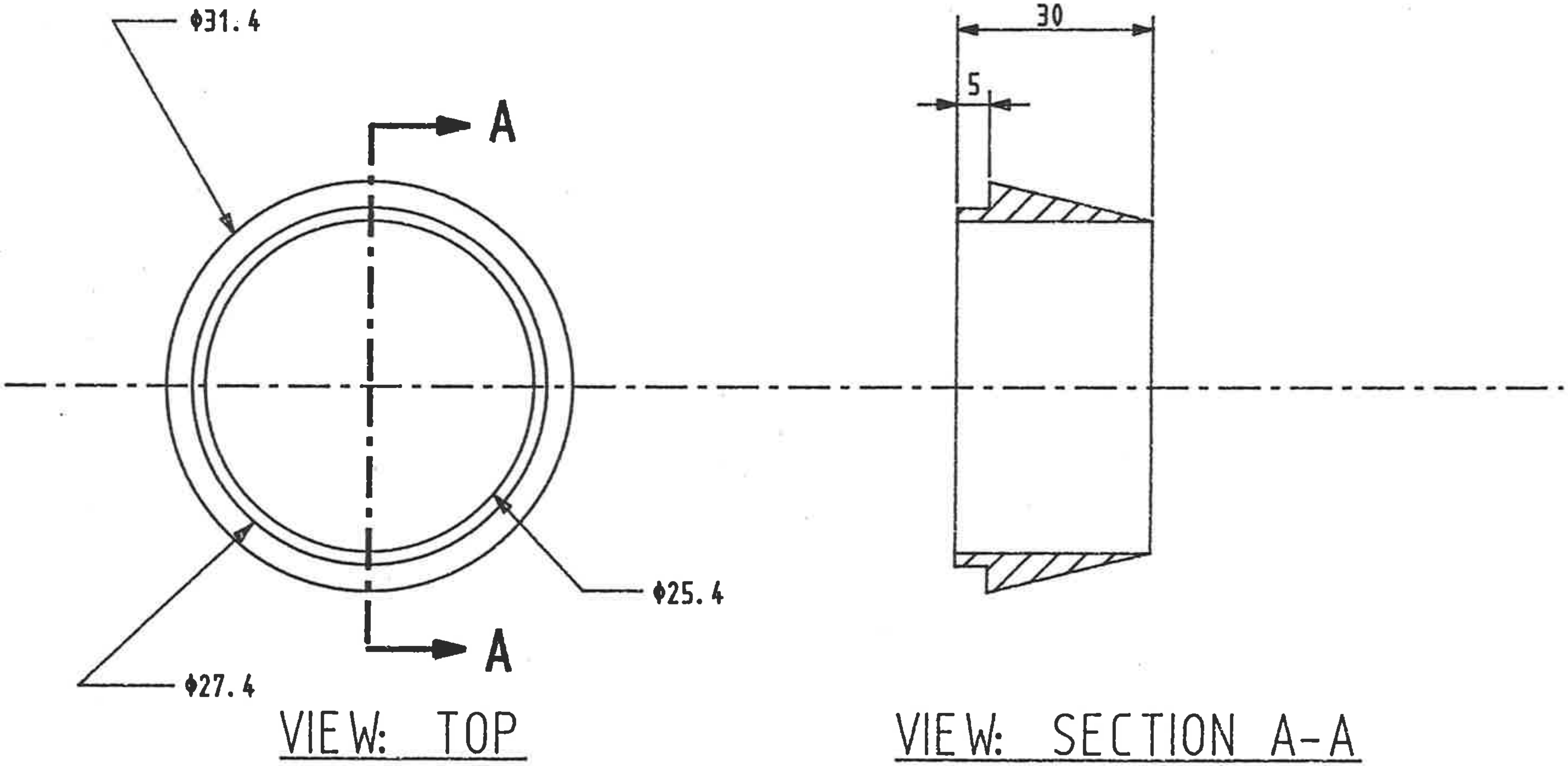

NOTE: (1) MATERIAL: BRASS

(2) DIAMETER OF SHIM TO MATCH SMOOTHLY WITH DIAMETER OF NOZZLE.

(3) DIAMETER TO MATCH INNER FLOW BRASS TUBE DIAMETER.

(4) ALL DIMENSIONS IN mm.

TITLE: NOZZLE SUPPORTING SHIM		
CLIENT: UNIVERSITY OF ADELAIDE		
VIEW: SHOWN	SCALE: 2:1	DATE: SEPT 28 1989
DRAWN BY: THOMAS KIEBERT		DRWG No 10
CHECKED BY:		DATE:

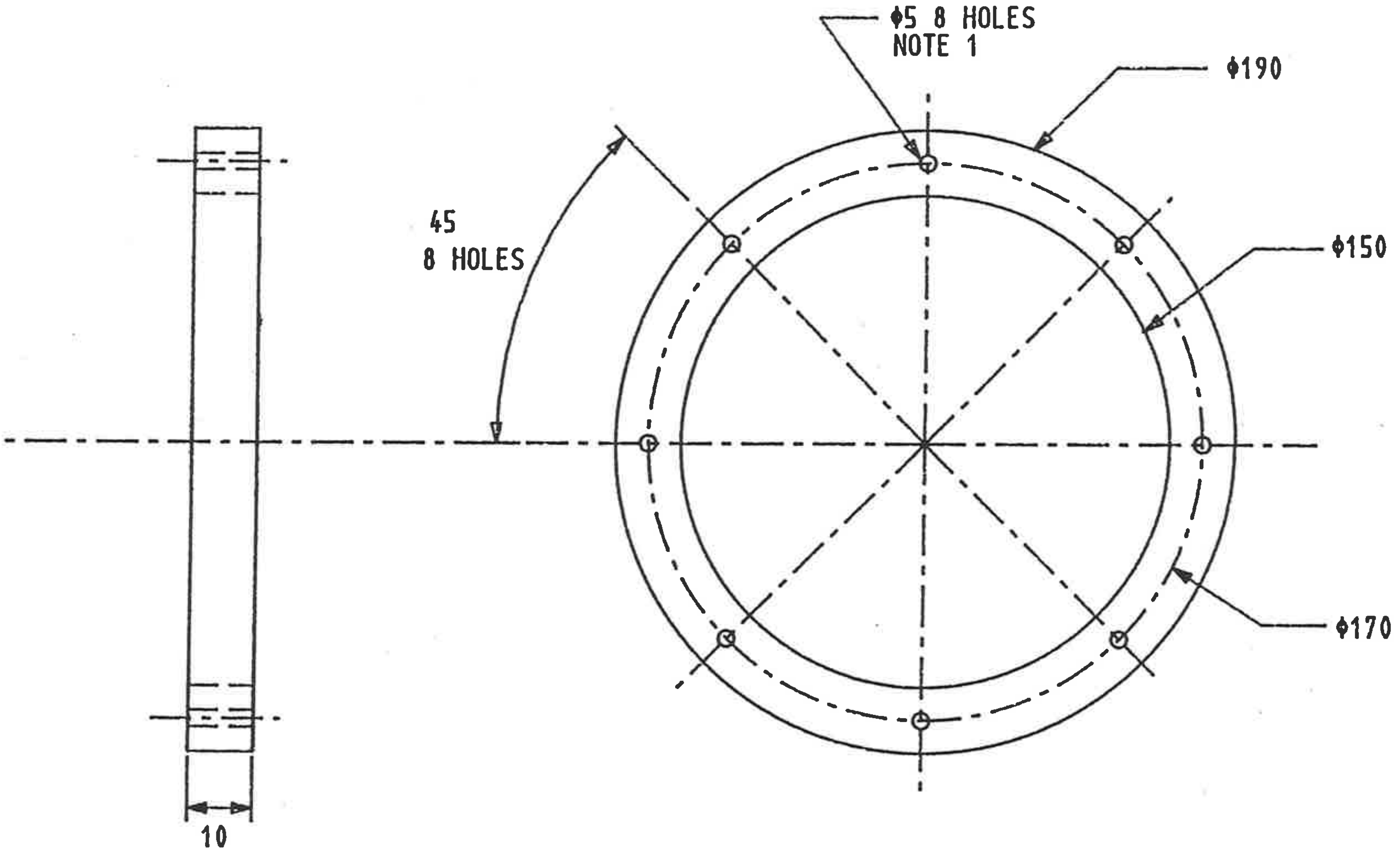

NOTE: (1) DRILLED THROUGH TO ACCEPT M5 SOCKET HEAD MOUNTING SCREWS

(2) MATERIAL: PERSPEX

(3) MOUNTING RING TO BE GLUED TO SHROUD.

(4) ALL DIMENSIONS IN mm.

TITLE: SHROUD MOUNTING RING		
CLIENT: UNVERSITY OF ADELAIDE		
VIEW: SHOWN	SCALE: 1:2	DATE: OCT 11 1989
DRAWN BY: THOMAS KIEBERT		DRWG No 11
CHECKED BY:	DATE:	

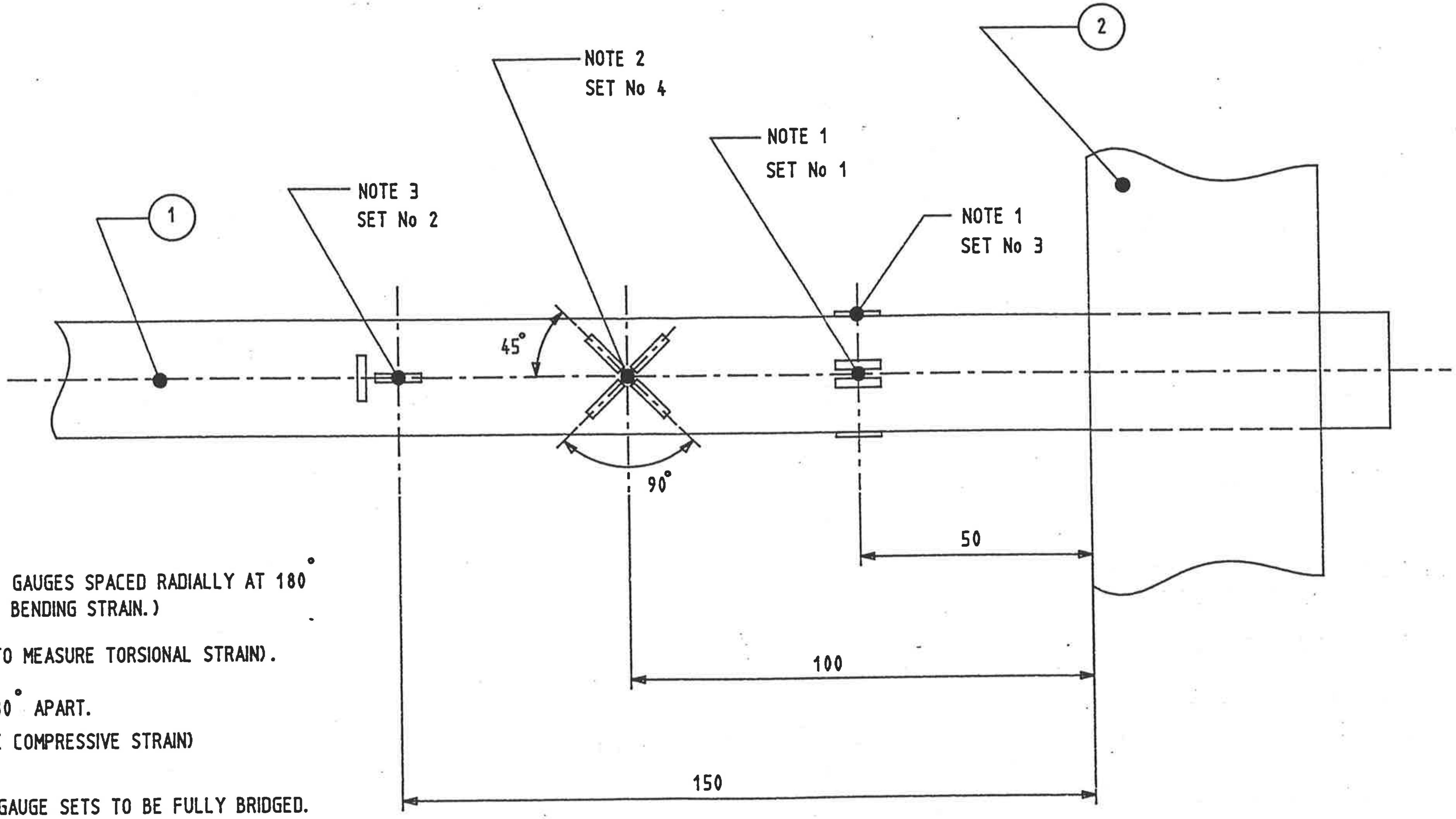

NOTE : (1) 2 SETS OF 2 GAUGES SPACED RADIALLY AT 180°
(TO MEASURE BENDING STRAIN.)

(2) 4 GUAGES (TO MEASURE TORSIONAL STRAIN).

(3) 2 T-SETS 180° APART.
(TO MEASURE COMPRESSIVE STRAIN)

(4) ALL STRAIN GAUGE SETS TO BE FULLY BRIDGED.

PART	QTY	DESCRIPTION	MATERIAL DIMENSIONS
2	1	BASE PLATE	STEEL
1	1	INNER FLOW SUPPLY TUBE	BRASS TUBE - 25.4 X 1100 LONG WALL THICKNESS - 0.9

TITLE: PLACEMENT OF STRAIN GUAGES ON INNER SUPPLY TUBE
CLIENT: UNIVERSITY OF ADELAIDE
VIEW: SECTION | SCALE: 1:1 | DATE: OCT 26 1989
DRAWN BY: THOMAS KIEBERT | DRWG No 12
CHECKED BY: | DATE:

APPENDIX B

Ancillary Equipment

Solid State Pressure Sensors/Low Level 170PC Series

MOUNTING DIMENSIONS (For reference only)

Gage Types

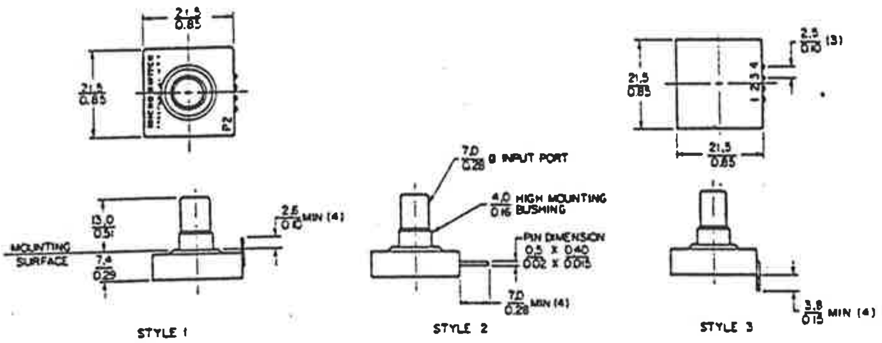

Terminals
1 — Vs (+)
2 — Output A
3 — Ground (−)
4 — Output B

Differential Types

Mounting Hardware

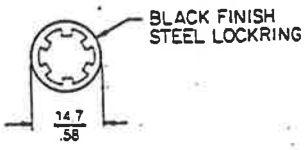

Catalog listings are shown with terminal style 1. To order style 2 (or 3), substitute the number 2 (or 3) for the 1 at the end of the listing.

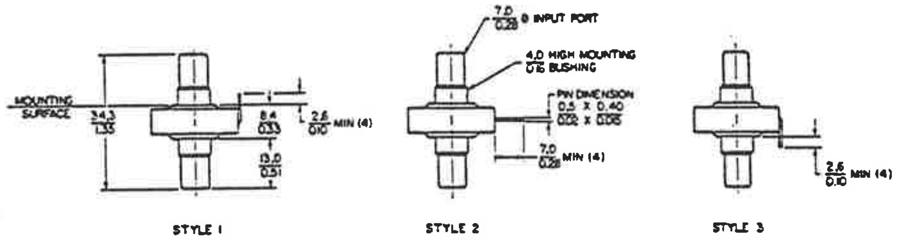

170PC CONSTRUCTION

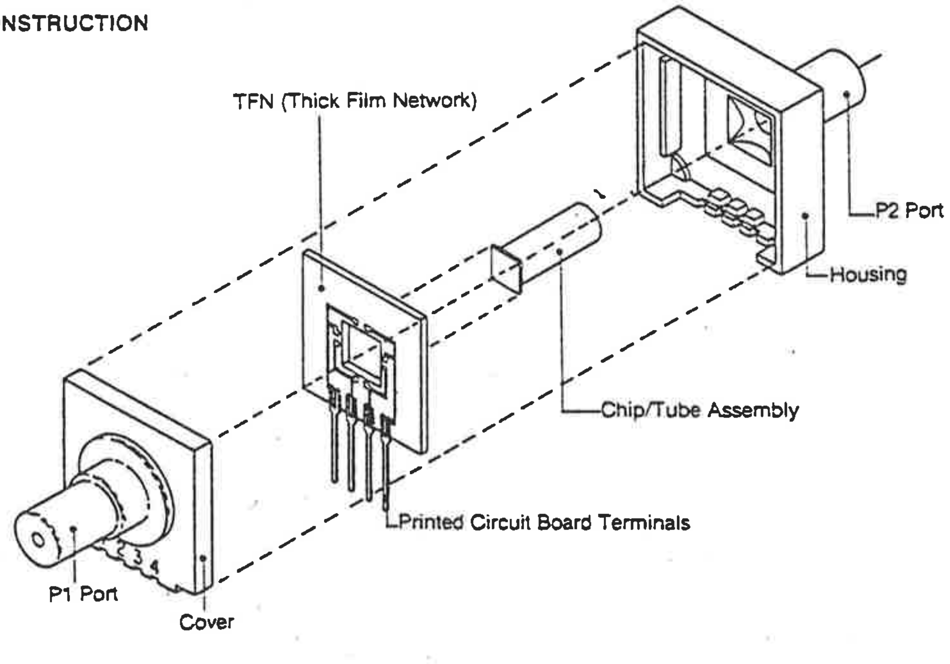

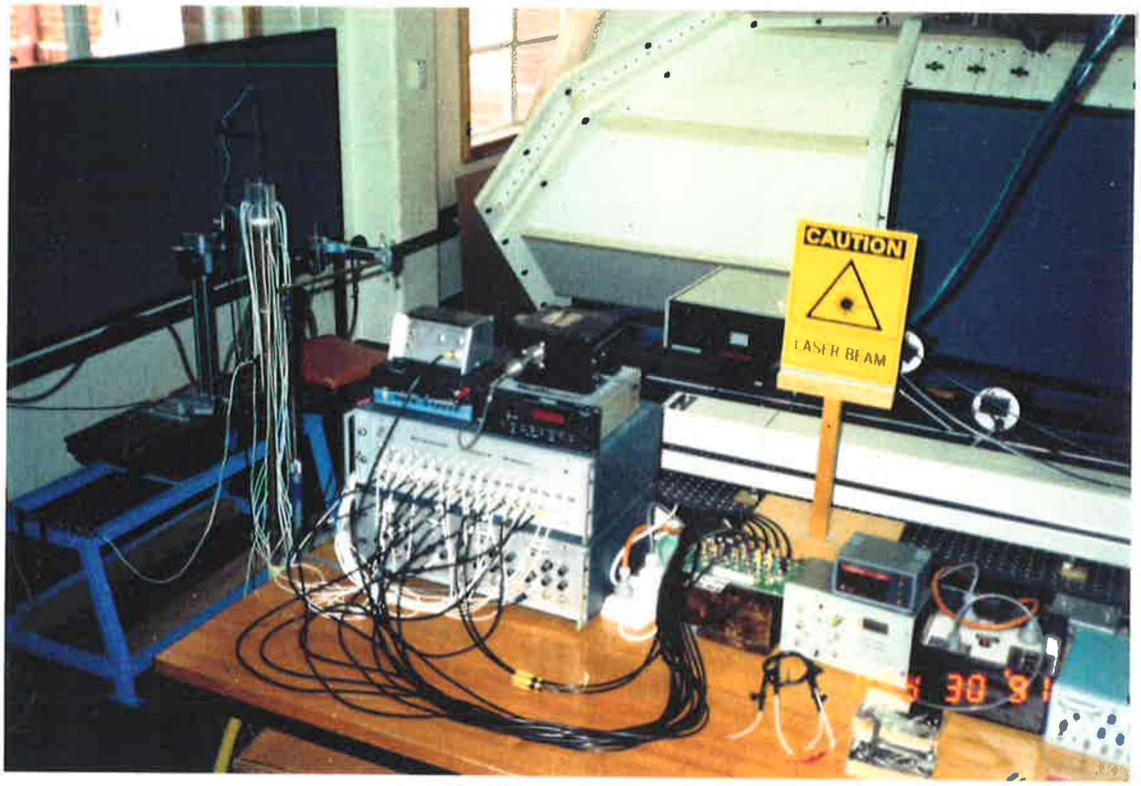

Photgraph showing hot-wire mounted on the 2-axis traverse table with pressure tappings connected to the differential pressure transducer array and associated instrumentation in the foreground. Laser orintation can be seen in the background.

APPENDIX C

Supplementary Experimental Data

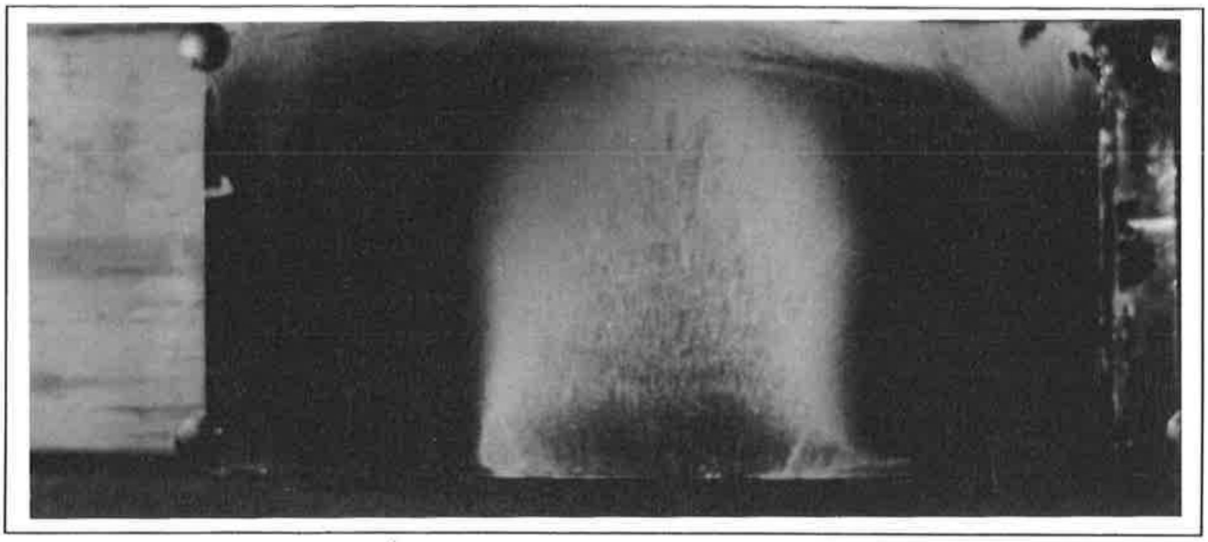

Figure C.1. Photograph of the unrolled sleeve inserted into the cavity, coated with china-clay and exposed to the flow at Re_t = 72,000 and AR = 0.11.

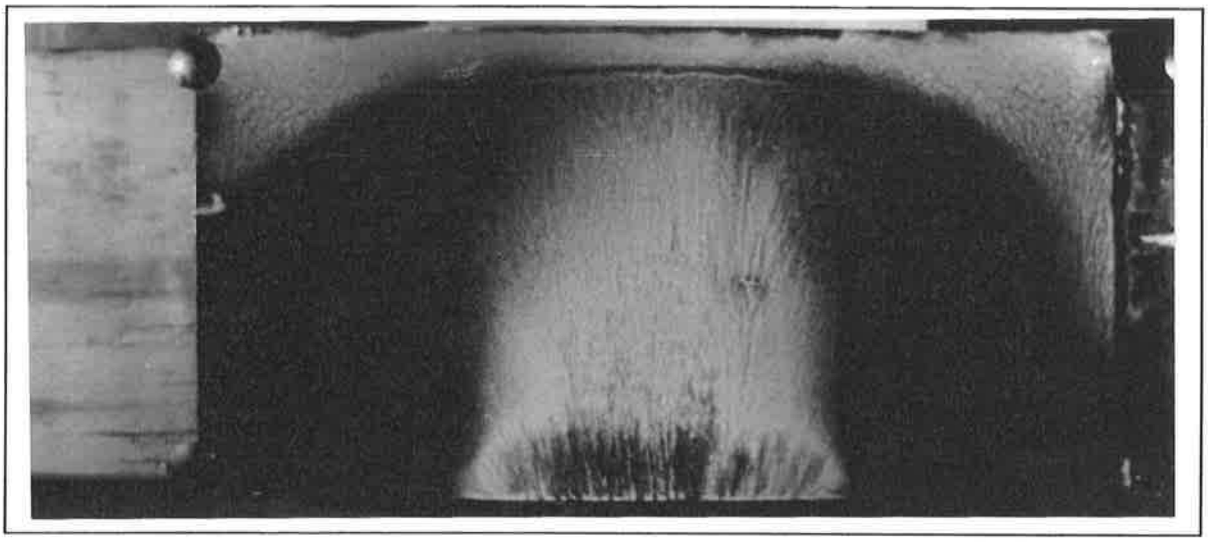

Figure C.2. Photograph of the unrolled sleeve inserted into the cavity, coated with china-clay and exposed to the flow at Re_t = 72,000 and AR = 0.17.

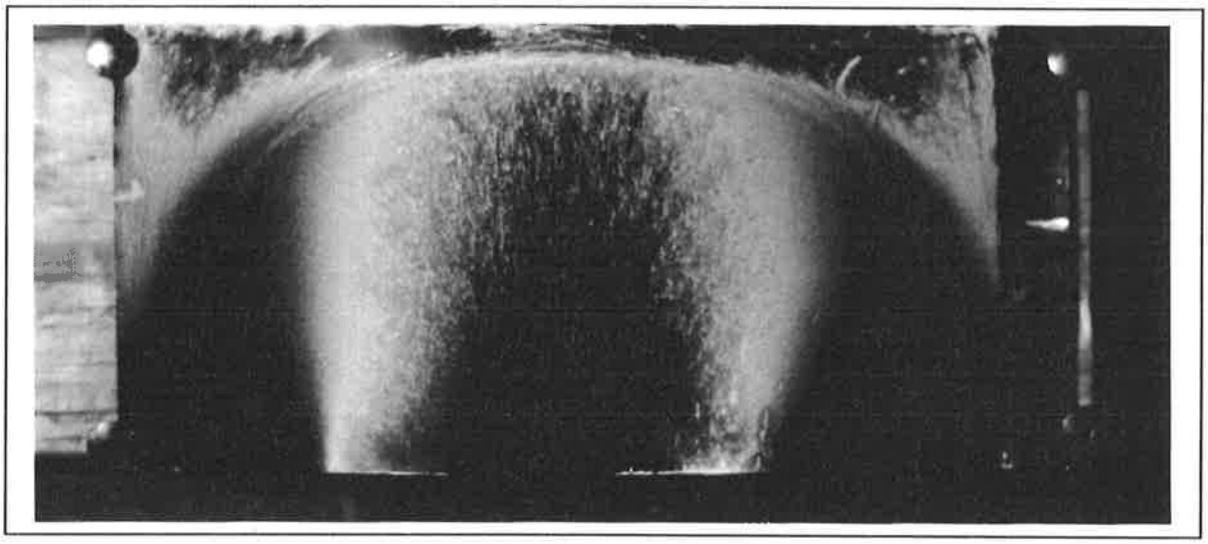

Figure C.3. Photograph of the unrolled sleeve inserted into the cavity, coated with china-clay and exposed to the flow at Re_t = 72,000 and AR = 0.25.

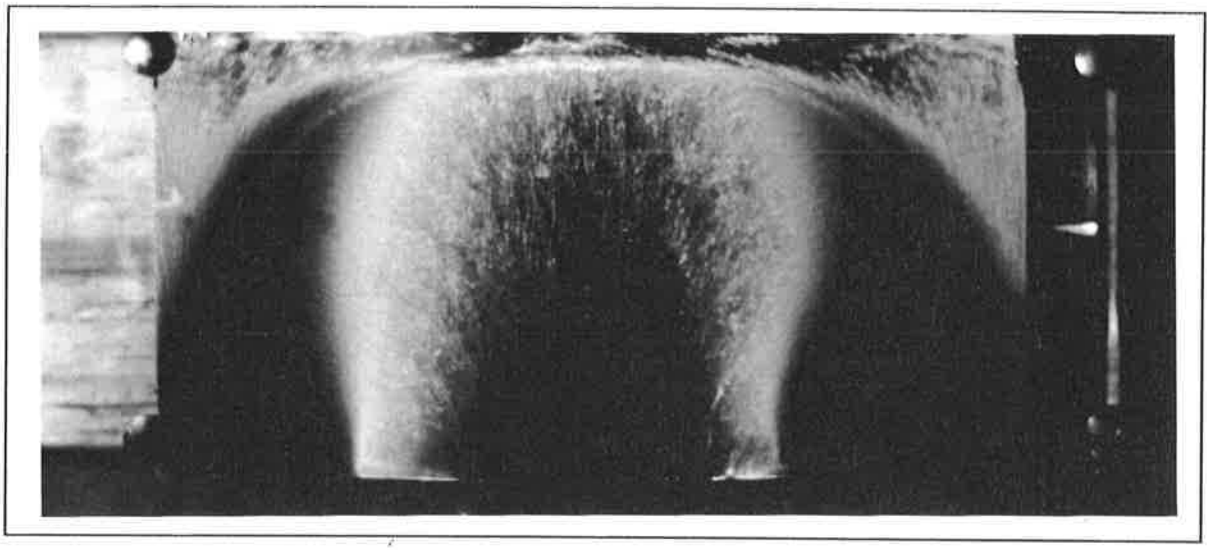

Figure C.4. Photograph of the unrolled sleeve inserted into the cavity, coated with china-clay and exposed to the flow at Re_t = 72,000 and AR = 0.34.

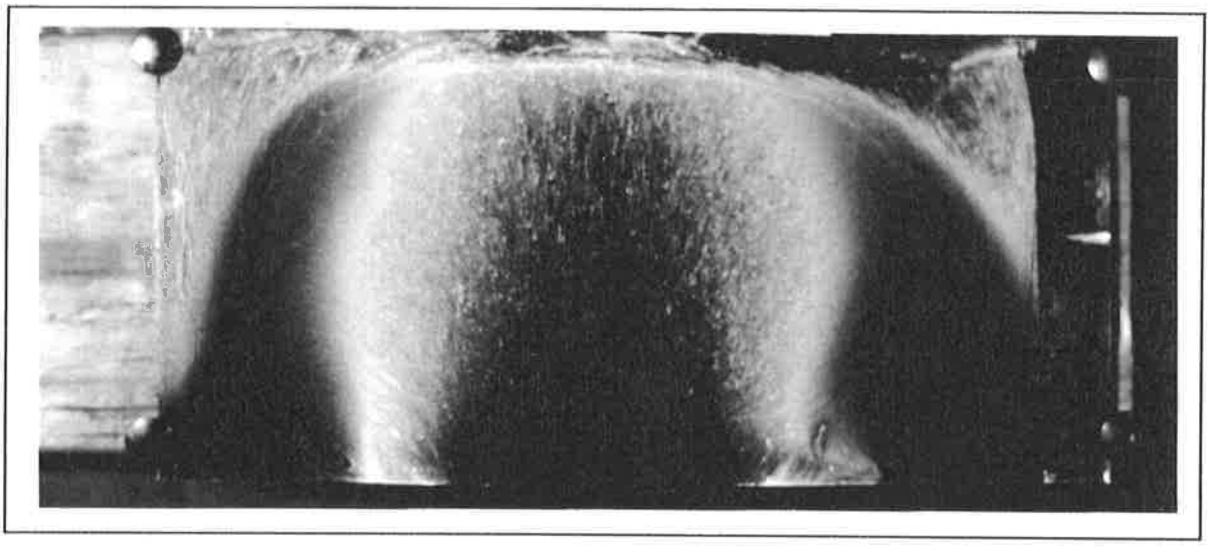

Figure C.5. Photograph of the unrolled sleeve inserted into the cavity, coated with china-clay and exposed to the flow at Re_t = 72,000 and AR = 0.44.

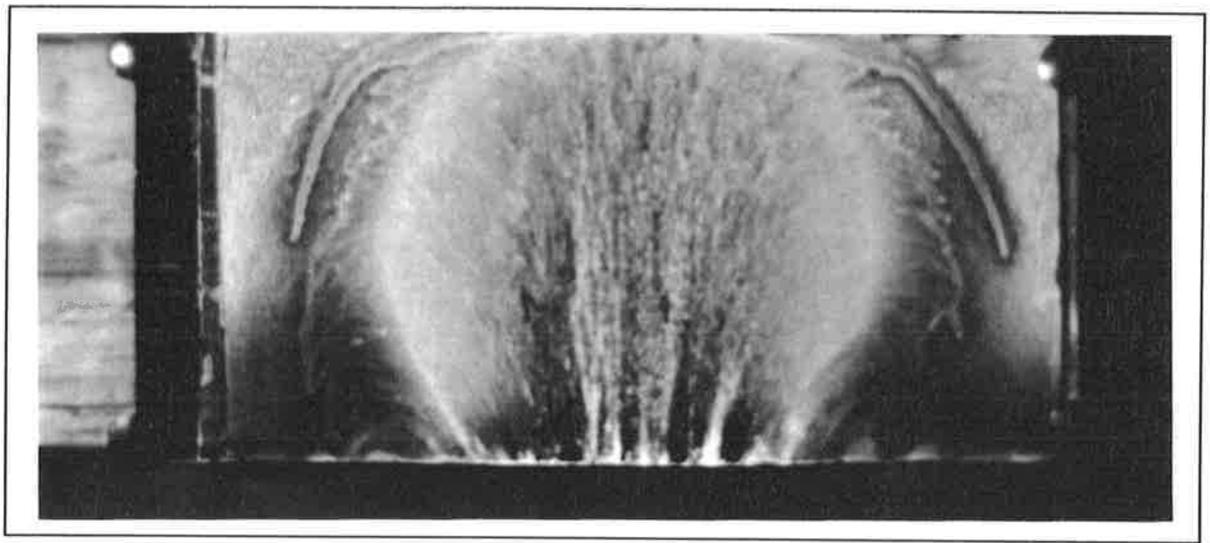

Figure C.4. Photograph of the unrolled sleeve inserted into the cavity, coated with china-clay and exposed to the flow at Re_t = 72,000 and AR = 0.83.

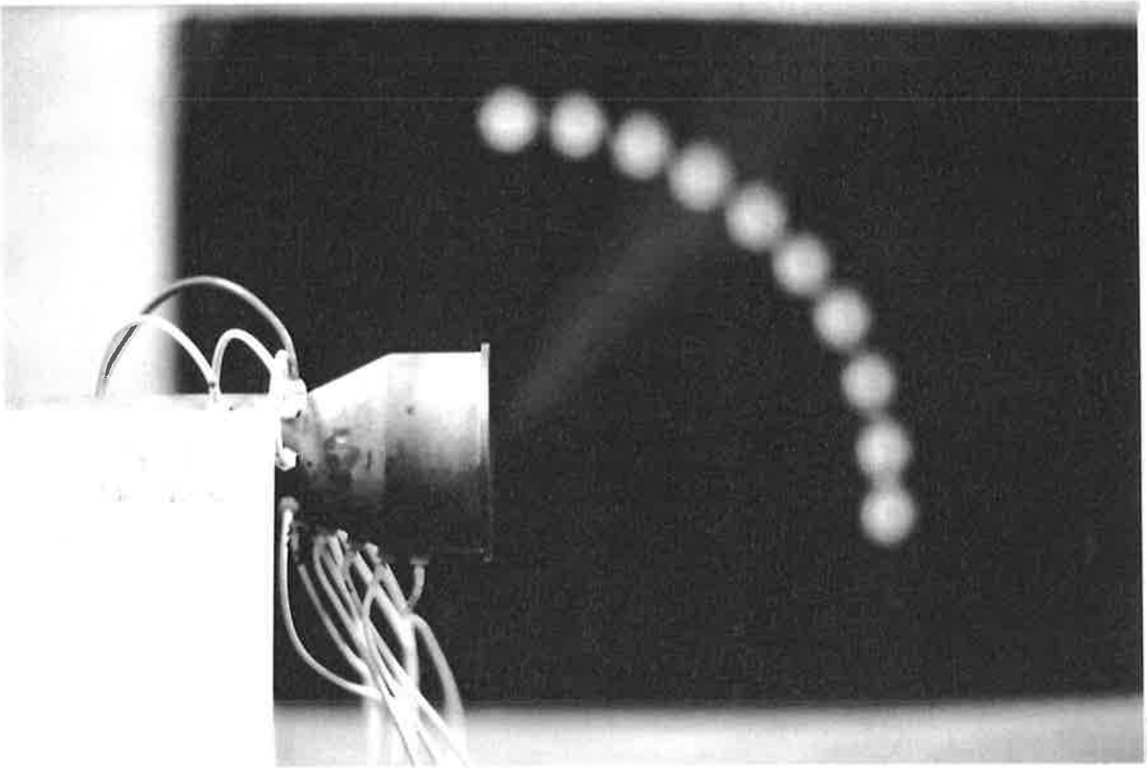

Figure C. 7 Deflected jet exiting CD Nozzle, visualised by seeding the jet viewed in natural light at Re = 27,000 and AR = 0.11.

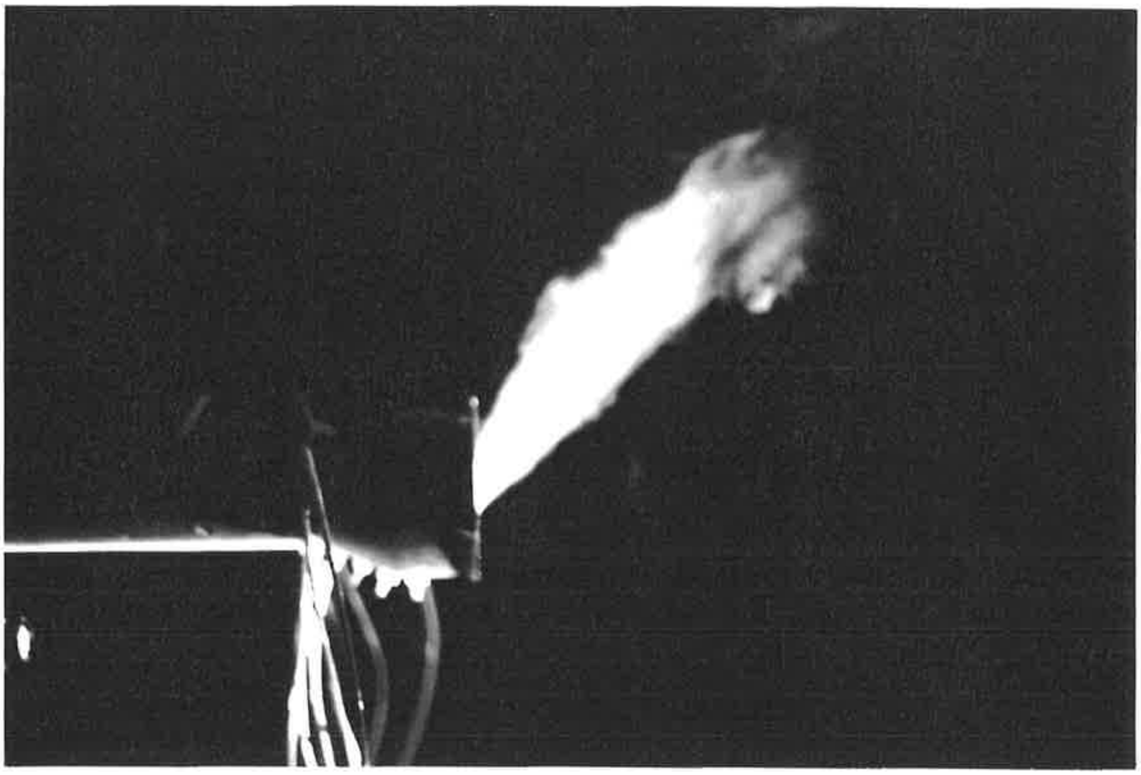

Figure C. 8 Deflected jet exiting CD Nozzle, visualised by seeding the jet viewed with laser sheet at Re = 1400 and AR = 0.11.

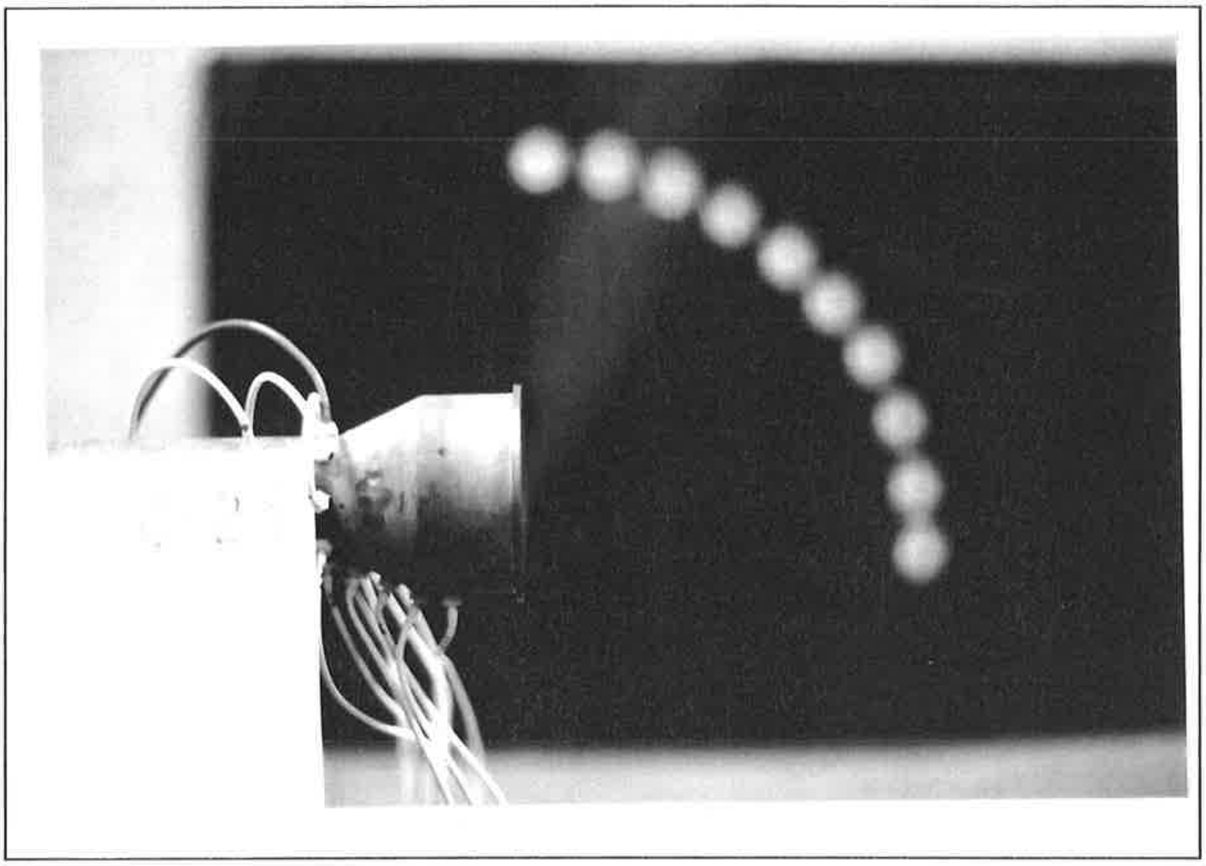

Figure C. 9 Deflected jet exiting CD Nozzle, visualised by seeding the jet viewed in natural light at Re = 27,000 and AR = 0.17.

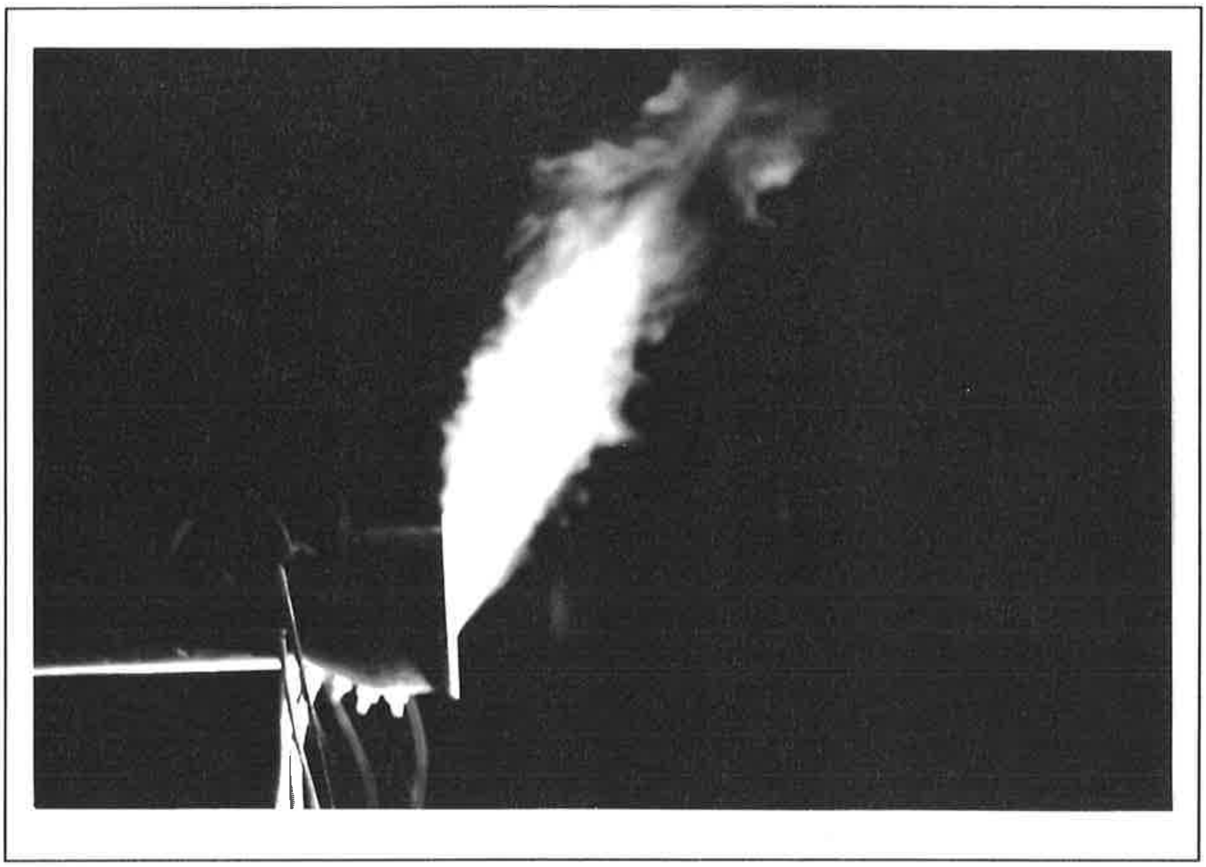

Figure C. 10 Deflected jet exiting CD Nozzle, visualised by seeding the jet viewed with laser sheet at Re = 1400 and AR = 0.17.

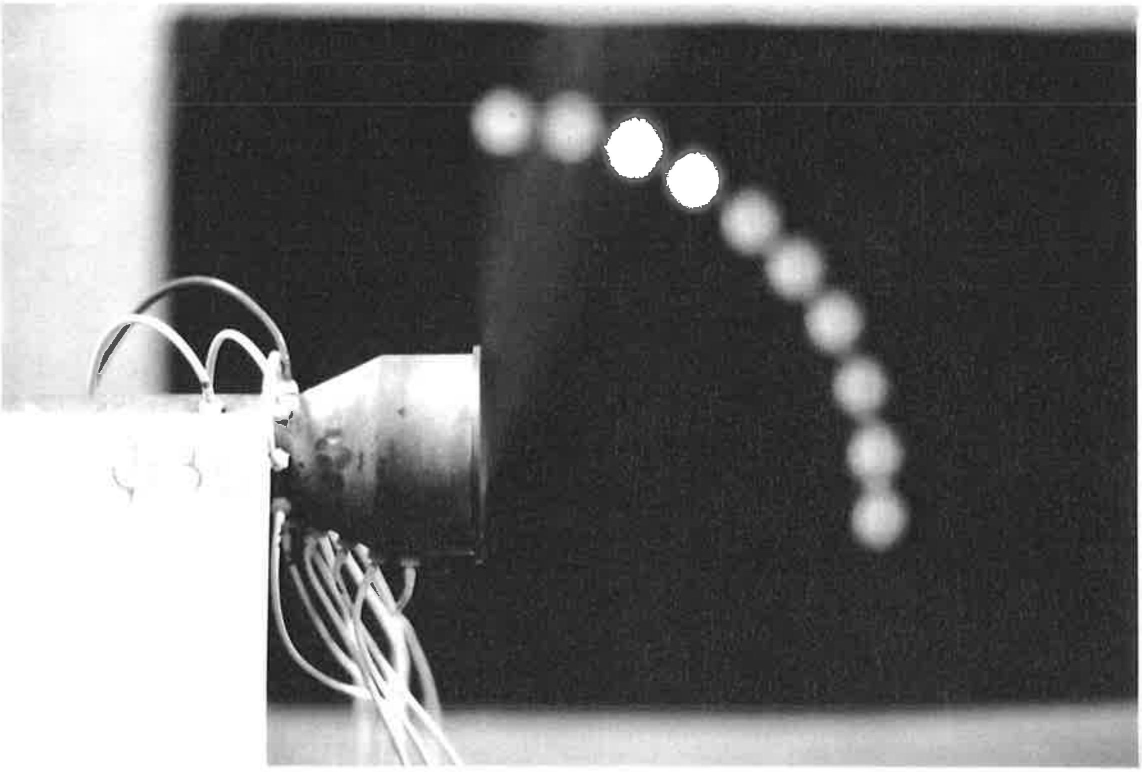

Figure C. 11 Deflected jet exiting CD Nozzle, visualised by seeding the jet viewed in natural light at Re = 27,000 and AR = 0.25.

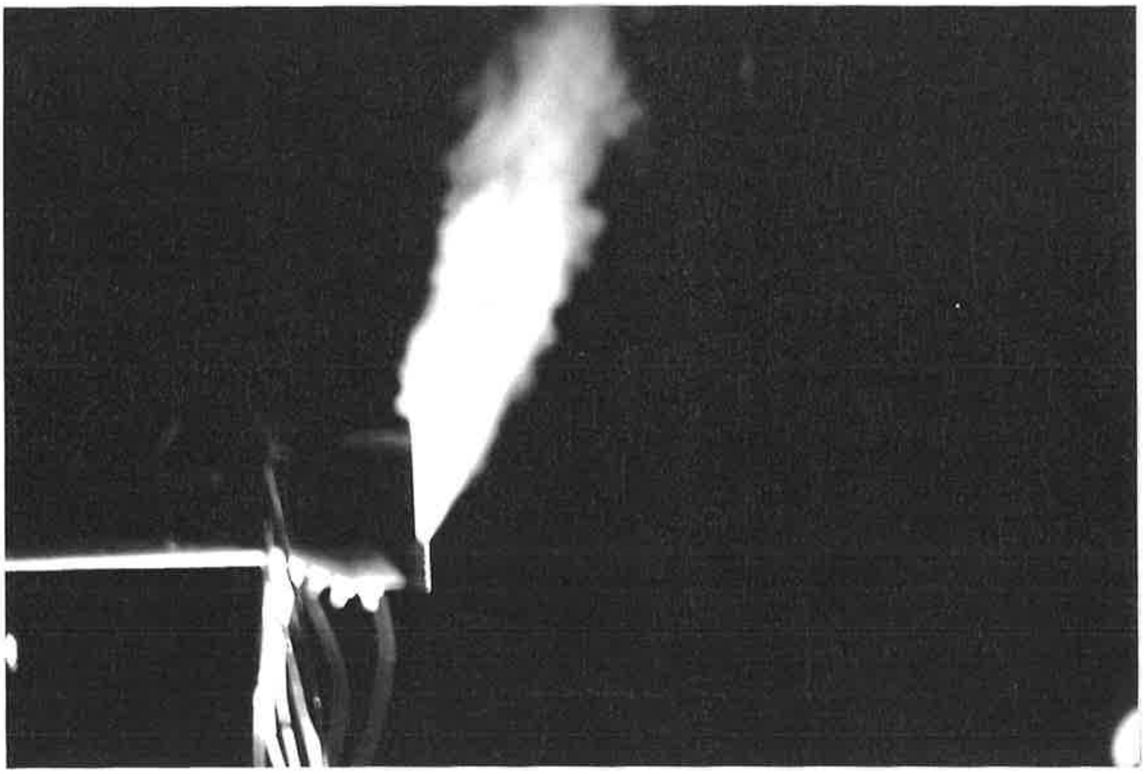

Figure C. 12 Deflected jet exiting CD Nozzle, visualised by seeding the jet viewed with laser sheet at Re = 1400 and AR = 0.25.

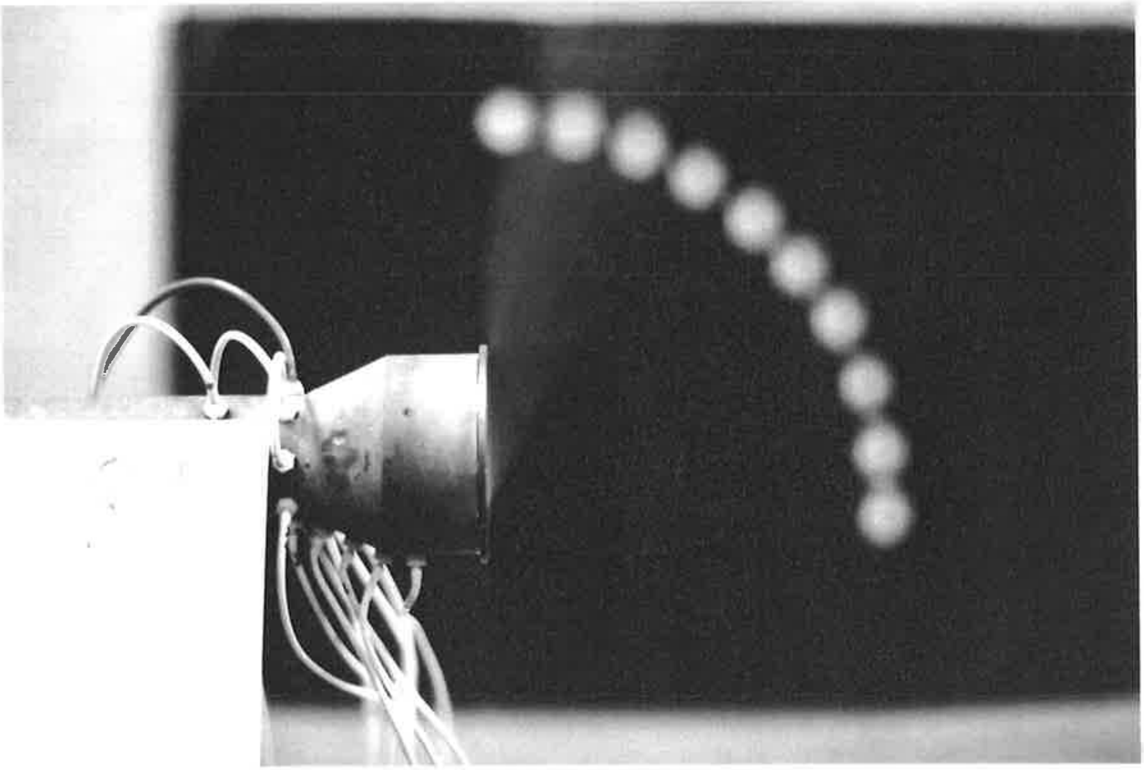

Figure C. 13 Deflected jet exiting CD Nozzle, visualised by seeding the jet viewed in natural light at Re = 27,000 and AR = 0.34.

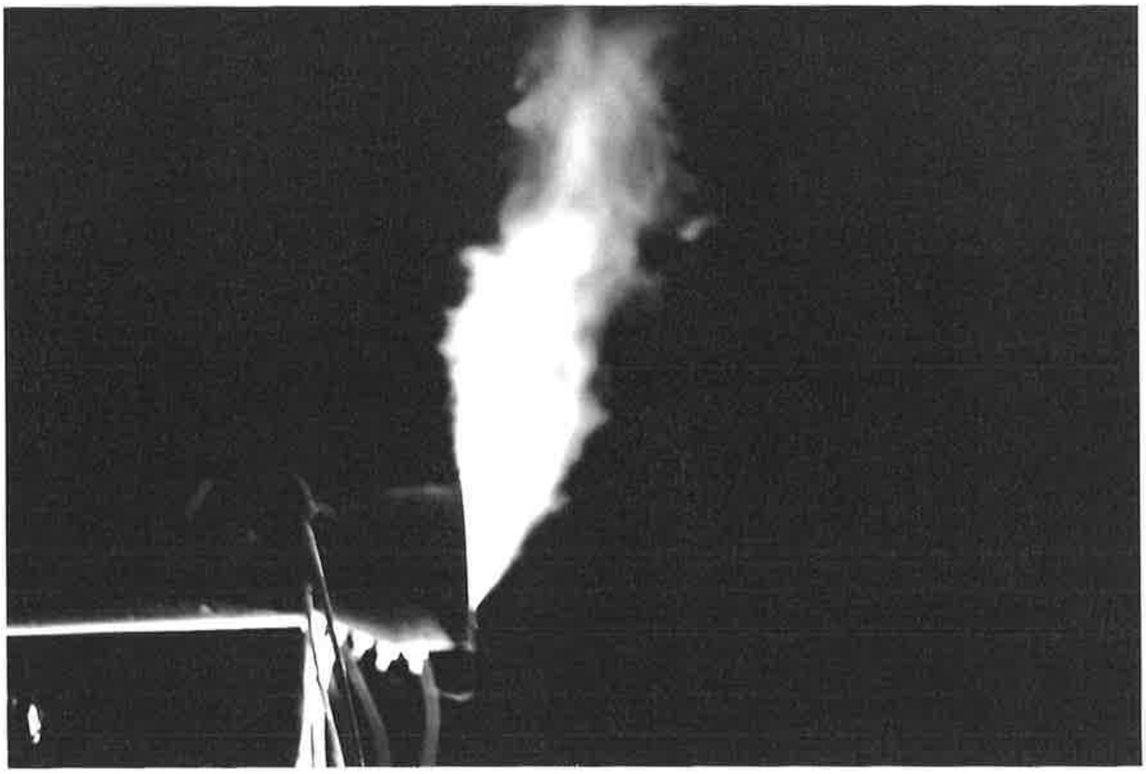

Figure C. 14 Deflected jet exiting CD Nozzle, visualised by seeding the jet viewed with laser sheet at Re = 1400 and AR = 0.34.

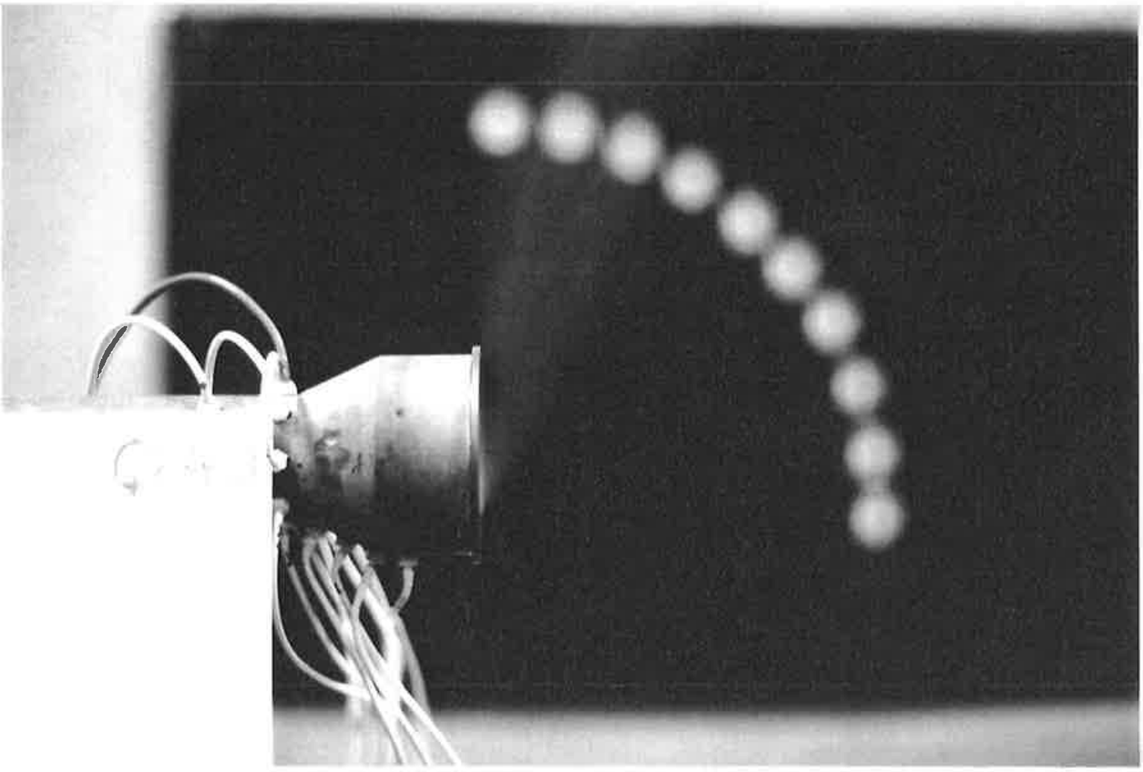

Figure C. 15 Deflected jet exiting CD Nozzle, visualised by seeding the jet viewed in natural light at Re = 27,000 and AR = 0.44.

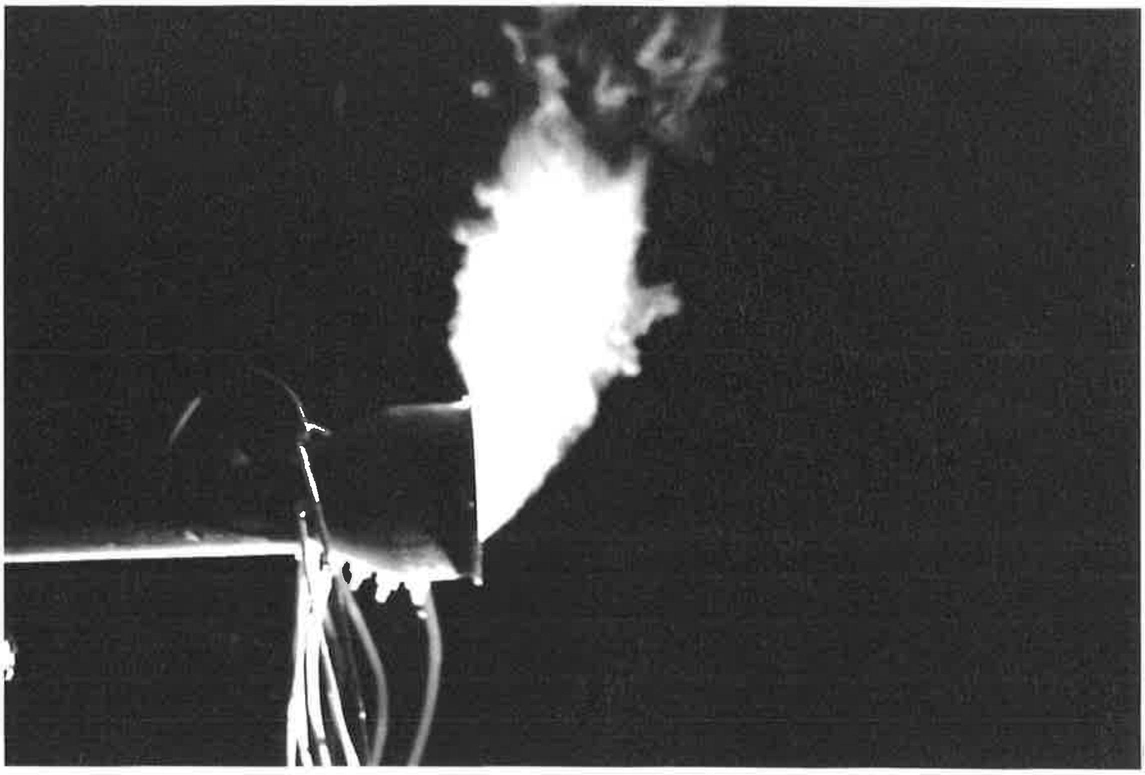

Figure C. 16 Deflected jet exiting CD Nozzle, visualised by seeding the jet viewed with laser sheet at Re = 1400 and AR = 0.44.

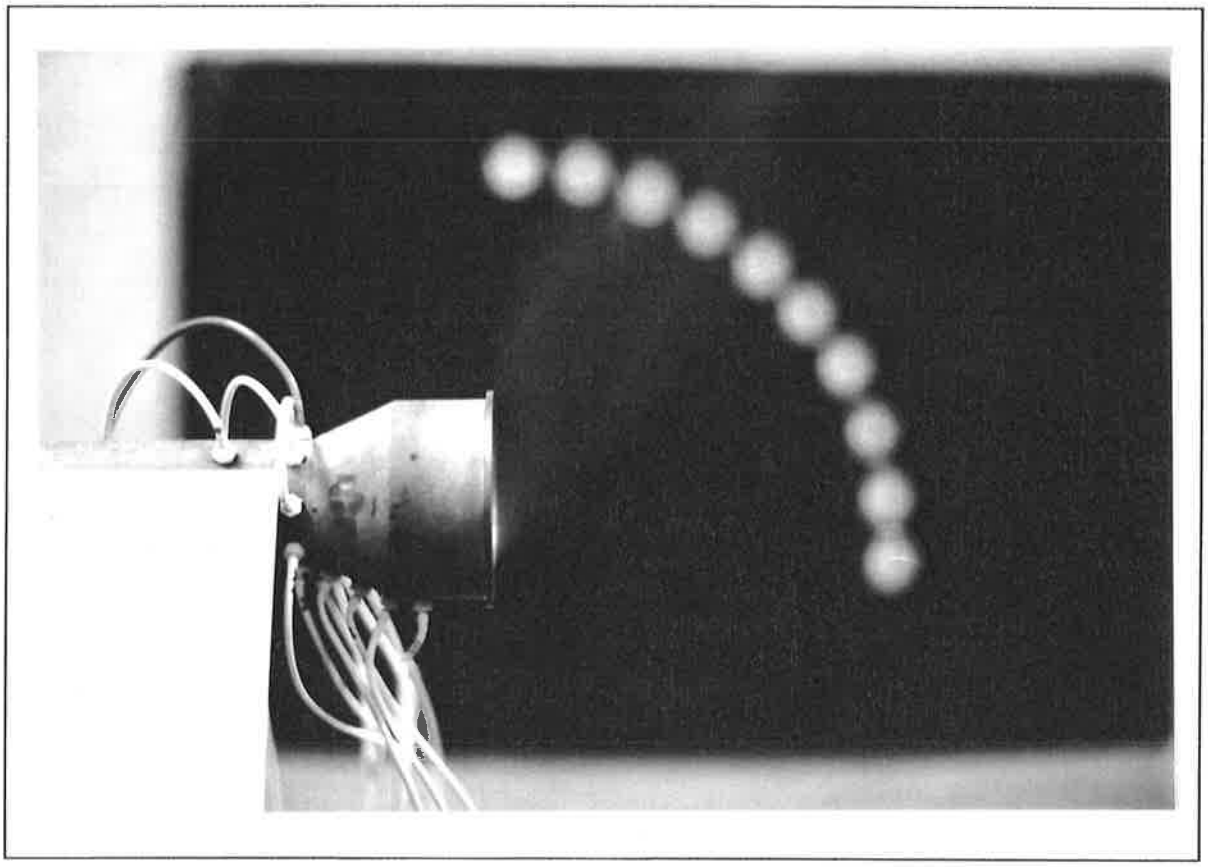

Figure C. 17 Deflected jet exiting CD Nozzle, visualised by seeding the jet viewed in natural light at Re = 27,000 and AR = 0.56.

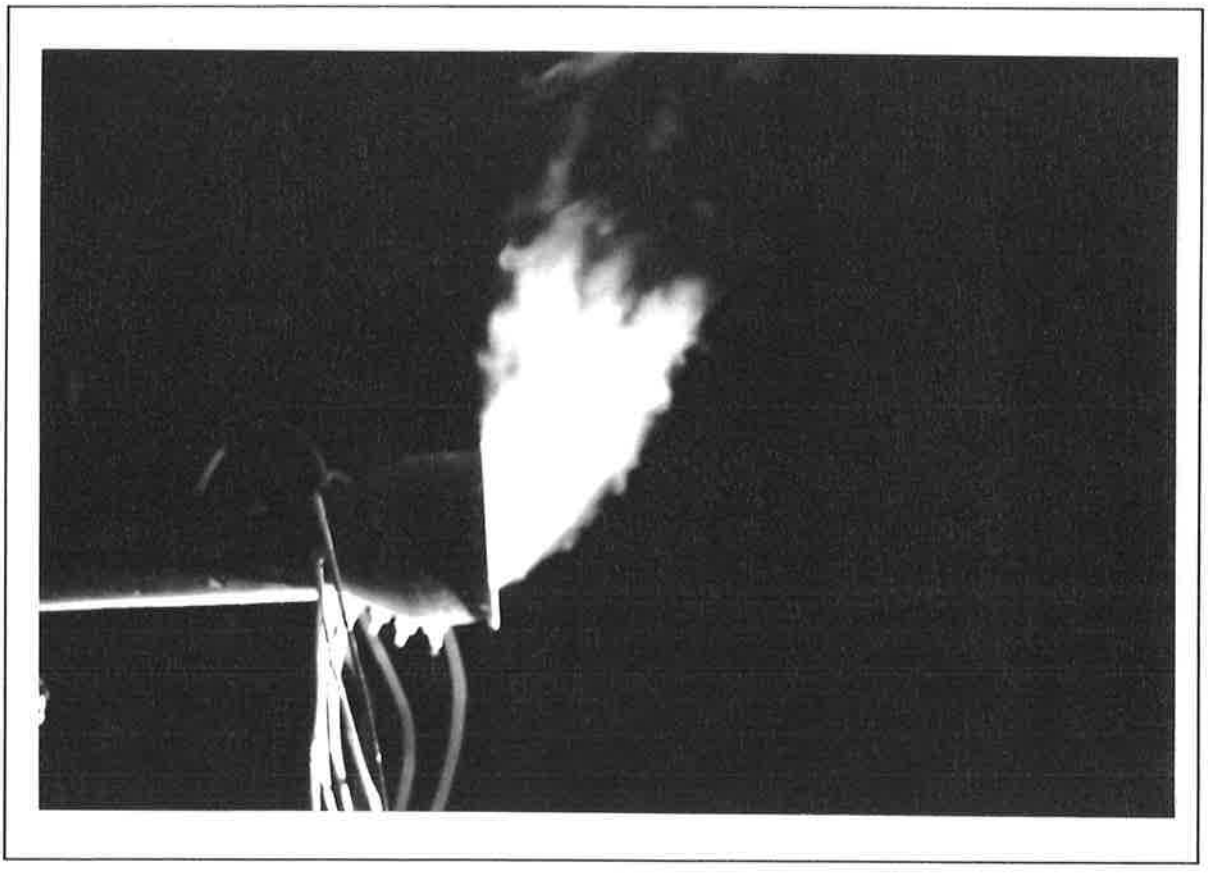

Figure C. 18 Deflected jet exiting CD Nozzle, visualised by seeding the jet viewed with laser sheet at Re = 1400 and AR = 0.56

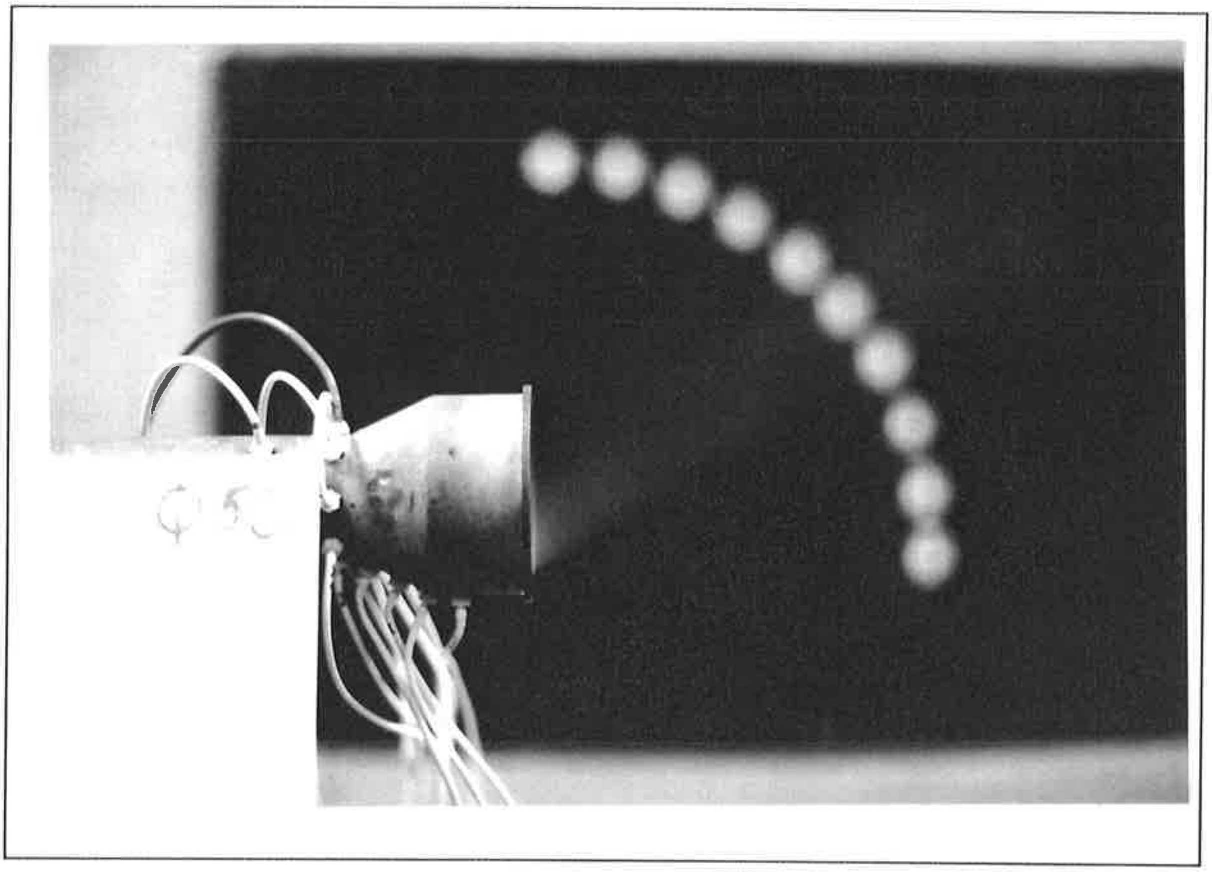

Figure C. 19 Deflected jet exiting CD Nozzle, visualised by seeding the jet viewed in natural light at Re = 27,000 and AR = 0.69.

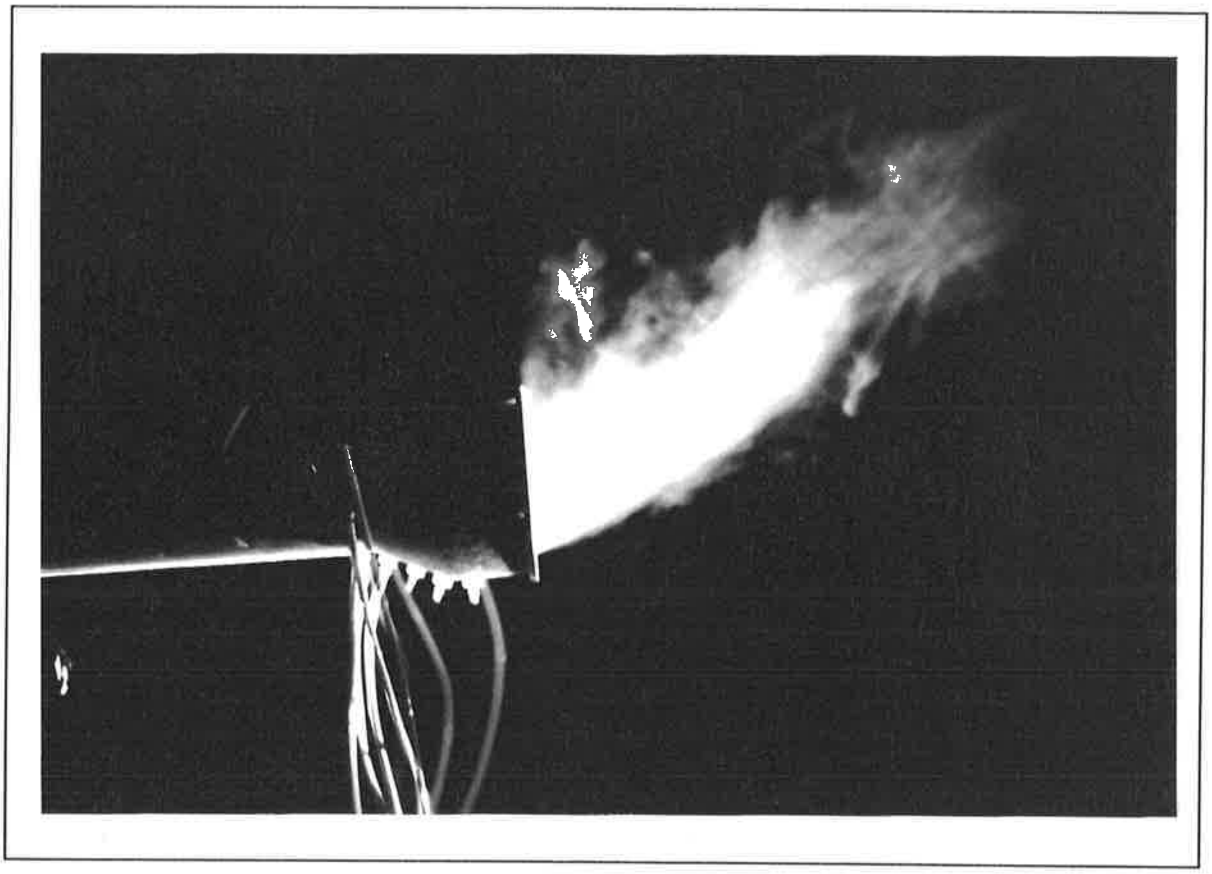

Figure C. 20 Deflected jet exiting CD Nozzle, visualised by seeding the jet viewed with laser sheet at Re = 1400 and AR = 0.69

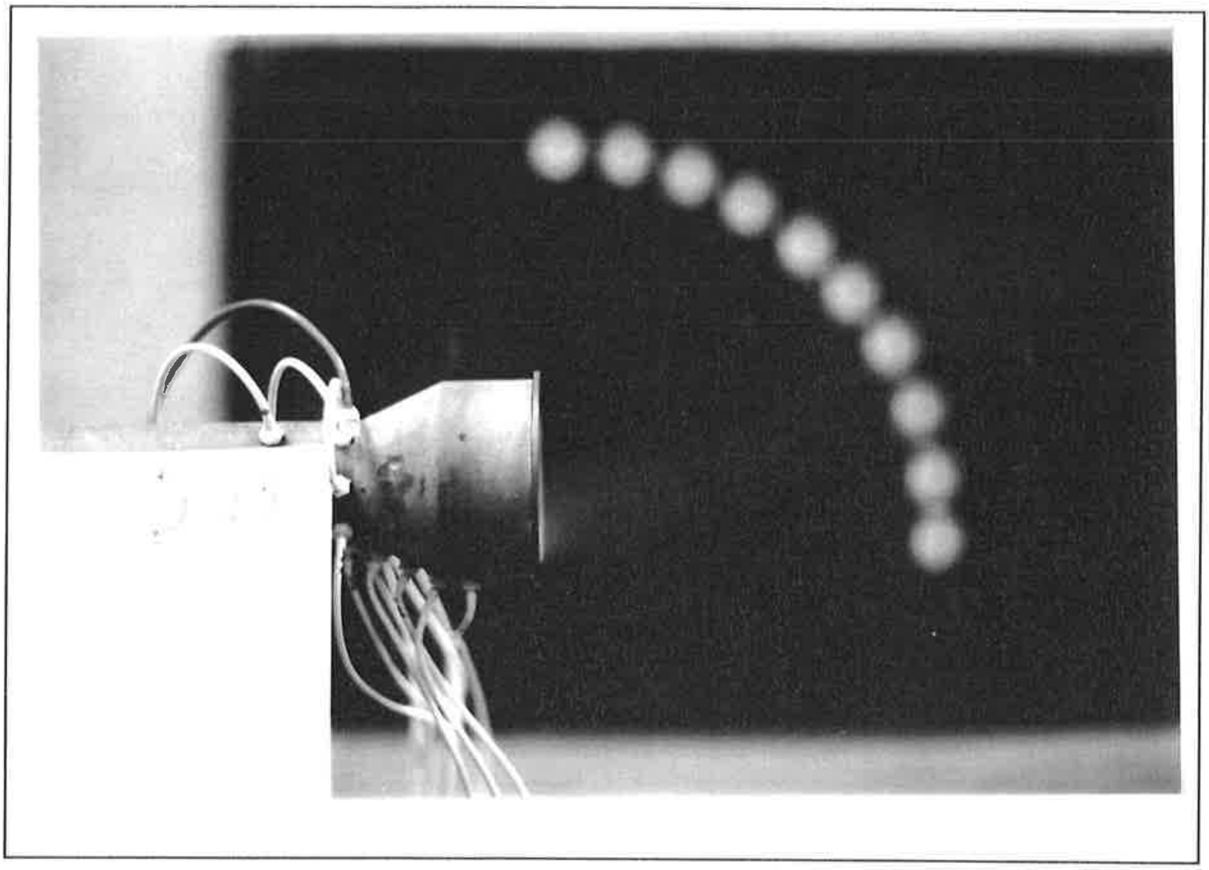

Figure C. 21 Deflected jet exiting CD Nozzle, visualised by seeding the jet viewed in natural light at Re = 27,000 and AR = 0.83

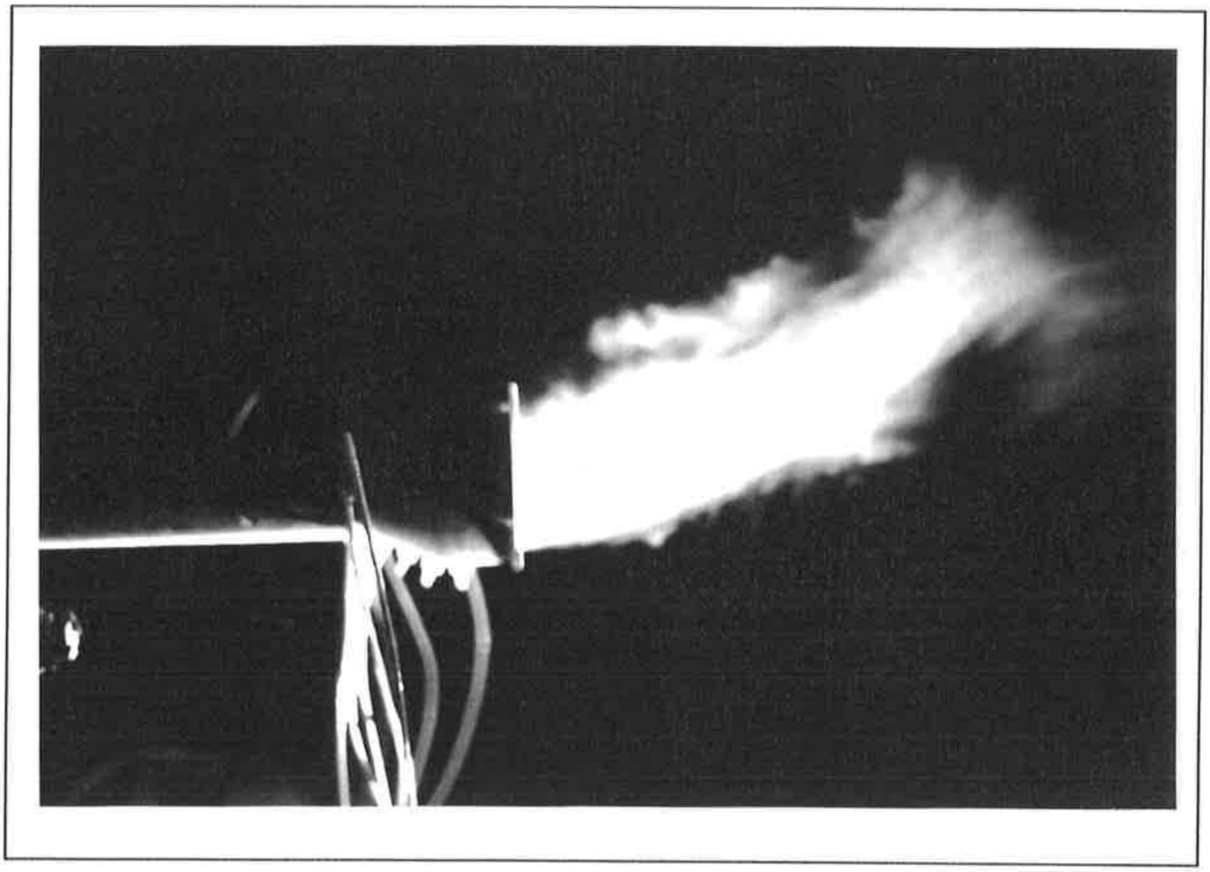

Figure C. 22 Deflected jet exiting CD Nozzle, visualised by seeding the jet viewed with laser sheet at Re = 1400 and AR = 0.83.

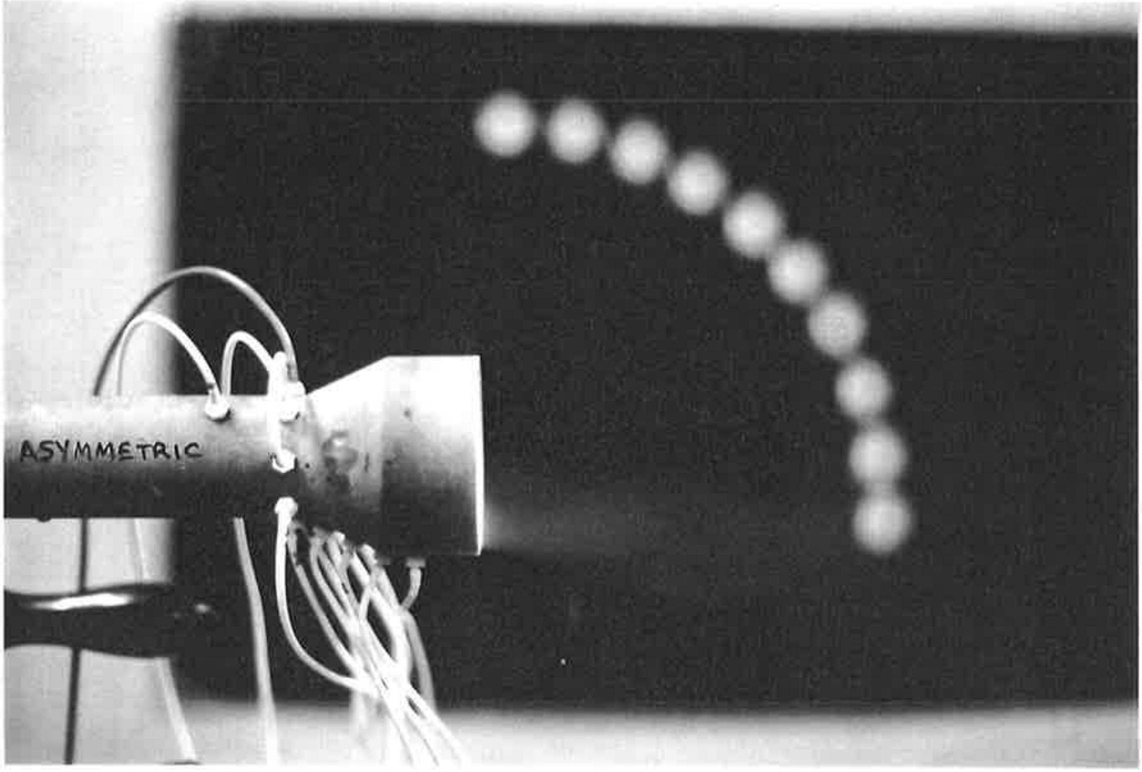

Figure C. 23 Jet exiting CD Nozzle, visualised by seeding the jet viewed in natural light at Re = 27,000 and AR = 1. Asymmetric flow.

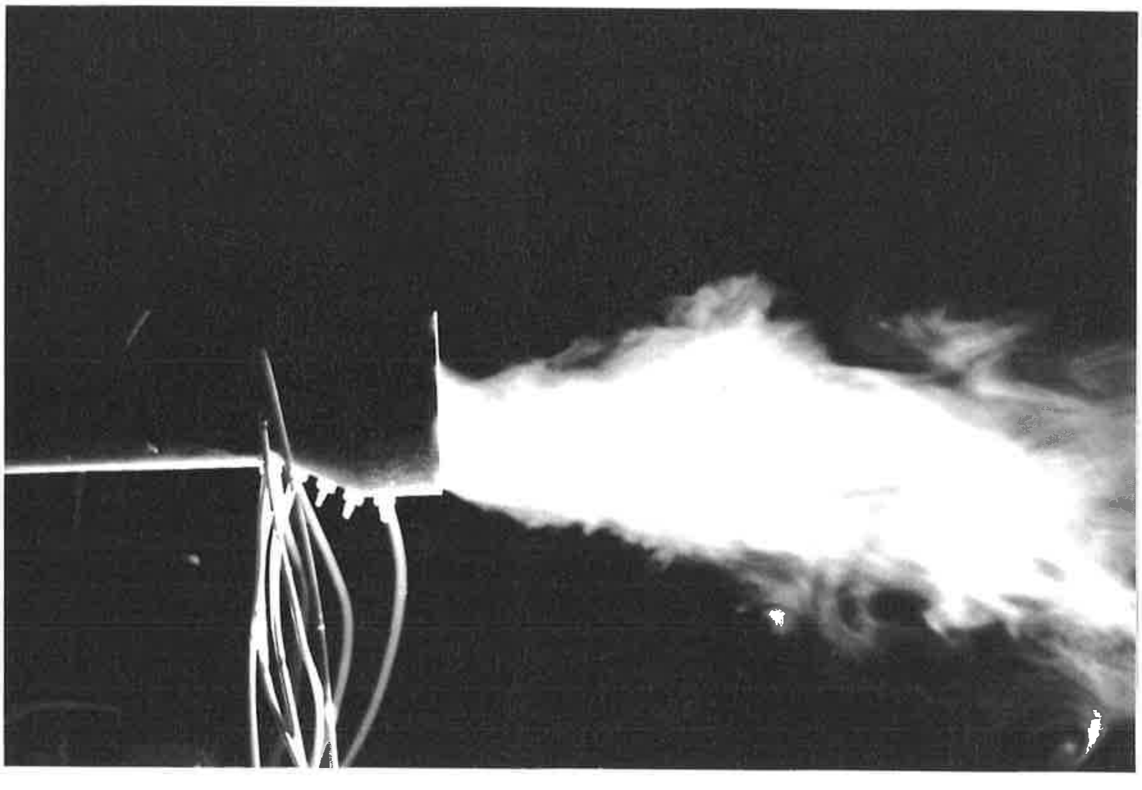

Figure C. 24 Jet exiting CD Nozzle, visualised by seeding the jet viewed with laser sheet at Re = 1400 and AR = 1. Asymmetric flow.

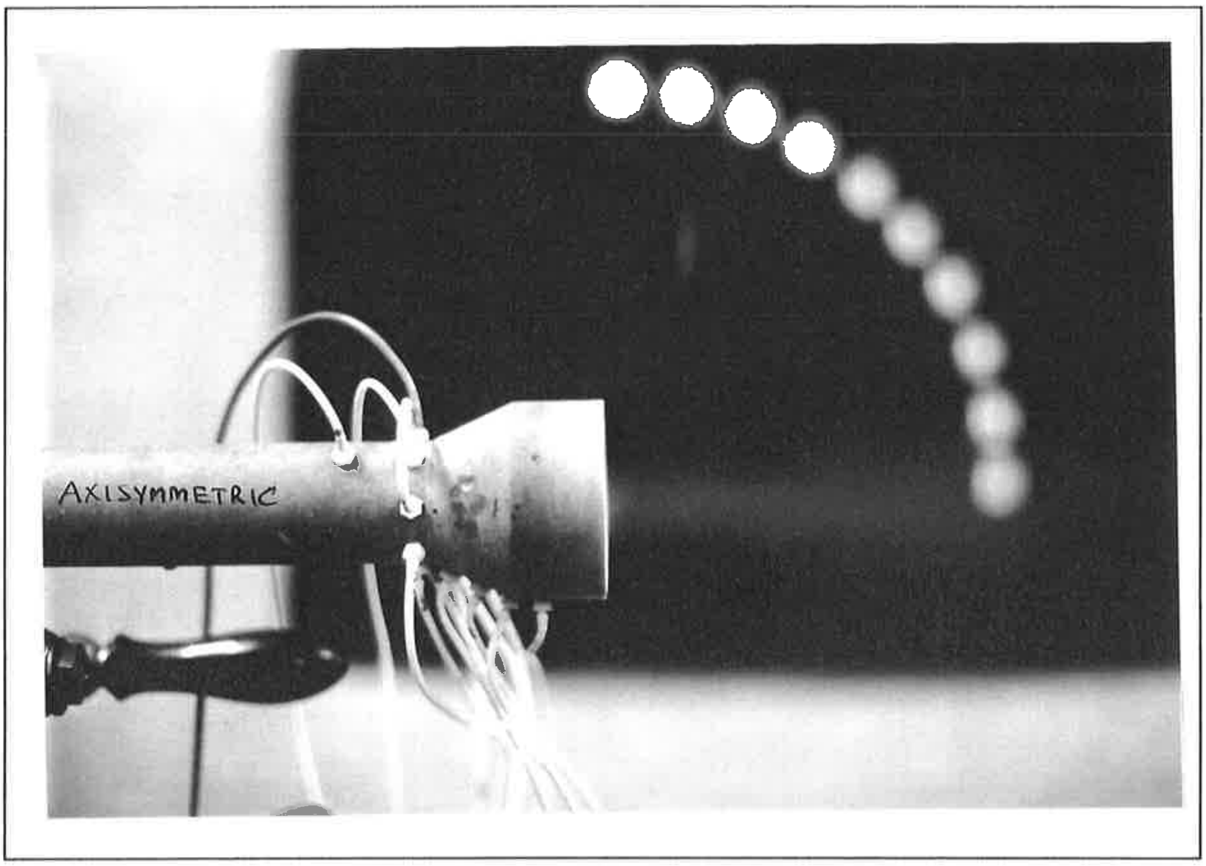

Figure C. 25 Jet exiting CD Nozzle, visualised by seeding the jet viewed in natural light at Re = 27,000 and AR = 1. Axisymmetric flow.

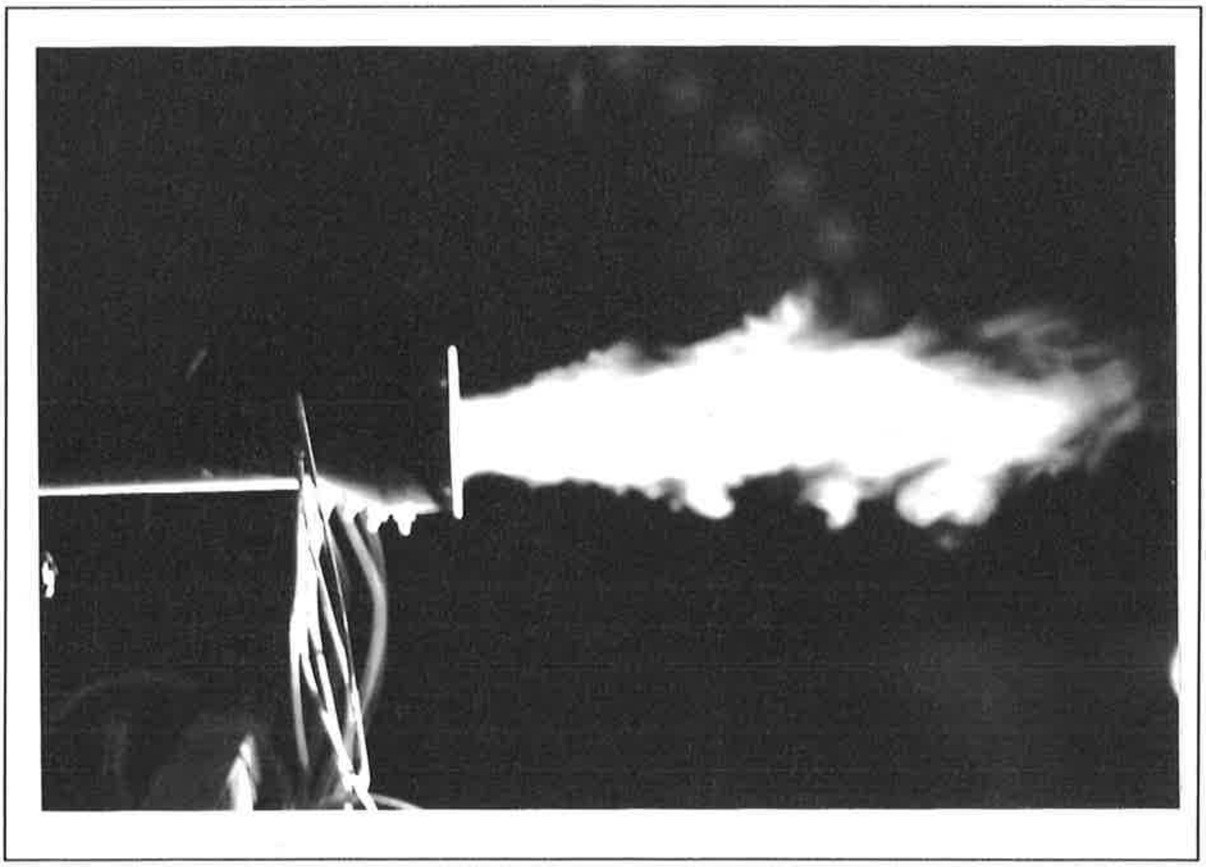

Figure C. 26 Jet exiting CD Nozzle, visualised by seeding the jet viewed with laser sheet at Re = 1400 and AR = 1. Axisymmetric flow.